Author:
Singh, Suresh

Title:
A clash of clades

the evolution and ecology of terrestrial amniotes through the Permo-Triassic.

A clash of clades: the evolution and ecology of terrestrial amniotes through the Permo-Triassic.

By

Suresh Anmol Singh

School of Earth Sciences

University of Bristol

A dissertation submitted to the University of Bristol in accordance with the requirements for the award of the degree of Doctor of Philosophy in the Faculty of Science.

February 2021

Word Count: 88,029

Abstract

The late Palaeozoic and early Mesozoic saw the birth of modern terrestrial ecosystems and clades as tetrapods embarked on conquest of the land. The onset of full tetrapod terrestrialisation in the Carboniferous sparked diversification that saw two amniote clades become the principal actors in the terrestrial realm, the Synapsida and Archosauromorpha, which came to dominate terrestrial faunas in the late Palaeozoic and early Mesozoic, respectively. Their patterns of diversification may help shed light on the way intrinsic and extrinsic pressures direct the course of evolution, as their relative success ebbed and flowed against a backdrop of the profound environmental changes that punctuated their evolution. Extrinsic changes are undoubted agents of macroevolutionary change, as they are associated with multiple mass extinction events and faunal turnovers. Extinction events help reset eco-evolutionary dynamics by giving new or minor clades the chance to diversify across previously occupied niches, but what drives differential survival and success through these events and in their aftermath? Here, I investigate how susceptibility to extinction and radiation are linked to ecology, as an animal's ecology determines its capacity to respond to environmental changes and their potential intrinsic interactions, which are key to survival and success through and after extinction events. Using the functional anatomy of synapsids and archosauromorphs through the late Palaeozoic and early Mesozoic macroevolution, I assess how their ecology varied in response to intrinsic and extrinsic changes to identify the key driving forces behind their macroevolution. I find that morpho-functional diversity is highly segregated by clade, particularly through times of environmental stability, reflecting strong niche partitioning and intrinsic constraint. However, I find the largest changes in ecomorphology are associated with large-scale extrinsic events, with the loss of competitors through these events often preceding eco-morphological diversification in the survivors. Consequently, intrinsic factors such as innate anatomy and competition appear to be key controls on ecological diversity, but environmental events are the primary drivers of large-scale changes in a clade's macroevolution.

Author Declaration

I declare that the work in this dissertation was carried out in accordance with the requirements of the university's regulations and code of practice for research degree programmes and that it has not been submitted for any other academic award. Except where indicated by specific reference in the text, the work is the candidate's own work. Work done in collaboration with, or with the assistance of others is indicated as such. Any views expressed in this dissertation are those of the author.

Suresh Anmol Singh

15th February 2021

Acknowledgements

I would like to express my sincerest gratitude to the Faculty of Science for funding my PhD studentship, and to my supervisors, Professors Michael J. Benton and Emily J. Rayfield, for their guidance and support throughout.

I thank the following institutions for allowing me to access their collections to gather data: The Museum of Natural History, London (NHMUK), The New Mexico Museum of Natural History & Science (NMMNHS), The Field Museum of Natural History, Chicago (FMNH), and The American Museum of Natural History, New York (AMNH).

I would also like to thank my friends and colleagues without whom, this body of work would not exist. Firstly, I would like to thank Dr Pamela Gill for her encouragement all those years ago following our meeting on the Access to Bristol scheme. Her encouragement was instrumental in my choice to study palaeontology at Bristol. Professor Christine Janis, for her insight, advice, and humour throughout this work and on other concurrent projects.

Holly Betts, Eloise Hunt, Avita Kaur, Logan King, Morten Lunde Nielsen, Klara Nordén, Gary Pontgratz-Coleman, Samantha Royle, Fiann Smithwick, Thomas Stubbs, Rhiannon Terrett, and Vishruth Venkat all have my sincere thanks for being such an integral part of my time as a PhD student and providing so many fond memories. Finally, special mention must be made of the following people: William Anderson, Charlie Delbridge, Armin Elsler, Catherine Klein, Nuria Melisa Morales Garcia, Amanpreet Kaur Nandhra, James Lewis, David Nash, Evan Saitta, Benjamin Search, Max Stockdale, Catherine Strickson, Marta Zaher, and Steven Zhang. Their stout support during the difficult times through this undertaking was a blessing for which I remain ever grateful.

Co-author Contributions

I declare that I received resources and guidance from colleagues that was integral to this entire body of work, and therefore outline this assistance here:
Specific contributions for each body of work are presented at the beginning of each chapter, but I mention here that the bulk of these resource contributions came from Dr Armin Elsler, who provided the chronostratigraphic data used to mark taxon first and last appearances, the Log^{10} femur length data that is used as a proxy for body size, and time-calibrated phylogenetic trees for the primary two clades of interest, the Synapsida and Archosauromorpha. He also ran the evolutionary rates analyses presented in Chapter 2. Dr Thomas Stubbs provided training and support to run the morphometric analyses. Professors Emily Rayfield and Michael Benton provided guidance and comments on the overall thesis concept and guidance on drafting the chapters.

I collected all the mandibular and dental data and carried out the morphometric, disparity, and macroevolutionary modelling analyses, as well as the phylogenetic imputations of missing data. The work presented here represents 90% of my own independent work. Chapters where co-author contribution was greater than 10% will be highlighted.

Dedication

Dedicated to my mother and aunt who have always pushed me to pursue my passions. All my work and efforts here would not have been possible without their enduring encouragement and support.

Table of Contents

List of Figures

List of Tables

Chapter 1 - Introduction

1.1 Macroevolution during the late Palaeozoic and early Mesozoic

How do the physical and biological aspects of the biosphere drive the tempo and mode of evolution? Such a question has been asked repeatedly by evolutionary biologists since the inception of the field (Simpson, 1944; 1953; Maynard Smith, 1989; Vrba, 1995), and remains the fundamental driver of much study today. Contemplating the drivers of evolution through deep time has led to dichotomous debate within macroevolutionary study over the primacy of intrinsic or extrinsic drivers. Proponents of extrinsic power argue that large-scale events such as climatic shifts and pulses of volcanism affect the greatest control on macroevolution, based on the coincidence of large-scale faunal turnovers and peaks in extinction and origination associated with such events (Lu et al., 2006; Alroy, 2008; Myers and Saupe, 2013; Hull, 2015). The view of primarily extrinsic control is characterised as the 'Court Jester' model (CJM) (Benton, 2009). In contrast, the advocates of intrinsic power use extensive microevolutionary evidence for how ecological interactions (Brown and Wilson, 1956; Schluter, 1994; Pigot et al., 2016; Yuan et al., 2020) between taxa can affect phenotypic and ultimately evolutionary changes to argue that intrinsic factors represent the primary control on macroevolution, encapsulated by the 'Red Queen' model (RQM) of Van Valen (1973), which extrapolated microevolutionary patterns to explain patterns of extinction across taxonomic levels through deep time. The dichotomy is partially driven by differences in perspective, epitomised in the general division of evolutionary biologists and palaeobiologists between the two viewpoints.
The spatio-temporal and taphonomic inconsistencies of the fossil record (Raup, 1972; Benton et al., 2000; Smith, 2001; Kidwell and Holland, 2002; Purnell and Donoghue, 2005; Valentine et al., 2009; Benson et al., 2010; Benson and Butler, 2011; Mannion et al., 2011; Dunhill et al., 2014) offer a coarse and intermittent view of palaeodiversity that better illustrates the broad spatio-temporal impacts of extrinsic changes/events, rather than the low-level, population dynamics that summarise the biotic conflict and coevolutionary interactions critical to the RQM (Jablonksi, 2009; Benton, 2009; Ezard et al., 2016). The increasing availability of big datasets and phylogenetic analytical methods is pushing the reconciliation of these camps through growing discussion and recognition that such dichotomous surmising of macroevolution as being primarily driven by extrinsic or intrinsic poorly reflects the real complexity of how these drivers work (Jablonski, 2003; Venditti et al., 2010; Rabosky, 2013; Quental and Marshall, 2013; Voje et al., 2015; Strotz et al., 2018)

The late Palaeozoic and early Mesozoic offer great opportunity for investigation of these phenomena as this interval of Earth history witnessed the foundation of modern terrestrial ecosystems and eco-evolutionary dynamics as tetrapods colonised the land and diversified (Olson,

1966; Sues, and Reisz, 1998; Benton, 2014; Coates et al., 2008). Many important modern clades trace their emergence as common components in modern faunas to this time. The lepidosaurs and lissamphibians trace their origins to this interval, as do key insect clades such as the flies and beetles, as well as multiple groups of ferns and conifers (Benton, 2016; Sues and Fraser, 2010; Kustatscher et al., 2018). Two great amniote clades also emerged as the predominant tetrapods in terrestrial ecosystems, the Synapsida and Archosauromorpha (Olson, 1982; Romer, 1966; Benton, 2014). Great taxonomic and ecological diversity saw these clades dominate terrestrial faunas in the Permian and early Mesozoic, respectively (Benton, 2014; 2020; Sahney et al., 2010; Sahney and Benton, 2008; Dunne et al., 2018; Rubidge and Sidor, 2001; Kemp, 2005; Ezcurra et al., 2020). Both also evolved similar intrinsic innovations to improve locomotory (Blob, 2001; Rubidge and Sidor, 2001; Ezcurra et al., 2020) and metabolic (Kemp, 2006b; Rey et al., 2017; Rubidge and Sidor, 2001; Benton, 2020) efficiency. Their reigns as have left a lasting legacy on biodiversity as the they produced the two key clades that current faunas, mammals, and birds (Benton, 2014).

Evolution was also subject to multiple extrinsic changes as global climates oscillated between icehouse and greenhouse conditions through the late Palaeozoic (Cleal and Thomas, 2005; DiMichele et al., 2009; Parrish, 1995), then between humid and drier climates in the early Mesozoic (Simms and Ruffel, 1990; Preto et al., 2010; Ruhl et al., 2011; Dubiel et al., 2011) (Fig. 1.1.1). Much of this change can be linked to large-scale tectonic changes, with multiple large igneous province (LIP) volcanic episodes occurring through this interval (Ernst et al., 2020; Benton, 2016; Kravchinsky, 2012). Most notably, this interval includes two of the 'Big five' mass extinctions driven by LIPs – the Permo-Triassic mass extinction (PTME) and Triassic-Jurassic mass extinction (TJE), driven by the Siberian Traps (Erwin et al, 2002**;** Joachimski et al., 2012; Yin and Song, 2013; Wu et al., 2021) and the Central Atlantic Magmatic Province volcanism, respectively (Tegner et al., 2020; Wignall and Atkinson, 2020; Benton et al., 2004) (Fig. 1.1.1). A host of smaller events have now been recognised within the late Palaeozoic and early Mesozoic (Fig. 1.1.1). Ongoing study has suggested another major mass extinction event at the end of the Capitanian (ECE) likely driven by the Emeishan LIP (He et al., 2007; Bond et al., 2010; Yin and Song, 2013; Rampino and Shen, 2021). Deeper eco-environmental changes have also been recognised through both the Carboniferous-Permian transition and Carnian, with both subject to deep floral turnovers/changes (Falcon-Lang and DiMichele, 2010; Kustatscher et al., 2018, McGhee, 2018). The Carboniferous-Permian transition marked a shift to drier climatic conditions and terrestrial faunas as the Late Paleozoic Ice Age began to end (Reisz, 1972; McGhee, 2018; Huttenlocker et al., 2021), with the changes being tied to the decline of the lycopod rainforests in the Kasimovian, an event known as the Carboniferous Rainforest Collapse (CRC) that is associated with the rise of amniote tetrapods (Sahney et al., 2010;

Dunne et al., 2018; Pardo et al., 2019) (Fig. 1.1.1). The Carnian has recently been acknowledged as marking an intense oscillation between dry and humid global climates, with the interval (234-232 Ma) now known as the Carnian Pluvial Event (CPE) (Bernardi et al., 2018; Benton et al., 2018; Dal Corso et al., 2020). Finally, the early Toarcian has long been known as an period of environmental upheaval in the oceans with a well-documented pulse of ocean acidification and anoxia (Bailey et al., 2003; Caruthers et al., 2013), but new studies have now started to identify broader environmental upheaval in terrestrial environments (Slater et al., 2019; Mander and McElwain, 2019; Pol et al., 2020; Ruebsam and Schwark, 2021). All of these global climatic changes drove significant restructuring of terrestrial floras and so marked changes in terrestrial habitats (Cleal and Thomas, 2005; Pfefferkorn et al., 2008; Falcon-Lang and DiMichele, 2010; Kustatscher et al., 2018; Cascales–Miñana and Cleal, 2012). These climatic changes often coincided with mass extinction events and faunal turnovers (Fig. 1.1.1) that effectively reset of ecosystems (Van Valen, 1984; Benton et al., 2004; Sahney and Benton, 2010). Furthermore, all are associated with significant faunal turnovers that saw the radiation of new clades and decline of previously prevalent and diverse (dominant) clades.

The repeated destruction and reestablishment of complex ecosystems offers further opportunity to explore the interplay of extrinsic and intrinsic macroevolutionary drivers and their impacts on successive clades during this time are manifested in the fossil record. Multiple biotic recoveries in this interval also provide a good chance to observe the enigmatic impacts of intrinsic interactions. Increasing taxonomic diversity logically suggests increasing ecological diversity through greater niche specialisation (Simpson, 1955; Schluter, 2000; Losos and Mahler, 2010) and so with greater ecological diversity, it is likely that food chains become more multifaceted with multiple trophic interactions creating highly complex trophic networks (Benton et al., 2004; Sahney and Benton, 2010; Roopnarine et al., 2019). Increasing ecological interactions, such as predation and resource competition, may also have driven greater ‘ecological conflict’; these taxa exist in opposition through pursuing their own interests, e.g., the predator wants eat the prey, but the prey doesn’t want to be eaten, or two different herbivores both want to maximise their intake of a particular resource so adapt to better exploit said resource (Romer, 1967; Bakker, 1975; Rabosky and Lovette, 2008; Rabosky, 2013). Such interactions are traditionally thought to have played a significant role in key faunal turnovers such as the shift from synapsid to archosauromorph and pseudosuchian to dinosaur faunal prevalence within the Mesozoic (Charig, 1984; Bakker, 1972; Bonaparte, 1982). Indeed, the minimisation of such conflict is the basis for each of the main types of ecological opportunity that promote radiations: 1) the extinction of competitors, 2) the emergence

of new niches/resources, 3) the evolution of innovations that unlock access to new resources (Simpson, 1953; Schluter, 2000).

Palaeobiological study of such patterns have become increasingly focused on disparity as the functional utility of morphology (Foote 1994; Alfaro et al., 2004; Brusatte et al., 2008; Sakamoto, 2010; Anderson et al., 2011; Stubbs et al., 2013; Grossnickle and Polly, 2013; Foth et al., 2017; Ezcurra and Butler, 2018; Brocklehurst, 2019; Brocklehurst and Brink, 2017; Grossnickle, 2020, Button and Zanno, 2020) allows the tracking of diversification alongside morpho-functional and ecological evolution, highlighting the impacts of specific traits on evolutionary success (Roy, 1996; Eble, 2000; Wagner & Estabrook, 2014). The wider context of such patterns must be considered as it is ultimately the interaction of organisms with the wider world and their relative performance against coeval taxa and environmental changes that dictate the course of evolution. Consequently, the form and function of synapsid and archosauromorph trophic ecomorphology are explored here to better understand how ecological clashes and climatic upheaval brought forth the ecological structures and clades that underpin modern biodiversity. Here, I investigate the trophic evolution of the Synapsida and Archosauromorpha, approaching their macroevolution from both a clade and guild perspective to highlight how intrinsic and extrinisc pressures drove the differential success of particular taxonomic and/or ecological groups, culminating in a detailed examination of how success or extinction relates to the broader interplay between both forms of macroevolutionary drivers and a confluence of ideal circumstances.

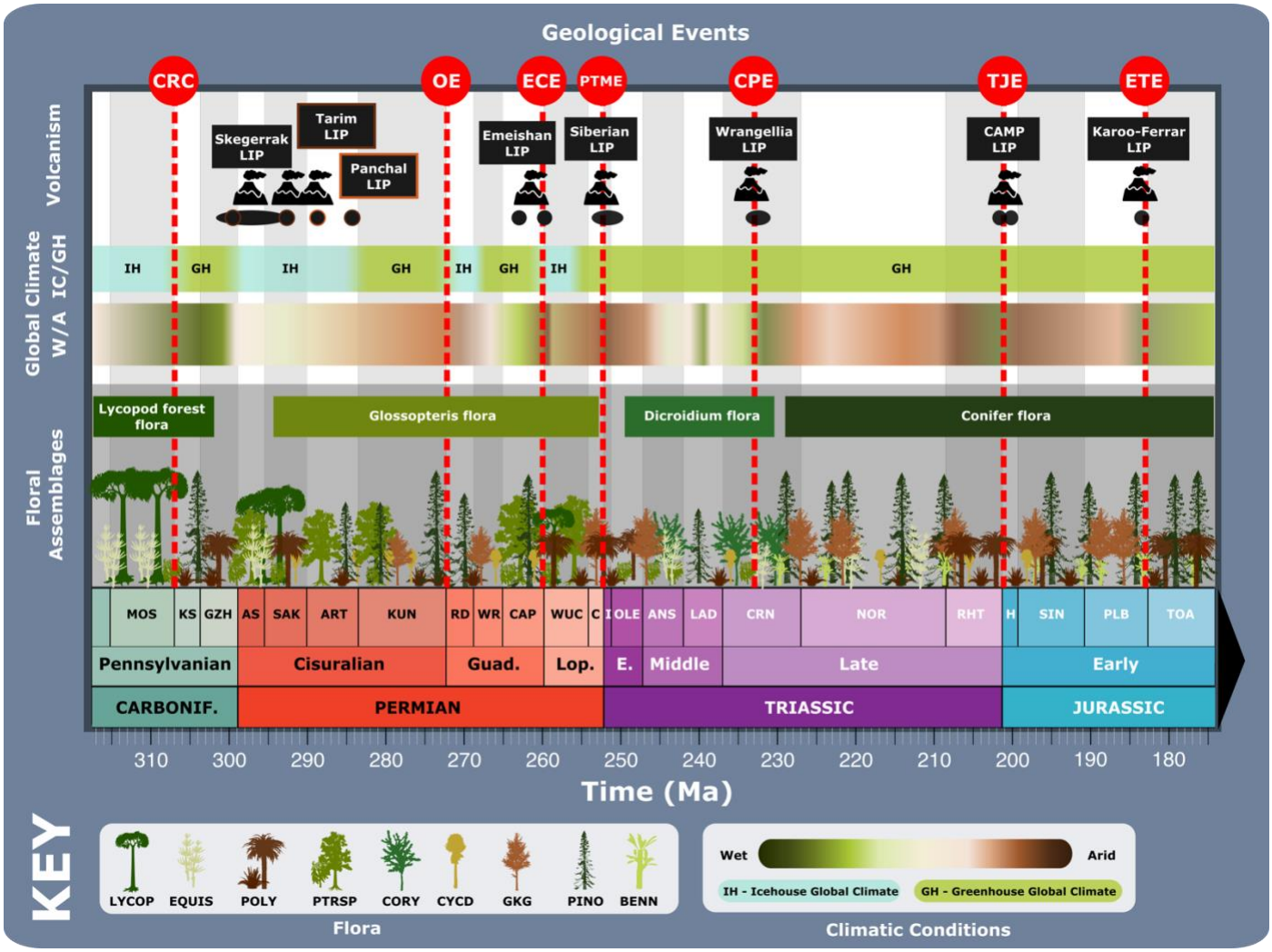

Figure 1.1.1. Key environmental changes through the late Palaeozoic and early Mesozoic. Changes from glacial (icehouse) to interglacial (greenhouse), and wet to arid climates shown by stripe colour gradients (McGhee, 2018; Ernst et al., 2020; Falcon-Lang and DiMichele, 2010; Preto et al., 2010; Chandler et al., 1992; Slater et al., 2019; Dal Corso et al., 2020). Key volcanic events indicated by graphic, with pulses indicated by black circles (Ernst et al., 2020; Chen and Xu, 2020; Benton, 2016; Kravchinsky, 2012). Predominant vegetation (Cleal and Thomas, 2005, Pfefferkorn et al., 2008; Kustatscher et al., 2018; van de Schootbrugge et al., 2009; McElwain et al., 1999; Anderson and Holmes, 2008; Dilcher et al., 2004; Tewari et al., 2012; Bernardes-de-Oliveira et al., 2016) indicated by tree silhouettes. Abbreviations: ANS, Anisian. ART, Artinskian. AS, Asselian. BENN, Bennettitales. C, Changhsingian. CAP, Capitanian. CORY, Corystospermaceae. CPE, Carnian pluvial event. CRC, Carboniferous rainforest collapse. CRN, Carnian. CYCD, Cycadophyta. E, Early. ECE, End-Capitanian extinction. EQUIS, Equisetidae. ETE, Early Toarcian event. GH, Greenhouse. GKG,

Ginkgoales. Guad, Guadalupian. GZH, Gzhelian. H, Hettangian. I, Induan. IH, Icehouse. KS, Kasimovian. KUN, Kungurian. LAD, Ladinian. LIP, Large igneous province. Lop, Lopingian. LYCO, Lycophyta. MOS, Moscovian. NOR, Norian. OE, Olson's extinction. OLE, Olenekian. PINO, Pinophyta. PLB, Pliensbachian. POLY, Polypodiopsida. PTME, Permo-Triassic mass extinction. PTRSP, Pteridospermales. RD, Roadian. RHT, Rhaetian. SAK, Sakmarian. SIN, Sinemurian. TJE, Triassic-Jurassic extinction event. TOA, Toarcian. WR, Wordian. WUC, Wuchiapingian.

1.2 The Synapsida

Synapsids are one of the great amniote clades, encompassing crown mammals as well as a host of extinct stem diversity. Their success is easily apparent given their contemporary domination of terrestrial faunas and colonisation of the aerial and marine realms (Kemp, 2005). Current mammalian prevalence marks an era of global dominance; the Cenozoic is characterised as the 'age of mammals'. Current supremacy marks a renaissance for synapsids as non-mammalian forms were the predominant terrestrial amniotes during the late Palaeozoic. Amniotes emerged in the Late Carboniferous (~320 Ma) and quickly radiated (Clack, 2002; Müller and Reisz 2005; Voigt and Ganzelewski, 2009), producing the synapsid and sauropsid lineages (Reisz, 1972; 2007). The oldest synapsid, *Archaeothyris florensis* is an ophiacodont, which suggests that the multiple clades of pelycosaur synapsid (Fig. 1.2.1) were already emerging in the Bashkirian, if the prevailing view of the synapsid phylogeny is correct (Reisz and Fröbisch, 2014; Brocklehurst et al., 2016). Further support for this comes from ichnofossil evidence from Germany that indicates large ophiacodont or even sphenacodont pelycosaurs were present in Bashkirian, underscoring a rapid increase in the body sizes of early synapsids soon after their emergence (Voigt and Ganzelewski, 2009). Reisz (1972) argues that such size increases allowed pelycosaurs to quickly establish themselves as the predominant terrestrial carnivores. The Late Carboniferous certainly saw the evolution of multiple carnivorous pelycosaur clades, and potentially the earliest therapsids, which represent the next grade of synapsid evolution (Kemp, 2006a; Rubidge and Sidor, 2001). In any case, pelycosaurs diversified and became the predominant large amniotes in most terrestrial faunas in the Pennsylvanian, as fully land-based ecosystems emerged through the Permo-Carboniferous (Olson, 1966; Benton, 2014; Coates et al., 2008). The rise of the amniotes (and thus synapsids) is attributed to the Kasimovian rainforest collapse (KRC), which occurred at the Moscovian-Kasimovian stage (~307 Ma). A shift from a glacial to interglacial climates at this boundary saw the decline of the giant lycopod-dominated rainforests that had prevailed for much of the Carboniferous (Cleal and Thomas, 2005; Pfefferkorn et al., 2008; Falcon-Lang and DiMichele, 2010). Though the diversification

mechanism remains hotly debated, amniotes were clear beneficiaries of this extrinsic change, becoming more abundant within terrestrial ecosystems (Sahney et al., 2010; Dunne et al., 2018). All pelycosaur clades diversified during this time, radiating across carnivorous and herbivorous niches (Romer and Price, 1940; Kemp, 2005; Benton, 2014). Glacial resurgence in the Early Permian brought drier and cooler climatic conditions that entrenched amniote dominance of terrestrial ecosystems, and saw further diversification within pelycosaurs, particularly the Sphenacodontidae and Edaphosauridae, which achieved greater body sizes and abundance (Olson, 1962; 1966; Gould, 1967; Brocklehurst et al., 2013). Global warming through the Artinskian – Kungurian (Chen and Xu, 2020; REF) saw a decline in pelycosaur diversity that culminated in the end-Kungurian extinction, known as Olson's extinction (OE) (Olson, 1982; Sahney and Benton, 2008; Brocklehurst et al., 2017). The decline of tropical, everwet, everwarm environments saw the extinction of all pelycosaur clades besides the Caseidae and Varanopidae, but more significantly saw the emergence of the Therapsida (Kemp, 2006a).

The origins of therapsids are clouded in uncertainty as the explosion of diversity in the late Roadian-early Wordian marks their earliest appearance in the fossil record (Olson, 1962; 1966; Chudinov, 1965; Benton, 2014). It is universally agreed that therapsids are the sister group to the sphenacodontids (Kemp, 2006a; Rubidge and Sidor, 2001), with the highly derived sphenacodontid, *Tetraceratops insignis* likely exhibiting similar traits to the first therapsids (Spindler, 2020). The sudden prevalence of therapsids and their faunal replacement of the pelycosaurs has been attributed by Kemp (2006) to ecological opportunism as supposed tolerance for cooler conditions permitted therapsid survival as such conditions prevailed in the Middle Permian. In any case, the therapsids attained greater ecological diversity towards the end of the Middle Permian, with radiations in the Wordian and Capitanian that saw basal then neotherapsids diversify (Fig. 1.2.1) (Olson, 1962; 1966; Sennikov, 1996; Rubidge and Sidor, 2001; Kemp, 2005). The end-Guadalupian extinction event is now recognised as a severe mass extinction (Retallack et al., 2006; Sahney and Benton, 2008; Clapham et al., 2009; Day et al., 2015; Rampino et al., 2019), that brought profound biotic changes including a turnover in terrestrial faunas. Biarmosuchians and dinocephalians were superseded by anomodonts and theriodonts (Benton et al., 2004; Sahney and Benton, 2008). The Late Permian marked the peak of non-mammalian synapsid faunal dominance, recording their greatest diversity and disparity (Benton et al., 2004; Kammerer, 2009; Botha and Huttenlocker, 2021) , hosting a wide diversity of herbivorous anomodonts as well as multiple clades of carnivorous theriodonts (Olson, 1966; Bakker, 1975; Benton et al., 2004) (Fig. 1.2.1), and saw great innovation in their feeding (Crompton, 1963; Rubidge and Sidor, 2001; Kemp, 2005; Lautenschlager et al., 2018; King et al., 1989) and locomotory anatomy (Blob, 1998; 2001; Rubidge and Sidor, 2001; Kemp, 2005;

Jones et al., 2018), as well as physiological changes indicative of endothermy (Bennett and Ruben, 1986; Ruben et al., 2012; Rubidge and Sidor, 2001; Kemp, 2006b; Hopson, 2012; Faure-Brac and Cubo, 2020; Benton, 2020).

Therapsid faunal predominance was shattered in the devastation of the Permo-Triassic mass extinction event (PTME) (Erwin et al, 2002; Benton et al., 2004; Kemp, 2005; Saunders and Reichow, 2009; Sookias et al., 2012; Fröbisch, 2013). Only the dicynodonts and eutheriodonts survived the PTME, and though they initially appeared to retain their place as the predominant large terrestrial amniotes, the Triassic marked their slow decline and relegation to lower levels of terrestrial food webs (Rubidge and Sidor, 2001; Sookias et al., 2012; Sidor et al., 2013; Benton, 2020). The extinction of therocephalians in the Middle Triassic (Brocklehurst, 2019) and dicynodonts at the end of the Triassic (Ruta et al., 2013b) left only one remaining lineage of synapsids that had emerged from within the cynodonts, the mammals (Kemp, 2005, Ruta et al., 2013a). Mammals would become highly successful through the remainder of the Mesozoic, achieving great diversity and disparity (Close et al., 2015; Luo, 2007; Meng, 2014), but terrestrial supremacy in the Mesozoic belonged to the dinosaurs.

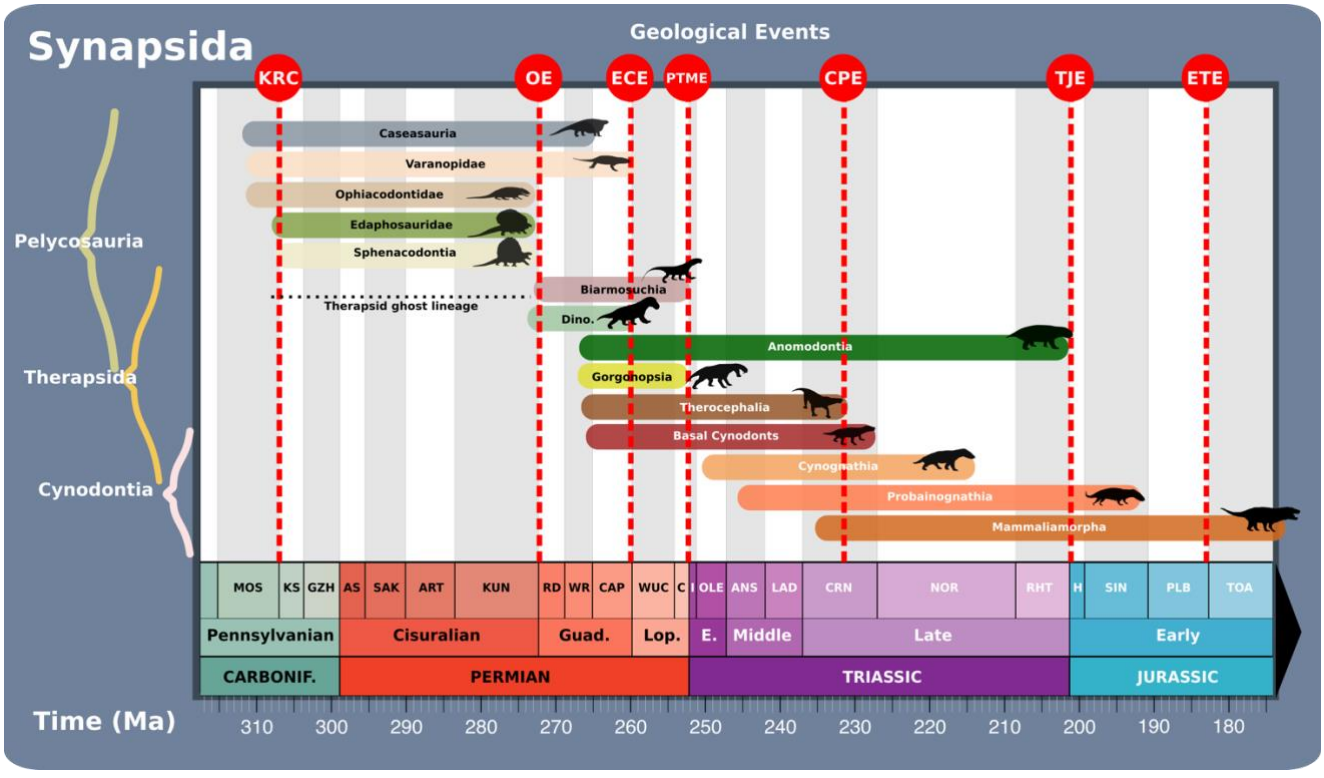

Figure 1.2.1. Range chart of the Synapsida through the late Palaeozoic and early Mesozoic. Abbreviations: ANS, Anisian. ART, Artinskian. AS, Asselian. C, Changhsingian. CAP, Capitanian. CPE, Carnian pluvial event. CRN, Carnian. Dino, Dinocephalia. E, Early. ECE,

End-Capitanian extinction. ETE, Early Toarcian event. Guad, Guadalupian. GZH, Gzhelian. H, Hettangian. I, Induan. KS, Kasimovian. KRC, Kasimovian rainforest collapse. KUN, Kungurian. LAD, Ladinian. Lop, Lopingian. MOS, Moscovian. NOR, Norian. OE, Olson's extinction. OLE, Olenekian. PLB, Pliensbachian. PTME, Permo-Triassic mass extinction. RD, Roadian. RHT, Rhaetian. SAK, Sakmarian. SIN, Sinemurian. TJE, Triassic-Jurassic extinction event. TOA, Toarcian. WR, Wordian. WUC, Wuchiapingian. Ranges based on Benton et al., (2013).

1.3 The Archosauromorpha

The sauropsids experienced notable success during the Late Palaeozoic, with parareptiles and captorhinid eureptiles enjoying great taxonomic and ecological diversity during this interval but although they were prominent within terrestrial faunas, they were not as ubiquitous as the synapsids (Olson, 1962; Brocklehurst et al., 2017; 2020). It was in the Triassic that the diapsids began to proliferate, and one clade rapidly emerged to fill many of the niches vacated by the therapsids, the Archosauromorpha. Originating in the mid-late Permian, archosauromorphs were initially negligible components within terrestrial faunas (Benton et al., 2004; Ezcurra et al., 2014; Ezcurra and Butler, 2018), but they gained in prominence towards the end of the Permian with the evolution of large, specialised taxa, such as the hypercarnivorous *Archosaurus rossicus* (Sennikov and Golubev, 2006). Through the course of the Triassic, they would evolve across a variety of niches, entering the marine and aerial realms (Ezcurra and Butler, 2018; Ezcurra et al., 2020; Foth et al., 2017), ultimately becoming the dominant terrestrial amniotes, leaving remaining synapsids in a diminished role within terrestrial ecosystems (Bakker, 1972; Bonaparte, 1982; Benton et al., 2004; Sues and Fraser, 2010; Sookias et al., 2012). The first big radiation of the Archosauromorpha occurred in the Anisian, which saw their diversification across a variety of niches in terrestrial and marine settings, and across the herbivore and carnivore guilds (Ezcurra et al., 2014; Stocker et al., 2016; Foth et al., 2017; Ezcurra and Butler, 2018; Ezcurra et al., 2020). The diversification of new specialised taxa in the Anisian helped drive the reestablishment of complex ecosystems by creating new links within terrestrial trophic networks (Benton et al., 2004; 2013; Wei et al., 2015). Within this newfound diversity, archosaurs arose to more prominent ecological positions with the evolution of specialised hypercarnivorous pseudosuchians and herbivorous dinosauromorphs (Stubbs et al., 2013; Nesbitt et al., 2017; Hoffman et al. 2019).

The onset of the Late Triassic saw basal archosauromorphs and archosauriforms supplanted by archosaurs (Fig. 1.3.1) in an apparent extinction event within the Carnian or at the Carnian-Norian boundary (Benton, 1983; 2004; Brusatte et al., 2008; Benton et al., 2018; Irmis, 2011; Mancuso et al., 2020), that has been associated with the Carnian Pluvial Event (CPE) (Bernardi et al., 2018;

Benton et al., 2018; Dal Corso et al., 2020). Dinosaurs emerged as a significant component in terrestrial faunas during this time, with recent studies suggesting a causal link to the CPE (Bernardi et al., 2018; Benton et al., 2018). Pseudosuchians and dinosaurs jointly dominated terrestrial ecosystems, and whilst dinosaurs dominated the herbivore guild (Barrett et al., 2010), pseudosuchians were much more ecologically diverse, spread across the carnivore and herbivore guilds, and occupying positions as the top predators within most terrestrial faunas (Bonaparte, 1982; Benton, 1983; Brusatte et al., 2008; Benton et al., 2014). The end of the Late Triassic saw significant declines in archosaur diversity and disparity (Brusatte et al., 2008; Stubbs et al., 2013; Foth et al., 2017; Ezcurra and Butler, 2018; Allen et al., 2018). This interval of extinction is somewhat poorly understood as although there is a clear mass extinction at the Triassic-Jurassic boundary, there is additional evidence to suggest this event was protracted across multiple pulses of extinction through the Rhaetian (Sephton et al., 2002; Rigo et al., 2020; Wignall & Atkinson 2020). Pseudosuchians were hit particularly hard by the end-Triassic extinction (ETE), whereas dinosaurs appear to have been less affected (Brusatte et al., 2008; Stubbs et al., 2013; Foth et al., 2017; Ezcurra and Butler, 2018). This allowed dinosaurs to quickly repopulate devastated terrestrial faunas and secure faunal dominance by becoming the predominant large tetrapods in most terrestrial faunas (Benton, 1983; Brusatte et al., 2008; Langer et al., 2010; Benton et al., 2014), which would endure to the end of the Mesozoic.

The succession of faunal turnovers that cemented archosauromorph prevalence and saw further turnovers within the Archosauromorpha have been heavily studied as part of the wider debate on macroevolutionary drivers. Patterns of archosauromorph evolution in the early Mesozoic have been cited in support of the primacy of intrinsic or extrinsic drivers; the outcome of each turnover has been attributed in either case to competitive superiority or environmental forcing (Charig, 1984; Bakker, 1972; Bonaparte, 1982; Benton, 1983; 1989; Brusatte et al., 2008; Benton et al., 2014).

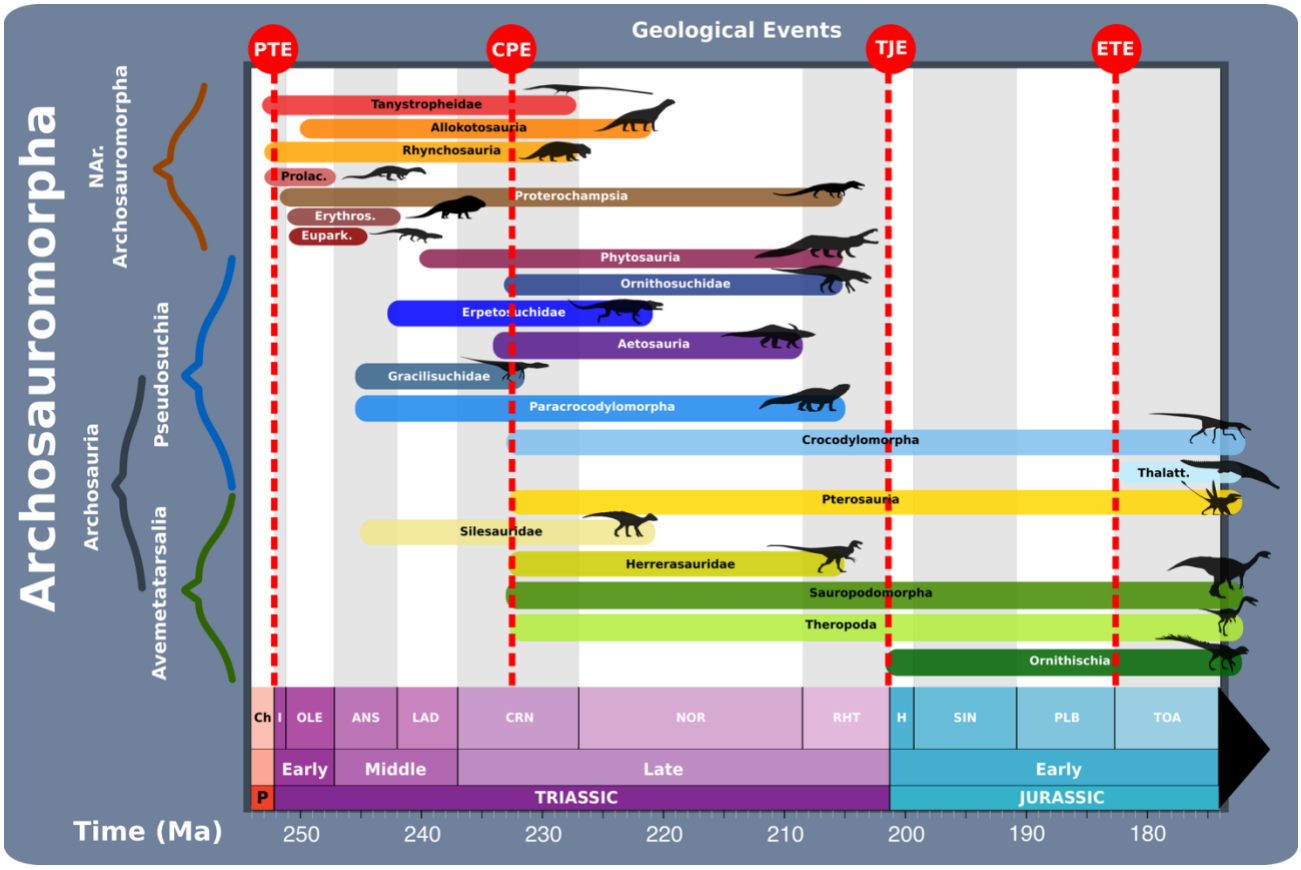

Figure 1.2.1. Range chart of the Archosauromorpha through the early Mesozoic.

First and Last appearances of key clades illustrated. Abbreviations: ANS, Anisian. Ch, Changhsingian. CPE, Carnian pluvial event. CRN, Carnian. Erythros, Erythrosuchidae. Eupark. Euparkeriidae. ETE, Early Toarcian event. H, Hettangian. I, Induan. LAD, Ladinian. NAr, Non-archosaur. NOR, Norian. OLE, Olenekian. P, Permian. PLB, Pliensbachian. Prolac, Prolacertidae. PTME, Permo-Triassic mass extinction event. RHT, Rhaetian. SIN, Sinemurian. Thalatt, Thalattosuchia. TJE, Triassic-Jurassic extinction event. TOA, Toarcian. Ranges based on Benton et al., (2013).

Chapter 2 - Trophic evolution during the radiation of a clade.

2.1 - An ecological perspective on the radiations and success of the Archosauromorpha through the early Mesozoic.

Authors: Suresh Singh, Armin Elsler, Tom Stubbs, Emily Rayfield, and Mike Benton.

Chapter Contributions and Acknowledgements

I designed the study, collected the mandibular and dental morphological data, and conducted all the morphometric and ancestral trait estimation analyses and wrote the chapter. A.E. provided the chronostratigraphic, femur length, and phylogenetic data and calculated the rates of evolution. He also helped with sourcing images. T.S. provided support with R coding. E.R. and M.J.B. provided guidance and comments on the chapter. My contributions represent 85% of the material in this chapter.

All silhouettes created by S.S., but some are vectorised from artwork by Felipe Alves Elias (https://www.paleozoobr.com/) and Jeff Martz (United States National Park Service).

Abstract

Archosauromorphs (crocodilians, birds, dinosaurs, and relatives) showed two substantial diversification events in the Triassic and Jurassic, each following global devastation. Each marked steps in the rise to dominance of dinosaurs, setting the scene for the remainder of the Jurassic and Cretaceous. Yet the ecological basis for their success remains underexplored beyond generic comparisons of disparity, with overall niche diversity of the Archosauromorpha largely hidden across more focused literature. Here, I use morphometric and multivariate phylogenetic comparative methods to chart and investigate archosauromorph trophic ecomorphology within the wider context of the times they lived. By assessing ecomorphology through time I identify common patterns of ecomorphological evolution highlighting the prevalence of convergence within the Archosauromorpha and the antiquity of many archosaurian morphotypes. Furthermore, I also find that the radiations in the aftermath of mass extinction mark key junctions in archosauromorph macroevolution with these events being the primary intervals of broad ecomorphological change. The success of clades such as the dinosaurs came from ecological opportunities combined with

intrinsic adaptability and the magnitude of ecological pressure applied by contemporary taxa following extinction events, highlighting the importance of considering ecology during studies of macroevolution.

Introduction

The Archosauromorpha emerged within the late Permian and underwent several radiations in the early Mesozoic, which helped establish their prevalence across global faunas for the remainder of the era (Ezcurra et al., 2020). Their first known radiation occurred in the Middle Triassic following the unprecedented ecological opportunity and devastation of the Permo-Triassic mass extinction (PTME). Severely depleted diversity in the aftermath allowed extensive diversification by survivors across a variety of niches (Ezcurra and Butler, 2018). Their later radiations are also associated with environmental upheavals through the early and closing stages of the Late Triassic, namely the Carnian Pluvial Event (CPE) (Bernardi et al., 2018) and Triassic-Jurassic extinction (TJE) (Allen et al., 2018), respectively. Through these radiations, the radiating clades attained faunal prevalence/dominance as archosauromorphs supplanted parareptiles and therapsids in the Middle Triassic, archosaurs fully supplanted their earlier archosauromorph predecessors at the onset of the Late Triassic, and dinosaurs overtook the pseudosuchians in the Early Jurassic (Sues and Fraser, 2010; Benton, 2016). Across these events, archosauromorphs managed to colonise terrestrial, marine, and aerial niches (Foth et al., 2017; Brusatte et al., 2008; Ezcurra and Butler, 2018). The Archosauromorpha have been heavily discussed within the wider context of underlying drivers of macroevolution, with proposals that their radiations and changes in clade-wise faunal prevalence are driven by intrinsic or extrinsic ecological opportunity: intrinsic (biological) explanations include innovations that boosted locomotory and/or metabolic efficiency in terms of 'competitive superiority' over their contemporaries allowing the superior taxa to displace incumbents from their niches (Charig, 1984; Bakker, 1972; Bonaparte, 1982). Indeed, competition is heavily cited in classic studies of archosauromorph evolution during the Triassic, with the supposed competitive superiority of successive clades, (particularly dinosaurs) being cited as the reason for their success (Charig, 1984; Bakker, 1972; Bonaparte, 1982). Extrinsic drivers include opportunism in the aftermaths of mass extinctions caused by significant climatic and environmental changes (Benton, 1987; Brusatte et al., 2008; Ezcurra and Butler, 2018).

Accrediting trends in macroevolution to either intrinsic or extrinsic drivers remains challenging because they operate on different spatiotemporal scales, and high-quality data are required (Jablonski, 2008; Benton, 2009; Ezard et al., 2016). Intrinsic interactions are an important force in microevolution and may modulate evolution through 'Red Queen' dynamics (Van Valen,

1973; Thompson, 2006; Voje et al., 2015). The recurring pattern of extensive taxonomic and ecological radiations (Lu et al., 2006; Alroy, 2008) in the aftermath of extinction events suggests that such intrinsic interactions played an important role in regulating speciation through diversity-dependent controls (Rabosky, 2013). The removal of intrinsic pressures is the underlying basis of ecological opportunity, in which mass extinctions remove competitor taxa and so enable survivors to diversify (Schluter, 2000). Understanding these pressures remains difficult but such pressures may be detectable in comparisons of postulated ecological and biomechanical functions of ancient species; for example, coexisting ecologically similar taxa may show ecomorphological divergence through time as they evolve to avoid competition (Martin and Harding, 1981; Pfennig and Murphy, 2000; Pritchard and Schluter, 2001). In such cases, comparative studies of palaeoecomorphology across closely related taxa are well suited to evaluating potential competitive pressures. Indeed, recent studies show that competitive pressures can manifest in the ecomorphological diversification dynamics of allegedly competing clade (Silvestro et al., 2015; Liow et al., 2015; Pires et al., 2015; Condamine et al., 2020).

By quantitatively investigating the morpho-functional trophic anatomy of the Archosauromorpha using morphometric methods, I infer and assess the ecological diversity of archosauromorphs through the early Mesozoic and chart the tempo and mode of their ecological evolution. Using inferred changes in ecology, I attempt to link patterns of morpho-functional change to wider changes in the environment, from and intrinsic (potential competitors) and extrinsic (large-scale climatic changes) perspective. I also identify the predominant patterns of ecomorphological evolution to identify common drivers or processes by which changes in dentition, mandibular anatomy, and body size may have repeatedly enabled new archosauromorph clades to establish themselves across so many niches in terrestrial ecosystems.

Materials and Methods

Taxonomic sampling and data collection. I compiled a list of all valid tetrapod taxa from Early Triassic to Early Jurassic, using a published dataset (Benton et al., 2013a) and the latest literature to incorporate new taxa and taxonomic revisions. The stratigraphic ranges of these taxa were updated to substage level following the designations of Benton et al. (2013). Absolute age assignments were based on the 2019 version of the International Chronostratigraphic Chart (Cohen et al., 2019). Our analysis was generally conducted at genus level to maintain a balance between availability of data and confidence in taxon diagnosis; in fact, most genera are monospecific. I generally used a single specimen per genus in this study, so I cannot account for varying levels of intraspecific variation; a true measure of total disparity would ideally include multiple specimens per taxon. Where

intraspecific variation had been reported, I included more than one species for those genera, for example three species of the rhynchosaur *Hyperodapedon*: *H. gordoni*, *H. huxleyi* and *H. sanjuanensis*, from Europe, India, and South America respectively as these were abundant and widespread taxa showing intrageneric shape variation.

I compiled photographs and specimen drawings from the literature alongside photographs taken during museum collection visits, taking care to exclude damaged, distorted, and juvenile material. The sampling presented here represent all taxa found for which there is sufficient mandibular data and in total contains 173 archosauromorph genera and a total of 176 taxa that included 23 non-archosauriform archosauromorphs, 15 non-archosaur archosauriforms, 64 pseudosuchians (including 11 phytosaurs), and 73 avemetatarsalians (featuring 58 dinosauromorphs).

Morphometric data. This study focuses on the mandible (lower jaw) as it is highly linked to feeding and has a well-established usage in the literature (Anderson et al., 2008; Stubbs et al., 2013; Maclaren et al., 2017; Grossnickle, 2020). Dental morphology is also included here to further refine interpretations of feeding mechanics as tooth shape is a highly plastic aspect of functional morphology that closely related to diet (Evans et al., 2007; Wilson et al., 2012; Melstrom, 2017).

Maximum femur length was used as a proxy for overall body size, as although this metric is less accurate than some size estimation methods such as that of Campione and Evans (2012; 2020), it is more easily sampled from the literature, which enables comprehensive study of size dynamics across our taxa. As part of the appendicular skeleton, femur length relates to locomotory and supportive functions, making it a fairly strong approximation of overall body size (Campione and Evans, 2020). This metric was further preferred to skull length as the archosauromorpha fossil record features an abundance of limb material relative to cranial remains (Ezcurra and Butler, 2018). Furthermore, skull size is often uncoupled from overall size (Millien and Bovy, 2010), particularly within archosauromorphs as demonstrated by the smaller skull sizes of the sauropodomorphs, which are the largest taxa within this study. Femur length also has a proven track record of use across an array of clades in the literature (Sookias et al., 2012; O'Gorman and Hone, 2012; Puttick et al., 2014).

Phylogenetic trees. The archosauromorph supertree is based on the tree of Ezcurra et al., (2017), which forms the scaffold of the current tree. Recent studies have produced some uncertainty on the phylogeny of both clades, with Baron et al., (2017) proposing an alternative Ornithoscelida topology for dinosaurs. I focus on established topologies to avoid unnecessary controversy. Additional taxa

were added to both trees using Mesquite 3.51 (Maddison and Maddison, 2018). Time-scaling was applied following the methodology of Lloyd et al. (2016).

Morphometric methods. I used both geometric morphometric (GM) and functional morphometric (FM) methods to precisely detail morphofunctional jaw evolution across the Archosauromorpha. Using both methods allows for examination of changes in mandibular morphology alongside (clearly defined) biomechanical utility. GM methods capture the overall shape of the element of interest and FM methods capture biomechanical properties of the element and can thus give insight into function. These two methods can (Eble, 2004; Hetherington et al., 2015), but do not necessarily overlap in their results, since shape variation may be non-independent of some functional traits due to a variety of factors such phylogenetic heritage, taxonomic scaling, or methodological choices (Meloro et al., 2011; Brusatte et al., 2011; Koch et al., 2017; Schaeffer et al., 2019).

Using both types of metric also allowed us to account for discrepancies between biomechanical and morphological patterns of disparity (Anderson et al., 2011; Stubbs et al., 2013), discriminating between shape data integrating various cladistic and functional traits, and clear, ecologically relevant functional measurements. GM methods assess shape variation via user-defined landmarks and Cartesian coordinates, whereas FM methods use continuous functional measurements such as mechanical advantage (MA) and aspect ratio, which reflect biting efficiency and jaw robusticity respectively (Button et al., 2014; MacLaren et al., 2017). I used both Procrustes aligned landmark data and standardised functional measurement data (SFMD) that were collected following an established methodology employed across a range of previous studies of tetrapod feeding morphology (Stubbs et al., 2013; Button et al., 2014; MacLaren et al., 2017; Sakamoto et al., 2010).

Shape data. Archosauromorphs encompass a wide range of mandible morphologies making it difficult to identify more than a small number of homologous landmark points. I opted for a relaxed landmarking regime, in which I used four fixed landmarks and connected them with four semi-landmarked curves comprising 55 semi-landmarks in total (Fig. 2.1.1). Hence, our landmarking regime focuses on overall shape (type 2 landmarking), rather than contacts between bones of the mandible (type 1 landmarking). Type 1 landmarking was impractical as points of bone articulation/sutures were not clearly visible across our specimens due to the aforementioned shape variability, and varying states of preservation across specimens. Furthermore, homologies were difficult to easily ascertain because of the wide phylogenetic range of the included genera.

Images were digitally landmarked using tpsDig2 (Rohlf, 2010), with fixed landmarks placed at homologous points on each mandible and semi-landmarks equally spaced along curves between the fixed landmarks. I used tpsUtil (Rohlf, 2013) to enable semi-landmarks to slide along their respective curves during the Procrustes transformation using the chord–min d^2 sliding method that allows each semi-landmark to slide along a chord between the two adjacent landmarks. Procrustes transformation was carried out using tpsRelW (Rohlf, 2015) to remove the effects of mandible size and orientation from the landmark data and to generate aligned coordinates.

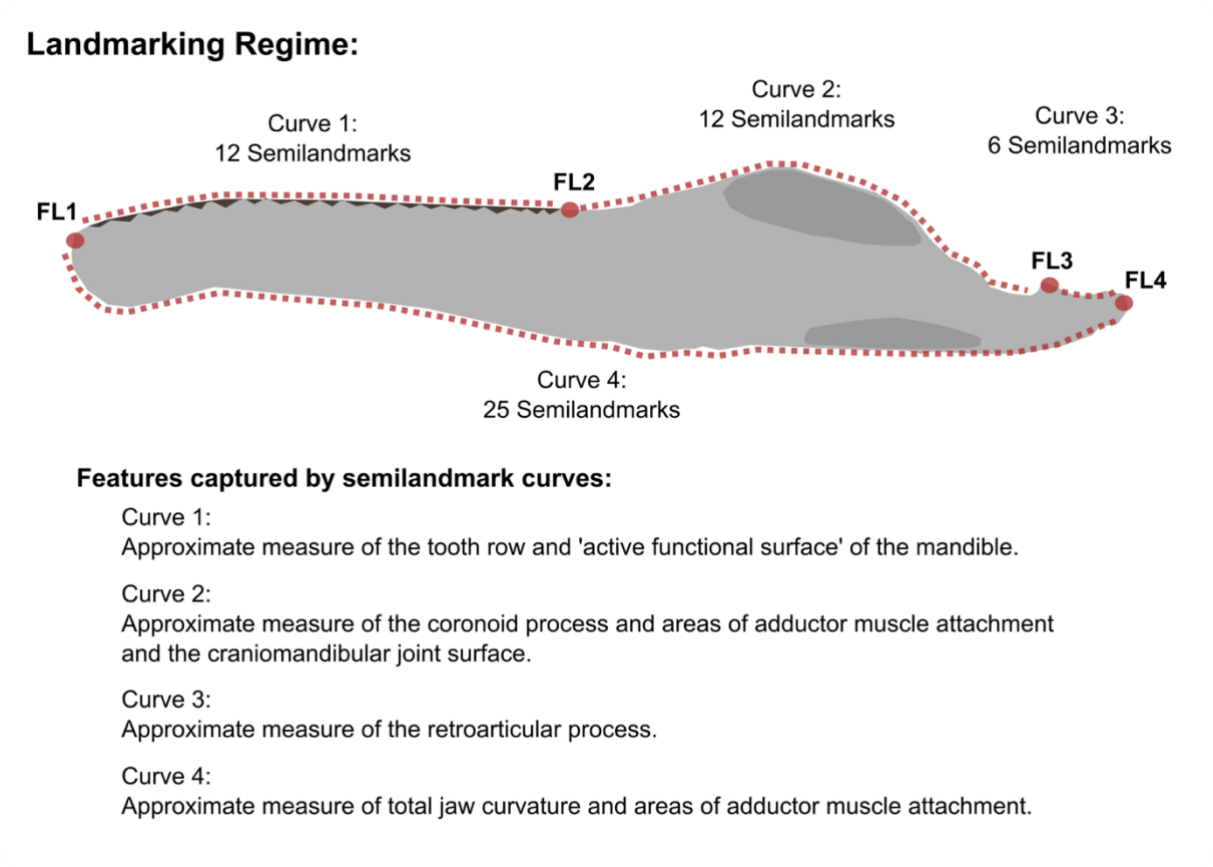

Figure 2.1.1. Geometric morphometric landmarking regime. a). Landmarking Regime: FL = Fixed Landmarks: 1). Anterior-most tip of the mandible, 2). Posterior-most tip of the toothrow, 3). Beginning of the jaw articulation, 4). Posterior-most tip of the mandible.

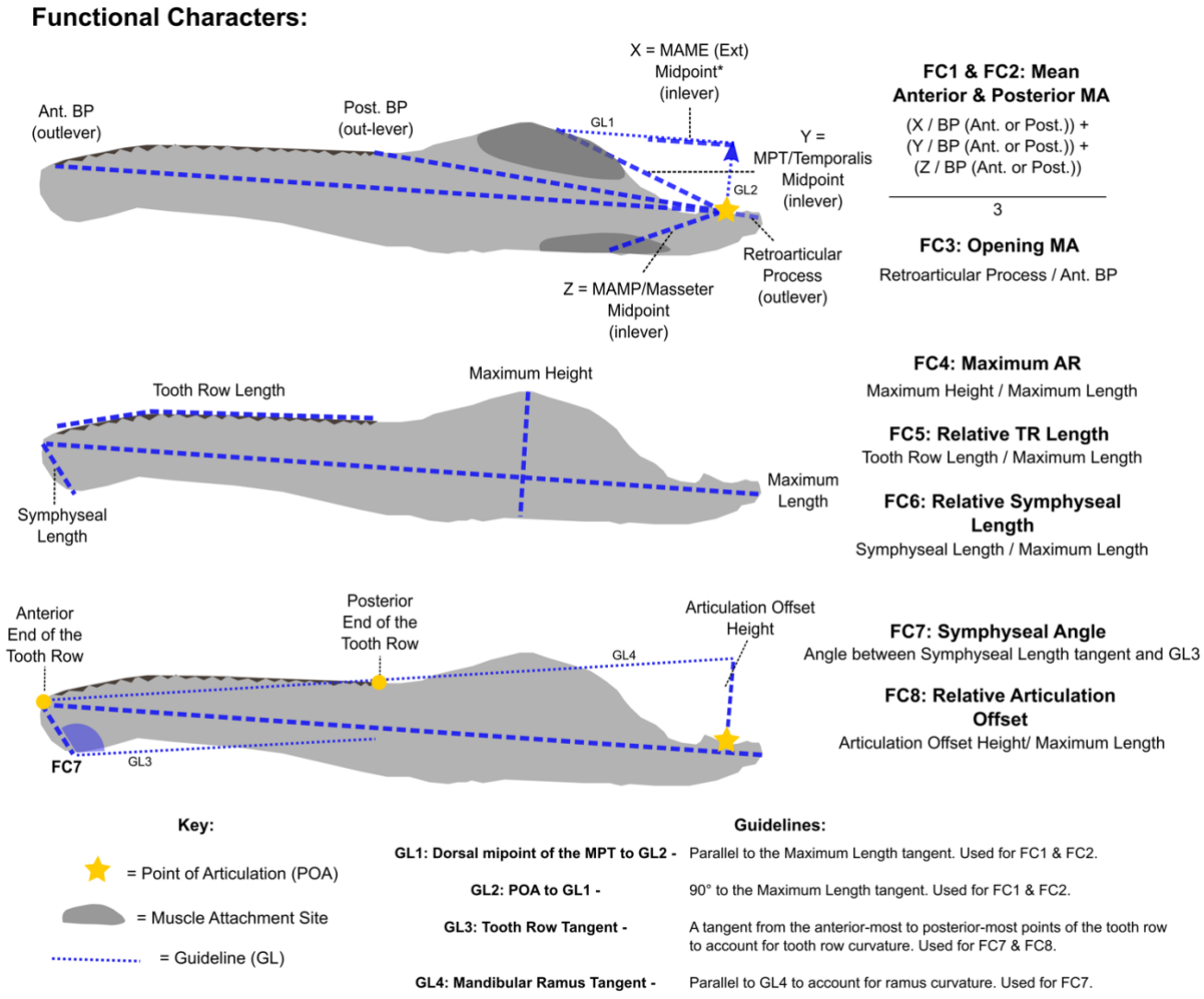

Figure 2.1.2. Mandibular functional character measurements. Functional Characters = FC: 1). Mean Anterior Mechanical Advantage, 2). Mean Posterior Mechanical Advantage, 3). Opening Mechanical Advantage, 4). Relative Maximum Aspect Ratio, 5). Relative Toothrow Length, 6). Relative Symphysis Length, 7). Symphyseal angle, 8). Relative Articulation Offset. *X not included for taxa with derived mammalian jaw joint, and mean calculation is adjusted accordingly.

Functional data. I collected data for eight functional characters using measurements taken from our mandible images (Fig. 2.1.2). These measurements, taken with ImageJ (Schneider et al., 2012), relate to dimensions between relevant areas of muscle attachment, articulation, and overall mandible shape that capture important biomechanical properties related to feeding ecology, which have been

used in multiple studies to characterise mandibular function (Stubbs et al., 2013; Button et al., 2014; MacLaren et al., 2017; Sakamoto et al., 2010). Functional Characters:

1. Mean Anterior Mechanical Advantage: A measure of biting efficiency at the anterior of the mandible (Westneat, 1994). This is the ratio of the inlever to the outlever, using the distance from the jaw joint to the anterior-most tip of the toothrow/dentary as the outlever. The distance from the jaw adductor muscle attachment to the jaw joint represents the inlever. This ratio of inlever to outlever gives the lowest possible value of MA.
2. Mean Posterior Mechanical Advantage: A measure of biting efficiency at the posterior of the mandible (Westneat, 1994). This is the ratio of the inlever to the outlever, using the distance from the jaw joint to the posterior-most point of the toothrow/dentary as the outlever. The distance from the jaw adductor muscle attachment to the jaw joint represents the inlever. This ratio of inlever to outlever gives the highest possible value of MA.
3. Opening Mechanical Advantage: A measure of biting velocity (Westneat, 1994). This is the ratio of the maximum inlever to the maximum outlever, using the distance from the jaw joint to the posterior-most point of the mandible/retroarticular process for the inlever, and using the distance from the jaw joint to the posterior-most point of the toothrow/dentary as the outlever. Opening MA is linked to feeding patterns and prey selection (Anderson and Westneat, 2007; Stubbs et al., 2013).

   Characters 1-3 are based on using lever mechanics to describe mandibular function, with the jaw acting as a third-order lever system (Westneat, 1994; 2004). The adductor musculature acts as the input force, the craniomandibular joint acts as the fulcrum and the output force is exerted along the toothrow/shearing surface. Herbivores often exhibit higher MA values than faunivores (Stayton, 2006). Levers are measured from the craniomandibular joint/jaw articulation. Taxa with low MA exhibit weak, rapid bites (Wainwright and Richard, 1995; Stubbs et al., 2013), whilst taxa with a strong bite force have a high MA.
4. Relative Maximum Aspect Ratio: A proxy for the second moment of area, previously used in 2D analyses of jaw mechanics (Anderson, 2011; Stubbs et al., 2013). Generated by dividing the maximum depth of the mandible by its total length. The second moment of area is typically used to assess the resistance of a beam to bending under loading and when applied to jaws gives indication of the pressures experienced during biting. It essentially requires calculation of the cross-sectional area of the mandible, and so needs additional measurements that were often not available from lateral view images sourced from the literature. In most wide-ranging macroevolutionary analyses of anatomy (Anderson, 2011; Stubbs et al., 2013, MacLaren et al., 2017; Kilbourne, & Hutchinson, 2019), the second

moment of area calculations assume a generalised jaw shape, treating it as a cylinder or rectangular beam, and this 2D approach takes this principle further by making a more basic approximation of the jaw that doesn't require 3D data. Most mandibles primarily experience dorsoventral stress during feeding function, the maximum aspect ratio measurement used here captures a more general approximation of dorsoventral robusticity and therefore, represents a measure of flexural stiffness (MacLaren et al., 2017) that can be widely applied across all sampled taxa.

5. Relative Toothrow Length: A measure of relative length of the dentition and its purported importance in trophic behaviour (Button et al., 2014). Generated by dividing the length of the toothrow/shearing surface by the total length of the mandible. A longer toothrow enables a greater range of MA along the jaw and likely increased use of the dentition in jaw functionality (either for food ingestion or processing/mastication). Herbivores tend to show relatively shortened toothrows compared to faunivores and omnivores (Sues, 2000).
6. Relative Symphysis Length: A measure of symphyseal robusticity generated by dividing the length of the symphysis by the total length of the mandible. The symphysis is subject to significant bending, shear, and torsional stress during biting action and so is highly related to transmission of muscle and biting force and feeding ecology and overall jaw mechanics (Daegling, 2001; Jones et al., 2012).
7. The symphyseal angle is measured between the ventral jaw line and a line parallel to the long axis of the mandibular symphysis. It affects symphyseal resistance to the bending, shear, and torsional stresses that occur during the bite cycle (Daegling, 2001). The symphyseal angle is known to affect food processing in modern herbivorous rhynchocephalians (Jones et al., 2012) and is of major importance in the mechanical response of modern crocodylians to biting, twisting, and shaking (Porro et al., 2011; Walmsley et al., 2013).
8. Relative Offset of Articulation: The articulation offset is measured as the length of the line perpendicular to the tangent of the mandibular toothrow (extrapolated from the anterior and posterior ends of the toothrow to account for jaw curvature) which intersects the articular joint (Anderson et al., 2011; MacLaren et al., 2017). This value is then divided by the total jaw length. An offset between the toothrow and jaw articulation affects dental occlusion and leverage of the jaw musculature (Janis, 1995). A small articulation offset indicates 'scissor-like' occlusion, which is typical of carnivorous taxa. Herbivores generally exhibit greater toothrow-articular offset as this enables simultaneous occlusion along the entirety of the toothrow, supporting gripping & crushing actions (Ramsay and Wilga, 2007).

Principal component analysis. To identify the major axes of variation, the shape-aligned coordinate data and functional measurement matrix were subjected to principal component analyses (PCAs). A PCA transforms total variation into a matrix of independent variables (PC axes). For the PCA analyses, I used packages in R (R Core Team, 2018), including geomorph (Adams and Otárola-Castillo, 2013) for the aligned coordinate data, and FactoMineR (Le et al., 2008) for the functional measurements; and to also centre and z-transform the data prior to a PCA following established protocols to mitigate issues of heteroscedasticity (Button and Zanno, 2020; Button et al., 2014). The first two PC axes account for the largest proportions of variation of all axes and were used to plot morphospace occupation. In chapter 4.2, an alternative PCA was also carried out using an alternative data standardisation to assess the robusticity of the PCA results. The resulting morphospaces differ (Supplementary Fig. 4.2.S2) as a result of the different treatment of the underlying trait data, but the overall results remain consistent across all methods and do not change the broader findings presented in the main chapter text, and so further use of the alternative treatments were not carried out for other chapters. The resulting shape and functional PC scores were subjected to a Mantel test using the ade4 R package (Dray, 2007) to test for a correlative relationship between mandibular form and function. Functional character contour plots were generated using the akima package (Akima and Gebhardt, 2016), with linear interpolation of functional and PC data for all taxa generating functional data for all areas of occupied morphospace.

Calculations of disparity through time. Disparity is a measure of morphological diversity that is calculated using the volume and extent of morphospace occupation. To explore patterns of shape and functional disparity, I calculated phylogenetic disparity using time-slices (Guillerme and Cooper, 2018) to generate within-bin sum of variance (SOV) using the DispRity R package (Guillerme, 2018). SOV was used to plot temporal disparity patterns as it is more resistant to sampling biases and therefore a better reflection of true patterns of disparity (Butler et al., 2012). I used 1000 cycles of bootstrapping to provide 95% confidence intervals. SOV were calculated using all PC axes. Our plots were generated in R using the calibrate (Graffelman, 2013) and strap (Bell and Lloyd, 2014) packages. Morphospace packing' (heavy taxon clustering within morphospace) has been shown to reduce disparity by lowering the average dissimilarity, despite the overall morphospace area/volume remaining stable (Smithwick et al., 2018; Nordén et al., 2018). Consequently, I plotted disparity alongside substage level, time-slices of morphospace in order to avoid misinterpreting the disparity results.

To quantitatively assess the significance of changes in morphospace through time, a one-way non-parametric analysis of variance (NPMANOVA) using a Euclidean similarity index was applied at epoch and stage-level in PAST (Hammer et al., 2001) (version 3.24) to the aligned landmark shape data and functional SFMD. Bonferroni corrections were also applied owing to the multiple comparisons carried out. Additionally, Wang's permutational analysis (Brusatte et al, 2014) was used to ascertain statistically significant differences in mandibular shape and function between clades. The analysis was run in R using code obtained from Foffa et al., (2018) and used 500 replications.

The phylogenetic disparity of different taxonomic groups was subjected to macroevolutionary modelling using the DispRity R package (Guillerme and Cooper, 2018) to test whether their disparity trends followed a Brownian Motion, Early Burst, Ornstein-Uhlenbeck/Constraint, Trend, or Stasis model of macroevolution. Resulting weighted Akaike Information Criterion (AIC) and log-likelihood values were used to assess model fit/support (Supplementary Table 2.1.3).

Phylogenetic comparative methods. To more comprehensively study ecomorphology across the Archosauromorpha, ancestral state estimations were applied to generate data for taxa without femoral data and for ancestral nodes. Where femoral material did not exist, basal skull length was used if available to estimate femur length via generalized least squares (GLS) regressions, implemented in R using the nlme package (Pinheiro et al., 2017). This was carried out under three varying assumptions to account for different correlation structures using the corPagel function from the ape package (Paradis et al., 2015; Paradis and Schliep, 2019). The first two structures investigated assumed non-existent or strong phylogenetic signal, whereas the third allowed phylogenetic signal to be estimated following the approach of Benson et al. (2018). Model fitting and parameter estimation were run using maximum likelihood and time-scaled trees, with the models evaluated using the corrected Akaike information criterion (Akaike, 1974; Sugiura, 1978; Burnham and Anderson, 2002). The data was $\log_{10}$ transformed prior to modelling. Additional taxa without femoral data that were discovered following the initial estimation of femur lengths were also included by using a multi-rate Brownian motion model of phylogenetic character reconstruction to impute the missing femur length data (O'Meara et al., 2006; Revell and Collar, 2009) with the mvMORPH package (Clavel et al., 2015). Estimations of ancestral PC scores and body sizes (the $\log_{10}$ transformed femur length) were also generated using a Maximum Likelihood approach via the 'FastAnc' function of the phytools R package (Revell, 2012). Resulting body size values mapped onto the phylogeny using the 'ggtree' R package (Yu, 2020) (Fig. 3.1.5b).

Rates of morphological and functional evolution were calculated by Armin Elsler. BayesTraits V2.0.2 (Pagel and Meade, 2013; Venditti et al., 2011) was used to estimate multivariate variable rates models for all eight fPCs and 13 PCs axes, which represent 100% and 90% of mandibular function and shape variation, respectively. All PCs were not used for the shape rates analysis to avoid problems with non-convergence. The rate analyses used the Markov chain Monte Carlo (MCMC) method to run variable rates independent contrast models for multiple timescaled trees. Each tree was run for 110,000,000 iterations for each tree and sampled at 10,000 iteration intervals, with 10,000,000 iterations being discarded as burn-in. The marginal likelihood of the models was calculated using the stepping stone sampler (Xie et al., 2011) in BayesTraits, with 1000 stones and 100,000 iterations per stone. The mean phylogenetically corrected evolutionary rates were calculated from across all trees using the Variable Rates Post Processor (Sakamoto et al., 2019) with 1,000 time slices per tree (Venditti et al., 2011; Sakamoto and Venditti, 2018). The final rates results were applied to a strict consensus tree based on all timescaled trees, with mean branch lengths and mean rate scalars using ggtree (Yu et al., 2017).

Results

Archosauromorph morpho-functional diversity. The extents of mandibular form and functional diversity are illustrated using morphospaces constructed from the primary axes of variation, as determined by principal component analysis (PCA) of geometric morphometric (GM) and standardised linear measurement (SLM) data (See methods) (Figs. 2.1.1-2). The foremost axes of shape (Fig. 2.1.3a) and functional (Fig. 2.1.3c) variation are displayed in the primary morphospaces composed of (functional) principal components (fPCs/PCs) 1 and 2. Patterns of shape and functional morphospace occupation show strong similarities, which was confirmed as statistically significant by a Mantel test ($p=<0.001$, $r=0.660$); however, this likely stems from the SLMs denoting functionally relevant aspects of jaw shape. To examine the sometimes-decoupled relationship between form and function more precisely (Stubbs et al., 2013; Lautenschlager et al., 2017), the functional SLMs were mapped onto the primary shape morphospace using linear interpolation (Fig. 2.1.3b). Most characters, particularly the mean anterior mechanical advantage (MAMA), relative maximum aspect ratio (RMAR), show a gradual distribution across morphospace, but symphyseal angle (SA) and mean posterior mechanical advantage (MPMA) show greater heterogeneity, illustrating greater archosauromorph experimentation with these traits. The relative shortening or elongation of the mandible across PC 1 is the main mode of shape variation and the strong graduation of functional values indicates it is closely related to changes in MAMA, RMAR, and relative symphyseal length (RSL). The deflection of the dentary illustrated along PC 2 marks the second major aspect of

morphological variation and is directly linked to the offset between jaw articulation and anterior-most bite point. Higher opening MAs and thus slower bite speeds are associated with the lower half of the shape morphospace. The fPC loadings (Table 2.1.1) highlight biting efficiency as the strongest positive determinants of the functional morphospace, with anterior and posterior MA bearing the greatest positive load in fPC1 and the second highest load for fPC2, respectively. fPC1 and fPC2 were also strongly linked to the RMAR and the relative toothrow length (RTL), whilst fPC3 was largely controlled by the symphyseal angle (SA). Taxa are highly clustered in the centre of functional morphospace representing the mean archosauromorph jaw shape, and this highly concentrated distribution is also present in ancillary morphospaces constructed using fPC/PC 3 (Supplementary Fig. 2.1.1). PC3 appears to reflect the relative positioning of the coronoid process along the surangular, whereas fPC3 is controlled by the symphyseal angle (Table 2.1.1). fPC3 appears to show slightly similar clade distributions across the morphospace to fPC1 and 2, highlighting symphyseal morphology as a highly plastic aspect of archosauromorph mandibular anatomy. Overall consideration of the primary and ancillary morphospaces (Fig. 2.1.3; Supplementary Fig. 2.1.1), which represent a total of 66% and 69% of overall shape and functional mandibular variation, respectively, indicates high morpho-functional conservatism within archosauromorph mandibles. There appears to no relationship between body size and mandibular shape, with a heterogeneous distribution of large and small sizes across shape morphospace (Fig. 2.1.3a). However, larger body sizes appear to be concentrated within the central region of the functional morphospace (Fig. 2.1.3b), indicating minimal jaw deviation from the mean archosauromorph morphology among larger taxa.

The concentrations of taxa within different areas of the shape and functional morphospaces reveals that non-archosaur archosauromorphs (NAAs), pseudosuchians and avemetatarsalians explored slightly different areas of morphospace associated with different diets (Fig. 2.1.4). NAA morphospace occupation (MO) extends all across overall archosauromorph MO, with their subclades being more broadly distributed within their total MO. In contrast, archosaur MO is highly concentrated and largely responsible for the morphospace packing at the centre (Figs. 2.1.3-4). These pattens of strong archosauromorph mandibular similarity are evident from comparison of functional characters (Fig. 2.1.5). The most morphologies distributed in negative (f)PC1 morphospace are highly elongate, longirostrine morphologies that are optimised for a raptorial function, possessing high bite speeds as indicated by their lower MA, and longer toothrows (Fig. 2.1.3b, 4), These morphologies are dominated by clades such as the phytosaurs and thalattosuchians (Fig. 2.1.4) and their thick conidont dentition (Fig. 2.1.6a), reflects a focus on prey capture with differences in robusticity indicating preferences for smaller or larger tetrapod prey (Fig. 2.1.3-6).

These patterns are replicated further towards the centre of the morphospace in taxa possessing less elongated mandibles (pterosaurs and tanystropheids) (Fig. 2). However, these taxa are much smaller in overall size and possessed thin conidont teeth suggestive of a preference for less robust prey, most probably insects or fish (Fig. 2.1.4, 6a). Central areas of morphospace are heavily shared by faunivorous NAAs, pseudosuchians and avemetatarsalians, such as erythrosuchids (Maidment et al., 2020), herrerasaurids (Pacheco et al., 2019), and theropods (Sakamoto, 2011). The increasingly upwardly deflected dentaries, increased robusticity and higher MAMA and opening MA (OMA) values towards the upper-righthand quadrant of morphospace (Figs. 2.1.3-4) denotes progressively powerful, stress-resistant bites, indicative of hypercarnivory. They possess either thick conidont or ziphodont teeth, which highlights an inclination towards slicing or penetrative tooth function (Hendrickx et al., 2015) (Figs. 2.1.4—6).

Taxa found at the very centre and trailing towards the lower areas of PC/fPC 2 possessed weaker bites and more gracile mandibles, marking a transition from generalised faunivory (mesocarnivory) to omnivory and finally herbivory. These 'central herbivores' are characterised by downwardly deflected dentaries, robust symphyses and folidont dentitions (Figs. 2.1.3-6), suggesting optimisation for cropping vegetation (Galton, 1985). This area is mostly occupied by sauropodomorphs but also features allokotosaurid azendohsaurs. This may indicate that the well-established dental shift from ziphodonty to folidonty, and the gradual changes in mandibular morphology reported here (Fig. 2.1.3-4) as sauropodomorphs became more herbivorous (Galton, 1985; Barrett and Upchurch, 2007, 2014), are part of an 'adaptive pathway' established by earlier archosauromorphs. The more 'positive' regions of morphospace are dominated by clades typically regarded as highly specialised herbivores such as the rhynchosaurs and ornithischians (Ezcurra et al., 2016; Barrett, 2014; Singh et al., 2021). Aetosaurs are also found within this morphospace. These morphologies are characterised are very robust with shorter toothrows and show high (particularly posterior) MA values and slower bite speeds. The folidont or bulbous dentitions of these taxa are well-suited to shearing or pulping vegetation (Hendrickx et al., 2015) (Fig. 2.1.6a). These traits are suggestive of strong oral comminution. The contrasting suites of adaptations indicate two main modes of herbivory among archosauromorph herbivores, with the 'ingestion specialist' azendohsaurs and sauropodomorphs pursuing generalised bulk feeding strategies, whilst 'comminution specialists' pursued more specialised browsing, perhaps on tougher vegetation (Weishampel and Norman, 1989; Barrett, 2014; Nabavizadeh, 2020). Interestingly, aetosaur morphospace sits halfway between the two aforementioned modes of herbivory and suggests that they exploited a novel niche within the herbivore guild.

Table 2.1.1. Character loadings for functional principal component analysis.

Abbreviations: fPC, Functional principal component. MA, Mechanical advantage.

Characters	fPC1	fPC2	fPC3	fPC4	fPC5	fPC6	fPC7	fPC8
Mean Anterior MA	0.512187	-0.084188	-0.101240	-0.375721	0.037473	0.421114	-0.221501	0.592754
Mean Posterior MA	0.291645	0.650229	-0.047848	0.025605	0.074851	0.339962	-0.317942	-0.516658
Opening MA	0.274688	-0.180369	0.290095	0.706164	-0.496522	0.186678	-0.147474	0.077842
Max Aspect Ratio	0.507634	0.197980	-0.077842	-0.037918	-0.180800	-0.113805	0.804331	-0.055003
Relative Toothrow Length	-0.267118	0.669460	0.001834	0.298422	0.071916	-0.106572	0.060798	0.609250
Relative Symphyseal Length	0.444620	0.064698	0.295764	-0.057829	0.137496	-0.754154	-0.343877	0.037448
Symphyseal Angle	-0.014334	-0.024376	0.796212	-0.015114	0.478650	0.281168	0.238382	-0.005599
Quadrate Articular Offset	0.224092	-0.213140	-0.419301	0.515213	0.678666	0.011292	0.048779	-0.001647

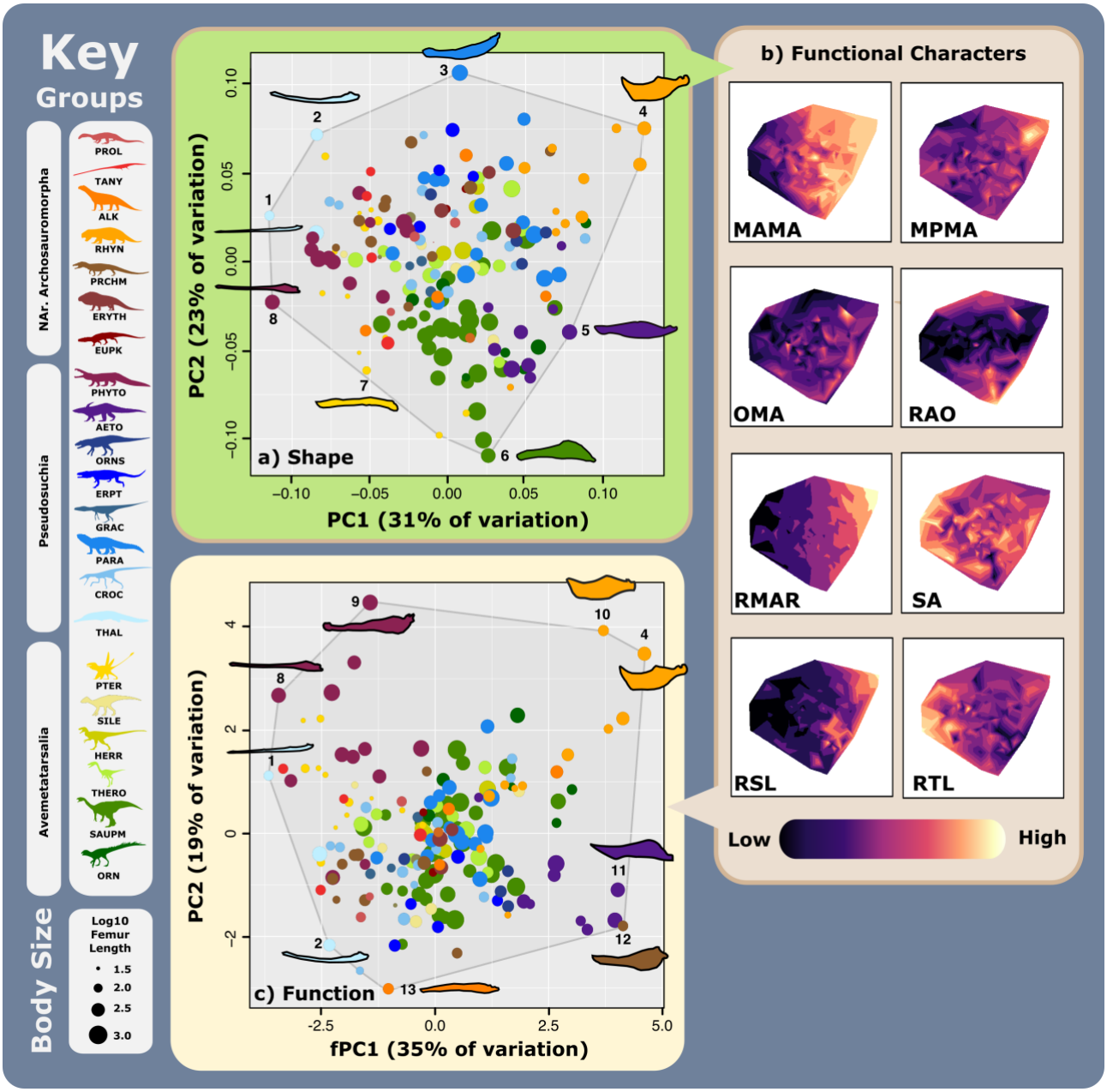

Figure 2.1.3. Early Mesozoic archosauromorph mandibular morpho-functionality and body size. (a) Shape morphospaces. (b) Contour plot of (interpolated) functional character data mapped onto shape morphospace. Magnitude of functional character values indicated by colour gradient. (c) Functional morphospaces. Taxon size (log_{10} femur length) indicated by point size. Abbreviations: MAMA, Mean anterior mechanical advantage. MPMA, Mean posterior mechanical advantage. OMA, Opening mechanical advantage. PC, Principal component. RAO, Relative articulation offset. RMAR, Relative maximum aspect ratio. RSL, Relative symphyseal length. RTL, Relative toothrow length. SA, Symphyseal angle. Taxa: 1. *Pelagosaurus typus*. 2. *Platysuchus multiscrobiculatus*. 3. *Batrachotomus*

kupferzellensis. 4. *Hyperodapedon huxleyi*. 5. *Lotosaurus adentus*. 6. *Sarahsaurus aurifontanalis*. 7. *Dorygnathus banthensis*. 8. *Mystriosuchus planirostris*. 9. *Machaeroprosopus gregorii*. 10. *Hyperodapedon sanjuanensis*. 11. *Longosuchus meadei*. 12. *Vancleavea campi*. 13. *Teraterpeton hrynewichorum*.

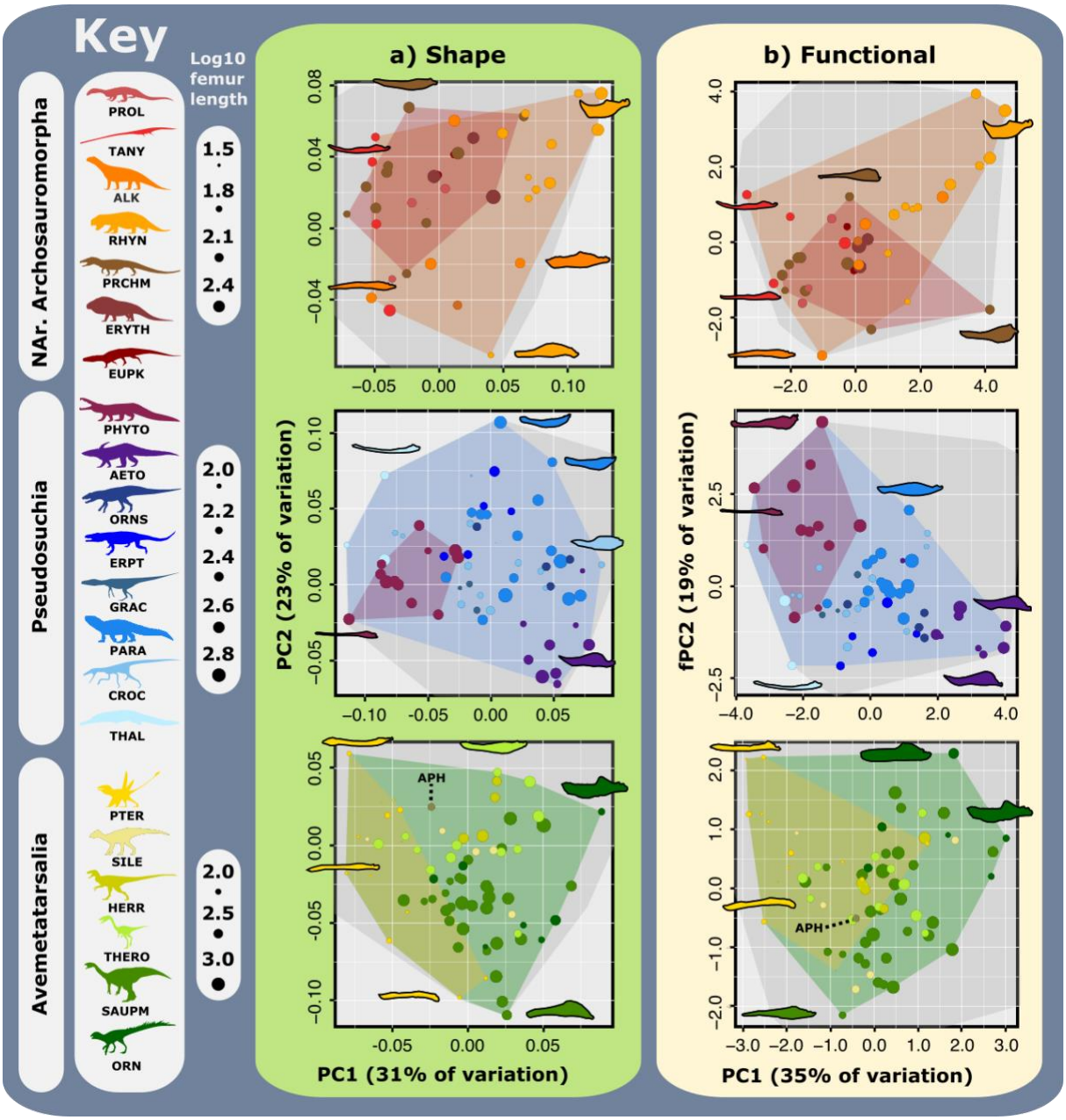

Figure 2.1.4. Clade distributions of shape and functional morphospace for early Mesozoic archosauromorphs. Taxon size (log_{10} femur length) indicated by point size. Grey shaded area represents overall archosauromorph morphospace occupation. Abbreviations: AETO, Aetosauria. ALK, Allokotosauria. APH, Aphanosauria. CROC, Crocodylomorpha. ERPT, Erpetosuchidae. ERYTH, Erythrosuchidae. EUPK, Euparkeriidae. GRAC, Gracilisuchidae. HERR,

Herrerasauridae. NAr, Non-archosaur. ORN, Ornithischia. ORNS, Ornithosuchidae. PARA, Paracrocodylomorpha. PC, Principal component. PHYTO, Phytosauria. PRCHM, Proterochampsia. PROL, Prolacertidae. PTER, Pterosauria. RHYN, Rhynchosauria. SAUPM, Sauropodomorpha. SILE, Silesauridae. TANY, Tanystropheidae. THAL, Thalattosuchia. THERO, Theropoda.

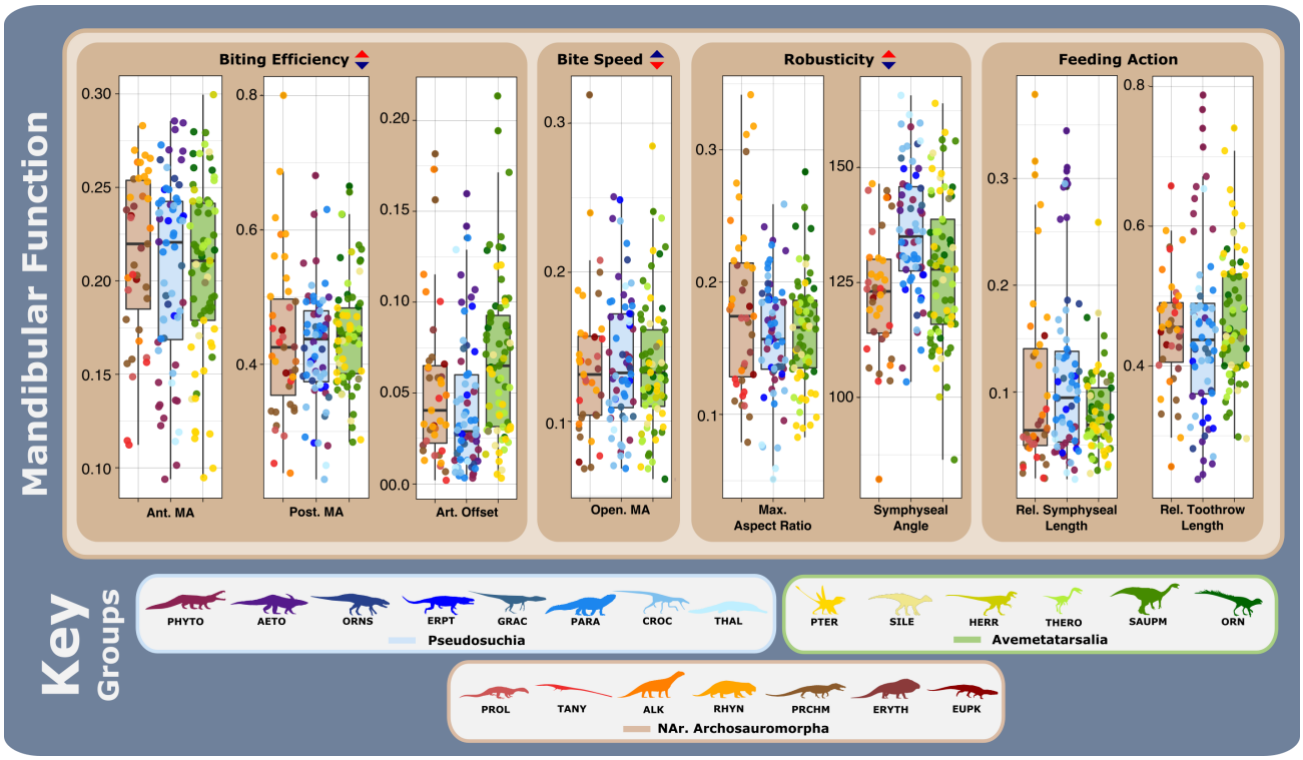

Figure 2.1.5. Mandibular functionality of early Mesozoic archosauromorphs. Mandibular functional trait variation. Abbreviations: AETO, Aetosauria. ALK, Allokotosauria. Ant, Anterior. APH, Aphanosauria. CROC, Crocodylomorpha. ERPT, Erpetosuchidae. ERYTH, Erythrosuchidae. EUPK, Euparkeriidae. GRAC, Gracilisuchidae. HERR, Herrerasauridae. MA, Mechanical advantage. Max, Maximum. NAr, Non-archosaur. ORN, Ornithischia. ORNS, Ornithosuchidae. PARA, Paracrocodylomorpha. PC, Principal component. PHYTO, Phytosauria. Post, Posterior. PRCHM, Proterochampsia. PROL, Prolacertidae. PTER, Pterosauria. Rel. Relative. RHYN, Rhynchosauria. SAUPM, Sauropodomorpha. SILE, Silesauridae. TANY, Tanystropheidae. THAL, Thalattosuchia. THERO, Theropoda.

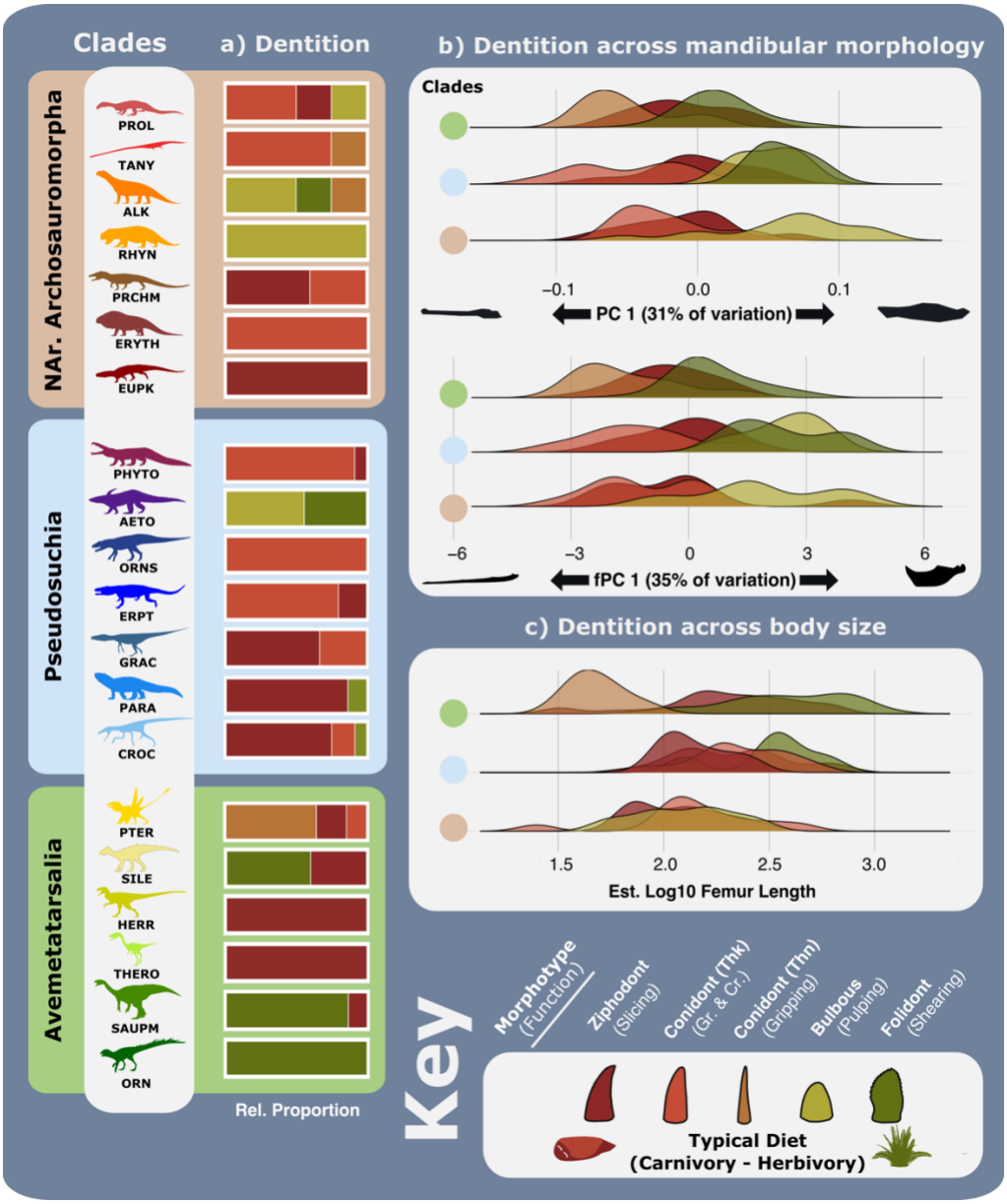

Figure 2.1.6. Dental diversity of early Mesozoic archosauromorphs. Tooth morphology classified using the designations of Hendrickx et al. (2015). (a) Prevailing tooth type of different archosauromorph clades. (b) Tooth types across mandibular shape (top) and functional (bottom) morphologies. (c) Tooth types across different body sizes. Abbreviations: AETO, Aetosauria. ALK, Allokotosauria. APH, Aphanosauria. Cr, Crushing. CROC, Crocodylomorpha. ERPT, Erpetosuchidae. ERYTH, Erythrosuchidae. Est, Estimated. EUPK, Euparkeriidae. Gr, Gripping. GRAC, Gracilisuchidae. HERR, Herrerasauridae. NAr, Non-archosaur. ORN, Ornithischia. ORNS, Ornithosuchidae. PARA, Paracrocodylomorpha. PC, Principal component. PHYTO, Phytosauria. PRCHM, Proterochampsia. PROL, Prolacertidae. PTER, Pterosauria. Rel. Relative. RHYN, Rhynchosauria. SAUPM, Sauropodomorpha. SILE, Silesauridae. TANY, Tanystropheidae. THAL, Thalattosuchia. THERO, Theropoda.

Archosauromorph trophic ecologies. Patterns of mandibular MO allow exploration of the differences in mandibular functionality and so likely jaw action during feeding (Anderson et al., 2008; Stubbs et al., 2013; Maclaren et al., 2017; Grossnickle, 2020). By combining this information with general dental morphologies (Evans et al., 2007; Wilson et al., 2012; Melstrom, 2017) and body size (Carbone et al., 2011; Clauss et al., 2013; Benson et al., 2018; Brocklehurst et al., 2019), I can precisely examine archosauromorph niche specialisation:

I. **Non-Archosaur Archosauromorphs.** NAAs show the greatest overall mandibular disparity (Fig. 2.1.8a) encompassing morphologies across almost the entire spectrum of the primary morphospaces (Figs. 2.1.3-4), highlighting their remarkable mandibular plasticity and hint that the convergent morphologies of later archosaurs (Stocker et al., 2016) were evolved using the adaptive/developmental pathways established by NAAs (Figs. 2.1.4, 7, 9b) (Button and Zanno, 2020; Singh et al., 2021). The earliest archosauromorphs were generalist faunivores as illustrated by the MO of the Prolacertidae, which are perhaps the basal-most archosauromorph clade (Figs. 2.1.3-4). Prolacertid mandibles were relatively straight with uniform depth and weak symphyses that are better suited to higher biting speeds than biting power (Figs. 2.1.3-5). Their MO is concentrated within central regions of morphospace but show a binary distribution between fairly thin (gracile) and thicker (robust) morphologies (Figs. 2.1.3-4). Their dentition is primarily thick conidont, which reflects their raptorial jaw functionality (Fig. 2.1.6a). However, the smallest taxa in the Early Triassic had ziphodont dentitions, whereas larger taxa possessed thick conidont teeth, and the latest taxon included here, *Malerisaurus robinsonae,* had a more bulbous dentition, reflecting shifting dietary preferences through prolacertid evolution within generalised faunivorous niches, with thick conidonty perhaps indicating greater range of prey and bulbous dentitions marking a shift to more durophagous diets.

   Tanystropheids developed more gracile mandibular morphologies and dentition, with their jaws and anterior teeth being very lightly built and thin, with variation appearing to be focused on the curvature of the dentary, with an upturned dentary supposedly enhancing raptorial abilities through the “curved bone effect” (Ma et al., 2021). This study considers the anterior teeth, but more detailed examination of the posterior dentition shows that tanystropheids has complex cusped posterior teeth, which highlights further dietary specialisation, with anterior conidont dentition being highly focused towards prey capture, and the posterior to prey processing. Their jaws present low MAMA suggesting a preference for faster rather than powerful bites (Fig. 2.1.5). These traits suggest adaptation

to catching small, elusive prey, such as fish or motile marine invertebrates as suggested in previous studies (Spiekman et al., 2020).

The allokotosaurians exhibited high jaw disparity compared to other NAAs as illustrated from their relatively broad MO (Fig. 2.1.4). Their MO encompasses more mesofaunivorous to herbivorous adaptation, with azendohsaurs evolving jaws highly reminiscent of sauropodomorphs, with highly robust, ventrally deflected dentaries and symphyses, as well as folidont dentitions (Fig. 2.1.6a). These traits represent adaptations to better resist stresses on the jaw and increase the shearing ability of the teeth and were also developed in sauropodomorphs during their dietary shift towards herbivory (Galton, 1985; Barrett, 2014). In combination with further convergent evolution of larger sizes and longer necks (Flynn et al., 2010), these ecomorphological traits suggest azendohsaur trophic ecologies as high-level, browsing herbivores. Trilophosaurids show highly variable jaws, with *Trilophosaurus buettneri* and *Teraterpeton hrynewichorum* exhibiting contrasting morphologies. *Trilophosaurus* had a relatively deep, robust jaw morphology, whereas *Teraterpeton* possessed an extended, gracile jaw much like the tanystropheids, with a downturned dentary as seen in sauropodomorphs. Both taxa possessed somewhat bulbous cusped teeth, but the dentition did not extend along the full margin of the dentary, with the anterior of the jaws being edentulous. The robust dentition of the trilophosaurs is suggestive of feeding on tough, fibrous materials, but the differences in jaw morphology highlight different dietary specialisations. The jaw of *Trilophosaurus* appears focused towards resisting strong stresses and creating higher bite forces, and so indicate heavy comminution. The slender jaws of *Teraterpeton* are primarily adapted for speed with low MA, but the deflected dentary suggests some reinforcement of the anterior jaws to higher stresses during action (Ma et al., 2017). Consequently, *Teraterpeton* appears to show adaptation towards a 'plucking' action and indicates a trophic ecology of selective herbivory or insectivory, whereas *Trilophosaurus* appears to have been more of a generalist herbivore. An herbivorous diet for *Trilophosaurus* is supported by the broadness of its abdomen, as a large stomach is often present in herbivores to ferment and digest vegetation.

Rhynchosaurs show the greatest jaw modification through the course of their evolution, with a clear transition from mandibular morphologies that were similar to that of many early sauropodomorphs to highly compact, beak-like forms by the end of the temporal range (Figs. 2.1.3-4, 7). This evolution saw strong optimisation of MA, with the increasingly hooked morphology focusing greater bite force at the anterior tip of the jaw and reinforcing it against stresses during biting, indicating increasingly powerful piercing jaw function (Fig.

2.1.5). Their bulbous dentition and high posterior MA are indicative of durophagous feeding and strong comminution, indicating a likely diet of fibrous vegetation (Figs. 2.1.5-6). This specialisation appears to have shown concerted development in the Carnian with the evolution of the Hyperodapedontinae (Fig. 2.1.7a).

Non-archosaur archosauriform mandibles fall within central areas of morphospace (Figs. 2.1.3-4) and typically balanced between the dentary and mandibular body (surangular and angular), with a relatively even depth throughout the jaw. However, there is variation with some, particularly later, archosauriforms showing more extended, slender dentaries reflecting more mesocarnivorous diets as these jaws are less optimised for resisting the high stresses of prey capture/subdual. Euparkeriid and erythrosuchid mandibles are remarkably similar in morphology with relatively greater depth across the jaw and slightly upturned dentaries. As such, they likely fed on comparably sized prey as their jaws are relatively robust and resistant to the stresses associated with gripping struggling prey. Euparkeriid ziphodonty suggests greater adaptation to slice through prey tissue and their small size suggests a propensity to tackle relatively robust prey for their size (Fig. 2.1.6a). The thick conidont teeth of erythrosuchids are more suited to puncturing prey tissue and gripping prey (Fig. 2.1.6a). As such, it seems likely that erythrosuchids engaged in more dynamic interactions with their prey, with jaw function directed towards holding and injuring prey. Proterochampsians show greater elongation of their jaws highlighting a trade-off of power and robusticity for speed, indicating optimisation to catching prey that were less likely to or unable to resist predation. This morphofunction trade-off within non-archosaur archosauriforms is most extreme in *Doswellia sixmilensis,* which possessed a highly longirostrine mandible. This morph would be further developed by pseudosuchian archosaurs.

II. **Pseudosuchians.** Pseudosuchians show similar mandibular evolution to non-archosaur archosauriforms, with their jaws ranging from highly elongate and straight, to more compact and curved, reflecting contrasting enhancement of biting speed or efficiency. Their earliest evolution points to almost parallel evolution as proterochampsians with a shift towards more longirostrine jaws within the phytosaurs, which represent the earliest pseudosuchians, if not their closest relatives (Ezcurra et al., 2016) (Figs. 2.1.3-4). *Diandongosuchus fuyuanensis* is the basal-most known phytosaur (Stocker et al., 2017) and exhibits a jaw morphology highly reminiscent of mesocarnivorous archosauriforms, but more derived phytosaurs echo the evolution of *Doswellia,* evolving more elongate, slender mandibles.

Longirostrine dentaries are ubiquitous across phytosaurs, and variation is instead focused on the mandibular body. Consequently, phytosaurs may also be divided between robust (e.g., *Machaeroprosopus* and *Brachysuchus*) and gracile (e.g., *Mystriosuchus* and *Parasuchus*) forms. Both groups exhibit low MAMA but high MPMA and OMA (Fig. 2.1.5). The robust forms show a gradually deeper dentary towards the posterior of the mandible and an expanded mandibular body, indicating greater jaw musculature. Contrastingly, the gracile forms maintain a relatively constant and typically thin depth across most of the dentary, with the transition from the mandibular corpus to the body being much more abrupt. These differences reflect varying levels of muscle development and bite force, as well as an inclination towards either more (robust forms) or less combative (gracile forms) prey. Phytosaur dentition is overwhelmingly conidont and further supports a highly raptorial jaw function (Fig. 2.1.6a).

Early pseudosuchian evolution appears to mark a period of major experimentation with jaw morphology as the two earliest clades within/near the origin of Pseudosuchia show the most novel mandibular morphologies of the entire clade: phytosaurs with the development of high speed, elongate jaws, and aetosaurs with powerful, robust jaws and heavily derived symphyses. Aetosaurs developed greater robusticity by increasing the relative depth of the jaw across its entirety, with further reinforcement of the symphysis by the development of an extended symphyseal buttress (Fig. 2.1.5). The symphyses are also rather pointed and would suggest very precise bites, perhaps in a rather 'plucking' fashion (Figs. 2.1.4-5). Enlargement of the mandibular body in larger aetosaurs such as *Desmatosuchus spurensis,* reflects increased robusticity as well as increased musculature as illustrated by high MAMA and MPMA (Figs. 2.1.4-5). Smaller taxa such as *Stenomyti huangae* likely exhibited weaker, faster bites, but these were still comparatively strong for pseudosuchians. Aetosaur dentition is rather variable (Reyes et al., 2020) but overall either rather bulbous or folidont, with more folidont dentition being primarily found in larger taxa (Fig. 2.1.6a). As such, these animals were adapted for strong, slow bites and likely fed on tough material. The slower speeds and folidonty of larger taxa support more herbivorous diets in these aetosaurs, but their jaw functionality is unlike any other archosauromorph herbivores. Consequently, larger taxa probably heavily featured vegetation within their diets (Crompton and Attridge, 1986), but overall aetosaurs diets may have been more diverse. The relatively slow bite speeds and strong bite forces suggest that aetosaurs may have been opportunistic faunivores, scavenging carcasses. Apparent suitability to scratch-digging in aetosaurs (Dróżdż, 2018) and a broad abdominal trunk (Desojo et al., 2013) may however

suggest a diet focused on other floral resources, namely roots and tubers. Regardless, these results suggest broad dietary diversity within aetosaurs and somewhat concurs with recent studies of aetosaur ecomorphology (Desojo and Vizcaíno, 2009; Desojo et al., 2013; Reyes et al., 2020).

Later pseudosuchian evolution is more constrained but shows distinct trends in their mandibular evolution. The ornithosuchids represent the most basal hypercarnivorous pseudosuchians, with their compact jaws showing much greater robusticity and larger areas of muscle attachment. In contrast, the erpetosuchids show little development of the mandibular body, with their jaw evolution focused on the relative upwards deflection of the dentary. Consequently, both clades showed hypercarnivorous adaptation, but directed towards different aspects of jaw function; ornithosuchids enhanced overall bite force through increased MA, to presumably increase the damage inflicted on prey during prey capture. In contrast, erpetosuchids improved their gripping capabilities to stop prey escaping during prey capture. As such their prey capture methods likely differed with ornithosuchids likely having to get quite close to their prey before attacking to maximise their chances of catching the prey in their shorter jaws and inflicting their powerful bites, as such they were perhaps better suited to preying on large prey compared to themselves. Erpetosuchids were probably more suited to tackling comparatively smaller prey with their jaw optimisation of capturing rather than injuring prey.

Interestingly, these two pathways of mandibular development are combined within the more derived Paracrocodylomorpha, which show mandibular development across the MO of both ornithosuchids and erpetosuchids (Fig. 2.1.4). Changes in paracrocodylomorph MO through time shows their mandibular evolution focused first on enhancing their jaw musculature and expansion of the areas of jaw adductor muscle attachment and then on improving grip by experimenting with the upward deflection of the dentary (Fig. 2.1.7a). Nonetheless, almost all paracrocodylomorphs possessed moderately high anterior and posterior MA (Fig. 2.1.5), with larger taxa such as loricatans, *Postosuchus kirkpatricki* and *Saurosuchus galilei* exhibiting the greatest MA values. These loricatan taxa typically possessed a relatively reduced corpus, creating a very squat, robust jaw. These jaws are well suited to exerting powerful bites and resisting high stresses during jaw action. The relatively large ziphodont dentitions present in most loricatans combined with the high power, high robusticity jaws suggests a powerful bite dedicated to penetrating and removing large chunks prey flesh, and the slower bite speeds as a result of adaptation for high power suggest the employment of one or two debilitating bites to quickly subdue prey before they

can escape, with the upward deflection of the dentary in some taxa further reducing the ability of the prey to escape.

The relatively slender but un-extended jaws of the gracilisuchids highlights these animals as being more mesocarnivorous than previously discussed pseudosuchians, with more emphasis on speed and prey capture. Interestingly, gracilisuchid MO is most similar to later crocodylomorphs. The lightly built nature of their jaws and smaller sizes (Figs. 2.1.3-4) suggests generalised faunivory within basal crocodylomorphs, with later evolution of the thalattosuchians seeing crocodylomorph entry into MO previously dominated by phytosaurs. Within the early Mesozoic, thalattosuchians apparently only converged upon the gracile phytosaur forms. Early Jurassic crocodylomorphs showed much greater disparity than the other pseudosuchian clades with their MO encompassing longirostrine and more compact jaws, highlighting greater dietary diversity within crocodylomorphs.

III. **Avemetatarsalians.** The overall MO of the avemetatarsalians, particularly the dinosauromorphs, is quite conservative when considered alongside other archosauromorphs with their overall morphospace sitting within the central regions of overall archosauromorph MO. The reconstruction of *Yarasuchus deccanensis* (Sen, 2005) is included to provide tentative estimation of aphanosaurian mandibular morphology and give some idea of trophic ecology at the base of Avemetatarsalia (Nesbitt et al., 2017) (Fig. 2.1.4). *Yarasuchus* sits within the central areas of morphospace, alongside small crocodylomorphs, immediately signalling mesocarnivory. Indeed, the mandible of *Yarasuchus* is slender with an obtuse symphysis and a relatively long toothrow that exhibits low MA, implying a low-stress, high speed raptorial functionality that would suit a mesocarnivorous trophic ecology (Figs. 2.1.3, 5).

Pterosaurs further push mandibular adaptation towards high speed, raptorial functionality by heavily reducing MAMA and OMA (Fig. 2.1.5), becoming extremely slender and gracile (Figs. 2.1.3-4). Their small sizes and the lightly built nature of their jaws and thin conidont dentitions (Figs. 2.1.3-4, 6) suggest a preference for slippery, gracile small prey such as insects or fish. However, there is strong variation across PC/fPC 2 highlighting strong variation in the curvature of their jaws and the symphyses. The upwardly deflected jaws of some pterosaurs largely conform with heightened gripping and raptorial functionality, but a downward deflection is typically associated with herbivory in sauropodomorphs and azendohsaurs, which is unlikely to be analogous in pterosaurs. The functional significance of the downward deflection is to enhance the stress resistance of the symphysis (Ma et al.,

2017) and so may indicate a feeding strategy involving higher stress in these pterosaurs. Furthermore, this deflection also results in slight reorientation of the anterior teeth, directing them to point forward and so perhaps improving piercing functionality. The downwardly deflected dentaries appear to be more prevalent in the older taxa, suggesting this was the basal pterosaur morpho-functionality, and their jaws became more gracile and adapted for speed through their evolution, reflecting perhaps increasing proficiency with life on the wing.

Dinosauromorph mandibular evolution appears to show a clear trend towards increased biting efficiency and robusticity (Fig. 2.1.8c), but their morphologies are comparatively conservative compared to the other archosauromorphs. The greatest novelty of early Mesozoic dinosauromorph mandibular morphology is the downward deflection of the dentary, with these mandibular morphologies being somewhat unique to sauropodomorphs; the clade is largely responsible for the expansion of overall archosauromorph MO into more PC2/fPC2 negative regions of morphospace (Figs. 2.1.3-4). Nonetheless, deflected dentaries are also present in the azendohsaurs underlining that sauropodomorphs were re-treading and further expanding on the mandibular evolution of earlier archosauromorphs (Stocker et al., 2016). Increased symphyseal robusticity is an adaptation for stress mitigation reflecting the heightened focus of forces and stresses at the rostral-most point of the mandible and indicating more cropping and pulling material (vegetation) (Lautenschlager, 2017). Shifts in dental morphology mark the second major aspect of variation in sauropodomorph trophic morphology with teeth shifting from ziphondont to folidont (Fig. 2.1.6a) and eventually more spatulate forms (Galton, 1985; Barrett, 2014). There is also some pseudo-heterodonty present in the tooth morphology across the toothrow (Weishampel and Norman, 1989), which is not precisely assessed here, but this variation along an extended toothrow (Fig. 2.1.5) suggests an extended bite, with the anterior of the jaw focused on cropping, and the posterior directed more towards shearing vegetation. The reduction in the toothrow in later, larger sauropodomorphs (Figs. 2.1.3-4, 7) suggests greater focus on the anterior cropping function.

Silesaurids show parallel patterns of mandibular, dental and (to a lesser extent) size evolution as sauropodomorphs in their transition from carnivorous to herbivorous diets (Figs. 2.1.3-6). Given these similarities in their morphological evolution, the divergent fortunes of silesaurids and sauropodomorphs through the Late Triassic is intriguing. It appears that the main difference in their morphologies considered here is their overall size (Fig. 2.1.4). The mandibles of the earliest silesaurids were fairly similar to the

crocodylomorphs, being quite slender, but not to the same extent as the pterosaurs. The larger taxa such as *Asilisaurus kongwe* and *Silesaurus opolensis*, are typically more sauropodomorph-like. However, the jaw morphology of *Pisanosaurus mertii* shows that later silesaurids also developed biting efficiency by expanding their jaw musculature as illustrated by posterior expansion of the mandible and a more prominent coronoid process. Nevertheless, this interpretation is tentative due to the uncertain classification of *Pisanosaurus* between Silesauridae and Ornithischia (Müller and Garcia, 2020).

Ornithischian mandibular morphology shows strong reinforcement along the dentary, but most notable is their development of a distinct coronoid process, greater than that seen in other early Mesozoic archosauromorphs, to bolster the jaw musculature (Figs. 2.1.3-5). This morphological evolution appears directed towards producing a precise, powerful cropping bite. Optimisation for power appears to be a hallmark of ornithischian mandibular evolution, with all members showing strong MA and robusticity (Fig. 2.1.5). The smaller (heterodontosaurid) taxa appear to have developed the most efficient jaws with high anterior and posterior MA (Figs. 2.1.3-4). The high MPMA of ornithischians indicates higher bite force directed towards the back of the toothrow, suggesting a strong masticatory function. *Scelidosaurus harrisonii* shows slight symphyseal deflection and relatively greater anterior MA compared to other ornithischians, suggesting further enhancement of cropping over masticatory function in the earliest thyreophorans.

The MO of herrerasaurids and theropods does not differ much from that of the pseudosuchian carnivores, suggesting strong similarities in their trophic ecologies (Fig. 2.1.3). Herrerasaurid jaws are generally all quite robust with relatively high MA at the anterior and posterior of the toothrow, highlighting a similar hypercarnivorous functionality to straight-jawed loricatan pseudosuchians. Large theropods such as *Dilophosaurus wetherilli* also exhibited these hypercarnivorous morphologies, but interestingly, large theropods also exhibited more slender jaws, typical of smaller mesocarnivorous archosauromorphs, meaning theropods appear to have developed much larger sizes across the breadth of their mandibular MO, breaking with a pattern of limited size ranges in other carnivorous archosauromorph clades. Herrerasaurids possessed high MAMA but low OMA suggesting adaptations to increase both biting power and speed (Fig. 2.1.5). Theropods exhibit much greater variation in MAMA and OMA, but show relatively higher MPMA, with MPMA being consistent across most theropod taxa, indicating greater bite forces directed towards the back of the toothrow. These subtle differences point to slightly different jaw action between herrerasaurids and theropods, with the herrerasaurids placing greater

emphasis on penetrative bites, maximising power and speed at the jaw anterior, whereas theropod biting was typically weaker but showed greater distribution of bite force along the entire breadth of the toothrow.

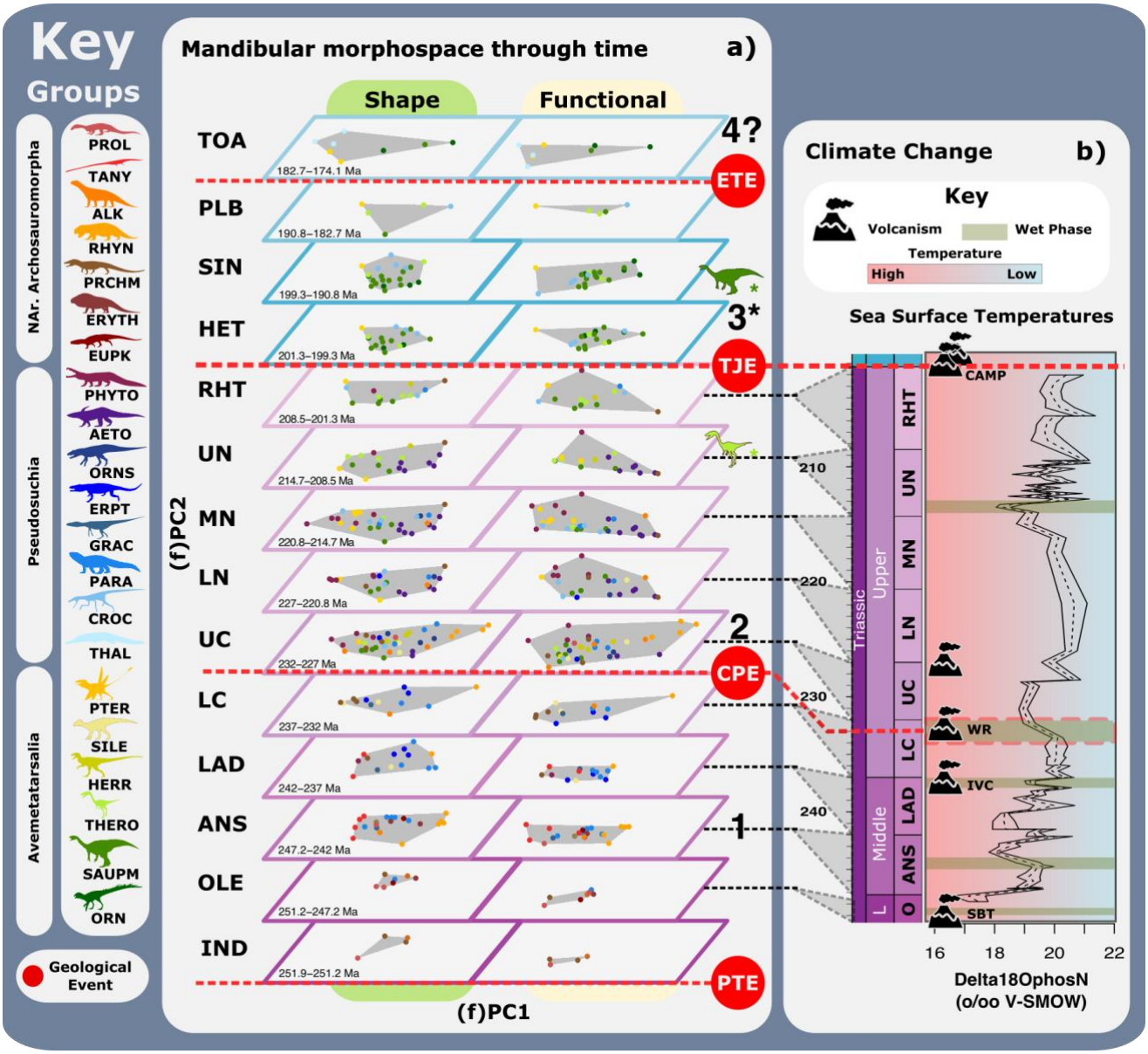

Figure 2.1.7. Mandibular shape and functional morphospace occupation of early Mesozoic archosauromorphs through time. (a) Shape and functional morphospace time-slices at stage and substage levels. (b) Sea surface temperatures and environmental changes through the Triassic from Trotter et al., (2015). Major extrinsic, environmental events are shown by the dashed red line. Humid intervals illustrated by shaded bands. Radiations are numbered. *Extended dinosaur diversification across the Triassic-Jurassic boundary illustrated by silhouettes of theropods in the Upper Norian and sauropodomorphs in the Hettangian. Abbreviations: AETO,

Aetosauria. ALK, Allokotosauria. ANS, Anisian. APH, Aphanosauria. CAMP, Cental Atlantic Magmatic Province. CPE, Carnian Pluvial Event. CROC, Crocodylomorpha. ERPT, Erpetosuchidae. ERYTH, Erythrosuchidae. ETE, Early Toarcian event. EUPK, Euparkeriidae. GRAC, Gracilisuchidae. HERR, Herrerasauridae. HET, Hettangian. IND, Induan. IVC, Italian volcanic centre. LAD, Ladinian. L. CRN, Lower Carnian. L. NOR, Lower Norian. M. NOR, Middle Norian. NAr, Non-archosaur. OLE, Olenekian. ORN, Ornithischia. ORNS, Ornithosuchidae. PARA, Paracrocodylomorpha. PC, Principal component. PHYTO, Phytosauria. PLB, Pliensbachian. PRCHM, Proterochampsia. PROL, Prolacertidae. PTER, Pterosauria. PTE, Permo-Triassic extinction. RHT, Rhaetian. RHYN, Rhynchosauria. SAUPM, Sauropodomorpha. SILE, Silesauridae. SIN, Sinemurian. TANY, Tanystropheidae. THAL, Thalattosuchia. THERO, Theropoda. TJE, Triassic-Jurassic extinction. TOA, Toarcian. U. CRN, Upper Carnian. U. NOR, Upper Norian. WR, Wrangellian eruptions.

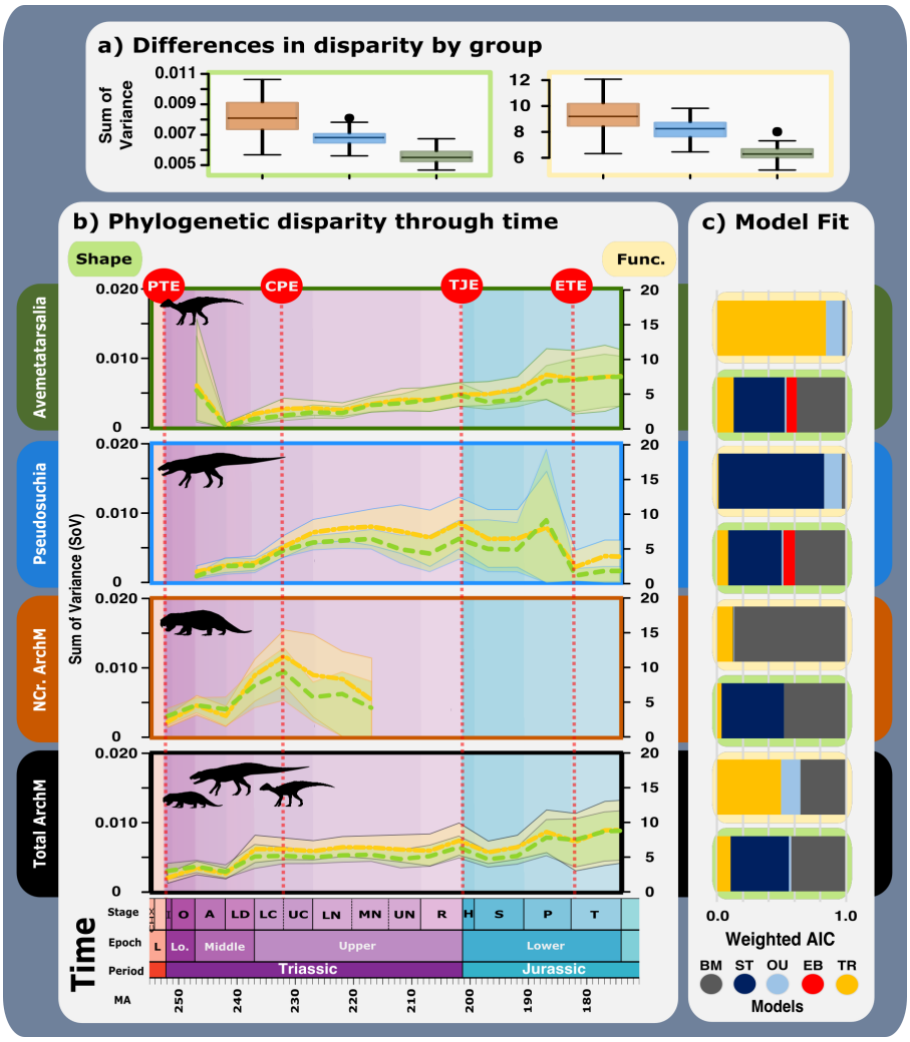

Figure 2.1.8. Mandibular shape and functional disparity of early Mesozoic archosauromorphs through time. (a) Overall shape and functional disparity across the Archosauromorpha. (b)

Phylogenetic shape and functional disparity per (sub)stage. (c) Macroevolutionary model support for archosauromorph morpo-functional evolution. Major extrinsic, environmental events are shown by the dashed red line. Abbreviations: A, Anisian. ArchM, Archosauromorpha. BM, Brownian motion. CHX, Changhsingian. CPE, Carnian Pluvial Event. EB, Early burst. ETE, Early Toarcian event. H, Hettangian. I, Induan. LD, Ladinian. LC, Lower Carnian. LN, Lower Norian. MN, Middle Norian. NCr, Non-archosaur. O, Olenekian. OU, Ornstein-Uhlenbeck. P, Pliensbachian. PTE, Permo-Triassic extinction. R, Rhaetian. S, Sinemurian. ST, Stasis. TJE, Triassic-Jurassic extinction. T, Toarcian. TR, Trend. UC, Upper Carnian. UN, Upper Norian.

Archosauromorph ecomorphological diversification through time. Dividing the mandibular shape and functional primary morphospaces (Fig. 2.1.3a, c) by stage (Fig. 2.1.7a) shows patterns of morpho-functional expansion and contraction through time. The abundance of taxa within the morphospace reflects the prevalence of different archosauromorph clades, given the positive relationship between diversity, faunal abundance, and taxon sampling. Overall trends in mandibular ecomorphological evolution are also illustrated using sum of variance (SOV) obtained from phylogenetic time-slices (Guillerme and Cooper, 2018) (Fig. 2.1.8) as a clear numerical measure of mandibular form and functional diversity. Overall, we see a pattern of decreasing disparity through archosauromorph evolution, with NAAs exhibiting much greater mandibular disparity than pseudosuchians, and pseudosuchians exhibiting much greater mandibular disparity than avemetatarsalians (Fig. 2.1.8a) (Foth et al., 2017; Ezcurra and Butler, 2018). I

Archosauromorph MO in the Early Triassic was largely contained within central (faunivorous) regions of shape and functional morphospaces, and grew from the Anisian onwards (Figs. 2.1.3, 7a). As archosauriforms, the presence of proterochampsians in the Induan indicates the prior emergence of more basal archosauromorph clades, and current phylogenetic evidence points to an initial diversification of NAAs in the Late Permian, following the End-Guadalupian extinction event (Ezcurra et al., 2020). Ancestral state estimation of mandibular morpho-function suggests this first radiation was rapid and quite morphologically diverse (Fig. 2.1.9). However, most Permian archosauromorphs were likely generalist faunivores, although archosauriforms became specialised hypercarnivores through the attainment of larger sizes towards the end of the Permian (Fig. 2.1.9b). Indeed, the earliest archosauriform, *Archosaurus rossicus*, from the Late Permian of Eastern Europe, supposedly reached lengths of approximately 3 metres (Sennikov and Golubev, 2006). The Middle Triassic archosauromorph radiation was driven by non-archosaur archosauromorphs and pseudosuchians, with NAAs showing particularly high mandibular morpho-functional disparity (Fig. 2.1.8) as they colonised new niches, moving beyond general faunivory, to become specialised herbivores

(rhynchosaurs), piscivores (tanystropheids), and hypercarnivores (erythrosuchids). The pseudosuchians diversification was gradual and concentrated within faunivorous morphospace (Figs. 2.1.8-9). The Anisian diversification of the first pseudosuchians echoed that of non-archosaur archosauriforms by also developing greater variation in body size (Fig. 2.1.9b). Pseudosuchians also expanded their mandibular morpho-functionality with their disparity growing through the Middle Triassic (Fig. 2.1.8b). Larger sizes and prevalent ziphodonty (Fig. 2.1.6a) highlight further archosauriform and pseudosuchian specialisation as terrestrial hypercarnivores. Trends in pseudosuchians and NAAs diverged in the Ladinian as NAA MO declined with remaining taxa distributed within peripheral regions of overall archosauromorph MO, while pseudosuchians expanded into hypercarnivorous morphologies, highlighting an archosauromorph turnover within the carnivore guild as pseudosuchians overtook non-archosaur archosauriforms as the largest terrestrial carnivores (Fig. 2.1.7a).

The Carnian Pluvial Event saw the interchange between NAA and archosaur predominance as pseudosuchians and avemetatarsalians became the primary constituents of archosauromorph morphospace. The onset of the Late Triassic saw the archosaurs diversify with the late Carnian featuring a strong diversity of terrestrial archosaurs, particularly herbivores, as well as semi-aquatic phytosaurs and aerial pterosaurs (Fig. 2.1.8a). The Carnian-Norian boundary saw the extinction of most remaining NAAs and a shift in dinosaur MO as sauropodomorphs shift into more herbivorous regions of central morphospace. The Norian saw relative stability of overall archosauromorph MO, but this was largely maintained by the survival of the most extreme archosaur morphologies in phytosaur (semo-aquatic) and aetosaur (herbivorous?) pseudosuchians. Within the centre of morphospace, there were a series of changes that reflect shifts in terrestrial archosaur communities, particularly within the faunivore guild. The Norian saw a turnover in pseudosuchian diversity as faunivorous paracrocodylomorphs were largely ‘replaced’ by crocodylomorphs, with remaining non-crocodylomorph pseudosuchians going extinct in the Rhaetian. Pseudosuchian decline is contrasted by dinosaur success as sauropodomorphs and theropods became more significant elements of archosaur diversity through the closing stages of the Triassic (Fig. 2.1.7a). Consequently, dinosaurs had already become prominent across faunivorous and herbivorous niches prior to the End-Triassic mass extinction (ETE), which cemented dinosaur terrestrial dominance by wiping out the majority of remaining terrestrial pseudosuchians. Dinosaurs radiated in the Early Jurassic, expanding their overall MO as sauropodomorphs, theropods and ornithischians all became more disparate (Fig. 2.1.8b). This was most pronounced in ornithischians as they radiated into morphospace once held by aetosaurs and rhynchosaurs. Theropods became the predominant megacarnivores as illustrated by their larger sizes (Fig. 2.1.3) and hypercarnivorous mandibular morphologies (Fig. 2.1.7a). Even

surviving crocodylomorphs became more disparate, re-entering the herbivore guild and establishing their core niche as terrestrial mesocarnivores. However, the Pliensbachian marks an abrupt change in archosaur ecomorphology as crocodylomorphs return to semi-aquatic niches with the evolution of the thalattosuchians. This is perhaps more marked in the disparity curves which shows a sharp peak in pseudosuchian disparity in the Pliensbachian, followed by a sharp drop towards a low base in the Toarcian (Fig. 2.1.8b). While pseudosuchian mandibular disparity fell following this Early Toarcian Event (ETE), avemetatarsalian disparity plateaued, marking the culmination of their trend towards greater disparity (Fig. 2.1.8c; Supplementary Table 2.1.3).

Bayesian estimation of the rates of mandibular shape and functional evolution using PC data reveals strong rate homogeneity across the archosauromorph tree, particularly for functional evolution, further highlighting conservative nature of their evolution (Fig. 2.1.9a). Rate heterogeneity is present as higher rates are scattered throughout the tree, with some clades such as the pterosaurs, phytosaurs, rhynchosaurs and herrerasaurids all showing relatively high evolutionary rates. The clade with the highest rates were rhynchosaurs, particularly the hyperodapedontine rhynchosaurs, which developed some of the most extreme morphologies of all early Mesozoic archosauromorphs, just prior to their extinction through the Carnian-Norian transition (Figs. 2.1.3, 9-10). Macroevolutionary modelling of disparity trends did not support an early burst of shape or functional diversity (Fig. 2.1.8c), but it seems that evolutionary rates were higher during the earliest cladogenesis. This is most apparent at the base of the Dinosauria, with basal sauropodomorphs and herrerasaurids showing high evolutionary rates, but it can be seen across the NAAs, pseudosuchians and avemetatarsalians, and in the overall Archosauromorpha when viewed in their entirety, with NAAs generally exhibiting much higher overall rates than archosaurs (Fig. 2.1.10). Interestingly, this contrast in rates between NAAs and archosaurs extends further, as slow rates are only found within archosaurs, most notably within crocodylomorphs and massopodan sauropodomorphs. Furthermore, evolutionary rates remained relatively high within NAAs throughout their range. Rates of mandible shape evolution appear to gradually decline through the early Mesozoic, whereas functional rates are largely static (Fig. 2.1.10a). However, there are pulses of increased rates that correspond to the Induan, Anisian, CPE, and TJE, and the Pliensbachian-Toarcian boundary. Barring the Induan and Toarcian peaks, these intervals of high rates are recovered here as being associated with archosauromorph radiations: NAAs in the Anisian, archosaurs at the CPE, and dinosaurs at the TJE (Figs. 2.1.7a, 10a). The high rates reflect the combined rapidity of lineage diversification and morphological evolution during these events. As such the Induan and early Toarcian rate pulses may hint at hidden diversifications during these intervals.

Patterns of mandibular shape and functional evolution are quite similar across NAAs, pseudosuchians and avemetatarsalians (Fig. 2.1.4), but their body size evolution shows clear differences, indicative of increasing archosaur experimentation with varying overall body size (Fig. 2.1.9b). NAAs do not show much size variation with only erythrosuchids and hyperodapedontid rhynchosaurs reaching markedly larger sizes, but archosaurs saw increasingly greater variation in size, with pseudosuchians and then dinosauromorphs developing larger sizes. This demonstrates an interesting contrast in ecomorphological evolution from NAAs to archosaurs, with NAAs developing high mandibular disparity but little size diversity, whereas archosaurs developed greater size ranges but increasingly reduced mandibular disparity (Figs. 2.1.8a, 9b).

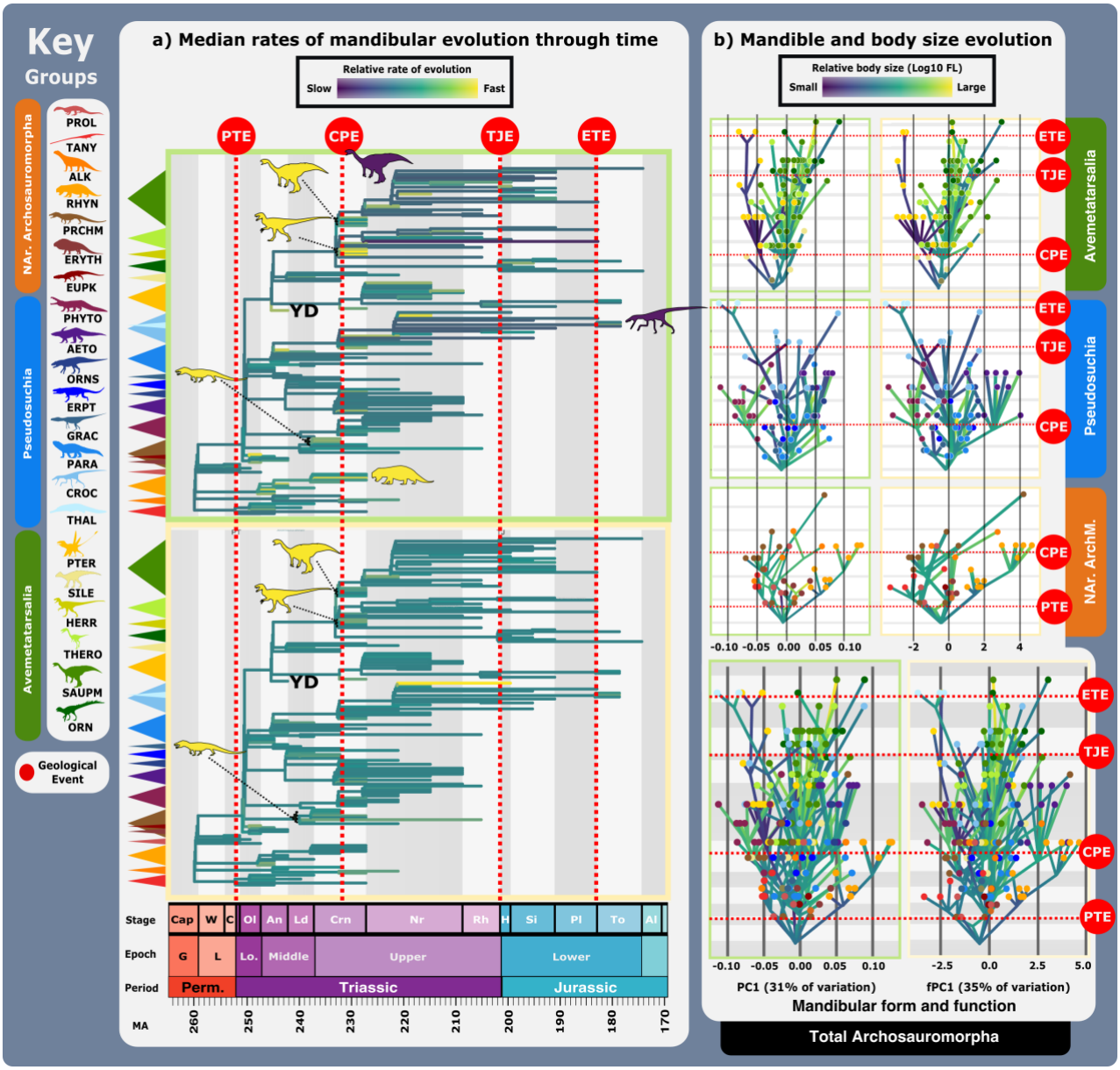

Figure 2.1.9. Tempo and mode of shape and functional mandibular evolution across early Mesozoic archosauromorphs. (a) Rates of shape and functional mandibular evolution across the Archosauromorpha. (b) Patterns of mandibular shape and functional evolution alongside changes in body size. Silhouettes in (a) indicate notably fast (yellow) or slow (purple) evolution. Major extrinsic, environmental events are shown by the dashed red line. Abbreviations: AETO, Aetosauria. Al, Aalenian. ALK, Allokotosauria. An, Anisian. C, Changhsingian. Cap, Capitanian. CPE, Carnian Pluvial Event. Crn, Carnian. CROC, Crocodylomorpha. ERPT, Erpetosuchidae. ERYTH, Erythrosuchidae. ETE, Early Toarcian event. EUPK, Euparkeriidae. G, Guadalupian. GRAC, Gracilisuchidae. H, Hettangian. HERR, Herrerasauridae. IND, Induan. LAD, Ladinian. L, Lopingian. Lo, Lower. NAr, Non-archosaur. Nr, Norian. Ol, Olenekian. ORN, Ornithischia. ORNS, Ornithosuchidae. PARA, Paracrocodylomorpha. PC, Principal component. PHYTO, Phytosauria. Pl, Pliensbachian. PRCHM, Proterochampsia. PROL, Prolacertidae. PTER, Pterosauria. PTE, Permo-Triassic extinction. Rh, Rhaetian. RHYN, Rhynchosauria. SAUPM, Sauropodomorpha. SILE, Silesauridae. Si, Sinemurian. TANY, Tanystropheidae. THAL, Thalattosuchia. THERO, Theropoda. TJE, Triassic-Jurassic extinction. To, Toarcian. U. CRN, Upper Carnian. U. NOR, Upper Norian. W, Wuchiapingian. YD, *Yarasuchus deccanensis*.

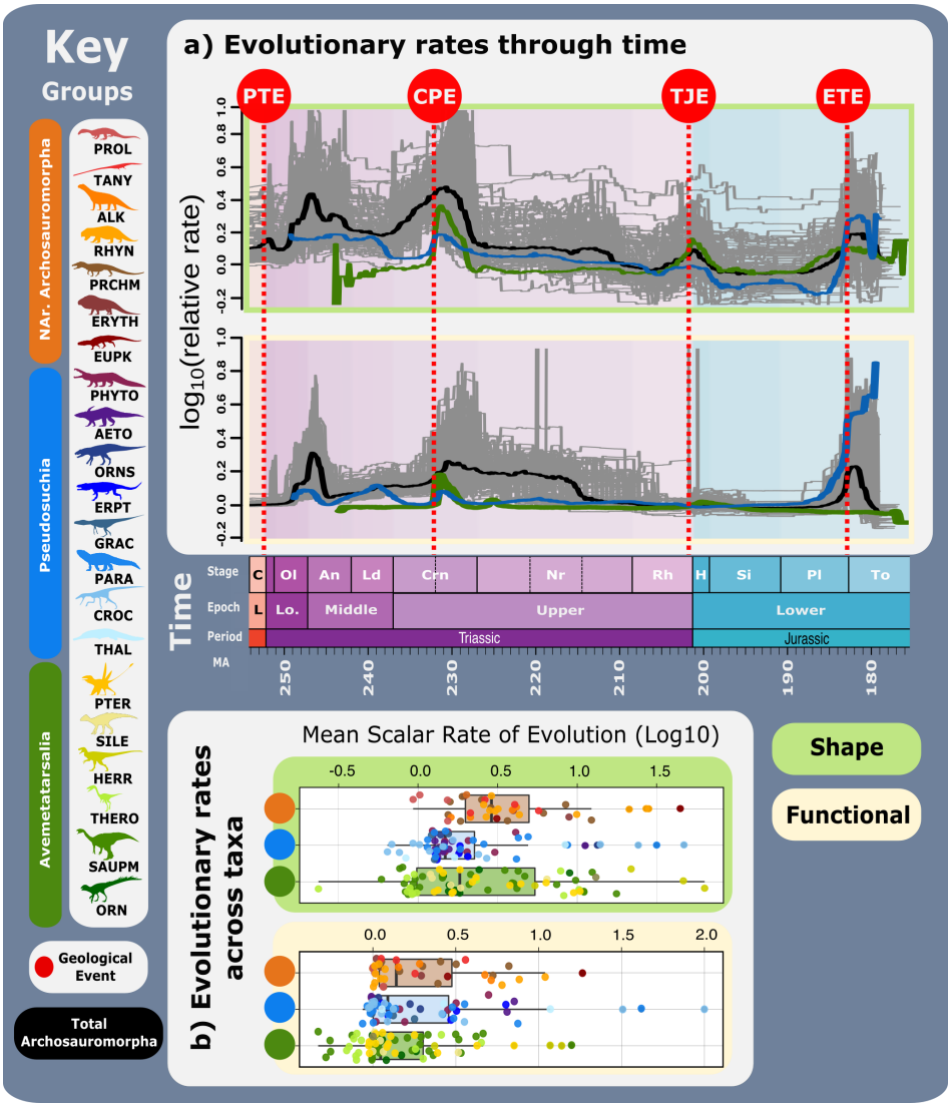

Figure 2.1.10. Rates of shape and functional mandibular evolution across early Mesozoic archosauromorphs. (a) Overall clade rates of shape and functional mandibular evolution through time. (b) Clade-wise differences in rates of shape and functional mandibular evolution across the Archosauromorpha. Abbreviations: AETO, Aetosauria. Al, Aalenian. ALK, Allokotosauria. An, Anisian. C, Changhsingian. Cap, Capitanian. CPE, Carnian Pluvial Event. Crn, Carnian. CROC, Crocodylomorpha. ERPT, Erpetosuchidae. ERYTH, Erythrosuchidae. ETE, Early Toarcian event. EUPK, Euparkeriidae. G, Guadalupian. GRAC, Gracilisuchidae. H, Hettangian. HERR, Herrerasauridae. IND, Induan. LAD, Ladinian. L, Lopingian. Lo, Lower. NAr, Non-archosaur. Nr, Norian. Ol, Olenekian. ORN, Ornithischia. ORNS, Ornithosuchidae. PARA, Paracrocodylomorpha. PC, Principal component. PHYTO, Phytosauria. Pl, Pliensbachian. PRCHM, Proterochampsia. PROL, Prolacertidae. PTER, Pterosauria. PTE, Permo-Triassic extinction. Rh, Rhaetian. RHYN, Rhynchosauria. SAUPM, Sauropodomorpha. SILE, Silesauridae. Si, Sinemurian. TANY, Tanystropheidae. THAL, Thalattosuchia. THERO,

Theropoda. TJE, Triassic-Jurassic extinction. To, Toarcian. U. CRN, Upper Carnian. U. NOR, Upper Norian. W, Wuchiapingian.

Discussion

Ecomorphological convergence, competition, and replacement. Taxa typically strive to maximise their exploitation of available resources whilst minimising the costs of competition through niche partitioning, and so the ecological diversity of coexisting clades is connected (Aristide and Morlon, 2019; Finke and Snyder 2008). Competition is heavily cited in classic studies of archosauromorph evolution as the driving force of the faunal turnovers of the early Mesozoic, with the supposed competitive superiority of successive clades, (particularly dinosaurs) cited as the source of their success (Charig, 1984; Bakker, 1972; Bonaparte, 1982). Competition requires conflicting exploitation of the same resources and as such would suggest some ecological similarity between competitors (Darwin, 1859). Recent studies have found broad differences in overall morphology across pseudosuchians and dinosaurs (Brusatte et al., 2008, 2010), and within the herbivore guild (Singh et al., 2021). In this comprehensive study of early Mesozoic archosauromorph mandibular disparity, I find strong overlap between the mandibular MO of NAAs, pseudosuchians and dinosaurs, focused within faunivorous niches (Figs. 2.1.3, 4). Whilst this may indicate strong potential for competition, a temporal breakdown reveals that much of this overlap represents convergent evolution at different times. Contemporaneous MO overlap is quite rare through the early Mesozoic. This is particularly true within archosaurs during the latest Triassic as although hypercarnivorous paracrocodylomorph pseudosuchians and theropod dinosaurs share similar morphospace and sizes (Fig. 2.1.3), they did not coexist as theropods only evolved these mandibular morphologies following the decline and extinction of paracrocodylomorphs. From their emergence in the late Carnian, theropod MO remained largely separate from that of paracrocodylomorphs until the late Norian (Figs. 2.1.7a), which marked the onset of declining pseudosuchian MO, evolutionary rates (Figs. 2.1.9-10), and diversity (Toljagić and Butler, 2013). Theropod MO in the Upper Norian and Rhaetian is indicative of increasingly hypercarnivorous ecologies and their increasing prevalence within the carnivore guild. Growing evidence from phylogenetic (Pol et al., 2021) and ichnofossil (Da Silva et al., 2012; Lucas et al., 2006) evidence supports an increase in saurischian diversity and body sizes around the TJB that may extend as far back as the late Norian–Rhaetian boundary (Upchurch et al., 2011). Rates of evolution show no distinct changes, but this interval marks the point at which the rates of dinosaur evolution begin to overtake pseudosuchians as a prelude to their short-term rates boost at the Triassic-Jurassic boundary (TJB) (Fig. 2.1.10a).

Whilst the TJE has traditionally marked a distinct beginning of dinosaur domination of terrestrial faunas (Brusatte et al., 2008; Sues and Fraser, 2010), my results support a pre-TJE increase in dinosaur ecological diversity and a stepwise takeover of terrestrial ecosystems, with morphospace expansions in the carnivore guild by theropods in the Upper Norian-Rhaetian, and then the herbivore guild by sauropodomorphs and ornithischians in the Hettangian (Fig. 2.1.7a). This pattern potentially supports the idea of separate extinction pulses at the Norian-Rhaetian boundary and TJB (Sephton et al., 2002; Rigo et al., 2020; Wignall & Atkinson 2020). Both dinosaurian morphospace expansions follow apparent pseudosuchian declines within those respective dietary guilds (Fig. 2.1.7a). These pseudosuchian declines may reflect poor sampling, as specialised terrestrial pseudosuchians are known from this interval (Melstrom and Irmis, 2019), but the present patterns of mandibular evolution demonstrate a pattern of dinosaur eco-morphological radiation following the loss of pseudosuchians competitors, highlighting the opportunistic nature of the rise of the dinosaurs (Benton, 1983; 1989). This suggests some diversity-dependent controls on terrestrial archosaur evolution (Rabosky and Lovette, 2008) as pseudosuchians and dinosauromorphs coexisted for approximately 45 million years, yet both clades show rather segregated MO for much of that interval; dinosauromorph diversification was primarily focused within generalised faunivorous and, later, specialised herbivorous niches (Figs. 2.1.4, 7a, 9) (Galton, 1985; Muller and Garcia, 2019). Pseudosuchians dominated the carnivore guild, with the only dinosauromorph coeval convergence of herrerasaurids and loricatan pseudosuchians in the Upper Carnian being relatively short-lived (Figs. 2.1.4, 7a, 9). Rather than directly competing, it appears that both clades engaged in broad niche-partitioning. Dinosaur ecological diversification into new ecospace only occurred following pseudosuchian decline and/or withdrawal from said ecospace, suggesting the prevalence of pseudosuchians through the Upper Carnian and Lower-Middle Norian was an intrinsic constraint on dinosaur macroevolution.

I find one clear example of apparent niche overlap in the Anisian, during which, basal archosauriform and pseudosuchian (Anisian) MO overlapped heavily within the central carnivorous regions of morphospace (Fig. 2.1.4, 7a). This apparent niche-overlap was relatively short-lived as basal archosauriforms vacated these niches by the Ladinian. Intriguingly, archosauriforms exhibited relatively higher evolutionary rates (Fig. 2.1.9a) than their pseudosuchian ‘rivals’. High rates of trait evolution reflects rapid morphological change within a short space of time, and so could reflect two ecological scenarios: i) the removal of ecological constraints enabling unbounded evolution across a wide range of morphologies either through the loss of competitors or entry into uncontested ecospace – an ‘ecological release’ (Cox and Ricklefs, 1977), or ii) strong selective pressures requiring rapid morphological evolution to minimise such stresses following ‘Red Queen’ patterns (Van Valen,

1973). Within these potentially competing Anisian carnivores, it was the pseudosuchians that ultimately outlasted their competitors, despite showing no obvious morpho-functional mandibular superiority and lower evolutionary rates. Ladinian archosauriforms withdrew from hypercarnivore niches and shifted into mesocarnivorous morphospace, possibly reflecting competitive displacement by pseudosuchians and so a Red Queen scenario. A potential driver of pseudosuchian success over archosauriforms may be their improved locomotory or respiratory efficiency and so an example of competitive replacement (Charig, 1984; Bonaparte, 1984; Bakker, 1972). However, there are other ways to explain this pattern, such as convergent allopatric specialisation, or if sympatric, low competitive pressures due to high resource availability, or niche-differentiation manifesting instead in alternative aspects of anatomy or behaviour (Patterson et al., 2003; White et al., 2007; McPhee et al., 2017; Hoffman et al., 2019). Furthermore, the speeds of these turnovers are unknown, so rapid displacements as would be consistent with the competitive replacement model (Benton, 1987) cannot be confirmed. In our study, coeval archosauromorphs show greater morpho-functional separation than convergence, highlighting a drive to avoid competition through niche partitioning (Finke and Snyder, 2008).

Environmental influences on early Mesozoic archosauromorph diversification. The timings of the archosauromorph radiations through the early Mesozoic (Fig. 2.1.7) hint at the importance of extrinsic changes as drivers of macroevolutionary patterns. Changes in environmental conditions affect resource diversity and availability (Cascales-Miñana et al., 2010), as well as impact different clades based on their physiological preferences (Liu et al., 2021). Clearly environmental stability is a key factor in setting the limits of ecological diversity as environmental instability supports the long-term survival of generalists (Roopnarine et al., 2007) as specialisation requires secure resource availability so that the benefits of increased niche efficiency outweigh the costs of reduced trophic flexibility (Smith and Szathmary, 1997; Van Valkenburgh et al., 2004; Ramiadantsoa et al., 2018). Therefore, the capacity to diversify explosively is dependent on stable access to bountiful resources, which is partially, possibly predominantly dependant on stabile environmental conditions.

Environmental controls on diversification dynamics are perhaps most apparent in the reestablishment of stable climates following the PTE and TJE. The aftermath of the PTE saw dramatic spatiotemporal oscillations in the carbon cycle, global temperatures and sea-levels and typically high global temperatures prevail through the Early Triassic (Payne and Kump, 2007; Irmis and Whiteside, 2012; Sun et al., 2012; Trotter et al., 2015; Li et al., 2016) (Fig. 2.1.7b). The end of these oscillations and the onset of cooler climates in the Anisian (Preto et al., 2010; Chen and Benton, 2012; Miller and Baranyi, 2019) coincides with increasing archosauromorph mandibular morpho-functional MO and

disparity (Figs. 2.1.7-8) that reflects increasing trophic diversity. This pattern in archosauromorphs links in with broader biotic patterns of increasing niche specialisation and guild complexity in the terrestrial and marine realms (Benton et al., 2004; 2013; Wei et al., 2015; Foth et al., 2017; Ezcurra and Butler, 2018). Climatic instability also predominated through the TJE, as temperature trends rapidly shifted between global cooling and warming at the onset of the Early Jurassic (Bacon et al., 2013; Baghli et al., 2020; Steinthorsdottir et al., 2021; Ruebsam and Schwark, 2021). This instability is further illustrated by the proliferation of fern-dominated 'disaster floras' and a drop in floral diversity across the TJB (McElwain et al., 1999; van de Schootbrugge et al., 2009). Floral diversity patterns indicate that terrestrial environments did not restabilise until around three to four million years after the TJE within the Sinemurian (McElwain et al., 2007). The return of floral/environmental stability appears to approximately coincide with pulses of archosauromorph diversification (Fig. 2.1.9), slight archosauromorph mandibular morphospace expansion and increased morphospace packing (Figs. 2.1.7-8). Indeed, we find two pulses of diversification within the Sinemurian across both dinosaurs and crocodylomorphs (Fig. 2.1.9). Both pulses of archosauromorph MO expansion (Fig. 2.1.7a) are associated with marked changes in interclade MO (see 1 and 3 on Fig. 2.1.7a), with archosaurs and dinosaurs, respectively becoming much more prominent.

Changes in environmental conditions can be directly related to patterns of archosauromorph diversity when supposedly herbivorous taxa are considered because of their clear link to climatically-controlled food resources – vegetation. Dramatic climatic and floral shifts during the Carnian Pluvial Event (~234-232 Ma) saw global climates change from arid to humid and back again (Preto et al., 2010; Miller and Baranyi, 2019; Kustatscher et al., 2018; Bernardi et al., 2018; Dal Corso et al., 2020; Mancuso et al., 2020). The CPE is associated with a faunal turnover that saw radiating archosaurs overtake non-archosaur archosauromorphs and therapsids as the predominant taxa in terrestrial ecosystems, particularly within the herbivore guild (Benton, 1983; Crompton and Attridge, 1986; Sues and Fraser, 2010; Benton et al., 2018). This is perhaps reflected here with the expansion of archosauromorph mandibular morphospace across the CPE, reflecting increasing herbivorous archosauromorph diversity and increasing specialisation illustrated across basal archosauromorphs (allokotosaurs and rhynchosaurs), pseudosuchians (aetosaurs) and dinosauromorphs (silesaurids) (Fig. 2.1.7a). Further shifts occurred at the Carnian-Norian boundary with sauropodomorph MO expansion confirming dinosaur entry into the herbivore guild (Fig. 2.1.7a). The establishment of sauropodomorphs and aetosaurs in the herbivore guild coincided with the decline of the rhynchosaurs (Ezcurra et al., 2016) and dicynodonts (Fröbisch, 2008; Ruta et al., 2013) (Fig. 2.1.7a). The Carnian-Norian transition marks the broad decline of non-archosaur archosauromorphs, which are reduced to specialist elements such as *Vancleavea campi* in the later Triassic (Figs. 2.1.7a, 9a).

Low morpho-functional convergence between prevailing archosaur herbivores and the last rhynchosaurs (Figs. 2.1.3-4) indicate divergent trophic strategies. Therefore, it appears archosaur niche choice was probably key to their success following the CPE as those niches ultimately proved more sustainable than the waning rhynchosaurs. The ability to process tough vegetation through strong masticatory systems or gizzards has been argued as evidence for archosaur domination of the herbivore guild (Crompton and Attridge, 1986; Farlow, 1987). This argument is compelling as the pattern of archosaur consolidation within herbivorous morphospace following the CPE roughly corresponds with the end of the '*Dicroidium* flora' and increasing gymnosperm prevalence (Bonaparte, 1982; Benton, 1983; Kustatscher et al., 2018). However, rhynchosaurs possessed powerful shearing jaws with multiple rows of bulbous teeth (Figs. 2.1.4, 6a) (Benton, 1984) that were well-suited to tough vegetation, so this hypothesis requires further examination. This differential survivorship may point to wider differences in the size and posture of archosaur herbivores (Sookias et al., 2012: Ezcurra and Butler, 2018) as being key; larger size and more efficient support could have better supported larger stomachs, maximising hind-gut fermentation, and efficient digestion of plant material (Clauss et al., 2013). Support for floral influence of archosaur evolution appears strong, as it seems that floral diversity changes drove the extinction of many low-level browsing herbivores at the TJB, because sauropodomorphs were the only large terrestrial herbivores to survive the TJE (Weishampel, 1984; Galton, 1985; Parrish, 2006; Sander et al., 2011). Sauropodomorph MO and diversity increased across the T-J boundary moving further into morphospace associated with greater MA, suggestive of further herbivorous specialisation (Fig. 2.1.7a). Furthermore, the diversification of ornithischians into morphospace representing greater MPMA and robusticity (Figs. 2.1.3-4, 7a, 9) and consistent with greater herbivorous specialisation occurs within the Sinemurian, alongside the return of climatic stability and floral diversity, particularly within the mid-level vegetation (McElwain et al., 2007; Mander et al., 2013).

A similar interval of climatic and floral upheaval is suggested during Pliensbachian-Toarcian boundary as the later Pliensbachian saw a brief transition to cooler moist climates before warmer conditions returned in the Toarcian alongside more extreme seasonality, particularly in the early part of the Toarcian (Slater et al., 2019; Mander and McElwain, 2019; Pol et al., 2020; Ruebsam and Schwark, 2021). The Pliensbachian-Toarcian climatic shift saw a corresponding turnover in conifers and from seed fern to cycads with further floral turnovers in the prevailing vegetation occurring later in the Toarcian (Slater et al., 2019). There are potential signs of an ecologically expansive (Fig. 2.1.7a) and rapid archosaur radiation comparable to that of the Anisian in the Toarcian, as evolutionary rates show a marked increase (Fig. 2.1.10a). Furthermore, there is notable morphospace expansion in the Pliensbachian and again in the Toarcian, although this is largely driven by crocodylomorph

diversification within aquatic niches and improved sampling of pterosaurs. Poor sampling and edge effects precludes detailed interpretation of this increase in morphological diversity, but recent studies encompassing the Early-Middle Jurassic transition show a marked diversification of theropod (Rauhut and Pol, 2019) and sauropod (Pol et al., 2020) dinosaurs, supporting a real radiation at the Pliensbachian-Toarcian boundary. Indeed, there is a transition from prosauropod to sauropod dominance across the Early-Middle Jurassic transition (Pol et al., 2020) echoing the earlier turnover in terrestrial herbivores in the Upper Carnian and potentially supporting wider environmental and floral changes as a prime driver of macroevolution during this interval (Bonaparte, 1982; Benton, 1983; Pol et al. 2020).

Archosauromorph trophic dynamics during the recovery from mass extinction. Extinction events drive large biotic turnovers as the magnitudes of these events dictate the extent of ecological opportunity in their aftermath, as the greater the biotic devastation, the greater the collapse of ecosystems and removal of related competitive constraints, allowing the diversification of different clades and thereby driving biotic turnovers. The PTE and THE are two of the biggest mass extinction events in Earth history and are similar in terms of the post-extinction ecological opportunities they provided. Both were driven by large-scale volcanism, the Siberian Traps flood basalt (Renne et al., 1995; Saunders and Reichow, 2009; Burgess et al., 2017) and Central Atlantic Magmatic Province (CAMP) eruptions (Hesselbo et al., 2002; Ruhl et al., 2011; Tegner et al., 2020), respectively (Fig. 2.1.7b). Both devastated global faunas, hugely opening up ecospace for survivors to exploit (Benton, 1983; 1987), and both saw archosauromorph radiations in their aftermath (Fig. 2.1.7a). Archosauromorphs were presumably severely affected by the PTE alongside other terrestrial tetrapod clades (Benton and Newell, 2014; Lungmus and Angielczyk, 2019; MacDougall et al., 2019). However, their poor Permian fossil record (Martinelli et al., 2017) precludes direct comparison of archosauromorph mandibular disparity change through the PTE and TJE. Through the TJE, overall MO is reduced but remains largely consistent with its pre-TJE distribution, with the major change being the relative redistribution of MO between clades within the bounds of existing MO; dinosaurs expanded their MO and became a greater proportion of overall archosauromorph diversity (Fig. 2.1.7a). Looking at the Olenekian and Sinemurian, it appears that after each extinction event there was some small morphospace expansion followed by lineage diversification within the existing bounds of morphospace to produce stronger taxon clustering. However, there are noticeable differences in MO (Fig. 2.1.7) and rates of evolution (Fig. 2.1.10a) in the 10 million years after each extinction event that point to divergent patterns of recovery. By the Ladinian, archosauromorph MO encompassed much greater morphological variation compared to immediately following the PTE,

whereas Pliensbachian is still rather similar, (if somewhat reduced) to Hettangian MO (Fig. 2.1.7a). The radiation of dinosaurs following the TJE is largely derived by lineage diversification over broad morpho-functional radiation, with the only significant expansion of dinosaur morphospace being driven by the ornithischians entering more specialised herbivorous morphologies (Figs. 2.1.4, 7a). Rates of evolution help to clarify these changes by showing much higher rates of mandibular shape and functional evolution following the PTE than the TJE (Fig. 2.1.10a). Consequently, there was greater mandibular form and functional experimentation in the 10 million years following the PTE compared to the TJE.

Divergent patterns of recovery may reflect the 'base' levels of morpho-functional diversity prior to these extinction events. The strong increases in disparity and evolutionary rates in the Anisian (Figs. 2.1.7-9) epitomise a broad adaptive radiation, with archosauromorphs radiating into new specialised herbivorous and piscivorous niches, quite different from the generalised faunivory of earlier archosauromorphs. On the other hand, the Early Jurassic dinosaur radiation began from a much wider base as theropods (and sauropodomorphs to a lesser extent) appear to have undergone ecological diversification without intensive speciation in the Upper Norian, prior to the TJE (Figs. 2.1.7a, 9). As such, there was less need for substantial mandibular evolution than in the Early to Middle Triassic to exploit newly available niches across faunivorous and herbivorous guilds as such morpho-functionality already existed. Additionally, dinosaurian mandibular morphologies were conservative, and overall, quite utilitarian (Figs. 2.1.3-4), further supporting them in their ability to pursue more generalist ecologies, which, combined with the removal of competitive constraints during the TJE, enabled sauropodomorph lineage diversification in the Early Jurassic (Fig. 2.1.7a). This is illustrated in the nature of the Early Jurassic dinosaur diversification with low mandibular disparity, which represents the duplication of existing ecomorphologies, with only modest mandibular modifications (Figs. 2.1.7-8). The lack of comparable competitors in the Early Jurassic, unlike in the Early Triassic (Benton and Newell, 2014), and thus a source of strong selective pressures on dinosaur evolution, likely acted on the hierarchical nature of morphological evolution (Slater and Friscia, 2019) by concentrating adaptive evolution within more plastic areas of anatomy such as the dentition (Karagic et al., 2020), minimising the signal of dinosaur ecological diversification in this study. I find relatively slower mandibular evolutionary rates in Early Jurassic dinosaurs (Figs. 2.1.9-10), but other studies report increased dental complexity in sauropodomorphs (Galton, 1985) and ornithischians (Porro et al., 2010) during this interval, supporting the assumption that dental evolution may best capture the ecomorphological signal of the Early Jurassic dinosaur ecological radiation. Presuming a similar pattern of recovery in the Early Jurassic as in the Early Triassic, more extensive mandibular modification would have followed as stable climates and resources returned,

restoring 'normal' ecological dynamics and strong selective pressures. The slow shift in ornithischian MO through the Early Jurassic into morphospace previously held by rhynchosaurs and aetosaurs may reflect this process (**Fig. 2.1.7a**). Body size differences would also likely have played a key role in stratifying these dinosaur-dominated ecosystems, given the close phylogenetic relatedness and ecomorphological similarity of taxa in these Early Jurassic faunas (Mallon et al., 2013; Benson et al., 2014).

Diversification dynamics and drivers of early Mesozoic archosauromorph macroevolution.
Differences in ecomorphology across the Archosauromorpha reveal interesting patterns that may shed light on the overall drivers of archosauromorph macroevolution during the early Mesozoic. Rising mandibular disparity in the Archosauromorpha from the onset of the Induan reflects the development of more complex trophic networks through the Early - Middle Triassic (Fig. 2.1.8), with an increasingly diverse array of small herbivorous and mesocarnivorous basal archosauromorphs supporting larger non-archosaur archosauriform and pseudosuchian hypercarnivores. The Middle – Late Triassic transition saw pseudosuchians and dinosauromorphs become increasingly prevalent and diverse, with their evolution concentrated within different trophic niches. The CPE marked a major boost to the archosaur takeover of terrestrial ecosystems with dinosaur and pseudosuchian entry into the herbivore guild and the decline of remaining NAAs (Fig. 2.1.7). Dinosaurs overtook pseudosuchians in two-steps across the latest Triassic and Early Jurassic, becoming the predominant carnivores and then herbivores following pseudosuchian declines within those guilds. The loss of most pseudosuchians in the TJE saw dinosaurs radiate, developing morphologies similar to those see in prior archosauromorphs. However, archosaur convergent evolution was not limited to dinosaurs, with surviving crocodylomorph pseudosuchians replicating the longirostrine morphologies of earlier archosauriforms in the Norian and phytosaurs towards the end of the Early Jurassic.

The timings and scope of the archosauromorph radiations following the PTE and TJE illustrate that environmental stability (Preto et al., 2010) and increasing ecological complexity in the terrestrial and marine realms (Benton et al., 2004; 2013; Wei et al., 2015) are integrally linked, with the abundance and diversity of resources supporting trophic specialisation as represented by growing mandibular MO (Figs. 2.1.7-8) upon the reestablishment of climatic stability. Changes in resources, particularly in the flora (Kustatscher et al., 2018; McElwain et al., 2007) were the likely stimulus of the archosaur radiation across the herbivore guild in the Carnian (Figs. 2.1.4-7a).

The archosauromorph radiations following the PTE and TJE highlight how the adaptive capacity of a clade and the survivor community composition can shape clade diversification dynamics; the relatively unspecialised morpho-functionalities of archosauromorphs in the Early

Triassic and dinosaurs through the Late Triassic – Early Jurassic likely supporting their radiations in the aftermath of mass extinction (Figs. 2.1.3-4, 7a) in a 'generalist bonanza'. The inherent level of ecomorphological specialisation acts in conjunction with the presence/absence of comparable competitors to control the magnitude of ensuing trait evolution, with greater specialisation and morpho-functional diversity in Triassic archosauromorphs likely driven by a scramble for resources/ecospace by contemporaneous parareptiles and synapsids. The lack of such comparable competitors for Early Jurassic dinosaurs produced less impetus for greater niche specialisation and thus less mandibular morpho-functional modification.

Whilst I highlight intrinsic factors such as adaptability and competitive constraints, I also find little evidence of active competitive replacement, with the only potential scenario of such being between carnivorous non-archosaur archosuriforms and pseudosuchians in the Middle Triassic. The rise of the dinosaurs, long discussed as a potential example of active competitive replacement (Charig, 1984), likely occurred via a passive model of replacement, with the prior loss of pseudosuchians as well as other terrestrial tetrapod taxa (Sues and Fraser, 2010) being necessary for further dinosaurian trophic diversification (Fig. 2.1.7a). Inverse patterns of pseudosuchian and dinosaur ecological diversity highlights how the ecological relationships between contemporaneous taxa can shape macroevolution. Nonetheless, my findings also suggest that further investigation is required, focusing on postcranial morphology. Morphological diversification is exemplified within mandibular morphology in basal archosauromorphs, but I find relatively greater experimentation with size in archosauriforms (Figs. 2.1.4, 9b). The archosauriform tendency to modify size may also relate to wider changes in locomotion (Ezcurra and Butler, 2018). As such, findings here of divergence of diversification dynamics in the archosauromorph radiations of the Middle Triassic and Early Jurassic may relate to this increasing focus on postcranial modification through archosauriform evolution. Indeed, examining these changes alongside dietary ecology may further clarify how ecology shaped the macroevolution of the Archosauromorpha through the early Mesozoic.

Supplementary Materials:

Supplementary Figures:

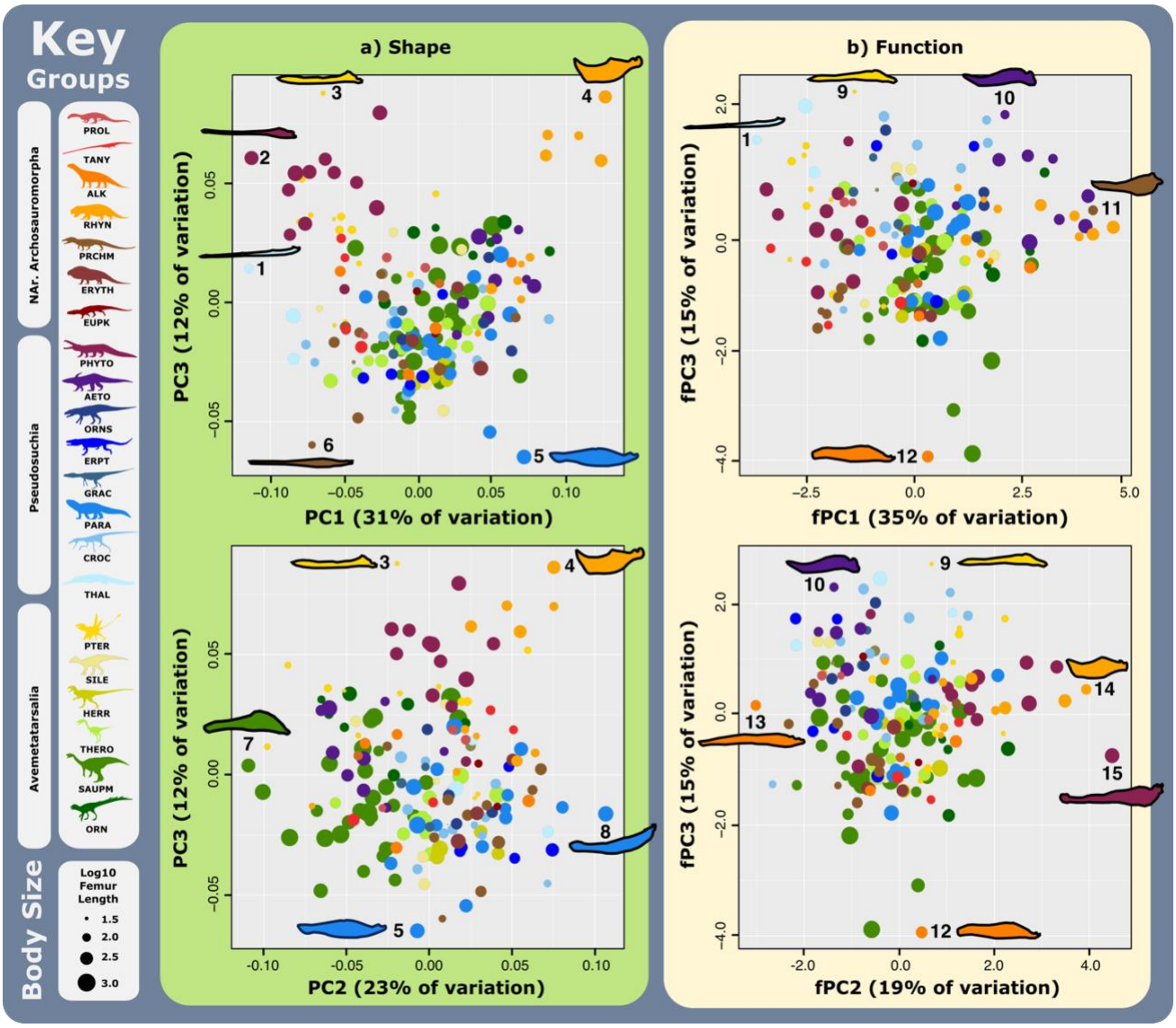

Supplementary Figure 2.1.S1. Secondary shape and functional morphospace for early Mesozoic archosauromorphs. Taxon size (log_{10} femur length) indicated by point size. Grey shaded area represents overall archosauromorph morphospace occupation. Abbreviations: AETO, Aetosauria. ALK, Allokotosauria. APH, Aphanosauria. CROC, Crocodylomorpha. ERPT, Erpetosuchidae. ERYTH, Erythrosuchidae. EUPK, Euparkeriidae. GRAC, Gracilisuchidae. HERR, Herrerasauridae. NAr, Non-archosaur. ORN, Ornithischia. ORNS, Ornithosuchidae. PARA, Paracrocodylomorpha. PC, Principal component. PHYTO, Phytosauria. PRCHM,

Proterochampsia. PROL, Prolacertidae. PTER, Pterosauria. RHYN, Rhynchosauria. SAUPM, Sauropodomorpha. SILE, Silesauridae. TANY, Tanystropheidae. THAL, Thalattosuchia. THERO, Theropoda. Taxa: 1. *Pelagosaurus typus*. 2. *Mystriosuchus planirostris*. 3. Carniadactylus rosenfeldi. 4. *Hyperodapedon huxleyi*. 5. *Effigia okeeffeae*. 6. *Chanaresuchus bonapartei*. 7. *Sarahsaurus aurifontanalis*. 8. *Batrachotomus kupferzellensis 9. Bergamodactylus wildi.* 10. *Aetosaurus ferratus*. 11. *Vancleavea campi*. 12. *Azendohsaurus madagaskarensis*. 13. *Teraterpeton hrynewichorum*. 14. *Hyperodapedon sanjuanensis*. 15. *Machaeroprosopus gregorii*.

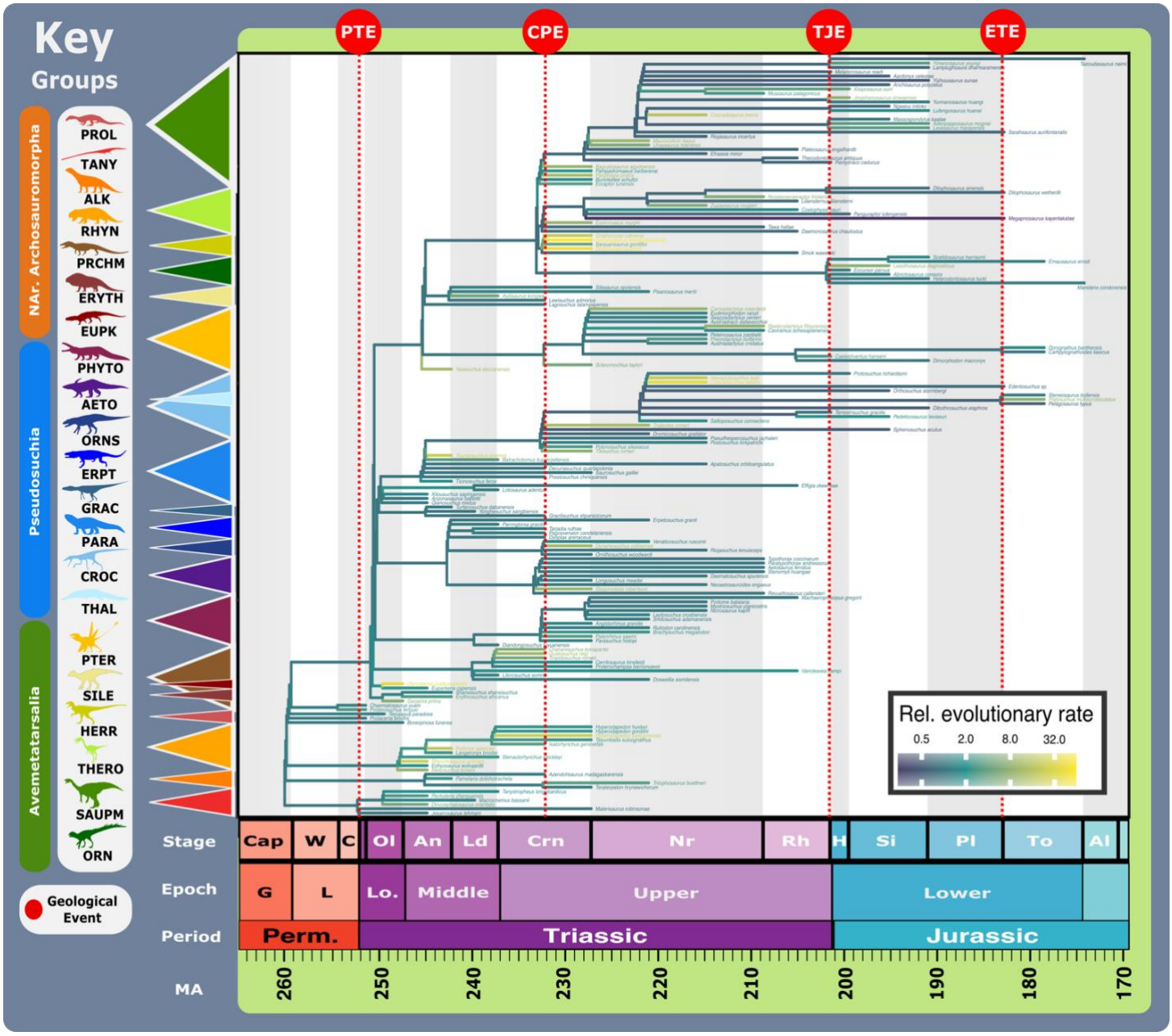

Supplementary Figure 2.1.S2. Rates of mandibular shape evolution across early Mesozoic archosauromorphs. Rates of mandibular shape evolution across the Archosauromorpha. Major extrinsic, environmental events are shown by the dashed red line. Abbreviations: AETO, Aetosauria. Al, Aalenian. ALK, Allokotosauria. An, Anisian. C, Changhsingian. Cap, Capitanian. CPE, Carnian Pluvial Event. Crn, Carnian. CROC, Crocodylomorpha. ERPT, Erpetosuchidae. ERYTH, Erythrosuchidae. ETE, Early Toarcian event. EUPK, Euparkeriidae. G, Guadalupian. GRAC, Gracilisuchidae. H, Hettangian. HERR, Herrerasauridae. IND, Induan. LAD, Ladinian. L, Lopingian. Lo, Lower. NAr, Non-archosaur. Nr, Norian. Ol, Olenekian. ORN, Ornithischia. ORNS, Ornithosuchidae. PARA, Paracrocodylomorpha. PC, Principal component. PHYTO, Phytosauria. Pl, Pliensbachian. PRCHM, Proterochampsia. PROL, Prolacertidae. PTER, Pterosauria. PTE, Permo-Triassic extinction. Rh, Rhaetian. RHYN, Rhynchosauria. SAUPM, Sauropodomorpha. SILE, Silesauridae. Si, Sinemurian. TANY, Tanystropheidae. THAL, Thalattosuchia. THERO, Theropoda. TJE, Triassic-Jurassic extinction. To, Toarcian. U. CRN, Upper Carnian. U. NOR, Upper Norian. W, Wuchiapingian.

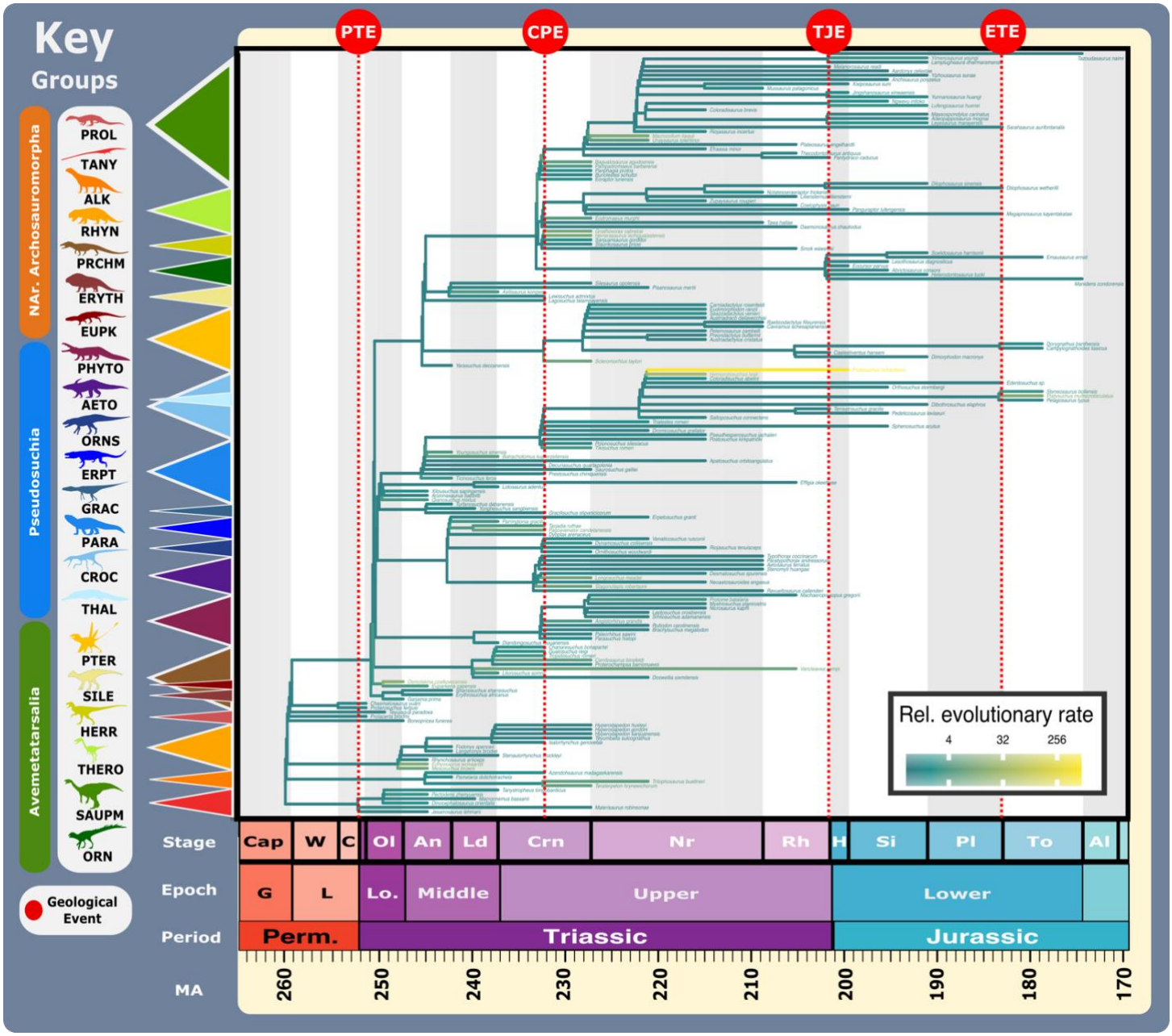

Supplementary Figure 2.1.S3. Rates of mandibular functional evolution across early Mesozoic archosauromorphs. Rates of mandibular functional evolution across the Archosauromorpha. Major extrinsic, environmental events are shown by the dashed red line. Abbreviations: AETO, Aetosauria. Al, Aalenian. ALK, Allokotosauria. An, Anisian. C, Changhsingian. Cap, Capitanian. CPE, Carnian Pluvial Event. Crn, Carnian. CROC, Crocodylomorpha. ERPT, Erpetosuchidae. ERYTH, Erythrosuchidae. ETE, Early Toarcian event. EUPK, Euparkeriidae. G, Guadalupian. GRAC, Gracilisuchidae. H, Hettangian. HERR, Herrerasauridae. IND, Induan. LAD, Ladinian. L, Lopingian. Lo, Lower. NAr, Non-archosaur. Nr, Norian. Ol, Olenekian. ORN, Ornithischia. ORNS, Ornithosuchidae. PARA,

Paracrocodylomorpha. PC, Principal component. PHYTO, Phytosauria. Pl, Pliensbachian. PRCHM, Proterochampsia. PROL, Prolacertidae. PTER, Pterosauria. PTE, Permo-Triassic extinction. Rh, Rhaetian. RHYN, Rhynchosauria. SAUPM, Sauropodomorpha. SILE, Silesauridae. Si, Sinemurian. TANY, Tanystropheidae. THAL, Thalattosuchia. THERO, Theropoda. TJE, Triassic-Jurassic extinction. To, Toarcian. U. CRN, Upper Carnian. U. NOR, Upper Norian. W, Wuchiapingian.

Supplementary Tables:

Supplementary Table 2.1.1. Archosauromorph shape and functional phylogenetic disparity at stage level. Minimum and maximum bounds for 95% confidence intervals included. Abbreviations: Max, Maximum. Min, Minimum. SOV, Sum of Variance.

Age (Ma)	Shape			Function		
	SOV	Min	Max	SOV	Min	Max
	Archosauromorpha					
251.9	0.0029472	0.00169231	0.00408318	2.159815	1.380262	2.908646
246.9	0.00361878	0.0027206	0.00452965	3.598567	2.632836	4.590497
241.9	0.00284852	0.00193679	0.00386448	2.790335	2.016343	3.572129
236.9	0.00508865	0.00334611	0.00685381	6.37602	4.407223	8.415099
231.9	0.00518188	0.00404073	0.00644672	6.373699	4.855031	8.006133
226.9	0.00496753	0.00405389	0.00581959	6.090414	4.808338	7.616343
221.9	0.00525982	0.00425905	0.00627496	6.664346	5.289085	8.218838
216.9	0.00534918	0.0043738	0.0063594	6.612566	4.978542	8.313922
211.9	0.00471416	0.00342288	0.00606376	6.321037	4.48832	8.462097
206.9	0.00513013	0.00365879	0.00674754	6.150133	3.914212	8.604163
201.9	0.00643448	0.0048646	0.0080805	7.617841	5.475535	10.205653
196.9	0.00468177	0.00352583	0.00593097	5.909612	4.252776	7.557883
191.9	0.00515789	0.0039672	0.00649238	6.674132	4.878975	8.412218
186.9	0.00786909	0.00521127	0.0104866	8.903483	5.865583	12.112305
181.9	0.00752679	0.0035556	0.01061893	7.471585	3.192438	11.600784
176.9	0.0087678	0.00441814	0.01161474	9.130601	3.99639	13.366732
174.1	0.00885701	0.00454907	0.01178143	9.214396	4.316107	13.534736
	Non-Archosaur Archosauromorpha					
251.9	0.00293773	0.00161997	0.00405931	2.147223	1.331882	2.994011
246.9	0.00457095	0.00345154	0.00565794	4.544324	3.156696	6.010706
241.9	0.00395624	0.00154743	0.0057446	3.018226	1.462209	4.453498
236.9	0.00748132	0.00419825	0.00991074	8.999861	5.197375	11.355778

231.9	0.00946092	0.00527029	0.01294691	11.776663	7.471264	15.610944
226.9	0.00572943	0.00218514	0.00792495	8.996204	2.854792	14.925793
221.9	0.00621113	0	0.00943443	8.417978	0	12.458101
216.9	0.0041768	0	0.0080323	5.353448	0	11.488086
211.9	NA	NA	NA	NA	NA	NA
206.9	NA	NA	NA	NA	NA	NA
201.9	0.00577157	0	0.02020718	10.360956	0	39.33672
196.9	NA	NA	NA	NA	NA	NA
191.9	NA	NA	NA	NA	NA	NA
186.9	NA	NA	NA	NA	NA	NA
181.9	NA	NA	NA	NA	NA	NA
176.9	NA	NA	NA	NA	NA	NA
174.1	NA	NA	NA	NA	NA	NA
	Pseudosuchia					
251.9	NA	NA	NA	NA	NA	NA
246.9	0.00097846	0.0005197	0.00141076	1.668779	0.8414876	2.53855
241.9	0.00245668	0.00125453	0.00370312	2.583156	1.5577414	3.627074
236.9	0.00254643	0.00149196	0.00353303	2.940508	1.8682995	3.987586
231.9	0.00477984	0.00377046	0.00571432	5.342476	3.7944584	7.008388
226.9	0.00590949	0.00482046	0.00692077	7.435903	5.6852574	9.32821
221.9	0.00618748	0.00504952	0.00728094	8.023859	6.2126505	10.03354
216.9	0.00644937	0.0049468	0.00782324	8.264574	5.502485	10.828745
211.9	0.0049155	0.00286589	0.00700719	7.568866	4.3379272	11.454981
206.9	0.00429566	0.00162715	0.006952	6.681619	2.4309516	10.692185
201.9	0.0064382	0.00346163	0.0091608	8.795151	4.9991981	12.571734
196.9	0.00497306	0.00165503	0.00924081	6.476233	2.2954923	10.754188
191.9	0.00488104	0.00161867	0.00881784	6.523933	2.3255378	10.754123
186.9	0.0091753	0	0.01956354	8.136314	0	16.370853
181.9	0.00107254	0.00021094	0.00209344	2.37769	0.3048407	4.820084
176.9	0.00174822	0	0.00238891	3.949439	0	6.304805
174.1	0.00173881	0	0.00238891	3.873731	0	6.304805
	Avemetatarsalia					
251.9	NA	NA	NA	NA	NA	NA
246.9	0.00550708	0.00086417	0.01347438	6.255586	1.17600072	16.009471
241.9	0.00032592	5.4304E-05	0.00064184	0.386324	0.02676979	0.8005438
236.9	0.00136165	0.00057558	0.0019061	2.121432	0.96092775	2.7130049
231.9	0.00183014	0.00107627	0.00263309	2.857531	1.55633921	4.4006205
226.9	0.00231052	0.00141975	0.00337247	2.935999	1.92731725	4.0252513
221.9	0.00219669	0.0013842	0.00310679	2.662747	1.75649593	3.7224741
216.9	0.00335646	0.00234627	0.00446354	3.534408	2.36707162	4.7741942

211.9	0.00361175	0.00244511	0.00492162	4.197002	2.66033644	5.8197508
206.9	0.00409497	0.00242702	0.00605391	4.11147	2.48096188	5.94601
201.9	0.00483878	0.00319788	0.0066414	4.954172	3.19255896	6.659633
196.9	0.00380294	0.00273265	0.00494012	4.989049	3.35102023	6.8322334
191.9	0.00416983	0.00311267	0.00519269	5.734672	3.93713022	7.5497552
186.9	0.00681685	0.00419581	0.00912221	7.836698	4.19320315	11.6474059
181.9	0.00706761	0.00237716	0.01014321	7.183655	2.10673423	11.3711896
176.9	0.00745976	0.00303073	0.01079555	7.527199	2.47474831	12.153285
174.1	0.00748466	0.00321384	0.01050925	7.608653	3.28198017	11.5096182

Supplementary Table 2.1.2. NPMANOVA results for overall archosauromorph shape and functional disparity changes through stages. Abbreviations: L., Lower. M., Middle. Max, Maximum. Min, Minimum. Sq, Squares. U., Upper.

Stage	Timebin (Ma)	Sum of Sq.	Mean Sq.	F Model	R^2	P
	Shape					
Induan	t251.9to251.2	0.00701	0.007009	1.0628	0.00566	0.332
Olenekian	t251.2to247.2	0.00995	0.009949	1.5084	0.00804	0.155
Anisian	t247.2to242	0.0195	0.019499	2.9564	0.01575	0.019
Ladinian	t242to237	0.01307	0.013069	1.9815	0.01056	0.067
L_Carnian	t237to232	0.01607	0.016065	2.4358	0.01297	0.028
U_Carnian	t232to227	0.01323	0.013231	2.006	0.01069	0.057
L_Norian	t227to220.83	0.00912	0.00912	1.3827	0.00737	0.178
M_Norian	t220.83to214.67	0.0115	0.011502	1.744	0.00929	0.111
U_Norian	t214.67to208.5	0.00786	0.007864	1.1923	0.00635	0.27
Rhaetian	t208.5to201.3	0.01563	0.015633	2.3703	0.01263	0.026
Hettangian	t201.3to199.3	0.00677	0.006772	1.0267	0.00547	0.382
Sinemurian	t199.3to190.8	0.03206	0.032061	4.861	0.02589	0.001
Pliensbachian	t190.8to182.7	0.00499	0.004994	0.7571	0.00403	0.564
Toarcian	t182.7to174.1	0.00952	0.009523	1.4438	0.00769	0.149
	Residuals	1.06188	0.006596	0.85762		
Overall	Total	1.23817	1			
Stage	**Function**					
Induan	t251.9to251.2	5.48	5.483	0.7062	0.00389	0.612
Olenekian	t251.2to247.2	10.69	10.692	1.3771	0.00759	0.235
Anisian	t247.2to242	4.43	4.432	0.5708	0.00315	0.724
Ladinian	t242to237	15.95	15.945	2.0536	0.01132	0.076
L_Carnian	t237to232	7.66	7.66	0.9866	0.00544	0.395
U_Carnian	t232to227	16.68	16.677	2.1478	0.01184	0.06
L_Norian	t227to220.83	9.51	9.509	1.2247	0.00675	0.285

M_Norian	t220.83to214.67	2.92	2.917	0.3757	0.00207	0.882
U_Norian	t214.67to208.5	8.08	8.083	1.041	0.00574	0.391
Rhaetian	t208.5to201.3	17.83	17.832	2.2967	0.01267	0.051
Hettangian	t201.3to199.3	11.57	11.568	1.4899	0.00822	0.169
Sinemurian	t199.3to190.8	34.56	34.562	4.4514	0.02455	0.003
Pliensbachian	t190.8to182.7	4.2	4.205	0.5415	0.00299	0.768
Toarcian	t182.7to174.1	8.37	8.37	1.0779	0.00594	0.356
	Residuals	1250.06	7.764	0.88783		
Overall	Total	1408	1			

Supplementary Table 2.1.3. Support for different macroevolutionary models of mandibular functional disparity evolution. Weighted Aikake Information Criterion and log-likelihood values for each model. Abbreviations: BIA, Biarmosuchia. BM, Brownian motion. BSL SYN, Basal-most synapsids. CYN, Cynodontia. DIN, Dinocephalia. EB, Early Burst. GRG, Gorgonopsia, Log. Lik, Log likelihood. OU, Ornstein-Uhlenbeck. SPH, (Non-therapsid) Sphenacodontia. THR, Therocephalia. W. AIC, Weighted Aikake Information Criterion.

Models			**BM**	**EB**	**OU**	**Stasis**	**Trend**
Shape	**Total ArchM**	**W. AIC**	0.426	0.001	0.019	0.449	0.106
		Log. Lik.	65.55	60.92	65.65	65.60	65.65
	Bsl. ArchM	**W. AIC**	0.483	0	0	0.484	0.033
		Log. Lik.	23.93	19.29	24.03	23.93	24.04
	Psd	**W. AIC**	0.397	0.088	0.016	0.412	0.088
		Log. Lik.	52.83	52.87	52.96	52.87	52.86
	Avm	**W. AIC**	0.381	0.080	0.018	0.393	0.128
		Log. Lik.	52.65	52.68	53.11	52.68	53.15
Function	**Total ArchM**	**W. AIC**	0.355	0	0.152	0	0.492
		Log. Lik.	-28.7	-71.4	-26.3	-37.8	-26.9
	Bsl. ArchM	**W. AIC**	0.869	0	0.003	0.006	0.122
		Log. Lik.	-17.6	-79.4	-15.8	-22.5	-16.8
	Psd	**W. AIC**	0.037	0	0.136	0.818	0.008
		Log. Lik.	-45	-229	-41	-42	-45
	Avm	**W. AIC**	0.030	0	0.127	0	0.843
		Log. Lik.	-23.7	-60.7	-18.7	-36.3	-18.8

Supplementary Table 2.1.4. Clade-wise differences in mandibular shape and functional disparity. Resulting differences in disparity from Wang's permutational analysis (Brusatte et al, 2014). Abbreviations: Avm, Avemetatarsalia. Bsl ArchM, Basal (Non-Archosaur) Archosauromorpha. EXP, Expected difference. OB, Observed differences. Psd, Pseudosuchia.

Groups		**Bsl. ArchM**			**Psd**		
		EXP	**OB**	**P**	**EXP**	**OB**	**P**
Shape	**Psd**	0.000008	0.001	0.49			
	Avm	0.00002	0.002	0.108	0.000004	-0.001	0.27
Function	**Psd**	0.062472	1.29	0.284			
	Avm	0.001518	3.18	0.004	0.001176	-1.885	0.006

Supplementary Table 2.1.5. Clade-wise differences in mandibular functional characters. Statistical differences in functional characters as determined by Mann-Whitney U pairwise comparisons. Abbreviations: Avm, Avemetatarsalia. Bonf. Bonferroni corrected. Bsl ArchM, Basal (Non-Archosaur) Archosauromorpha. MAMA, Mean anterior mechanical advantage. MPMA, Mean posterior mechanical advantage. OMA, Opening mechanical advantage. Psd, Pseudosuchia. RAO, Relative articulation offset. RMAR, Relative maximum aspect ratio. RSL, Relative symphyseal length. RTL, Relative toothrow length. SA, Symphyseal angle.

Functional Characters		Bsl. ArchM - Psd	Bsl. ArchM -AvM	Psd - AvM
	P	0.3677	0.3628	0.8444
	Bonf. P	1	1	1
MAMA	U	1115	1274	2290
MPMA	P	0.9919	0.3628	0.3285

	Bonf. P	1	1	0.9855
	U	1246	1274	2109
	P	0.6125	0.9756	0.5444
	Bonf. P	1	1	1
OMA	U	1173	1418	2195
	P	0.1466	0.2337	0.6646
	Bonf. P	0.4398	0.701	1
RMAR	U	1034	1228	2235
	P	0.4443	0.7928	0.1919
	Bonf. P	1	1	0.5756
RTL	U	1135	1380	2033
	P	0.2605	0.8642	**0.03818**
	Bonf. P	0.7814	1	0.1145
RSL	U	1082	1395	1855
	P	**0.00**	0.1394	**0.002239**
	Bonf. P	**0.00004**	0.4182	**0.006716**
SA	U	607	1181	1627
	P	0.1429	**0.025**	**0.000131**
	Bonf. P	0.4286	0.075	0.**0003931**
RAO	U	1032	1056	1449

Chapter 3 - Guild Evolution through the Permian – Early Jurassic

3.1. Establishment of the carnivore guild: the rise of synapsid carnivores through the late Palaeozoic.

Authors: Suresh Singh, Armin Elsler, Tom Stubbs, Emily Rayfield, and Mike Benton.

Chapter Contributions and Acknowledgements

I designed the study, collected the morphological data, and conducted all the analyses and wrote the chapter. A.E. provided the phylogeny, chronostratigraphic and femur length data and helped with image collection. T.S., E.R. and M.J.B. provided guidance and comments on the chapter. My contributions represent 95% of the material in this chapter.

I thank Christine Janis for providing literature and constructive commentary. All silhouettes were created by me.

Abstract

Non-mammalian synapsids established themselves as the foremost terrestrial predators through the late Palaeozoic despite successive extinction events, acting as apex predators in rich ecological communities by the latest Permian. Given their close phylogenetic relatedness, competition was presumably a strong pressure on the evolution of carnivorous synapsids, shaping their ecologies as they sought to minimise competitive constraints, much like extant mammalian predators in diverse carnivore communities. Nonetheless, the influence of competitive pressures through deep time remains unclear, especially as ecosystems have changed dramatically through the Phanerozoic. Using morphometric and phylogenetic comparative methods, I track synapsid carnivore ecomorphology and evolution through the formation of the first complex, terrestrial tetrapod ecosystems during the latest Carboniferous and Permian (307-251.9 Ma). I identify several functional feeding groups and trends indicative of niche partitioning, with diversification patterns showing coupled pulses of size and feeding ecomorphology differentiation, highlighting the rapid development of complex trophic networks in the late Palaeozoic.

Introduction

Ecological interactions between species are key selective pressures that can drive behavioural shifts that ultimately promote phenotypic change (Brown and Wilson, 1956; Van Valen, 1973; Schluter, 1994; Pigot et al., 2016; Yuan et al., 2020). Such interactions are perhaps most apparent between coexisting large carnivores; mammalian predators in African savannah communities can modify their hunting behaviours to reduce interspecific competition (Durant, 2000; Linnell and Strand, 2000; Fedriani et al., 2000; Caro and Stoner, 2003; Périquet and Revilla, 2015). Given the fact that the material properties of flesh and bone have presumably remained constant through geological time, competition is thought to have been a primary driver of large carnivore diversification, with resultant resource partitioning repeatedly producing shearing and crushing ecomorphs through mammalian evolutionary history (Van Valkenburgh and Wayne, 2010; Goswami and Friscia, 2010; Silvestro et al., 2015; Pires et al., 2015). Furthermore, competition has been implicated in multiple turnovers within Cenozoic carnivore faunas, with newly evolving (or arriving) predators outcompeting incumbent forms and driving them to extinction (Savage, 1977; Van Valkenburgh, 1999; Friscia and Van Valkenburgh, 2010; Wang et al., 2008). Studies of such ecosystems over the past 66 Myr provide outcomes I can comprehend in terms of modern ecosystems, but what about much older predators? Competitive influences on the macroevolution of predators through most of the Phanerozoic remain poorly understood (Hautmann, 2020). Here, I explore some of the earliest terrestrial ecosystems, seeking to understand whether they share aspects of competitive dynamics seen in extant ecosystems and how such dynamics influenced carnivore macroevolution.

In the terrestrial realm, diverse tetrapod ecosystems emerged during the Carboniferous (358.9–298.9 Ma) and developed greater complexity through the Permian (298.9–251.9 Ma), with late Permian faunas hosting trophic networks of various specialised herbivores and carnivores (Olson, 1962; Benton et al., 2004; Sahney and Benton, 2008; Sahney et al., 2010; Dunne et al., 2018). Throughout the Late Palaeozoic, synapsids dominated the carnivore guild (Romer and Price., 1940; Kemp, 2005; Benton, 2014). Basal, 'pelycosaur-grade' synapsids quickly assumed predatory roles within the earliest terrestrial amniote communities in the Late Carboniferous (Kemp, 1982), with sphenacodontian pelycosaurs becoming the predominant large terrestrial carnivores of the Early Permian (Romer and Price., 1940; Kemp, 2005). Despite a series of extinction events (Benton, 2014), synapsids maintained and monopolised large carnivore niches through the Middle and Late Permian, with diversifications of basal therapsids (biarmosuchians and dinocephalians) in the Guadalupian, followed by gorgonopsians and therocephalians in the Lopingian (Kemp 1982; 2005). Synapsid monopolisation of the terrestrial carnivore guild offers an interesting opportunity to study guild dynamics during the foundation of terrestrial ecosystems (DiMichele et al., 1992; Hautmann, 2020),

and the potential macroevolutionary impacts of competitive pressures during the Palaeozoic, which is comparatively unexplored when compared to key Mesozoic and Cenozoic radiations, such as that of the dinosaurs in the Jurassic (Benton, 1984; Brusatte et al., 2008; Langer et al., 2010) and mammals in the Palaeogene (Meredith et al., 2011; Halliday and Goswami, 2015; Grossnickle and Newham, 2016).

Ecological similarity among multiple, closely related, sympatric lineages should theoretically generate strong intrinsic selective pressures (Darwin, 1859; Pyron et al., 2015). Consequently, strong intraguild competition would have been a powerful selective pressure on the trophic ecology of synapsid carnivores as coexisting taxa in successive faunas through the late Palaeozoic sought to maximise feeding efficiency by minimising competitive constraints (Slater and Friscia, 2019). Long-term ecological divergence drives morphological evolution and so may capture these intrinsic pressures in the disparity of synapsid functional morphology. Using morphometric and macroevolutionary analytical methods, I detail the functional aspects of food ingestion and prey capture by carnivorous Palaeozoic synapsids to determine niche characteristics and dimensions and assess the potential for competition (Singh et al., 2021). I also incorporate patterns of body size evolution across the synapsid carnivore guild, reflecting its strong influence on mammalian carnivore ecology (Ramesh et al., 2012) to further refine estimations of competition potential. Exploring both sets of traits reveals the rapid emergence of niche partitioning in the Late Carboniferous, with differences in size and feeding functionality becoming increasingly apparent through the Permian. This confirms that the increasing diversity of synapsid carnivores was enabled by diversifying diets and feeding modes, which together contributed to rapidly expanding complexity of terrestrial ecosystems. Patterns of niche partitioning in Palaeozoic synapsid carnivores echo those of extant large mammalian carnivores, indicating remarkable continuity in guild dynamics across hundreds of millions of years, from the first emergence of such systems on Earth to the present day.

Materials and Methods

Ecomorphological inferences. Anatomy can be indicative of ecology as different parts are often adapted to specific functions, enabling inferences of the ecology of extinct organisms (Seilacher, 1970). Mandibular morphology is principally devoted to feeding (processing and ingestion) and has been used extensively to study trophic macroevolution (Slater et al., 2009; Sakamoto, 2010; Grossnickle and Polly, 2013; Stubbs et al., 2013; Maclaren et al., 2017; Grossnickle, 2020). Cranial morphology may exhibit greater modification that potentially offers more specific insights on feeding preferences, but it also serves additional neurosensory and perhaps ornamental functions

that can obscure interpretations of trophic ecology. Consequently, this study focuses on mandibular form and function.

Taxonomic sampling and data collection. A list of all valid synapsid carnivore taxa from the Late Carboniferous to Early Triassic was compiled alongside their stratigraphic ranges using the published dataset of Benton et al. (2013a), and recent literature used to integrate subsequently described taxa and taxonomic and stratigraphic revisions. Absolute age assignments were to stage level and based on the 2019 version of the International Chronostratigraphic Chart (Cohen et al., 2019). This analysis was mostly conducted at a genus level to maintain a balance between availability of data and confidence in taxon diagnosis as most genera are monospecific. Consequently, I typically used a single specimen per genus. This unfortunately discounts assessment of intraspecific variation, which would require significantly more sampling. However, I used multiple specimens per genus where multiple species were available; this may bias our morphometric analyses, but basal-most synapsids possess much greater species diversity per genus than their therapsid relatives, and I would otherwise ignore much basal synapsid diversity, particularly during their zenith in the Early Permian. The genera with multiple species are: *Dimetrodon (D. grandis, D. limbatus, D. loomisi, D. milleri,* and *D. natalis)*, *Haptodus* (*H. garnettensis* and *H. baylei*), *Ophiacodon (O. uniformis, O. mirus,* and *O. retroversus)*, *Sphenacodon* (*S. ferocior* and *S. ferox*), *Aloposaurus* (*A. gracilis and A. tenuis*), *Inostrancevia* (*I. alexandri* and *I. latifrons*), and *Sauroctonus* (*S. parringtoni* and *S. progressus*). I compiled photographs and specimen drawings from the literature alongside photographs taken during museum collection visits of complete mandibles in lateral view.

Maximum femur length was used as a measure of overall body size, as these data are widely available from published literature, enabling comprehensive study of size dynamics across taxa. Femur length was preferable to skull length as cranial morphology often does not show a fixed scaling relationship with overall size across a wide phylogenetic range (Millien and Bovy, 2010), and this is especially apparent within synapsids, when the 'pea-headed' caseids are considered (Romer and Price, 1940). The locomotory and supportive function of the limbs makes their characteristics a strong approximation of overall body size (Campione and Evans, 2020). Where femoral material did not exist, basal skull length was used if available to estimate femur length via generalized least squares (GLS) regressions, implemented in R using the nlme package (Pinheiro et al., 2017). This was carried out under three varying assumptions to account for different correlation structures using the corPagel function from the ape package (Paradis et al., 2015; Paradis and Schliep, 2019). The first two structures investigated assumed non-existent or strong phylogenetic signal, whereas the third allowed phylogenetic signal to be estimated following the approach of Benson et al. (2018). Model

fitting and parameter estimation were run using maximum likelihood and time-scaled trees, with the models evaluated using the corrected Akaike information criterion (Akaike, 1974; Sugiura, 1978; Burnham and Anderson, 2002). The data was $\log_{10}$ transformed prior to modelling. Estimation of femur length from basal skull length was necessary due to preservation biases in the synapsid fossil record; the synapsid fossil record is primarily based on cranial remains and appendicular fossils, particularly complete specimens are rare. Consequently, the limb fossil record of non-mammalian synapsids is rather poor and dominated by basal synapsids such the sphenacodontians (Lungmus and Angielczyk, 2019). Furthermore, the limb materials present often are incomplete and so ineligible for our study. This lack of data also precluded use of more accurate methods of size estimation, such as the mass estimations used by Campione and Evans., (2012; 2020), which requires calculation of the circumference of the upper limbs (femur and humerus, if quadrupedal). Nonetheless, femur length has a proven track record of use across a wide array of clades in the literature (Sookias et al., 2012; O'Gorman and Hone, 2012; Puttick et al., 2014). Additional taxa without femoral data that were discovered following the initial estimation of femur lengths were also included by using a multi-rate Brownian motion model of phylogenetic character reconstruction to impute the missing femur length data (O'Meara et al., 2006; Revell and Collar, 2009) with the mvMORPH package (Clavel et al., 2015).

This study encompasses a total of 122 taxa representing 111 genera. The sample includes two eothyridids, 12 varanopids, five ophiacodonts, 15 sphenacodonts, 14 biarmosuchians, 10 dinocephalians, 27 gorgonopsians, 28 therocephalians, and nine cynodonts. Basal dinocephalians were included alongside the anteosaurids as the diets of the basal taxa are poorly resolved and have been suggested as omnivorous (King, 1988). All fossil specimens used in this study were assessed to ensure damaged, distorted, and juvenile material were excluded where discernible/possible. I also recorded functional data from 23 extant taxa (10 reptiles, eight canids, and five felids) to better interpret non-mammalian synapsid trophic ecology.

Phylogeny. I use an informal supertree based on Brocklehurst et al. (2016), which expanded and modified character matrices used by Reisz and Fröbisch (2014), and Benson (2012). Varanopids have recently been suggested as diapsids rather than basal synapsids (Ford and Benson, 2020), marking a major potential change in the synapsid phylogeny. However, Ford and Benson (2020) stress the extreme uncertainty of this topology and highlight the need for more attention to the interrelationships of basal amniotes. Further, more recent anatomical study of varanopids supports their traditional inclusion as synapsids (Bazzana et al., 2021)., and I follow this traditional cladistic placement. Additional taxa were added to both trees using Mesquite 3.51 (Maddison and Maddison,

2018). Time-scaling was applied following the methodology of Lloyd et al. (2016) using the Hedman algorithm (Hedman, 2010).

Morphometric analyses. To clearly understand changes in trophic ecomorphology, a combination of geometric morphometric (GM) and functional morphometric (FM) methods are used, following the approach of Singh et al. (2021). By assessing mandibular form and function, I can better understand ecomorphological evolution and partially mitigate the divergent impacts of phylogenetic heritage, taxonomic scaling, or methodological choices (Anderson et al., 2011; Meloro et al., 2011; Brusatte et al., 2011; Koch et al., 2017; Schaeffer et al., 2019). The GM methods use user-defined landmarks and Cartesian coordinates to capture shape variation, whereas FM methods use standardised functional measurements (SFM) (See Supplement) that reflect clear, ecologically relevant aspects of jaw function.

Synapsid evolution encompasses significant changes in jaw anatomy, particularly through the transition from basal synapsids to therapsids (Kemp 1982), and the evolution of mammals (Lautenshlager et al., 2017). A Type I landmarking regime focusing on biologically relevant, homologous points is classically preferred for morphometric studies, but it is often impractical due to difficulties in identifying homologous points of bone articulation across a phylogenetically diverse range of taxa and poor specimen preservation. Furthermore, it could be argued that a Type I approach using landmarks based on anatomical contacts could increase the degree of phylogenetic signal in any results as the landmarking regime is inherently based on features heavily controlled by phylogeny. I adopted a Type II approach as although it may lack the capacity to clearly assess modular changes in the jaw and the mechanical evolution that may entail, the focus on overall shape provides a flexible framework capable of assessing broader patterns of trophic ecology across the wide diversity of non-mammalian synapsids and potentially in future, other tetrapod clades.

Our regime uses four fixed homologous landmarks, connected by four semi-landmarked curves comprised of a total of 55 semi-landmarks, placed equidistantly along each curve (Supplementary Fig. 3.1.S1). Images were digitally landmarked using tpsDig2 (Rohlf, 2010), and processed in tpsUtil (Rohlf, 2013) to enable semi-landmarks to slide along their respective curves during the Procrustes transformation, which was applied in tpsRelW (Rohlf, 2015). I used the chord–min d^2 sliding method that restricts semi-landmark movement along a chord between the two adjacent landmarks. The Procrustes transformation removes the effects of mandible size and orientation from the landmark data and to generate aligned coordinate data. The FM used eight functional characters using measurements taken from the mandible images (Supplementary Fig. 3.1.S2), using ImageJ

(Schneider et al., 2012). These measurements capture aspects of mandibular functionality such as areas of muscle attachment, articulation, and overall mandible shape, which have been used to characterise overall mandibular function and interpret feeding ecology (Stubbs et al., 2013; Button et al., 2014; MacLaren et al., 2017; Sakamoto et al., 2010) (See Supplementary Methods). Significant differences between clades across each functional character were identified using a pairwise Mann-Whitney U test (Supplementary Data). Overall differences in jaw shape and function between clades were assessed via one-way non-parametric analysis of variance (NPMANOVA). NPMANOVA calculates and compares centroids and surrounding spread of data for each group (timebin). The analysis was applied to the aligned landmark shape data and functional SFMD using a Euclidean similarity index to identify overlap in data distributions between timebins at epoch and stage-level. I used Bonferroni corrections to minimise Type I errors stemming from multiple comparisons.

The shape-aligned coordinate data and SFMD were subjected to separate principal component analyses (PCAs) to identify the major axes of form and functional variation, using geomorph (Adams and Otárola-Castillo, 2013) for the GM data, and FactoMineR (Le et al., 2008) for the FM data. The functional measurement data was centred and standardised using a z-transformation prior to the PCA to mitigate heteroscedasticity (Button and Zanno, 2020). Whilst alternative data standardisations can be used (Benvenuto et al., 2020), Singh et al., (2021) found that these variants produced minor differences in subsequent analyses that did not affect overall findings. The resulting first two PC axes were used to plot morphospace occupation as they reflect the greatest aspects of variation. The PC scores were also used alongside the functional character data to generate contour plots of different functions across morphospace using linear interpolations via the akima package (Akima and Gebhardt, 2016).

Calculations of disparity through time. To measure morphological diversity (disparity), I calculated within-bin sum of variance (SOV) to assess changes in shape and functional disparity through time. SOV is quite resistant to sampling biases and so provides robust temporal patterns of disparity (Butler et al., 2012). Other metrics such as sum of ranges can better account for 'morphospace packing', where strong concentrations of taxa within morphospace produce lower disparity values (Smithwick et al., 2018; Nordén et al., 2018), but these metrics are less resilient to sampling differences between timebins (Guillerme et al., 2020). I used the dispRity package (Guillerme, 2018) following a phylogenetic time-slice approach (Guillerme and Cooper, 2018) to generate SOV through time for different clades. All PC axes were used in the calculations using 1000 cycles of bootstrapping to provide 95% confidence intervals and rarefaction to minimum timebin sample size to account for differences in sampling per subset. I plotted shape and functional SOV alongside substage level,

time-slices of morphospace using the calibrate (Graffelman, 2013) and strap (Bell and Lloyd, 2014) packages. NPMANOVA with a Bonferroni correction was also used to identify significant shape and functional changes through time at stage-level using all PC scores.

Consensus cluster methods. To identify the niches of synapsid carnivores through the Palaeozoic from direct ecomorphological data, I use the consensus clustering approach of Singh et al., (2021). This method requires minimal prior input or supervision and uses different hierarchical and partition clustering algorithms (Kaufman and Rousseeuw, 2009) to produce robust, objective feeding functional groups (FFGs) (Singh et al., 2021). The distinct functional and ecological utility of the functional measurements enables clearer interpretations of likely feeding behaviour relative to shape data, which carries greater phylogenetic signal and neglects important features such as such muscle attachment positions. Therefore, the consensus cluster approach was applied to the functional data. The SFM were used to generate a Euclidean distance matrix that was subjected to hierarchical, K-means and partitioning around medioids (PAM) clustering analyses using the 'eclust' function of the FactoExtra package (Kassambara and Mundt, 2017). I used a defined cluster (K) range (3–10) (Madhulatha, 2011) using gap statistic values generated from 2000 bootstrap cycles. The results were evaluated using the 'cluster.stats' function from the fpc R package (Hennig, 2019) using silhouette metrics to illustrate clustering performance and phylogenetic signal using external validation metrics (Kaufman and Rousseeuw, 2009) (Supplementary Tables 3.1.9-10). The different cluster results were compared to generate composite groups based on classification consensus; these composite groups became our FFGs. Majority rule was used to designate the typical FFGs of clades based on the classification their taxa classified here.

A linear discriminant analysis (LDA) was used to assess the robusticity of the consensus cluster FFsG classifications (Foffa et al., 2018). The LDA was implemented with a jack-knifing test in PAST (version 3.24) (Hammer et al., 2001) using all functional PC scores, and correctly classified 86% of taxa. Classification differences typically occurred in taxa at the margins of their respective consensus cluster FFsG. (Supplementary Fig. 3.1.S7). Therefore, these taxa potentially exhibited trophic ecologies in-between the core FFsGs, highlighting the troughs in the adaptive landscape of Palaeozoic synapsid carnivores and the reality that realised niches exist within a spectrum, varying considerably depending on a range of factors such as the conspecifics present and available habitat resources (Shipley et al., 2009). An LDA was also used to classify the FFsG of ancestral taxa based on ancestral state reconstructions of functional PC scores to plot trends in FFsG body size through time (Fig. 3.1.8).

Phylogenetic methods. The functional phylogenetic disparity of different taxonomic groups was subjected to macroevolutionary modelling using the DispRity R package (Guillerme and Cooper, 2018) to test whether their disparity trends followed a Brownian Motion, Early Burst, Ornstein-Uhlenbeck/Constraint, Trend, or Stasis model of macroevolution. Resulting weighted Akaike Information Criterion (AIC) and log-likelihood values were used to assess model fit/support (Supplementary Table 3.1.11).

Ancestral states for FFsG, Functional PC scores, and body size were reconstructed for nodes across the synapsid phylogeny to better understand the ecomorphological diversification patterns of synapsid carnivores through the late Palaeozoic. Discrete FFsG character states were reconstructed using the 'ace' function of the ape R package (Paradis and Schliep, 2019) using Maximum Likelihood estimations (Barrett et al., 2015; Yang et al., 2019). Given the general uncertainty regarding niche boundaries and therapsid deviation from typical rules of mammalian carnivore specialisation (Brocklehurst, 2019), I ran trait estimations under a conservative equal rates and more derived, symmetrical rates model of character transition, which allows different rates between pairs of states (Pagel, 1994). These estimations are presented on a time-scaled phylogeny using the strap R package (Bell and Lloyd, 2014) (Fig. 3.1.5a). The log-likelihood results for the equal (-179.04) and symmetrical (-144.33) rates models showed significantly higher support for the reconstructions obtained under a symmetrical model (Supplementary Fig. 3.1.S7; Fig. 3.1.7). Estimations of ancestral functional PC scores and body sizes (the $\log_{10}$ transformed femur length) were also generated using a Maximum Likelihood approach via the 'FastAnc' function of the phytools R package (**Revell, 2012**). Resulting body size values mapped onto the phylogeny using the 'ggtree' R package (**Yu, 2020**) (Fig. 3.1.5b). The reconstructed fPC scores were used to classify the FFsG of ancestral nodes and their estimated body size was used alongside taxon body sizes to plot mean body size per FFsG through the late Palaeozoic (Fig. 3.1.9).

Results

Synapsid carnivore mandibular morphofunctional diversity. Mandibular form and function were examined using geometric morphometric landmark data (Supplementary Fig. 3.1.S1) and standardised functional measurements (SFM) (Supplementary Fig. 3.1.S2) (See Methods) to capture shape and functional variation, respectively. Both form and function are considered here, as though linked (Eble, 2004; Hetherington et al., 2015), they do not necessarily follow the same trends (Brusatte et al., 2011; Koch et al., 2017; Schaeffer et al., 2019). The landmark and SFM data were subjected to principal component analyses (PCA) to identify the primary axes of variation, which are illustrated as morphospaces constructed from the first two principal components (PCs) of each

analysis. These morphospaces represent 27.8% and 12.9% of total shape variation and 37.1.% and 23.5% of total functional variation. PC1 illustrates that mandibular form (Fig. 3.1.1a) varies most significantly through the changing depth of the symphysis and mandibular body, as well as the overall curvature of the mandibular ramus. PC2 identifies the changing prominence of a coronoid process as a further major aspect of shape variation. Mapping functional data across the shape morphospace using linear interpolations (Akima and Gebhardt, 2016) reveals marked heterogeneity in functionality across jaw shape, particularly in mean posterior mechanical advantage (MPMA), opening mechanical advantage (OMA), and symphyseal angle (SA) (Fig. 3.1.1b). Nonetheless, broad patterns are present; PC1 negatively relates to mean anterior mechanical advantage (MAMA), maximum aspect ratio (MAR), and relative symphyseal length (RSL), but has a positive relationship with relative toothrow length (RTL). Relative articulation offset (RAO) is bimodally distributed across PC2. The functional morphospace (Fig. 3.1.1c) generated from the SLMs (Fig. 3.1.1b) shows that taxa are principally distinguished by MAMA, MAR, and RTL along functional PC (fPC) 1 (Supplementary Table 3.1.2). RTL and OMA are strongly represented via positive distributions across fPC2. Anterior and posterior mechanical advantage (MA) are key aspects of jaw functional variation, being the respective prime determinants of fPC1 and fPC2 (Supplementary Table 3.1.2). Consideration of body size represented using $\log_{10}$ femur length shows that mandibular robusticity and biting efficiency scale positively with size.

Both form and functional morphospaces illustrate parallel progressions through the evolution of basal synapsids and therapsids, from relatively gracile, elongate mandibles towards more robust morphologies capable of more powerful bites (Fig. 3.1.1). Basal synapsids and therapsids are distinguished principally by RTL due to the shortening of the toothrow and increasing prominence of the postdentary bones in therapsids (Kemp, 2005). Both groups occupy similar extents of shape morphospace despite differences in sampling, but therapsids show much greater functional morphospace occupation (MO). Secondary morphospaces constructed using (f)PC 3 (9.3% and 11.4% of shape and functional variation, respectively) also show basal synapsids and therapsids distributed broadly in parallel across shape morphospace (Supplementary Fig. 3.1.S3a), and greater therapsid functional MO (Supplementary Fig. 3.1.S3b). PC3 captures the relative size and curvature of the mandibular body, most distinctively in the surangular, whereas fPC3 somewhat exemplifies the curvature of the ramus. Subclade patterns of MO highlight strong trends in mandibular form and function through synapsid evolution, highlighted in macroevolutionary modelling by the recovery of strongest support for a trend pattern of morphological evolution across all synapsid clades except biarmosuchians (Brownian motion) and cynodonts (stasis) (Table 3.1.11). Basal synapsids developed increasing robusticity and enlargement of the mandibular body from varanopids and ophiacodonts

to non-therapsid sphenacodontians (NTS) (Fig. 3.1.1; Supplementary Fig. 3.1.S4). This pattern extends to therapsids, as taxa within multiple clades (particularly gorgonopsians) evolved more robust morphologies with reinforcement focused on the symphysis, but some taxa also contrastingly evolved highly gracile morphologies with curved mandibular rami (Fig. 3.1.1). Divergence between gorgonopsians and therocephalians is apparent in their functional character ranges, indicating optimisations for power or speed, respectively (Supplementary Fig. 3.1.S4). Cynodont MO intriguingly overlaps basal synapsid and therapsid MO, highlighting the early origins of the mammalian jaw structure with optimisation of posterior biting efficiency and relatively large toothrows (Supplementary Fig. 3.1.S4). PERMANOVA further reveals significant differences in the jaw form and function between most synapsid groups, highlighting the disparity of the clade (Supplementary Tables 3.1.2-3).

Temporal patterns of synapsid carnivore mandibular evolution. Mandibular morphofunctional evolution through time is illustrated by dividing the shape and functional morphospaces (Fig. 3.1.1a, c) by geological stage (Fig. 3.1.2a). Mandibular form and functional MO in basal synapsids began to increase in the Late Carboniferous across the Kasimovian-Gzhelian boundary and a marked expansion followed at the onset of the Permian driven by increasingly robust sphenacodontians. Basal synapsid MO remained largely static through the Early Permian until it collapsed at the end of the Kungurian, with the extinction of ophiacodonts and sphenacodontids (Fig. 3.1.2). However, when morphofunctional disparity is viewed via sum of variance curves generated using phylogenetic time-slicing to incorporate unsampled lineages (**Guillerme and Cooper, 2018**), differences between Cisuralian stages become more apparent (Fig. 3.1.3). Basal synapsid shape disparity (Fig. 3.1.3a), but not functional disparity (Fig. 3.1.3b) expanded through the Cisuralian. Shape and functional disparity peaked at the Sakmarian-Artinskian transition but declined in the Artinskian, as shape and functional disparity trends in basal synapsids diverged. Artinskian NTS exhibited reduced functional disparity but increased shape disparity, whereas basal-most synapsid shape and functional disparity remained stable, and functionally overtook NTS. The extinction event at the end of the Early Permian, known as Olson's extinction (OE) saw the extinction of all basal synapsids except varanopids and caseids (Fig. 3.1.2b) (Olson**,** 1982). Surviving varanopids developed more powerful jaw capabilities, expanding their MO following Olson's extinction (Fig. 3.1.2a). However, the dominant carnivores of the Middle Permian were the therapsids.

The earliest known therapsids appeared in the Roadian with fairly robust mandibles that typically lacked prominent coronoid processes; they are distributed within the central regions of overall shape and functional morphospace, adjacent to the MO of earlier NTS (Figs. 3.1.1-2a). Rising

phylogenetic disparity indicates that early therapsid diversification was likely concentrated within the Roadian (Fig. 3.1.3), with biarmosuchian and dinocephalian MO showing they had established the core of therapsid MO for the remainder of the Permian by the Wordian. The extent of biarmosuchian MO across robust and gracile morphologies highlights early therapsid experimentation with jaw musculature and foreshadows the later split in theriodont morphofunctional evolution (Fig. 3.1.2a). The emergence of theriodonts appears to have instigated greater morphospace separation between all therapsid clades (Fig. 3.1.2a), and saw early gorgonopsians and therocephalians diverge from their common ecomorphology in the Capitanian, focused in the morphospace zone that represents heavily robust, powerful jaws (Figs. 3.1.1; 2a). The End-Capitanian extinction event (ECE) and extinction of dinocephalians and most biarmosuchians saw the evolution of larger gorgonopsians with more robust jaws, whereas therocephalians inversely diversified across more gracile forms, captured in their increasing disparity through the Late Permian (Figs. 3.1.1-3**;** Supplementary Fig. 3.1.S8)**.** Surviving biarmosuchians persisted into the Wuchiapingian with much reduced mandibular form and functional MO (Figs. 3.1.2). The Late Permian marked the first appearance of basal cynodonts in central areas of morphospace, but their MO shifted from the Wuchiapingian to the Changhsingian (Figs. 3.1.1-2), denoting evolution of extremely robust mandibles with large coronoid processes and optimisation of their MPMA. These cynodonts and a handful of mostly gracile-jawed therocephalians were the only synapsid carnivores to survive the Permo-Triassic mass extinction (PTME) (Fig. 3.1.2). Therocephalians were the largest remaining carnivores, but the sizes of surviving eutheriodonts are generally quite similar and much reduced in comparison to their Changhsingian ranges (Sigurdson et al., 2012; Huttenlocker, 2014).

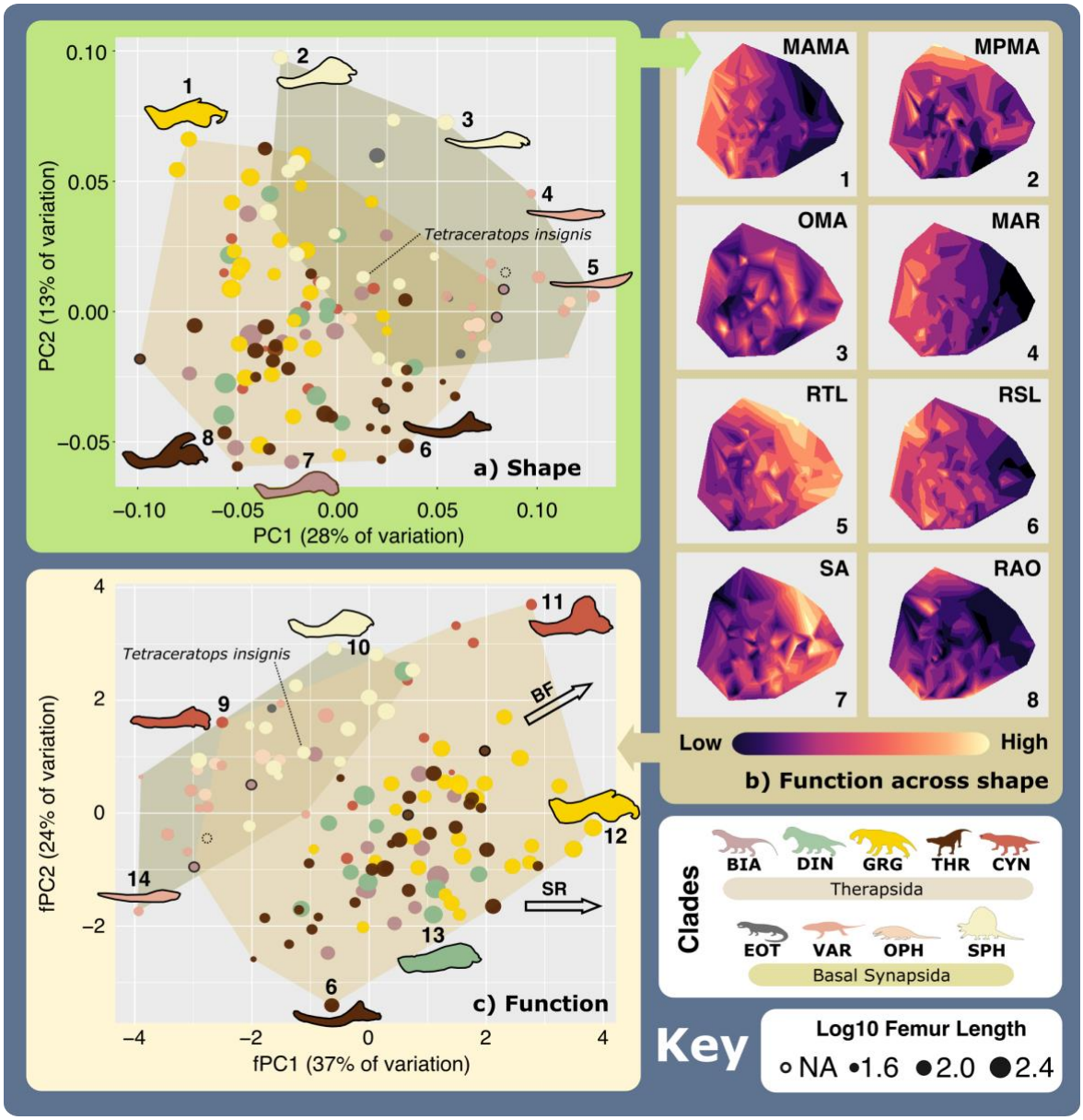

Figure 3.1.1. Synapsid carnivore mandibular morpho-functional diversity. a) Mandibular shape morphospace. b) Mandibular functional characters mapped across shape morphospace. (Colour gradient reflects functional character values – see scale.) c) Mandibular functional morphospace, with arrows showing general functional trends. Mandible silhouettes: 1. *Smilesaurus ferox*, 2. *Sphenacodon ferox*, 3. *Secodontosaurus obtusidens*, 4. *Microvaranops parentis*, 5. *Varanodon agilis*, 6. *Lycideops longiceps*, 7. *Lobalopex mordax*, 8. *Ictidosaurus angusticeps*, 9. *Procynosuchus delaharpeae*, 10. *Dimetrodon milleri*, 11. *Vetusodon elikhulu*, 12. *Dinogorgon rubidgei,* 13. *Deuterosaurus biarmicus*. 14. *Mycterosaurus longiceps*. Abbreviations: BF, Biting force. BIA, Biarmosuchia. CYN, Cynodontia. DIN, Dinocephalia. EOT, Eothyrididae and assorted Casesauria. GRG, Gorgonopsia, MAMA, Mean anterior mechanical advantage. MAR, Maximum aspect ratio.

MPMA, Mean posterior mechanical advantage. OMA, Opening mechanical advantage. OPH, Ophiacodontidae. RAO, Relative articulation offset. RSL, Relative symphyseal length. RTL, Relative toothrow length. SA, Symphyseal angle. SPH, Sphenacodontia (non-therapsid). SR, Symphyseal robusticity. THR, Therocephalia. VAR, Varanopidae.

Table 3.1.1. Functional principal component analysis character loadings. Abbreviation: fPC, functional principal component. MA, mechanical advantage.

Functional Characters	**Functional Principal Components**							
	fPC1	fPC2	fPC3	fPC4	fPC5	fPC6	fPC7	fPC8
C1. Mean Anterior MA	0.4888	0.2748	-0.0185	0.2044	0.0482	-0.2974	-0.4591	0.5847
C2. Mean Posterior MA	0.0417	0.6794	0.1057	0.1756	-0.2916	0.0708	-0.2793	-0.5715
C3. Opening MA	-0.1404	0.4650	0.2329	-0.4273	0.7207	0.0162	0.0662	0.0563
C4. Maximum Aspect Ratio	0.4584	0.2533	-0.1062	0.2033	0.0148	-0.1814	0.7988	-0.0430
C5. Relative Toothrow Length	-0.4294	0.3777	0.0535	0.0587	-0.3847	0.3683	0.2403	0.5703
C6. Relative Symphyseal Length	0.4494	-0.0183	-0.3250	-0.1082	0.1306	0.8098	-0.0867	-0.0064
C7. Symphyseal Angle	-0.3136	0.0032	-0.2228	0.7820	0.4758	0.1084	-0.0357	-0.0319
C8. Quadrate Articular Offset	0.2117	-0.1985	0.8745	0.2770	0.0394	0.2649	0.0475	0.0159

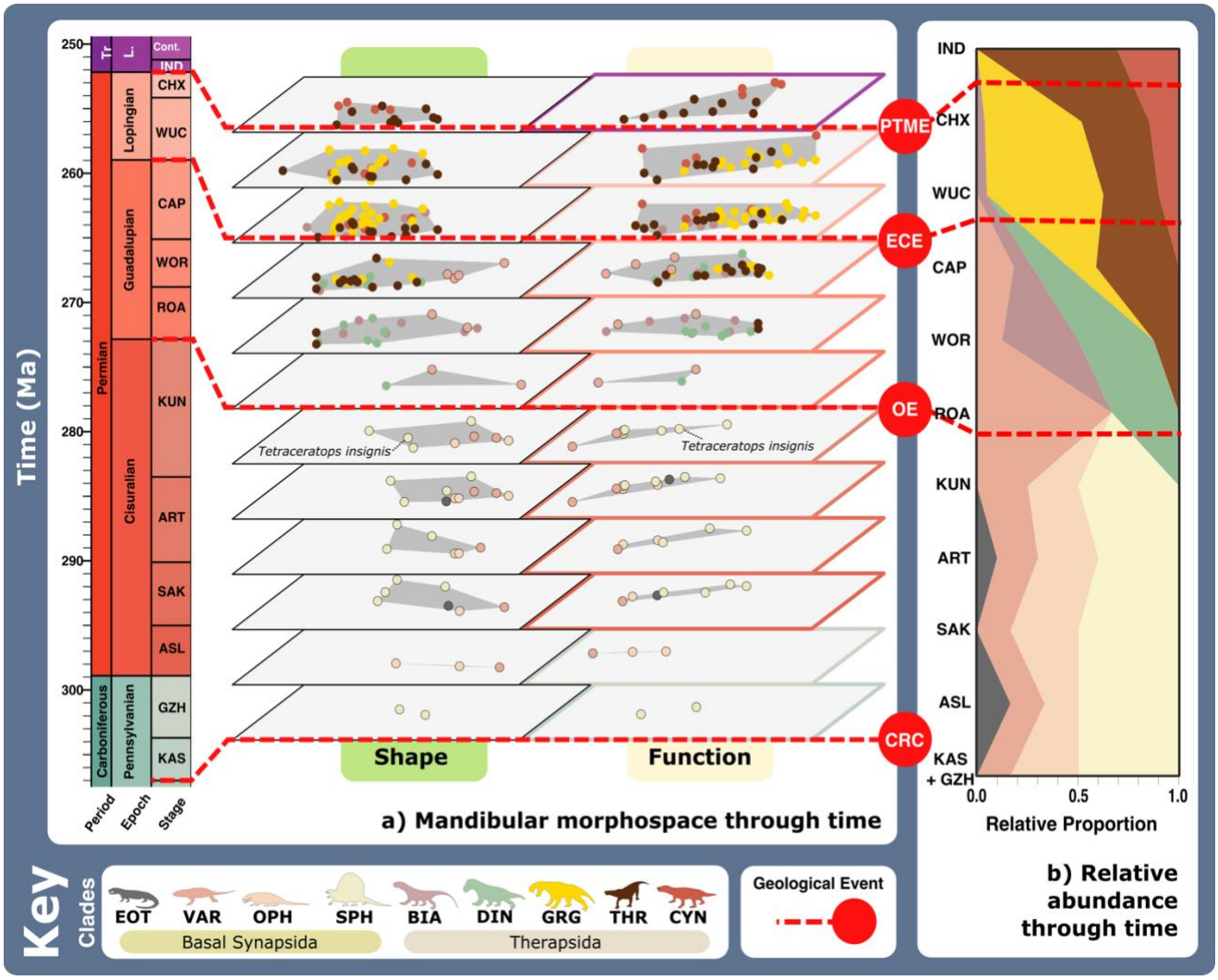

Figure 3.1.2. Synapsid carnivore mandibular morpho-functional evolution and relative abundance through time. a) Mandibular shape and functional morphospace changes through the late Palaeozoic. Morphospace margin colours correspond to colours of the relevant timebin on the stratigraphic chart. b) Relative proportions of different taxonomic groups per timebin through the late Palaeozoic. Abbreviations: ART, Artinskian. ASL, Asselian. BIA, Biarmosuchia. CAP, Capitanian. CHX, Changhsingian. CRC, Carboniferous rainforest collapse. CYN, Cynodontia. DIN, Dinocephalia. ECE, End-Capitanian extinction. EOT, Eothyrididae and assorted Casesauria. GRG, Gorgonopsia, GZH, Gzhelian. IND, Induan. KAS, Kasimovian. KUN, Kungurian. OE, Olson's extinction. OPH, Ophiacodontidae. PENN, Pennsylvanian. PTME, Permo-Triassic mass extinction. SAK, Sakmarian. SPH, Sphenacodontia (non-therapsid). ROA, Roadian. THR, Therocephalia. VAR, Varanopidae. WOR, Wordian. WUC, Wuchiapingian.

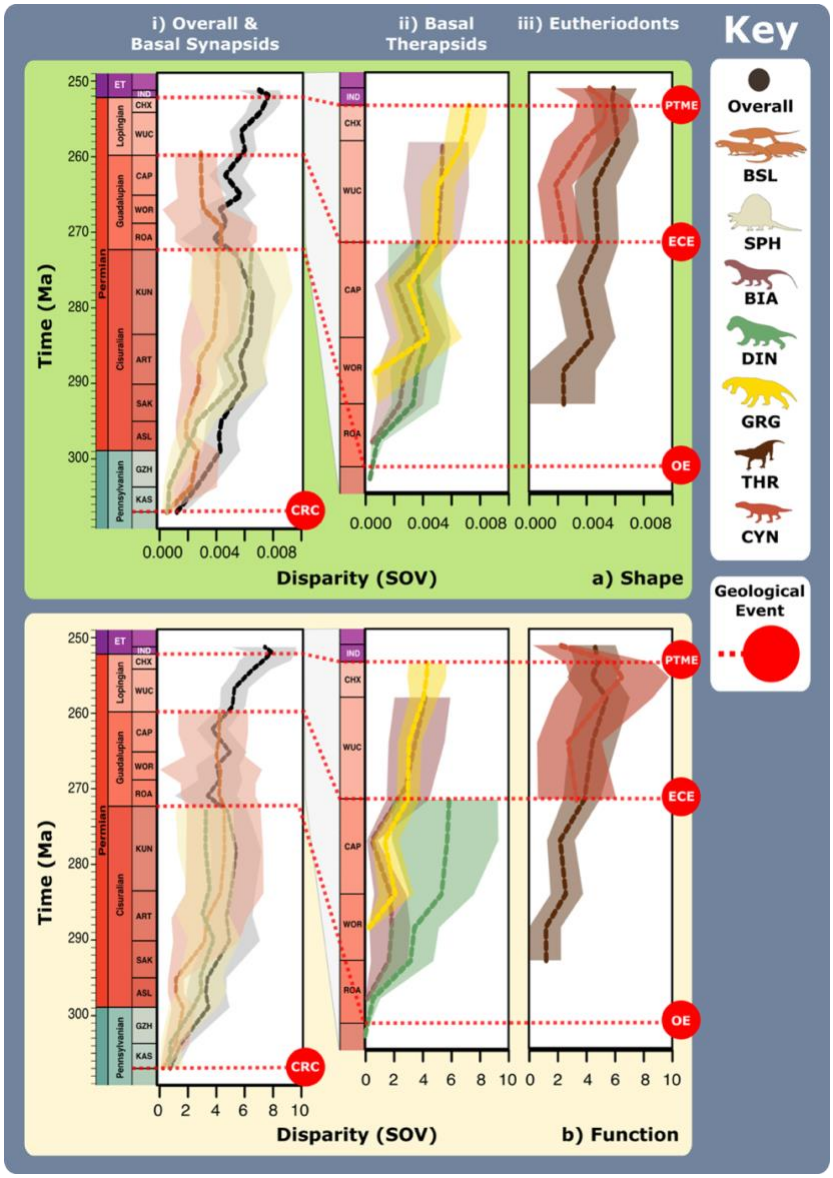

Figure 3.1.3. Synapsid carnivore mandibular shape and functional phylogenetic disparity through the late Palaeozoic. a) Shape and b) functional sum of variance calculated for each time bin for carnivorous synapsid groups using phylogenetic time-slicing **(Guillerme and Cooper, 2018),** divided into: i) Basal synapsids, ii) Basal therapsids, and iii) Eutheriodonts. Significant geological events also highlighted. 'Overall' represents all carnivorous synapsids. Shaded 95% confidence intervals shown for each curve. N=123. Abbreviations: ART, Artinskian. ASL, Asselian. BIA, Biarmosuchia. BSL, Basal-most synapsids (eothyridids, varanopids, and ophiacodonts). CAP, Capitanian. CHX, Changhsingian. CRC, Carboniferous rainforest collapse. CYN, Cynodontia. DIN, Dinocephalia. ECE, End-Capitanian extinction. GRG, Gorgonopsia, GZH, Gzhelian. IND, Induan. KAS, Kasimovian. KUN, Kungurian. OE, Olson's extinction. PENN, Pennsylvanian. PTME, Permo-Triassic mass extinction. SAK,

Sakmarian. SPH, Sphenacodontia (non-therapsid). ROA, Roadian. THR, Therocephalia. WOR, Wordian. WUC, Wuchiapingian.

Synapsid carnivore feeding strategies. Three feeding functional groups (FFGs) are identified using the consensus cluster method of Singh et al., (2021) to categorise taxa quantitatively using their functional SLMs. Qualitative examination of FFG functionality led us to characterise these groups as raptorial specialists, power shearers, and speed specialists (Supplementary Fig. 3.1.S5). The FFGs show broad phylogenetic segregation as basal synapsids are largely confined to the raptorial specialist FFG, reflecting their primitive jaw functionality (Fig. 3.1.1c), as well as strong phylogenetic controls on mandibular ecomorphology (Carmul and Polly, 2005; Raia et al., 2010). Nonetheless, functionality is an important discriminant of mandibular anatomy as illustrated by external validation metrics that reveal low correspondence between cluster classifications and phylogeny at higher taxonomic levels (Supplementary Table 3.1.9). Each FFG was subjected to further cluster analyses to identify more specific subgroups potentially overlooked in the original analyses, revealing a total of seven feeding functional subgroups (FFsGs) (Fig. 3.1.4; Supplementary Fig. 3.1.S6a). The FFsG classifications were validated using a jack-knifed, linear discriminant analysis (LDA) (Foffa et al., 2018) (Supplementary Fig. 3.1.S6b).

Raptorial specialists are defined by gracile, longirostrine mandibles and lengthy toothrows (Supplementary Fig. 3.1.S5) and subdivided into the gracile mesocarnivore (GM) and primitive hypercarnivore (PH) subgroups by differences in jaw robusticity and biting efficiency (Fig. 3.1.4). Varanopids and ophiacodonts form the majority of GM, but larger, more robust members of both clades and most sphenacodontids are PH (Figs. 3.1.4-5). Low MAMA, MPMA, and robusticity highlights raptorial specialist adaptation for speed, but speed specialists take this strategy further by also developing lower OMA to further enhance bite speeds (Westneat, 1994; Stubbs et al., 2013). Speed specialists are divided into grip and rip attackers (GRA) and rapid attack specialists (RAS). The RAS show extreme adaptations for bite speed, heavily reducing their mandibular robusticity and biting power (Fig. 3.1.4). Speed specialists are the most taxonomically diverse FFG, encompassing most therapsids, but particularly therocephalians, which predominantly comprise the RAS (Fig. 3.1.4). Power shearers feature the most robust and mechanically efficient mandibles with particularly strong symphyseal reinforcement (Supplementary Fig. 3.1.S5; Fig. 3.1.4). These overwhelmingly comprise large gorgonopsians and basal therocephalians, although the majority of cynodonts and a few species of *Dimetrodon* and *Sphenacodon* also belong to this FFG within the power bite specialist (PBS) subgroup (Figs. 3.1.4-5; Supplementary Figs. 3.1.S5-6a). Shearing bite specialists (SBS) form the core of the group, but power bite specialists (PBS) and sabretooth

specialists (SS) represent distinct variations on the power shearer feeding mode, opting to maximise biting efficiency along the entire toothrow or at the anterior of the dentary (Fig. 3.1.4). The SS are dominated by rubidgeine gorgonopsids, which were the largest and most heavily built gorgonopsians (Kammerer, 2016; 2018).

FFsG prevalence though time shows that trophic diversity increased from the Pennsylvanian to the Cisuralian (Fig. 3.1.6), with reconstructions of FFsGs across the synapsid phylogeny dating the origin of synapsid carnivore diversity to a radiation across GM and PH FFsGs in the middle Kasimovian (Fig. 3.1.7a; Supplementary Fig. 3.1.S7). Power bite specialist sphenacodontians also originated in the Kasimovian, with mandibular morphofunctional diversification and concurrent increases in body size (Figs. 3.1.2, 7) indicating a decisive shift towards macrocarnivore niches through the Carboniferous-Permian transition and further synapsid ecological specialisation in the carnivore guild. Through the early Cisuralian, PBS became larger and less numerous perhaps highlighting their monopolisation of hypercarnivorous niches as PH concurrently declined in abundance and size (Figs. 3.1.6-8; Supplementary Fig. 3.1.S8**).** Olson's extinction saw varanopids become the dominant the raptorial specialists, encompassing a wider range of sizes (Figs. 3.1.6-7; Supplementary Fig. 3.1.S8b). Therapsid emerged across all FFGs in the Middle Permian, but predominantly as speed specialists and power shearers (Figs. 3.1.6-7**).** Prevalence among basal therapsids and ancestral state reconstructions indicate the speed specialist FFG was plesiomorphic for therapsids and appeared in the Kungurian, with power shearers evolving as part of a later therapsid radiation in the Roadian (Fig. 3.1.5-7; Supplementary Fig. 3.1.S7). Two additional therapsid radiations followed in the Capitanian that saw new FFsGs emerge and greater FFsG size differentiation, demonstrating further specialisations within the carnivore guild (Figs. 3.1.6-8). The End-Capitanian extinction triggered a rise in dominance by highly specialised FFsGs (sabretooth and rapid attack specialists) coupled with increasing taxonomic segregation within FFGs as gorgonopsians and therocephalians became the predominant power shearers and speed specialists, respectively (Fig. 3.1.6). The Late Permian saw complex patterns of niche partitioning with power shearing gorgonopsians as the top macropredator roles, and smaller speed specialists typically occupying mesopredator niches, split between smaller gorgonopsian, therocephalian and biarmosuchian GRAs (Figs. 3.1.6-7). Therocephalians also expanded into the smaller-sized RAS FFG. Interestingly, the PTME did not decimate synapsid carnivore feeding functionality as the core shearing bite specialist and grip and rip attacker subgroups survived into the Triassic, populated exclusively by small eutheriodonts (Figs. 3.1.6-8; Supplementary Fig. 3.1.S8). However, the Triassic marked the end of synapsid domination of the carnivore guild with new archosauromorph carnivores replacing synapsids as the top predators in terrestrial ecosystems (Benton, 1987).

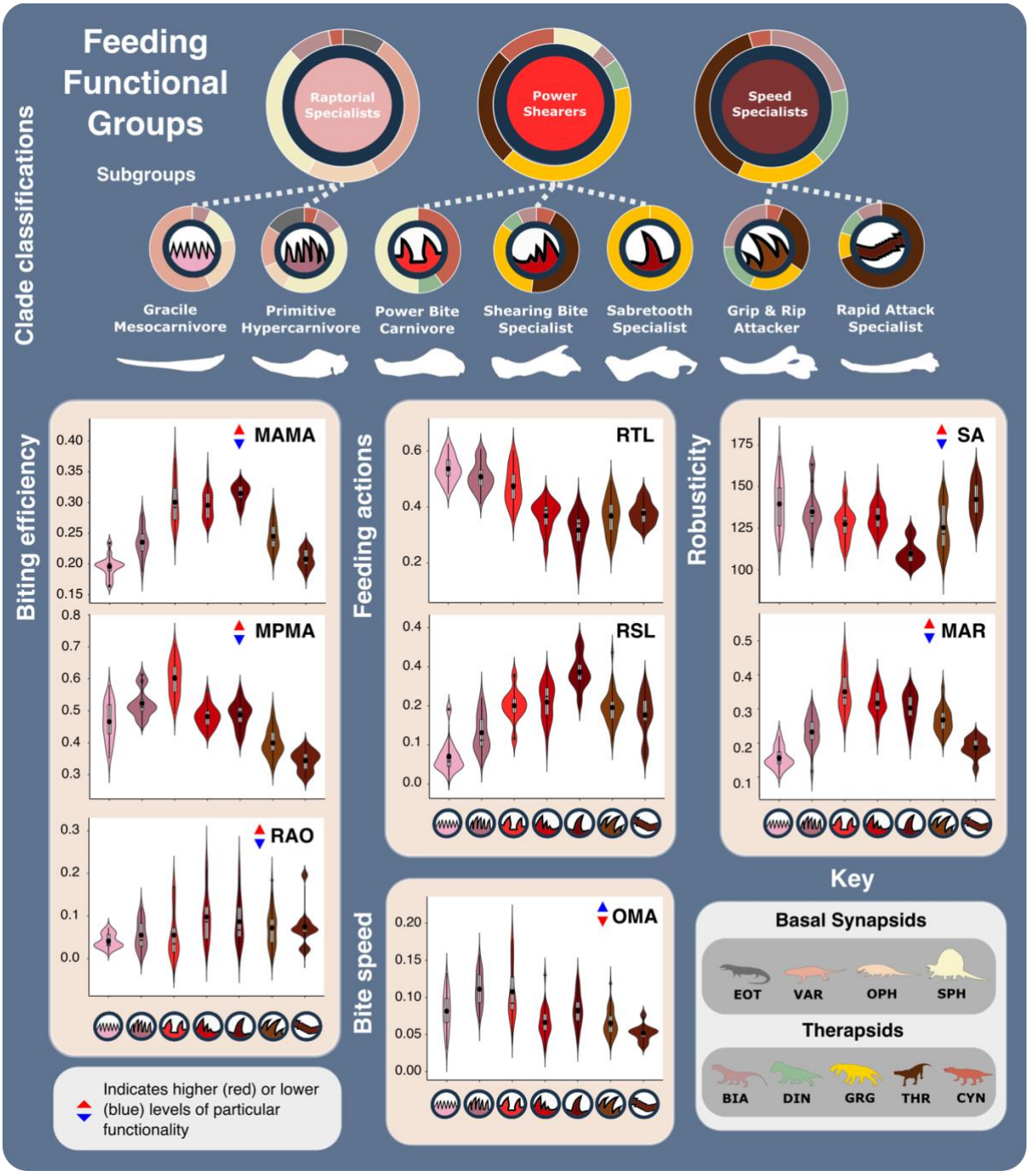

Figure 3.1.4. Synapsid carnivore feeding functional subgroup mandibular characteristics. The feeding functional subgroup mandibular functional character (Supplementary methods) distributions illustrated using violin and box plots. Feeding functional group compositions illustrated using ring plots detailing relative proportions of different taxonomic groups. Mean values indicate by black dots. Coloured arrows indicate whether values increase (red) or decrease (blue) relevant mandible functionality. N=123. Mandible silhouettes (left to

right): *Varanodon agilis*, *Tetraceratops insignis*, *Dimetrodon grandis*, *Sauroctonus parringtoni*, *Smilesaurus ferox*, *Annatherapsidus petri*, *Tetracynodon darti*. Abbreviations: BIA, Biarmosuchia. CYN, Cynodontia. DIN, Dinocephalia. EOT, Eothyrididae and assorted Casesauria. GRG, Gorgonopsia, MAMA, Mean anterior mechanical advantage. MAR, Maximum aspect ratio. MPMA, Mean posterior mechanical advantage. OMA, Opening mechanical advantage. OPH, Ophiacodontidae. RAO, Relative articulation offset. RSL, Relative symphyseal length. RTL, Relative toothrow length. SA, Symphyseal angle. SPH, Sphenacodontia (non-therapsid). THR, Therocephalia. VAR, Varanopidae.

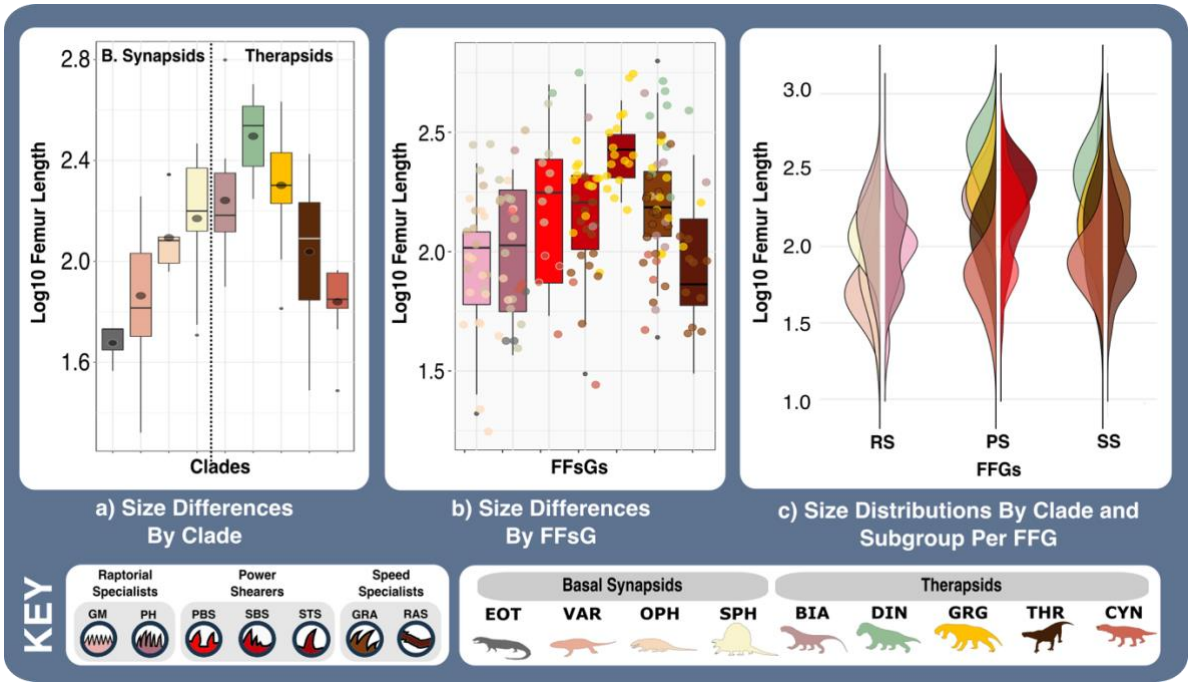

Figure 3.1.5. Synapsid carnivore size distributions by taxonomic and feeding functional subgroup a) Boxplots illustrating body size (log_{10} femur length) distributions by taxonomic group. Dotted line represents divide between basal synapsids and therapsids. b) Boxplots illustrating body size (log_{10} femur length) distributions by feeding functional subgroup with taxonomic groups indicated by points. c) Distribution plots illustrating the body size ranges of and taxonomic groups and feeding functional subgroups within each feeding functional group. N=123. Abbreviations: BIA, Biarmosuchia. CYN, Cynodontia. DIN, Dinocephalia. EOT, Eothyrididae and assorted Casesauria. FFGs, Feeding functional groups. FFsG, Feeding functional subgroups. GM, Gracile mesocarnivore. GRA, Grip and rip attacker. GRG, Gorgonopsia, OPH, Ophiacodontidae. PBS, Power bite specialist. PH, Primitive hypercarnivore. PS, Power shearer. RAS, Rapid attack specialist. RS, Raptorial specialist. SBS,

Shearing bite specialist. SPH, Sphenacodontia (non-therapsid). SS, Speed specialist. STS, Sabretooth specialist. THR, Therocephalia. VAR, Varanopidae.

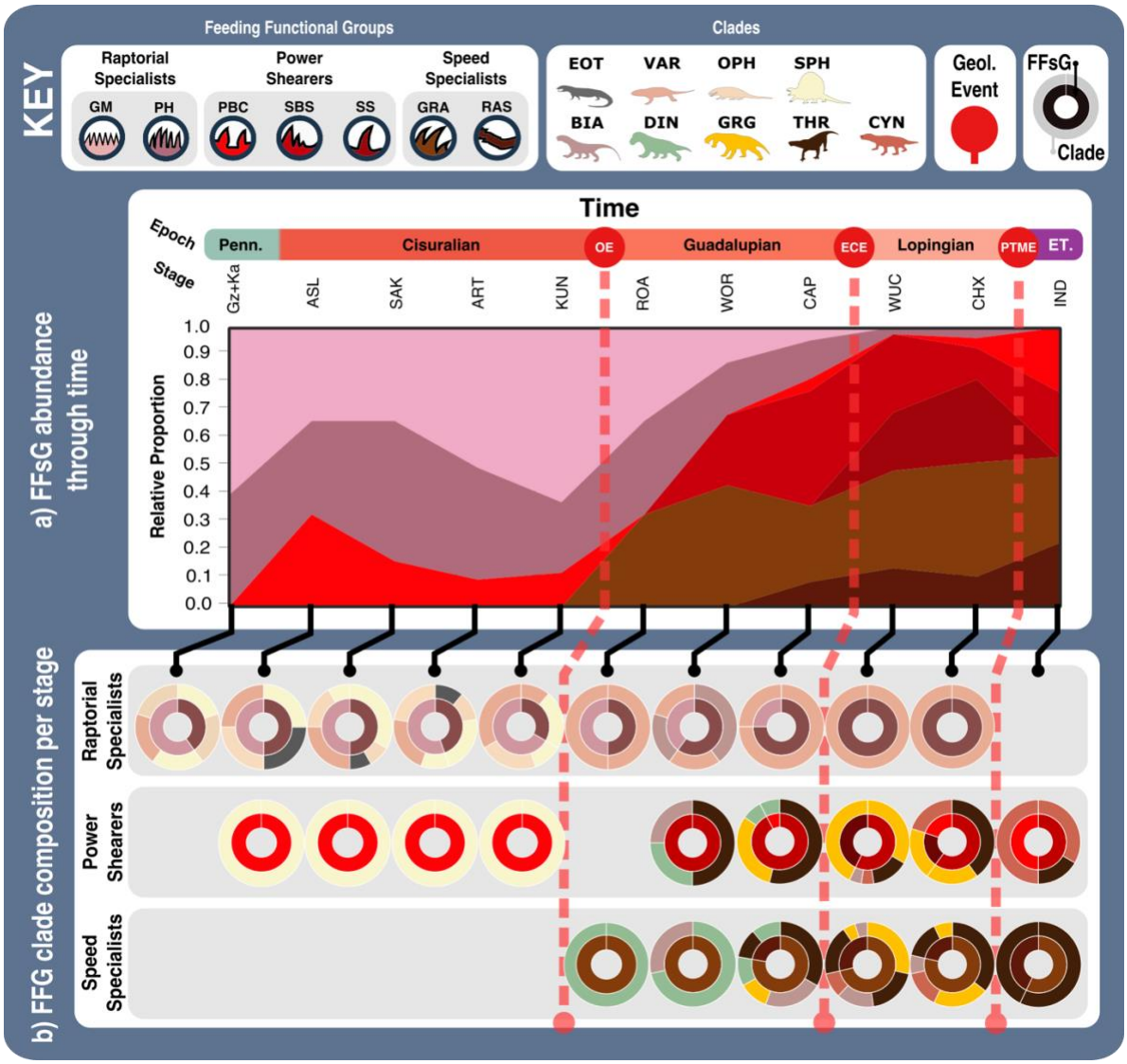

Figure 3.1.6. Synapsid carnivore feeding functional subgroups through the late Palaeozoic. a) Relative abundance through time of different feeding functional (sub)groups. b) Composition of each feeding functional group by feeding functional subgroup and clade per timebin. Key geological events shown. Epochs are colour coded by period: Carboniferous (green), Permian (orange), and Triassic (purple). N=123. Abbreviations: ART, Artinskian. ASL, Asselian. BIA, Biarmosuchia. CAP, Capitanian. CHX, Changhsingian. CYN, Cynodontia. DIN, Dinocephalia. ECE, End-Capitanian extinction. EOT, Eothyrididae and assorted Casesauria. ET, Early Triassic. FFsG, Feeding functional subgroup. GM, Gracile mesopredators. GRA, Grip and rip attackers. GRG, Gorgonopsia, Gz, Gzhelian. IND, Induan. Ka, Kasimovian. KUN,

Kungurian. OE, Olson's extinction. OPH, Ophiacodontidae. PBC, Power bite carnivores. PENN, Pennsylvanian. PH, Primitive hypercarnivores. PTME, Permo-Triassic mass extinction. SAK, Sakmarian. SBS, Shearing bite specialists. SPH, Sphenacodontia (non-therapsid). SS, Sabretooth specialists. RAS, Rapid attack specialists. ROA, Roadian. THR, Therocephalia. VAR, Varanopidae. WOR, Wordian. WUC, Wuchiapingian.

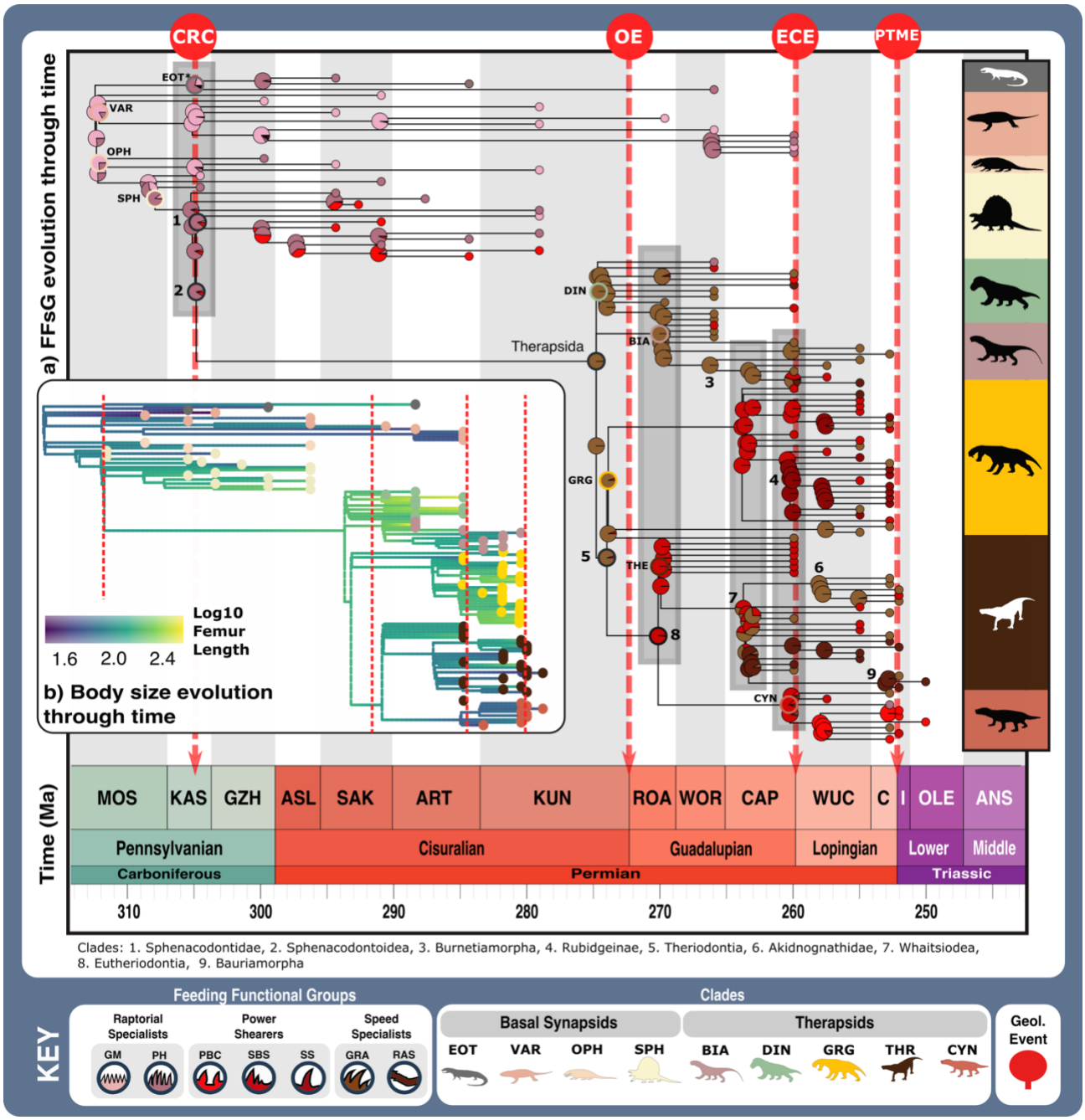

Figure 3.1.7. Synapsid carnivore ecomorphological evolution through the late Palaeozoic.

a) Feeding functional subgroup states cross the carnivorous synapsid phylogeny with

reconstructed ancestral character state likelihoods under a symmetrical rates model of character transitions denoted by pie charts at node positions. Positions of key clades indicated by numbers in bold across the phylogeny. Pulses of diversification highlighted with shaded boxes. b) Body size evolution across the carnivorous synapsid phylogeny through time. Body size represented by Log_{10} femur length, with colour denoting low or high values (see scale). Key geological events shown. N=123. Abbreviations: ART, Artinskian. ASL, Asselian. BIA, Biarmosuchia. CAP, Capitanian. CHX, Changhsingian. CYN, Cynodontia. DIN, Dinocephalia. ECE, End-Capitanian extinction. EOT, Eothyrididae and assorted Casesauria. ET, Early Triassic. FFsG, Feeding functional subgroup. GM, Gracile mesopredators. GRA, Grip and rip attackers. GRG, Gorgonopsia, Gz, Gzhelian. IND, Induan. Ka, Kasimovian. KUN, Kungurian. MOS, Moscovian. OE, Olson's extinction. OPH, Ophiacodontidae. PBS, Power bite specialists. PENN, Pennsylvanian. PH, Primitive hypercarnivores. PTME, Permo-Triassic mass extinction. SAK, Sakmarian. SBS, Shearing bite specialists. SPH, Sphenacodontia (non-therapsid). SS, Sabretooth specialists. RAS, Rapid attack specialists. ROA, Roadian. THR, Therocephalia. VAR, Varanopidae. WOR, Wordian. WUC, Wuchiapingian.

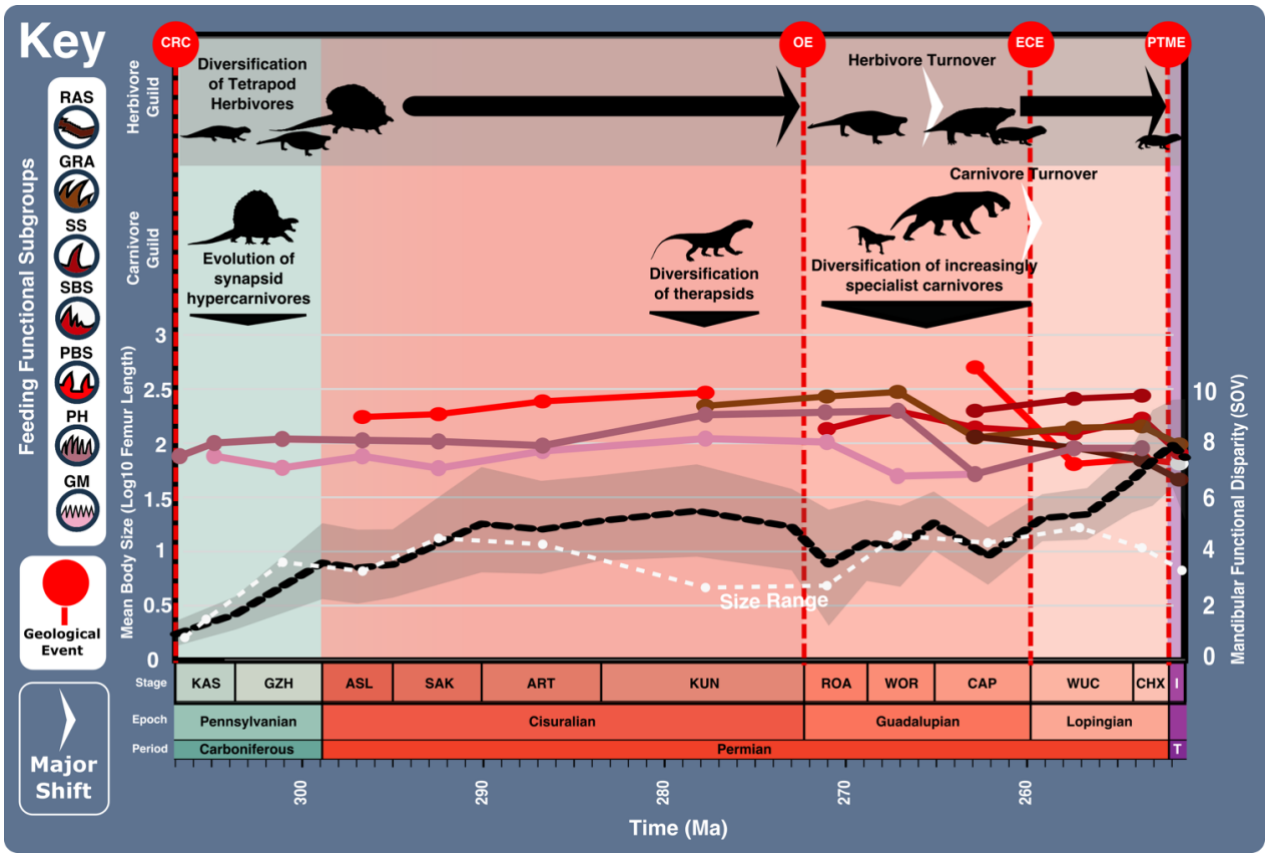

Figure 3.1.8. Key changes in synapsid carnivore ecomorphology and their prey diversity through the Palaeozoic. Trends in synapsid carnivore ecomorphology through the late Palaeozoic: feeding functional subgroup mean body size incorporating reconstructed ancestral size data with FFsG classification determined using linear discriminant analysis (coloured lines with circle points), overall body size range (white dashed line), and mandibular functional disparity with 95% confidence intervals (black dashed line with shading). Shown alongside concurrent changes in the carnivore and herbivore guild. Key geological events also shown. Abbreviations: ART, Artinskian. ASL, Asselian. CAP, Capitanian. CHX, Changhsingian. ECE, End-Capitanian extinction. GM, Gracile mesopredators. GRA, Grip and rip attackers. GZH, Gzhelian. I, Induan. KAS, Kasimovian. KUN, Kungurian. OE, Olson's extinction. PBS, Power bite specialists. PENN, Pennsylvanian. PH, Primitive hypercarnivores. PTME, Permo-Triassic mass extinction. SAK, Sakmarian. SBS, Shearing bite specialists. SOV, Sum of variance. SS, Sabreteeth specialists. RAS, Rapid attack specialists. ROA, Roadian. T, Triassic. WOR, Wordian. WUC, Wuchiapingian.

Discussion

Modes of synapsid carnivory. The feeding mechanics employed by basal synapsids were largely the same as in sauropsid reptiles (Cleuren and Vree, 1992), but therapsids developed more complex jaws that reflected the progressive redevelopment of synapsid jaw mechanics and contrasting optimisations for speed or power, echoing the functional divergence between extant canids and felids (Van Valkenburgh and Jenkin, 2002; Kemp, 1982; Ivakhnenko, 2008). It is harder to use modern mammals as analogues for some of the earliest synapsids which shared more phylogenetically with sauropsids (Supplementary Fig. 3.1.S4). For example, extant felids and canids engage in grappling or social prey capture methods (Murray et al., 1995) that were likely unavailable to non-mammalian synapsids with their primitive, sprawling posture (Van Valkenburgh, 1999; Benton, 2021). Furthermore, non-mammalian synapsids employed a kinetic inertial biting system, and lacked masseter musculature and carnassial teeth, which are key features in carnivoran mammal evolution (Van Valkenburgh, 1999; Van Valkenburgh and Jenkin, 2002; Goswami and Friscia, 2010). Carnivoran evolution is heavily focused towards optimising carnassial functionality (Van Valkenburgh, 1999) with mammals exhibiting extremely high MPMA **(**Supplementary Fig. 3.1.S4), but equivalent changes in things like snout length and ramus curvature still modify the same functional properties (e.g., posterior MA) in nonmammalian therapsids. Consequently, absolute, and relative functional similarities with mammalian carnivores allow some inferences of prey selection and capture by therapsid carnivores. Carnivores apply a combination of compressive, shearing,

tearing, and puncture damage to subdue prey (Cabon et al., 2015), and each aspect preferentially acts in different ways to incapacitate prey. Puncture and compressive injuries can extend damage deeper within prey tissue, potentially extending to vital internal anatomy, whereas shearing and tearing are focused on causing tissue and blood loss (Cowell et al., 1989; Davidson et al., 1998). The mix of damage inflicted likely depended on the relative robusticity of the predator's jaws and of their prey.

Raptorial and speed specialists are both optimised for speed, but raptorial specialists show wider distribution of bite force along their toothrow, improving their gripping ability. Speed specialists opt to further enhance bite speed by heavily reducing jaw robusticity. Further adaptations in both FFGs such as curved dentaries further help prey capture by varying the angle of teeth, allowing them to pin smaller prey in place (Figs. 3.1.4; 9; Supplementary Fig. 3.1.S6). Relative robusticity gives some indication of likely prey preferences as gracile GM and RAS are ill-suited to high stresses associated with large prey capture and probably favoured smaller prey that were unable to resist, such as insects, fish and small tetrapods. Rapid head movements were likely employed by varanopids (Bazzana et al., 2021), and given their basal-most phylogenetic position, such behaviour could be plesiomorphic for synapsids. Therefore, the raptorial specialist emphasis on speed and grip suggests they quickly grasped prey, using their long toothrow and high posterior biting efficiency to hold prey in place, with rapid head movements enabling greater penetration and tearing damage, much like extant monitor lizards. The shortening of the toothrow and strengthening of the symphysis in therapsids (Fig. 3.1.1; Supplementary Fig. 3.1.S4) reflects a shift in jaw function from gripping to penetration, followed by divergent optimisations, some for speed and some for power, producing speed specialists and power shearers.

I propose that the initial killing behaviour of the first therapsids followed a speed-specialist mode, which was to employ quick, penetrating bites, overcoming prey with multiple bites as required by prey resistance, incapacitating the prey before it could escape (Valkenburgh and Ruff, 1987). Differences in relative jaw robusticity between raptorial specialists and speed specialists reflect increasing discrepancies in the size of potential prey animals, in which GRA likely preyed on relatively smaller prey than PH. Elongate GRA jaws are unsuited to extended struggles with large prey, and in any case GRA predators show a wide size range, which together suggest they probably focussed on smaller and less combative prey, which could be subdued more quickly as the size disparity enabled infliction of relatively greater compressive and shearing damage (Van Valkenburgh, 2007) (Figs. 3.1.4-5, 9; Supplementary Fig. 3.1.S6). This 'harrying' speed specialist prey capture mode (Fig. 3.1.9) is consistent with jaw and neck muscle development across the basal synapsid-therapsid transition (Kemp, 2005) and is reminiscent of canid killing modes. However,

canids are pursuit predators, which is unlikely in therapsids due to their more primitive locomotory abilities; therapsids probably engaged in low-energy stalking like most extant large felids, deploying their killing bite(s) once within striking distance (MacDonald et al., 2010).

Robust speed specialists were probably able to target more similarly sized prey, which gives some indication of how power shearers evolved. The brevirostrine power-shearers maximised anterior bite force and symphyseal resistance to torsional stresses to amplify penetrative biting power and inflict deeper wounds on their prey and cause heavier trauma, thereby incapacitating prey more quickly (Walmsley et al., 2013) (Fig. 3.1.9). Optimising flesh removal over grip suggests that power-shearers employed few or perhaps a single powerful bite to quickly disable prey of up to equal or greater sizes, much like extant large felids (Valkenburgh and Ruff, 1987; Murray et al., 1995; Brahman et al., 2004). This adaptation to hunting large prey is pursued to the extreme by the sabretooth specialist subgroup exclusively populated by large gorgonopsians with hypertrophied canines (Lautenschlager et al., 2020) (Figs. 3.1.4-5). High MPMA in power bite specialists enhanced grip during prey capture and suggests more durophagous feeding. However, differences in size (Fig. 3.1.5), dentition (Huttenlocker et al., 2021) and musculature (Lautenschlager et al., 2017) point to divergent ecologies among power bite specialists, with hypercarnivory in the large sphenacodontids and mesocarnivory in the cynodonts.

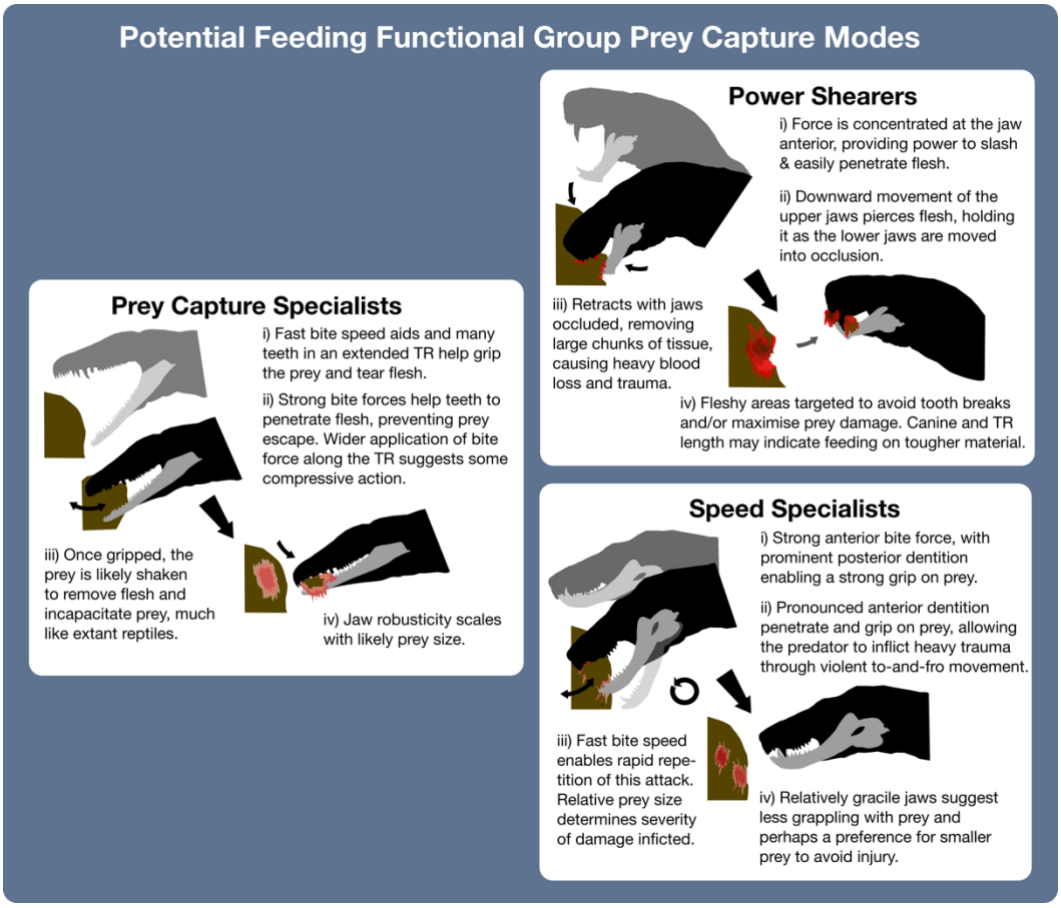

Figure 3.1.9. Potential prey capture modes of each synapsid carnivore feeding functional group. Outline of the different prey capture methods utilised by the three feeding functional groups, as suggested by overall interpretation of mandibular functional traits. Abbreviations. TR, Toothrow.

Synapsid carnivore niche dynamics through the late Palaeozoic. Niche partitioning enables sympatric taxa to avoid excessive competitive pressure by minimising intraguild interactions (Hutchinson, 1959; Finke and Snyder 2008). Niche partitioning is widely reported from both extant (Durant, 2000; Linnell and Strand, 2000; Caro and Stoner, 2003) and extinct communities (Sereno et al., 1996; Mallon and Anderson, 2013; Button et al., 2014; Rivals and Lister, 2016), underscoring its spatiotemporal prevalence. High morphological and size differentiation indicates niche partitioning in extant carnivores, with larger carnivores generally preying on larger prey (Durant, 1998; Slater et al., 2009; Ramesh et al., 2012). Divergent FFG and size distributions (Supplementary Fig. 3.1.S8), particularly in therapsids, suggest prevalent niche partitioning by synapsid carnivores, with pulses of synapsid diversification corresponding to FFG subdivision (Fig. 3.1.7a) and increasing size range (Fig. 3.1.8) reflecting further niche specialisation as carnivore diversity increased. This is most apparent in

the late Capitanian radiation, which saw strong partitioning by size and jaw anatomy between a variety of specialist FFsGs, producing Late Permian predator communities that included large megapredatory gorgonopsians, mid-sized mesopredatory therocephalians, and small insectivorous therocephalians and cynodonts (Figs. 3.1.2, 5-8). The speed specialists show the most complex patterns of niche partitioning, with akidognathid therocephalians taking the role of largest GRAs and gorgonopsians vying with the remaining biarmosuchians for mid-sized GRA niches (Fig. 3.1.7; Supplementary Fig. 3.1.S8).

This trophic complexity is highlighted by high body size ranges across the ECE and Late Permian despite the loss of the large dinocephalians (Fig. 3.1.8; Supplementary Fig. 3.1.S8). Niche partitioning in Late Permian theriodonts is interesting because early therocephalians and gorgonopsians were similarly sized SBS in the Capitanian (Figs. 3.1.5-6; Supplementary Fig. 3.1.S8b), exhibiting functional similarities such as modified jaw adductor musculature to maximise muscle force at different points in their bite cycle and extend their gape (Crompton, 1963; Kemp, 2005). Both also reinforced their jaw articulation to support their derived musculature and resist disarticulation during prey capture (Parrington, 1959; Kemp, 1969). Yet gorgonopsians overtook therocephalians as the predominant power shearers across the ECE, with the further evolution of the hypercarnivorous sabretooth specialists reflecting their elevation to top predators (Figs. 3.1.1-2, 6, 7b). Therocephalians made a rare synapsid shift from hyper to mesocarnivory (Brocklehurst, 2019), by becoming smaller mesopredators and insectivores (Figs. 3.1.1, 5). Eutheriodont mesocarnivore specialisation in the Changhsingian laid the foundations for their survival through the PTME, as generalist therocephalian and durophagous cynodont capabilities increased their trophic adaptability, enabling them to cope with the environmental devastation of the PTME and ensuing resource instability (Roopnarine et al., 2007; Payne and Kump, 2007; Irmis and Whiteside, 2012; Sun et al., 2012; Li et al., 2016).

Patterns of theriodont niche partitioning may perhaps reveal long-term ecological displacement (Grant and Grant, 2008) within synapsid carnivore faunas. The basal to theriodont therapsid turnover in the Middle Permian (Figs. 3.1.2, 6) illustrates how competition influenced synapsid macroevolution, with dinocephalians and biarmosuchians exhibiting different adaptive responses to adjust their niche breath in response to new theriodont competitors. Dinocephalian size and robusticity enabled them to vacate contested ecospace as medium carnivores by becoming increasingly large PS; this specialisation as top predators left them extremely vulnerable to eco-environmental changes and likely contributed to their extinction in the ECE. Biarmosuchians were constrained by larger dinocephalians and new smaller-equivalently sized theriodonts, and their macroevolution highlights this high ecological constraint with the clade vacating the PS FFG, and

surviving exclusively as speed specialists. However, the radiation of speed specialist therocephalians and smaller gorgonopsians in the latest Capitanian brought renewed competitive pressures within this FFG, driving a declining role for biarmosuchians in Late Permian terrestrial faunas (Figs. 3.1.1-2, 5-7). These changes in clade morphospace occupation and FFG through time suggest intraguild dynamics played a key role in eco-evolutionary shifts and the earliest example of such a shift indicates that strong competitive pressures may have originated early in the development of terrestrialised tetrapod faunas. Ophiacodonts and sphenacodontians diverged from shared morphospace through the Carboniferous-Permian boundary (Fig. 3.1.2) with differences in jaw morphofunction and postcranial anatomy (Romer and Price, 1940; Laurin and de Buffrénil, 2016) suggesting stratification of ophiacodonts and sphenacodontians into medium and large terrestrial carnivore niches between semi-aquatic and terrestrial habitats in the Early Permian (Fig. 3.1.7b**;** Supplementary Fig. 3.1.S8).

Synapsid predator-prey coevolution. Prey size, abundance and diversity are key controls on carnivore ecology, constraining the degree of trophic specialisations available to sympatric carnivores in their drive to minimise competitive pressures by partitioning prey resources (Palomares and Caro, 1999; Caro and Stone, 2003; Ramesh et al., 2012; Tucker and Rogers, 2014). As such, changes in prey diversity produce consequent changes in their predators, determining levels of intraguild competition, foraging behaviour and size (Palomares and Caro, 1999; Caro and Stone, 2003; Carbone et al., 2013). The onset of drier conditions in the Late Carboniferous (DiMichele et al., 2009) instigated an increasing shift towards fully terrestrialised food webs (Olson, 1966; Benton, 2014; Coates et al., 2008; Sahney et al., 2010; Dunne et al., 2018; Pardo et al., 2019), with further increases in aridity and seasonality through the Permian propelling the shift towards dry, heterogeneous terrestrial environments as the Late Palaeozoic ice age ended (Parrish, 1995). These environmental changes undoubtedly changed the resources available to terrestrial animals, with new plants providing new food resources for herbivores (McGhee, 2018). The combination of new environments and prey resources created an array of selection pressures acting across carnivore anatomy, pushing key advances in synapsid macroevolution:

- **Carboniferous origins of synapsid carnivore guild dominance -** Increasing guild complexity and more dynamic palaeoecological interactions may also reflect the increasing terrestrialisation of tetrapods through the late Palaeozoic as tetrapod faunas became increasingly entrenched inland and independent of aquatic resources (Sahney et al., 2010; Dunne et al., 2018; Pardo et al., 2019). Resulting increases in habitat heterogeneity would have demanded greater locomotory

efficiency from tetrapods, and focused predator-prey interactions in fully terrestrial settings (Bakker, 1975). From the Moscovian onwards, increasing seasonality and aridity created more heterogeneous environments, with the transformation of stable wetlands into more variable fluvial floodplains by the end of the Late Carboniferous (Parrish, 1995; DiMichele et al., 2009; 2011; Huttenlocker et al., 2021). This increasing habitat variability and ensuing prey diversity split between more terrestrial and aquatic resources manifests in the increasing size range and mandibular disparity of basal synapsids that reflects increasing synapsid experimentation with specialised carnivory through the Carboniferous (Figs. 3.1.2-3, 6-8).

- **Diversification of predatory modes in the Permian -** Heightened aridity in the Early Permian pushed tetrapods further inland (McGhee, 2018), creating new niches for fully terrestrialised carnivores. Synapsids evidently exploited these niches as illustrated in their increasing range of body sizes and the evolution of more hypercarnivorous power bite specialists (Figs. 3.1.7, 8; Supplementary Fig. 3.1.S7). Synapsid specialisation as active carnivores in the Moscovian (Fig. 3.1.7), as well as their evolution of heterodonty (Huttenlocker et al., 2021) and the inherent adaptations of amniotes to survive in drier climates (Reisz, 1972) combined to give synapsids the advantage over diapsids and temnospondyl amphibians when colonising the carnivore guild through the Carboniferous-Permian transition. Temnospondyls were top carnivores during the Carboniferous (Benton, 2014), but despite appendicular adaptation for improved terrestrial locomotion (Romer, 1966), their physiological and reproductive ties to wetter environments limited their ability to exploit carnivorous niches in the drier Early Permian (Sahney et al., 2010), and this reduced the competition faced by synapsids from established large carnivores for new carnivore niches created by the new communities of herbivorous diadectids, captorhinids, caseids, and edaphosaurids (Olson, 1962; 1966; Brocklehurst and Brink, 2017; Brocklehurst et al., 2020). However, large basal synapsids and temnospondyls likely engaged in spatial niche partitioning between drier and wetter environments in the Early Permian as large synapsids and large temnospondyls such as *Eryops megacephalus* reached comparable sizes, but temnospondyl sizes range often extending to larger sizes than coexisting piscivorous synapsids in semi-aquatic environments (Romer 1966; Benton, 2014; Van Valkenburgh and Jenkins, 2002). Niche partitioning between synapsids and temnospondyls, and between basal-most synapsids and sphenacodontians, reflects spatial specialisation as a consequence of each clade's suitability to terrestrial predation (Bakker, 1975); sphenacodontians exhibit greater postcranial robusticity and postural changes that are indicative of more efficient terrestrial locomotion (Gould, 1967),

allowing them to better adapt to increasingly land-based predator-prey interactions than coeval ophiacodonts or water-bound temnospondyls (**Olson, 1966; Brocklehurst and Brink, 2017**).

- **Dynamic trophic interactions and key advances in therapsid evolution –** Patterns of synapsid carnivore faunal succession may also relate to a drive towards 'all-terrain, all-weather' (ATAW) mobility (and foraging capability). The rise of therapsids in the Middle Permian is also attributed to enhanced suitability to dry environments as well as the ecological release following Olson's extinction (Palomares et al., 1998; Kemp, 2005; Berger & Gese, 2007). The first therapsids were likely small-medium sized speed specialists (Figs. 3.1.5, 7; Supplementary Fig. 3.1.S7), with *Tetraceratops insignis* offering a glimpse of stem therapsid ecomorphology (Spindler, 2020); its strong mandibular robusticity, mid-range biting efficiency and moderate bite speed suggest it was an active predator (Fig. 3.1.1). Comparison of *Tetraceratops* and basal therapsid jaw morphofunction with Kungurian sphenacodontids indicates low potential for competition (Figs. 3.1.1, 6-7; Supplementary Fig. 3.1.S4**).** Furthermore, basal-most therapsid (biarmosuchian) postcranial morphology closely resembles that of sprawling sphenacodontids (Kemp, 1978; 2005) dispelling ideas of significant early therapsid locomotive superiority. Greater therapsid ecomorphological diversity and body sizes following Olson's extinction is consistent with a passive opportunistic replacement model for the basal synapsid-therapsid turnover (Cleal and Thomas, 2005; Kemp, 2005) (Figs. 3.1.1-2, 5, 7; Supplementary Fig. 3.1.S7). However, the evolution of more slender limbs and parasagittal gaits in theriodonts (Sues, 1986; Sigogneau-Russell, 1989; Kemp, 1978; 2005) illustrates their increasing locomotory efficiency, and this may have influenced patterns of niche partitioning and evolution in later therapsids. The evolution of greater locomotory efficiency provided theriodonts with a competitive advantage over biarmosuchians and dinocephalians, allowing theriodonts to engage in more dynamic predator-prey interactions. This may have enabled theriodonts to engage in more efficient foraging and so overtake basal therapsids within carnivorous niches through the Capitanian (Fig. 3.1.6). High intrinsic pressure stemming from highly diverse carnivore communities from the Capitanian onwards would have been a strong driver for the evolution of improved locomotory efficiency in synapsid carnivores. Greater speed or endurance would help carnivores to engage in different hunting strategies, and increased efficiency may have supported the eutheriodont trophic shift towards targeting smaller, more active prey in the Late Permian. Furthermore, the adaptive flexibility offered by greater locomotory efficiency may have driven gorgonopsian-therocephalian niche partitioning between power-shearer and speed specialist FFGs (Figs. 3.1.6-7) as it allowed therocephalians to break out of their Wordian hypercarnivorous niches into fast,

small mesocarnivore roles (Brocklehurst, 2019) that were largely unavailable to gorgonopsians. Intriguingly, synapsid endothermy supposedly originated in the Capitanian (Kemp, 2006b; Benton, 2020) and may stem from this heightened intrinsic pressure as it drove niche partitioning into more specialised mesocarnivorous niches, with these smaller carnivores requiring more regular nourishment (Bakker, 1975; Kemp, 2006b; Hopson, 2012; De Cuyper et al., 2019).

New herbivores created new prey resources for carnivores supporting the early synapsid shift from mesocarnivory to primitive hypercarnivory in the Late Carboniferous (Figs. 3.1.2, 6-8). The decisive shift from lycophyte rainforests to fern-dominated, fluvial environments in the Kasimovian (DiMichele et al., 2009; 2011; Huttenlocker et al., 2021), saw the first radiation of tetrapod herbivores, establishing diverse herbivore faunas that persisted through the Early Permian (Olson, 1962; 1966; Sues and Reisz, 1998; Brocklehurst and Brink, 2017; Brocklehurst et al., 2020), mirroring the relative stasis of carnivorous basal synapsids (Fig. 3.1.2). The evolution of terrestrial megapredatory therapsids in the Middle Permian coincided with the reestablishment of favourable climatic conditions (Metcalfe et al., 2015) and successive diversifications of large synapsid and parareptile herbivores (Olson, 1962; 1966; Brocklehurst et al., 2013; 2020) (Fig. 3.1.8). The impacts of increasing large herbivore diversity are demonstrated in the shared evolution of traits reflecting increasing tetrapod on tetrapod predation across therapsid carnivores. Dinocephalians, biarmosuchians and gorgonopsians all evolved interdigitating upper and lower incisors, enlarged canines, highly developed reflected laminae and robust symphyses, alongside larger body sizes (Figs. 3.1.1-2, 7) (Romer, 1966; Kemp, 1969; 2005). Gorgonopsians also developed propalinal lower jaw movement to enable wider gapes and rapid tooth replacement (Hopson, 1964; Kemp, 1969; Bendel et al., 2018; Lautenschlager et al., 2020). Furthermore, increased robusticity, particularly in dinocephalians and rubidgeine gorgonopsids (Kammerer, 2011; 2016) (Figs. 3.1.1-2; Supplementary Fig. 3.1.S4), supported greater resistance to internal and external loads during prey capture and highlights further specialisation to megacarnivory (Slater et al., 2009). The increased energetic constraints on larger carnivores (Stephens and Krebs, 1986; Williams et al., 2014) would have driven more antagonistic interference competition, echoing size-based intraguild relationships in present faunas (Caro and Stone, 2003; Périquet and Revilla, 2015), forcing further niche partitioning of available prey resources and boosting carnivore ecomorphological diversity. Increasing ecomorphological segregation between FFGs and clades (Figs. 3.1.2, 6-8; Supplementary Fig. 3.1.S8) illustrates the intrinsic origins of high ecological diversity in the synapsid carnivore communities of the late Palaeozoic (Benton et al., 2004; Roopnarine and Angielczyk, 2012). Carnivore diversification

through the late Palaeozoic fostered ecosystem complexification; new taxa added complexity to terrestrial ecosystems by installing multiple levels within their trophic networks, with the evolution of sphenacodontian hypercarnivores in the Carboniferous and neotherapsids in the Capitanian adding progressively more dynamism to terrestrial predator-prey interactions. The concurrence of intense intervals of carnivore size and mandibular evolution with changes in herbivore faunas (Fig. 3.1.8) indicates a co-macroevolutionary relationship through deep time (Olson, 1966; Brocklehurst et al, 2013; 2020; Reisz and Fröbisch, 2014). These findings support a “Red Queen” macroevolutionary dynamic (Van Valen, 1973; Quental and Marshall, 2013; Voje et al., 2015; Condamine et al., 2019; Hautmann, 2020), and stress how macroevolution reflects the intersection of extrinsic and intrinsic selective pressures.

Supplementary Materials:

Supplementary Methods.

Functional Characters:

1. Mean Anterior Mechanical Advantage: A measure of biting efficiency at the anterior of the mandible (Westneat, 1994). This is the ratio of the inlever to the outlever, using the distance from the jaw joint to the anterior-most tip of the toothrow/dentary as the outlever. The distance from the jaw adductor muscle attachment to the jaw joint represents the inlever. This ratio of inlever to outlever gives the lowest possible value of MA.
2. Mean Posterior Mechanical Advantage: A measure of biting efficiency at the posterior of the mandible (Westneat, 1994). This is the ratio of the inlever to the outlever, using the distance from the jaw joint to the posterior-most point of the toothrow/dentary as the outlever. The distance from the jaw adductor muscle attachment to the jaw joint represents the inlever. This ratio of inlever to outlever gives the highest possible value of MA.
3. Opening Mechanical Advantage: A measure of biting velocity (Westneat, 1994). This is the ratio of the maximum inlever to the maximum outlever, using the distance from the jaw joint to the posterior-most point of the mandible/retroarticular process for the inlever, and using the distance from the jaw joint to the posterior-most point of the toothrow/dentary as the outlever. Opening MA is linked to feeding patterns and prey selection (Anderson and Westneat, 2007; Stubbs et al., 2013).

   Characters 1-3 are based on using lever mechanics to describe mandibular function, with the jaw acting as a third-order lever system (Westneat, 1994; 2004). The adductor musculature acts as the input force, the craniomandibular joint acts as the fulcrum and the output force is exerted along the toothrow/shearing surface. Herbivores often exhibit higher MA values than faunivores (Stayton, 2006). Levers are measured from the craniomandibular joint/jaw articulation. Taxa with low MA exhibit weak, rapid bites (Wainwright and Richard, 1995; Stubbs et al., 2013), whilst taxa with a strong bite force have a high MA. It should be noted that use of mean MA values for characters 1 and 2 rather than MA for each of the main jaw muscle groups probably reduces the signal of therapsid jaw musculature modifications. This is further compounded by the emergence of the therapsid reflected lamina of the angular, which is thought to anchor additional muscles originating from the pectoral girdle that acted as a primitive version of the digastric muscle seen in modern mammals (Kemp, 2005).

4. Relative Maximum Aspect Ratio: A proxy for the second moment of area, previously used in 2D analyses of jaw mechanics (Anderson, 2011; Stubbs et al., 2013). Generated by dividing the maximum depth of the mandible by its total length. The second moment of area is typically used to assess the resistance of a beam to bending under loading and when applied to jaws gives indication of the pressures experienced during biting. It essentially requires calculation of the cross-sectional area of the mandible, and so needs additional measurements that were often not available from lateral view images sourced from the literature. In most wide-ranging macroevolutionary analyses of anatomy (Anderson, 2011; Stubbs et al., 2013, MacLaren et al., 2017; Kilbourne, & Hutchinson, 2019), the second moment of area calculations assume a generalised jaw shape, treating it as a cylinder or rectangular beam, and this 2D approach takes this principle further by making a more basic approximation of the jaw that doesn't require 3D data. Most mandibles primarily experience dorsoventral stress during feeding function, the maximum aspect ratio measurement used here captures a more general approximation of dorsoventral robusticity and therefore, represents a measure of flexural stiffness (MacLaren et al., 2017) that can be widely applied across all sampled taxa.
5. Relative Toothrow Length: A measure of relative length of the dentition and its purported importance in trophic behaviour (Button et al., 2014). Generated by dividing the length of the toothrow/shearing surface by the total length of the mandible. A longer toothrow enables a greater range of MA along the jaw and likely increased use of the dentition in jaw functionality (either for food ingestion or processing/mastication). Herbivores tend to show relatively shortened toothrows compared to faunivores and omnivores (Sues, 2000).
6. Relative Symphysis Length: A measure of symphyseal robusticity generated by dividing the length of the symphysis by the total length of the mandible. The symphysis is subject to significant bending, shear, and torsional stress during biting action and so is highly related to transmission of muscle and biting force and feeding ecology and overall jaw mechanics (Daegling, 2001; Jones et al., 2012).
7. The symphyseal angle is measured between the ventral jaw line and a line parallel to the long axis of the mandibular symphysis. It affects symphyseal resistance to the bending, shear, and torsional stresses that occur during the bite cycle (Daegling, 2001). The symphyseal angle is known to affect food processing in modern herbivorous rhynchocephalians (Jones et al., 2012) and is of major importance in the mechanical response of modern crocodylians to biting, twisting, and shaking (Porro et al., 2011; Walmsley et al., 2013).

8. Relative Offset of Articulation: The articulation offset is measured as the length of the line perpendicular to the tangent of the mandibular toothrow (extrapolated from the anterior and posterior ends of the toothrow to account for jaw curvature) which intersects the articular joint (Anderson et al., 2011; MacLaren et al., 2017). This value is then divided by the total jaw length. An offset between the toothrow and jaw articulation affects dental occlusion and leverage of the jaw musculature (Janis, 1995). A small articulation offset indicates 'scissor-like' occlusion, which is typical of carnivorous taxa. Herbivores generally exhibit greater toothrow-articular offset as this enables simultaneous occlusion along the entirety of the toothrow, supporting gripping & crushing actions (Ramsay and Wilga, 2007).

Supplementary Materials

Supplementary Figures.

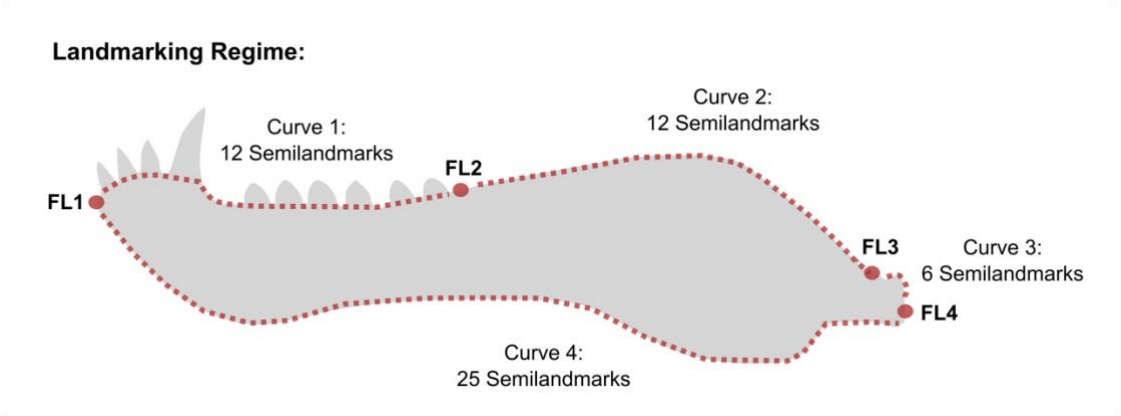

Supplementary Figure 3.1.S1. Landmarking regime for shape geometric morphometric analyses. morphospaces. Fixed landmarks (four) and semi-landmark curves (totalling 55 semi-landmarks) represented by circles and dotted lines, respectively. Abbreviations: FL, Fixed landmark.

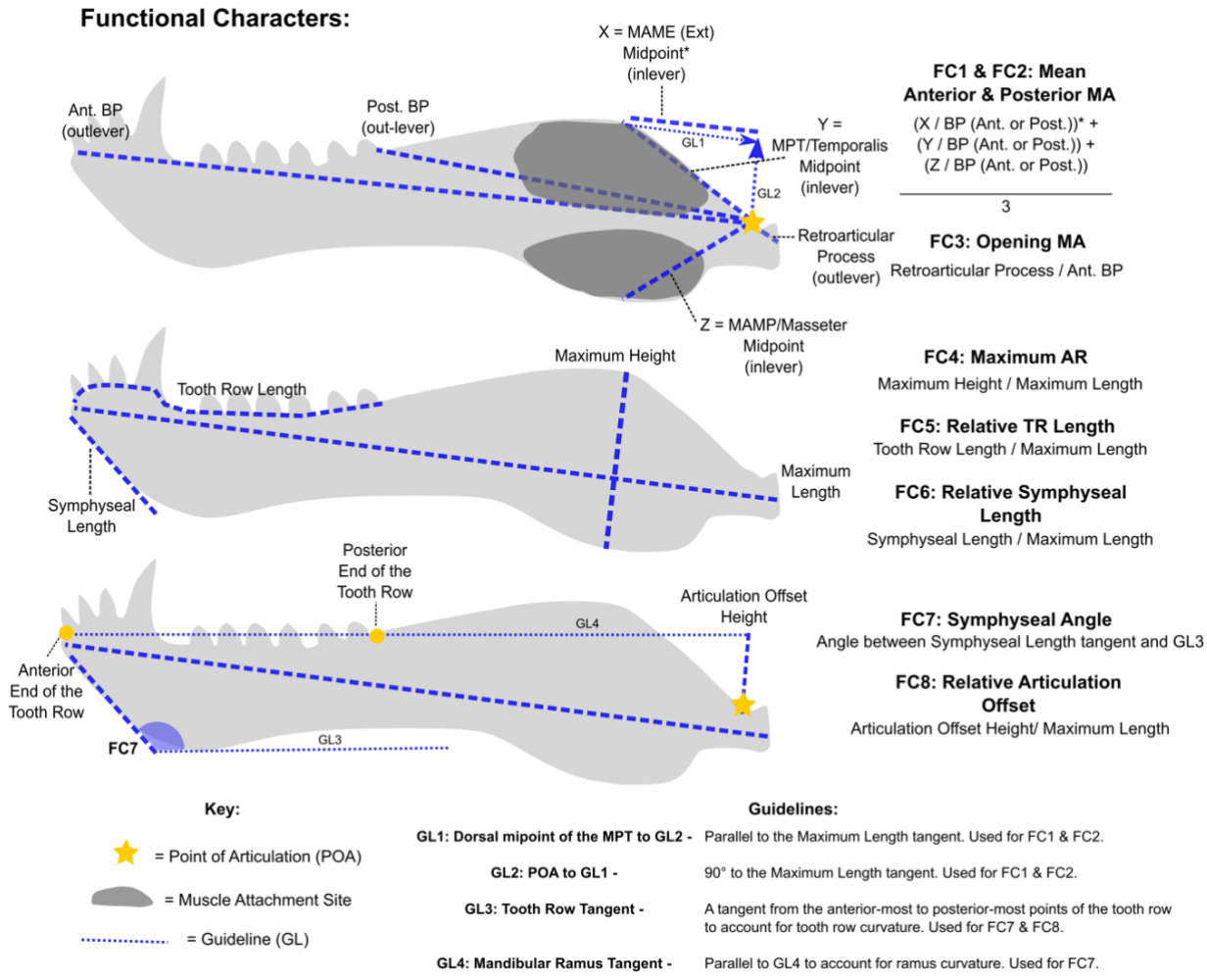

Supplementary Figure 3.1.S2. Functional linear measurement and character guide. Guide illustrating the linear measurements recorded from the lateral view images of synapsid mandibles, and how these measurements were used to calculate the functional character data. Functional Characters = FC: 1). Mean Anterior Mechanical Advantage, 2). Mean Posterior Mechanical Advantage, 3). Opening Mechanical Advantage, 4). Relative Maximum Aspect Ratio, 5). Relative Toothrow Length, 6). Relative Symphysis Length, 7). Symphyseal angle, 8). Relative Articulation Offset. Abbreviations: Ant, Anterior. BP, Biting point. Ext, External. Post, Posterior.

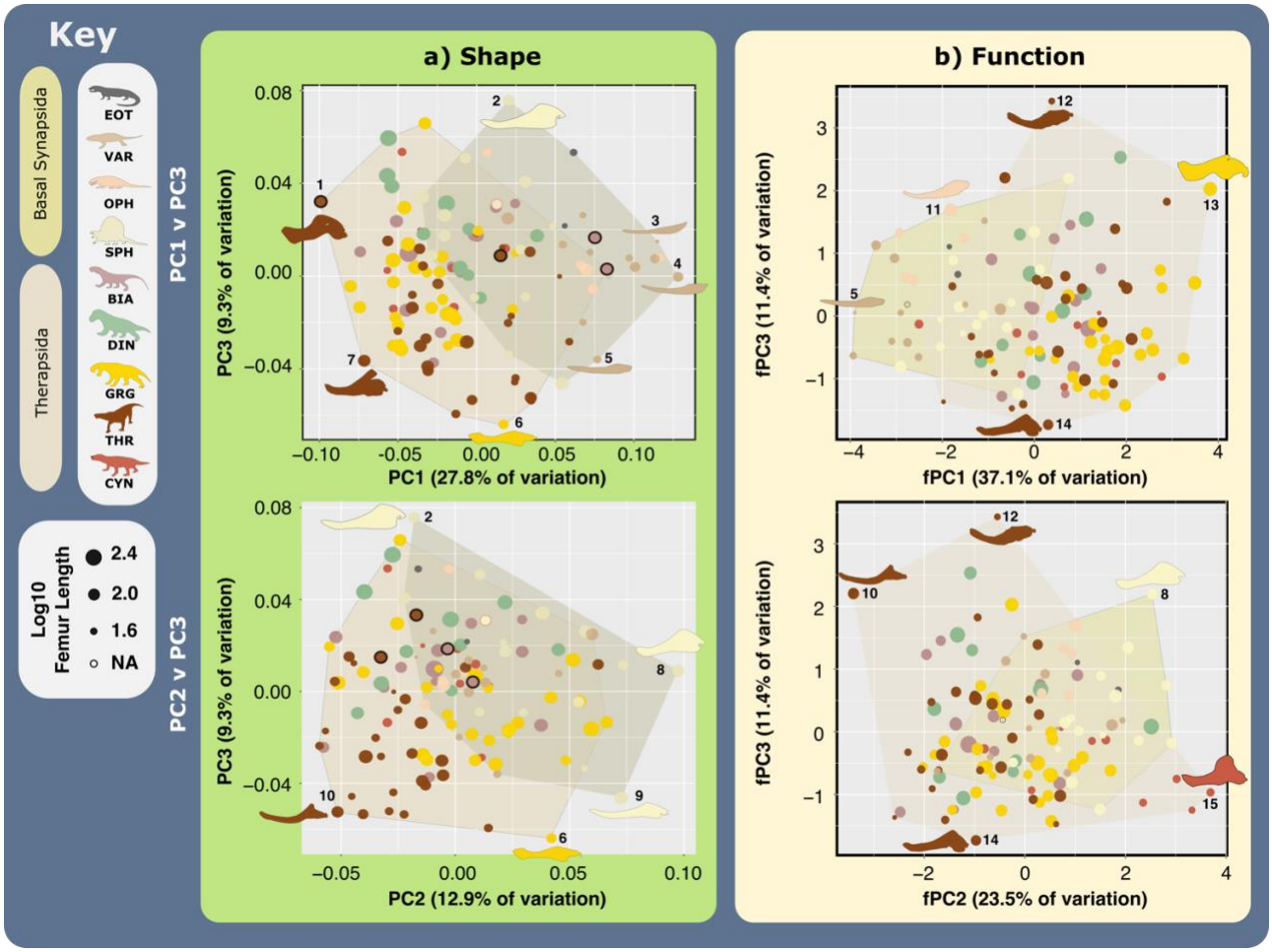

Supplementary Figure 3.1.S3. Secondary synapsid carnivore mandibular morphofunctional morphospaces. Secondary morphospaces showing distribution of taxa across principal component three. a) Mandibular shape morphospaces. b) Mandibular functional morphospaces. Overall basal synapsid and therapsid morphospace occupation shown through shaded convex hulls. N=123. Mandible silhouettes: 1. Purlovia maxima, 2. Dimetrodon natalis, 3. *Archaeovenator hamiltonensis*, 4. *Varanodon agilis*, 5. *Mycterosaurus longiceps*, 6. *Aleurosaurus felinus*, 7. *Glanosuchus macrops*, 8. *Sphenacodon ferox*, 9. *Secodontosaurus obtusidens*, 10. *Lycideops longiceps,* 11. *Ophiacodon retroversus*, 12. *Ophidostoma tartarinovi*, 13. *Dinogorgon rubidgei,* 14. *Viatokosuchus sumini*, 15. *Vetusodon elikhulu*. Abbreviations: BIA, Biarmosuchia. CYN, Cynodontia. DIN, Dinocephalia. EOT, Eothyrididae. fPC, functional principal component. GRG, Gorgonopsia, OPH, Ophiacodontidae. PC, Principal component. SPH, Sphenacodontia (non-therapsid). THR, Therocephalia. VAR, Varanopidae.

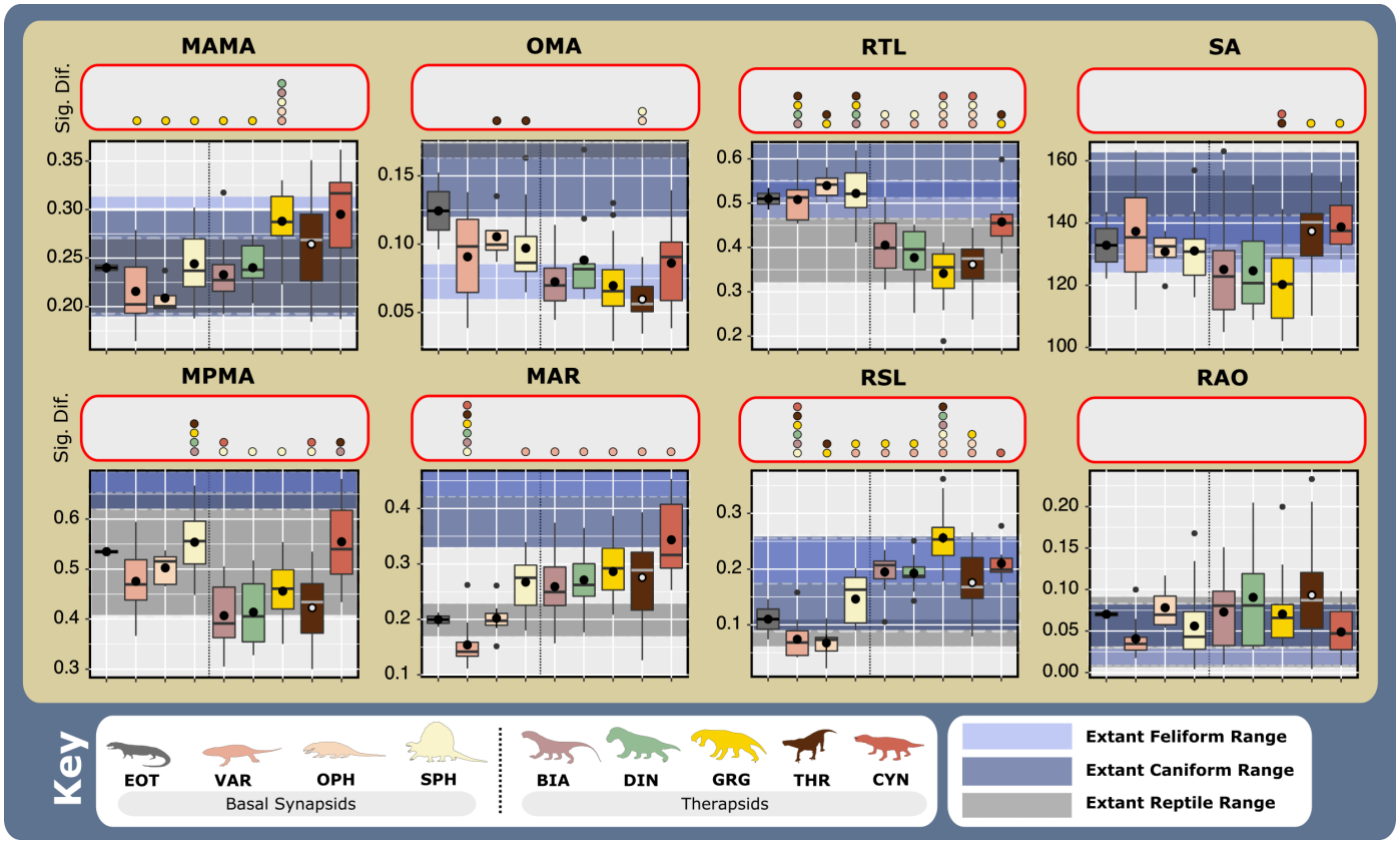

Supplementary Figure 3.1.S4. Synapsid carnivore mandibular functional character distributions. Boxplots illustrating group ranges across all functional characters with extant mammalian and reptile ranges (shaded). Statistically significant differences (<0.05) between groups highlighted by clade colour-coded circles. N=123. Abbreviations: BIA, Biarmosuchia. CYN, Cynodontia. DIN, Dinocephalia. EOT, Eothyrididae and assorted Casesauria. GRG, Gorgonopsia, MAMA, Mean anterior mechanical advantage. MAR, Maximum aspect ratio. MPMA, Mean posterior mechanical advantage. OMA, Opening mechanical advantage. OPH, Ophiacodontidae. RAO, Relative articulation offset. RSL, Relative symphyseal length. RTL, Relative toothrow length. SA, Symphyseal angle. SPH, Sphenacodontia (non-therapsid). THR, Therocephalia. VAR, Varanopidae.

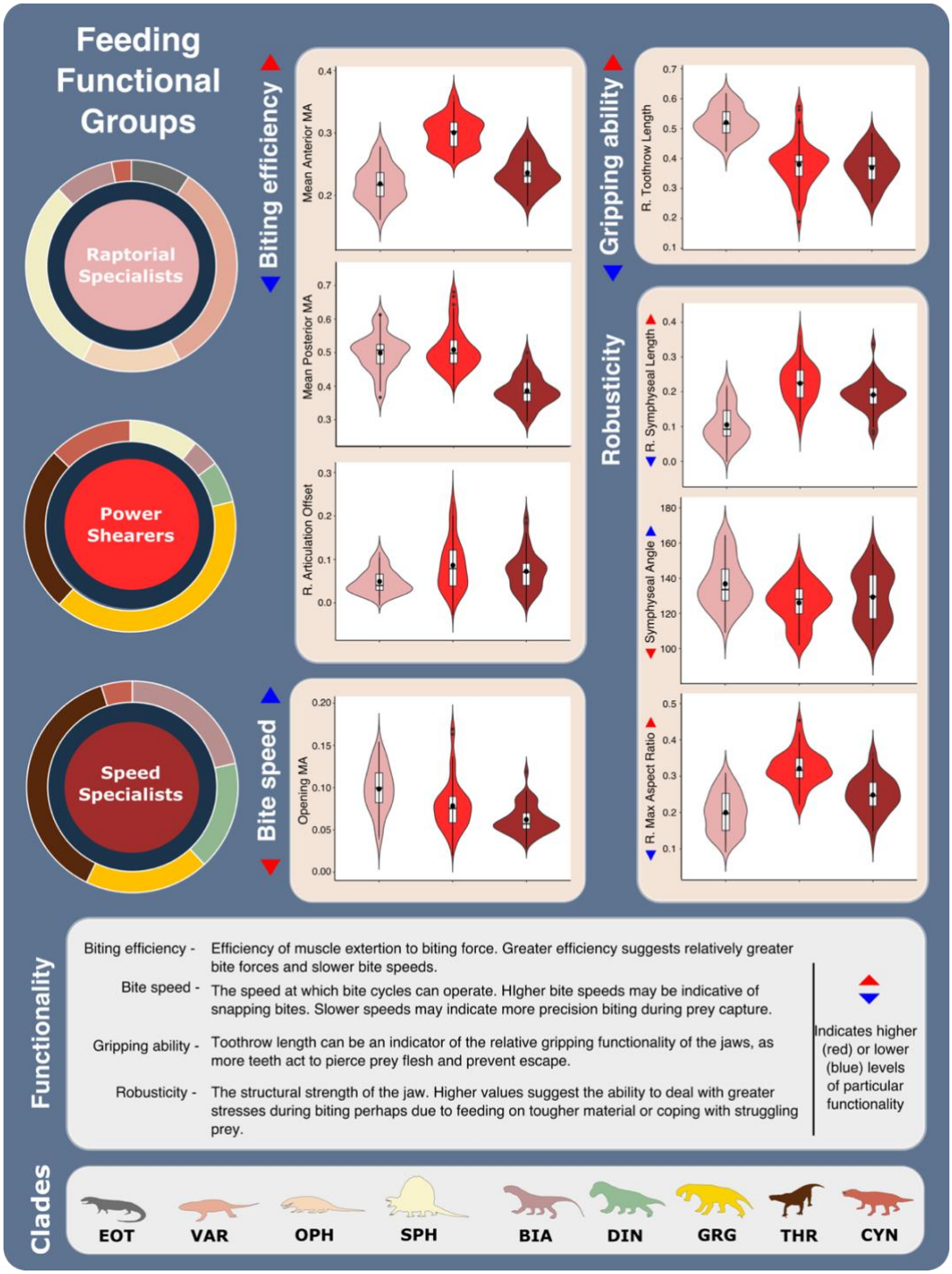

Supplementary Figure 3.1.S5. Synapsid carnivore feeding functional group mandibular characteristics. The feeding functional group mandibular functional character distributions illustrated using violin and box plots. Feeding functional group compositions illustrated using ring plots detailing relative proportions of different taxonomic groups. Mean values indicate by black dots. Coloured arrows indicate whether values increase (red) or decrease (blue)

relevant mandible functionality. N=123. Abbreviations: BIA, Biarmosuchia. CYN, Cynodontia. DIN, Dinocephalia. EOT, Eothyrididae and assorted Casesauria. GRG, Gorgonopsia, MAMA, Mean anterior mechanical advantage. MAR, Maximum aspect ratio. MPMA, Mean posterior mechanical advantage. OMA, Opening mechanical advantage. OPH, Ophiacodontidae. RAO, Relative articulation offset. RSL, Relative symphyseal length. RTL, Relative toothrow length. SA, Symphyseal angle. SPH, Sphenacodontia (non-therapsid). THR, Therocephalia. VAR, Varanopidae.

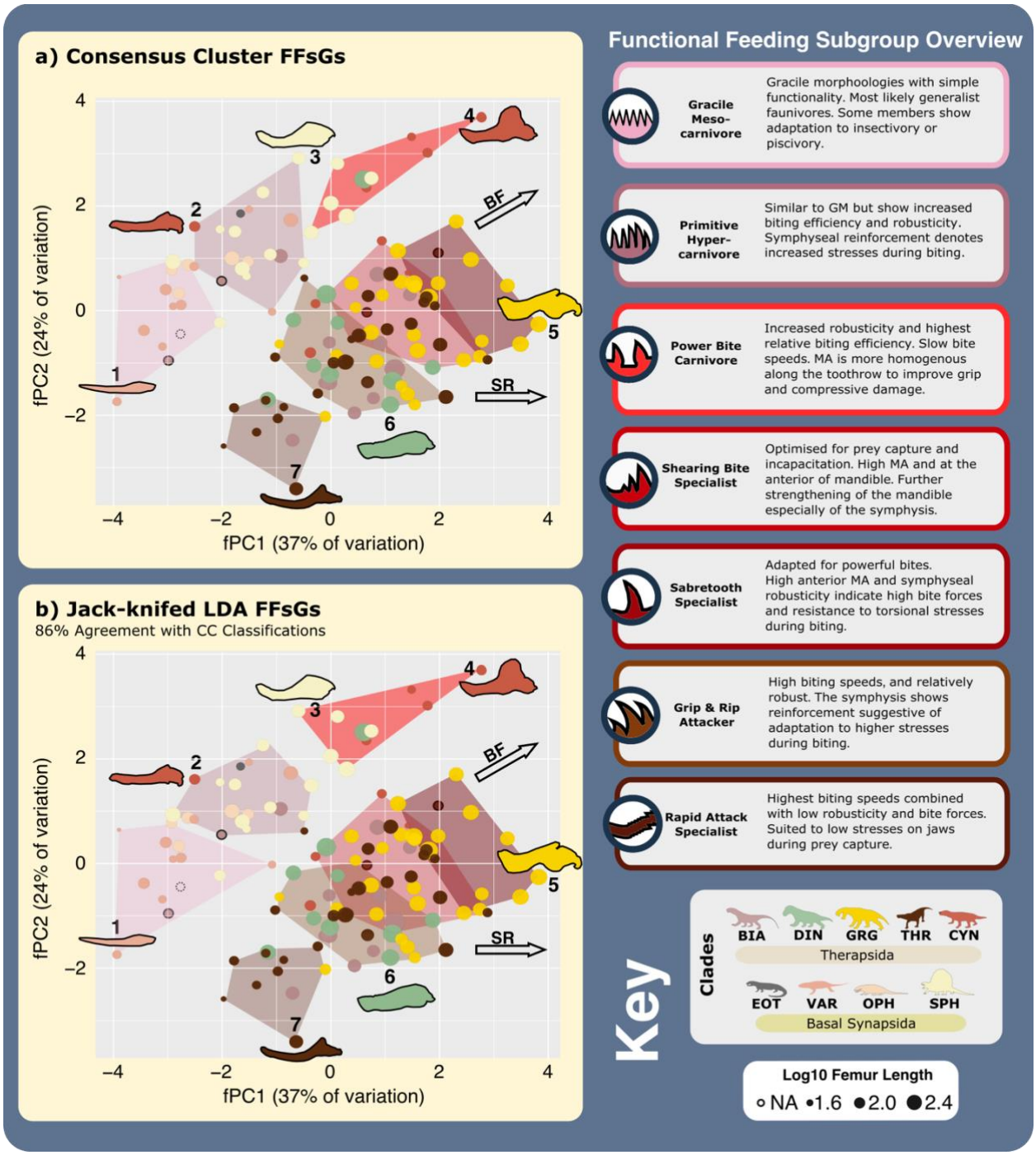

Supplementary Figure 3.1.S6. Synapsid carnivore feeding functional group validation.
a) Consensus cluster analysis feeding functional subgroups of synapsid carnivores mapped onto their functional morphospace. b) The feeding functional subgroups of synapsid carnivores resulting from a linear discriminant analysis after a jack-knifing test, mapped onto the functional morphospace. N=123. Abbreviations: BF, Biting force. BIA, Biarmosuchia. CC, Consensus cluster. CYN, Cynodontia. DIN, Dinocephalia. EOT, Eothyrididae and assorted Casesauria. FFsGs, Feeding functional subgroups. fPC, Functional principal components. GM, Gracile mesocarnivores. GRG, Gorgonopsia, LDA, Linear discriminant analysis. MA, Mechanical advantage. OPH, Ophiacodontidae. SPH, Sphenacodontia (non-therapsid). SR, Symphyseal robusticity. THR, Therocephalia. VAR, Varanopidae.

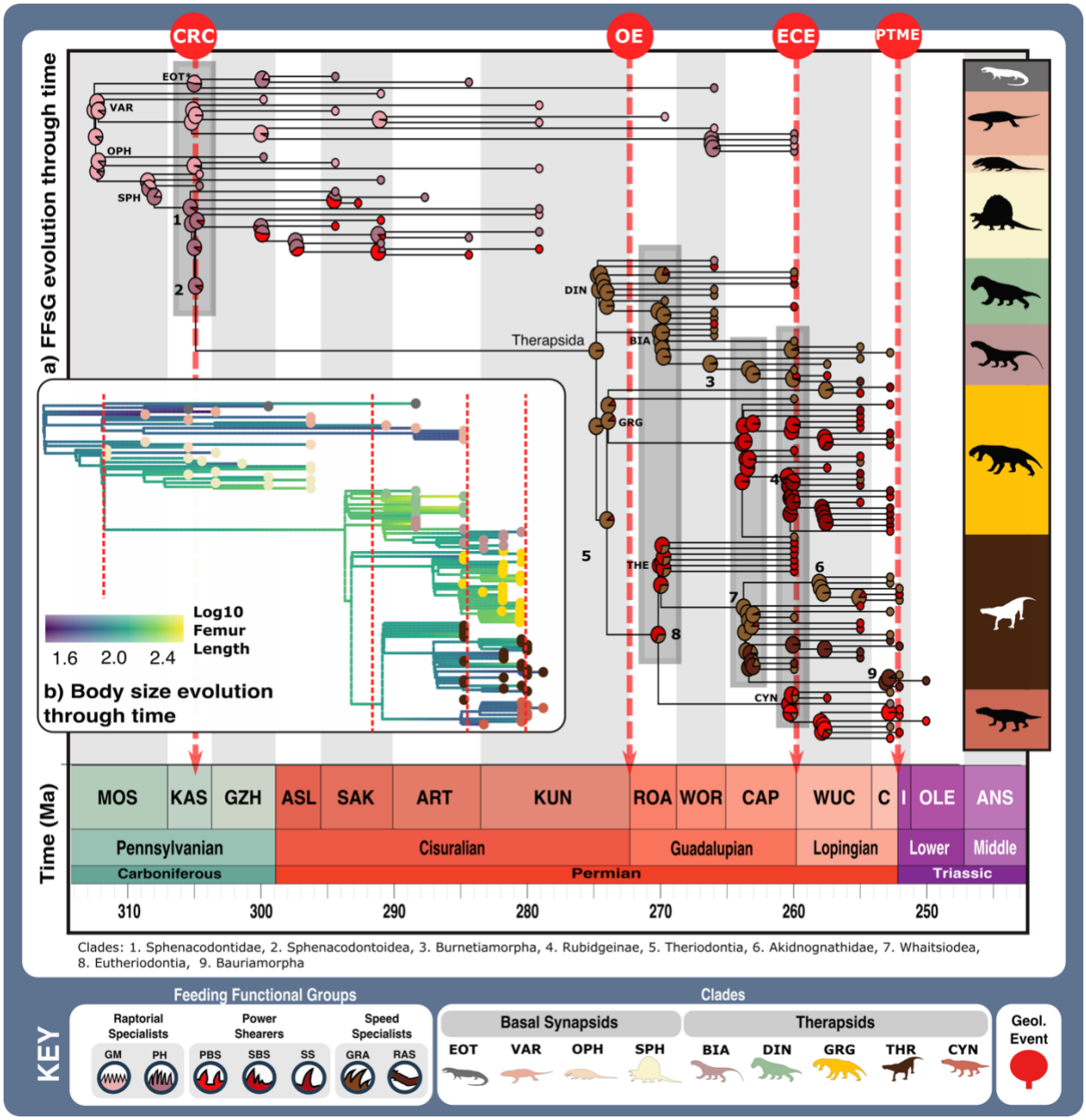

Supplementary Figure 3.1.S7. Alternative synapsid carnivore ecomorphological evolution through the late Palaeozoic. a) Feeding functional subgroup states cross the carnivorous synapsid phylogeny with reconstructed ancestral character state likelihoods under an equal rates model of character transitions denoted by pie charts at node positions. Positions of key clades indicated by numbers in bold across the phylogeny. Pulses of diversification highlighted with shaded boxes. b) Body size evolution across the carnivorous synapsid phylogeny through time. Body size represented by Log_{10} femur length, with colour denoting low or high values (see scale). Key geological events shown. N=123. Abbreviations: ART, Artinskian. ASL, Asselian. BIA, Biarmosuchia. CAP, Capitanian. CHX, Changhsingian. CYN, Cynodontia. DIN, Dinocephalia. ECE, End-Capitanian extinction. EOT, Eothyrididae and

assorted Casesauria. ET, Early Triassic. FFsG, Feeding functional subgroup. GM, Gracile mesopredators. GRA, Grip and rip attackers. GRG, Gorgonopsia, Gz, Gzhelian. IND, Induan. Ka, Kasimovian. KUN, Kungurian. MOS, Moscovian. OE, Olson's extinction. OPH, Ophiacodontidae. PBS, Power bite specialists. PENN, Pennsylvanian. PH, Primitive hypercarnivores. PTME, Permo-Triassic mass extinction. SAK, Sakmarian. SBS, Shearing bite specialists. SPH, Sphenacodontia (non-therapsid). SS, Sabretooth specialists. RAS, Rapid attack specialists. ROA, Roadian. THR, Therocephalia. VAR, Varanopidae. WOR, Wordian. WUC, Wuchiapingian.

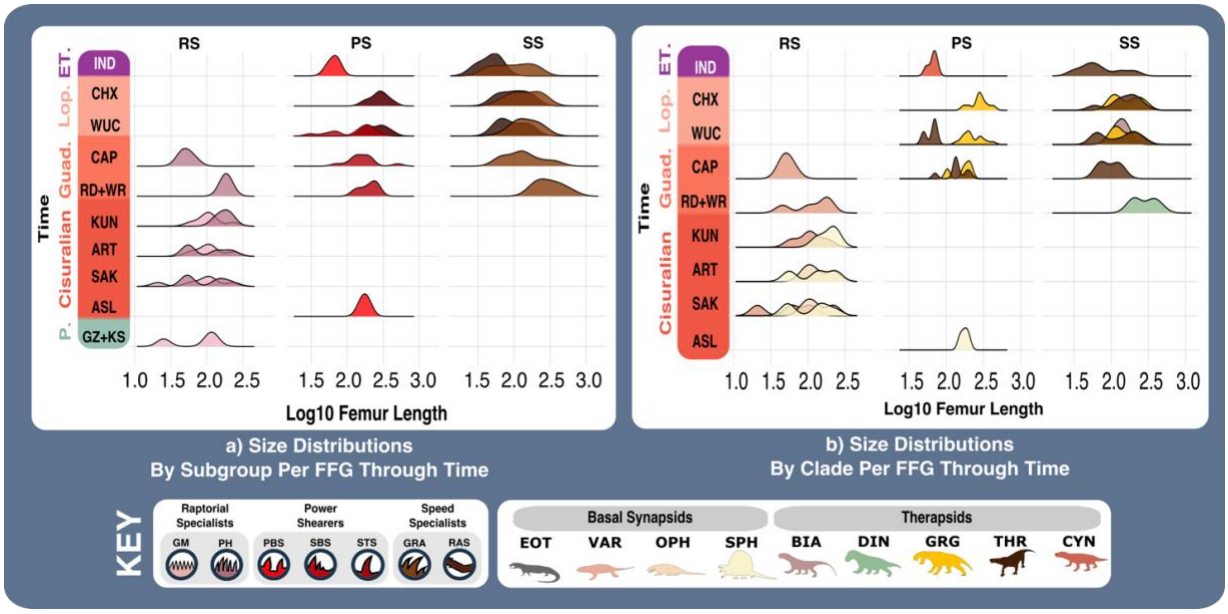

Supplementary Figure 3.1.S8. Synapsid carnivore size distributions by taxonomic and feeding functional group through the late Palaeozoic a) Distribution plots illustrating the body size ranges of feeding functional subgroups within each feeding functional group per timebin through the late Palaeozoic. b) Distribution plots illustrating the body size ranges of different taxonomic groups within each feeding functional group per timebin through the late Palaeozoic. Body size represented by $\log_{10}$ femur length. N=123. Abbreviations: ART, Artinskian. ASL, Asselian. BIA, Biarmosuchia. CAP, Capitanian. CHX, Changhsingian. CYN, Cynodontia. DIN, Dinocephalia. ET, Early Triassic. EOT, Eothyrididae and assorted Casesauria. FFG, Feeding functional group. FFsG, Feeding functional subgroup. GM, Gracile mesocarnivores. GRA, Grip and rip attacker. GRG, Gorgonopsia, GUAD, Guadalupian. GZH, Gzhelian. IND, Induan. LOP, Lopingian. OPH, Ophiacodontidae. PBS, Power bite specialist. PH, Primitive hypercarnivore. PS, Power shearer. RAS, Rapid attack specialist. RD, Roadian. RS, Raptorial specialist. SAK, Sakmarian. SBS, Shearing bite specialist. SPH, Sphenacodontia

(non-therapsid). SS, Speed specialist. STS, Sabretooth specialist. THR, Therocephalia. VAR, Varanopidae. WR, Wordian. WUC, Wuchiapingian.

Supplementary Tables.

Supplementary Table 3.1.1. PERMANOVA results for shape differences between synapsid carnivore clades. Abbreviations: BIA, Biarmosuchia. Bonf, Bonferroni-corrected. CYN, Cynodontia. DIN, Dinocephalia. EOT, Eothyrididae. GRG, Gorgonopsia, OPH, Ophiacodontidae. SPH, Sphenacodontia. SS, Sum of squares. THR, Therocephalia. VAR, Varanopidae.

Clade	Result	EOT	VAR	OPH	SPH	BIA	DIN	GRG	THR	CYN
EOT	**Raw P**		0.0319	0.3284	0.0244	0.0345	0.0158	0.0024	0.0067	0.0176
	Bonf. P		1	1	0.8784	1	0.5688	0.0864	0.2412	0.6336
	F		2.178	1.222	2.686	2.501	3.517	3.565	2.836	3.725
VAR	**Raw P**			0.0128	0.0001	0.0001	0.0001	0.0001	0.0001	0.0001
	Bonf. P			0.4608	0.0036	0.0036	0.0036	0.0036	0.0036	0.0036
	F			2.737	10.01	11.23	15.28	19.15	14.51	13.98
OPH	**Raw P**				0.0006	0.0012	0.0011	0.0001	0.0001	0.0007
	Bonf. P				0.0216	0.0432	0.0396	0.0036	0.0036	0.0252
	F				4.79	5.404	8.398	7.946	5.2	6.914
SPH	**Raw P**					0.0006	0.0001	0.0001	0.0001	0.0002
	Bonf. P					0.0216	0.0036	0.0036	0.0036	0.0072
	F					3.826	5.428	6.885	7.836	3.785
BIA	**Raw P**						0.1392	0.0001	0.0074	0.0004
	Bonf. P						1	0.0036	0.2664	0.0144
	F						1.5	3.999	2.558	3.469
DIN	**Raw P**							0.0003	0.0007	0.0001
	Bonf. P							0.0108	0.0252	0.0036
	F							3.636	3.763	3.771
GRG	**Raw P**								0.0001	0.0002
	Bonf. P								0.0036	0.0072
	F								6.15	3.682

THE	**Raw P**									0.0007
	Bonf. P									0.0252
	F									3.483
CYN	**Raw P**									
	Bonf. P									
	F									
Total	**Total SS**	1.0								
	Within-group SS	0.7								
	P	0.0001								
	F	6.107								

Supplementary Table 3.1.2. PERMANOVA results for functional differences between synapsid carnivore clades. Abbreviations: BIA, Biarmosuchia. Bonf, Bonferroni-corrected. CYN, Cynodontia. DIN, Dinocephalia. EOT, Eothyrididae. GRG, Gorgonopsia, OPH, Ophiacodontidae. SPH, Sphenacodontia. SS, Sum of squares. THR, Therocephalia. VAR, Varanopidae.

Clade	Result	EOT	VAR	OPH	SPH	BIA	DIN	GRG	THR	CYN
EOT	**Raw P**		0.3426	0.3843	0.4721	0.0243	0.0442	0.002	0.3426	0.0947
	Bonf. P		1	1	1	0.8748	1	0.072	0.0792	1
	F		1.133	0.9989	0.8613	3.132	2.367	6.851	4.074	2.598
VAR	**Raw P**			0.2115	0.0003	0.0001	0.0001	0.0001	0.0001	0.0001
	Bonf. P			1	0.0108	0.0036	0.0036	0.0036	0.0036	0.0036
	F			1.476	7.288	10.76	9.808	33.82	17.55	13.6
OPH	**Raw P**				0.0115	0.0002	0.0002	0.0001	0.0001	0.0021
	Bonf. P				0.414	0.0072	0.0072	0.0036	0.0036	0.0756
	F				3.208	7.373	6.274	20.08	10.29	8.906
SPH	**Raw P**					0.0001	0.0001	0.0001	0.0001	0.0032
	Bonf. P					0.0036	0.0036	0.0036	0.0036	0.1152
	F					9.477	7.64	22.85	15.84	4.409
BIA	**Raw P**						0.7373	0.0001	0.0105	0.0002

	Bonf. P						1	0.0036	0.378	0.0072
	F						0.5847	6.734	3.341	7.908
DIN	**Raw P**							0.0005	0.0228	0.0012
	Bonf. P							0.018	0.8208	0.0432
	F							4.685	2.725	5.924
GRG	**Raw P**								0.0001	0.0001
	Bonf. P								0.0036	0.0036
	F								9.974	9.065
THE	**Raw P**									0.0001
	Bonf. P									0.0036
	F									8.26
CYN	**Raw P**									
	Bonf. P									
	F									
Total	**Total SS**	976								
	Within-group SS	590								
	P	0.0001								
	F	9.239								

Supplementary Table 3.1.3. PERMANOVA results for significant differences between synapsid carnivore mandibular shape and function between geological stages. Abbreviations: ART, Artinskian. ASL, Asselian. Bonf. Bonferroni corrected. CAP, Capitanian. CHX, Changhsingian. GZH, Gzhelian. IND, Induan. KAS, Kasimovian. KUN, Kungurian. SAK, Sakmarian. ROA, Roadian. WOR, Wordian. WUC, Wuchiapingian.

	Shape			**Function**		
Stage Transitions	P	Bonf. P	F	P	Bonf. P	F
KAS>GZH	0.3003	1	1.434	0.205	1	1.766
GZH>ASL	0.285	1	1.187	0.2056	1	1.527
ASL>SAK	0.7297	1	0.555	0.6513	1	0.6113

SAK>ART	0.9754	1	0.2388	0.9582	1	0.1822
ART>KUN	0.9812	1	0.2344	0.8697	1	0.3373
KUN>ROA	0.9027	1	0.3793	0.6179	1	0.6559
ROA>WOR	0.1649	1	1.512	0.1686	1	1.544
WOR>CAP	0.3566	1	1.045	0.3913	1	1.019
CAP>WUC	0.0723	1	1.641	0.0153	1	2.905
WUC>CHX	0.9998	1	0.2543	0.8109	1	0.4438
CHX>IND	0.1737	1	1.334	0.1181	1	1.812
Total	0.0001	-	3.071	0.0001	-	5.384
Total sum of squares:	1.491			1452		
Within-group sum of squares:	1.234			1065		

Supplementary Table 3.1.4. PERMANOVA results for significant differences between synapsid carnivore mandibular shape and function between feeding functional groups. Abbreviations: Bonf. Bonferroni corrected. SS, Sum of squares.

Feeding Functional Group	**Result**	**Power Specialists**		**Speed Specialists**	
		Shape	**Function**	**Shape**	**Function**
Raptorial Specialists	**Raw P**	0.0001	0.0001	0.0001	0.0001
	Bonf. P	0.0003	0.0003	0.0003	0.0003
	F	25.87	47.66	15.76	37.14
Power Specialists	**Raw P**			0.0001	0.0001
	Bonf. P			0.0003	0.0003
	F			8.171	26.71
Total		**Shape**		**Function**	
	Total SS	1.003		976	
	Within-group SS	0.7867		602.3	
	P	0.0001		0.0001	
	F	16.35		36.92	

Supplementary Table 3.1.5. PERMANOVA results for significant differences in synapsid carnivore mandibular shape between feeding functional subgroups. Abbreviations: Bonf. Bonferroni corrected. SS, Sum of squares.

Feeding Functional Group	Result	Gracile Meso-carnivore	Primitive Hyper-carnivore	Power Bite Specialist	Shearing Bite Specialist	Sabretooth Specialist	Grip and Rip Attacker	Rapid Attack specialist
Gracile Meso-carnivore	**Raw P**		0.0001	0.0001	0.0001	0.0001	0.0001	0.0001
	Bonf. P		0.0021	0.0021	0.0021	0.0021	0.0021	0.0021
	F		5.884	18.07	23.04	20.58	19.96	7.076
Primitive Hyper-carnivore	**Raw P**			0.0001	0.0001	0.0001	0.0001	0.0001
	Bonf. P			0.0021	0.0021	0.0021	0.0021	0.0021
	F			6.679	10.51	10.63	8.666	5.742
Power Bite Specialist	**Raw P**				0.0021	0.0001	0.0001	0.0001
	Bonf. P				0.0441	0.0021	0.0021	0.0021
	F				2.592	3.553	5.526	9.809
Shearing Bite Specialist	**Raw P**					0.0001	0.0006	0.0001
	Bonf. P					0.0021	0.0126	0.0021
	F					3.273	2.761	7.566
Sabretooth Specialist	**Raw P**						0.0001	0.0001
	Bonf. P						0.0021	0.0021
	F						6.195	9.327
Grip and Rip Attacker	**Raw P**							0.0001
	Bonf. P							0.0021
	F							4.612
Rapid Attack specialist	**Raw P**							
	Bonf. P							
	F							
Total	**Total SS**			1.003				

	Within-group SS	0.6882
	P	0.0001
	F	8.764

Supplementary Table 3.1.6. PERMANOVA results for significant differences in synapsid carnivore mandibular function between feeding functional subgroups. Abbreviations: Bonf. Bonferroni corrected. SS, Sum of squares.

Feeding Functional Group	Result	Gracile Meso-carnivore	Primitive Hyper-carnivore	Power Bite Specialist	Shearing Bite Specialist	Sabretooth Specialist	Grip and Rip Attacker	Rapid Attack specialist
Gracile Meso-carnivore	**Raw P**		0.0001	0.0001	0.0001	0.0001	0.0001	0.0001
	Bonf. P		0.0021	0.0021	0.0021	0.0021	0.0021	0.0021
	F		10.28	28.13	49.37	52.98	33.52	17.4
Primitive Hyper-carnivore	**Raw P**			0.0001	0.0001	0.0001	0.0001	0.0001
	Bonf. P			0.0021	0.0021	0.0021	0.0021	0.0021
	F			10.67	24.84	32.11	28.47	24.84
Power Bite Specialist	**Raw P**				0.0001	0.0001	0.0001	0.0002
	Bonf. P				0.0021	0.0021	0.0021	0.0042
	F				11.47	10.21	23.05	29.93
Shearing Bite Specialist	**Raw P**					0.0001	0.0001	0.0001
	Bonf. P					0.0021	0.0021	0.0021
	F					23.89	13.04	23.89
Sabretooth Specialist	**Raw P**						0.0001	0.0001
	Bonf. P						0.0021	0.0021
	F						15.05	31.97
	Raw P							0.0001
	Bonf. P							0.0021

Grip and Rip Attacker	**F**							8.971
Rapid Attack specialist	**Raw P**							
	Bonf. P							
	F							
Total	**Total SS**			976				
	Within-group SS			445.4				
	P			0.0001				
	F			22.83				

Supplementary Table 3.1.7. Mann-Whitney U test results for significant body size changes in synapsid carnivores between geological stages. Abbreviations: ART, Artinskian. ASL, Asselian. Bonf. Bonferroni corrected. CAP, Capitanian. CHX, Changhsingian. GZH, Gzhelian. IND, Induan. KAS, Kasimovian. KUN, Kungurian. SAK, Sakmarian. ROA, Roadian. WOR, Wordian. WUC, Wuchiapingian.

	Body Size		
Stage>Transitions	P	Bonf. P	U Value
KAS>GZH	0.7728	1	3
GZH>ASL	0.2997	1	4.5
ASL>SAK	0.9362	1	17
SAK>ART	0.786	1	27
ART>KUN	0.5329	1	32.5
KUN>ROA	0.9187	1	11
ROA>WOR	0.2565	1	11.5
WOR>CAP	0.0322	1	87.5
CAP>WUC	0.5651	1	431
WUC>CHX	0.4066	1	491.5
CHX>IND	0.0006	0.03847	46

Supplementary Table 3.1.8. Internal validation statistics for cluster configurations. Results for analyses run with all taxa, and each identified functional feeding group. Abbreviations: FFG, Feeding functional group. MDB, mean distance between cluster centroids. MDC, mean distance from cluster

centroid. PAM, partition around medoids. pF Value, pseudo F value. WSS, within cluster sum of squares.

Internal Validation Index	Data	Clustering Methods		
		Hierarchical	K-means	PAM
WSS	All Taxa	914.7134	596.4908	597.3226
	FFG1	145.131	145.131	145.131
	FFG2	186.527	184.6536	201.9363
	FFG3	113.1085	111.3767	133.4041
MDC	All Taxa	3.727941	3.023226	3.024016
	FFG1	2.574005	2.574005	2.574005
	FFG2	2.76468	2.749539	2.87168
	FFG3	2.589147	2.578228	2.800941
MDB	All Taxa	3.854758	4.199812	4.202307
	FFG1	3.160952	3.160952	3.160952
	FFG2	3.61181	3.622567	3.524632
	FFG3	3.22876	3.254656	3.048589
pF Value	All Taxa	1.034018	1.389182	1.389645
	FFG1	1.228029	1.228029	1.228029
	FFG2	1.306412	1.317518	1.227377
	FFG3	1.247036	1.262362	1.088416
Dunn Index	All Taxa	0.1010731	0.1636738	0.1883225
	FFG1	0.2438311	0.2438311	0.2438311
	FFG2	0.2481868	0.2283256	0.264629
	FFG3	0.3003869	0.2486065	0.3155862

Supplementary Table 3.1.9. External validation statistics for different cluster configurations. Examination of the agreement between cluster groups and phylogenetic groups, at broad and higher taxonomic resolution (**See Supplementary Data SX**), during identification of functional feeding groups and subgroups. Abbreviations: FFG, Feeding functional group. PAM, partition around medoids.

External Index	Data	Hierarchical		K-means		PAM	
		Broad	Higher	Broad	Higher	Broad	Higher
Corrected Rand Index	All Taxa	0.1852451	0.1163629	0.1852451	0.02217388	0.04268881	0.02706362
	FFG1	-0.03047528	0.01332104	-0.03047528	0.01332104	-0.03047528	0.01332104
	FFG2	0.2353576	0.142697	0.2353576	0.142697	0.1624334	0.1006176
	FFG3	0.08697908	0.09867758	0.04132803	0.053041	0.003285492	0.00740442
Meila's VI Index	All Taxa	2.1159	2.557417	2.813495	3.269911	2.751141	3.21913
	FFG1	1.860208	2.256557	1.860208	2.256557	1.860208	2.256557
	FFG2	1.45274	1.924394	1.45274	1.924394	1.663936	2.057649
	FFG3	1.969793	1.891421	1.992029	1.913657	1.999068	1.929383

Supplementary Table 3.1.10. Support for different macroevolutionary models of mandibular functional disparity evolution. Weighted Aikake Information Criterion and log-likelihood values for each model. Abbreviations: BIA, Biarmosuchia. BM, Brownian motion. BSL SYN, Basal-most synapsids. CYN, Cynodontia. DIN, Dinocephalia. EB, Early Burst. GRG, Gorgonopsia, Log. Lik, Log likelihood. OU, Ornstein-Uhlenbeck. SPH, (Non-therapsid) Sphenacodontia. THR, Therocephalia. W. AIC, Weighted Aikake Information Criterion.

Models			BM	EB	OU	Stasis	Trend
Taxonomic Groups	BSL SYN	W. AIC	0.36	0	0.08	0	0.57
		Log. Lik.	-18.8	-34.7	-18.8	-33.7	-16.8
	SPH	W. AIC	0.4	0.01	0.05	0.001	0.55
		Log. Lik.	-10.4	-11.8	-10.4	-16.5	-7.9
	BIA	W. AIC	0	81.06	3.86	0.77	3.07
		Log. Lik.	0.49	0	0.07	0.33	0.11
	DIN	W. AIC	0.4	0	0.01	0.02	0.57
		Log. Lik.	-14	-114	-14	-17	-11
	GRG	W. AIC	11.25	41.11	15.85	14.64	0
		Log. Lik.	0.004	0	0	0.001	0.1
	THE	W. AIC	0.03	0	0.01	0	0.97
		Log. Lik.	-14.5	-31.7	-14.1	-19	-8.8
	CYN	W. AIC	6.56	19.85	10	0	16.54
		Log. Lik.	0.04	0	0.01	0.96	0

Supplementary Table 3.1.11. Cluster analysis results for feeding functional groups. Colour coded to improve group recognition.

Abbreviations: HC, Hierarchical. KM, K-means. PAM, Partition around medioids.

Clade	Taxa	HC	Taxa	KM	Taxa	PAM	Taxa	consensus
Biarmosuchia	Alrausuchus tagax	1	Alrausuchus tagax	1	Alrausuchus tagax	1	Alrausuchus tagax	1
Biarmosuchia	Biarmosuchus tener	1	Biarmosuchus tener	1	Biarmosuchus tener	1	Biarmosuchus tener	1
Biarmosuchia	Herpetoskylax hopsoni	1	Herpetoskylax hopsoni	1	Herpetoskylax hopsoni	1	Herpetoskylax hopsoni	1
Biarmosuchia	Hipposaurus	1	Hipposaurus	1	Hipposaurus	1	Hipposaurus	1
Biarmosuchia	Ictidorhinus	1	Ictidorhinus	1	Ictidorhinus	1	Ictidorhinus	1
Biarmosuchia	Lemurosaurus pricei	1	Lemurosaurus pricei	1	Lemurosaurus pricei	1	Lemurosaurus pricei	1
Biarmosuchia	Lende chiweta	1	Lende chiweta	1	Lende chiweta	1	Lende chiweta	1
Biarmosuchia	Lobalopex mordax	1	Lobalopex mordax	1	Lobalopex mordax	1	Lobalopex mordax	1
Biarmosuchia	Phthinosaurus borissiaki	1	Phthinosaurus borissiaki	1	Phthinosaurus borissiaki	1	Phthinosaurus borissiaki	1
Biarmosuchia	Proburnetia viatkensis	1	Proburnetia viatkensis	1	Proburnetia viatkensis	1	Proburnetia viatkensis	1
Cyndontia	Dvinia prima	1	Dvinia prima	1	Dvinia prima	1	Dvinia prima	1
Dinocephalia	Australosyodon nyaphuli	1	Nanictosaurus kitchingi	1	Nanictosaurus kitchingi	1	Nanictosaurus kitchingi	1
Dinocephalia	Deuterosaurus biarmicus	1	Australosyodon nyaphuli	1	Australosyodon nyaphuli	1	Australosyodon nyaphuli	1
Dinocephalia	Pampaphoneus biccai	1	Deuterosaurus biarmicus	1	Deuterosaurus biarmicus	1	Deuterosaurus biarmicus	1
Dinocephalia	Syodon biarmicum	1	Pampaphoneus biccai	1	Pampaphoneus biccai	1	Pampaphoneus biccai	1
Dinocephalia	Tapinocaninus	1	Syodon biarmicum	1	Syodon biarmicum	1	Syodon biarmicum	1
Dinocephalia	Titanophoneus potens	1	Tapinocaninus	1	Tapinocaninus	1	Tapinocaninus	1
Gorgonopsia	Aelurosaurus	1	Titanophoneus potens	1	Titanophoneus potens	1	Titanophoneus potens	1
Gorgonopsia	Lycaenops ornatus	1	Aelurosaurus	1	Aelurosaurus	1	Aelurosaurus	1

Gorgonopsia	Nochnitsa geminidens	1	Aloposaurus gracilis	1	Aloposaurus gracilis	1	Aloposaurus gracilis	1
Gorgonopsia	Scylacops capensis	1	Aloposaurus tenuis	1	Aloposaurus tenuis	1	Aloposaurus tenuis	1
Therocephalia	Choerosaurus dejageri	1	Arctops willistoni	1	Arctops willistoni	1	Arctops willistoni	1
Therocephalia	Ericiolacerta parva	1	Inostrancevia latifrons	1	Inostrancevia latifrons	1	Inostrancevia latifrons	1
Therocephalia	Jiufengia jiai	1	Lycaenops ornatus	1	Lycaenops ornatus	1	Lycaenops ornatus	1
Therocephalia	Karenites ornamentatus	1	Nochnitsa geminidens	1	Nochnitsa geminidens	1	Nochnitsa geminidens	1
Therocephalia	Lycideops longiceps	1	Scylacops capensis	1	Scylacops capensis	1	Scylacops capensis	1
Therocephalia	Mupashi migrator	1	Annatherapsidus petri	1	Annatherapsidus petri	1	Annatherapsidus petri	1
Therocephalia	Olivierosuchus parringtoni	1	Choerosaurus dejageri	1	Choerosaurus dejageri	1	Choerosaurus dejageri	1
Therocephalia	Scalopodon tenuisfrons	1	Ericiolacerta parva	1	Ericiolacerta parva	1	Ericiolacerta parva	1
Therocephalia	Scaloposaurus constrictus	1	Ictidosuchoides longiceps	1	Ictidosuchoides longiceps	1	Ictidosuchoides longiceps	1
Therocephalia	Tetracynodon darti	1	Jiufengia jiai	1	Jiufengia jiai	1	Jiufengia jiai	1
Therocephalia	Viatkosuchus sumini	1	Karenites ornamentatus	1	Karenites ornamentatus	1	Karenites ornamentatus	1
Biarmosuchia	Leucocephalus wewersi	2	Lycideops longiceps	1	Lycideops longiceps	1	Lycideops longiceps	1
Biarmosuchia	Phthinosuchus discors	2	Moschorhinus kitchingi	1	Moschorhinus kitchingi	1	Moschorhinus kitchingi	1
Cyndontia	Charassognathus gracilis	2	Mupashi migrator	1	Mupashi migrator	1	Mupashi migrator	1
Cyndontia	Nanictosaurus kitchingi	2	Olivierosuchus parringtoni	1	Olivierosuchus parringtoni	1	Olivierosuchus parringtoni	1
Cyndontia	Platycraniellus elegans	2	Scalopodon tenuisfrons	1	Scalopodon tenuisfrons	1	Scalopodon tenuisfrons	1
Cyndontia	Progalesaurus lootsbergensis	2	Scaloposaurus constrictus	1	Scalopolacerta hoffmanni	1	Scaloposaurus constrictus	1

Cyndontia	Thrinaxodon liorhinus	2	Tetracynodon darti	1	Scaloposaurus constrictus	1	Tetracynodon darti	1
Cyndontia	Vetusodon elikhulu	2	Theriognathus microps	1	Tetracynodon darti	1	Theriognathus microps	1
Dinocephalia	Jonkeria sp	2	Viatkosuchus sumini	1	Theriognathus microps	1	Viatkosuchus sumini	1
Dinocephalia	Sinophoneus yumenensis	2	Leucocephalus wewersi	2	Viatkosuchus sumini	1	Leucocephalus wewersi	2
Gorgonopsia	Aelurognathus tigriceps	2	Phthinosuchus discors	2	Leucocephalus wewersi	2	Phthinosuchus discors	2
Gorgonopsia	Aloposaurus gracilis	2	Charassognathus gracilis	2	Phthinosuchus discors	2	Charassognathus gracilis	2
Gorgonopsia	Aloposaurus tenuis	2	Galesaurus planiceps	2	Charassognathus gracilis	2	Galesaurus planiceps	2
Gorgonopsia	Arctognathus	2	Platycraniellus elegans	2	Galesaurus planiceps	2	Platycraniellus elegans	2
Gorgonopsia	Arctops willistoni	2	Progalesaurus lootsbergensis	2	Platycraniellus elegans	2	Progalesaurus lootsbergensis	2
Gorgonopsia	Clelandina rubidgei	2	Thrinaxodon liorhinus	2	Progalesaurus lootsbergensis	2	Thrinaxodon liorhinus	2
Gorgonopsia	Cyonosaurus longiceps	2	Vetusodon elikhulu	2	Thrinaxodon liorhinus	2	Vetusodon elikhulu	2
Gorgonopsia	Dinogorgon rubidgei	2	Anteosaurus	2	Vetusodon elikhulu	2	Anteosaurus	2
Gorgonopsia	Dixeya	2	Jonkeria sp	2	Anteosaurus	2	Jonkeria sp	2
Gorgonopsia	Eriphostoma microdon	2	Sinophoneus yumenensis	2	Jonkeria sp	2	Sinophoneus yumenensis	2
Gorgonopsia	Gorgonops torvus	2	Aelurognathus tigriceps	2	Sinophoneus yumenensis	2	Aelurognathus tigriceps	2
Gorgonopsia	Inostrancevia alexandri	2	Arctognathus	2	Aelurognathus tigriceps	2	Arctognathus	2
Gorgonopsia	Inostrancevia latifrons	2	Clelandina rubidgei	2	Arctognathus	2	Clelandina rubidgei	2
Gorgonopsia	Leontosaurus vanderhorsti	2	Cynariops robustus	2	Clelandina rubidgei	2	Cynariops robustus	2

Gorgonopsia	Pravoslavlevia parva	2	Cyonosaurus longiceps	2	Cynariops robustus	2	Cyonosaurus longiceps	2
Gorgonopsia	Rubidgea atrox	2	Dinogorgon rubidgei	2	Cyonosaurus longiceps	2	Dinogorgon rubidgei	2
Gorgonopsia	Sauroctonus parringtoni	2	Dixeya	2	Dinogorgon rubidgei	2	Dixeya	2
Gorgonopsia	Sauroctonus progressus	2	Eriphostoma microdon	2	Dixeya	2	Eriphostoma microdon	2
Gorgonopsia	Smilesaurus ferox	2	Gorgonops torvus	2	Eriphostoma microdon	2	Gorgonops torvus	2
Gorgonopsia	Suchogorgon golubevi	2	Inostrancevia alexandri	2	Gorgonops torvus	2	Inostrancevia alexandri	2
Gorgonopsia	Sycosaurus nowaki	2	Leontosaurus vanderhorsti	2	Inostrancevia alexandri	2	Leontosaurus vanderhorsti	2
Gorgonopsia	Viatkogorgon ivakhnenkoi	2	Pravoslavlevia parva	2	Leontosaurus vanderhorsti	2	Pravoslavlevia parva	2
Sphenacodontia	Dimetrodon grandis	2	Rubidgea atrox	2	Pravoslavlevia parva	2	Rubidgea atrox	2
Sphenacodontia	Dimetrodon limbatus	2	Sauroctonus parringtoni	2	Rubidgea atrox	2	Sauroctonus parringtoni	2
Sphenacodontia	Sphenacodon ferocior	2	Sauroctonus progressus	2	Sauroctonus parringtoni	2	Sauroctonus progressus	2
Sphenacodontia	Sphenacodon ferox	2	Smilesaurus ferox	2	Sauroctonus progressus	2	Smilesaurus ferox	2
Therocephalia	Annatherapsidus petri	2	Suchogorgon golubevi	2	Smilesaurus ferox	2	Suchogorgon golubevi	2
Therocephalia	Glanosuchus macrops	2	Sycosaurus nowaki	2	Suchogorgon golubevi	2	Sycosaurus nowaki	2
Therocephalia	Gorynychus masyutinae	2	Viatkogorgon ivakhnenkoi	2	Sycosaurus nowaki	2	Viatkogorgon ivakhnenkoi	2
Therocephalia	Hofmeyria atavus	2	Dimetrodon grandis	2	Viatkogorgon ivakhnenkoi	2	Dimetrodon grandis	2
Therocephalia	Ictidosaurus augusticeps	2	Dimetrodon limbatus	2	Dimetrodon grandis	2	Dimetrodon limbatus	2
Therocephalia	Ictidosuchoides longiceps	2	Pantelosaurus saxonicus	2	Dimetrodon limbatus	2	Pantelosaurus saxonicus	2

Therocephalia	Lycosuchus vanderrieti	2	Sphenacodon ferox	2	Pantelosaurus saxonicus	2	Sphenacodon ferocior	2
Therocephalia	Mirotenthes digitipes	2	Glanosuchus macrops	2	Sphenacodon ferocior	2	Sphenacodon ferox	2
Therocephalia	Moschorhinus kitchingi	2	Gorynychus masyutinae	2	Sphenacodon ferox	2	Glanosuchus macrops	2
Therocephalia	Ophidostoma tatarinovi	2	Hofmeyria atavus	2	Glanosuchus macrops	2	Gorynychus masyutinae	2
Therocephalia	Pristerognathus polyodon	2	Ictidosaurus augusticeps	2	Gorynychus masyutinae	2	Hofmeyria atavus	2
Therocephalia	Promoschorhynchus	2	Lycosuchus vanderrieti	2	Hofmeyria atavus	2	Ictidosaurus augusticeps	2
Therocephalia	Purlovia maxima	2	Mirotenthes digitipes	2	Ictidosaurus augusticeps	2	Lycosuchus vanderrieti	2
Therocephalia	Scalopolacerta hoffmanni	2	Ophidostoma tatarinovi	2	Lycosuchus vanderrieti	2	Mirotenthes digitipes	2
Therocephalia	Scylacosaurus sclateri	2	Pristerognathus polyodon	2	Mirotenthes digitipes	2	Ophidostoma tatarinovi	2
Therocephalia	Theriognathus microps	2	Promoschorhynchus	2	Ophidostoma tatarinovi	2	Pristerognathus polyodon	2
Therocephalia	Zorillodontops gracilis	2	Purlovia maxima	2	Pristerognathus polyodon	2	Promoschorhynchus	2
Biarmosuchia	Niaftasuchus zekkeli	3	Scylacosaurus sclateri	2	Promoschorhynchus	2	Purlovia maxima	2
Biarmosuchia	Nikkasaurus tatarinovi	3	Zorillodontops gracilis	2	Purlovia maxima	2	Scylacosaurus sclateri	2
Biarmosuchia	Reiszia gubini	3	Niaftasuchus zekkeli	3	Scylacosaurus sclateri	2	Zorillodontops gracilis	2
Biarmosuchia	Tetraceratops insignis	3	Nikkasaurus tatarinovi	3	Zorillodontops gracilis	2	Niaftasuchus zekkeli	3
Cyndontia	Galesaurus planiceps	3	Reiszia gubini	3	Niaftasuchus zekkeli	3	Nikkasaurus tatarinovi	3
Cyndontia	Procynosuchus delaharpeae	3	Tetraceratops insignis	3	Nikkasaurus tatarinovi	3	Reiszia gubini	3

Dinocephalia	Anteosaurus	3	Procynosuchus delaharpeae	3	Reiszia gubini	3	Tetraceratops insignis	3
Eothyridae	Eothyris parkeyi	3	Eothyris parkeyi	3	Tetraceratops insignis	3	Procynosuchus delaharpeae	3
Eothyridae	Vaughnictis smithae	3	Vaughnictis smithae	3	Procynosuchus delaharpeae	3	Eothyris parkeyi	3
Gorgonopsia	Cynariops robustus	3	Ophiacodon mirus	3	Eothyris parkeyi	3	Vaughnictis smithae	3
Ophiacodontidae	Ophiacodon mirus	3	Ophiacodon retroversus	3	Vaughnictis smithae	3	Ophiacodon mirus	3
Ophiacodontidae	Ophiacodon retroversus	3	Ophiacodon uniformis	3	Ophiacodon mirus	3	Ophiacodon retroversus	3
Ophiacodontidae	Ophiacodon uniformis	3	Stereorachis dominans	3	Ophiacodon retroversus	3	Ophiacodon uniformis	3
Ophiacodontidae	Stereorachis dominans	3	Varanosaurus acutirostris	3	Ophiacodon uniformis	3	Stereorachis dominans	3
Ophiacodontidae	Varanosaurus acutirostris	3	Cutleria sp	3	Stereorachis dominans	3	Varanosaurus acutirostris	3
Sphenacodontia	Cutleria sp	3	Dimetrodon loomisi	3	Varanosaurus acutirostris	3	Cutleria sp	3
Sphenacodontia	Dimetrodon loomisi	3	Dimetrodon milleri	3	Cutleria sp	3	Dimetrodon loomisi	3
Sphenacodontia	Dimetrodon milleri	3	Dimetrodon natalis	3	Dimetrodon loomisi	3	Dimetrodon milleri	3
Sphenacodontia	Dimetrodon natalis	3	Eohaptodus garnettensis	3	Dimetrodon milleri	3	Dimetrodon natalis	3
Sphenacodontia	Eohaptodus garnettensis	3	Haptodus baylei	3	Dimetrodon natalis	3	Eohaptodus garnettensis	3
Sphenacodontia	Haptodus baylei	3	Ianthodon schultzei	3	Eohaptodus garnettensis	3	Haptodus baylei	3
Sphenacodontia	Ianthodon schultzei	3	Palaeohatteria longicaudata	3	Haptodus baylei	3	Ianthodon schultzei	3

Sphenacodontia	Palaeohatteria longicaudata	3	Secodontosaurus obtusidens	3	Ianthodon schultzei	3	Palaeohatteria longicaudata	3
Sphenacodontia	Pantelosaurus saxonicus	3	Sphenacodon ferocior	3	Palaeohatteria longicaudata	3	Secodontosaurus obtusidens	3
Sphenacodontia	Secodontosaurus obtusidens	3	Scalopolacerta hoffmanni	3	Secodontosaurus obtusidens	3	Aerosaurus wellesi	3
Varanopidae	Aerosaurus wellesi	3	Aerosaurus wellesi	3	Aerosaurus wellesi	3	Anningia megalops	3
Varanopidae	Anningia megalops	3	Anningia megalops	3	Anningia megalops	3	Archaeovenator hamiltonensis	3
Varanopidae	Archaeovenator hamiltonensis	3	Archaeovenator hamiltonensis	3	Archaeovenator hamiltonensis	3	Ascendonanus nestleri	3
Varanopidae	Ascendonanus nestleri	3	Ascendonanus nestleri	3	Ascendonanus nestleri	3	Elliotsmithia longiceps	3
Varanopidae	Elliotsmithia longiceps	3	Elliotsmithia longiceps	3	Elliotsmithia longiceps	3	Euromycter rutenus	3
Varanopidae	Euromycter rutenus	3	Euromycter rutenus	3	Euromycter rutenus	3	Heleosaurus scholtzi	3
Varanopidae	Heleosaurus scholtzi	3	Heleosaurus scholtzi	3	Heleosaurus scholtzi	3	Mesenosaurus romeri	3
Varanopidae	Mesenosaurus romeri	3	Mesenosaurus romeri	3	Mesenosaurus romeri	3	Microvaranops parentis	3
Varanopidae	Microvaranops parentis	3	Microvaranops parentis	3	Microvaranops parentis	3	Mycterosaurus longiceps	3
Varanopidae	Mycterosaurus longiceps	3	Mycterosaurus longiceps	3	Mycterosaurus longiceps	3	Varanodon agilis	3
Varanopidae	Varanodon agilis	3	Varanodon agilis	3	Varanodon agilis	3	Varanops brevirostris	3
Varanopidae	Varanops brevirostris	3	Varanops brevirostris	3	Varanops brevirostris	3	Scalopolacerta hoffmanni	?

Supplementary Table 3.1.12. Cluster analysis results for feeding functional subgroups. Colour coded to improve group recognition.

Abbreviations: HC, Hierarchical. KM, K-means. PAM, Partition around medioids.

Clade	Taxa	HC	Taxa	KM	Taxa	PAM	Taxa	Consensus
Group 1								
Biarmosuchia	Niaftasuchus zekkeli	1	Niaftasuchus zekkeli	2	Niaftasuchus zekkeli	1	Niaftasuchus zekkeli	2
Biarmosuchia	Reiszia gubini	1	Reiszia gubini	2	Procynosuchus delaharpeae	1	Reiszia gubini	2
Biarmosuchia	Tetraceratops insignis	1	Tetraceratops insignis	2	Vaughnictis smithae	1	Tetraceratops insignis	2
Cyndontia	Procynosuchus delaharpeae	1	Procynosuchus delaharpeae	2	Ophiacodon mirus	1	Procynosuchus delaharpeae	2
Eothyridae	Eothyris parkeyi	1	Eothyris parkeyi	2	Ophiacodon retroversus	1	Eothyris parkeyi	2
Ophiacodontidae	Ophiacodon retroversus	1	Vaughnictis smithae	2	Ophiacodon uniformis	1	Vaughnictis smithae	2
Ophiacodontidae	Stereorachis dominans	1	Ophiacodon retroversus	2	Stereorachis dominans	1	Ophiacodon retroversus	2
Sphenacodontia	Cutleria sp	1	Stereorachis dominans	2	Varanosaurus acutirostris	1	Stereorachis dominans	2
Sphenacodontia	Dimetrodon loomisi	1	Cutleria sp	2	Cutleria sp	1	Cutleria sp	2
Sphenacodontia	Dimetrodon milleri	1	Dimetrodon loomisi	2	Dimetrodon loomisi	1	Dimetrodon loomisi	2
Sphenacodontia	Dimetrodon natalis	1	Dimetrodon milleri	2	Dimetrodon natalis	1	Dimetrodon milleri	2
Sphenacodontia	Eohaptodus garnettensis	1	Dimetrodon natalis	2	Secodontosaurus obtusidens	1	Dimetrodon natalis	2
Sphenacodontia	Haptodus baylei	1	Eohaptodus garnettensis	2	Aerosaurus wellesi	1	Eohaptodus garnettensis	2

Sphenacodontia	Palaeohatteria longicaudata	1	Haptodus baylei	2	Archaeovenator hamiltonensis	1	Haptodus baylei	2
Sphenacodontia	Secodontosaurus obtusidens	1	Palaeohatteria longicaudata	2	Ascendonanus nestleri	1	Palaeohatteria longicaudata	2
Varanopidae	Anningia megalops	1	Anningia megalops	2	Mesenosaurus romeri	1	Anningia megalops	2
Varanopidae	Elliotsmithia longiceps	1	Elliotsmithia longiceps	2	Mycterosaurus longiceps	1	Elliotsmithia longiceps	2
Varanopidae	Euromycter rutenus	1	Euromycter rutenus	2	Varanodon agilis	1	Euromycter rutenus	2
Varanopidae	Heleosaurus scholtzi	1	Heleosaurus scholtzi	2	Varanops brevirostris	1	Heleosaurus scholtzi	2
Biarmosuchia	Nikkasaurus tatarinovi	2	Nikkasaurus tatarinovi	1	Nikkasaurus tatarinovi	2	Nikkasaurus tatarinovi	1
Eothyridae	Vaughnictis smithae	2	Ophiacodon mirus	1	Reiszia gubini	2	Ophiacodon mirus	1
Ophiacodontidae	Ophiacodon mirus	2	Ophiacodon uniformis	1	Tetraceratops insignis	2	Ophiacodon uniformis	1
Ophiacodontidae	Ophiacodon uniformis	2	Varanosaurus acutirostris	1	Eothyris parkeyi	2	Varanosaurus acutirostris	1
Ophiacodontidae	Varanosaurus acutirostris	2	Ianthodon schultzei	1	Dimetrodon milleri	2	Ianthodon schultzei	1
Sphenacodontia	Ianthodon schultzei	2	Secodontosaurus obtusidens	1	Eohaptodus garnettensis	2	Secodontosaurus obtusidens	1
Varanopidae	Aerosaurus wellesi	2	Aerosaurus wellesi	1	Haptodus baylei	2	Aerosaurus wellesi	1
Varanopidae	Archaeovenator hamiltonensis	2	Archaeovenator hamiltonensis	1	Ianthodon schultzei	2	Archaeovenator hamiltonensis	1
Varanopidae	Ascendonanus nestleri	2	Ascendonanus nestleri	1	Palaeohatteria longicaudata	2	Ascendonanus nestleri	1
Varanopidae	Mesenosaurus romeri	2	Mesenosaurus romeri	1	Anningia megalops	2	Mesenosaurus romeri	1

Varanopidae	Microvaranops parentis	2	Microvaranops parentis	1	Elliotsmithia longiceps	2	Microvaranops parentis	1
Varanopidae	Mycterosaurus longiceps	2	Mycterosaurus longiceps	1	Euromycter rutenus	2	Mycterosaurus longiceps	1
Varanopidae	Varanodon agilis	2	Varanodon agilis	1	Heleosaurus scholtzi	2	Varanodon agilis	1
Varanopidae	Varanops brevirostris	2	Varanops brevirostris	1	Microvaranops parentis	2	Varanops brevirostris	1
Group 2								
Biarmosuchia	Leucocephalus wewersi	1	Leucocephalus wewersi	2	Leucocephalus wewersi	1	Leucocephalus wewersi	2
Biarmosuchia	Phthinosuchus discors	1	Phthinosuchus discors	2	Charassognathus gracilis	1	Phthinosuchus discors	2
Cyndontia	Charassognathus gracilis	1	Charassognathus gracilis	2	Platycraniellus elegans	1	Charassognathus gracilis	2
Cyndontia	Platycraniellus elegans	1	Platycraniellus elegans	2	Sinophoneus yumenensis	1	Platycraniellus elegans	2
Dinocephalia	Jonkeria sp	1	Jonkeria sp	2	Aelurognathus tigriceps	1	Jonkeria sp	2
Dinocephalia	Sinophoneus yumenensis	1	Sinophoneus yumenensis	2	Arctognathus	1	Sinophoneus yumenensis	2
Gorgonopsia	Cynariops robustus	1	Cynariops robustus	2	Clelandina rubidgei	1	Cynariops robustus	2
Gorgonopsia	Cyonosaurus longiceps	1	Cyonosaurus longiceps	2	Cynariops robustus	1	Cyonosaurus longiceps	2
Gorgonopsia	Gorgonops torvus	1	Eriphostoma microdon	2	Dinogorgon rubidgei	1	Eriphostoma microdon	2
Gorgonopsia	Sauroctonus parringtoni	1	Sauroctonus parringtoni	2	Dixeya	1	Gorgonops torvus	2
Gorgonopsia	Sauroctonus progressus	1	Sauroctonus progressus	2	Eriphostoma microdon	1	Sauroctonus parringtoni	2

Gorgonopsia	Suchogorgon golubevi	1	Suchogorgon golubevi	2	Gorgonops torvus	1	Sauroctonus progressus	2
Gorgonopsia	Sycosaurus nowaki	1	Sycosaurus nowaki	2	Inostrancevia alexandri	1	Suchogorgon golubevi	2
Gorgonopsia	Viatkogorgon ivakhnenkoi	1	Viatkogorgon ivakhnenkoi	2	Pravoslavlevia parva	1	Sycosaurus nowaki	2
Therocephalia	Glanosuchus macrops	1	Glanosuchus macrops	2	Rubidgea atrox	1	Viatkogorgon ivakhnenkoi	2
Therocephalia	Gorynychus masyutinae	1	Gorynychus masyutinae	2	Sycosaurus nowaki	1	Glanosuchus macrops	2
Therocephalia	Hofmeyria atavus	1	Hofmeyria atavus	2	Glanosuchus macrops	1	Gorynychus masyutinae	2
Therocephalia	Ictidosaurus augusticeps	1	Ictidosaurus augusticeps	2	Hofmeyria atavus	1	Hofmeyria atavus	2
Therocephalia	Lycosuchus vanderrieti	1	Lycosuchus vanderrieti	2	Ictidosaurus augusticeps	1	Ictidosaurus augusticeps	2
Therocephalia	Mirotenthes digitipes	1	Mirotenthes digitipes	2	Lycosuchus vanderrieti	1	Lycosuchus vanderrieti	2
Therocephalia	Ophidostoma tatarinovi	1	Ophidostoma tatarinovi	2	Mirotenthes digitipes	1	Mirotenthes digitipes	2
Therocephalia	Pristerognathus polyodon	1	Pristerognathus polyodon	2	Ophidostoma tatarinovi	1	Ophidostoma tatarinovi	2
Therocephalia	Promoschorhynchus	1	Promoschorhynchus	2	Purlovia maxima	1	Pristerognathus polyodon	2
Therocephalia	Scylacosaurus sclateri	1	Scylacosaurus sclateri	2	Scylacosaurus sclateri	1	Promoschorhynchus	2
Therocephalia	Zorillodontops gracilis	1	Zorillodontops gracilis	2	Zorillodontops gracilis	1	Scylacosaurus sclateri	2
Gorgonopsia	Aelurognathus tigriceps	3	Aelurognathus tigriceps	3	Phthinosuchus discors	2	Zorillodontops gracilis	2

Gorgonopsia	Arctognathus	3	Arctognathus	3	Galesaurus planiceps	2	Aelurognathus tigriceps	3
Gorgonopsia	Clelandina rubidgei	3	Clelandina rubidgei	3	Progalesaurus lootsbergensis	2	Arctognathus	3
Gorgonopsia	Dinogorgon rubidgei	3	Dinogorgon rubidgei	3	Thrinaxodon liorhinus	2	Clelandina rubidgei	3
Gorgonopsia	Dixeya	3	Dixeya	3	Vetusodon elikhulu	2	Dinogorgon rubidgei	3
Gorgonopsia	Eriphostoma microdon	3	Gorgonops torvus	3	Cyonosaurus longiceps	2	Dixeya	3
Gorgonopsia	Inostrancevia alexandri	3	Inostrancevia alexandri	3	Leontosaurus vanderhorsti	2	Inostrancevia alexandri	3
Gorgonopsia	Leontosaurus vanderhorsti	3	Leontosaurus vanderhorsti	3	Sauroctonus parringtoni	2	Leontosaurus vanderhorsti	3
Gorgonopsia	Pravoslavlevia parva	3	Pravoslavlevia parva	3	Sauroctonus progressus	2	Pravoslavlevia parva	3
Gorgonopsia	Rubidgea atrox	3	Rubidgea atrox	3	Smilesaurus ferox	2	Rubidgea atrox	3
Gorgonopsia	Smilesaurus ferox	3	Smilesaurus ferox	3	Suchogorgon golubevi	2	Smilesaurus ferox	3
Therocephalia	Purlovia maxima	3	Purlovia maxima	3	Viatkogorgon ivakhnenkoi	2	Purlovia maxima	3
Cyndontia	Galesaurus planiceps	2	Galesaurus planiceps	1	Gorynychus masyutinae	2	Galesaurus planiceps	1
Cyndontia	Progalesaurus lootsbergensis	2	Progalesaurus lootsbergensis	1	Pristerognathus polyodon	2	Progalesaurus lootsbergensis	1
Cyndontia	Thrinaxodon liorhinus	2	Thrinaxodon liorhinus	1	Promoschorhynchus	2	Thrinaxodon liorhinus	1
Cyndontia	Vetusodon elikhulu	2	Vetusodon elikhulu	1	Anteosaurus	3	Vetusodon elikhulu	1
Dinocephalia	Anteosaurus	2	Anteosaurus	1	Jonkeria sp	3	Anteosaurus	1

Sphenacodontia	Dimetrodon grandis	2	Dimetrodon grandis	1	Dimetrodon grandis	3	Dimetrodon grandis	1
Sphenacodontia	Dimetrodon limbatus	2	Dimetrodon limbatus	1	Dimetrodon limbatus	3	Dimetrodon limbatus	1
Sphenacodontia	Pantelosaurus saxonicus	2	Pantelosaurus saxonicus	1	Pantelosaurus saxonicus	3	Pantelosaurus saxonicus	1
Sphenacodontia	Sphenacodon ferocior	2	Sphenacodon ferocior	1	Sphenacodon ferocior	3	Sphenacodon ferocior	1
Sphenacodontia	Sphenacodon ferox	2	Sphenacodon ferox	1	Sphenacodon ferox	3	Sphenacodon ferox	1
Group 3								
Biarmosuchia	Alrausuchus tagax	1	Alrausuchus tagax	2	Alrausuchus tagax	1		
Biarmosuchia	Biarmosuchus tener	1	Biarmosuchus tener	2	Biarmosuchus tener	1		
Biarmosuchia	Herpetoskylax hopsoni	1	Herpetoskylax hopsoni	2	Herpetoskylax hopsoni	1		
Biarmosuchia	Hipposaurus	1	Hipposaurus	2	Hipposaurus	1		
Biarmosuchia	Ictidorhinus	1	Ictidorhinus	2	Ictidorhinus	1		
Biarmosuchia	Lemurosaurus pricei	1	Lemurosaurus pricei	2	Lemurosaurus pricei	1		
Biarmosuchia	Lobalopex mordax	1	Lobalopex mordax	2	Lobalopex mordax	1		
Biarmosuchia	Phthinosaurus borissiaki	1	Phthinosaurus borissiaki	2	Phthinosaurus borissiaki	1		
Cynodontia	Dvinia prima	1	Dvinia prima	2	Dvinia prima	1		
Cynodontia	Proburnetia viatkensis	1	Proburnetia viatkensis	2	Proburnetia viatkensis	1		
Dinocephalia	Australosyodon nyaphuli	1	Australosyodon nyaphuli	2	Australosyodon nyaphuli	1		
Dinocephalia	Deuterosaurus biarmicus	1	Deuterosaurus biarmicus	2	Deuterosaurus biarmicus	1		
Dinocephalia	Moschorhinus kitchingi	1	Moschorhinus kitchingi	2	Moschorhinus kitchingi	1		

Dinocephalia	Nanictosaurus kitchingi	1	Nanictosaurus kitchingi	2	Nanictosaurus kitchingi	1		
Dinocephalia	Syodon biarmicum	1	Syodon biarmicum	2	Syodon biarmicum	1		
Gorgonopsia	Aloposaurus gracilis	1	Aloposaurus gracilis	2	Aloposaurus gracilis	1		
Gorgonopsia	Aloposaurus tenuis	1	Aloposaurus tenuis	2	Aloposaurus tenuis	1		
Gorgonopsia	Arctops willistoni	1	Arctops willistoni	2	Arctops willistoni	1		
Gorgonopsia	Inostrancevia latifrons	1	Inostrancevia latifrons	2	Inostrancevia latifrons	1		
Gorgonopsia	Tapinocaninus	1	Tapinocaninus	2	Tapinocaninus	1		
Gorgonopsia	Titanophoneus potens	1	Titanophoneus potens	2	Titanophoneus potens	1		
Therocephalia	Annatherapsidus petri	1	Annatherapsidus petri	2	Annatherapsidus petri	1		
Therocephalia	Ictidosuchoides longiceps	1	Ictidosuchoides longiceps	2	Ictidosuchoides longiceps	1		
Therocephalia	Jiufengia jiai	1	Jiufengia jiai	2	Jiufengia jiai	1		
Therocephalia	Karenites ornamentatus	1	Karenites ornamentatus	2	Karenites ornamentatus	1		
Therocephalia	Lycaenops ornatus	1	Lycaenops ornatus	2	Lycaenops ornatus	1		
Therocephalia	Nochnitsa geminidens	1	Nochnitsa geminidens	2	Nochnitsa geminidens	1		
Therocephalia	Olivierosuchus parringtoni	1	Olivierosuchus parringtoni	2	Olivierosuchus parringtoni	1		
Therocephalia	Scalopolacerta hoffmanni	1	Scalopolacerta hoffmanni	2	Scalopolacerta hoffmanni	1		
Therocephalia	Scylacops capensis	1	Scylacops capensis	2	Scylacops capensis	1		
Therocephalia	Theriognathus microps	1	Theriognathus microps	2	Theriognathus microps	1		
Therocephalia	Viatkosuchus sumini	1	Viatkosuchus sumini	2	Viatkosuchus sumini	1		

Biarmosuchia	Lende chiweta	2	Lende chiweta	1	Lende chiweta	2		
Biarmosuchia	Lycideops longiceps	2	Lycideops longiceps	1	Lycideops longiceps	2		
Dinocephalia	Pampaphoneus biccai	2	Pampaphoneus biccai	1	Pampaphoneus biccai	2		
Gorgonopsia	Aelurosaurus	2	Aelurosaurus	1	Aelurosaurus	2		
Gorgonopsia	Mupashi migrator	2	Mupashi migrator	1	Mupashi migrator	2		
Therocephalia	Choerosaurus dejageri	2	Choerosaurus dejageri	1	Choerosaurus dejageri	2		
Therocephalia	Ericiolacerta parva	2	Ericiolacerta parva	1	Ericiolacerta parva	2		
Therocephalia	Scalopodon tenuisfrons	2	Scalopodon tenuisfrons	1	Scalopodon tenuisfrons	2		
Therocephalia	Scaloposaurus constrictus	2	Scaloposaurus constrictus	1	Scaloposaurus constrictus	2		
Therocephalia	Tetracynodon darti	2	Tetracynodon darti	1	Tetracynodon darti	2		

3.2 The Triassic radiation of tetrapod herbivory

Niche partitioning shaped herbivore macroevolution through the early Mesozoic.

Chapter Published: Singh, S. A., Elsler, A., Stubbs, T. L., Bond, R., Rayfield, E. J., & Benton, M. J. (2021). Niche partitioning shaped herbivore macroevolution through the early Mesozoic. *Nature communications*, *12*(1), 1-13.

Chapter Contributions and Acknowledgements

I collected most of the images, all the shape and functional data, conducted the analyses, constructed the figures, and wrote the manuscript. A.E. provided the chronostratigraphic data and helped with image collection. T.S. helped design the morphometric analyses and write the R codes used. R.B. contributed some images. E.R. and M.J.B. provided guidance and comments on the study concept and revised the manuscript. All authors discussed the results and helped draft and revise the manuscript. My contributions represent 90% of the material in this chapter.

I thank David Button for help in data collection early in this project, and Christine Janis for providing literature and constructive commentary. I also thank reviewers Nicolas Campione, Caleb Brown, and David Polly for their insightful comments and suggestions in greatly improving this work. All silhouettes created by S.S., but some are vectorised from artwork by Felipe Alves Elias (https://www.paleozoobr.com/) and Jeff Martz (United States National Park Service).

Abstract

The Triassic (252–201 Ma) marks a major punctuation in Earth history, when ecosystems rebuilt themselves following the devastating Permian-Triassic mass extinction. Herbivory evolved independently several times as ecosystems comprising diverse assemblages of therapsids, parareptiles and archosauromorphs rose and fell, culminating in a world dominated by dinosaurs. It was assumed that dinosaurs prevailed either through long-term competitive replacement of the incumbent clades or rapidly and opportunistically following one or more extinction events. Here I use functional morphology and ecology to explore herbivore morphospace through the Triassic and Early Jurassic. I identify five main herbivore guilds (ingestion generalists, prehension specialists, durophagous specialists, shearing pulpers, and heavy oral processors), and find that herbivore clades generally avoided competition by almost exclusively occupying different guilds. Major ecosystem remodelling was triggered multiple times by large-scale climatic and environmental changes, and previously dominant herbivores were marginalised by newly emerging forms. Dinosaur dominance

was a mix of opportunity, following disaster, combined with competitive advantage in their new world.

Introduction

Terrestrial ecosystems underwent significant remodelling during the Triassic via floral and faunal turnovers that established many of the structural elements found within modern ecosystems. The preceding Permian-Triassic mass extinction (PTME), 252 Ma, is said to have reset the whole evolution of life (Van Valen, 1984; Benton et al., 2004). Palaeozoic tetrapod survivors of the PTME, such as procolophonid parareptiles and dicynodont therapsids, were superseded by new archosauromorph and mammaliaform clades (Benton, 2016; Sues and Fraser, 2010). The turnovers established dinosaurs as the predominant terrestrial tetrapods for the remainder of the Mesozoic and saw the emergence of key modern groups such as lissamphibians (frogs and relatives), turtles, lepidosaurs (lizards and relatives), crocodylomorphs, and mammals, as well as flies and beetles (Benton, 2016; Sues and Fraser, 2010) and several families of ferns and conifers (Kustatscher et al., 2018).

The evolution of tetrapods through the Triassic, with the eventual success of the dinosaurs, is a classic example of a biotic replacement (Benton, 1987; 2009) for which two explanatory models have been proposed. The first, the 'competitive replacement model' (CRM) is that archosauromorphs/ dinosaurs outcompeted their rivals because of their more efficient locomotion, respiration, thermoregulation, and/or feeding habits (Charig, 1984; Bakker, 1972; Zawiskie, 1986). The CRM occurred in two steps, with archosauromorphs first outcompeting and replacing therapsids in the carnivore guild, and then in the herbivore guild, in the Middle and Late Triassic respectively (Charig, 1984). The second model, the 'opportunistic replacement model' (ORM) focuses on the role of extrinsic environmental perturbations in enabling an opportunistic diversification of archosauromorphs/ dinosaurs following the extinction of competitor groups (Benton, 1983). New evidence for the ORM is the discovery that the Carnian Pluvial Event (CPE), 233–232 Ma, was a turning point for terrestrial ecosystems; this was a time when climates switched rapidly from arid to humid and back to arid conditions, causing significant extinctions among plants and among the herbivores that depended on them, and further enabling explosive diversification of herbivorous dinosaurs (Bernardi et al., 2018; Benton et al., 2018). There have been similar debates over competitive and opportunistic models as explanations for many large-scale biotic replacements through geological time (Benton, 2009), and the Triassic example explored here can act as an exemplar for study of these other events.

Recent work on Triassic tetrapods has changed our understanding of the pattern of biotic replacement but has not resolved the tension between CR and OR models. For example, despite their success, early dinosaurs show no apparent superiority, possessing lower morphological disparity than contemporaneous pseudosuchians (or crurotarsans, crocodile-line archosaurs) (Brusatte et al., 2008; Ezcurra and Butler, 2018, Ezcurra et al., 2020), and no long-term evolutionary drive or extinction resilience (Sookias et al., 2012; Allen et al., 2019). Recent discoveries of silesaurids (the dinosaur sister-group) from the Middle Triassic and potential uncertainty regarding the classification of the silesaurids as potential ornithischian dinosaurs now suggest earlier origins for dinosaurs, potentially as early as the Early Triassic (Nesbitt et al., 2017; Müller and Garcia, 2020), and the extinction of the last non-mammaliaform therapsids towards the end of the Late Triassic (Sulej and Niedźwiedzki, 2019). This newly extended span of coexistence across the entire Triassic challenges old assumptions of archaic therapsid capabilities. All these points indicate the need for deeper study.

Here, I explore diversity dynamics and eco-morphospaces to investigate the timing of functional and ecological changes between the key clades through the Triassic. I limit our study to the herbivores as they are the basis of the tetrapod food chains, and by far the most abundant animals in each ecosystem. As primary consumers, herbivores constitute the interface between flora and fauna, acting as indicators of wider eco-environmental change (Pringle et al., 2011). Further, they generally had robust skeletons that are extensively preserved, and the phylogenetics and feeding functions of all key clades have been previously studied.

Materials and methods

Taxonomic sampling and data collection. I compiled a list of all valid herbivorous tetrapod taxa from Early Triassic to Early Jurassic, using a published dataset (Benton et al., 2013a) and the latest literature to incorporate new taxa and taxonomic revisions. The stratigraphic ranges of these taxa were updated to substage level following the designations of Benton et al. (2013a). Absolute age assignments were based on the 2019 version of the International Chronostratigraphic Chart (Cohen et al., 2019). Assemblage data was gathered from Benton et al. (2018) for herbivore-rich early Mesozoic fossil localities and updated using published literature to include new taxa.

Our analysis was generally conducted at genus level to maintain a balance between availability of data and confidence in taxon diagnosis; in fact, most genera are monospecific. I generally used a single specimen per genus in this study, so I cannot account for varying levels of intraspecific variation; a true measure of total disparity would ideally include multiple specimens per taxon. Where intraspecific variation had been reported, I included more than one species for those genera,

for example three species of the rhynchosaur *Hyperodapedon*: *H. gordoni*, *H. huxleyi* and *H. sanjuanensis*, from Europe, India, and South America respectively, and four of *Lystrosaurus*: *L. hedini*, *L. maccaigi*, *L. murrayi*, and *L. robustus* from locations in China, South Africa, and India. These were abundant and widespread taxa showing intrageneric shape variation. I also included all available cynognathian cynodonts, as some genera characterised as carnivores were found by isotopic analysis to have also fed on vegetation (Botha et al., 2005), so omnivory may have been common within this group.

I compiled photographs and specimen drawings for 128 genera from the literature, taking care to exclude damaged, distorted, and juvenile material. These represent all taxa for which there is sufficient data for inclusion. The sample of 136 images includes 23 procolophonoid parareptiles, 22 dicynodont anomodonts, 17 cynognathian cynodonts, six tritylodont mammals, three bauriid therocephalians, seven ornithischian and 29 sauropodomorph dinosaurs, two silesaurids, eight aetosaurs, four pseudosuchians, and 15 non-archosaur archosauromorphs (Supplementary Data S3.2.12).

Geometric and functional morphometrics. I used both geometric morphometric (GM) and functional morphometric (FM) methods to generate a detailed account of morphological and functional evolution in herbivorous tetrapod jaws. Using both methods allows for examination of changes in mandibular morphology alongside (clearly defined) biomechanical utility. GM methods capture the overall shape of the element of interest and FM methods capture biomechanical properties of the element and can thus give insight into function. These two methods can, but do not necessarily overlap in their results since shape variation may be non-independent of some functional traits. Using both types of metrics also allowed us to account for discrepancies between biomechanical and morphological patterns of disparity (Eble, 2004; Hetherington et al., 2015). GM methods assess shape variation via user-defined landmarks and Cartesian coordinates, whereas FM methods use continuous functional measurements such as mechanical advantage (MA) and aspect ratio, which reflect biting efficiency and jaw robusticity respectively (Button et al., 2014; MacLaren et al., 2017). I used both Procrustes aligned landmark data and standardised functional measurement data (SFMD) that were collected following the methodology of previous studies of tetrapod feeding morphology (Stubbs et al., 2013; Button et al., 2014; MacLaren et al., 2017; Sakamoto et al., 2010).

Shape data. Herbivorous tetrapods encompass a wide range of mandible morphologies making it difficult to identify more than a small number of homologous landmark points. I opted for a relaxed

landmarking regime, in which I used four fixed landmarks and connected them with four semi-landmarked curves comprising 55 semi-landmarks in total (Supplementary Fig. 2.1.1). Hence, our landmarking regime focuses on overall shape (type 2 landmarking), rather than contacts between bones of the mandible (type 1 landmarking). Type 1 landmarking was impractical as contacts were not clearly visible across our specimens due to the aforementioned shape variability, and homologies were hard to ascertain because of the wide phylogenetic range of the included genera. Images were digitally landmarked using tpsDig2 (Rohlf, 2010), with fixed landmarks placed at homologous points on each mandible and semi-landmarks equally spaced along curves between the fixed landmarks. I used tpsUtil (Rohlf, 2013) to enable semi-landmarks to slide along their respective curves during the Procrustes transformation using the chord–min d^2 sliding method that allows each semi-landmark to slide along a chord between the two adjacent landmarks. Procrustes transformation was carried out using tpsRelW (Rohlf, 2015) to remove the effects of mandible size and orientation from the landmark data and to generate aligned coordinates.

Functional data. I collected data for eight functional characters using measurements taken from our mandible images (Supplementary Table S3.2.1; Supplementary Fig. 2.1.2). These measurements, taken with ImageJ (Schneider et al., 2012), capture important biomechanical properties of the mandible related to feeding ecology and have been used in multiple studies to characterise mandibular function (Stubbs et al., 2013; Button et al., 2014; MacLaren et al., 2017; Sakamoto et al., 2010). Functional Characters:

1. Mean Anterior Mechanical Advantage: A measure of biting efficiency at the anterior of the mandible (Westneat, 1994). This is the ratio of the inlever to the outlever, using the distance from the jaw joint to the anterior-most tip of the toothrow/dentary as the outlever. The distance from the jaw adductor muscle attachment to the jaw joint represents the inlever. This ratio of inlever to outlever gives the lowest possible value of MA.
2. Mean Posterior Mechanical Advantage: A measure of biting efficiency at the posterior of the mandible (Westneat, 1994). This is the ratio of the inlever to the outlever, using the distance from the jaw joint to the posterior-most point of the toothrow/dentary as the outlever. The distance from the jaw adductor muscle attachment to the jaw joint represents the inlever. This ratio of inlever to outlever gives the highest possible value of MA.
3. Opening Mechanical Advantage: A measure of biting velocity (Westneat, 1994). This is the ratio of the maximum inlever to the maximum outlever, using the distance from the jaw joint to the posterior-most point of the mandible/retroarticular process for the inlever, and using the distance from the jaw joint to the posterior-most point of the toothrow/dentary as

the outlever. Opening MA is linked to feeding patterns and prey selection (Anderson and Westneat, 2007; Stubbs et al., 2013).

   a. Characters 1-3 are based on using lever mechanics to describe mandibular function, with the jaw acting as a third-order lever system (Westneat, 1994; 2004). The adductor musculature acts as the input force, the craniomandibular joint acts as the fulcrum and the output force is exerted along the toothrow/shearing surface. Herbivores often exhibit higher MA values than faunivores (Stayton, 2006). Levers are measured from the craniomandibular joint/jaw articulation. Taxa with low MA exhibit weak, rapid bites (Wainwright and Richard, 1995; Stubbs et al., 2013), whilst taxa with a strong bite force have a high MA.

4. Relative Maximum Aspect Ratio: A proxy for the second moment of area, previously used in 2D analyses of jaw mechanics (Anderson, 2011; Stubbs et al., 2013). Generated by dividing the maximum depth of the mandible by its total length. The second moment of area is typically used to assess the resistance of a beam to bending under loading and when applied to jaws gives indication of the pressures experienced during biting. It essentially requires calculation of the cross-sectional area of the mandible, and so needs additional measurements that were often not available from lateral view images sourced from the literature. In most wide-ranging macroevolutionary analyses of anatomy (Anderson, 2011; Stubbs et al., 2013, MacLaren et al., 2017; Kilbourne, & Hutchinson, 2019), the second moment of area calculations assume a generalised jaw shape, treating it as a cylinder or rectangular beam, and this 2D approach takes this principle further by making a more basic approximation of the jaw that doesn't require 3D data. Most mandibles primarily experience dorsoventral stress during feeding function, the maximum aspect ratio measurement used here captures a more general approximation of dorsoventral robusticity and therefore, represents a measure of flexural stiffness (MacLaren et al., 2017) that can be widely applied across all sampled taxa.
5. Relative Toothrow Length: A measure of relative length of the dentition and its purported importance in trophic behaviour (Button et al., 2014). Generated by dividing the length of the toothrow/shearing surface by the total length of the mandible. A longer toothrow enables a greater range of MA along the jaw and likely increased use of the dentition in jaw functionality (either for food ingestion or processing/mastication). Herbivores tend to show relatively shortened toothrows compared to faunivores and omnivores (Sues, 2000).
6. Relative Symphysis Length: A measure of symphyseal robusticity generated by dividing the length of the symphysis by the total length of the mandible. The symphysis is subject to

significant bending, shear, and torsional stress during biting action and so is highly related to transmission of muscle and biting force and feeding ecology and overall jaw mechanics (Daegling, 2001; Jones et al., 2012).

7. The symphyseal angle is measured between the ventral jaw line and a line parallel to the long axis of the mandibular symphysis. It affects symphyseal resistance to the bending, shear, and torsional stresses that occur during the bite cycle (Daegling, 2001). The symphyseal angle is known to affect food processing in modern herbivorous rhynchocephalians (Jones et al., 2012) and is of major importance in the mechanical response of modern crocodylians to biting, twisting, and shaking (Porro et al., 2011; Walmsley et al., 2013).
8. Relative Offset of Articulation: The articulation offset is measured as the length of the line perpendicular to the tangent of the mandibular toothrow (extrapolated from the anterior and posterior ends of the toothrow to account for jaw curvature) which intersects the articular joint (Anderson et al., 2011; MacLaren et al., 2017). This value is then divided by the total jaw length. An offset between the toothrow and jaw articulation affects dental occlusion and leverage of the jaw musculature (Janis, 1995). A small articulation offset indicates 'scissor-like' occlusion, which is typical of carnivorous taxa. Herbivores generally exhibit greater toothrow-articular offset as this enables simultaneous occlusion along the entirety of the toothrow, supporting gripping & crushing actions (Ramsay and Wilga, 2007).

Principal component analysis. To identify the major axes of variation, the shape-aligned coordinate data and functional measurement matrix were subjected to principal component analyses (PCAs). A PCA transforms total variation into a matrix of independent variables (PC axes). For the PCA analyses, I used packages in R (R Core Team, 2018), including geomorph (Adams and Otárola-Castillo, 2013) for the aligned coordinate data, and FactoMineR (Le et al., 2008) for the functional measurements; and to also centre and z-transform the data prior to a PCA following established protocols to mitigate issues of heteroscedasticity (Button and Zanno, 2020; Button et al., 2014). The first two PC axes account for the largest proportions of variation of all axes and were used to plot morphospace occupation. Alternative standardisation and additional (linear and non-linear) dimensional scaling analyses were also carried out to assess the robusticity of the PCA results. reported above (see supplement). The resulting morphospaces differ (**Supplementary Fig. 3.2.S2**) because of the different treatment of the underlying trait data, but the overall results remain consistent across all methods and do not change the broader findings presented in the main chapter text.

The first and second principal components were used to plot morphospace occupation, with these components amounting to 32% and 14% of total shape variation, and 42% and 16% of total functional variation respectively, constituting the maximum morphological variation within two components. Functional character contour plots were generated using the akima package (Akima and Gebhardt, 2016), with linear interpolation of functional and PC data for all taxa generating functional data for all areas of occupied morphospace.

Cluster analyses. I used the SFMD to define functional feeding groups (FFGs) because these traits have known links to feeding ecology and diet in extant taxa (Wainwright, 2007), hence allowing us to interpret differences in disparity from an eco-functional perspective rather than more ambiguous comparisons of shape. It should be noted that our functional characters do feature characters based on functionally important aspects of shape, which may yield some similarities if the cluster analyses were applied to shape rather than functional data. However, landmark data encapsulates a greater level of shape detail whilst disregarding aspects such muscle attachment positions, and so I would still expect different results between cluster analyses run using either the functional or shape landmark data.

Boundaries between dietary niches become increasingly ambiguous as classifications move beyond broad groupings such as herbivore or carnivore, and generalist or specialist. Modern studies illustrate that realized niches are not set-in stone, but often conditional on factors such as the conspecifics present and available habitat resources (Shipley et al., 2009; Abraham et al., 2019). Such niche flexibility and our focus on niches within one particular guild led us to employ a combination of hierarchical and partition clustering methods: hierarchical, K-means and partitioning around medioids (PAM) (Kaufman and Rousseeuw, 2009). These methods group taxa into clearly defined 'hard' clusters using machine-learning algorithms that require minimal prior input, thus bolstering the objectivity of resulting cluster groups. All analyses are unsupervised and use different clustering algorithms, which complement each other when used in combination. Agglomerative hierarchical clustering is a distance-based method that uses a 'bottom-up' approach to assign taxa to progressively larger groupings, whereas K-means and PAM are partition methods that use randomly selected centroids/medoids to assemble optimal cluster configurations based on cluster cohesion and separation (Kaufman and Rousseeuw, 2009). K-means clustering focuses on minimising the sum of squared Euclidean distances and uses artificial centroids, whilst PAM tries to minimise the sum of general pairwise dissimilarities and uses real data-points (medoids) as the centroids and is also considered more robust to outliers and noise within the data (Kassambara and Mundt, 2017). Comparison of the K-means and PAM results may help address the inherent ambiguity between

niches as they enable identification of core groupings within each cluster that would ideally form a firm basis for a distinct functional feeding group. K-means may better identify these FFG cores but struggle with classifying peripheral taxa. In contrast, PAM can recover irregular cluster configurations, which may more accurately reflect niche-spaces within the overall morphospace. These partition methods complement the hierarchical cluster analysis, which forms a tree based on phenetic similarities and thereby assumes a parsimonious regime of trait evolution, as K-means and PAM methods do not attempt to find broader linkages beyond the immediate similarity between taxa. These assumptions on the connectivity between taxa and clusters helps our combined approach identify robust FFGs that reflect the phylogenetic distances between clades, whilst still acknowledging the common selective pressures in pursuit of similar dietary niches. Further methodological studies exploring the distribution of niches within ecospaces may provide greater clarity on the accuracy of these clustering methods, and so identify which method may better reflect reality and should be favoured in future studies.

The three separate analyses were applied to a Euclidean distance matrix generated using the SFMD. Using Euclidean distances is an appropriate choice given our continuous multivariate dataset and the aim to use the magnitude of differences between taxa to determine separate groups, as well as enabling use of subsequent partition clustering methods. The hierarchical analysis was carried out first to explore the clustering present within our taxa as the agglomerative process enables identification of the clusters and subclusters present, as well as the degree of separation between these groupings. These results inform the subsequent K-means and PAM analyses, which both require a user-defined range of cluster combinations to test (Madhulatha, 2011). The cluster analyses were run in R using the 'eclust' function from the FactoExtra package (Kassambara and Mundt, 2017), with the partition methods identifying the optimal number of clusters from within our defined cluster (K) range (4–10) using gap statistic values generated from 2000 bootstrap cycles. The hierarchical analysis was also rerun using the defined K range to generate clear cluster classifications. The results from these the cluster analyses were validated using the 'cluster.stats' function from the fpc R package (Hennig, 2019). Resulting cluster 'silhouette' metrics (Kaufman and Rousseeuw, 2009) illustrate the performance of each method in distinguishing clusters and assigning taxa. The cluster analysis results were used to generate composite groups to act as our FFGs, based on patterns of consensus in the distribution of taxa across clusters. Where possible, I used lower-level taxonomic groupings to increase FFG assignment accuracy. FFGs were assigned to clades based on which groups held the majority of a clade's taxa. This approach enabled us to better compare taxa in different assemblages in the later assessment of potential competition. This coarse classification scheme may conceal the true levels of feeding diversity present, but because many

assemblages feature taxa not included in this analysis, I felt that this cautious approach would ensure a more robust assessment of potential competition. Further study utilising new and alternative aspects of feeding anatomy (such as dentition) may enable higher resolution classification of feeding diversity in future.

Many (predominantly sauropsid) taxa were recovered within a single cluster group, and while I termed this group 'ingestion generalists', I felt this grouping provided little diagnostic use as an FFG in our investigations of potential competition. Therefore, I re-ran the above cluster procedures using only the ingestion generalist taxa to recover more details of potential clade-level competition, and I then identified three FFsGs (basal generalists, tough generalists, and light oral processors).

Calculations of disparity through time. Disparity is a measure of morphological diversity that is calculated using the volume and extent of morphospace occupation. To explore patterns of shape and functional disparity, mean pairwise distances (MPD) were calculated as the disparity metric using a Euclidean distance matrix generated from the aligned landmark data. MPD is a fairly conservative measure of disparity and although it may not fully illustrate the extent of occupied morphospace, it is also fairly resistant to sample size inconsistencies and an effective metric for measuring relative changes in morphospace (Ciampaglio et al., 2001), which is of key interest to the study. I used 1000 cycles of bootstrapping to provide 95% confidence intervals. MPD were calculated using all PC axes. Our plots were generated in R using the calibrate (Graffelman, 2013) and strap (Bell and Lloyd, 2014) packages. Morphospace packing' (heavy taxon clustering within morphospace) has been shown to reduce disparity by lowering the average dissimilarity, despite the overall morphospace area/volume remaining stable (Smithwick et al., 2018; Nordén et al., 2018). Consequently, I plotted MPD alongside substage level, time-slices of morphospace to avoid misinterpreting the disparity results.

To quantitatively assess the significance of changes in morphospace through time, a one-way non-parametric analysis of variance (NPMANOVA) was applied in PAST (Hammer et al., 2001) (version 3.24). NPMANOVA calculates and compares centroids and surrounding spread of data for each group (timebin) using distance metrics. The analysis was applied to the aligned landmark shape data and functional SFMD, using a Euclidean similarity index to test for differences between timebins at epoch and stage-level. Bonferroni corrections were also applied owing to the multiple comparisons carried out.

Calculations of divergence through time. To quantify the contrasting eco-evolutionary trajectories of the three main clades analysed here (Archosauromorpha, Therapsida and Parareptilia), I

calculated the mean shape and functionality for each clade at stage level using the aligned landmark shape data and functional SFMD. The mean values were subsequently used to generate Euclidean distance matrixes for the shape and functional data respectively.

Results and Discussion

Triassic herbivore ecomorphological feeding guilds. I use herbivorous tetrapod jaws as an ecomorphological proxy and consider variation in both shape and function. After applying a PCA, the first and second principal components were used to plot morphospace occupation, with these components amounting to 32% and 14% of total shape variation, and 42% and 16% of total functional variation respectively, constituting the maximum morphological variation within two components. Archosauromorphs and therapsids occupy different areas of shape morphospace with almost no overlap (Fig. 3.2.1a). The main discrimination between these two clades is along the major axis of variation, principal component (PC) 1, while PC2 discriminates therapsid subgroups, but not the sauropsids, which remain clustered on PC2. This pattern of greater sauropsid conservatism relative to synapsids appears to remain consistent in morphospaces generated from combinations of the first three PCs (Supplementary Fig. 3.2.S1). Two clades crosscut this general pattern: the areas of morphospace occupied by rhynchosaurs (Archosauromorpha) and procolophonoids (Parareptilia) overlap with other sauropsids as well as with therapsids (Fig. 3.2.1a). This functional-ecological discrimination between the two major tetrapod clades, including the ancestors of modern birds and crocodilians on the one hand (archosauromorphs) and mammals on the other (therapsids) helps explain how both clades survived and neither overwhelmed the other, despite evidence for arms races between both through the Triassic (Brusatte et al., 2008; Sookias et al., 2012; Benton et al., 2014).

Contour mapping of the functional characters (Methods 2.2) helps to reveal how jaw shape reflects function (Fig. 3.2.1b–i). The sauropsid-therapsid division along PC1 appears closely linked with anterior (Fig. 3.2.1b) and posterior (Fig. 3.2.1c) mechanical advantage (MA) and maximum aspect ratio (MAR) (Fig. 3.2.1e), reflecting biting efficiency and speed, and jaw robusticity. PC2 reflects a more complex pattern and appears to document the opening MA (Fig. 3.2.1d), relative symphyseal length (RSL) (Fig. 3.2.1g), and articulation offset (AO) (Fig. 3.2.1i), reflecting the speed of jaw opening, anterior robusticity, and efficiency of jaw lever mechanics respectively. These functional characters were used to generate a separate jaw 'functional' morphospace (Fig. 3.2.1j) in which PC contribution scores indicate that functional PC1 (fPC1) is equally dependent on posterior MA, anterior MA, and MAR, while fPC2 is dominated by the opening MA and AO (Table 3.2.1). Taxon distribution is more extended along fPC2, but the functional morphospace shows largely the same

patterns as seen in the shape morphospace (Fig. 3.2.1j and Supplementary Fig. 3.2.S2). In the functional morphospace, only the rhynchosaurs overlap with therapsids in the functional morphospace, and they occupy a space between cynognathian cynodonts and dicynodonts, rather than being associated more closely with dicynodonts as in the shape morphospace (Fig. 3.2.1a).

Triassic therapsid jaws were highly efficient, granting them relatively high power and speed, as shown by the shape and functional morphospaces (Fig. 3.2.1a, j). Therapsids have relatively compressed mandibles (Fig. 3.2.1a) that maximise the areas of muscle attachment, increasing MA (Fig. 3.2.1b–c). Among therapsids, eutheriodonts developed this characteristic further, diverging from other taxa in terms of the greater compression of their mandibles and the reduced offset between tooth row and jaw joint. This progression continues through the successive positions in morphospace of the bauriid therocephalians, cynognathian cynodonts and tritylodont mammaliamorphs. Relative expansion of the tooth row (Fig. 3.2.1f) and development of the jaw musculature supports therapsid optimisation for powerful bites. The more anterior positioning of the adductor musculature in dicynodonts manifests as the highest anterior and posterior MA values of any group with the quadrate-articular jaw joint. Tooth row expansion and low opening MA in eutheriodonts indicates power was directed towards oral processing/mastication, while dicynodont edentulism supports optimisation for a powerful, shearing bite (Weishampel and Norman, 1989).

Triassic sauropsid jaws were relatively less mechanically efficient typically being slower and less optimised for the transmission of biting power (Fig. 3.2.1a-d) but follow similar trends to therapsids in developing comminution ability. Sauropodomorphs and allokotosaurs diverged from these trends, opting for fairly quick but weak bites with relatively large tooth rows to optimise ingestion of vegetation. Aetosaurs, ornithischians and some procolophonoids exhibit morphologies that mechanically improved on the basal morphology of the sauropodomorphs and allokotosaurs, with greater MA and robusticity, although jaw closure was notably slower. This may suggest greater cropping ability and further herbivorous specialisation. Rhynchosaurs show similar trends in developing their jaw musculature, exhibiting MA values (Fig. 3.2.1b–d) that converge towards those of therapsids. Leptopleuronine procolophonids are interesting in that their jaws were very stout with slower bite speed and high MA, suggesting they were feeding on very hard/ tough materials. The expansion of the tooth row in aetosaurs, ornithischians and rhynchosaurs suggests they were emulating the eutheriodonts in developing more effective mastication. Consequently, early Mesozoic herbivores can be subdivided broadly by their preference for gut or oral processing (Fritz et al., 2011). Different groups of therapsids and sauropsids followed common adaptive pathways as specialised herbivores: as phylogenetic contingency combined with ecology to produce convergent

forms. This pattern has already been observed among dinosaurs (Button and Zanno, 2020) and our results suggest it runs even deeper in the tetrapod tree.

Regional mapping on the functional morphospace plot (Fig. 3.2.1j) shows qualitative groupings that may reflect different functional feeding groups (FFG) or guilds. To quantitatively identify these FFGs, three separate cluster analyses were run using a distance matrix of the standardised functional data. All methods gave similar results with regards to the separation and stability of the cluster groups but disagree over the precise groups (Supplementary Table 3.2.3-4). External validation metrics were used to assess how closely the cluster groups corresponded with broad and higher resolution taxonomic groupings (Supplementary Data 3.2.S14), which highlighted the relatively strong phylogenetic control on mandibular morpho-function (Supplementary Table 3.2.4; Supplementary Data 3.2.S14). By removing inconsistent taxa and looking for consensus among the three sets of cluster results, I identified five main FFGs: the ingestion generalists (relatively unspecialised), the prehension specialists (stronger, larger bites), the durophagous specialists (slow, powerful bites), the shearing pulpers (that cut and smash plant food), and the heavy oral processors (using teeth to reduce the food). Many sauropsid taxa were recovered within the ingestion generalist FFG, and so the clustering methodology was repeated with the ingestion generalists in an effort to generate higher resolution functional feeding subgroups (FFsG) for use in analysis of potential competition (Supplementary Data 3.2.S5-S6). This allowed identification of three additional FFsG within the ingestion generalist group: the basal generalists, tough generalists and light oral processors.

Dissecting the functional properties within each of the FFGs enables us to determine the likely feeding specialisations (Fig. 3.2.2) and track their prevalence through geological time (Fig. 3.2.3). MA is the main discriminant for our FFGs. The FFGs show that therapsid herbivores fall into three FFGs, and archosauromorphs into two groups. However, the identification of the FFsG shows that archosauromorph morpho-functional differences are more subtle than those present in therapsids, illustrating the varying levels of specialisation and phylogenetic constraints within the two clades. I note that only two FFGs include both therapsids and sauropsids, the ‘shearing pulper’ group, including both hyperodapedontine rhynchosaurs and dicynodonts, and the light oral processor subgroup of the ingestion generalists, which included both archosauromorph rhynchosaurs and trilophosaurs and bauriid therocephalians. Sauropsids show much greater FFG variability within clades than therapsids, where feeding mode is largely common to the entire clade (Fig. 3.2.2; Supplementary Data 3.2.S5-S6). This may reflect greater ecological diversification within sauropsid clades as a result of being relatively unspecialised compared to contemporaneous therapsid herbivores, which were already quite specialised at the onset of the Mesozoic. This contrast in

specialisation granted sauropsids greater freedom to diversify across different guilds, despite therapsids possessing more mechanically efficient jaws (Fig 3.2.2).

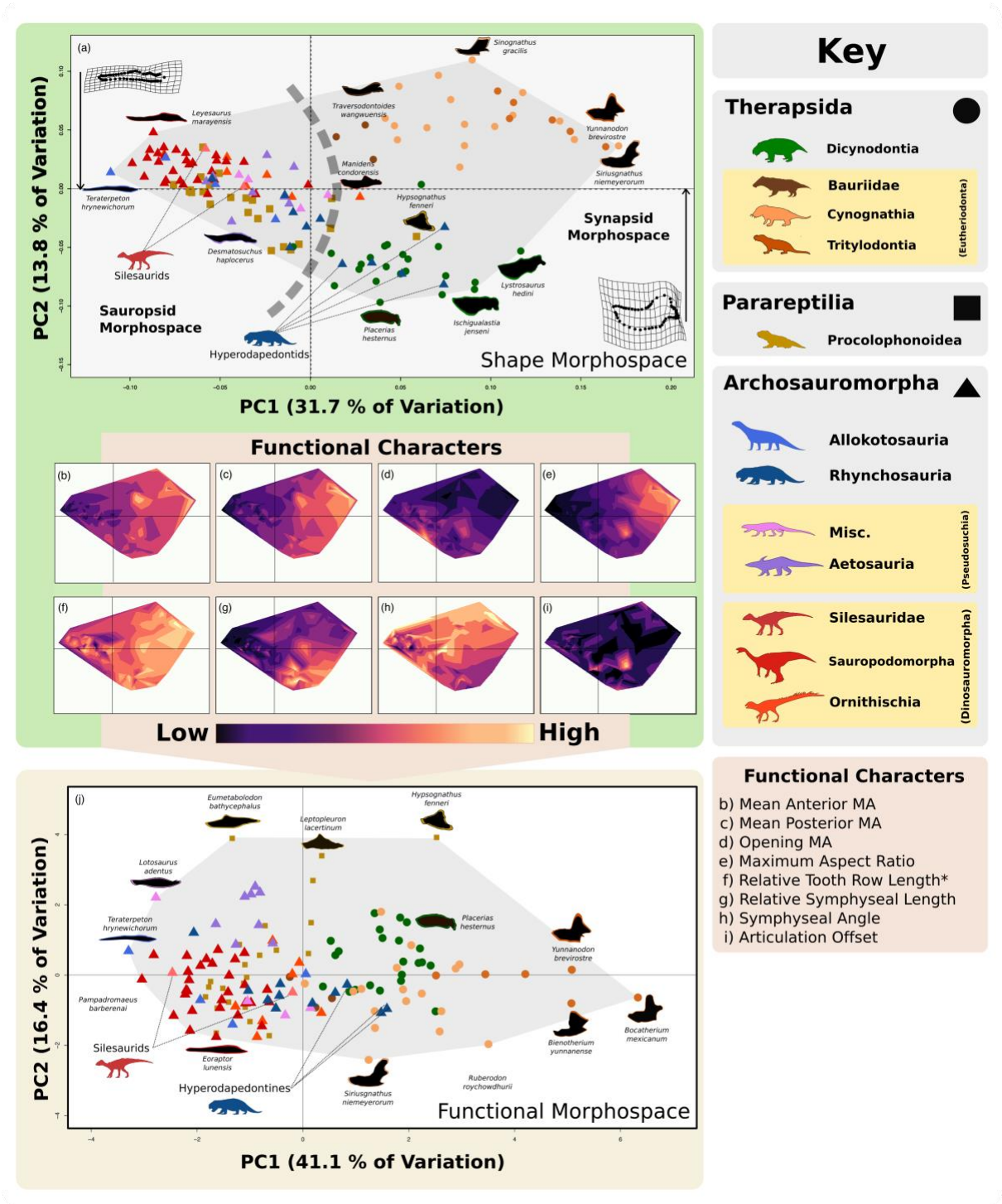

Figure 3.2.1. Shape and functional morphospace occupation of early Mesozoic herbivores. (a) shape morphospace based on geometric morphometric data. (b–i) Contour plot of (interpolated) functional character data mapped onto shape morphospace. Magnitude of functional character values indicated by colour gradient. (j) Functional

morphospace based on the above functional characters. Abbreviations: Misc., Miscellaneous pseudosuchians. MA, Mechanical advantage. *Tooth row length or length of the mandibular functional surface.

Table 3.2.1. Character loadings to functional principal component (fPC) scores using Z-transformed data. (Results presented in main text.) Abbreviations: MA, Mechanical advantage.

Functional Characters	fPC 1	fPC 2	fPC 3	fPC 4	fPC 5	fPC 6	fPC 7	fPC 8
Mean Anterior MA	0.4934625	0.24667339	-0.0900206	0.00786307	-0.1050386	-0.3682956	-0.4319062	0.59520067
Mean Posterior MA	0.5254681	-0.0619115	0.06039547	-0.0601783	0.2154931	-0.0632664	-0.4132983	-0.7010889
Opening MA	-0.1631619	0.5947072	0.14454208	-0.2878902	0.7146802	0.01233845	0.02485324	0.06626129
Max Aspect Ratio	0.495494	0.08422196	-0.0582864	0.21013936	0.1223364	-0.2877307	0.77419792	-0.0519512
Relative Toothrow Length	0.2882966	-0.5297162	0.33770575	0.07496055	0.4259769	0.43923177	-0.0005719	0.37714757
Relative Symphyseal Length	0.3340768	0.23554854	0.06918551	-0.622936	-0.4008042	0.49565115	0.18327337	0.0130569
Symphyseal Angle	0.1052323	0.16547329	-0.765179	0.31068997	0.158592	0.49986206	-0.065635	0.01400572
Quadrate Articular Offset	0.0494548	0.4594403	0.50953734	0.61569542	-0.2225842	0.29825801	-0.0688771	-0.0671866

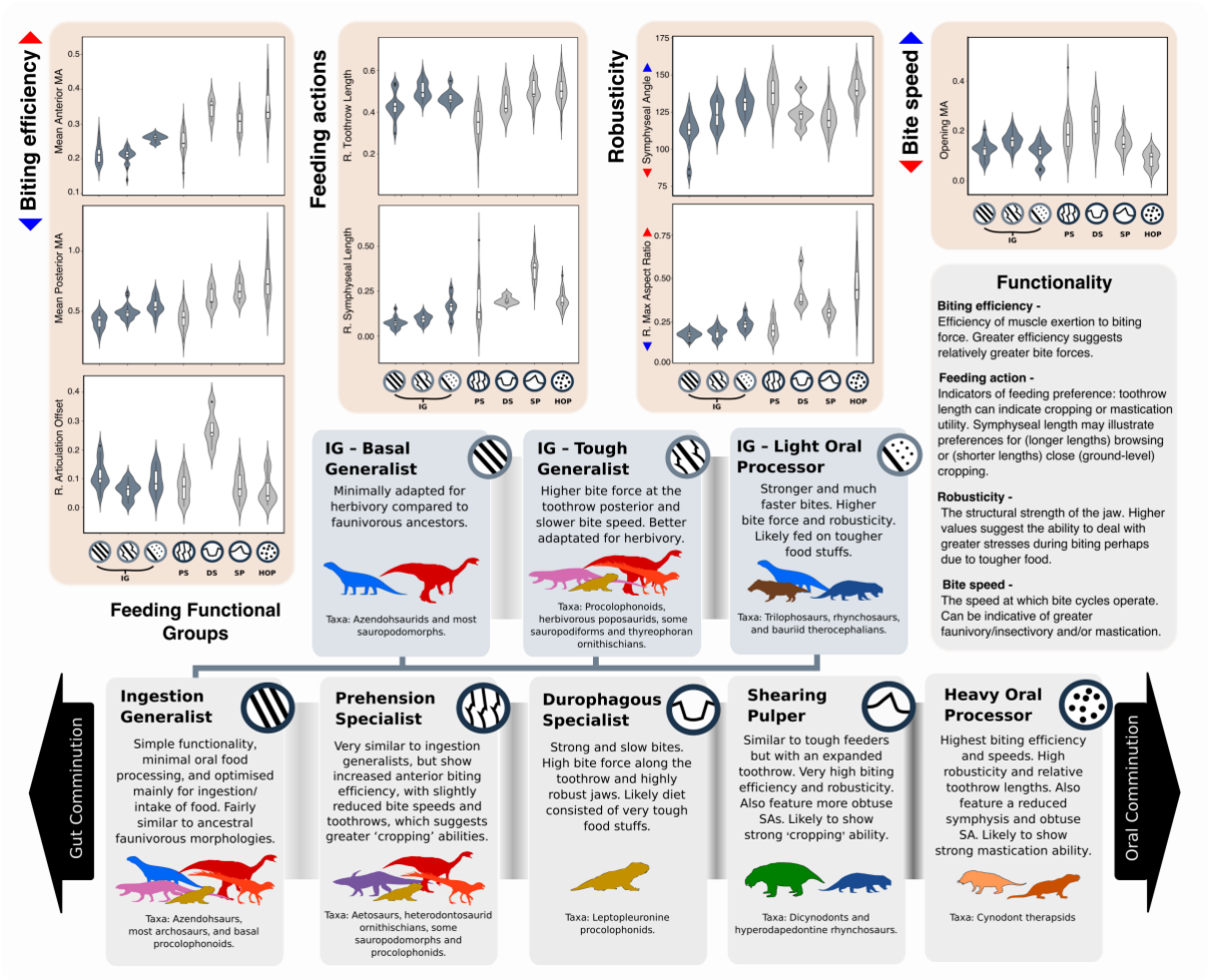

Figure 3.2.2. Functional feeding groups of early Mesozoic herbivores. Characteristics of the different functional feeding groups with silhouettes of the taxa that exhibit these feeding modes (see Fig. 1 for silhouette key). Preference of each group for gut or oral processing/comminution of food is indicated. The strength of separation between the groups is illustrated by the darkness of the band connecting each FFG description box. Violin plots show taxon density. Box plots showing median value and upper and lower quartiles, with whisker illustrating standard deviation. Abbreviations: DS, durophagous specialist. HOP, heavy oral processor. IG, ingestion generalist. PS, prehension specialist. SP, shearing pulper. SA, symphyseal angle.

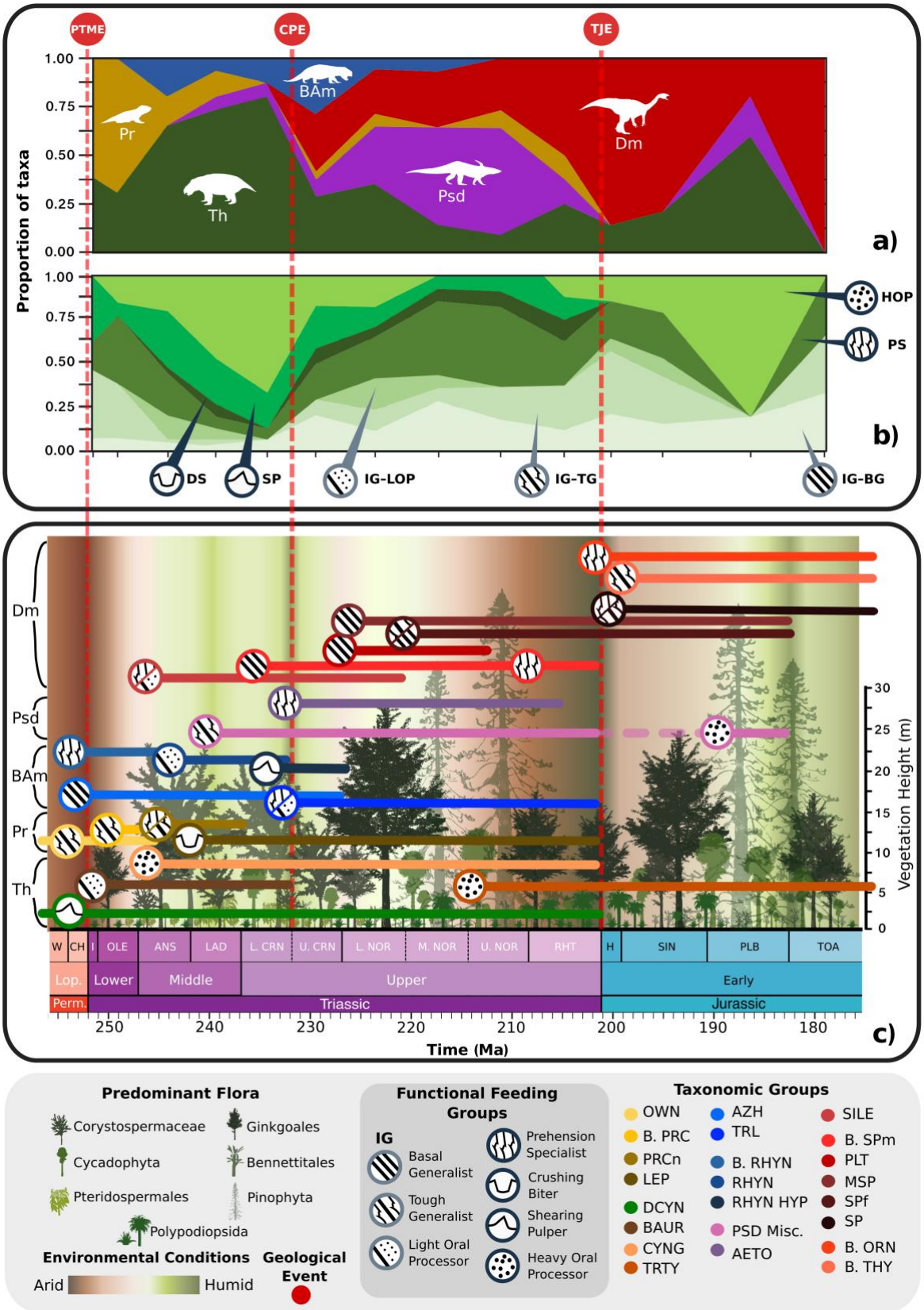

Figure 3.2.3. Functional feeding groups of early Mesozoic herbivores through time. a). The relative species richness of different clades through time. b). The relative richness of different functional feeding groups through time. c). Distribution of functional feeding

groups across different taxonomic groups and subgroups of herbivores is indicated. Clade and guild changes shown at the midpoints for each stage/substage in panels a and b. Temporal ranges of the groups are based on first and last fossil occurrence dates, highlighting the span of ecological prominence for each group. Environmental changes from arid to humid shown by background colour gradient. Predominant vegetation (Kustatscher et al., 2018; van de Schootbrugge et al., 2009; McElwain et al., 1999) and characteristic vegetation (relative) height (Anderson and Holmes, 2008; Dilcher et al., 2004) indicated by tree silhouettes. Abbreviations: Geological Events: PTME, Permian-Triassic mass extinction. CPE, Carnian Pluvial Event. TJE, Triassic-Jurassic mass extinction. Feeding Functional Groups: BG, basal generalist. DS, durophagous specialist. HOP, heavy oral processor. IG, ingestion generalist. LOP, light oral processor. PS, prehension specialist. SP, shearing pulper. TG, tough generalist. Larger Clades: Dm, Dinosauromorpha. Psd, Pseudosuchia. BAm, Basal Archosauromorpha. Pr, Parareptilia. Th, Therapsida. Taxonomic Groups: Parareptilia: OWN, Owenettidae. B. PRC, Basal Procolophonidae. PRCn, Procolophoninae. LEP, Leptopleuroninae. Therapsida: DCYN, Dicynodontia. BAUR, Bauriidae. CYNG, Cynognathia. TRTY, Tritylodontia. Archosauromorpha: ALLOK, Allokotosauria. B. RHYN, Basal Rhynchosauria. RHYN, Rhynchosauridae. RHYN HYP, Hyperodapedontinae. PSD Misc., Miscellaneous Pseudosuchia. AETO, Aetosauria. SILE, Silesauridae. B. SPm, Basal Sauropodomorpha. PLT, Plateosauridae. MSP, (non-sauropodiform) Massopoda. SPf, (non-sauropod) Sauropodiformes. SP, Sauropoda. B. ORN, Basal Ornithischia. B. THY, Basal Thyreophora. TRL, Trilophosauria.

Niche partitioning and competition avoidance. Were different clades of herbivores apparently competing for the same resources and in the same way? It seems not. I find that differences in jaw morphology are highly constrained by phylogeny and our FFGs do closely reflect phylogenetic groupings. Such phylogenetic structuring does not preclude meaningful functional interpretation of our FFGs to study divergent feeding strategies (Caumul and Polly, 2005; Raia et al., 2010); this simply reflects that morphology and thus functionality is highly controlled by phylogeny. The distinction between the areas of morphospace occupied by therapsids and archosauromorphs (Fig. 3.2.1a) represents their fundamentally different feeding priorities, in which archosauromorphs optimised prehension and therapsids optimised comminution. Therapsids appear to have consistently enhanced biting power, possessing greater MA than most sauropsids, and this may reflect differences in the primary jaw adductor musculature of sauropsids (pterygoideus) and therapsids (adductor mandibularis) (Olson, 1961). Sauropsid jaw mechanics are less efficient compared to

therapsids, but it is clear that sauropsids, particularly the archosaurs achieved significantly larger body sizes than therapsids (Sookias et al, 2012). Therefore, it appears that sauropsids favoured increasing their bite forces through boosting jaw muscle mass and the absolute power involved, rather than improve efficiency. Their separation in morphospace suggests broad-scale niche partitioning between members of these two clades, guided in part by phylogenetic constraint. Nonetheless, our patterns of shape and functional morphospace occupation show how both groups converged from basal amniote (faunivorous) morphologies (Janis and Keller, 2001) towards a common amniote-specific form of herbivory (Sues and Reisz, 1998).

At the level of FFGs, minimal overlap between the various therapsid and archosauromorph clades confirms that these herbivores were not in competition for most of the early Mesozoic, contrary to the competitive model (Fig. 3.2.3). When our FFGs are applied at ecosystem level for different localities (Fig. 3.2.4; Supplementary Data 3.2.S11, Table 3.2.6), I find that most co-occurring taxa belonged to different FFGs. Examples of coexisting herbivores with the same feeding functionality (Supplementary Table 3.2.5), and thus possibly competing, include procolophonids, bauriids and rhynchosaurs in the Early Triassic, hyperodapedontine rhynchosaurs and dicynodonts in the Lower Ischigualasto Formation (Carnian), and within dinosaur-dominated assemblages of the latest Triassic and Early Jurassic (Fig. 3.2.3), which is expected as most of these dinosaur groups have been shown to employ similar 'orthal' jaw mechanics (Nabavizadeh, 2020). Widespread morphological dissimilarity suggests highly diverse herbivore communities from around the globe such as in the Santa Maria (Brazil), Ischigualasto (Argentina), and Lossiemouth (UK) formations (Fig. 3.2.4) were sustained by niche partitioning, which enables ecologically similar taxa to coexist by diverging from each other in their demands on resources (Hutchinson, 1959; Finke and Snyder, 2008). The subdivision of resources by specialisation towards separate niches minimizes resource competition, whilst boosting feeding efficiency, and thus the chances of survival (Hardin, 1960; MacArthur, 1972; Tilman, 1982).

Our FFGs are broadly defined, so even these examples of possible competition may be exaggerated. The further identification of large subgroups within the ingestion generalist FFG (Fig. 3.2.2) highlights this, as use of these subgroups dramatically reduced the occurrences of potential trophic conflict (Supplementary Data 3.2.S11). Additionally, in the Carnian examples, the kannemeyeriiform dicynodonts were much larger (Keyser, 1974) and lacked the dental plates of rhynchosaurs (Benton, 1984). These two clades may well have specialised on different plant food while coexisting within the same broadly defined feeding guild. Further, among the Late Triassic herbivorous dinosaurs that also coexisted within broad feeding guilds (Fig. 3.2.3), niche partitioning has been noted already among sauropodomorph dinosaurs, expressed in their body size (McPhee et

al., 2015) and postural disparity (McPhee et al., 2018). Further evidence of tetrapod niche differentiation may be found in their dentition (Hoffman et al., 2019), body size (White et al, 2007), limb anatomy (Lungmus and Angielczyk, 2019), and even spatiotemporal behaviour (Patterson et al., 2003). Therefore, other aspects of ecology may support divergent trophic strategies and the avoidance of competition within these groups, although further comparative studies are needed. Competition between Early Triassic diapsids is more convincing as there are greater levels of coexistence, similarities between sizes, and abundances where found together (Supplementary Data S10).

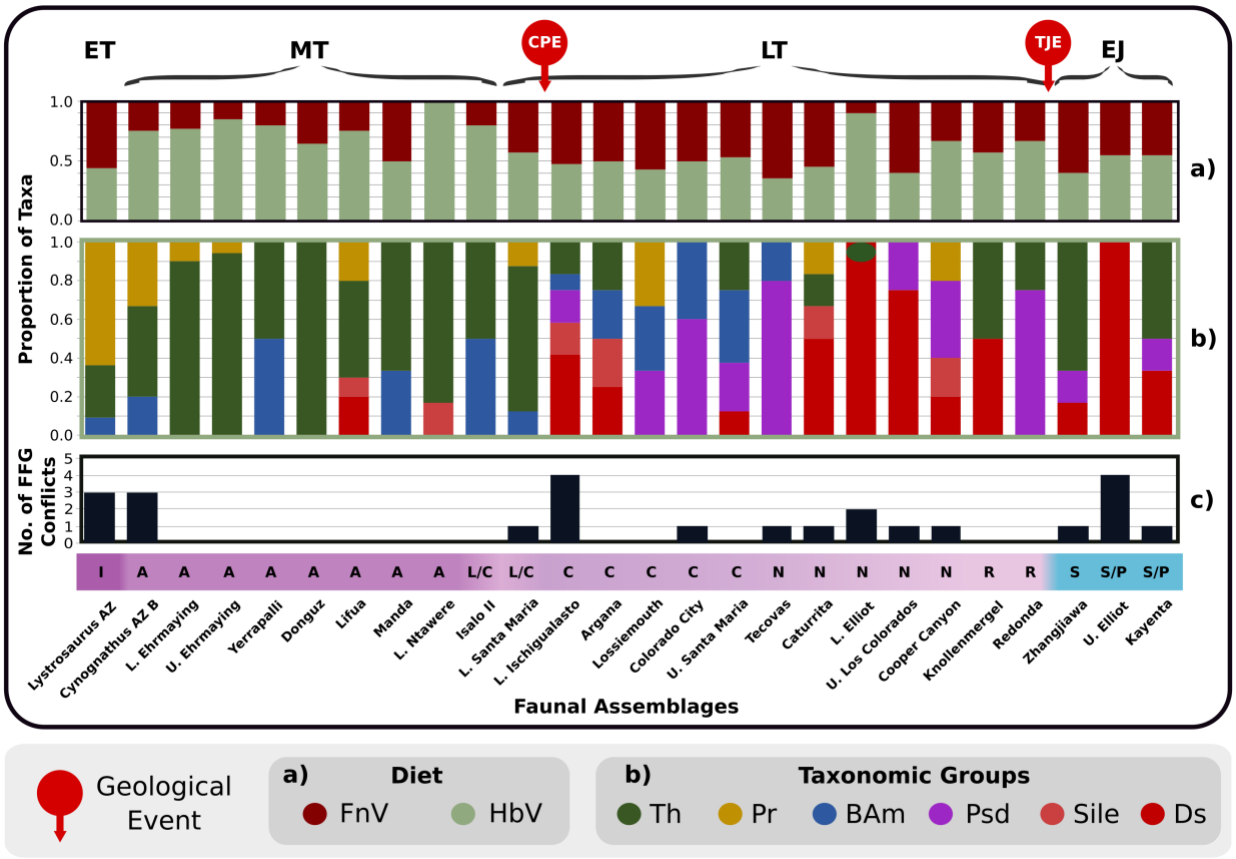

Figure 3.2.4. Relative faunal abundances and potential competitive trophic conflicts within early Mesozoic assemblages through time. (a) The relative abundance of faunivores and herbivores. (b) The relative species richness of different therapsids and sauropsid clades. (c) The number of feeding functional group (FFG) conflicts in each assemblage. Abbreviations: Geological Events: CPE, Carnian Pluvial Event. TJE, Triassic-Jurassic mass extinction. Epochs: EJ, Early Jurassic. ET, Early Triassic. LT, Late Triassic. MT, Middle Triassic. Diet: FnV, Faunivores. HbV, Herbivores. Taxonomic groups: BAm, Basal

Archosauromorpha. Ds, Dinosauria. Pr, Parareptilia. Psd, Pseudosuchia. Sile, Silesauridae. Th, Therapsida.

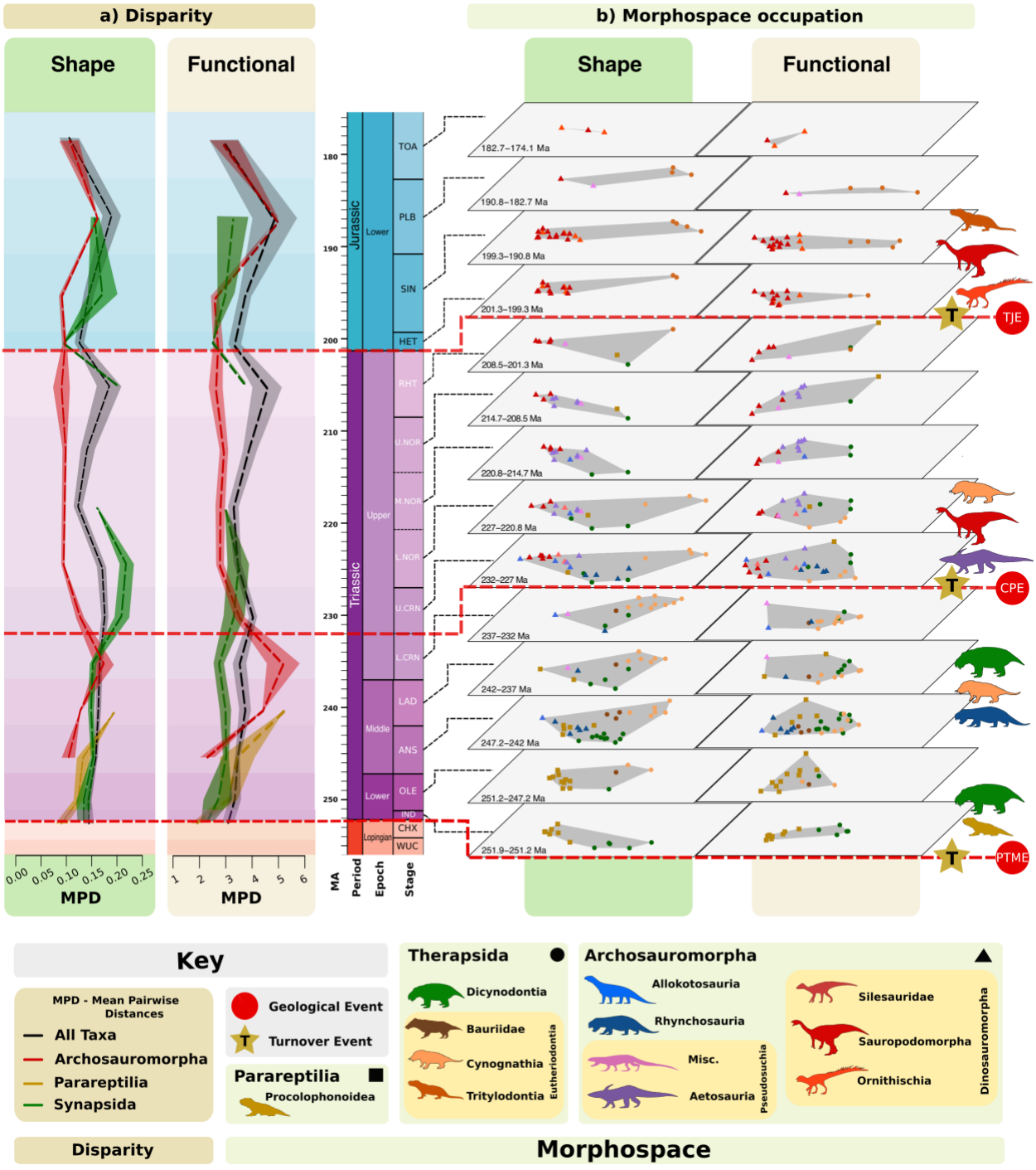

Figure 3.2.5. The shape and functional disparity and morphospace occupation of early Mesozoic herbivores through time. (a) Shape (Procrustes variance) and functional (sum of variance) disparity of Archosauromorpha, Therapsida, and Parareptilia. (b) Shape and functional morphospace time-slices at stage and substage levels. Major extrinsic,

environmental events are shown by the dashed red line. Faunal turnovers are highlighted by stars. Abbreviations: Misc., Miscellaneous pseudosuchians. PTME, Permo-Triassic mass extinction. CPE, Carnian Pluvial Event. TJE, Triassic-Jurassic extinction.

Temporal trends: changing of the guilds. Patterns of shape and functional disparity through geological time (Fig. 3.2.5a) generally show near reciprocal traces for therapsids and archosauromorphs – when values for one clade are trending upwards, those for the other are trending downwards. This is particularly apparent in the lower Carnian and Rhaetian. However, this pattern appears to vanish in the Norian, possibly due to poor sampling of the therapsids. Crossovers occur at the times of the Carnian Pluvial Event, 233 Ma, and in the aftermath of the Triassic-Jurassic mass extinction (TJE), 201 Ma. Comparison of trends in disparity with MO shows that the peaks correspond to either intervals of highly disparate diversification as in the archosauromorph radiation in the Middle Triassic or contrastingly, heavy decline and the survival of disparate taxa as seen in the last dicynodonts and parareptiles (Fig. 3.2.5b). The troughs in disparity typically and counter-intuitively indicate clade 'success' in the form of morphospace packing of a particular mandibular functional-morphology, epitomised in the relatively morphologically limited diversification of sauropodomorphs in the Late Triassic ((Fig. 3.2.5b). Given the lack of competitive potential between herbivorous clades, these reciprocal trends in disparity likely reflect the suitability and adaptive potential of these clades to prevailing conditions (Fig. 3.2.3). Both metrics broadly agree, showing rising archosauromorph shape and functional disparity through the Early and Middle Triassic, and then higher values for therapsids through most of the Late Triassic, and equivalent values in the Early Jurassic. Interestingly, this concordance breaks down in the Early Jurassic as a disconnect appears within therapsids (tritylodonts), with high shape disparity producing rather low functional disparity.

Dividing the shape and functional morphospaces temporally as stacked plots shows more detail of how different herbivorous clades waxed and waned (Fig. 3.2.5b). Herbivore guilds in the Early Triassic were dominated by procolophonoids and dicynodonts. During the Middle Triassic, parareptile disparity fell as the Early Triassic disaster fauna was complemented by new groups such as the gomphodont cynognathian cynodonts and archosauromorph allokotosaurs and rhynchosaurs. Archosauromorph disparity also increased as diversity increased with the emergence of new groups with new forms and functions, such as the rhynchosaurs and allokotosaurs. Therapsid disparity remained stable with the diversification of many morphologically similar kannemeyeriform dicynodonts masking the new diversity of cynodonts.

Near the beginning of the Late Triassic, the CPE marked a substantial change, as rhynchosaurs and dicynodonts disappeared or reduced to very low diversity and abundance, and archosauromorph herbivores took over (Benton; 1983; Benton et al., 2018; Bernardi et al., 2018). These were initially aetosaurs and sauropodomorph dinosaurs and, while expanding in diversity, their disparity declined (Fig. 3.2.5a) because new taxa were morphologically conservative, exhibiting limited variance and emerging within the existing morphospace of each respective clade (Fig. 3.2.5b). At the same time, all other herbivore clades declined, with remaining (parareptile and dicynodont) taxa shifting towards the extreme edges of their former morphospace occupancy. Cynognathians also dwindled in the early Norian. This transition within the herbivore guilds marks a shift from oral to gut processing among most large terrestrial herbivores (Fritz et al., 2011) (Figs. 3.2.2, 3.2.3, 3.2.5b).

During the Norian and Rhaetian, herbivore diversity and disparity gradually declined with only dinosaur and mammalian herbivores surviving into the Jurassic. Both groups underwent morphological and taxonomic radiations in the Early Jurassic, with dinosaurs and mammals typically occupying the roles of large and small herbivores, respectively. There was also a brief reappearance of pseudosuchian herbivores. I note that through the course of the early Mesozoic, sauropsid and therapsid morphospace became increasingly distanced from each other, with further comparison of the distances between therapsid and archosauromorph morphospace centroids showing that this separation accelerated at the onset of the Late Triassic (Supplementary Table 3.2.11).

At epoch scale, NPMANOVA identified significant shifts in morphospace occupation between the Early and Middle Triassic (shape and function: $p = 0.02$). At stage level, only the Olenekian-Anisian transition shows a significant shift in both shape and functional morphological diversity (shape: $p = 0.009$, function: $p = 0.007$) (Supplementary Table 3.2.13). These results denote the distinct shift from disaster faunas through the Early Triassic, marked by repeated climate perturbations, to the more stable conditions of the mid-Anisian onwards and faunal recovery from the PTME (Payne et al., 2004; Chen and Benton, 2012). The transitions between the lower Carnian-upper Carnian and Sinemurian-Pliensbachian were identified as being significant to shape but not function ($p = 0.01$ and 0.03) (Supplementary Table 3.2.13). These results for the Carnian are tantalising and tentatively highlight the impacts of the CPE as an important macroevolutionary event (Benton et al., 2018). Furthermore, at the $p < 0.1$ significance level, the functional differences between these two transitions are recovered as significant ($p = 0.06$ and 0.05), as well as the Pliensbachian-Toarcian transition ($p = 0.1$). However, it must be noted that if a Bonferroni correction is applied, I am unable to recover any significant results for stage transitions.

I recognise a repeated pattern in the replacements in herbivore guilds that coincided with the three crisis events:

- In the case of the PTME, so many clades had been entirely wiped out by the severity of the extinction that the few species of procolophonoids and dicynodonts that survived (Benton et al., 2004; Fröbisch, 2008) would likely have occupied a much-reduced ecospace relative to the latest Permian. Whilst procolophonoids began to decline in the Anisian, dicynodonts radiated alongside new rhynchosaurs and cynognathians. These clades came to dominate Middle Triassic herbivore guilds.
- The CPE hit these dominant groups hard, with survivors hanging on in the peripheries of their former morphological and functional space (Fig. 3.2.5b). Through the Norian and Rhaetian, these taxa became further confined to extreme areas of morphospace, whilst new archosaurian herbivores radiated.
- The TJE saw the extinction of the last procolophonoids, dicynodonts and cynognathians, (rhynchosaurs having already succumbed to extinction in the early Norian), as well as the aetosaurs, which had been important elements within Norian faunas (Fig. 3.2.3c). Though they vanished at the TJE, I find that these taxa actually began to decline during the Norian (Fig 3.2.5). The decline in these formerly dominant groups is mirrored by expansion of new dinosaur and mammalian herbivore clades. Despite also suffering severe declines in MO through the latest Triassic, both groups radiated in the Early Jurassic, moving into space vacated by aetosaurs and cynognathians, respectively. The Early Jurassic fossil record is limited, but total herbivore shape and function space were later refilled by sauropodomorph and ornithischian dinosaurs, as well as new mammalian clades.

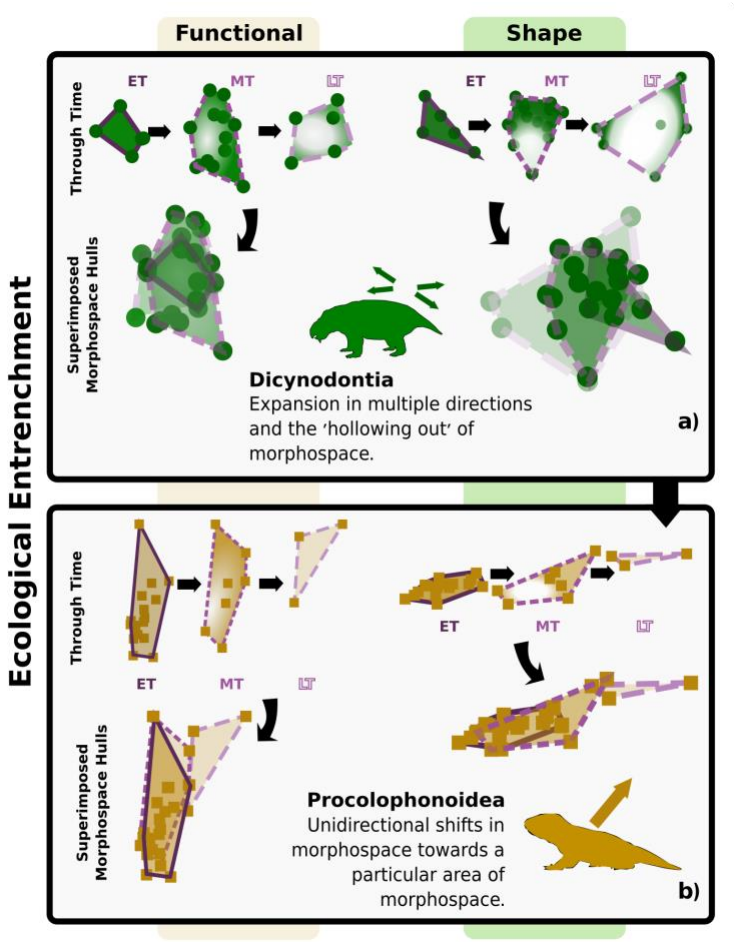

Figure 3.2.6. Ecological entrenchment illustrated using morphospace occupation through time. The isolated shape and functional morphospace convex hulls for two clades (dicynodonts and procolophonoids) from each epoch are shown in isolation and then overlaid over each other to showcase their pattern of morphospace decline through time. Abbreviations: Epochs: EJ, Early Jurassic. ET, Early Triassic. LT, Late Triassic. MT, Middle Triassic.

This pattern of marginalisation seen in both shape and function space (Fig. 3.2.5b) documents how stressed clades apparently 'retreat' into specialised niches at the periphery of their former occupancy. Sampling issues may confound observation of this pattern at stage level, but epoch-level comparisons of morphospace occupation highlights this pattern of declining disparity in certain clades through the Triassic (Fig. 3.2.6). This is seen three times through the Triassic and Early Jurassic, as the last parareptiles, rhynchosaurs and dicynodonts were pushed to peripheral positions in shape and function space after the rigours of the three mass extinction events (PTME, CPE, TJE). Likely then, the last survivors of each of these clades had become trophic specialists. As specialists, dicynodonts, hyperodapedontine rhynchosaurs and leptopleuronine procolophonids were

potentially more constrained than the new archosaur herbivores in shifting their diets towards the new prevailing flora. Survivors became further entrenched within specialist niches and rare following the crises. In becoming highly specialised, these groups were forced along an evolutionary ratchet (Van Valkenburgh et al., 2004) that amplified extinction risk as the environment changed and those niches disappeared. Specialists may outcompete generalists where high-quality resources are readily available and stable (Ramiadantsoa et al., 2018).

Consequently, this trophic specialism in combination with reduced abundance suggests this 'ecological entrenchment' is possibly correlated with geographic retrenchment to where preferred (floral) resources remained abundant, with the reduction in numbers and geographic spread exacerbating extinction risk (Gaston, 1998; Dunhill and Wills, 2015). 'Marginal' morphospace occupation may be followed by further restriction of MO to a smaller subset of morphospace (Fig. 3.2.5b and 3.2.6), which may relate to further 'hyper-specialisation' or perhaps the ongoing loss of refugia as conditions became increasingly adverse. Nonetheless, poor sampling is an acute issue, particularly as these clades approached extinction in the Late Triassic, so further study is required to test these tentative interpretations. Ecological entrenchment may have served to minimise competitive pressures and prolong survival in the face of increasingly heterogenous environmental conditions and new competitors that were able to better colonise/exploit predominant plant resources.

Extrinsic controls on herbivore macroevolution. Triassic climates oscillated between acute humid and extended dry phases (Preto et al., 2010), and these fluctuations triggered widespread and significant remodelling of terrestrial floras (Kustatscher et al., 2018; Cascales–Miñana and Cleal, 2012). Floral turnovers coincided with pulses of change in herbivore guilds. The transition from palaeophytic to mesophytic plant assemblages through the Ladinian and Carnian (Cascales–Miñana and Cleal, 2012) coincided with reduced morphospace packing by non-archosaurian herbivores (Figs. 3.2.3c and 3.2.5b). Herbivore functional diversity among dinosaurs and pseudosuchians expanded following the CPE. Widespread wetter climates in the CPE (Baranyi et al., 2019; Simms and Ruffel, 1990) may have triggered radiations of Bennettitales, Gnetales, and modern ferns and conifers[5], associated with the expansion of archosaurian herbivore diversity and taxon density within archosaur morphospace, which counter-intuitively reduced archosaur disparity (Fig. 3.2.5a). Increased morphospace packing by archosaurian herbivores (Fig. 3.2.5b) tentatively suggests that the increased prominence of some gymnosperms as arid conditions returned in the Norian (Cascales–Miñana and Cleal, 2012) may be linked to the survival of archosaur herbivores, particularly sauropodomorphs through the Carnian-Norian transition, whilst other herbivore groups perished.

The CPE was critical in triggering the decisive switch from dominance by therapsids as herbivores to the real beginning of the 'age of dinosaurs' (Figs. 3.2.3, 3.2.4, 3.2.5). Before the CPE, rhynchosaurs and dicynodonts comprised 50–80% of individuals within well sampled faunas, whereas after the CPE they had dwindled to low abundance, and aetosaurs and sauropodomorph dinosaurs replaced them numerically, in some Norian faunas comprising 80–90% of individuals (Benton et al., 2018). The decline of rhynchosaurs and dicynodonts has been previously linked to the decline of the '*Dicroidium* flora' (Fig. 3.2.3c) (Benton, 1983; Crompton and Attridge, 1986). This may reflect wider changes in the availability of water and floral resources at the end of the CPE as the climate became drier and more seasonal (Simms and Ruffel, 1990; Spalletti et al., 2003). Furthermore, morphological features potentially suggest that many of the 'seedferns' which dominated the *Dicroidium* flora may have had similar growth regimes and nutritional value as Gingkoales (Axsmith et al., 2000), which were potentially more nutritionally richer food for herbivores than the ferns and conifers that became more prominent through the Late Triassic (Hummel et al., 2008; Spalletti et al., 2003; Cascales–Miñana and Cleal, 2012). The TJE saw the end of aetosaurs, but sauropodomorphs continued to diversify and retained their ecological dominance as large herbivores, alongside the newly diversifying ornithischian dinosaurs.

The CPE did not cause the extinction of rhynchosaurs and dicynodonts but made them rare (Figs. 3.2.3 and 3.2.4). Rhynchosaurs went extinct in the early Norian (Ezcurra et al., 2016), whereas dicynodonts survived to the end of the Triassic, but at reduced diversity, abundance, and disparity (Ruta et al., 2013b; Racki and Lucas, 2018). This example shows the value of metrics of ecological abundance rather than species richness. Dicynodonts survived within wetter environments, even within dinosaur-dominated ecosystems (Dzik et al., 2008). Some of these latest taxa, such as *Lisowicia bojani* in Poland, even achieved huge body sizes that rivalled those of contemporaneous large sauropodomorphs (Sulej and Niedźwiedzki, 2019; Romano and Manucci, 2020). The survival of kannemeyeriform dicynodonts might be because their typically large body sizes enabled them to explore wider geographic areas in search of suitable habitats. Nonetheless, they went extinct at the end of the Triassic alongside aetosaurs and cynognathian cynodonts (Sues and Fraser, 2010) (Fig. 3.2.3c). The end-Triassic saw widespread deforestation alongside a dramatic reorganisation of global floras that favoured ferns, at the expense of tropical flora (van de Schootbrugge et al., 2009; McElwain et al., 1999). Sparsely vegetated floras dominated by ferns would have served as a poor food resource for large herbivores (Soh et al., 2017) and therefore may be linked to the extinction of most large herbivores (including the aforementioned clades). The only large herbivores that remained prevalent through the end-Triassic were the sauropodomorphs; given they share the ingestion generalist FFG with many pseudosuchian herbivores that perished in the TJE, it seems that

sauropodomorph success was not a result of novel jaw/feeding mechanics. This lack of mandibular functional superiority, when considered alongside the observation that all other large herbivores were largely low- to mid-level browsers, suggests that sauropodomorph success may stem from their ability to feed on higher, canopy-level vegetation by virtue of their larger sizes and long necks (Sander et al., 2011).

I find that the largest episodes of morphospace expansion occur during the supposed recovery intervals of mass extinction events, with some surviving clades (particularly dinosaurs) showing much greater MO than before the extinction event (Fig. 3.2.5b). Morphospace expansion following the PTME occurs relatively quickly compared to the TJE, suggesting a relatively faster ecological recovery. Following the PTME and the loss of most species, total herbivore disparity and FFGs reached maximum levels in the Anisian, whereas following the TJE, the rebound in morphological diversity was modest, even by the end of the Early Jurassic. However, there is an edge effect here as I have not continued the analysis into the Middle Jurassic, and there may be sampling problems, as there are few well documented terrestrial tetrapod faunas in the Sinemurian and Pliensbachian. The inclusion of later dinosaur taxa and the overall diversification of dinosaurs in the Jurassic would likely yield a greater diversity of FFG in the later Jurassic than seen at the end of the Early Jurassic. Furthermore, it is likely that the FFGs (light oral processors, shearing pulpers, and durophagous specialists) that disappeared within the Triassic would re-emerge as the climatic conditions stabilised from the end-Triassic event and terrestrial floras recovered (Cascales–Miñana and Cleal, 2012; Simms and Ruffel, 1990); the resurgence of floral diversity would likely have spurred new herbivorous diversification in both dinosaurs and mammals. The lost and depleted guilds identified here were likely restored as new dinosaurian and mammalian herbivores evolved through the later Mesozoic. Previous work highlights the prevalence of convergent evolution within dinosaurs (Button and Zanno, 2020), and this is recognised here with repeated patterns of specialisation towards higher biting efficiency and greater oral processing in procolophonoids, rhynchosaurs, aetosaurs and ornithischians (Figs. 3.2.1 and 3.2.2). The prevalence of these patterns across quite phylogenetically distant clades emphasises that ecomorphs can disappear and reappear as conditions permit. This is further illustrated by the continuation of the prehension specialist FFG through the TJE with minimal change (Fig. 3.2.3b), despite the loss of its main constituent clade, the aetosaurs. The extinction of the aetosaurs in the TJE was offset by the emergence of heterodontosaurid ornithischians and likely later thyreophorans as the Jurassic progressed and they followed the common ‘herbivore adaptive pathway’ (Figs. 3.2.2 and 3.2.3c). Aetosaurs-thyreophoran convergent evolution was not limited to jaw mechanics as ankylosaurs evolved similar armoured morphologies, and ecologies as large, quadrupedal, low-level feeders. However, these later thyreophorans developed more complex and

powerful jaw mechanics (Nabavizadeh, 2020), allowing them to diverge from aetosaurs and exploit different niches as specialised herbivores.

Our study shows substantial ecological shifts occurred mostly at times of environmental instability, with only incremental development of ecospace during times of relative stability. This highlights a fluctuation between times of normal or 'Red Queen' evolution typified by adaptation to intrinsic pressures, punctuated by times of crisis or 'Court Jester' evolution, when large-scale extrinsic events provide the dominant selective pressures (Benton, 2009). Our results confirm recent findings using model-based analyses that intrinsic, competitive interactions are the key to maintaining stasis within community assemblages through deep time (Ramiadantsoa et al., 2018; Roopnarine et al., 2019). Stasis is the norm, characterised by relatively stable climates and floras and honing of the adaptations of herbivores and slow expansion of morphospace occupation through biotic interaction.

The environmental perturbations of the three global crises, all involving sharp global warming, extremes of humidity and aridity, and acid rain nearly but not quite killed off the dominant incumbent herbivores. The few survivors endured at the periphery of their former shape and function spaces, perhaps ecologically marginalized due to loss of food sources or because other surviving herbivores monopolised the newly prevalent vegetation. Episodes of instability mark a flip from dominance of competitive ability as the key driver of evolution to opportunism in perturbed times when the winners and losers might reflect entirely different selective advantages.

Supplementary Materials

Supplementary Methods

Alternative data transformation methods: In order to assess trophic macroevolution using multivariate data, I applied principal component analyses (PCAs) to the shape-aligned coordinate data and functional measurement matrix. The functional dimensional scaling was executed using multiple procedures to offset the impacts of potential violations of the data assumptions in a PCA. A z-standardisation to the continuous character data prior to running the PCA was applied following the procedures of many previous studies[1,3–6]. I also explored the impact of using an additional logit standardisation on the proportional ratio characters (all characters barring the symphyseal angle) prior to the z transformation using the gtools R package[7]. This was done to enable our data to better fulfil the linear assumptions of subsequent analyses and test the potential impacts of non-linearity in our data, which is often an issue of ratio data[8]. As a monotonic function, the logit transformation has become a favoured option for linearising proportional data, particularly when variance stabilisation is no longer a prime concern as is the case with non-binomial ratios [9]. The transformation proved inapplicable to two tritylodont taxa (*Bienotherium* and *Bocatherium*) due to their exceedingly high posterior mechanical advantage values, meaning this character was automatically adjusted to the mean values for these taxa in a PCA. However, I used the 'fill.missing' function from the nbpMatching package[10] to impute the missing values using the greatest correlation with the best linear combination of the other characters.

The resulting morphospaces show subtle differences (Supplementary Fig. S4-S5), likely due to the different algorithms employed by each method. Comparison of the different results shows that the broad patterns of different groupings and associations tend to remain constant, with an additional Procrustes correlation analysis conducted using the vegan r package[11] finding strong correlation between the z and logit transformed PCA scores (Supplementary Table 4). The are some slight differences on the lower PC axes that result from emphasis being placed on different characters (Supplementary Table 1). This nonetheless alters the placement of some taxa, mainly the aetosaurs and the leptopleuronid procolophonids.

Feeding functional subgroup cluster analyses: A disproportionately large number of (predominantly sauropsid) taxa were recovered within a single cluster group, and while I termed this group 'ingestion generalists', I felt this grouping provided little diagnostic use as an FFG in our investigations of potential competition. Therefore, I re-ran the above cluster procedures using only

the ingestion generalist taxa to recover more details of potential clade-level competition, and I then identified three FFsGs (basal generalists, tough generalists, and light oral processors).

I further tested the robusticity of our FFGs by running the above cluster analyses and FFG construction using data subject to alternative standardisation (see supplement). The resulting FFGS show some classification differences within the sauropsids and a shift in the boundary of the ingestion generalists and prehension specialists (Supplementary Data 3.2.S15 and Supplementary Fig. S6). These differences reflect the strong levels of morphological conservatism within the sauropsids and key changes in the relative importance of our functional characters. However, the core assortment of taxa in each FFG largely remains and the alternative FFG results do not change the conclusions presented here.

Alternative cluster analysis. Subtle differences in the PCA results led us to further test the robusticity of the functional feeding group (FFG) assignments by rerunning the cluster analyses using the logit transformed data. The resulting FFGs show close similarities to those derived from the z transformed data (Supplementary Fig. S3.2.4). However, there are some prominent differences within the sauropsids as the logit cluster results (Supplementary Data S15) show that the tough generalist and light oral processor functional feeding subgroups remain largely intact but are now grouped with prehension specialists instead of the ingestion generalists. Additionally, the unique durophagous specialist FFG populated exclusively by the leptopleuronid procolophonids are now grouped with the shearing pulper group. These changes reflect the impact of the logit transformation on the relative weighting of the functional characters, with the relative articulation offset character in particular losing discriminatory power and being reflected in lower PC axes (Supplementary Table 3). It should be noted the relative articulation offset was a character that distinguished the durophagous specialists in the main (z transformed) results (Fig. 3.2.2). The differences evidently stem from the alternative treatment of the data, but I also suggest that this is a result of the strong sauropsid morpho-functional conservatism as highlighted in the discussion. The general indistinctiveness of niche boundaries combined with high levels of similarity between sauropsid taxa means that changes to classifications for taxa on the peripherals of cluster 'cores' is not unexpected. Indeed, I notice that the cluster cores remain largely intact, affirming the general robusticity of our FFGs.

The slight differences noted here should not be overlooked, but as the fundamental relationships that are key to our later competition analyses remain relatively constant, and so I retain the 'z transformed only' PCA results as they offer greater discrimination between groups and enable more coherent comparison with previous studies of some of the amniote groups presented

here[1,3]. The logit results do not dispute the core findings of this study which identify stronger support for potential competition between sauropsids, particularly the archosaurs, rather than between sauropsids and synapsids in the Triassic.

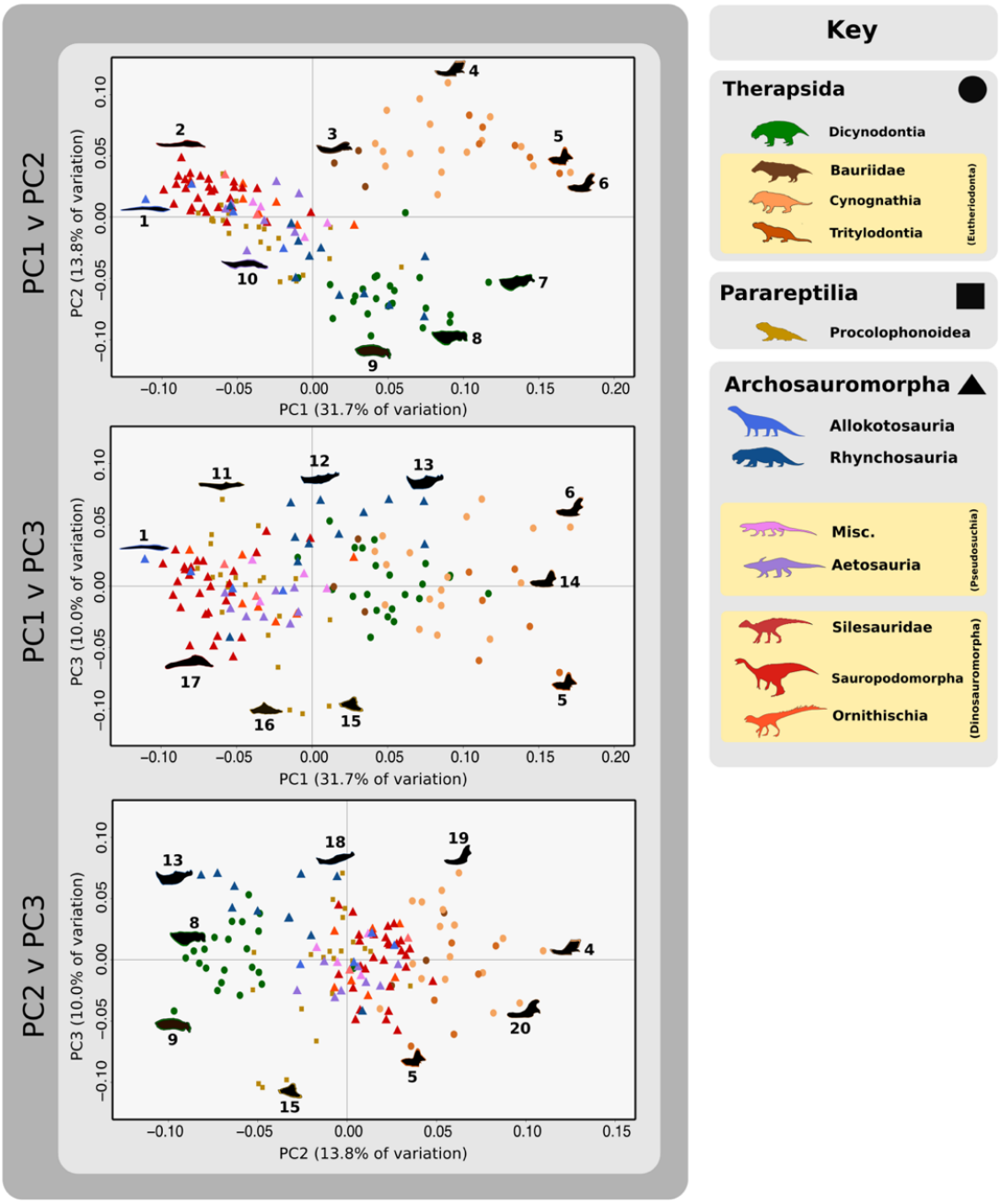

Supplementary Figure 3.2.S1. Early Mesozoic herbivore shape morphospaces using combinations of the first three principal components. Mandible silhouettes = 1. *Teraterpeton hrynewichorum*. 2. *Leyesaurus marayensis,* 3. *Traversodontoides wanguensis*. 4. *Sinognathus gracilis.* 5. *Yunnanodon brevirostre.* 6. *Siriusgnathus niemeyerorum*. 7.

Lystrosaurus hedini, 8. *Ischigualastia jenseni*, 9. *Placerias hesternus*. 10. *Desmatosuchus haplocerus*, 11. *Kitchingnathus untabeni*, 12. *Fondonyx spenceri*, 13. *Hyperodapedon huxleyi*, 14. *Ruberodon roychowdhurii*, 15. *Hypsognathus fenneri*. 16. *Leptopleuron lacertinum*, 17. *Sarahsaurus aurifontanalis*, 18. *Stenaulorhynchus sp*., 19. *Pascualgnathus polanskii*, 20. *Dadadon isaloi*.

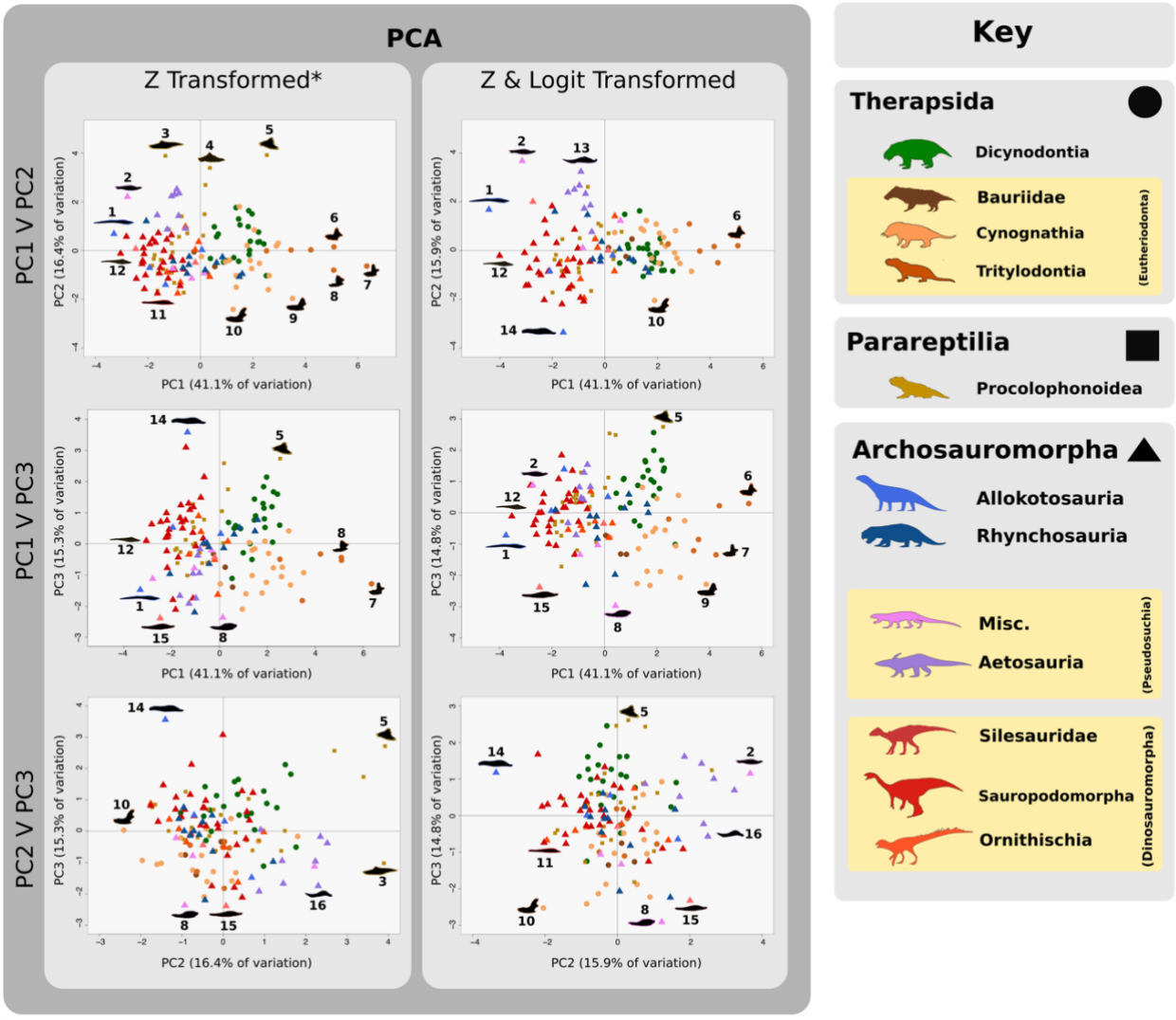

Supplementary Figure 3.2.S2. Early Mesozoic herbivore functional morphospace results from PCA using only z and z and logit transformed data. Mandible silhouettes = 1. *Teraterpeton hrynewichorum*. 2. *Lotosaurus adentus,* 3. *Eumetabolodon bathycephalus*. 4. *Leptopleuron lacertinum.* 5. *Hypsognathus fenneri*. 6. *Yunnanodon brevirostre.* 7. *Bocatherium mexicanum*. 8. *Bienotherium yunnanense*. 9. *Ruberodon roychowdhurii*. 10. *Siriusgnathus niemeyerorum*. 11. *Eoraptor lunensis*. 12. *Pampadromaeus barberenai*. 13.

Stenomyti huangae. 14. *Azendohsaurus madagaskarensis.* 15. *Silesurus opolensis*. 16. *Stagonolepis robertsoni.*

Biting efficiency
Mean Anterior MA
Mean Posterior MA
R. Articulation Offset
Feeding actions
R. Toothrow Length
R. Symphyseal Length
Robusticity
Symphyseal Angle
R. Max Aspect Ratio
Bite speed
Opening MA
Key
Feeding Functional Groups
Ingestion Generalist
Prehension Specialist
Durophagous Specialist
Shearing Pulper
Heavy Oral Processor
Indicates higher (red) or lower (blue) levels of particular functionality
Functionality
Biting efficiency - Efficiency of muscle extertion to biting force. Greater efficiency suggests relatively greater bite forces.
Feeding action - Indicators of feeding preference: toothrow length can indicate cropping or mastication utility. Symphyseal length may illustrate preferences for (longer lengths) browsing or (shorter lengths) close (ground-level) cropping.
Robusticity - The structural strength of the jaw. Higher values suggest the ability to deal with greater stresses during biting perhaps due to tougher food.
Bite speed - The speed at which bite cycles can operate. Can be indicative of greater faunivory/insectivory and/or mastication.
Gut Comminution
Ingestion Generalist
Simple functionality, minimal oral food processing, and optimised mainly for ingestion/ intake of food. Fairly similar to ancestral faunivorous morphologies.
Predominant taxa: Azendohsaurs, most archosaurs, and basal procolophonoids.
Prehension Specialist
Very similar to ingestion generalists, but show increased anterior biting efficiency, with slightly reduced bite speeds and toothrows, which suggests greater 'cropping' abilities.
Predominant taxa: Aetosaurs, heterodontid ornithischians, and some sauropodomorphs and procolophonids.
Durophagous Specialist
Strong and slow bites. High bite force along the toothrow and highly robust jaws. Likely diet consisted of very tough food stuffs.
Predominant taxa: Leptopleuronid procolophonids.
Shearing Pulper
Similar to tough feeders but with an expanded toothrow. Very high biting efficiency and robusticity. Also feature more obtuse SAs. Likely to show strong 'cropping' ability.
Predominant taxa: Dicynodonts and hyperodapedontine rhynchosaurs.
Heavy Oral Processor
Highest biting efficiency and speeds. High robusticity and relative toothrow lengths. Also feature a reduced symphysis and obtuse SA. Likely to show strong mastication ability.
Predominant Taxa: Cynodont therapsids
Oral Comminution

Supplementary Figure 3.2.S3. Early Mesozoic herbivore feeding functional group characters – first step results. Feeding action characteristics not suitable for red/blue description as indicative of varying bite mechanics suggestive of different feeding. Abbreviations: MA, Mechanical advantage. R, Relative.

Oral Comminution
Gut Comminution
Ingestion Generalist
Simple functionality, minimal oral food processing, and optimised mainly for ingestion/ intake of food. Very similar to ancestral faunivorous morphologies.
Predominant taxa: Azendohsaurs, most sauropodomorphs, and basal procolophonoids.
Prehension Specialist
Similar to ingestion generalists, but show increased anterior biting efficiency, with slightly reduced bite speeds and toothrows, which suggests greater 'cropping' abilities.
Predominant taxa: Pseudosuchians, ornithischians and later procolophonids.
Shearing Pulper
Similar to tough feeders but with an expanded toothrow. Very high biting efficiency and robusticity. Also feature more obtuse SAs. Likely fed on very tough plant material.
Predominant taxa: Dicynodonts, leptopleuronid procolophonids and hyperodapedontine rhynchosaurs.
Heavy Oral Processor
Highest biting efficiency and speeds. High robusticity and relative toothrow lengths. Also feature a reduced symphysis and obtuse SA. Likely to show strong mastication ability.
Predominant Taxa: eutheriodont therapsids
Functionality
Biting efficiency - Efficiency of muscle extertion to biting force. Greater efficiency suggests relatively greater bite forces.
Feeding action - Indicators of feeding preference: toothrow length can indicate cropping or mastication utility. Symphyseal length may illustrate preferences for (longer lengths) browsing or (shorter lengths) close (ground-level) cropping.
Robusticity - The structural strength of the jaw. Higher values suggest the ability to deal with greater stresses during biting perhaps due to tougher food.
Bite speed - The speed at which bite cycles can operate. Can be indicative of greater faunivory/insectivory and/or mastication.
Biting efficiency
Mean Anterior MA
Mean Posterior MA
R. Articulation Offset
Feeding actions
R. Toothrow Length
R. Symphyseal Length
Robusticity
Symphyseal Angle
R. Max Aspect Ratio
Bite speed
Opening MA
Key
Feeding Functional Groups
Ingestion Generalist
Prehension Specialist
Shearing Pulper
Heavy Oral Processor
Indicates higher (red) or lower (blue) levels of particular functionality

Supplementary Figure 3.2.S4. Early Mesozoic herbivore feeding functional group characters for logit data. Feeding action characteristics not suitable for red/blue description as indicative of varying bite mechanics suggestive of different feeding. Abbreviations: MA, Mechanical advantage. R, Relative.

Supplementary Table 3.2.1. Character loadings to functional principal component (fPC) scores using logit and Z-transformed data. Abbreviations: MA, Mechanical advantage. *Character not subject to logit transformation.

Functional Characters	fPC 1	fPC 2	fPC 3	fPC 4	fPC 5	fPC 6	fPC 7	fPC 8
Mean Anterior MA	0.49503534	0.23122617	0.10536859	0.04964019	-0.1273287	-0.3363787	-0.1565343	0.73078148
Mean Posterior MA	0.49693454	-0.1216105	0.07959073	-0.1474894	0.18112881	-0.1646706	-0.6462706	-0.4822753
Opening MA	-0.1806332	0.32970026	0.53062276	-0.5059771	0.55308876	-0.0403764	0.09063646	0.07310027
Max Aspect Ratio	0.49570689	0.05747547	0.00678971	0.12181526	0.13688021	-0.3172677	0.71115436	-0.3330926
Relative Toothrow Length	0.26850726	-0.6430047	-0.1077064	-0.0763911	0.47019064	0.39168346	0.11757984	0.32968526
Relative Symphyseal Length	0.3813682	0.21990249	0.22890568	-0.2835418	-0.4432088	0.67654042	0.11067584	-0.0837695
Symphyseal Angle*	0.10931081	0.59506341	-0.4519173	0.31625262	0.44803486	0.34126223	-0.1116049	-0.0074124
Quadrate Articular Offset	-0.0124778	-0.0618631	0.657821	0.72019698	0.08993274	0.1728038	-0.0731168	-0.0361939

Supplementary Table 3.2.2. Symmetric Procrustes analysis results. Illustrates the degree of correlation between the functional principal component scores generated using alternate data transformation regimes: using a Z-transformation and using both logit and Z-transformations.

Symmetric Procrustes Analysis Results	
Procrustes Sum of Squares	0.05407
Correlation in a symmetric Procrustes rotation	0.9726
Significance	0.0001

Supplementary Table 3.2.3. Internal validation statistics for different cluster configurations. Abbreviations: PAM, partition around medoids. WSS, within cluster sum of squares. MDC, mean distance from cluster centroid. MDB, mean distance between cluster centroids. pF Value, pseudo F value.

Clustering Method	WSS	MDC	MDB	pF Value	Dunn Index
Hierarchical	528.7776	2.667516	4.158011	1.558758	0.1247351
K-means	495.668	2.605416	4.16443	1.598375	0.1466154
PAM	543.0932	2.683238	4.062733	1.514116	0.06729752

Supplementary Table 3.2.4. External validation statistics for different cluster configurations. Abbreviations: PAM, partition around medoids. WSS, within cluster sum of squares. MDC, mean distance from cluster centroid. MDB, mean distance between cluster centroids. pF Value, pseudo F value.

Phylogenetic Groups	Corrected Rand Index		Meila's VI Index	
	Broad Clades	Higher Resolution Clades	Broad Clades	Higher Resolution Clades
Hierarchical	0.2871463	0.08786818	1.947933	2.703176
K-means	0.3190135	0.1046528	1.824302	2.567004
PAM	0.341187	0.1223362	1.939353	2.603949

Supplementary Table 3.2.5. Feeding functional group conflicts within early Mesozoic assemblages. The total proportions herbivore and herbivorous dinosaur species also shown. Clades: B. PrcD, Basal Procolophonidae. B. RhyncD, Basal Rhynchosauridae. ProcN, Procolophoninae. RhyncD, Rhynchosauridae. Hyp. RhyncD, Hyperodapedontin**e** Rhynchosauridae. Lept. PrcD, Leptopleuronine Procolophonidae. B. SauropodM, Basal Sauropodomorpha. B. Thyreophora, Basal Thyreophora. Misc. Psd, Miscellaneous Pseudosuchia. Assemblage data from the Early Tetrapod Dataset (ETD) by Benton et al., (2013).

Assemblages	Potential FFG Conflicts	Groups Involved	Conflict FFG
Lystrosaurus AZ	3	Procolophonoidea	IG - Tough Generalists
Cynognathus AZ (B)	3	Rhynchosaurs, Procolophonidae, and Bauriidae	IG - Tough Generalists, IG – Light Oral Processors, Prehension Specialists
Lower Ehrmaying	0		
Upper Ehrmaying	0		
Yerrapalli	0		
Donguz	0		
Lifua	0		
Manda	0		
Lower Ntawere	0		
Isalo II	0		
Lower Santa Maria	1	Dicynodonts and Hyperodapedontine rhynchosaurs	Shearing Pulpers
Lower Ischigualasto	4	Silesauridae and Aetosauria and Poposauridae	Prehension Specialists
		Dicynodonts and Hyperodapedontine rhynchosaurs	Shearing Pulpers
Argana	0		
Lossiemouth	0		
Colorado City	1	Trilophosaurs and Aetosaurs	Prehension Specialists

Santa Maria U	0		
Tecovas	1	Trilophosaurs and Aetosaurs	Prehension Specialists
Caturrita	1	Sauropodomorpha	IG - Basal Generalists
Lower Elliot	2	Sauropodomorpha	IG - Basal Generalists
		Thyreophoran Ornithischians and Sauropodiformes	IG - Tough Generalists
Los Colorados U	1	Sauropodomorphs	IG - Basal Generalists
Cooper Canyon	1	Shuvosaurids and Aetosaurs	Prehension Specialists
Knollenmergel	0		
Redonda	0		
Zhangjiawa	1	Sauropodomorpha and Pseudosuchia	Prehension Specialists
Kayenta	1	Misc. Pseudosuchia and Tritylodontia	Heavy Oral Processors
Upper Elliot	4	Thyreophoran Ornithischians, Sauropodiformes and Sauropods	IG - Tough Generalists
		Ornithischians and Sauropods	Prehension Specialists

Supplementary Table 3.2.6. Results for herbivore shape and functional disparity at stage level with minimum and maximum bounds for 95% confidence intervals.

Abbreviations: L., Lower. M., Middle. Max, Maximum. Min, Minimum. MPD, Mean pairwise distance. U., Upper.

	Timebin	Shape			Function		
		MPD	MPD min	MPD max	MPD	MPD min	MPD max
Total herbivore disparity	Induan	0.1445887	0.13483597	0.1542025	3.100405	2.873077	3.326893
	Olenekian	0.1432726	0.13699571	0.1495954	3.429627	3.194541	3.672072
	Anisian	0.1579298	0.15496873	0.1608701	3.466344	3.376638	3.55972
	Ladinian	0.162579	0.15765787	0.1674503	3.752859	3.536768	3.969487
	L. Carnian	0.1652017	0.15989481	0.1706082	3.538404	3.289624	3.785865
	U. Carnian	0.1750951	0.16897517	0.1813733	4.04509	3.905203	4.183961
	L. Norian	0.1668659	0.15825504	0.1756525	3.488175	3.33425	3.640399
	M. Norian	0.1235526	0.11549975	0.131735	3.309642	3.10023	3.516843
	U. Norian	0.1447827	0.13058011	0.1593925	4.068642	3.690119	4.464911
	Rhaetian	0.183866	0.15975648	0.2073251	4.598277	4.053449	5.15978
	Hettangian	0.1261408	0.11740697	0.1352225	3.3409	3.094312	3.585143
	Sinemurian	0.1447199	0.13545447	0.1540862	3.741877	3.509254	3.982271
	Pliensbachian	0.1880424	0.17090689	0.2064568	4.863254	4.055635	5.700277
	Toarcian	0.1064164	0.08799137	0.1248414	2.932972	2.387499	3.478445

Supplementary Table 3.2.7. Results for archosauromorph shape and functional disparity at stage level with minimum and maximum bounds for 95% confidence intervals. Abbreviations: L., Lower. M., Middle. Max, Maximum. Min, Minimum. MPD, Mean pairwise distance. U., Upper.

	Timebin	Shape			Function		
		MPD	MPD min	MPD max	MPD	MPD min	MPD max
Archosauromorpha disparity	Induan	NA	NA	NA	NA	NA	NA
	Olenekian	NA	NA	NA	NA	NA	NA
	Anisian	0.10474423	0.09228994	0.1175903	2.307067	2.015081	2.565871
	Ladinian	0.1278479	0.1278479	0.1278479	4.426436	4.426436	4.426436
	L. Carnian	0.17397138	0.1560309	0.19191187	5.197552	4.563563	5.831541
	U. Carnian	0.12729403	0.1196138	0.13517212	3.54249	3.355211	3.72607
	L. Norian	0.09847115	0.09385611	0.10321581	2.747459	2.580191	2.920414
	M. Norian	0.09658072	0.09307374	0.10005029	2.8028	2.615463	2.984609
	U. Norian	0.10157567	0.09590351	0.10746544	3.079998	2.822621	3.342785
	Rhaetian	0.09058495	0.0762065	0.10703437	2.636028	2.368081	2.894308
	Hettangian	0.09746722	0.09331604	0.10178418	2.710316	2.523729	2.899712
	Sinemurian	0.09116253	0.08783565	0.09440833	2.579776	2.425916	2.737153
	Pliensbachian	0.16169554	0.16169554	0.16169554	5.004178	5.004178	5.004178
	Toarcian	0.10641641	0.08799137	0.12484144	2.932972	2.387499	3.478445

Supplementary Table 3.2.8. Results for parareptile shape and functional disparity at stage level with minimum and maximum bounds for 95% confidence intervals. Abbreviations: L., Lower. M., Middle. Max, Maximum. Min, Minimum. MPD, Mean pairwise distance. U., Upper.

	Timebin	Shape			Function		
		MPD	MPD min	MPD max	MPD	MPD min	MPD max
Parareptilia disparity	Induan	0.09149552	0.07986558	0.1035187	1.914165	1.702471	2.127557
	Olenekian	0.12351262	0.11468565	0.1320419	3.093589	2.756892	3.446809
	Anisian	0.13327885	0.12129245	0.146882	3.445285	2.796384	4.119149
	Ladinian	0.19631361	0.19631361	0.1963136	5.265504	5.265504	5.265504
	L. Carnian	NA	NA	NA	NA	NA	NA

	U. Carnian	NA	NA	NA	NA	NA	NA
	L. Norian	NA	NA	NA	NA	NA	NA
	M. Norian	NA	NA	NA	NA	NA	NA
	U. Norian	NA	NA	NA	NA	NA	NA
	Rhaetian	NA	NA	NA	NA	NA	NA
	Hettangian	NA	NA	NA	NA	NA	NA
	Sinemurian	NA	NA	NA	NA	NA	NA
	Pliensbachian	NA	NA	NA	NA	NA	NA
	Toarcian	NA	NA	NA	NA	NA	NA

Supplementary Table 3.2.9. Results for therapsid shape and functional disparity at stage level with minimum and maximum bounds for 95% confidence intervals.

Abbreviations: L., Lower. M., Middle. Max, Maximum. Min, Minimum. MPD, Mean pairwise distance. U., Upper.

	Timebin	**Shape**			**Function**		
		MPD	**MPD min**	**MPD max**	**MPD**	**MPD min**	**MPD max**
Therapsida disparity	Induan	0.1338565	0.1221877	0.145506	2.278369	2.065287	2.499334
	Olenekian	0.1344112	0.120528	0.1469067	2.716522	2.157714	3.25092
	Anisian	0.1530128	0.1481407	0.1577795	3.019929	2.916729	3.12159
	Ladinian	0.1489864	0.1430042	0.1549179	2.998761	2.77864	3.21537
	L. Carnian	0.1522754	0.146442	0.1583021	2.750761	2.559374	2.944616
	U. Carnian	0.2089568	0.194219	0.2222803	3.309207	2.914151	3.714083
	L. Norian	0.2178604	0.2035501	0.2305253	3.497063	3.067216	3.894637
	M. Norian	0.1589451	0.1589451	0.1589451	2.987786	2.987786	2.987786
	U. Norian	NA	NA	NA	NA	NA	NA
	Rhaetian	0.2031484	0.2031484	0.2031484	3.739695	3.739695	3.739695
	Hettangian	0.0949083	0.0949083	0.0949083	2.511281	2.511281	2.511281
	Sinemurian	0.1710371	0.142037	0.198981	2.987366	2.677312	3.332465
	Pliensbachian	0.1558767	0.1479013	0.1638522	3.287281	2.687763	3.8868
	Toarcian	NA	NA	NA	NA	NA	NA

Supplementary Table 3.2.10. Shape and functional differences through time by clade. Euclidean distances of taxa in successive timebins. The mean change between timebins is highlighted in bold, with greater than average changes in italic. Abbreviation: ANS, Anisian. CRN, Carnian. HET, Hettangian. IND, Induan. LAD, Ladinian. M, Middle. NOR, Norian. OLE, Olenekian. PLB, Pliensbachian. RHT, Rhaetian. SIN, Sinemurian. TOA, Toarcian.

Raw distances	**PR GM Distance**	**PR FM Distance**	**ThP GM Distance**	**ThP FM Distance**	**Arch GM Distance**	**Arch FM Distance**
IND to OLE	0.037588717	0.765074367	*0.09602917*	*2.550595194*	NA	NA
OLE to ANS	0.040774895	1.159737606	0.046512798	1.194520406	NA	NA
ANS to LAD	0.081554452	*2.11375207*	0.037871321	0.699428297	*0.054723111*	*1.304334986*
LAD to L. CRN	*0.132998282*	*2.855256367*	0.037419148	0.710375579	*0.060287797*	*1.726533898*
L. CRN to U. CRN	NA	NA	*0.082236526*	1.205805001	*0.051580074*	*1.365566866*
U. CRN to L. NOR	NA	NA	0.027494766	0.553003559	0.031315572	0.616074704
L. NOR to M. NOR	NA	NA	*0.097036481*	*2.221965681*	0.013964427	0.529565097
M. NOR to U. NOR	NA	NA	*0.079472209*	*1.499415491*	0.012741677	0.23603122
U. NOR to RHT	NA	NA	*0.101573793*	*1.876759861*	*0.052903971*	*1.655405751*
RHT to HET	NA	NA	*0.100056957*	*2.219552363*	*0.043658529*	0.835106611
HET to SIN	NA	NA	0.05032122	0.890317593	0.020617797	0.619080702
SIN to PLB	NA	NA	*0.100408418*	1.020866782	*0.056729342*	*1.38183536*
PLB to TOA	NA	NA	NA	NA	*0.078989447*	*1.489050518*
Mean distance	**0.073229086**	**1.723455102**	**0.066336469**	**1.248363408**	**0.042809224**	**1.05013389**

Supplementary Table 3.2.11. Shape and functional distances between clade centroids through time. Abbreviations: ArchM, Archosauromorpha. L., Lower. M., Middle. PR, Parareptile. ThP, Therapsida. U., Upper.

Timebin	Shape			Function		
	PR-ArchM	PR-ThP	ThP-ArchM	PR-ArchM	PR-ThP	ThP-ArchmM
Induan	NA	0.15146122	NA	NA	3.67097459	NA
Olenekian	NA	0.11826611	NA	NA	2.57805223	NA
Anisian	0.0737323	0.12273283	0.09999322	2.11020391	3.17294226	2.72344546
Ladinian	0.10877199	0.13086032	0.12029713	2.30554529	3.29815755	3.75491724
L. Carnian	NA	NA	0.12204885	NA	NA	3.54875186
U. Carnian	NA	NA	0.13903228	NA	NA	3.21130891
L. Norian	NA	NA	0.14027829	NA	NA	3.14123974
M. Norian	NA	NA	0.16783183	NA	NA	4.07636575
U. Norian	NA	NA	0.18671158	NA	NA	4.33655353
Rhaetian	NA	NA	0.17741984	NA	NA	4.38859378
Hettangian	NA	NA	0.18974149	NA	NA	4.66900132
Sinemurian	NA	NA	0.18521242	NA	NA	4.76454108
Pliensbachian	NA	NA	0.17210496	NA	NA	4.88224895
Toarcian	NA	NA	NA	NA	NA	NA

Supplementary Table 3.2.12. PERMANOVA results for statistical significance of shape and functional morphospace changes through stage and epoch transitions.

Abbreviation: Bonf., Bonferroni Corrected.

Stages						
Transitions	**Shape**			**Function**		
	P	**$P^{Bonf.}$**	**F**	**P**	**$P^{Bonf.}$**	**F**
Induan > Olenekian	0.511	1	0.8631	0.5591	1	0.7772
Olenekian > Anisian	0.0476	1	1.997	0.0498	1	2.292
Anisian > Ladinian	0.6695	1	0.7421	0.8269	1	0.4646
Ladinian > Lower Carnian	0.6698	1	0.7422	0.8782	1	0.3761
Lower Carnian > Upper Carnian	0.0123	1	2.823	0.0656	1	2.212
Upper Carnian > Lower Norian	0.9572	1	0.3515	0.9501	1	0.2209
Lower Norian > Middle Norian	0.7476	1	0.6261	0.3125	1	1.191
Middle Norian > Upper Norian	0.9945	1	0.2587	0.9989	1	0.05569
Upper Norian > Rhaetian	0.8055	1	0.4335	0.5248	1	0.8009
Rhaetian > Hettangian	0.5804	1	0.7746	0.7916	1	0.4803
Hettangian > Sinemurian	0.9573	1	0.3318	0.7218	1	0.4476
Sinemurian > Pliensbachian	0.0332	1	2.773	0.0519	1	2.976
Pliensbachian > Toarcian	0.163	1	1.561	0.0951	1	2.288
Total MANOVA	0.0001		1.931	0.0005		1.913
Total sum of squares:	2.879			1654		
Within-group sum of squares:	2.541			1461		
Epochs						
Early Triassic > Middle Triassic	0.0223	0.1338	2.292	0.0222	0.1332	2.719
Middle Triassic > Late Triassic	0.0532	0.3192	1.933	0.1265	0.759	1.698
Late Triassic > Early Jurassic	0.1977	1	1.325	0.2324	1	1.34
Total MANOVA	0.0041		2.182	0.0268		1.958
Total sum of squares:	2.129			1216		
Within-group sum of squares:	2.038			1169		

Supplementary Table 3.2.13. Feeding functional (sub)group classifications.

Classification codes: IG, Ingestion generalist. ARCHM, Archosauromorpha. Bsl, Non-archosaur archosauromorphs. AlloK, Allokotosauria. Az, Azendohsauria. TrL, Trilophosauria. Rhynch, Rhynchosauria. DINOSM, Dinosauromorpha. DINO, Dinosauria. ORN, Ornithischia. THY, Thyreophora. B, Basal Sauropodomorpha. SpdF, Sauropodiformes. MSSPd, Massopoda. Mss, Massospondylidae. PLT, Plateosauridae. Spd, Sauropoda. PSD, Pseudosuchia. AETO, Aetosauria. Aet, Aetosaurinae. Desm, Desmatosuchinae. Misc, Miscellaneous - a mixture of herbivorous taxa from across the Pseudosuchia. PR, Parareptilia. OW, Owenettidae. Prcd, Procolophonidae. Prcn, Procolophoninae. Lep, Leptopleuroninae. Cyn, Cynodontia. CYNOG, Cynognathia. TRAV. Traversodontidae. Gmp, Gomphodontosuchinae. TRIR, Trirachodontidae. DCYN, Dicynodontia. KEY, Kannemeyeriidae. LYST, Lystrosauridae. ShN, Shansiodontidae. StL, Stahleckeriidae. MML, Mammaliamorpha. THERO, Therocephalia. BAU, Bauriidae.

Taxa	Clade	FFG Name
Azendohsaurus madagaskarensis	AlloK Az	IG Basal Generalists
Pamelaria dolichotrachela	AlloK Az	IG Basal Generalists
Emausaurus ernsti	DINO Orn Thy	IG Basal Generalists
Buriolestes schultzi	DINO SpdM B	IG Basal Generalists
Efraasia minor	DINO SpdM B	IG Basal Generalists
Eoraptor	DINO SpdM B	IG Basal Generalists
Pampadromaeus barberenai	DINO SpdM B	IG Basal Generalists
Panphagia protos	DINO SpdM B	IG Basal Generalists
Coloradisaurus	DINO SpdM Mss	IG Basal Generalists
Lufengosaurus	DINO SpdM Mss	IG Basal Generalists
Sarahsaurus aurifontanalis	DINO SpdM Mss	IG Basal Generalists
Plateosaurus engelhardti	DINO SpdM Plt	IG Basal Generalists
Riojasaurus	DINO SpdM Plt	IG Basal Generalists
Unaysaurus tolentinoi	DINO SpdM Plt	IG Basal Generalists
Aardonyx celestae	DINO SpdM SpdF	IG Basal Generalists
Chuxiongosaurus	DINO SpdM SpdF	IG Basal Generalists
Mussaurus patagonicus	DINO SpdM SpdF	IG Basal Generalists

Lasasaurus beltanae	PR B Prcd	IG Basal Generalists
Eocursor parvus	DINO Orn Thy	IG Tougher Generalists
Lesothosaurus diagnosticus	DINO Orn Thy	IG Tougher Generalists
Adeopapposaurus mognai	DINO SpdM Mss	IG Tougher Generalists
Massospondylus kaalae	DINO SpdM Mss	IG Tougher Generalists
Macrocollum itaquii	DINO SpdM Plt	IG Tougher Generalists
Tazoudasaurus naimi	DINO SpdM Spd	IG Tougher Generalists
Jingshanosaurus	DINO SpdM SpdF	IG Tougher Generalists
Lamplughsaura dharmaramensis	DINO SpdM SpdF	IG Tougher Generalists
Melanorosaurus	DINO SpdM SpdF	IG Tougher Generalists
Yizhousaurus sunae	DINO SpdM SpdF	IG Tougher Generalists
Coletta seca	PR B Prcd	IG Tougher Generalists
Contritosaurus simus	PR B Prcd	IG Tougher Generalists
Kitchingnathus untabeni	PR B Prcd	IG Tougher Generalists
Phaanthosaurus ignatjevi	PR B Prcd	IG Tougher Generalists
Sauropareion anoplus	PR B Prcd	IG Tougher Generalists
Candelaria barbouri	PR ow	IG Tougher Generalists
Owenetta kitchingorum	PR ow	IG Tougher Generalists
Orenburgia bruma	PR prcn	IG Tougher Generalists
Samaria concinna	PR prcn	IG Tougher Generalists
Thelephon contritus	PR prcn	IG Tougher Generalists
Timanophon raridentatus	PR prcn	IG Tougher Generalists
Effigia okeeffeae	Psd	IG Tougher Generalists
Revueltosaurus callenderi	Psd	IG Tougher Generalists
Trilophosaurus buettneri	AlloK TrL	IG Light Oral Processors
Rhynchosaurus articeps	B Rhync	IG Light Oral Processors
Fodonyx	Rhync	IG Light Oral Processors
Stenaulorhynchus sp	Rhync	IG Light Oral Processors
Pisanosaurus mertii	DINO M Sile	IG Light Oral Processors
Abrictosaurus consors	DINO Orn	IG Light Oral Processors
Scelidosaurus harrisonii	DINO Orn Thy	IG Light Oral Processors

Soturnia caliodon	PR lep	IG Light Oral Processors
Bauria cynops	Thero	IG Light Oral Processors
Traversodontoides wangwuensis	Thero	IG Light Oral Processors
Aetosaurus ferratus	Aet aet	Prehension Specialists
Paratypothorax andressorum	Aet aet	Prehension Specialists
Stenomyti huangae	Aet aet	Prehension Specialists
Typothorax	Aet aet	Prehension Specialists
Desmatosuchus haplocerus	Aet Des	Prehension Specialists
Longosuchus meadei	Aet Des	Prehension Specialists
Neoaetosauroides engaeus	Aet Des	Prehension Specialists
Stagonolepis robertsoni	Aet Des	Prehension Specialists
Teraterpeton hrynewichorum	AlloK TrL	Prehension Specialists
Eohyosaurus wolvaardti	B Rhync	Prehension Specialists
Mesosuchus browni	B Rhync	Prehension Specialists
Langeronyx brodiei	Rhync	Prehension Specialists
Silesaurus opolensis	DINO M Sile	Prehension Specialists
Heterodontosaurus tucki	DINO Orn	Prehension Specialists
Manidens condorensis	DINO Orn	Prehension Specialists
Bagualosaurus agudoensis	DINO SpdM B	Prehension Specialists
Pantydraco caducus	DINO SpdM B	Prehension Specialists
Thecodontosaurus sp	DINO SpdM B	Prehension Specialists
Leyesaurus marayensis	DINO SpdM Mss	Prehension Specialists
Yimenosaurus	DINO SpdM Spd	Prehension Specialists
Anchisaurus	DINO SpdM SpdF	Prehension Specialists
Yunnanosaurus huangi	DINO SpdM SpdF	Prehension Specialists
Tichvisnkia vjakkensis	PR B Prcd	Prehension Specialists
Owenetta rubidgei	PR ow	Prehension Specialists
Eumetabolodon bathycephalus	PR prcn	Prehension Specialists
Kapes bentoni	PR prcn	Prehension Specialists
Kapes majmesculae	PR prcn	Prehension Specialists
Procolophon trigoniceps	PR prcn	Prehension Specialists

Lotosaurus	Psd	Prehension Specialists
Shansiodon	DCYN Shan	Prehension Specialists
Langbergia modisei	Cyn Trir	Prehension Specialists
Placerias	Dcyn Sthl	Durophagous Specialists
Sinognathus gracilis	Cyn Trir	Durophagous Specialists
Hypsognathus fenneri	PR lep	Durophagous Specialists
Leptopleuron lacertinum	PR lep	Durophagous Specialists
Mandaphon nadra	PR lep	Durophagous Specialists
Dolichuranus primaevus	DCYN Kan	Shearing Pulpers
Kannemeyeria latirostris	DCYN Kan	Shearing Pulpers
Moghreberia nmachouensis	DCYN Kan	Shearing Pulpers
Parakannemeyeria ningwuensis	DCYN Kan	Shearing Pulpers
Shaanbeikannemeyeria buerdongia	DCYN Kan	Shearing Pulpers
Sinokannemeyeria yingchiaoensis	DCYN Kan	Shearing Pulpers
Wadiasaurus indicus	DCYN Kan	Shearing Pulpers
Xiyukannemeyeria brevirostris	DCYN Kan	Shearing Pulpers
Lystrosaurus hedini	DCYN Lyst	Shearing Pulpers
Lystrosaurus maccaigi	DCYN Lyst	Shearing Pulpers
Lystrosaurus murrayi	DCYN Lyst	Shearing Pulpers
Lystrosaurus robustus	DCYN Lyst	Shearing Pulpers
Myosaurus	DCYN Lyst	Shearing Pulpers
Rhinodicynodon gracile	DCYN Shan	Shearing Pulpers
Tetragonias njalilus	DCYN Shan	Shearing Pulpers
Angonisaurus cruickshanki	Dcyn Sthl	Shearing Pulpers
Dinodontosaurus	Dcyn Sthl	Shearing Pulpers
Ischigualastia jenseni	Dcyn Sthl	Shearing Pulpers
Jachaleria colorata	Dcyn Sthl	Shearing Pulpers
Stahleckeria potens	Dcyn Sthl	Shearing Pulpers
Isalorhynchus genovefae	Rhync	Shearing Pulpers
Hyperodapedon gordoni	Rhync Hyp	Shearing Pulpers

Hyperodapedon huxleyi	Rhync Hyp	Shearing Pulpers
Hyperodapedon sanjuanensis	Rhync Hyp	Shearing Pulpers
Teyumbaita sulcognathus	Rhync Hyp	Shearing Pulpers
Exaeretodon argentinus	CYG GmpS	Heavy Oral Processors
Menadon besairiei	CYG GmpS	Heavy Oral Processors
Ruberodon roychowdhurii	CYG GmpS	Heavy Oral Processors
Cricodon metabolus	Cyn Trir	Heavy Oral Processors
Trirachodon	Cyn Trir	Heavy Oral Processors
Andescynodon	Cyn Trv	Heavy Oral Processors
Boreogomphodon jeffersoni	Cyn Trv	Heavy Oral Processors
Cynognathus crateronotus	Cyn Trv	Heavy Oral Processors
Dadadon isaloi	Cyn Trv	Heavy Oral Processors
Diademodon sp.	Cyn Trv	Heavy Oral Processors
Luangwa drysdalli	Cyn Trv	Heavy Oral Processors
Massetognathus pascuali	Cyn Trv	Heavy Oral Processors
Pascualgnathus polanskii	Cyn Trv	Heavy Oral Processors
Siriusgnathus niemeyerorum	Cyn Trv	Heavy Oral Processors
Traversodon stahleckeri	Cyn Trv	Heavy Oral Processors
Bienotherium yunnanense	Mml Trt	Heavy Oral Processors
Bocatherium mexicanum	Mml Trt	Heavy Oral Processors
Kayentatherium wellesi	Mml Trt	Heavy Oral Processors
Oligokyphus	Mml Trt	Heavy Oral Processors
Tritylodon	Mml Trt	Heavy Oral Processors
Yunnanodon	Mml Trt	Heavy Oral Processors
Edentosuchus	Psd	Heavy Oral Processors
Microgomphodon oligocynus	Thero	Heavy Oral Processors

Supplementary Table 3.2.14. Cluster analysis results for the main feeding functional groups. Colour coded to improve group recognition. Abbreviations: HC, Hierarchical. KM, K-means. PAM, Partition around medioids. Classification codes: ARCHM, Archosauromorpha. Bsl, Non-archosaur archosauromorphs. AlloK, Allokotosauria. Az, Azendohsauria. TrL, Trilophosauria. Rhynch, Rhynchosauria. DINOSM, Dinosauromorpha. DINO, Dinosauria. ORN, Ornithischia. THY, Thyreophora. B, Basal Sauropodomorpha. SpdF, Sauropodiformes. MSSPd, Massopoda. Mss, Massospondylidae. PLT, Plateosauridae. Spd, Sauropoda. PSD, Pseudosuchia. AETO, Aetosauria. Aet, Aetosaurinae. Desm, Desmatosuchinae. Misc, Miscellaneous - a mixture of herbivorous taxa from across the Pseudosuchia. PR, Parareptilia. OW, Owenettidae. Prcd, Procolophonidae. Prcn, Procolophoninae. Lep, Leptopleuroninae. Cyn, Cynodontia. CYNOG, Cynognathia. TRAV. Traversodontidae. Gmp, Gomphodontosuchinae. TRIR, Trirachodontidae. DCYN, Dicynodontia. KEY, Kannemeyeriidae. LYST, Lystrosauridae. ShN, Shansiodontidae. StL, Stahleckeriidae. MML, Mammaliamorpha. THERO, Therocephalia. BAU, Bauriidae.

Clade code	taxa	HC5	Clade code	taxa	KM5	Clade code	taxa	PAM5	consensus	taxa	FFG
AlloK	Azendohsaurus madagaskarensis	1	AlloK	Azendohsaurus madagaskarensis	2	AlloK	Azendohsaurus madagaskarensis	2	AlloK	Azendohsaurus madagaskarensis	1
AlloK	Pamelaria dolichotrachela	1	AlloK	Pamelaria dolichotrachela	2	AlloK	Pamelaria dolichotrachela	2	AlloK	Pamelaria dolichotrachela	1
AlloK	Trilophosaurus buettneri	1	AlloK	Trilophosaurus buettneri	2	B Rhync	Rhynchosaurus articeps	2	AlloK	Trilophosaurus buettneri	1
B Rhync	Rhynchosaurus articeps	1	B Rhync	Rhynchosaurus articeps	2	Rhync	Fodonyx	2	B Rhync	Rhynchosaurus articeps	1
Rhync	Fodonyx	1	Rhync	Fodonyx	2	Rhync	Stenaulorhynchus sp	2	Rhync	Fodonyx	1
Rhync	Stenaulorhynchus sp	1	Rhync	Stenaulorhynchus sp	2	DINO M Sile	Pisanosaurus mertii	2	Rhync	Stenaulorhynchus sp	1
Rhync Hyp	Teyumbaita sulcognathus	1	Psd	Effigia okeeffeae	2	DINO Orn Thy	Emausaurus ernsti	2	Psd	Effigia okeeffeae	1
Psd	Effigia okeeffeae	1	Psd	Revueltosaurus callenderi	2	DINO Orn Thy	Eocursor parvus	2	Psd	Revueltosaurus callenderi	1
Psd	Revueltosaurus callenderi	1	DINO M Sile	Pisanosaurus mertii	2	DINO Orn Thy	Lesothosaurus diagnosticus	2	DINO M Sile	Pisanosaurus mertii	1

DINO Orn	Abrictosaurus consors	1	DINO Orn	Abrictosaurus consors	2	DINO SpdM B	Buriolestes schultzi	2	DINO Orn	Abrictosaurus consors	1
DINO Orn	Heterodontosaurus tucki	1	DINO Orn Thy	Emausaurus ernsti	2	DINO SpdM B	Efraasia minor	2	DINO Orn Thy	Emausaurus ernsti	1
DINO Orn Thy	Emausaurus ernsti	1	DINO Orn Thy	Eocursor parvus	2	DINO SpdM B	Eoraptor	2	DINO Orn Thy	Eocursor parvus	1
DINO Orn Thy	Eocursor parvus	1	DINO Orn Thy	Lesothosaurus diagnosticus	2	DINO SpdM B	Pampadromaeus barberenai	2	DINO Orn Thy	Lesothosaurus diagnosticus	1
DINO Orn Thy	Lesothosaurus diagnosticus	1	DINO Orn Thy	Scelidosaurus harrisonii	2	DINO SpdM B	Panphagia protos	2	DINO Orn Thy	Scelidosaurus harrisonii	1
DINO Orn Thy	Scelidosaurus harrisonii	1	DINO SpdM B	Buriolestes schultzi	2	DINO SpdM Plt	Macrocollum itaquii	2	DINO SpdM B	Buriolestes schultzi	1
DINO SpdM B	Bagualosaurus agudoensis	1	DINO SpdM B	Efraasia minor	2	DINO SpdM Plt	Plateosaurus engelhardti	2	DINO SpdM B	Efraasia minor	1
DINO SpdM B	Buriolestes schultzi	1	DINO SpdM B	Eoraptor	2	DINO SpdM Plt	Riojasaurus	2	DINO SpdM B	Eoraptor	1
DINO SpdM B	Efraasia minor	1	DINO SpdM B	Pampadromaeus barberenai	2	DINO SpdM Plt	Unaysaurus tolentinoi	2	DINO SpdM B	Pampadromaeus barberenai	1
DINO SpdM B	Eoraptor	1	DINO SpdM B	Panphagia protos	2	DINO SpdM Mss	Adeopapposaurus mognai	2	DINO SpdM B	Panphagia protos	1
DINO SpdM B	Pampadromaeus barberenai	1	DINO SpdM Plt	Macrocollum itaquii	2	DINO SpdM Mss	Coloradisaurus	2	DINO SpdM Plt	Macrocollum itaquii	1
DINO SpdM B	Panphagia protos	1	DINO SpdM Plt	Plateosaurus engelhardti	2	DINO SpdM Mss	Lufengosaurus	2	DINO SpdM Plt	Plateosaurus engelhardti	1
DINO SpdM Plt	Macrocollum itaquii	1	DINO SpdM Plt	Riojasaurus	2	DINO SpdM Mss	Sarahsaurus aurifontanalis	2	DINO SpdM Plt	Riojasaurus	1
DINO SpdM Plt	Plateosaurus engelhardti	1	DINO SpdM Plt	Unaysaurus tolentinoi	2	DINO SpdM SpdF	Aardonyx celestae	2	DINO SpdM Plt	Unaysaurus tolentinoi	1
DINO SpdM Plt	Riojasaurus	1	DINO SpdM Mss	Adeopapposaurus mognai	2	DINO SpdM SpdF	Jingshanosaurus	2	DINO SpdM Mss	Adeopapposaurus mognai	1

DINO SpdM Plt	Unaysaurus tolentinoi	1	DINO SpdM Mss	Coloradisaurus	2	DINO SpdM SpdF	Lamplughsaura dharmaramensis	2	DINO SpdM Mss	Coloradisaurus	1
DINO SpdM Mss	Adeopapposaurus mognai	1	DINO SpdM Mss	Lufengosaurus	2	DINO SpdM SpdF	Melanorosaurus	2	DINO SpdM Mss	Lufengosaurus	1
DINO SpdM Mss	Coloradisaurus	1	DINO SpdM Mss	Massospondylus kaalae	2	DINO SpdM SpdF	Mussaurus patagonicus	2	DINO SpdM Mss	Massospondylus kaalae	1
DINO SpdM Mss	Lufengosaurus	1	DINO SpdM Mss	Sarahsaurus aurifontanalis	2	DINO SpdM SpdF	Yizhousaurus sunae	2	DINO SpdM Mss	Sarahsaurus aurifontanalis	1
DINO SpdM Mss	Massospondylus kaalae	1	DINO SpdM SpdF	Aardonyx celestae	2	DINO SpdM Spd	Tazoudasaurus naimi	2	DINO SpdM SpdF	Aardonyx celestae	1
DINO SpdM Mss	Sarahsaurus aurifontanalis	1	DINO SpdM SpdF	Chuxiongosaurus	2	PR B Prcd	Coletta seca	2	DINO SpdM SpdF	Chuxiongosaurus	1
DINO SpdM SpdF	Aardonyx celestae	1	DINO SpdM SpdF	Jingshanosaurus	2	PR B Prcd	Kitchingnathus untabeni	2	DINO SpdM SpdF	Jingshanosaurus	1
DINO SpdM SpdF	Chuxiongosaurus	1	DINO SpdM SpdF	Lamplughsaura dharmaramensis	2	PR B Prcd	Lasasaurus beltanae	2	DINO SpdM SpdF	Lamplughsaura dharmaramensis	1
DINO SpdM SpdF	Jingshanosaurus	1	DINO SpdM SpdF	Melanorosaurus	2	PR lep	Soturnia caliodon	2	DINO SpdM SpdF	Melanorosaurus	1
DINO SpdM SpdF	Lamplughsaura dharmaramensis	1	DINO SpdM SpdF	Mussaurus patagonicus	2	PR prcn	Orenburgia bruma	2	DINO SpdM SpdF	Mussaurus patagonicus	1
DINO SpdM SpdF	Melanorosaurus	1	DINO SpdM SpdF	Yizhousaurus sunae	2	PR prcn	Samaria concinna	2	DINO SpdM SpdF	Yizhousaurus sunae	1
DINO SpdM SpdF	Mussaurus patagonicus	1	DINO SpdM Spd	Tazoudasaurus naimi	2	PR prcn	Thelephon contritus	2	DINO SpdM Spd	Tazoudasaurus naimi	1

DINO SpdM SpdF	Yizhousaurus sunae	1	DINO SpdM Spd	Yimenosaurus	2	PR prcn	Timanophon raridentatus	2	PR ow	Candelaria barbouri	1
DINO SpdM Spd	Tazoudasaurus naimi	1	PR ow	Candelaria barbouri	2	Thero	Traversodontoides wangwuensis	2	PR ow	Owenetta kitchingorum	1
PR ow	Candelaria barbouri	1	PR ow	Owenetta kitchingorum	2	Aet aet	Aetosaurus ferratus	1	PR B Prcd	Coletta seca	1
PR ow	Owenetta kitchingorum	1	PR B Prcd	Coletta seca	2	AlloK	Teraterpeton hrynewichorum	1	PR B Prcd	Contritosaurus simus	1
PR ow	Owenetta rubidgei	1	PR B Prcd	Contritosaurus simus	2	B Rhync	Eohyosaurus wolvaardti	1	PR B Prcd	Kitchingnathus untabeni	1
PR B Prcd	Coletta seca	1	PR B Prcd	Kitchingnathus untabeni	2	B Rhync	Mesosuchus browni	1	PR B Prcd	Lasasaurus beltanae	1
PR B Prcd	Contritosaurus simus	1	PR B Prcd	Lasasaurus beltanae	2	Cyn Trir	Langbergia modisei	1	PR B Prcd	Phaanthosaurus ignatjevi	1
PR B Prcd	Kitchingnathus untabeni	1	PR B Prcd	Phaanthosaurus ignatjevi	2	DINO M Sile	Silesaurus opolensis	1	PR B Prcd	Sauropareion anoplus	1
PR B Prcd	Lasasaurus beltanae	1	PR B Prcd	Sauropareion anoplus	2	DINO Orn	Abrictosaurus consors	1	PR prcn	Orenburgia bruma	1
PR B Prcd	Phaanthosaurus ignatjevi	1	PR lep	Soturnia caliodon	2	DINO Orn	Heterodontosaurus tucki	1	PR prcn	Samaria concinna	1
PR B Prcd	Sauropareion anoplus	1	PR prcn	Orenburgia bruma	2	DINO Orn	Manidens condorensis	1	PR prcn	Thelephon contritus	1
PR lep	Soturnia caliodon	1	PR prcn	Samaria concinna	2	DINO SpdM B	Bagualosaurus agudoensis	1	PR prcn	Timanophon raridentatus	1
PR prcn	Orenburgia bruma	1	PR prcn	Thelephon contritus	2	DINO SpdM B	Pantydraco caducus	1	PR lep	Soturnia caliodon	1
PR prcn	Samaria concinna	1	PR prcn	Timanophon raridentatus	2	DINO SpdM B	Thecodontosaurus sp	1	Thero	Bauria cynops	1
PR prcn	Thelephon contritus	1	Thero	Bauria cynops	2	DINO SpdM Mss	Leyesaurus marayensis	1	Thero	Traversodontoides wangwuensis	1
PR prcn	Timanophon raridentatus	1	Thero	Traversodontoides wangwuensis	2	DINO SpdM Mss	Massospondylus kaalae	1	AlloK	Teraterpeton hrynewichorum	2

DCYN Kan	Kannemeyeria latirostris	1	Aet aet	Aetosaurus ferratus	4	DINO SpdM Spd	Yimenosaurus	1	B Rhync	Eohyosaurus wolvaardti	2
Aet aet	Aetosaurus ferratus	2	Aet aet	Paratypothorax andressorum	4	DINO SpdM SpdF	Anchisaurus	1	B Rhync	Mesosuchus browni	2
Aet aet	Paratypothorax andressorum	2	Aet aet	Stenomyti huangae	4	DINO SpdM SpdF	Chuxiongosaurus	1	Rhync	Langeronyx brodiei	2
Aet aet	Stenomyti huangae	2	Aet aet	Typothorax	4	DINO SpdM SpdF	Yunnanosaurus huangi	1	Aet aet	Aetosaurus ferratus	2
Aet aet	Typothorax	2	Aet Des	Desmatosuchus haplocerus	4	PR B Prcd	Contritosaurus simus	1	Aet aet	Paratypothorax andressorum	2
Aet Des	Desmatosuchus haplocerus	2	Aet Des	Longosuchus meadei	4	PR B Prcd	Phaanthosaurus ignatjevi	1	Aet aet	Stenomyti huangae	2
Aet Des	Longosuchus meadei	2	Aet Des	Neoaetosauroides engaeus	4	PR B Prcd	Sauropareion anoplus	1	Aet aet	Typothorax	2
Aet Des	Neoaetosauroides engaeus	2	Aet Des	Stagonolepis robertsoni	4	PR B Prcd	Tichvisnkia vjakkensis	1	Aet Des	Desmatosuchus haplocerus	2
Aet Des	Stagonolepis robertsoni	2	AlloK	Teraterpeton hrynewichorum	4	PR lep	Pentaedrusaurus ordosianus	1	Aet Des	Longosuchus meadei	2
AlloK	Teraterpeton hrynewichorum	2	B Rhync	Eohyosaurus wolvaardti	4	PR ow	Candelaria barbouri	1	Aet Des	Neoaetosauroides engaeus	2
B Rhync	Eohyosaurus wolvaardti	2	B Rhync	Mesosuchus browni	4	PR ow	Owenetta kitchingorum	1	Aet Des	Stagonolepis robertsoni	2
B Rhync	Mesosuchus browni	2	Cyn Trir	Langbergia modisei	4	PR ow	Owenetta rubidgei	1	Psd	Lotosaurus	2
DCYN Shan	Shansiodon	2	DINO M Sile	Silesaurus opolensis	4	PR prcn	Eumetabolodon bathycephalus	1	DINO M Sile	Silesaurus opolensis	2
Dcyn Sthl	Jachaleria colorata	2	DINO Orn	Heterodontosaurus tucki	4	PR prcn	Kapes bentoni	1	DINO Orn	Heterodontosaurus tucki	2
DINO M Sile	Silesaurus opolensis	2	DINO Orn	Manidens condorensis	4	PR prcn	Kapes majmesculae	1	DINO Orn	Manidens condorensis	2
DINO Orn	Manidens condorensis	2	DINO SpdM B	Bagualosaurus agudoensis	4	PR prcn	Procolophon trigoniceps	1	DINO SpdM B	Bagualosaurus agudoensis	2

DINO SpdM B	Pantydraco caducus	2	DINO SpdM B	Pantydraco caducus	4	Psd	Revueltosaurus callenderi	1	DINO SpdM B	Pantydraco caducus	2
DINO SpdM B	Thecodontosaurus sp	2	DINO SpdM B	Thecodontosaurus sp	4	Rhync	Langeronyx brodiei	1	DINO SpdM B	Thecodontosaurus sp	2
DINO SpdM Mss	Leyesaurus marayensis	2	DINO SpdM Mss	Leyesaurus marayensis	4	Aet aet	Paratypothorax andressorum	3	DINO SpdM Mss	Leyesaurus marayensis	2
DINO SpdM Spd	Yimenosaurus	2	DINO SpdM SpdF	Anchisaurus	4	Aet aet	Stenomyti huangae	3	DINO SpdM SpdF	Anchisaurus	2
DINO SpdM SpdF	Anchisaurus	2	DINO SpdM SpdF	Yunnanosaurus huangi	4	Aet aet	Typothorax	3	DINO SpdM SpdF	Yunnanosaurus huangi	2
DINO SpdM SpdF	Yunnanosaurus huangi	2	PR B Prcd	Tichvisnkia vjakkensis	4	Aet Des	Desmatosuchus haplocerus	3	DINO SpdM Spd	Yimenosaurus	2
PR B Prcd	Tichvisnkia vjakkensis	2	PR ow	Owenetta rubidgei	4	Aet Des	Longosuchus meadei	3	PR ow	Owenetta rubidgei	2
PR prcn	Eumetabolodon bathycephalus	2	PR prcn	Eumetabolodon bathycephalus	4	Aet Des	Neoaetosauroides engaeus	3	PR B Prcd	Tichvisnkia vjakkensis	2
PR prcn	Kapes bentoni	2	PR prcn	Kapes bentoni	4	Aet Des	Stagonolepis robertsoni	3	PR prcn	Eumetabolodon bathycephalus	2
PR prcn	Kapes majmesculae	2	PR prcn	Kapes majmesculae	4	Cyn Trir	Sinognathus gracilis	3	PR prcn	Kapes bentoni	2
PR prcn	Procolophon trigoniceps	2	PR prcn	Procolophon trigoniceps	4	DCYN Shan	Shansiodon	3	PR prcn	Kapes majmesculae	2
Psd	Lotosaurus	2	Psd	Edentosuchus	4	PR lep	Hypsognathus fenneri	3	PR prcn	Procolophon trigoniceps	2
Rhync	Langeronyx brodiei	2	Psd	Lotosaurus	4	PR lep	Leptopleuron lacertinum	3	DCYN Shan	Shansiodon	2
Dcyn Sthl	Placerias	3	Rhync	Langeronyx brodiei	4	PR lep	Mandaphon nadra	3	Cyn Trir	Langbergia modisei	2
PR lep	Hypsognathus fenneri	3	Cyn Trir	Sinognathus gracilis	1	Psd	Lotosaurus	3	Cyn Trir	Sinognathus gracilis	3
PR lep	Leptopleuron lacertinum	3	Dcyn Sthl	Placerias	1	AlloK	Trilophosaurus buettneri	4	PR lep	Hypsognathus fenneri	3
PR lep	Mandaphon nadra	3	PR lep	Hypsognathus fenneri	1	DCYN Kan	Dolichuranus primaevus	4	PR lep	Leptopleuron lacertinum	3

Cyn Trv	Andescynodon	5	PR lep	Leptopleuron lacertinum	1	DCYN Kan	Kannemeyeria latirostris	4	PR lep	Mandaphon nadra	3
DCYN Kan	Dolichuranus primaevus	5	PR lep	Mandaphon nadra	1	DCYN Kan	Moghreberia nmachouensis	4	Dcyn Sthl	Placerias	3
DCYN Kan	Moghreberia nmachouensis	5	PR lep	Pentaedrusaurus ordosianus	1	DCYN Kan	Parakannemeyeria ningwuensis	4	DCYN Kan	Dolichuranus primaevus	4
DCYN Kan	Parakannemeyeria ningwuensis	5	DCYN Kan	Dolichuranus primaevus	3	DCYN Kan	Shaanbeikannemeyeria buerdongia	4	DCYN Kan	Kannemeyeria latirostris	4
DCYN Kan	Shaanbeikannemeyeria buerdongia	5	DCYN Kan	Kannemeyeria latirostris	3	DCYN Kan	Sinokannemeyeria yingchiaoensis	4	DCYN Kan	Moghreberia nmachouensis	4
DCYN Kan	Sinokannemeyeria yingchiaoensis	5	DCYN Kan	Moghreberia nmachouensis	3	DCYN Kan	Wadiasaurus indicus	4	DCYN Kan	Parakannemeyeria ningwuensis	4
DCYN Kan	Wadiasaurus indicus	5	DCYN Kan	Parakannemeyeria ningwuensis	3	DCYN Kan	Xiyukannemeyeria brevirostris	4	DCYN Kan	Shaanbeikannemeyeria buerdongia	4
DCYN Kan	Xiyukannemeyeria brevirostris	5	DCYN Kan	Shaanbeikannemeyeria buerdongia	3	DCYN Lyst	Lystrosaurus hedini	4	DCYN Kan	Sinokannemeyeria yingchiaoensis	4
DCYN Lyst	Lystrosaurus hedini	5	DCYN Kan	Sinokannemeyeria yingchiaoensis	3	DCYN Lyst	Lystrosaurus maccaigi	4	DCYN Kan	Wadiasaurus indicus	4
DCYN Lyst	Lystrosaurus maccaigi	5	DCYN Kan	Wadiasaurus indicus	3	DCYN Lyst	Lystrosaurus murrayi	4	DCYN Kan	Xiyukannemeyeria brevirostris	4
DCYN Lyst	Lystrosaurus murrayi	5	DCYN Kan	Xiyukannemeyeria brevirostris	3	DCYN Lyst	Lystrosaurus robustus	4	DCYN Lyst	Lystrosaurus hedini	4
DCYN Lyst	Lystrosaurus robustus	5	DCYN Lyst	Lystrosaurus hedini	3	DCYN Lyst	Myosaurus	4	DCYN Lyst	Lystrosaurus maccaigi	4
DCYN Lyst	Myosaurus	5	DCYN Lyst	Lystrosaurus maccaigi	3	DCYN Shan	Rhinodicynodon gracile	4	DCYN Lyst	Lystrosaurus murrayi	4
DCYN Shan	Rhinodicynodon gracile	5	DCYN Lyst	Lystrosaurus murrayi	3	DCYN Shan	Tetragonias njalilus	4	DCYN Lyst	Lystrosaurus robustus	4
DCYN Shan	Tetragonias njalilus	5	DCYN Lyst	Lystrosaurus robustus	3	Dcyn Sthl	Angonisaurus cruickshanki	4	DCYN Lyst	Myosaurus	4
Dcyn Sthl	Angonisaurus cruickshanki	5	DCYN Lyst	Myosaurus	3	Dcyn Sthl	Dinodontosaurus	4	DCYN Shan	Rhinodicynodon gracile	4
Dcyn Sthl	Dinodontosaurus	5	DCYN Shan	Rhinodicynodon gracile	3	Dcyn Sthl	Ischigualastia jenseni	4	DCYN Shan	Tetragonias njalilus	4
Dcyn Sthl	Ischigualastia jenseni	5	DCYN Shan	Shansiodon	3	Dcyn Sthl	Jachaleria colorata	4	Dcyn Sthl	Angonisaurus cruickshanki	4

Dcyn Sthl	Stahleckeria potens	5	DCYN Shan	Tetragonias njalilus	3	Dcyn Sthl	Placerias	4	Dcyn Sthl	Dinodontosaurus	4
Rhync	Isalorhynchus genovefae	5	Dcyn Sthl	Angonisaurus cruickshanki	3	Dcyn Sthl	Stahleckeria potens	4	Dcyn Sthl	Ischigualastia jenseni	4
Rhync Hyp	Hyperodapedon gordoni	5	Dcyn Sthl	Dinodontosaurus	3	DINO Orn Thy	Scelidosaurus harrisonii	4	Dcyn Sthl	Jachaleria colorata	4
Rhync Hyp	Hyperodapedon huxleyi	5	Dcyn Sthl	Ischigualastia jenseni	3	Psd	Effigia okeeffeae	4	Dcyn Sthl	Stahleckeria potens	4
Rhync Hyp	Hyperodapedon sanjuanensis	5	Dcyn Sthl	Jachaleria colorata	3	Rhync	Isalorhynchus genovefae	4	Rhync	Isalorhynchus genovefae	4
CYG GmpS	Exaeretodon argentinus	4	Dcyn Sthl	Stahleckeria potens	3	Rhync Hyp	Hyperodapedon gordoni	4	Rhync Hyp	Hyperodapedon gordoni	4
CYG GmpS	Menadon besairiei	4	Rhync	Isalorhynchus genovefae	3	Rhync Hyp	Hyperodapedon huxleyi	4	Rhync Hyp	Hyperodapedon huxleyi	4
CYG GmpS	Ruberodon roychowdhurii	4	Rhync Hyp	Hyperodapedon gordoni	3	Rhync Hyp	Hyperodapedon sanjuanensis	4	Rhync Hyp	Hyperodapedon sanjuanensis	4
Cyn Trir	Cricodon metabolus	4	Rhync Hyp	Hyperodapedon huxleyi	3	Rhync Hyp	Teyumbaita sulcognathus	4	Rhync Hyp	Teyumbaita sulcognathus	4
Cyn Trir	Langbergia modisei	4	Rhync Hyp	Hyperodapedon sanjuanensis	3	Thero	Bauria cynops	4	Psd	Edentosuchus	5
Cyn Trir	Sinognathus gracilis	4	Rhync Hyp	Teyumbaita sulcognathus	3	CYG GmpS	Exaeretodon argentinus	5	Thero	Microgomphodon oligocynus	5
Cyn Trir	Trirachodon	4	CYG GmpS	Exaeretodon argentinus	5	CYG GmpS	Menadon besairiei	5	Cyn Trir	Cricodon metabolus	5
Cyn Trv	Boreogomphodon jeffersoni	4	CYG GmpS	Menadon besairiei	5	CYG GmpS	Ruberodon roychowdhurii	5	Cyn Trir	Trirachodon	5
Cyn Trv	Cynognathus crateronotus	4	CYG GmpS	Ruberodon roychowdhurii	5	Cyn Trir	Cricodon metabolus	5	Cyn Trv	Andescynodon	5
Cyn Trv	Dadadon isaloi	4	Cyn Trir	Cricodon metabolus	5	Cyn Trir	Trirachodon	5	Cyn Trv	Boreogomphodon jeffersoni	5
Cyn Trv	Diademodon	4	Cyn Trir	Trirachodon	5	Cyn Trv	Andescynodon	5	Cyn Trv	Cynognathus crateronotus	5
Cyn Trv	Luangwa drysdalli	4	Cyn Trv	Andescynodon	5	Cyn Trv	Boreogomphodon jeffersoni	5	Cyn Trv	Dadadon isaloi	5
Cyn Trv	Massetognathus pascuali	4	Cyn Trv	Boreogomphodon jeffersoni	5	Cyn Trv	Cynognathus crateronotus	5	Cyn Trv	Diademodon	5

Cyn Trv	Pascualgnathus polanskii	4	Cyn Trv	Cynognathus crateronotus	5	Cyn Trv	Dadadon isaloi	5	Cyn Trv	Luangwa drysdalli	5
Cyn Trv	Siriusgnathus niemeyerorum	4	Cyn Trv	Dadadon isaloi	5	Cyn Trv	Diademodon	5	Cyn Trv	Massetognathus pascuali	5
Cyn Trv	Traversodon stahleckeri	4	Cyn Trv	Diademodon	5	Cyn Trv	Luangwa drysdalli	5	Cyn Trv	Pascualgnathus polanskii	5
DINO M Sile	Pisanosaurus mertii	4	Cyn Trv	Luangwa drysdalli	5	Cyn Trv	Massetognathus pascuali	5	Cyn Trv	Siriusgnathus niemeyerorum	5
Mml Trt	Bienotherium yunnanense	4	Cyn Trv	Massetognathus pascuali	5	Cyn Trv	Pascualgnathus polanskii	5	Cyn Trv	Traversodon stahleckeri	5
Mml Trt	Bocatherium mexicanum	4	Cyn Trv	Pascualgnathus polanskii	5	Cyn Trv	Siriusgnathus niemeyerorum	5	CYG GmpS	Exaeretodon argentinus	5
Mml Trt	Kayentatherium wellesi	4	Cyn Trv	Siriusgnathus niemeyerorum	5	Cyn Trv	Traversodon stahleckeri	5	CYG GmpS	Menadon besairiei	5
Mml Trt	Oligokyphus	4	Cyn Trv	Traversodon stahleckeri	5	Mml Trt	Bienotherium yunnanense	5	CYG GmpS	Ruberodon roychowdhurii	5
Mml Trt	Tritylodon	4	Mml Trt	Bienotherium yunnanense	5	Mml Trt	Bocatherium mexicanum	5	Mml Trt	Bienotherium yunnanense	5
Mml Trt	Yunnanodon	4	Mml Trt	Bocatherium mexicanum	5	Mml Trt	Kayentatherium wellesi	5	Mml Trt	Bocatherium mexicanum	5
PR lep	Pentaedrusaurus ordosianus	4	Mml Trt	Kayentatherium wellesi	5	Mml Trt	Oligokyphus	5	Mml Trt	Kayentatherium wellesi	5
Psd	Edentosuchus	4	Mml Trt	Oligokyphus	5	Mml Trt	Tritylodon	5	Mml Trt	Oligokyphus	5
Thero	Bauria cynops	4	Mml Trt	Tritylodon	5	Mml Trt	Yunnanodon	5	Mml Trt	Tritylodon	5
Thero	Microgomphodon oligocynus	4	Mml Trt	Yunnanodon	5	Psd	Edentosuchus	5	Mml Trt	Yunnanodon	5
Thero	Traversodontoides wangwuensis	4	Thero	Microgomphodon oligocynus	5	Thero	Microgomphodon oligocynus	5	PR lep	Pentaedrusaurus ordosianus	?

Supplementary Table 3.2.15. Cluster analysis results for the ingestion generalist feeding functional group. Colour coded to improve group recognition. Abbreviations: HC, Hierarchical. KM, K-means. PAM, Partition around medioids. Classification codes: ARCHM, Archosauromorpha. Bsl, Non-archosaur archosauromorphs. AlloK, Allokotosauria. Az, Azendohsauria. TrL, Trilophosauria. Rhynch, Rhynchosauria. DINOSM, Dinosauromorpha. DINO, Dinosauria. ORN, Ornithischia. THY, Thyreophora. B, Basal Sauropodomorpha. SpdF, Sauropodiformes. MSSPd, Massopoda. Mss, Massospondylidae. PLT, Plateosauridae. Spd, Sauropoda. PSD, Pseudosuchia. AETO, Aetosauria. Aet, Aetosaurinae. Desm, Desmatosuchinae. Misc, Miscellaneous - a mixture of herbivorous taxa from across the Pseudosuchia. PR, Parareptilia. OW, Owenettidae. Prcd, Procolophonidae. Prcn, Procolophoninae. Lep, Leptopleuroninae. THERO, Therocephalia. BAU, Bauriidae.

Taxa	Clade	HC	Taxa	Clade	KM	Taxa	Clade	PAM	Taxa	consensus	Sub FFG
Azendohsaurus madagaskarensis	AlloK	1	Azendohsaurus madagaskarensis	AlloK	3	Azendohsaurus madagaskarensis	AlloK	1	Azendohsaurus madagaskarensis	AlloK	1
Lufengosaurus	DINO SpdM Mss	1	Pamelaria dolichotrachela	AlloK	3	Pamelaria dolichotrachela	AlloK	1	Pamelaria dolichotrachela	AlloK	1
Sarahsaurus aurifontanalis	DINO SpdM Mss	1	Emausaurus ernsti	DINO Orn Thy	3	Emausaurus ernsti	DINO Orn Thy	1	Emausaurus ernsti	DINO Orn Thy	1
			Buriolestes schultzi	DINO SpdM B	3	Lesothosaurus diagnosticus	DINO Orn Thy	1	Buriolestes schultzi	DINO SpdM B	1
Pamelaria dolichotrachela	AlloK	2	Efraasia minor	DINO SpdM B	3	Buriolestes schultzi	DINO SpdM B	1	Efraasia minor	DINO SpdM B	1
Buriolestes schultzi	DINO SpdM B	2	Eoraptor	DINO SpdM B	3	Efraasia minor	DINO SpdM B	1	Eoraptor	DINO SpdM B	1
Efraasia minor	DINO SpdM B	2	Pampadromaeus barberenai	DINO SpdM B	3	Eoraptor	DINO SpdM B	1	Pampadromaeus barberenai	DINO SpdM B	1

Pampadromaeus barberenai	DINO SpdM B	2	Panphagia protos	DINO SpdM B	3	Pampadromaeus barberenai	DINO SpdM B	1	Panphagia protos	DINO SpdM B	1
Panphagia protos	DINO SpdM B	2	Coloradisaurus	DINO SpdM Mss	3	Panphagia protos	DINO SpdM B	1	Lufengosaurus	DINO SpdM Mss	1
Coloradisaurus	DINO SpdM Mss	2	Lufengosaurus	DINO SpdM Mss	3	Adeopapposaurus mognai	DINO SpdM Mss	1	Sarahsaurus aurifontanalis	DINO SpdM Mss	1
Plateosaurus engelhardti	DINO SpdM Plt	2	Sarahsaurus aurifontanalis	DINO SpdM Mss	3	Coloradisaurus	DINO SpdM Mss	1	Coloradisaurus	DINO SpdM Mss	1
Unaysaurus tolentinoi	DINO SpdM Plt	2	Plateosaurus engelhardti	DINO SpdM Plt	3	Lufengosaurus	DINO SpdM Mss	1	Plateosaurus engelhardti	DINO SpdM Plt	1
Aardonyx celestae	DINO SpdM SpdF	2	Riojasaurus	DINO SpdM Plt	3	Sarahsaurus aurifontanalis	DINO SpdM Mss	1	Riojasaurus	DINO SpdM Plt	1
Chuxiongosaurus	DINO SpdM SpdF	2	Unaysaurus tolentinoi	DINO SpdM Plt	3	Plateosaurus engelhardti	DINO SpdM Plt	1	Unaysaurus tolentinoi	DINO SpdM Plt	1
Mussaurus patagonicus	DINO SpdM SpdF	2	Aardonyx celestae	DINO SpdM SpdF	3	Riojasaurus	DINO SpdM Plt	1	Aardonyx celestae	DINO SpdM SpdF	1
Lasasaurus beltanae	PR B Prcd	2	Mussaurus patagonicus	DINO SpdM SpdF	3	Unaysaurus tolentinoi	DINO SpdM Plt	1	Chuxiongosaurus	DINO SpdM SpdF	1
			Lasasaurus beltanae	PR B Prcd	3	Aardonyx celestae	DINO SpdM SpdF	1	Mussaurus patagonicus	DINO SpdM SpdF	1

Emausaurus ernsti	DINO Orn Thy	4				Chuxiongosaurus	DINO SpdM SpdF	1	Lasasaurus beltanae	PR B Prcd	1
Eocursor parvus	DINO Orn Thy	4	Eocursor parvus	DINO Orn Thy	1	Lamplughsaura dharmaramensis	DINO SpdM SpdF	1	Eocursor parvus	DINO Orn Thy	2
Lesothosaurus diagnosticus	DINO Orn Thy	4	Lesothosaurus diagnosticus	DINO Orn Thy	1	Mussaurus patagonicus	DINO SpdM SpdF	1	Lesothosaurus diagnosticus	DINO Orn Thy	2
Eoraptor	DINO SpdM B	4	Adeopapposaurus mognai	DINO SpdM Mss	1	Lasasaurus beltanae	PR B Prcd	1	Macrocollum itaquii	DINO SpdM Plt	2
Adeopapposaurus mognai	DINO SpdM Mss	4	Massospondylus kaalae	DINO SpdM Mss	1	Candelaria barbouri	PR ow	1	Adeopapposaurus mognai	DINO SpdM Mss	2
Massospondylus kaalae	DINO SpdM Mss	4	Macrocollum itaquii	DINO SpdM Plt	1				Massospondylus kaalae	DINO SpdM Mss	2
Macrocollum itaquii	DINO SpdM Plt	4	Tazoudasaurus naimi	DINO SpdM Spd	1	Eocursor parvus	DINO Orn Thy	3	Jingshanosaurus	DINO SpdM SpdF	2
Riojasaurus	DINO SpdM Plt	4	Jingshanosaurus	DINO SpdM SpdF	1	Massospondylus kaalae	DINO SpdM Mss	3	Lamplughsaura dharmaramensis	DINO SpdM SpdF	2
Tazoudasaurus naimi	DINO SpdM Spd	4	Lamplughsaura dharmaramensis	DINO SpdM SpdF	1	Macrocollum itaquii	DINO SpdM Plt	3	Melanorosaurus	DINO SpdM SpdF	2
Jingshanosaurus	DINO SpdM SpdF	4	Melanorosaurus	DINO SpdM SpdF	1	Tazoudasaurus naimi	DINO SpdM Spd	3	Yizhousaurus sunae	DINO SpdM SpdF	2

Lamplughsaura dharmaramensis	DINO SpdM SpdF	4	Yizhousaurus sunae	DINO SpdM SpdF	1	Jingshanosaurus	DINO SpdM SpdF	3	Tazoudasaurus naimi	DINO SpdM Spd	2
Melanorosaurus	DINO SpdM SpdF	4	Coletta seca	PR B Prcd	1	Melanorosaurus	DINO SpdM SpdF	3	Candelaria barbouri	PR ow	2
Yizhousaurus sunae	DINO SpdM SpdF	4	Contritosaurus simus	PR B Prcd	1	Yizhousaurus sunae	DINO SpdM SpdF	3	Owenetta kitchingorum	PR ow	2
Coletta seca	PR B Prcd	4	Kitchingnathus untabeni	PR B Prcd	1	Coletta seca	PR B Prcd	3	Coletta seca	PR B Prcd	2
Contritosaurus simus	PR B Prcd	4	Phaanthosaurus ignatjevi	PR B Prcd	1	Contritosaurus simus	PR B Prcd	3	Contritosaurus simus	PR B Prcd	2
Kitchingnathus untabeni	PR B Prcd	4	Sauropareion anoplus	PR B Prcd	1	Kitchingnathus untabeni	PR B Prcd	3	Kitchingnathus untabeni	PR B Prcd	2
Phaanthosaurus ignatjevi	PR B Prcd	4	Candelaria barbouri	PR ow	1	Phaanthosaurus ignatjevi	PR B Prcd	3	Phaanthosaurus ignatjevi	PR B Prcd	2
Sauropareion anoplus	PR B Prcd	4	Owenetta kitchingorum	PR ow	1	Sauropareion anoplus	PR B Prcd	3	Sauropareion anoplus	PR B Prcd	2
Candelaria barbouri	PR ow	4	Orenburgia bruma	PR prcn	1	Owenetta kitchingorum	PR ow	3	Orenburgia bruma	PR prcn	2
Owenetta kitchingorum	PR ow	4	Samaria concinna	PR prcn	1	Samaria concinna	PR prcn	3	Samaria concinna	PR prcn	2
Orenburgia bruma	PR prcn	4	Thelephon contritus	PR prcn	1	Timanophon raridentatus	PR prcn	3	Thelephon contritus	PR prcn	2
Samaria concinna	PR prcn	4	Timanophon raridentatus	PR prcn	1	Revueltosaurus callenderi	Psd	3	Timanophon raridentatus	PR prcn	2
Thelephon contritus	PR prcn	4	Effigia okeeffeae	Psd	1				Effigia okeeffeae	Psd	2

Timanophon raridentatus	PR prcn	4	Revueltosaurus callenderi	Psd	1	Trilophosaurus buettneri	AlloK	2	Revueltosaurus callenderi	Psd	2
Effigia okeeffeae	Psd	4				Rhynchosaurus articeps	B Rhync	2	Trilophosaurus buettneri	AlloK	3
Revueltosaurus callenderi	Psd	4	Trilophosaurus buettneri	AlloK	2	Pisanosaurus mertii	DINO M Sile	2	Rhynchosaurus articeps	B Rhync	3
			Rhynchosaurus articeps	B Rhync	2	Abrictosaurus consors	DINO Orn	2	Fodonyx	Rhync	3
Trilophosaurus buettneri	AlloK	3	Pisanosaurus mertii	DINO M Sile	2	Scelidosaurus harrisonii	DINO Orn Thy	2	Stenaulorhynchus sp	Rhync	3
Rhynchosaurus articeps	B Rhync	3	Abrictosaurus consors	DINO Orn	2	Soturnia caliodon	PR lep	2	Pisanosaurus mertii	DINO M Sile	3
Pisanosaurus mertii	DINO M Sile	3	Scelidosaurus harrisonii	DINO Orn Thy	2	Orenburgia bruma	PR prcn	2	Abrictosaurus consors	DINO Orn	3
Abrictosaurus consors	DINO Orn	3	Chuxiongosaurus	DINO SpdM SpdF	2	Thelephon contritus	PR prcn	2	Scelidosaurus harrisonii	DINO Orn Thy	3
Scelidosaurus harrisonii	DINO Orn Thy	3	Soturnia caliodon	PR lep	2	Effigia okeeffeae	Psd	2	Soturnia caliodon	PR lep	3
Soturnia caliodon	PR lep	3	Fodonyx	Rhync	2	Fodonyx	Rhync	2	Bauria cynops	Thero	3
Fodonyx	Rhync	3	Stenaulorhynchus sp	Rhync	2	Stenaulorhynchus sp	Rhync	2	Traversodontoides wangwuensis	Thero	3
Stenaulorhynchus sp	Rhync	3	Bauria cynops	Thero	2	Bauria cynops	Thero	2			
			Traversodontoides wangwuensis	Thero	2	Traversodontoides wangwuensis	Thero	2			
Bauria cynops	Thero	5									
Traversodontoides wangwuensis	Thero	5									

Supplementary Table 3.2.16. Assemblage data for herbivore and clade abundance within early Mesozoic faunas. Abbreviations: ArchM, Archosauromorpha AZ, Assemblage Zone. DinoM, Dinosauromorpha. FNV, Faunivorous. HBV, Herbivorous. L, Lower. No, Number. PR, Parareptile. Prop, Proportion. PSD, Pseudosuchia. Sin-Plb, Sinemurian-Pliensbachian. Sp. Species. THR, Therapsid. U, Upper.

Site	Location	Stage	No. of Sp.	HBV Sp.	FNV Sp.	HBV prop	FNV prop	HBV DinoM prop	HBV PSD prop	HBV ArchM prop	HBV THR prop	HBV PR prop
Lystrosaurus AZ	S Africa	Induan	25	11	14	0.440	0.560	0.000	0.000	0.091	0.273	0.636
Cynognathus AZ b	S Africa	Anisian L	20	15	5	0.750	0.250	0.000	0.000	0.200	0.467	0.333
Ehrmaying L	China	Anisian L	13	10	3	0.769	0.231	0.000	0.000	0.000	0.900	0.100
Ehrmaying U	China	Anisian U	20	17	3	0.850	0.150	0.000	0.000	0.000	0.941	0.059
Yerrapalli	India	Anisian U	5	4	1	0.800	0.200	0.000	0.000	0.500	0.500	0.000
Donguz	Russia	Anisian U	14	9	5	0.643	0.357	0.000	0.000	0.000	1.000	0.000
Lifua	Tanzania	Anisian U	12	9	3	0.750	0.250	0.222	0.000	0.000	0.556	0.222
Manda	Tanzania	Anisian U	6	3	3	0.500	0.500	0.000	0.000	0.333	0.667	0.000
Ntawere L	Zambia	Anisian U	6	6	0	1.000	0.000	0.000	0.000	0.000	0.833	0.000
Isalo II	Madagascar	Lad Carnian L	5	4	1	0.800	0.200	0.000	0.000	0.500	0.500	0.000
Santa Maria L	Brazil	Lad Carnian L	14	8	6	0.571	0.429	0.000	0.000	0.125	0.750	0.125
Ischigualasto L	Argentina	Carnian U	21	10	11	0.476	0.524	0.500	0.200	0.100	0.200	0.000
Argana	Morocco	Carnian U	6	3	3	0.500	0.500	0.333	0.000	0.333	0.333	0.000

Lossiemouth	UK	Carnian U	7	3	4	0.429	0.571	0.000	0.333	0.333	0.000	0.333
Colorado City	USA	Carnian U	10	5	5	0.500	0.500	0.000	0.600	0.400	0.000	0.000
Santa Maria U	Brazil	Carnian U	15	8	7	0.533	0.467	0.125	0.250	0.375	0.250	0.000
Tecovas	USA	Norian L	14	5	9	0.357	0.643	0.000	0.800	0.200	0.000	0.000
Caturrita	Brazil	Norian M	11	5	6	0.455	0.545	0.600	0.000	0.000	0.200	0.200
Lower Elliot	South Africa	Norian M	11	10	1	0.909	0.091	1.000	0.000	0.000	0.100	0.000
Los Colorados U	Argentina	Norian U	10	4	6	0.400	0.600	0.750	0.250	0.000	0.000	0.000
Cooper Canyon	USA	Norian U	6	4	2	0.667	0.333	0.250	0.500	0.000	0.000	0.250
Knollenmergel	Germany	Rhaetian	7	4	3	0.571	0.429	0.500	0.000	0.000	0.500	0.000
Redonda	USA	Rhaetian	6	4	2	0.667	0.333	0.000	0.750	0.000	0.250	0.000
Zhangjiawa	China	Sinemurian	15	6	9	0.400	0.600	0.167	0.167	0.000	0.667	0.000
Upper Elliot	South Africa	Sin Plb	20	11	9	0.550	0.450	1.000	0.000	0.000	0.000	0.000
Kayenta	USA	Sin Plb	11	6	5	0.545	0.455	0.333	0.167	0.000	0.500	0.000

Chapter 4 - The interplay between intrinsic and extrinsic macroevolutionary drivers

4.1 A clade in focus: Sauropodomorph success through the early Mesozoic.

Authors: Suresh Singh, Armin Elsler, Logan King, Tom Stubbs, Emily Rayfield, and Mike Benton.

Chapter Contributions and Acknowledgements

I designed the study, collected the morphological data, and conducted all the analyses and wrote the chapter. A. E. provided the phylogeny, chronostratigraphic and femur length data and helped with sourcing images. L. K., T. S., E. R. and M. J. B. provided guidance and comments on the chapter. My contributions represent 95% of the material in this chapter.

I thank Christine Janis for providing literature and constructive commentary. All silhouettes created by S. S., but some are vectorised from artwork by Felipe Alves Elias (https://www.paleozoobr.com/) and Jeff Martz (United States National Park Service).

Abstract

Sauropod dinosaurs were the largest animals ever to walk the planet, exhibiting great diversity and abundance through the Mesozoic. Their evolutionary success and gargantuan size attract much attention, but their origins from gracile, bipedal ancestors (‘prosauropods’) in the Late Triassic and Early Jurassic (237 – 174 Ma) remain obscure. The discovery of many new taxa has now clarified the morphological evolution of the unique sauropod body plan, but the ecological context of this transformation remains unclear. Sauropodomorphs became the preeminent large herbivores within most terrestrial faunas in the Late Triassic, in contrast to other large herbivores, which went extinct at the end of the Triassic. The underlying causes of exceptional prosauropod success remain unclear, and yet sauropodomorph success through this time was key to solidifying dinosaur terrestrial supremacy. Here I present a focused, quantitative morphometric analysis of early sauropodomorph and silesaurid ecomorphology through the early Mesozoic. By contrasting trends in dentition, mandibular morphology, and body size in these contemporaneous dinosauromorph clades, we find that changes in sauropodomorph ecomorphology coincide with intervals of floral change, beginning at the Carnian Pluvial Event, which marked the beginning of the novel sauropodomorph body-plan. We further identify that the adoption of larger body sizes at the Carnian-Norian transition was key to

sauropodomorph success; the adoption of bulk-feeding alongside the likely retention of faunivorous diets as juveniles enabled prosauropods to survive through intervals of poor-quality vegetation and environmental instability through the end of the Triassic. This resilience helped sauropodomorphs to emerge from the Triassic-Jurassic mass extinction as the only large, terrestrial herbivores. A depauperate herbivore guild fueled an opportunistic radiation of sauropodomorphs in the Early Jurassic, and the take-off of sauropod diversity and gigantism as climates stabilized and nutrient-rich floras returned. Sauropodomorph success and gigantism originated a mix of their unique biology and tough climatic conditions.

Introduction

Sauropod dinosaurs have challenged biologists because of their huge size, up to 70 tonnes (Sander et al., 2011; Benson et al., 2018) – how did they achieve the apparently impossible? Their ancestors were small, gracile, bipedal animals that emerged as key components of terrestrial faunas at the beginning of the Late Triassic in the Carnian (Cabreira et al., 2016). These non-sauropod sauropodomorphs are traditionally known as 'prosauropods' and established themselves as the predominant large herbivores within terrestrial faunas in the Late Triassic (Galton, 1985; Mannion et al., 2011), against a backdrop of significant environmental changes as pulses of volcanism drove strong changes in global climates and environments (Simms and Ruffel, 1990; Preto et al., 2010; Benton, 2016; Kustatscher et al., 2018). These climatic upheavals saw the decline and eventual extinction of all other supposed large herbivores such as the therapsid dicynodonts and pseudosuchian aetosaurs at the end of the Triassic (Barrett et al., 2010; Sues and Fraser, 2010). Mounting sauropodomorph faunal prominence is accompanied by the stepwise evolution of the novel sauropod body plan, a combination of traits ranging from cursoriality and quadrupedality to elongated necks and larger guts, that allowed sauropodomorphs to become the giant herbivores that became key components of terrestrial faunas worldwide for the remainder of the Mesozoic (Sander et al., 2011; Pol et al., 2021). Sauropodomorphs were the vanguard of dinosaur domination, becoming increasingly prevalent through the Late Triassic and Early Jurassic (237 – 174 Ma) (Brusatte et al., 2008; 2010; Benton et al., 2014). Yet the underlying basis for this exceptionalism remains unclear, particularly as sauropodomorphs were not the only dinosauromorph herbivores in the Triassic, with the Silesauridae having become members of the herbivore guild in the Middle Triassic (Müller and Garcia, 2020). These two clades both existed within the herbivore guild at the same time, yet only one would survive into the Jurassic. It has been proposed that sauropodomorphs were intrinsically better adapted than contemporary large herbivores to the conditions that prevailed through the early Mesozoic (Barrett et al., 2010, Benson et al., 2018).

Indeed, this interval saw dramatic reorganizations of terrestrial floras, as tough gymnosperm and nutrient-poor fern floras prevailed (Kustatscher et al., 2018, Gill et al., 2018). The ability to subsist on lower-quality vegetation is a supposed key adaptation in sauropods (Farlow, 1987; Sander et al., 2011), but it has not been rigorously tracked within early sauropodomorphs. Likewise, many aspects of the sauropodomorph morphology have been linked to their success, but these hypotheses have yet to be explicitly explored within an ecological and evolutionary context. Furthermore, new fossil evidence is now providing high resolution floral data that can help clarify the links between sauropodomorphs and vegetation (Pol et al., 2020; 2021). Variation in mandibular morphology, body size, and dentition provide robust evidence of ecological specialization (Anderson et al., 2011; Bonner, 2006; Larson et al., 2016; Eronen et al., 2010). Changes in these eco-functional traits when considered in the context of the changing flora and climates may illustrate how the ecology of sauropodomorphs and their silesaurid relatives evolved through time and how ecomorphological differences contributed to their divergent fortunes through the Late Triassic. By quantitatively assessing the ecologies of sauropodomorphs and silesaurids using morphometric analysis of dental, mandibular, and body size evolution, with additional attention on potential ontogenetic changes to feeding morphology, I offer an eco-morphological perspective on the factors that drove the rise of the sauropodomorphs.

Materials and Methods

Taxonomic sampling and data collection: I generated a list of all valid sauropodomorph taxa through the Triassic to Middle Jurassic by using an updated version of a published dataset (Benton et al., 2013), which included the latest new taxa and taxonomic revisions. Using this taxon list, I collected lateral view photographs and/or specimen drawings of mandibles from the literature, excluding heavily damaged and distorted specimens. This study was conducted at genus level to maintain effective representation of total sauropodomorph disparity at the highest-possible taxonomic resolution. Our final mandibular analysis includes 44 specimens, representing 40 genera (five silesaurids and 35 sauropodomorphs), including three specimens of *Massospondylus carinatus* and *Mussaurus patagonicus* at different stages of maturity (Supplementary Data S1). Femur length was used as a metric of body size, and a dataset of 69 genera (10 silesaurids and 49 sauropodomorphs) were obtained or estimated using published literature to chart body size evolution (Supplementary Data S2). Taxa without mandibular data were included to improve the overall accuracy of reported temporal trends in body size evolution. Taxon stratigraphic ranges were updated and recorded to substage level as designated by Benton et al. (2013). Absolute age assignments were based on the 2019 version of the International Chronostratigraphic Chart (Cohen

et al., 2013; International Commission on Stratigraphy, 2019). Taxa were classified by taxonomic groups according to the latest published literature; the precise definition of Sauropoda remains controversial, but I use the definitions outlined by McPhee et al. (2014) for Sauropodiformes and Salgado et al. (1997) for Sauropoda, both of which have been extensively used in the literature. I also acknowledge that the clade designations of some included taxa such as *Yimenosaurus youngi* remain untested and subject to revision. Nonetheless, the uncertainty of distinguishing advanced sauropodiforms and sauropodans was felt to not greatly impact the focus of this study and interpretation of the broader trends in sauropodomorph ecomorphology during the Late Triassic and into the Middle Jurassic.

Mandibular geometric and functional morphometrics: Geometric morphometric (GM) and functional morphometric (FM) methods were used to assess mandibular form and function, which are often closely linked. However, this relationship can be distorted by factors such as phylogeny (Meloro et al., 2011), so results may differ when assessing form and function (Anderson et al., 2011; Stubbs et al., 2013). While both shape and functional data are derived from the same mandibular morphologies, by using GM and FM metrics I was able to discriminate shape data integrating various cladistic and functional traits, and clear, ecologically relevant functional measurements.
To generate GM data (Supplementary Data S3), landmarks were digitally applied to the images using TPSDig2 (Rohlf, 2010). Our landmarking regime uses four fixed landmarks placed at homologous points of morphology, linked by four semi-landmarked curves made up of 55 semi-landmarks (Fig. 2.1.1). The varying state of preservation across our specimens rendered type 1 landmarking impractical as points of bone articulation and sutures were difficult to identify, and so a type 2 landmarking regime was selected (Bookstein, 1991). TPSUtil (Rohlf, 2013) was used to designate semi-landmark curves and TPSRelW (Rohlf, 2015) used to perform a Procrustes transformation to remove the effects of size and orientation from the landmark data and thereby generate Procrustes aligned landmark data.

Standardized linear measurement data (SLMD) ((Supplementary Data S4) were collected for eight functional characters using measurements taken from our mandible images (Fig. 2.1.2) in ImageJ (Schneider et al., 2012). Our functional characters were chosen to capture functionally important biomechanical properties related to feeding ecology that have been widely used before to characterize tetrapod mandibular function (Sakamoto, 2010; Anderson et al., 2011; Stubbs et al.,

2013; Button et al., 2017; MacLaren et al., 2017). (See supplementary methods for character descriptions).

Principal Component Analysis: The shape-aligned coordinate data and functional linear measurement matrix were subjected to principal component analyses (PCAs) in R using the *geomorph* package (Adams and Otárola-Castillo, 2013) for the shape data, and the *FactoMineR* package (Lê et al., 2008; Husson et al., 2018) for the functional measurements. The functional data were centered and standardized using a z-transformation prior to the PCA to mitigate issues of heteroscedasticity, in line with comparable contemporary studies (Button and Zanno, 2020). The first two PC axes account for the largest proportions of variation of all axes and were used to plot morphospace occupation. The shape morphospace represents 46.9% of total mandibular variation (25.9% on PC1 and 21% on PC2), and the functional morphospace represents 51.2% of total mandibular variation (31.7 % on PC1 and 19.5% on PC2). The morphospaces were plotted using the *ggplot2* R package (Wickham, 2016), with point size determined by $\log_{10}$ transformed femur length to represent body size.

NPMANOVA and Wang's permutational analysis (Brusatte et al, 2014) was used to ascertain statistically significant differences in mandibular shape and function between timebins and taxonomic groupings. The NPMANOVA was carried out at epoch and stage-level using PAST (Hammer et al., 2001) (version 3.24). A Euclidean similarity index was generated from the aligned landmark shape data and functional SLMD, and the analysis used Bonferroni corrections to minimise the errors stemming from multiple comparisons. Wang's permutational analysis was applied in R using code from (Foffa et al., 2018) using 500 replications.

Temporal Disparity Calculations: To measure disparity (morphological diversity), I used the *DispRity* R package (Guillerme, 2018), and generated sum of variance (SOV) results following a phylogenetic time-slice approach (Guillerme and Cooper, 2018) to incorporate unsampled lineages. The calculations were run with 1000 cycles of bootstrapping to provide 95% confidence intervals and rarefaction to minimum timebin sample size to mitigate differences in subset size. SOV was used to plot temporal disparity patterns as it is more resistant to sampling biases and therefore a better reflection of true patterns of disparity (Butler et al. 2012). Within-time-bin SOV were calculated using all PC axes. Our plots were generated in R using the *strap* package (Bell and Lloyd, 2014). As disparity is calculated using the volume and extent of morphospace occupation, changes in the density of morphospace occupation may skew disparity metrics (Smithwick and Stubbs, 2018; Norden et al., 2018). Consequently, temporal disparity was plotted alongside time-slices of our

morphospace to allow comparison of trends in disparity and patterns of morphospace occupation, and so avoid misinterpretation of morphological evolution.

Ancestral Character Estimation. Ancestral states for dentition type, PC scores, and body size were estimated for nodes across the sauropodomorph phylogeny to better understand the timings of trait change through their ecomorphological diversification. Discrete dental character states were reconstructed using the 'ace' function of the ape R package (Paradis and Schliep, 2019) using Maximum Likelihood estimations (Barrett et al., 2015; Yang et al., 2019). I ran trait estimations under a conservative equal rates (ER) and more derived, symmetrical (SYM) and all different (ARD) rates model of character transition (Pagel, 1994). These estimations are presented on a time-scaled phylogeny using the strap R package (Bell and Lloyd, 2014) (Fig. 3.1.5a). The log-likelihood results for the ER (-60.27), SYM (-52.73) and ARD (-47.07) rates models showed significantly higher support for the reconstructions obtained under a ARD model (Supplementary Fig. 3.1.S7; Fig. 3.1.7).

Ancestral estimations of continuous functional PC score (fPC) and body size (log_{10} transformed femur length) values were generated using a Maximum Likelihood approach via the 'FastAnc' function of the phytools R package (Revell, 2012). Resulting values were mapped onto the phylogeny using the 'ggtree' R package to create phenograms illustrating trait evolution through time (Yu, 2020) (Fig. 3.1.5b).

Results

Silesaurid and early Mesozoic sauropodomorph ecomorphology. Combining an overview of tooth morphotypes (Fig. 4.1.1a) with mandibular morphospaces (Figs. 4.1.1b and 1c) generated from geometric morphometric landmark data and biomechanical characters (Fig. 4.1.1d) allows differentiation of diets and feeding modes.

- **Dentition -** Tooth morphology (Fig. 4.1.1a) shifted from ziphodont-like dentitions in basal-most sauropodomorphs to leaf-shaped, lanceolate forms in later Triassic plateosaurids, massospondylids, and sauropodiforms (Galton, 1985). Prosauropod mandibular tooth crowns are typified by a distally angled apex with denticles along both mesial and distal edges. The denticles are generally fewer in number per millimeter than in more basal dinosaurs and are apically angled at approximately 45° from the long axis of the crown (Galton, 1985; Barrett and Upchurch, 2007). The dentary teeth are labiolingually wider at the base of the crown – a deviation from the blade-like crowns of basal members like *Buriolestes* (Cabreira et al., 2016). As sauropodomorphs evolved in the Jurassic, their teeth became more peg-like. However, this

trend is typically not found in Triassic and Early Jurassic forms with only a few exceptions such as *Yunnanosaurus* (Barrett and Upchurch, 2007).

- **Mandibular Morphology** - The shape morphospace represents 47.3% of total mandibular variation (29.8% on PC1 and 17.5% on PC2), and the functional morphospace represents 51.2% of total mandibular variation (32.5% on fPC1 and 18.9% on fPC2). Functional character loadings (Table 4.1.1) reveal that fPC 1 is controlled by maximum aspect ratio (MAR) and mean posterior mechanical advantage (MPMA), whereas fPC 2 is dominated by a combination of opening mechanical advantage (OMA), symphyseal angle (SA) and relative length of the toothrow (RLT). Basal sauropodomorphs and silesaurids occupy similar regions of morphospace, in an area characterised by being relatively slender with a slight taper through the dentary. These jaws show greater proficiency for speed than for biting efficiency. However, silesaurid shape and functional morphospace occupation (MO) is far greater and encompasses morphologies with more developed robusticity and biting efficiency (Fig. 4.1.1b-c), particularly along the posterior of the toothrow (Fig. 4.1.1c-d). Interestingly, the theocodontosaurid basal-most sauropodomorphs such as *Efraasia minor,* sit closer to these derived silesaurids (*Asilisaurus* kongwe and *Silesaurus opolensis*) in shape and function. However, whilst some later sauropodomorph taxa do converge on these supposedly herbivorous silesaurids (Martz and Small, 2019), most sauropodomorph morpho-functional evolution is directed towards strengthening of the dentary and maximising mean anterior mechanical advantage (MAMA). Plateosaurids occupy a small area of morphospace towards the centre of both morphospaces close to their Carnian predecessors, but this is a surprisingly broad area given their lack of representation within this analysis. The wide extent of plateosaurid functional morphospace occupation (MO) shows early experimentation MAMA modification (Fig. 4.1.1c).

  The massospondylids build on the MO of plateosaurids by further developing their mandibular robusticity and biting efficiency through expansion of the mandibular body and thickening of the dentary. Some taxa also show further symphyseal reinforcement with these taxa making the first major modifications of the dentary and symphysis through downward deflection of the jaw and reorientation of the symphyseal angle (SA), which would become a major aspect of later sauropodiform morpho-functional diversity. Sauropodiforms further build on these traits alongside additional extension the length of the symphysis. However, their evolution also saw a shortening of the toothrow, suggesting less emphasis on MPMA. The massospondylids and sauropodiforms occupy the greatest extents of overall morphospace. but their overall areas of MO show slight differences reflecting the divergences in their jaw morpho-function. This divergence is better illustrated when morphospaces are constructed using PC3

(13.1% of shape and 15.5% of functional variation), which shows these two groups are distinguished by their RTL and MAMA (Supplementary figure 4.1.1; Table 4.1.1).

Early sauropod MO encompasses a very broad extent of overall sauropodomorph MO, but their taxa are located at the peripheries in two distinct groups. In terms of shape, this manifests as a difference in dentary deflection either upwards or downwards, whereas functionally it reflects differences in the relative balance between MAMA and MPMA. Interestingly, this bimodal distribution does not match up from shape to function with different taxa constituting the groups in either morphospace, indicating a surprising degree of many-to-one mapping of functionality (Anderson et al., 2008). Nonetheless, a common trait of sauropods is heavy symphyseal development, stressing the importance to sauropods of increased robusticity and stability at the anterior of the jaw during biting (Lautenschlager, 2017).

Examination of the functional characters by group (Fig. 4.1.1d) highlights trends towards increasing jaw and particularly symphyseal robusticity as identified in previous studies (MacLaren et al., 2017; Button et al., 2017; 2019). Anterior and posterior mechanical advantage (MA) show an upward trend within non-sauropodans, but the range of functionality across almost all characters also increases reflecting increasing functional diversity through the course of sauropodomorph evolution. Only symphyseal length shows a clear and sustained trend of absolute increase through evolution. Plateosaurids appear to mark a morpho-functional bottleneck, although this may stem from poor sampling of this group. Such a functional bottleneck is also apparent in the sauropods and potentially indicates very specific eco-functionality and trophic ecologies for plateosaurids and sauropods. Massospondylids and sauropodiforms display the greatest ranges of functionality across the measured functional characters, particularly across relative toothrow length and aspect ratio.

- **Body Size** - Large body sizes are scattered across both morphospaces (Figs. 4.1.1b-c), though larger taxa are generally positioned towards the positive ends of PC and fPC 1. However, sauropods break this trend through their 'bimodal' distributions. I notice that intra-group size ranges seem consistent but there is a trend of increasing maximum size through sauropodomorph evolution, with the increase between basal sauropodomorphs to plateosaurids being the most extreme.

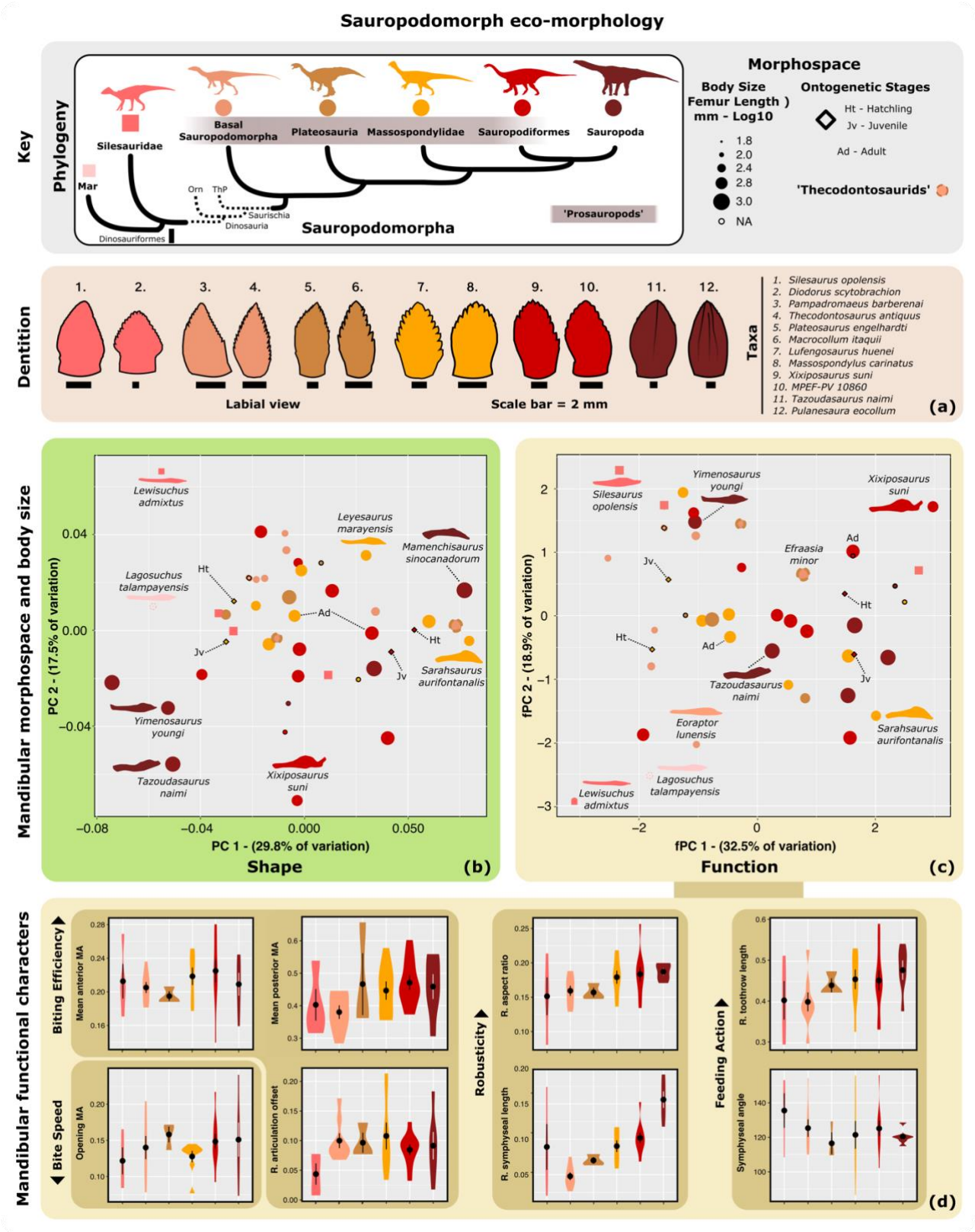

Figure 4.1.1. Silesaurid and sauropodomorph ecomorphology. Dental, mandibular and body size variation in Triassic and Early-Middle Jurassic sauropodomorphs. (a) Dental morphotypes. Scale bar = 2 millimeters. (b) Mandibular shape morphospace. (c) Mandibular

functional morphospace. Ontogenetic representatives of *Massospondylus carinatus* included in both morphospaces. (d) Mandibular functional character comparison. (n=44). Violin plots show taxon density. Box plots showing median value and upper and lower quartiles, with whisker illustrating standard deviation. Abbreviations: MA, mechanical advantage; R, relative; Mar, Marasuchidae; Orn, Ornithischia; ThP, Theropoda.

Table 4.1.1. Functional principal component analysis loadings. Abbreviations: fPC, Functional principal component. MAMA, Mean anterior mechanical advantage. MPMA, Mean posterior mechanical advantage. OMA, Opening mechanical advantage. RAO, Relative articulation offset. RMAR, Relative maximum aspect ratio. RSL, Relative symphyseal length. RTL, Relative toothrow length. SA, Symphyseal angle.

Functional Character	**fPC1**	**fPC2**	**fPC3**	**fPC4**	**fPC5**	**fPC6**	**fPC7**	**fPC8**
MAMA	0.4275	0.3505	-0.4114	0.0714	0.3438	-0.2102	0.1554	0.5775
MPMA	0.5004	-0.2445	0.0696	0.2285	0.5204	0.0043	0.2074	-0.5647
OMA	0.0060	0.3575	0.6972	-0.2813	0.1987	0.2407	0.4271	0.1644
RMAR	0.4626	0.2552	0.3154	-0.1649	-0.0416	-0.0728	-0.7648	-0.0481
RTL	0.2156	-0.6698	0.2642	0.2155	-0.0228	0.2811	-0.0906	0.5486
RSL	0.4351	0.1010	0.1337	0.2672	-0.7240	-0.2290	0.3600	-0.0703
SA	-0.1089	0.4068	-0.0213	0.7043	0.0056	0.5523	-0.1415	-0.0329
RAO	0.3243	-0.0090	-0.3901	-0.4717	-0.2121	0.6754	0.0879	-0.1057

Ontogeny. The mandibles of a hatchling and juvenile *Massospondylus carinatus* and *Mussaurus patagonicus* were included to investigate dietary changes through ontogeny as ontogenetic shifts in locomotion have been noted in some sauropodomorphs (Chapelle et al., 2019; Otero et al., 2019). Mandibular functional development through ontogeny (Fig. 4.1.2) reveals intriguing differences between these two taxa. In *Massospondylus* there is relatively greater improvement of anterior MA as overall biting efficiency improved during the growth from hatchlings into juveniles. This suggests that young animals fed by using powerful snapping bites and adults showed higher posterior biting efficiency. The deflection of the dentary and relative increase of the articular offset saw improved mandibular robusticity and biting efficiency in adults (Lautenschlager, 2017). Contrastingly, *Mussaurus* shows a more complex pattern of development with much less mandibular development through ontogeny as seen in *Massospondylus*. *Mussaurus* MPMA, RAO, RSL are generally constant,

with MAMA and SA showing modest declines and RTL and RMAR showing more notable increases from the hatchling to juvenile stage. MAMA increased but RAO, RMAR, RTL and SA all markedly decreased between adolescence and adulthood, indicating a more significant shift in jaw function between adolescence and adulthood. As such, it appears that *Mussaurus* showed an expected increase in jaw robusticity as they became juveniles, but became faster and less powerful, although they maintained already strong MPMA. The juvenile-adult transition in *Mussaurus* saw a marked shortening of the toothrow and reinforcement of the symphysis and is the greatest change in functionality seen through its ontogeny.

Collectively, this indicates an expected optimization through ontogeny to deal with tougher food material, but at different tempos. This may highlight differences in dietary evolution through ontogeny. *Mussaurus* jaw functionality was relatively constant from hatchlings to juveniles already exhibiting high biting efficiency and a suitability to tough foods unlike *Massospondylus*, which developed these capabilities more gradually through ontogeny. The limited scale of the changes between the hatchling and juvenile suggests a very early predisposition to herbivory as suggested by a juvenile *Mussaurus* already possessing similar if not greater relative functional capabilities than an adult Massospondylus. Dental ontogenetic changes in *Massospondylus carinatus* are not considered here for lack of available material, but well-preserved hatchling dentition in another massospondylid (*Lufengosaurus*) indicates that folidont dentition was present at birth (Reisz et al., 2020). It is unclear whether these features are a widespread condition, but if so, it would indicate that young massopodans were equipped from birth with a combination of teeth adapted for herbivory and their jaws became gradually adapted for feeding on tougher vegetation. It is possible that the much lower MA of the hatchling and juvenile *Massospondylus* compared to *Mussaurus* and distinctive shift to *Mussaurus*-levels of functionality into adulthood may indicate an overall greater dietary shift from insectivory/faunivory as juveniles to herbivory in adults (Montanucci, 1968; Gow, 1978; DeMar and Bolt, 1981), similar to that seen in modern iguanid lizards (Troyer, 1982). Mussaurus saw most jaw morpho-functional modification as it reached maturity with heavy modification of the symphysis and toothrow length, which suggests perhaps a shift within an already herbivorous diet towards feeding on tougher material and less focus on oral processing on food. Nonetheless, existing studies of sauropodomorph ontogeny (Reisz et al., 2005; Chapelle et al., 2019; Otero et al., 2019) indicate substantial variation across the clade, and I stress that further materials and study are needed to clarify whether these trophic shifts are ubiquitous across massospondylids and sauropodiforms. Nevertheless, this ontogenetic pathway of mandibular development mirrors the evolutionary trajectory of sauropodomorph jaw morphology through the Late Triassic (Figs. 4.1.1b and 4.1.1c) and may offer additional lines of inquiry for the acquisition of these features in sauropodomorphs.

Indeed, heterochronic shifts have been implicated in key evolutionary changes to sauropodomorph locomotion (Chapelle et al., 2019) and dentition (Reisz et al., 2020).

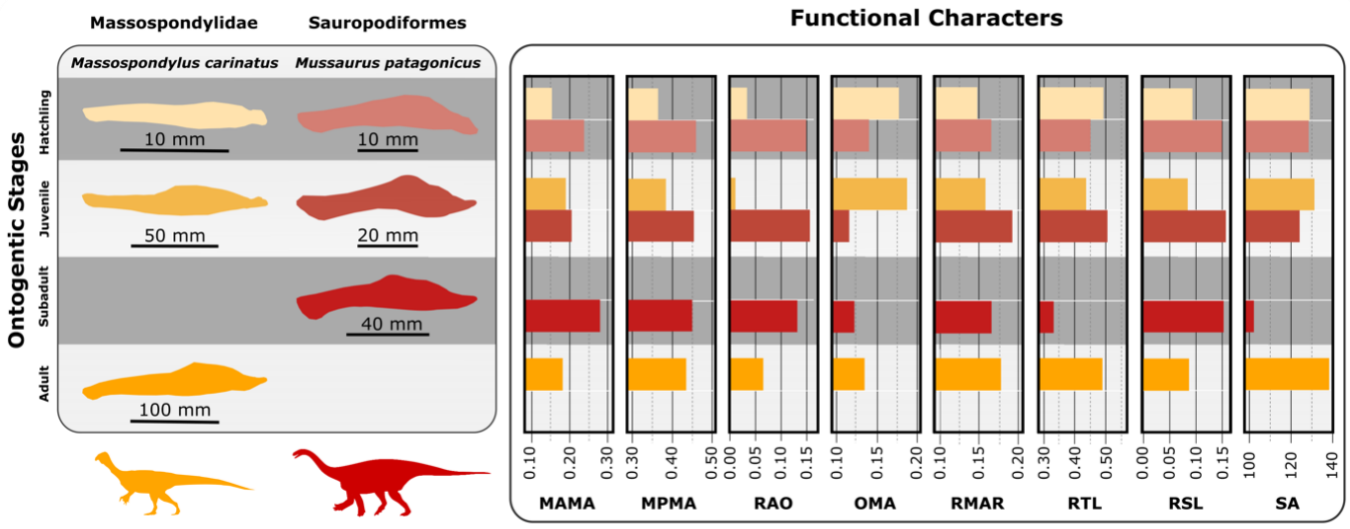

Figure 4.1.2. Sauropodomorph mandibular development through ontogeny. Mandibular morphological and functional changes through ontogeny within the taxa, *Massospondylus carinatus*. (n=3) and *Mussaurus patagonicus* (n=3). Abbreviations: MAMA, Anterior mechanical advantage; MPMA, Posterior mechanical advantage; OMA, Opening mechanical advantage; RAO, Relative articulation offset; RMAR, Relative maximum aspect ratio; RSL, Relative symphysis length; RTL, Relative toothrow length; SA, Symphyseal angle.

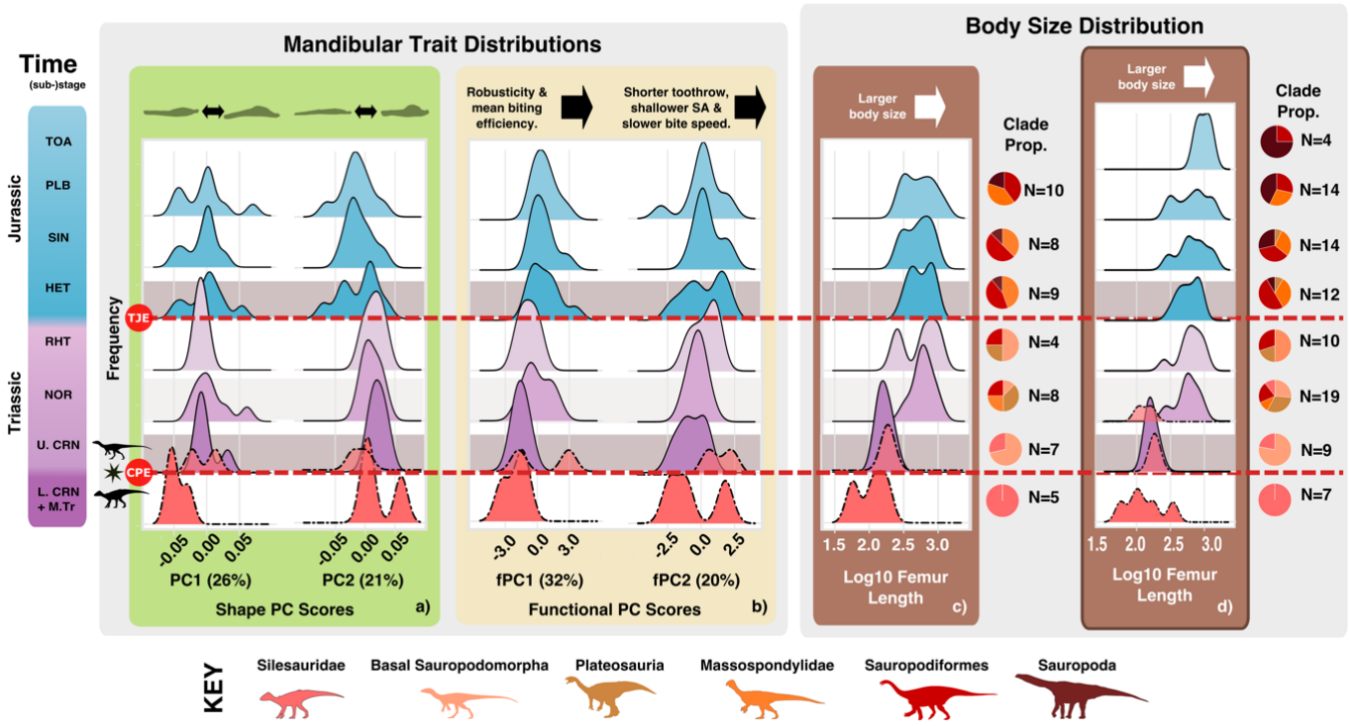

Figure 4.1.3. Changes in silesaurid and sauropodomorph mandibular morphofunctionality and body size through the Middle Triassic – Middle Jurassic. Shifts in silesaurid sauropodomorph (f)PC 1 and (f)PC2 score and log10 femur length through the Middle Triassic to Middle Jurassic. Silesaurid distributions indicated by dashed line. Clade proportions per timebin show. Shaded bands illustrate shifts in ecomorphology. Abbreviations: CPE, Carnian Pluvial Event. F, Functional. HET, Hettangian; L. CRN, Lower Carnian. LAD, Ladinian. M, Middle. NOR, Norian. PC, Principal Component. PLB, Pliensbachian. Prop. Proportion. RHT, Rhaetian. SA, Symphyseal angle. SIN, Sinemurian. TJE, Triassic-Jurassic Extinction. Tr, Triassic. TOA, Toarcian. U. CRN, Upper Carnian.

Ecomorphology Through Time. When overall changes in shape and functional PC score are broken down into trait distributions per timebin, additional patterns of morpho-functional change become apparent (Fig. 4.1.3). Silesaurid mandibular shape and function shifted across the Carnian Pluvial Event (CPE), becoming more robust with a shorter toothrow (Fig. 4.1.3; Supplementary Fig. 4.1.2). This change occurs alongside an increase in overall size (Fig 4.1.3c-d). Basal-most sauropodomorphs in the Upper Carnian appear to be somewhat dissimilar to the majority of pre-CPE silesaurids, represented by taxa such as *Lewisuchus admixtus.* Within sauropodomorphs, distributions across (f)PC1 and (f)PC2 indicate minimal variance through the Late Triassic, with the Triassic-Jurassic

extinction (TJE) marking a shift towards greater shape and functional diversity. However, it is also apparent that the shift towards greater functionality at the TJE is part of a wider gradual trend towards greater robusticity and biting efficiency (Fig. 4.1.3b). The aftermath of the TJE also appears mark a period of diversification as indicated by the broader distribution of shape and functional PC scores in the Hettangian compared to the Norian and Rhaetian. The end of the Hettangian saw a slight reduction in variation, with increasing consolidation of functionality around an apparent adaptive peak, although there is still experimentation with the length of the toothrow and symphyseal angle (Fig. 4.1.3b). Consideration of mandibular changes alongside changes in body size illustrate a slight difference in trends, with the gradual changes in jaw morphology and body size through the Triassic and Jurassic, but jaw morphofunction is punctuated by a shift at the TJE, whereas body size shows minor changes across this transition; rather the greatest shift in body size occurred at between the Upper Carnian and Norian (Fig. 4.1.3c-d). This highlights the Norian as the key stage of body size evolution for sauropodomorphs. There is an additional marked change in body sizes across the Pliensbachian – Toarcian transition, with a reduction in size variation around a larger mean (Fig. 4.1.3d). Overall, the most prominent trends in sauropodomorph mandibular evolution through the Middle Triassic to Middle Jurassic are towards increased overall and symphyseal robusticity (Fig. 4.1.3; Supplementary Fig. 4.1.2).

Further clarification of patterns of morphofunctional evolution are discerned through subdivision of the shape (Fig. 4.1.1b) and functional (Fig. 4.1.1c) morphospaces by time and the illustration of their sum of variance (SOV) through time as a distinct measure of disparity (Fig. 4.1.4). MO through the Late Triassic and Early Jurassic show similar patterns for shape and function variance. The differences in shape and functional MO between Middle Triassic – Lower Carnian silesaurids and Upper Carnian sauropodomorphs are more apparent when displayed as morphospace through time, and this is confirmed by permutational analysis ($p=0.067$ for shape and $p=0.000$ for function) (Supplementary Table 4.1.2). Basal-most sauropodomorphs in the Carnian show clustered MO, but the evolution of 'core prosauropods' (plateosaurids and massospondylids) across the Carnian-Norian transition saw a slight shift in overall sauropodomorph MO through expansion along PC1 and fPC1 (Fig. 4.1.4b). This was followed by a continued gradual shift in MO through the Norian. These variations in feeding morpho-function are largely paralleled by gradual increases in mean body size apart from a distinct increase in size through the Carnian-Norian transition (Figs. 4.1.3c-d, 4) that occurred alongside a shift in dentition, as curved and straight folidont teeth became the primary dentitions of Norian sauropodomorphs (Fig. 4.1.4a). Shape and functional MO shows a slight shift through the Norian, but the Middle Norian is poorly sampled (Fig. 4.1.4b) and contracted greatly in the Rhaetian. The Rhaetian contraction must also be viewed with

caution on account the poor sampling through this stage. interestingly, the Middle Norian represents a potential interval of significant mandibular evolution as the shift from the Lower and Middle Norian to the Upper Norian and Rhaetian marks a significant functional shift (p=0.03) in mandibular morphology (Supplementary Table 4.1.3). This may potentially reflect the appearance of the sauropodiforms, which appear in greater prevalence towards the end of the Norian (Fig. 4.1.4b).

Morphospace expansion and contraction through the Late Triassic is followed by a large shift through the TJE and further expansion (Fig. 4.1.4) driven by massospondylids and sauropodiforms. Disparity through time (Fig. 4.1.4c and Supplementary Table 4.1.1) illustrates this shift in mandibular MO across the TJE with an increase in disparity in the Hettangian. The TJE also exhibits the next major shift in dentition with the first appearance here of spatulate and lanceolate dentitions within sauropodomorphs. The change in MO from the Hettangian-Sinemurian is recovered as significant for mandibular shape (p=0.034) but not function (Supplementary Table 4.1.3), but this change represents morphospace packing as taxa populate existing morphospace rather than develop more extreme mandibular modification to expand overall MO (Fig. 4.1.4b). Shape and functional disparity declined accordingly in the Sinemurian (Fig. 4.1.4c). Interestingly, this phase of morphospace packing marks another notable increase in maximum body size (Figs. 4.1.3d, 4c). The Sinemurian-Pliensbachian shows another functionally nonsignificant, significant shift in mandibular shape (p=0.004), but insufficient sampling prevents clear observation of Pliensbachian and Toarcian mandibular MO, which are shown here combined (Fig. 4.1.4). Sauropodomorph shape MO for these combined stages is broad despite poor sampling but with reduced functionality; this is also reflected in the patterns of phylogenetic disparity, which shows an increase in shape disparity but a downturn in functional disparity at this time (Fig. 4.1.4c). Another dental shift also occurs during the Pliensbachian and Toarcian as remaining sauropodomorphs (largely early sauropods) adopted either spatulate or lanceolate dentitions (Fig. 4.1.4a). Furthermore, the Pliensbachian-Toarcian also saw an additional upward shift in body size (Fig. 4.1.4c), that is analogous to the shift at the Carnian-Norian boundary as it reflects a complete upward shift in size range (Fig. 4.1.3d).

The Middle Jurassic exhibits a further shift in dentition as lanceolate dentitions become more prevalent than spatulate forms (Fig. 4.1.4a), but MO and body size follow similar patterns as seen at the end of the Early Jurassic, which is curious, given it remains largely unchanged despite now being solely formed by sauropods. There was also a further increase in size and an increasing disconnect between mandibular shape and function as functionality becomes increasingly

specialised; these jaws were characterised by highly robust and lengthened symphyses and stronger MPMA (Fig. 4.1.1, 3-4b; Supplementary Fig. 4.1.2).

Incorporation of phylogenetic heritage potentially provides further clarity on the timing of the aforementioned shifts in dentition, mandibular morphofunction and body size (Fig. 4.1.5). Using ancestral trait estimation (Pagel, 1994), I pinpoint the evolution of folidonty in sauropodomorphs to the CPE, with the further shift from curved to straight folidont teeth occurring within the Lower Norian (Fig. 4.1.5a), alongside shifts representing a slight improvement in mandibular robusticity Fig. 4.1.5b) and a large increase in overall body size (Fig. 4.1.5c). The emergence of spatulate teeth in the Early Jurassic (Fig. 4.1.4a) is recovered as having likely emerged much earlier at the onset of the Rhaetian and possibly even within the Upper Norian (Fig. 4.1.5a). Further examination of sauropodomorph ecomorphology in this interval reveals that sauropodiforms developed highly robust and efficient mandibles towards the end of the Norian and Rhaetian, with the prevalence of enhanced mandibular functionality cooccurring alongside spatulate dentitions. Overall, it appears that much of the dental and mandibular ecomorphological change in non-sauropod massopodans through the Early Jurassic was based on the development of traits earlier in the Upper Norian and Rhaetian. This is also somewhat true for early sauropods, as their dental diversity and large body size is already present in the Rhaetian. However, early sauropod mandibular function saw a pulse of diversification in the Pliensbachian alongside greater prevalence of lanceolate teeth. Typically, sauropodomorph changes in dentition precede expansions of body size range, which in turn precede concerted shifts in mandibular modification.

Silesaurids exhibited rapid dental evolution with folidonty emerging from the ancestral ziphodont condition in the Ladinian. Silesaurids mandibular and body size evolution is limited compared to sauropodomorphs, with *Pisanosaurus mertii* representing the most derived silesaurid. This controversial taxon (Müller and Garcia, 2020) indicates strong herbivorous specialisation in silesaurids across the CPE through the development of highly robust and powerful jaws in the sulcimentisaurians (Fig. 4.1.5b). Whilst this is somewhat similar to later sauropodomorph mandibular evolution, it is not accompanied by an additional increase in body size. Most silesaurid size evolution appears to have occurred through the Anisian-Ladinian transition (Fig. 4.1.5c),

whereas mandibular diversification appears to be based mostly within the Lower Carnian (Fig. 4.1.5b).

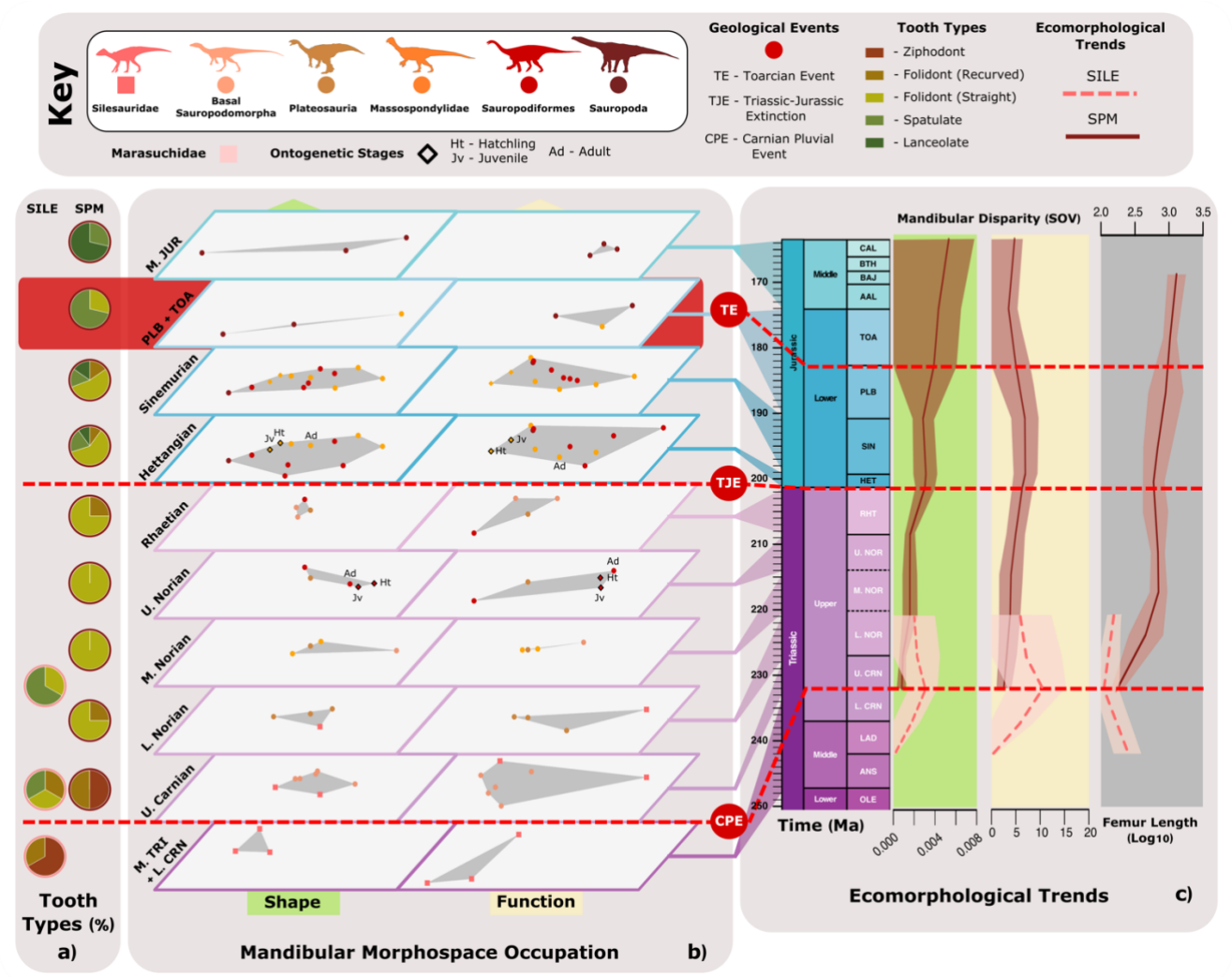

Figure 4.1.4. Sauropodomorph ecomorphological evolution through time.
Ecomorphological changes through the Middle Triassic - Middle Jurassic. (a) Proportional abundance of different tooth types per timebin. (b) Shape and functional mandibular morphospace occupation through time. Ontogenetic representatives of *Massospondylus carinatus* and *Mussaurus patagonicus* also included. (n=44) (c) Shape and functional mandibular disparity alongside body size range through time (n=69). Disparity plotted with 95% CI and mean body size plotted with standard deviation. Points on the body size plot represent individual taxa to give some idea of silesaurid body size in timebins with insufficient data. The underlying plotspace gradient illustrates the prevailing climatic conditions through time (6, 7). The Norian was subdivided on account of its lengthy duration. Insufficient sampling from the Ladinian, Pliensbachian and Toarcian meant taxa

from those time bins are plotted within adjacent bins. Abbreviations: AAL, Aalenian. ANS, Anisian. BAJ, Bajocian. BTH, Bathonian. CAL, Callovian. HET, Hettangian. L. CRN, Lower Carnian. L. NOR, Lower Norian. LAD, Ladinian. M. NOR, Middle Norian. OLE, Olenekian. OXF, Oxfordian. PLB, Pliensbachian. RHT, Rhaetian. SPM, Sauropodomorpha. SILE, Silesauridae. SIN, Sinemurian. SOV, Sum of variance. TOA, Toarcian. U. CRN, Upper Carnian. U. NOR, Upper Norian.

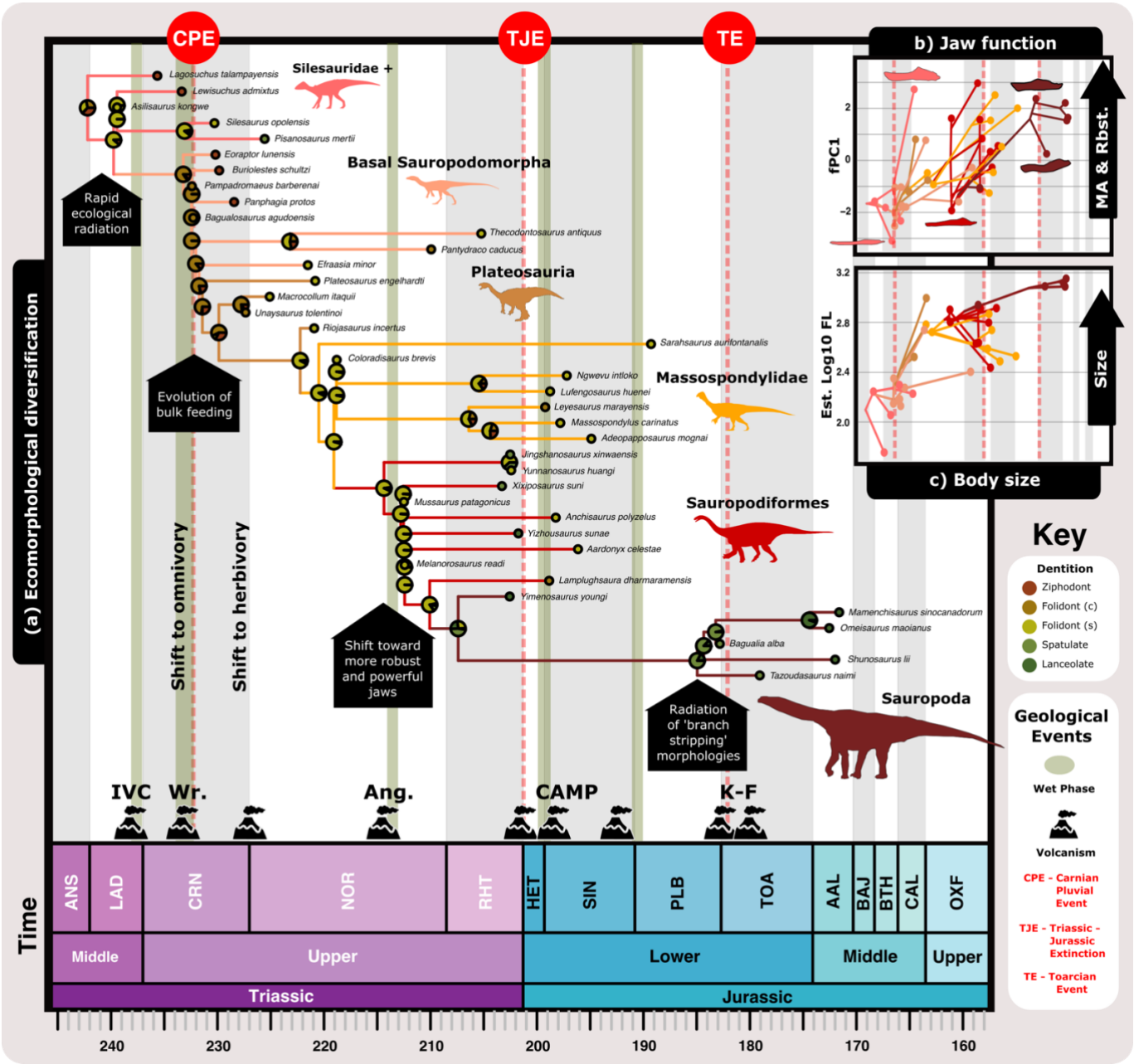

Figure 4.1.5. Changes in overall sauropodomorph and silesaurid ecomorphology through the early Mesozoic. Shifts in ecomorphology: a) ancestral state estimations of

dentition. b) phenogram showing primary mandibular functionality. c) phenogram showing body size. Illustrated alongside large volcanic events (Trotter et al., 2015; Rigo et al., 2020) and corresponding shifts in climate during the Late Triassic - Middle Jurassic. (n=44) Abbreviations: AAL, Aalenian. Ang. Angayucham Emplacement. ANS, Anisian. BAJ, Bajocian. BTH, Bathonian. CAL, Callovian. CAMP, Central Atlantic Magmatic Province. CPE, Carnian Pluvial Event. CRN, Carnian. Est. Estimated. FL, Femur length. fPC, Functional principal component. HET, Hettangian. IVC, Italian volcanic centre. LAD, Ladinian. NOR, Norian. OXF, Oxfordian. PLB, Pliensbachian. RHT, Rhaetian. SPM, Sauropodomorpha. SILE, Silesauridae. SIN, Sinemurian. SOV, Sum of variance. TE, Toarcian Event. TJE, Triassic-Jurassic Extinction. TOA, Toarcian. WR, Wrangellian eruptions.

Discussion

The Sauropodomorph Route to Megaherbivory. Sauropodomorph megaherbivory emerged in an efficient, stepwise fashion with changes in more plastic areas of anatomy preceding more significant change (Fig. 4.1.5). Changes in tooth morphology at the CPE supported their initial radiation and marked the first adaptive step towards herbivory. Carnian sauropodomorphs were morphologically conservative except in their dentition, which deviated in curvature and denticle orientation from typical faunivorous ziphodonty, creating a curved folidont tooth morphotype (Cabreira et al., 2016; Müller and Garcia, 2019). Such subtle dental modifications can permit low-fibre herbivory and suggests omnivory within some Carnian taxa (Melstrom, 2017; Hotton et al., 1997). Folidont dentitions provide a more continuous cutting surface and superior grip, thereby improving cropping abilities (Throckmorton, 1976). The shift from folidont to lanceolate and spatulate morphologies in later sauropodomorphs enhanced their cropping ability and so has been interpreted as representing greater herbivory (Galton, 1985; Barrett and Upchurch, 20017). Similar trends are noted within extant lizards (Montanucci, 1968; Stayton. 2006), as well as other herbivorous Mesozoic archosaurs (Martz and Small, 2019; Melstrom and Irmis, 2019; Weishampel and Norman, 1989). Mandibular modification was gradual and focused on improving cropping functionality by developing higher structural robusticity and anterior biting efficiency (Figs. 4.1.1 and 4.1.3) (Lautenschlager, 2017; Button and Zanno, 2020; Stayton, 2006). Low MA values in advanced sauropodiforms and sauropods possibly reflect the emergence of additional structural support in the form of lateral plates along the alveolar margins of the dentary (Barrett and Upchurch, 2007). They also correspond to the shift to spatulate and lanceolate dentitions, which may have acted in accordance with improvements to cropping efficacy to further reduce stresses on the mandible during feeding. Mandibular evolution is

primarily directed to maximizing ingestion with no development of oral or gut comminution (Nabavizadeh, 2019; Wings and Sander, 2007; Button et al., 2017).

High rates of ingestion and adaptation for food prehension over mastication implies optimization for bulk feeding and increases in body size suggest concurrent improvement in digestive efficiency through the development of intensive fermentation (gut-processing) (Sander et al., 2011; Clauss et al., 2013). Improved digestive efficiency alongside greater intake of food may have satisfied the higher absolute energy demands required to grow larger (Clauss et al., 2013). The onset of gut-processing may have fuelled the transition to obligate herbivory as fermentation can make herbivory more energetically favourable than omnivory (Bjorndal and Bolten, 1993), and the concurrent increases in body size would also have reduced relative energy demands, thereby permitting sauropodomorphs to subsist on (lower quality) vegetation (Hummel et al., 2008). The synchrony of shifts in feeding morphology alongside body size (Figs. 4.1.3-5) and other anatomical traits (McPhee et al., 2015; Rauhut et al., 2011), supports the 'cascade/correlated progression' model of evolution as outlined by Barrett and Upchurch (2007), and Sander (2013) for the evolution of sauropod gigantism. This cascade likely fuelled the larger sizes (>2 meters in length) that distinguished sauropodomorphs from contemporary herbivores; only the Rhaetian dicynodont, *Lisowicia bojani,* achieved comparable size (Sulej and Niedźviedzki, 2019; Romano and Manucci, 2019).

Silesaurids likely adopted herbivorous diets in the Middle Triassic in a similar way to sauropodomorphs. They also adopted some of the same changes to their anatomy in modifying their jaws to be more robust, with greater biting efficiency and even ventrally deflected dentaries (Fig. 4.1.4), but their morpho-functionality diverged (Fig. 4.1.4; Supplementary Table 4.1.4) as it appears silesaurids opted to pursue oral-processing of their food rather than bulk processing as seen in sauropodomorphs. Oral processing can be highly advantageous in that it allows for fairly strong digestive efficiency through greater comminution of food material prior to ingestion (Weishampel and Norman, 1989). However, this efficiency comes at a cost as it is more energy intensive as it relies on mechanical breakdown of the food by the herbivore (Sanson, 2006). In combination with their smaller sizes, this may have driven silesaurids to become more specialised browsing herbivores as increasing specialisation on available high-quality vegetation to meet their energetic and nutritional requirements. Indeed, this appears to manifest in the mandibular evolution of the sulcimentisaurians, which showed strong divergence from the carnivorous functionality as seen in more basal silesaurids such as *Lewisuchus admixtus,* particularly in their development of MPMA (Figs. 4.1.1, 3, 5). However, the likely efficiency gains of specialisation are tied to reduced ecological

flexibility and this may explain why silesaurids were unable to survive alongside the sauropodomorphs through the end-Triassic extinction.

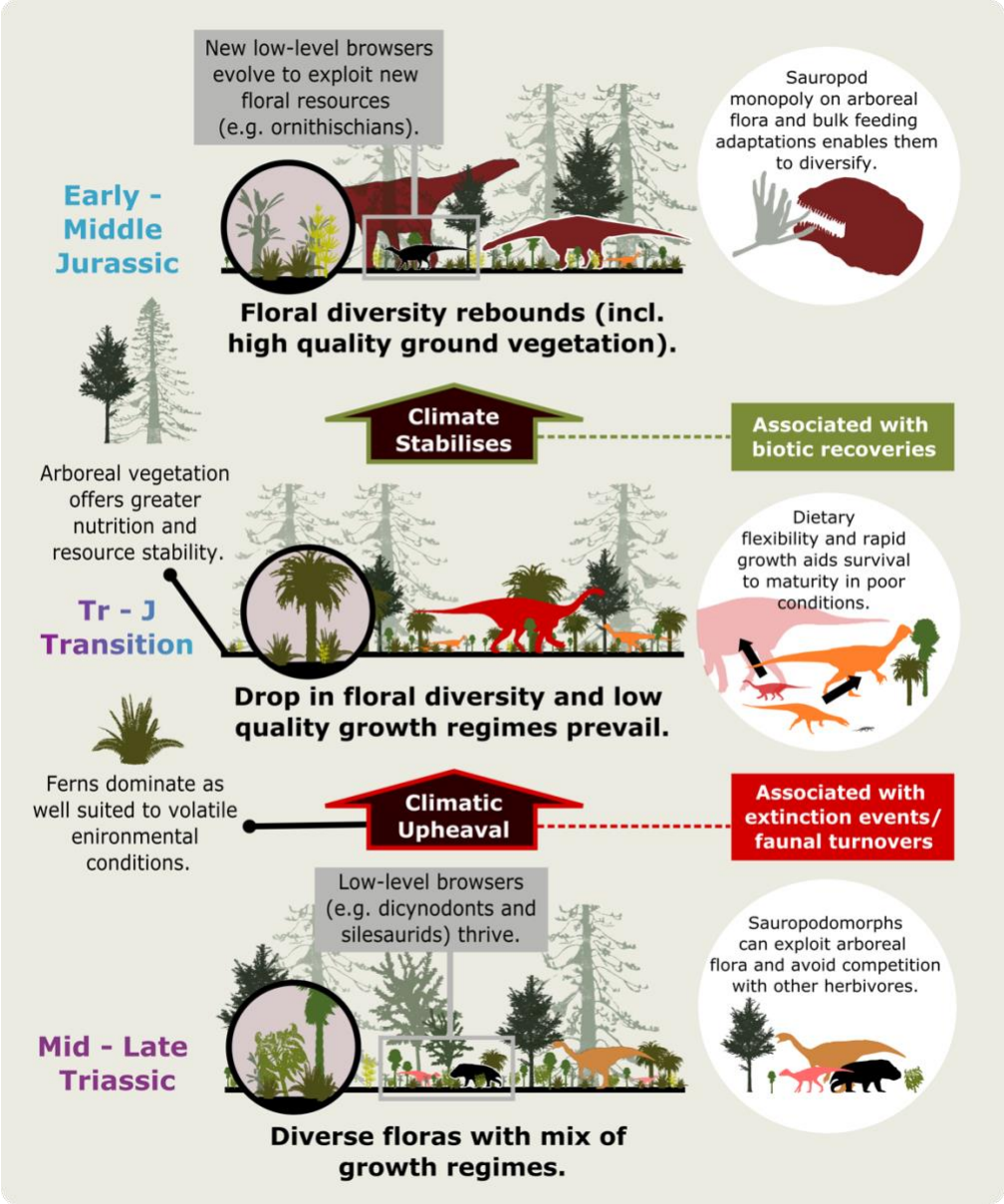

Figure 4.1.6. Extrinsic drivers of sauropodomorph macroevolution. Changes in terrestrial floras alongside key changes/traits that supported sauropodomorph success through the Late Triassic and Middle Jurassic. Changes in predominant flora shown (with additional magnification of undergrowth), illustrating the shift to gymnosperm floras in the Late Triassic (Kustatscher et al., 2018; Patterson and Mangerud, 2015), the prevalence of fern-dominant floras following the TJE (van de Schootbrugge et al., 2009; McElwain et al., 1999), the return of conifer-dominated forests in the Early Jurassic (Lindström et al., 2016),

and climatic instability in the Early Toarcian (Mander and McElwain, 2019). Abbreviations: J, Jurassic. Tr, Triassic.

Extrinsic Drivers of Sauropodomorph Macroevolution. Considerable ecomorphological shifts coincide with wider extrinsic changes (Fig. 4.1.5) and reflect the interactions between these animals and their changing environments. I note four major events/shifts that echo the faunal succession of sauropodomorphs (Pol et al., 2021):

1. Late Carnian: Ongoing phylogenetic uncertainty at the base of the Dinosauria (Baron et al., 2017; Müller and Garcia, 2020) suggests dinosaur origins in the Middle Triassic, yet the first unequivocal dinosaurs occur in the Late Carnian (Nesbitt et al., 2017). The sudden appearance of multiple dinosaur taxa has been tied to the CPE (Bernardi et al., 2018; Benton et al., 2018), an interval (234-232 Ma) of wetter climates (Simms and Ruffel, 1990; Baranyi et al., 2019) that also saw significant turnovers/diversifications of terrestrial floras (Cascales-Miñana and Cleal, 2012) and insects (Labandeira et al., 2016; Shcherbakov, 2008). Basal-most sauropodomorphs were largely faunivorous (Cabreira et al., 2016; Bronzanti et al., 2017), but subtle evolution from clear ziphodont to curved folidont dentitions (Figs. 4.1.4-5) hints at omnivory in some (Müller and Garcia, 2019). Rich plant and insect resources during the CPE provided ample opportunities for them to acquire the microbes necessary for plant digestion from the ingestion of herbivorous insects and/or detritus (Sues and Reisz, 1998), and augment their diets with vegetation. The CPE appears to be the likely catalyst for wider archosaur experimentation with herbivory, as seen in the morphological evolution of pseudosuchian aetosaurs (Desojo et al., 2013) and sulcimentisaurian silesaurids (Martz and Small, 2019) during their late Carnian diversifications. The dietary flexibility offered by omnivory may have contributed to the sudden appearance and increasing prominence of sauropodomorph dinosaurs in the late Carnian (Müller and Garcia, 2019; Benton, 1983), as the end of the CPE saw the onset of greater aridity and seasonality (Simms and Ruffel, 1990; Preto et al., 2010).

2. Carnian-Norian Transition: The CNT marks a concerted shift in dentition and body size reflecting greater herbivorous specialization and the likely onset of bulk-feeding (Figs. 4.1.3-5) during the evolution of 'core' prosauropods (plateosaurids and massospondylids) (McPhee et al., 2020). This increase in body sizes was modest compared to later sauropod evolution, but this change appears to be a key to sauropodomorph success by enabling them to engage in bulk-feeding. Wider extrinsic changes may have drove this evolution as changes in sauropodomorph trophic morphology and body size coincide with changes in flora at the onset of the Norian (Cascales-Miñana and Cleal, 2012). Thoughts that changes in prosauropod ecomorphology reflect adaptations to low-quality diets (Midgley et al., 2002) are challenged by recent analyses of the relationship between body size

and diet quality (Clauss et al., 2013) and the estimated nutritional quality of Mesozoic flora (Gill et al., 2018; Hummel et al., 2008). Rather recent study suggests this floral change saw a shift in nutritional content from ground to canopy level as terrestrial floras became more mesophytic and gymnosperm dominated (Kustatscher et al., 2018; Patterson and Mangerud, 2015) (Fig. 4.1.6). Undergrowth was generally dominated by ferns and their allies, which were relatively nutrient poor compared to canopy vegetation comprising gingkoes, conifers and bennettitales (Kustatscher et al., 2018; Hummel et al., 2008; Patterson and Mangerud, 2015; Soh et al., 2017). Being big, allowed core prosauropods to exploit these high-quality resources unlike contemporaneous herbivores such as aetosaurs, dicynodonts and rhynchosaurs, which were largely low-level browsers (Parrish, 2006; Barrett et al., 2010; Weishampel and Norman, 1989). Exclusive access to widely available, high-quality, but tough gymnosperm foliage is a strong selective force for increasing herbivorous specialization and body size and may explain prosauropod faunal dominance as these floras proliferated in the Norian (Benton, 1983).

3. Triassic-Jurassic Extinction: The eruption of the Central Atlantic Magmatic Province as the Pangaean supercontinent broke apart drove intense global warming and climatic oscillations at the end of the Triassic (Hesselbo et al., 2002; Ruhl et al., 2011; Tegner et al., 2020). This climatic upheaval may have been more protracted as recent studies indicate further volcanism at the Norian-Rhaetian transition and so a more extended extinction event with two pulses across the end of the Triassic (Sephton et al., 2002; Rigo et al., 2020; Wignall & Atkinson, 2020) (Fig. 2.1.5a). This interval of climate change is held responsible for the TJE, which saw the extinction of all other large herbivores (aetosaurs and dicynodonts) apart from sauropodomorphs (Sues and Fraser, 2010; Rigo et al., 2020). Sauropodomorph mandibular disparity and size range declined during the Rhaetian as environmental conditions worsened (Fig. 4.1.3). Yet, sauropodomorphs survived. The end-Triassic witnessed widespread deforestation and dramatic reorganization of global floras, with ferns flourishing as tropical flora suffered declining species richness and prevalence (van de Schootbrugge et al., 2009; McElwain et al., 1999; Bacon et al., 2013). Leaf functional traits reveal heightened adaptation to environmental stress during the TJE, and shifts to longer leaf lifespans, low nutrient concentrations and slow physiological rates (Soh et al., 2017; Bacon et al., 2013; Lindström et al., 2016). Bulk-feeding and larger body sizes would have allowed prosauropods to compensate for lower quality foliage at ground and canopy level during the TJE by increasing consumption with minimal effort (Sander et al., 2011). Further strengthening of the mandible symphysis and posterior biting efficiency (Fig. 4.1.1d) may reflect adjustment to tougher foliage, and a marked increase in body size may indicate further enhancement of bulk-feeding capabilities. The emergence of robust dental and mandibular morphologies in the Rhaetian across large sauropodiforms and sauropods

(Fig. 4.1.5) exemplifies this mechanism of sauropodomorph survival by showing it in its most extreme form. Massospondylids also show a similar pattern of development, although they also show greater diversity with the evolution of two apparent regimes, with smaller taxa developing more efficient MA but without significant symphyseal modification and the larger taxa following a similar path as sauropodiforms and sauropods. Potentially increased omnivory in juvenile massospondylids may have helped to balance foraging energy expenditure by permitting a wider resource base. Whereas sauropodiforms likely saw rapid ontogenetic growth to enable them to feed on ideal high canopy vegetation as soon as possible (Krupandan et al., 2018). Ontogenetic dietary flexibility and rapid growth supported higher likelihoods of survival to reproductive maturity, after which sauropodomorphs enjoyed exclusive access to canopy vegetation. Stronger population recovery potential via high turnover associated with oviparity and the capacity for rapid reproductive rates (Sander et al., 2011; Janis and Carrano, 1992) would also have promoted sauropodomorph survival through the TJE. Greater MO in the Hettangian (Fig. 4.1.4b) indicates greater trophic diversity and suggests that morphospace expansion was driven by the availability of vacant niche space, echoing the wider opportunistic radiation of dinosaurs post-TJE (Brusatte et al., 2008; 2020; Benton et al., 2014).

4. Sinemurian - Pliensbachian: Morphospace packing of advanced sauropodiforms and early sauropods illustrates the success of their feeding mode in the Early Jurassic. Comparatively reduced, more-rostrally positioned toothrows and shifts in anterior biting efficiency within stem and early sauropods (Figs. 4.1.1, 4.1.3) co-occur with muzzle width expansion (Rauhut et al., 2011) and more robust spatulate and lanceolate dentitions, possibly marking the emergence of 'branch stripping' feeding (Button et al., 2017). Whilst smaller Early Jurassic sauropodomorphs exhibited trophic morpho-functionality that predominated among core prosauropods (long toothrows with relatively high MA across the entire length, and ventrally deflected dentaries), these forms disappeared at the end of the Early Jurassic, during the late Pliensbachian, leaving only branch stripping morphologies in the Toarcian and into the Middle Jurassic. The greatest diversity of both forms in the Early Jurassic occurs in the Sinemurian which coincides with the apparent recovery of terrestrial floral diversity from the TJE within the middle of this stage (McElwain et al., 2007). Sauropods were likely present in the late Norian (Lallensack et al., 2017), but did not diversify until the Early Jurassic perhaps because of this lack of climatic stability (Chandler et al., 1992). Being already larger than contemporary herbivores in the Early Jurassic (Barrett et al., 2010), sauropods were ideally placed to exploit highly nutritious arborescent vegetation as conifer-dominated forests returned in the Sinemurian (Lindström et al., 2016) (Fig. 4.1.6). I note that sauropod diversity increased relative to prosauropods through the Toarcian. Newly discovered taxa further pinpoint the late Early Jurassic as the interval of

major sauropod diversification (Xu et al., 2018; Pol et al., 2020). A pulse of volcanism in the early Toarcian is linked to marine extinctions, and perhaps significant (floral) changes in the terrestrial realm (Mander and McElwain, 2019; Slater et al., 2019; Jansson et al., 2008). This environmental upheaval may therefore be linked to the rise of eusauropods at the end of the Early Jurassic. Indeed, these taxa show stronger ecomorphological specialisation towards the branch stripping functionality and bulk-feeding (Figs. 4.1.4-6).

Conclusions

In summary, sauropodomorphs underwent two radiations during the recovery intervals following mass extinctions linked to significant climatic events, and two shifts in both body size and dentition within the recovery phases of those extinctions (Fig. 4.1.6). Enhanced dietary efficiency enabled prosauropods to adapt to newly prevalent gymnosperm floras, and more importantly to poor-quality floras during episodes of poor climatic conditions. Dietary flexibility through ontogeny provided a further buffer against environmental instability. Whilst rapid growth allowed obligate herbivore sauropodiforms to quickly begin exploiting high-quality canopy vegetation in bulk. Sauropodomorph mandibular traits are not unique, being present in both silesaurids and some theropod clades (Cabreira et al., 2016; Button and Zanno, 2019; Nesbitt et al., 2017; Martz and Small, 2019). However, sauropodomorphs were able to maximise the utility of these traits through the boosting of their overall body sizes at the Carnian-Norian transition; getting larger enabled them to exploit new, superior resources and more efficiently process them via the adoption of bulk-feeding. This ability to exploit high level vegetation, alongside dietary resilience of bulk-feeding as obligate herbivores supported sauropodomorph success through the early Mesozoic. Further study is required to understand the underlying features that allowed sauropodomorphs to get so much larger than contemporaneous herbivore, including their silesaurid relatives. Nonetheless, it appears it was the coincidence of fortunate trait evolution and extrinsic changes that allowed sauropodomorphs to become the predominant large terrestrial herbivores in the Early Jurassic, eventually producing the unique form of megaherbivory seen in sauropods (Sander et al., 2011).

Supplementary Materials

Supplementary Methods.

Functional Characters:

1. Mean Anterior Mechanical Advantage: A measure of biting efficiency at the anterior of the mandible (Westneat, 1994). This is the ratio of the inlever to the outlever, using the distance from the jaw joint to the anterior-most tip of the toothrow/dentary as the outlever. The distance from the jaw adductor muscle attachment to the jaw joint represents the inlever. This ratio of inlever to outlever gives the lowest possible value of MA.
2. Mean Posterior Mechanical Advantage: A measure of biting efficiency at the posterior of the mandible (Westneat, 1994). This is the ratio of the inlever to the outlever, using the distance from the jaw joint to the posterior-most point of the toothrow/dentary as the outlever. The distance from the jaw adductor muscle attachment to the jaw joint represents the inlever. This ratio of inlever to outlever gives the highest possible value of MA.
3. Opening Mechanical Advantage: A measure of biting velocity (Westneat, 1994). This is the ratio of the maximum inlever to the maximum outlever, using the distance from the jaw joint to the posterior-most point of the mandible/retroarticular process for the inlever, and using the distance from the jaw joint to the posterior-most point of the toothrow/dentary as the outlever. Opening MA is linked to feeding patterns and prey selection (Anderson and Westneat, 2007; Stubbs et al., 2013).

Characters 1-3 are based on using lever mechanics to describe mandibular function, with the jaw acting as a third-order lever system (Westneat, 1994; 2004). The adductor musculature acts as the input force, the craniomandibular joint acts as the fulcrum and the output force is exerted along the toothrow/shearing surface. Herbivores often exhibit higher MA values than faunivores (Stayton, 2006). Levers are measured from the craniomandibular joint/jaw articulation. Taxa with low MA exhibit weak, rapid bites (Wainwright and Richard, 1995; Stubbs et al., 2013), whilst taxa with a strong bite force have a high MA.

4. Relative Maximum Aspect Ratio: A proxy for the second moment of area, previously used in 2D analyses of jaw mechanics (Anderson, 2011; Stubbs et al., 2013). Generated by dividing the maximum depth of the mandible by its total length. The second moment of area is typically used to assess the resistance of a beam to bending under loading and when applied to jaws gives indication of the pressures experienced during biting. It essentially requires

calculation of the cross-sectional area of the mandible, and so needs additional measurements that were often not available from lateral view images sourced from the literature. In most wide-ranging macroevolutionary analyses of anatomy (Anderson, 2011; Stubbs et al., 2013, MacLaren et al., 2017; Kilbourne, & Hutchinson, 2019), the second moment of area calculations assume a generalised jaw shape, treating it as a cylinder or rectangular beam, and this 2D approach takes this principle further by making a more basic approximation of the jaw that doesn't require 3D data. Most mandibles primarily experience dorsoventral stress during feeding function, the maximum aspect ratio measurement used here captures a more general approximation of dorsoventral robusticity and therefore, represents a measure of flexural stiffness (MacLaren et al., 2017) that can be widely applied across all sampled taxa.

5. Relative Toothrow Length: A measure of relative length of the dentition and its purported importance in trophic behaviour (Button et al., 2014). Generated by dividing the length of the toothrow/shearing surface by the total length of the mandible. A longer toothrow enables a greater range of MA along the jaw and likely increased use of the dentition in jaw functionality (either for food ingestion or processing/mastication). Herbivores tend to show relatively shortened toothrows compared to faunivores and omnivores (Sues, 2000).
6. Relative Symphysis Length: A measure of symphyseal robusticity generated by dividing the length of the symphysis by the total length of the mandible. The symphysis is subject to significant bending, shear, and torsional stress during biting action and so is highly related to transmission of muscle and biting force and feeding ecology and overall jaw mechanics (Daegling, 2001; Jones et al., 2012).
7. The symphyseal angle is measured between the ventral jaw line and a line parallel to the long axis of the mandibular symphysis. It affects symphyseal resistance to the bending, shear, and torsional stresses that occur during the bite cycle (Daegling, 2001). The symphyseal angle is known to affect food processing in modern herbivorous rhynchocephalians (Jones et al., 2012) and is of major importance in the mechanical response of modern crocodylians to biting, twisting, and shaking (Porro et al., 2011; Walmsley et al., 2013).
8. Relative Offset of Articulation: The articulation offset is measured as the length of the line perpendicular to the tangent of the mandibular toothrow (extrapolated from the anterior and posterior ends of the toothrow to account for jaw curvature) which intersects the articular joint (Anderson et al., 2011; MacLaren et al., 2017). This value is then divided by the total jaw length. An offset between the toothrow and jaw articulation affects dental

occlusion and leverage of the jaw musculature (Janis, 1995). A small articulation offset indicates 'scissor-like' occlusion, which is typical of carnivorous taxa. Herbivores generally exhibit greater toothrow-articular offset as this enables simultaneous occlusion along the entirety of the toothrow, supporting gripping & crushing actions (Ramsay and Wilga, 2007).

Supplementary Figures.

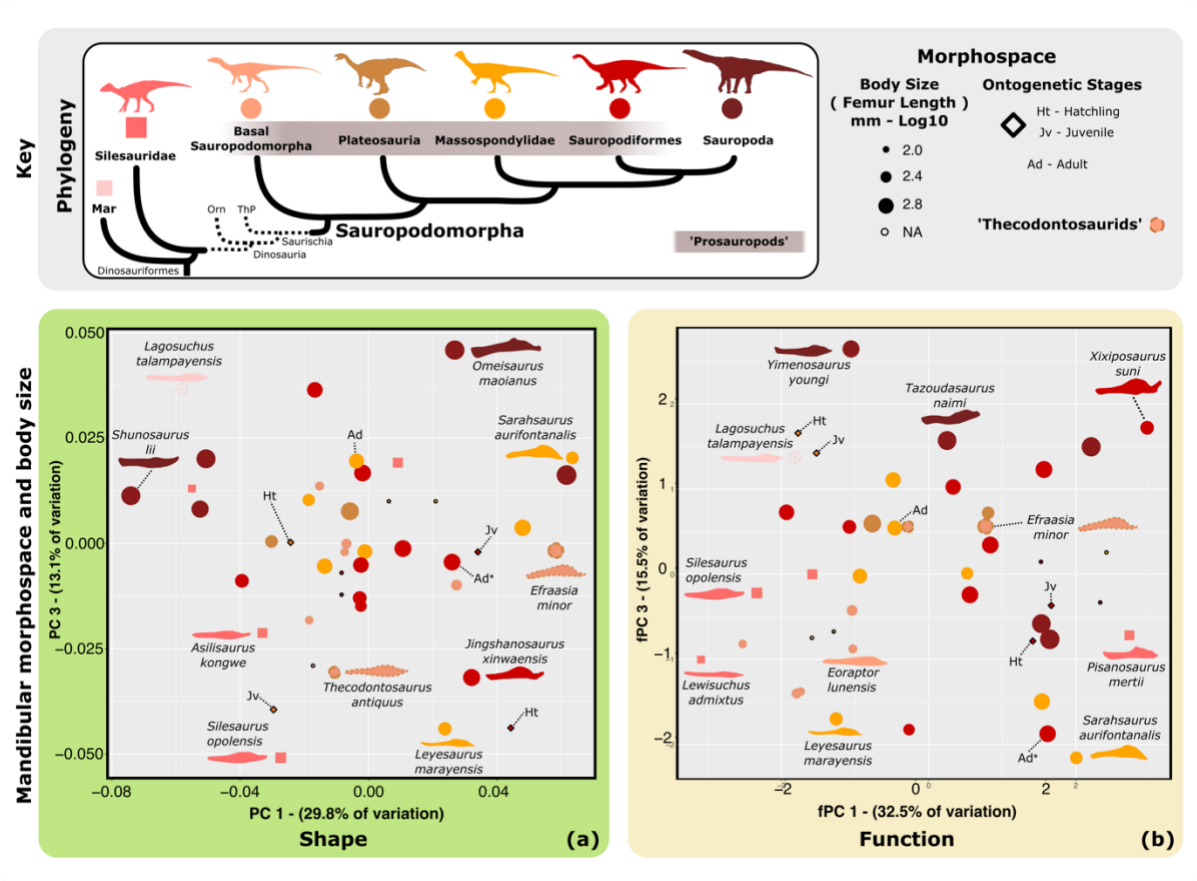

Supplementary Figure 4.1.S1. PC1 v PC3 shape and functional morphospaces. Mandibular and body size variation in Middle Triassic - Middle Jurassic silesaurids and sauropodomorphs. (a) Mandibular shape morphospace. (b) Mandibular functional morphospace. Ontogenetic representatives of *Massospondylus carinatus* and *Mussaurus patagonicus* included in both morphospaces. (n=44). Abbreviations: MA, mechanical advantage; R, relative; Mar, Marasuchidae; Orn, Ornithischia; ThP, Theropoda.

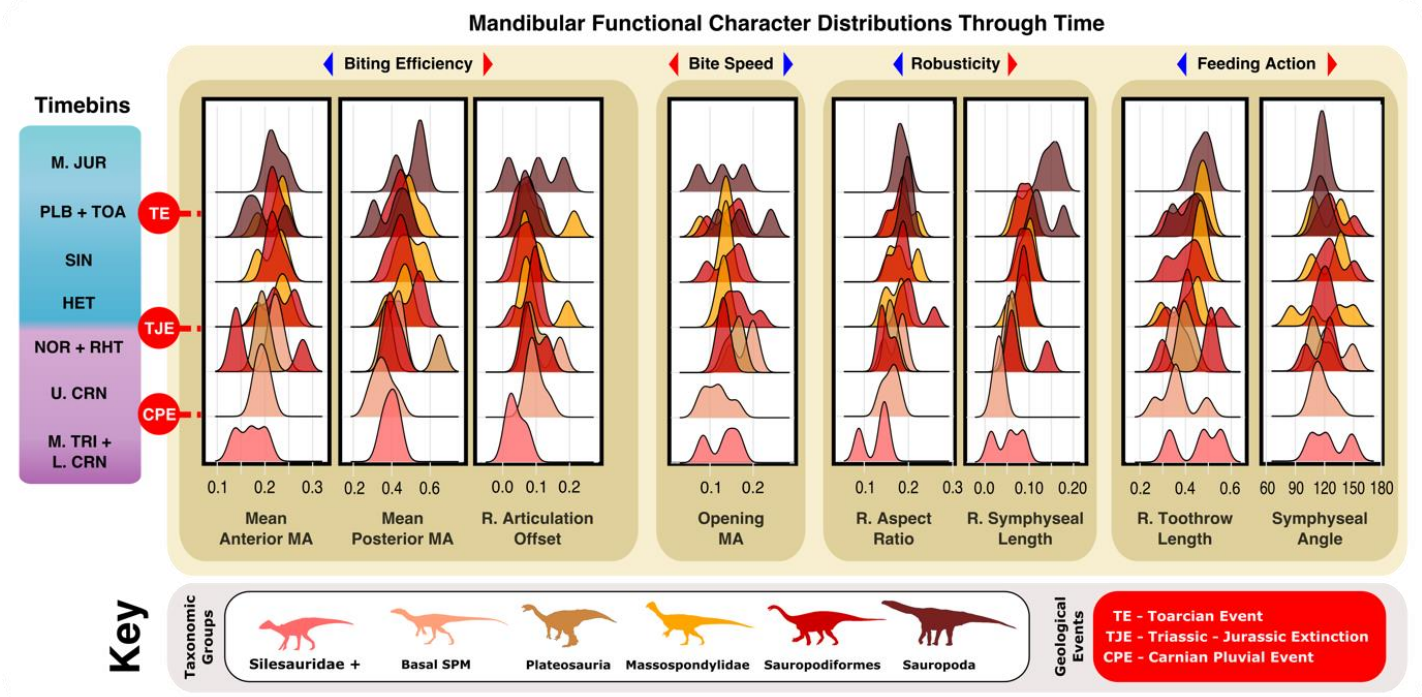

Supplementary Figure 4.1.S2. Changes in silesaurid ansd sauropodomorph mandibular functionality through the Middle Triassic – Middle Jurassic.

Shifts in sauropodomorph mandibular functional characters illustrated during the Middle Triassic to Middle Jurassic. Silesaurid distributions indicated by dashed line. (n=44) Abbreviations: CPE, Carnian Pluvial Event. F, Functional. HET, Hettangian; L. CRN, Lower Carnian. M, Middle. MA, Mechanical advantage. NOR, Norian. PLB, Pliensbachian. Prop, Proportion. R, Relative. RHT, Rhaetian. SA, Symphyseal angle. SIN, Sinemurian. TJE, Triassic-Jurassic Extinction. Tr, Triassic. TOA, Toarcian. U. CRN, Upper Carnian.

Supplementary Tables.

Supplementary Table 4.1.1. Phylogenetic disparity results for sauropodomorph shape and functional morphospace at stage level. Minimum and maximum bounds for 95% confidence intervals. Abbreviations: Max, Maximum. Min, Minimum. SOV, sum of variance.

Time (Ma)	Shape			Function		
	SOV	SOV Min	SOV Max	SOV	SOV Min	SOV Max
Sauropodomorpha						

232	0.00082	0.00033	0.00121	2.53695	1.02559	4.07627
227	0.00092	0.00060	0.00123	3.12333	1.39713	5.20156
220.83	0.00159	0.00089	0.00232	3.82853	1.56472	5.94916
214.67	0.00159	0.00089	0.00230	3.99523	1.58120	6.38510
208.5	0.00161	0.00111	0.00209	4.96033	3.05856	6.91495
201.3	0.00303	0.00212	0.00401	6.34184	4.22718	8.50688
199.3	0.00312	0.00193	0.00423	6.94269	4.53235	9.34733
190.8	0.00285	0.00185	0.00394	6.84533	4.05104	9.71557
182.7	0.00390	0.00000	0.00608	4.99900	0.00000	7.82733
174.1	0.00433	0.00000	0.00651	3.50535	0.00000	5.27007
163.5	0.00532	0.00000	0.00777	4.73608	0.00000	6.43770
Silesauridae						
242	0.00015	0.00000	0.00027	0.46615	0.00000	0.96511
237	0.00179	0.00000	0.00255	6.27865	0.00000	8.98032
232	0.00309	0.00149	0.00428	10.51805	3.36121	15.33522
227	0.00229	0.00000	0.00449	6.99868	0.00000	14.46008
220.83	0.00202	0.00000	0.00404	5.91329	0.00000	12.34507
214.67	NA	NA	NA	NA	NA	NA

Supplementary Table 4.1.2. Wang's permutation analysis results for statistically significant differences in mandibular shape and functional disparity between silesaurid and sauropodomorph clades. Abbreviations: B. SPM, Basal sauropodomorphs. Exp. Df, Expected difference. MSS, Massopodans (Non sauropodiform). Obs. Df, Observed difference. PLT, Platerosauria (Non massopodan). SILE, Silesauridae. SPD, Sauropod. SPF, Sauropodiform (Non sauropod).

Clades compared	Shape			Function		
	Obs. Df	Exp. Df	p value	Obs. Df	Exp. Df	p value
SILE > B. SPM	-0.002	0.000043	0.067	-7.95	-0.04719	0.000
B. SPM > PLT	-0.001	-0.0001	0.644	0.416	0.036232	0.868
PLT > MSS	0.002	0.0001	0.224	2.757	0.036654	0.408
MSS > SPF	0.001	-0.00003	0.306	-1.885	-0.028674	0.212
SPF > SPD	0.002	-0.00001	0.1	0.999	0.008072	0.62

Supplementary Table 4.1.3. Wang's permutation analysis results for statistically significant differences in sauropodomorph mandibular shape and functional disparity between timebins. Abbreviations: Exp. Df, Expected difference. HET, Hettangian. Jur. Jurassic. L + M. NOR, Lower and Middle Norian. M, Middle. Obs. Df, Observed difference. PLB + TOA, Pliensbachian and Toarcian. SIN, Sinemurian. Tr, Triassic. U. CRN, Upper Carnian. U. NOR + RHT, Upper Norian and Rhaetian.

Timebins compared	Shape			Function		
	Obs. Df	Exp. Df	p value	Obs. Df	Exp. Df	p value
U. CRN > L + M. NOR	0.001	0.000088	0.364	1.033	0.048868	0.612
L-M. NOR > U. NOR + RHT	0.001	0.000128	0.508	5.2	-0.094746	0.03
U. NOR + RHT > HET	0.002	0.000016	0.234	-1.13	0.017564	0.706
HET > SIN	-0.003	-0.000014	0.034	-4.242	-0.225546	0.136
SIN > PLB + TOA	0.005	0.00008	0.004	3.627	0.02974	0.202
PLB + TOA > M. Jur	0.001	-0.000106	0.6	-1.389	-0.135024	0.652

Supplementary Table 4.1.4. Wang permutation analysis results for statistically significant differences in mandibular shape and functionality between additional grouping by clade and/or time. Abbreviations: B. SPM, Basal sauropodomorphs. Exp. Df, Expected difference. J. Jurassic. NnSpd, Non-sauropod. Obs. Df, Observed difference. PostCrn, Post-Carnian. Sile, Silesauridae. Spm, Sauropodomorphs. Tr, Triassic.

Groups compared	Shape			Function		
	Obs. Df	Exp. Df	p value	Obs. Df	Exp. Df	p value
SILE > PostCrn. SPM	-0.002	0.000005	0.017	-6.57	0.115292	0.006
B. SPM > PostCrn. SPM	0	0.000032	1	1.387	-0.000729	0.396
PostCrn. SPM > J. NnSpd_SPM	0.001	-0.00002	0.343	0.312	0.058653	0.887

Conclusions - Macroevolutionary drivers and patterns across the late Palaeozoic and early Mesozoic

Understanding patterns of morphospace occupation may appear to be highly descriptive and perhaps repetitive, simply giving quantification to ideas expressed elsewhere, but the strength of these studies lies in their breadth and ability to quickly and fairly accurately outline the ecologies of many different taxa, enabling comprehension of ecological diversity across entire clades and periods. The study outlined here represents a detailed assessment of trophic ecology that tracked the rise and fall of different clades (Chapter 2) both within guilds (Chapter 3) and in-depth through specific intervals of Earth history (Chapter 4).

My studies of archosauromorph and synapsid trophic morphology find that patterns of morpho-functional diversification appear to follow largely punctuated patterns of change, with gradual trends interspersed with intervals of significant change. They also demonstrate the interplay between extrinsic and intrinsic controls on ecological diversity, as the return of environmental stability (Preto et al., 2010) is linked with the onset of successive archosauromorph radiations in the Middle Triassic and Early Jurassic, and therapsid radiations through the Permian (Figs. 2.1.7a; 3.1.2). Such environmental stability promotes trophic diversity by providing stable access to resources and allows a greater constancy of selective pressures that can further boost resource diversity and thus further ecological diversity (Cascales-Miñana et al., 2010). Instances of considerable ecological similarity are rare, but do exist, with non-archosaur archosauriforms and pseudosuchians in the Middle Triassic, demonstrating a potential pattern of ecological displacement. One more potential exampled of such displacement occurs between theriodonts and biarmosuchians during the Capitanian and Wuchiapingian. Increasing taxonomic diversity saw more limited exploration of potential mandibular morpho-function, with clade functional morphology becoming increasingly focused on particular niches. The psuedosuchians apparently acted as a suppressor on dinosaur evolution in the Late Triassic (Chapter 3.1), and eutherapsids on the theriodonts (Chapter 4.1) in the Permian, with the radiation of the supressed clades quickly following the extinction of their suppressors.

When trophic morphology by guild within closely related clades (Chapter 3.1) and between more phylogenetically distant clades (Chapter 3.2) are considered, I find a consistent drive to avoid competition through niche partitioning, with ecomorphological convergence rarely present in coexisting taxa. Within synapsids carnivores, where the mechanical requirements of feeding are fairly constant, shared mandibular and dental functional traits are quite common, echoing patterns

present across more recent mammalian evolution (Van Valkenburgh and Wayne, 2010). However, further niche partitioning occurs through varying overall body size (Figs. 3.1.7-8). Herbivory offers more freedom to modify trophic anatomy through specialisation to feed on specific plant materials, and so I find greater morphofunctional diversity within Triassic herbivores than in Permian predators. Nevertheless, it should be noted that this may reflect that the herbivore study was much more phylogenetically diverse encompassing sauropsids and synapsids. Regardless, mandibular morpho-function shows strong dissimilarity between clades (Figs. 3.2.3-4). Both studies highlight how environmental conditions dictate ecological diversity, with certain feeding functional groups only existing when permitted by extrinsic factors such as available flora or prey.

Nonetheless, the extinction of a clade may not have anything to do with conspecifics; in depth assessment of multiple aspects of anatomy within the context of broader background environmental change reveals that survival and success can hinge on key niche choices, such as the sauropodomorph choice to prioritise ingestion of food and bulk-feeding, or the silesaurid choice to pursue more specialised herbivory. Sauropodomorphs were able to capitalise on environmental changes and a fortuitous mosaic of traits that allowed them to survive, whilst herbivores such as the dicynodonts, which had persisted through multiple mass extinctions, and the silesaurids perished.

Apparent differences in survival despite minimal change across dentition, mandibular morphology and/or body size studied here highlights the need to investigate multiple aspects of ecomorphology, with such studies of modular evolution revealing more specific details of a clade's palaeoecology. The finding of greater size variation relative to mandibular variation in archosauriforms, and particularly in dinosaurs (Chapter 2) suggests that key differences in ecomorphology may be present in postcranial anatomy rather than the trophic anatomy assessed here. Indeed, my results suggest that postcranial, particularly locomotory anatomy is a key part of ecology that should not be overlooked. Species interactions such as predator-prey coevolution are dependent on taxa traversing terrain to get within range to interact, and thus locomotory ability represents an intersection between extrinsic and intrinsic selective pressures. Changes in locomotion may have profound impacts on a clade's macroevolution, by supporting clades within particular niches and environments, as with the development of strong forelimbs aiding in fossorial behaviour (Lungmus and Angielczyk, 2019), or rendering some ecologies untenable. The displacement of biarmosuchians by theriodont therapisds may stem from such lococmotory differences as their postcranial morphology closely resembles a sprawling sphenacodontid pelycosaurs, whereas theriodonts developed more slender limbs and more parasagittal gaits that are suggestive of greater agility and speed (Sues, 1986; Sigogneau-Russell, 1989; Kemp, 1978; 2005). The therapsid succession in the carnivore guild through the Middle-Late Permian may be related to a

drive for ‘all-terrain, all-weather’ (ATAW) hunting capability as indicated by increasing locomotory efficiency through therapsid evolution. Dinosaur locomotory agility has been implicated in their rise to faunal dominance through the faunal turnovers of the Late Triassic (Charig, 1984; Bakker, 1972; Bonaparte, 1982). Although such competitive replacement is unlikely (Benton, 1987; Brusatte et al., 2008), particularly in the herbivore guild (Chapter 3.2), when viewed in the wider environmental context, differences in locomotion may offer some insight into why dinosaurs emerged from the TJE with a rapid radiation whereas pseudosuchians were hit hard and showed more gradual recovery.

This study concludes that the actions of the ‘Court Jester’ and ‘Red Queen’ (Benton, 2009) are entwined, each impacting evolution in their own way that in combination, may mark the difference between survival and extinction, success or failure and the victor of the clash of clades. The findings of each chapter have repeatedly stressed the confluence of large-scale extrinsic events and intrinsic opportunity, or constraint are the determinants of great macroevolutionary change (Van Valen, 1984), but whilst these moments in time attract much attention, it is the intervals of stability that my findings suggest intrinsic controls on macroevolution are most apparent, and it is these moments that deserve greater scrutiny.

References

- Abraham, J. O., Hempson, G. P., and Staver, A. C. (2019). Drought-response strategies of savanna herbivores. *Ecology and Evolution.* 9, 7047-7056.
- Adam, P. J., & Berta, A. (2002). Evolution of prey capture strategies and diet in the Pinnipedimorpha (Mammalia, Carnivora). *Oryctos*, 4, 83-107.
- Adams, D.C. & Otárola-Castillo, E. (2013). geomorph: an R package for the collection and analysis of geometric morphometric shape data. *Methods in Ecology and Evolution.* 4, 393–399.
- Akaike, H. (1974). A new look at the statistical model identification. IEEE transactions on automatic control, 19(6), 716-7
- Akima, H. & Gebhardt, A. (2016). akima: Interpolation of Irregularly and Regularly Spaced Data. R package version 0.6-2
- Allen, B. J., Stubbs, T. L., Benton, M. J., & Puttick, M. N. (2019). Archosauromorph extinction selectivity during the Triassic–Jurassic mass extinction. *Palaeontology*, *62*(2), 211-224.
- Alroy, J. (2008). Dynamics of origination and extinction in the marine fossil record. *Proceedings of the National Academy of Sciences*, 105(Supplement 1), 11536-11542.
- Anderson, P. S., Friedman, M., Brazeau, M. D., & Rayfield, E. J. (2011). Initial radiation of jaws demonstrated stability despite faunal and environmental change. *Nature*, 476(7359), 206-209.
- Anderson, H. M. & Holmes, W. B. K. (2008). Stems with attached *Dicroidium* leaves from the Ipswich Coal Measures, Queensland, Australia. *Memoirs of the Queensland Museum.* 52, 1–12
- Anderson, P. S., & Westneat, M. W. (2006). Feeding mechanics and bite force modelling of the skull of Dunkleosteus terrelli, an ancient apex predator. *Biology Letters.* 3, 77-80.
- Aristide, L., & Morlon, H. (2019). Understanding the effect of competition during evolutionary radiations: an integrated model of phenotypic and species diversification. *Ecology Letters*, *22*(12), 2006-2017.
- Ashraf, A. R., Sun, Y., Sun, G., Uhl, D., Mosbrugger, V., Li, J., & Herrmann, M. (2010). Triassic and Jurassic palaeoclimate development in the Junggar Basin, Xinjiang, Northwest China—a review and additional lithological data. *Palaeobiodiversity and Palaeoenvironments*, *90*(3), 187-201.
- Axsmith, B. J., Taylor, E. L., Taylor, T. N., & Cuneo, N. R. (2000). New perspectives on the Mesozoic seed fern order Corystospermales based on attached organs from the Triassic of Antarctica. *American Journal of Botany*, *87*(6), 757-768.
- Bacon, K.L., Belcher, C.M., Haworth, M. and McElwain, J.C., (2013). Increased atmospheric SO_2 detected from changes in leaf physiognomy across the Triassic–Jurassic boundary interval of East Greenland. *PloS one*, *8*(4), p.e60614.

- Baghli, H., Mattioli, E., Spangenberg, J. E., Bensalah, M., Arnaud-Godet, F., Pittet, B., & Suan, G. (2020). Early Jurassic climatic trends in the south-Tethyan margin. *Gondwana Research*, *77*, 67-81.
- Bahram, R., Burke, J. E., & Lanzi, G. L. (2004). Head and neck injury from a leopard attack: case report and review of the literature. *Journal of oral and maxillofacial surgery*, *62*(2), 247-249.
- Bailey, T. R., Rosenthal, Y., McArthur, J. M., Van de Schootbrugge, B., & Thirlwall, M. F. (2003). Paleoceanographic changes of the Late Pliensbachian–Early Toarcian interval: a possible link to the genesis of an Oceanic Anoxic Event. *Earth and Planetary Science Letters*, *212*(3-4), 307-320.
- Bakker, R. T. (1972). Anatomical and ecological evidence of endothermy in dinosaurs. *Nature,* 238, 81–85
- Bakker, R. T. (1975). Experimental and fossil evidence for the evolution of tetrapod bioenergetics. In *Perspectives of biophysical ecology*. 365-399. Springer, Berlin, Heidelberg.
- Baranyi, V., Miller, C. S., Ruffell, A., Hounslow, M. W. & Kürschner, W. M. (2019). A continental record of the Carnian Pluvial Episode (CPE) from the Mercia Mudstone Group (UK): palynology and climatic implications. *Journal of the Geological Society.* 176(1), 149–166.
- Baron, M. G., Norman, D. B., & Barrett, P. M. (2017). A new hypothesis of dinosaur relationships and early dinosaur evolution. *Nature*, *543*(7646), 501-506.
- Barrett, P. M. (2014). Paleobiology of herbivorous dinosaurs. *Annual Review of Earth and Planetary Sciences*, *42*, 207-230.
- Barrett, P. M., Butler, R. J., & Nesbitt, S. J. (2010). The roles of herbivory and omnivory in early dinosaur evolution. Earth and Environmental Science Transactions of the Royal Society of Edinburgh, 101(3-4), 383-396.
- Barrett, P.M. and Upchurch, P. (2007). The evolution of feeding mechanisms in early sauropodomorph dinosaurs. Special Papers in Palaeontology *77*, 91–112.
- Barrett, P. M., Evans, D. C. & Campione, N. E. (2015). Evolution of dinosaur epidermal structures. Biology Letters. 11, 20150229
- Bell, M. A., & Lloyd, G. T. (2014). strap: Stratigraphic Tree Analysis for Palaeontology. R package version 1.4. https://CRAN.R-project.org/package=strap
- Bendel, E. M., Kammerer, C. F., Kardjilov, N., Fernandez, V., & Fröbisch, J. (2018). Cranial anatomy of the gorgonopsian Cynariops robustus based on CT-reconstruction. *PloS one*, 13(11), e0207367.
- Benevento, G. L. , Benson R. B. J., and Friedman M. (2019). Patterns of mammalian jaw ecomorphological disparity during the Mesozoic/Cenozoic transition. *Proceedings of the Royal Society B: Biological Sciences*. 286, 1902.

- Bennett, A. F., and J. A. Ruben. (1986). The metabolic and thermoregulatory status of therapsids. 207–218 in N. Hotton, P. D. Maclean, J. J. Roth, and E. C. Roth (eds.), The Ecology and Biology of Mammal-Like Reptiles. Smithsonian Institution Press, Washington, D.C.
- Benson R. B. J., (2012). Interrelationships of basal synapsids: cranial and postcranial morphological partitions suggest different topologies. Journal of Systematic Palaeontology, 10: 601–624.
- Benson, R. B. J. and Butler, R. J. (2011). Uncovering the diversification history of marine tetrapods: ecology influences the effect of geological sampling biases. *Geological Society, London, Special Publications*, 358, 191–208.
- Benson, R. B. J., Butler, R. J., Lindgren, J. and Smith, A. S. (2010). Mesozoic marine tetrapod diversity: mass extinctions and temporal heterogeneity in geological megabiases affecting vertebrates. *Proceedings of the Royal Society of London B*, 277, 829–834.
- Benson, R. B., Campione, N. E., Carrano, M. T., Mannion, P. D., Sullivan, C., Upchurch, P., & Evans, D. C. (2014). Rates of dinosaur body mass evolution indicate 170 million years of sustained ecological innovation on the avian stem lineage. *PLoS Biol*, *12*(5), e1001853.
- Benson, R. B., Hunt, G., Carrano, M. T., & Campione, N. (2018). Cope's rule and the adaptive landscape of dinosaur body size evolution. *Palaeontology*, *61*(1), 13-48.
- Benson R. B. J., Upchurch P. (2013). Diversity trends in the establishment of terrestrial vertebrate ecosystems: interactions between spatial and temporal sampling biases. Geology 41, 43–46.
- Benton, M. J. (1983). Dinosaur success in the Triassic: a noncompetitive ecological model. *The Quarterly Review of Biology*, 58(1), 29-55.
- Benton, M. J. (1984). Tooth form, growth, and function in Triassic rhynchosaurs (Reptilia, Diapsida). *Palaeontology*, 27, 4, 737–776.
- Benton, M. J. (1987). Progress and competition in macroevolution. *Biology Reviews,* 62, 305–338.
- Benton, M. J. (2009). The Red Queen and the Court Jester: species diversity and the role of biotic and abiotic factors through time. *Science,* 323, 728–732.
- Benton, M. J. (2014). Vertebrate palaeontology. John Wiley & Sons.
- Benton, M. J. (2016). The Triassic. *Current Biology*. 26, 1214–1218.
- Benton, M. J. (2020). The origin of endothermy in synapsids and archosaurs and arms races in the Triassic. *Gondwana Research*.
- Benton, M. J., & Newell, A. J. (2014). Impacts of global warming on Permo-Triassic terrestrial ecosystems. *Gondwana Research*, *25*(4), 1308-1337.
- Benton, M. J., Bernardi, M. & Kinsella, C. (2018). The Carnian Pluvial Episode and the origin of dinosaurs. *Journal of the Geological Society.* 175, 1019–1026.

- Benton, M.J., Forth, J. & Langer, M. C. (2014). Models for the rise of the dinosaurs. *Current Biology*. 24, 87–95.
- Benton, M. J., Ruta, M., Dunhill, A. M., & Sakamoto, M. (2013a). The first half of tetrapod evolution, sampling proxies, and fossil record quality. *Palaeogeography, Palaeoclimatology, Palaeoecology*, *372*, 18-41.
- Benton, M. J., Tverdokhlebov, V. P., and Surkov, M. V. (2004). Ecosystem remodelling among vertebrates at the Permian–Triassic boundary in Russia. *Nature*, *432*(7013), 97-100.
- Benton, M. J., Wills, M. A., & Hitchin, R. (2000). Quality of the fossil record through time. *Nature*, 403(6769), 534-537.
- Benton, M.J., Zhang, Q., Hu, S., Chen, Z.Q., Wen, W., Liu, J., Huang, J., Zhou, C., Xie, T., Tong, J. and Choo, B., (2013b). Exceptional vertebrate biotas from the Triassic of China, and the expansion of marine ecosystems after the Permo-Triassic mass extinction. *Earth-Science Reviews*, *125*, 199-243.
- Berger, K. & Gese, E. (2007). Does interference competition with wolves limit the distribution and abundance of coyotes? *Journal of Animal Ecology,* 76, 1075–1085.
- Bernardes-de-Oliveira, M.E.C., Kavali, P.S., Mune, S.E., Shivanna, M., de Souza, P.A., Iannuzzi, R., Jasper, A., Hoelzel, A., Boardman, D.R., Rohn, R. and Ricardi-Branco, F. (2016). Pennsylvanian–early cisuralian interglacial macrofloristic succession in Paraná Basin of the state of São Paulo. *Journal of South American Earth Sciences*, *72*, 351-374.
- Bernardi, M., Gianolla, P., Petti, F. M., Mietto, P., & Benton, M. J. (2018). Dinosaur diversification linked with the Carnian Pluvial Episode. *Nature Communications*, *9*(1), 1-10.
- Bjorndal, K. A., & Bolten, A. B. (1993). Digestive efficiencies in herbivorous and omnivorous freshwater turtles on plant diets: do herbivores have a nutritional advantage?. *Physiological Zoology*, *66*(3), 384-395.
- Blob R. W. (1998). *Mechanics of non-parasagittal locomotion in* alligator and iguana: *func- tional implications for the evolution of non- sprawling posture in the Therapsida*. PhD thesis, Univ. Chicago. 324.
- Blob, R. W. (2001). Evolution of hindlimb posture in nonmammalian therapsids: biomechanical tests of paleontological hypotheses. Paleobiology, 27(1), 14-38.
- Bonaparte, J. F. (1982). Faunal replacement in the Triassic of South America. *Journal of Vertebrate Paleontology*, *2*(3), 362-371.
- Bonaparte, J. F. (1984). Locomotion in rauisuchid thecodonts. *Journal of Vertebrate Paleontology*, *3*(4), 210-218.

- Bond, D. P., Hilton, J., Wignall, P. B., Ali, J. R., Stevens, L. G., Sun, Y., & Lai, X. (2010). The Middle Permian (Capitanian) mass extinction on land and in the oceans. *Earth-Science Reviews*, *102*(1-2), 100-116.
- Bonner, J. T. (2011). *Why size matters: from bacteria to blue whales*. Princeton University Press.
- Bookstein, F. L. (1997). *Morphometric tools for landmark data: geometry and biology*. Cambridge University Press.
- Botha, J., Lee-Thorp, J., & Chinsamy, A. (2005). The palaeoecology of the non-mammalian cynodonts Diademodon and Cynognathus from the Karoo Basin of South Africa, using stable light isotope analysis. *Palaeogeography, Palaeoclimatology, Palaeoecology*, *223*(3-4), 303-316.
- Botha, J., & Huttenlocker, A. (2021). Nonmammalian Synapsids. In *Vertebrate Skeletal Histology and Paleohistology* (pp. 550-563). Boca Raton and London: CRC Press.
- Brocklehurst, N. (2019). Morphological evolution in therocephalians breaks the hypercarnivore ratchet. Proceedings of the Royal Society B, 286(1900), 20190590.
- Brocklehurst, N., & Brink, K. S. (2017). Selection towards larger body size in both herbivorous and carnivorous synapsids during the Carboniferous. *Facets*, 2(1), 68-84.
- Brocklehurst, N., Day, M. O., Rubidge, B. S., and Fröbisch J. (2017). Olson's Extinction and the latitudinal biodiversity gradient of tetrapods in the Permian. Proc. R. Soc. B.28420170231
- Brocklehurst, N., Kammerer, C. F., Fröbisch, J. (2013). The early evolution of synapsids and the influence of sampling on their fossil record. *Paleobiology* 39, 470–490.
- Brocklehurst, N., Kammerer, C. F., & Benson, R. J. (2020). The origin of tetrapod herbivory: effects on local plant diversity. Proceedings of the Royal Society B, 287(1928), 20200124.
- Brocklehurst N, Ruta M, Müller J, Fröbisch J. (2015). Elevated extinction rates as a trigger for diversification rate shifts: early amniotes as a case study. Sci. Rep. 5, 17104.
- Bronzati, M., Rauhut, O. W., Bittencourt, J. S., & Langer, M. C. (2017). Endocast of the Late Triassic (Carnian) dinosaur Saturnalia tupiniquim: implications for the evolution of brain tissue in Sauropodomorpha. *Scientific reports*, *7*(1), 1-7.
- Brown, W. L., and Wilson, E. O. (1956). Character displacement. *Systematic zoology*, *5*(2), 49-64.
- Brusatte, S. L., Benton, M. J., Ruta, M. & Lloyd, G. T. (2008). The first 50 Myr of dinosaur evolution: macroevolutionary pattern and morphological disparity. *Biology Letters.* 4, 733–736.
- Brusatte, S. L., Nesbitt, S. J., Irmis, R. B., Butler, R. J., Benton, M. J., & Norell, M. A. (2010). The origin and early radiation of dinosaurs. *Earth-Science Reviews*, *101*(1-2), 68-100.
- Butler, R. J., Brusatte, S. L., Andres, B., & Benson, R. B. (2012). How do geological sampling biases affect studies of morphological evolution in deep time? A case study of pterosaur (Reptilia: Archosauria) disparity. Evolution: International Journal of Organic Evolution, 66(1), 147-162.

- Burgess, S. D., Muirhead, J. D., & Bowring, S. A. (2017). Initial pulse of Siberian Traps sills as the trigger of the end-Permian mass extinction. *Nature Communications*, *8*(1), 1-6.
- Burnham, K. P. and Anderson, D. R. (2010). Model Selection and Multimodel Inference (2nd ed.), Springer, New York
- Button, D. J., Barrett, P. M., & Rayfield, E. J. (2017). Craniodental functional evolution in sauropodomorph dinosaurs. *Paleobiology*, *43*(3), 435-462.
- Button, D.J., Rayfield, E.J. and Barrett, P.M., (2014). Cranial biomechanics underpins high sauropod diversity in resource-poor environments. *Proceedings of the Royal Society B: Biological Sciences*, *281*(1795), 20142114.
- Button, D. J. & Zanno, L. E. (2020). Repeated evolution of divergent modes of herbivory in non–avian dinosaurs. *Current Biology.* 30, 158–168.
- Cabon, Q., Deroy, C., Ferrand, F.X., Pillard, P., Cachon, T., Fau, D., Goy-Thollot, I., Viguier, E. and Carozzo, C., (2015). Thoracic bite trauma in dogs and cats: a retrospective study of 65 cases. Veterinary and Comparative Orthopaedics and Traumatology, 28(06), 448-454.
- Cabreira, S.F., Kellner, A.W.A., Dias-da-Silva, S., da Silva, L.R., Bronzati, M., de Almeida Marsola, J.C., Müller, R.T., de Souza Bittencourt, J., Batista, B.J.A., Raugust, T. and Carrilho, R., (2016). A unique Late Triassic dinosauromorph assemblage reveals dinosaur ancestral anatomy and diet. *Current Biology*, *26*(22), 3090-3095.
- Campione, N. E., & Evans, D. C. (2012). A universal scaling relationship between body mass and proximal limb bone dimensions in quadrupedal terrestrial tetrapods. *BMC biology*, *10*(1), 1-22.
- Campione, N. E., & Evans, D. C. (2020). The accuracy and precision of body mass estimation in non-avian dinosaurs. *Biological Reviews*, *95*(6), 1759-1797.
- Carbone, C., Pettorelli, N., & Stephens, P. A. (2011). The bigger they come, the harder they fall: body size and prey abundance influence predator–prey ratios. *Biology letters,* 7(2), 312-315.
- Caro T. M. and Stoner C. J., (2003). The potential for interspecific competition among African carnivores. Biological Conservation. 110:67–75.
- Caruthers, A. H., Smith, P. L., & Gröcke, D. R. (2013). The Pliensbachian–Toarcian (Early Jurassic) extinction, a global multi-phased event. *Palaeogeography, Palaeoclimatology, Palaeoecology*, *386*, 104-118.
- Cascales–Miñana, B. & Cleal, C. J. (2012). Plant fossil record and survival analyses. *Lethaia* 45, 71–82.
- Cascales-Miñana, B., Muñoz-Bertomeu, J., Ros, R., & Segura, J. (2010). Trends and patterns in the evolution of vascular plants: Macroevolutionary implications of a multilevel taxonomic analysis. *Lethaia*, *43*(4), 545-557.

- Caumul, R. & Polly, P. D. (2005). Phylogenetic and environmental components of morphological variation: skull, mandible, and molar shape in marmots (Marmota, Rodentia). *Evolution* 59, 2460–2472.
- Chandler, M. A., Rind, D., & Ruedy, R. (1992). Pangaean climate during the Early Jurassic: GCM simulations and the sedimentary record of paleoclimate. *Geological Society of America Bulletin*, *104*(5), 543-559.
- Chapelle, K. E., Benson, R. B., Stiegler, J., Otero, A., Zhao, Q., & Choiniere, J. N. (2020). A quantitative method for inferring locomotory shifts in amniotes during ontogeny, its application to dinosaurs and its bearing on the evolution of posture. *Palaeontology*, *63*(2), 229-242.
- Charig, A. J. (1984) Competition between therapsids and archosaurs during the Triassic period: a review and synthesis of current theories. *Symposia of the Zoological Society of London.* 52, 597–628.
- Chen, Z. Q. & Benton, M. J. (2012). The timing and pattern of biotic recovery following the end–Permian mass extinction. *Nature Geoscience.* 5, 375.
- Chen, J., & Xu, Y. G. (2020). Permian Large Igneous Provinces and Their Paleoenvironmental Effects. *Large Igneous Provinces: A Driver of Global Environmental and Biotic Changes*, 417-434.
- Ciampaglio, C. N., Kemp, M., & McShea, D. W. (2001). Detecting changes in morphospace occupation patterns in the fossil record: characterization and analysis of measures of disparity. *Paleobiology*, 27, 695-715.
- Cisneros, J. C., Abdala, F., Atayman-Güven, S., Rubidge, B. S., Şengör, A. C., & Schultz, C. L. (2012). Carnivorous dinocephalian from the Middle Permian of Brazil and tetrapod dispersal in Pangaea. Proceedings of the National Academy of Sciences, 109(5), 1584-1588.
- Clapham, M. E., Shen, S., & Bottjer, D. J. (2009). The double mass extinction revisited: reassessing the severity, selectivity, and causes of the end-Guadalupian biotic crisis (Late Permian). Paleobiology, 35(1), 32-50.
- Clauss, M., Steuer, P., Müller, D. W., Codron, D., & Hummel, J. (2013). Herbivory and body size: allometries of diet quality and gastrointestinal physiology, and implications for herbivore ecology and dinosaur gigantism. *PLoS One*, *8*(10), e68714.
- Clavel, J., Escarguel, G., and Merceron, G. (2015) mvMORPH: an R package for fitting multivariate evolutionary models to morphometric data. Methods in Ecology and Evolution, 6(11):1311-1319.
- Cleal, C. J., & Thomas, B. A. (2005). Palaeozoic tropical rainforests and their effect on global climates: is the past the key to the present?. *Geobiology*, *3*(1), 13-31.
- Cleuren, J., & de Vree, F. (1992). Kinematics of the jaw and hyolingual apparatus during feeding in Caiman crocodilus. *Journal of morphology*, *212*(2), 141-154.

- Close, R. A., Friedman, M., Lloyd, G. T., & Benson, R. B. (2015). Evidence for a mid-Jurassic adaptive radiation in mammals. *Current Biology*, *25*(16), 2137-2142.
- Coates, M.I., Ruta, M., and Friedman, M. (2008). Ever since Owen: Changing perspectives on the early evolution of tetrapods. *Annual Review of Ecology Evolution and Systematics*, 39, 571–592.
- Cohen, K. M., Finney, S. C., Gibbard, P. L. & Fan, J. X. (2013). The ICS international chronostratigraphic chart. *Episodes* 36, 199–204.
- Cohen, K. M., Harper, D. A. T., Gibbard, P. L. & Fan, J. X. (2019). ICS International Chronostratigraphic Chart 2019/05. International Commission on Stratigraphy, IUGS, www.stratigraphy.org
- Condamine, F. L., Rolland, J., Höhna, S., Sperling, F. A., and Sanmartín, I. (2018). Testing the role of the Red Queen and Court Jester as drivers of the macroevolution of Apollo butterflies. *Systematic Biology*, *67*(6), 940-964.
- Condamine, F. L., Silvestro, D., Koppelhus, E. B., and Antonelli, A. (2020). The rise of angiosperms pushed conifers to decline during global cooling. *Proceedings of the National Academy of Sciences*, *117*(46), 28867-28875.
- Cooney, C.R., Bright, J.A., Capp, E.J., Chira, A.M., Hughes, E.C., Moody, C.J., Nouri, L.O., Varley, Z.K. and Thomas, G.H., (2017). Mega-evolutionary dynamics of the adaptive radiation of birds. *Nature*, *542*(7641), 344-347.
- Cowell K, and Penwick C. (1989). Dog bite wounds: A study of 93 cases. *Compendium on continuing education for the practicing veterinarian*. 11:313–320.
- Cox, C. B. (1998). The jaw function and adaptive radiation of the dicynodont mammal-like reptiles of the Karoo basin of South Africa. *Zoological Journal of the Linnean Society*, *122*(1-2), 349-384.
- Cox, G. W., & Ricklefs, R. E. (1977). Species diversity and ecological release in Caribbean land bird faunas. *Oikos*, 113-122.
- Craine, J. M., & Dybzinski, R. (2013). Mechanisms of plant competition for nutrients, water and light. *Functional Ecology*, *27*(4), 833-840.
- Crompton, A. W. (1963). The evolution of the mammalian jaw. *Evolution*, 431-439.
- Crompton, A. W., & Attridge, J. (1986). Masticatory apparatus of the larger herbivores during Late Triassic and Early Jurassic times. *The Beginning of the Age of the Dinosaurs*, 223-236.
- Crompton, A. W., & Parker, P. (1978). Evolution of the mammalian masticatory apparatus: the fossil record shows how mammals evolved both complex chewing mechanisms and an effective middle ear, two structures that distinguish them from reptiles. *American Scientist*, *66*(2), 192-201.

- Crowell, J. (1999). Pre-Mesozoic ice ages: Their bearing on understanding the climate system. *Geological Society of America Memoir*, *192*, 1-106.
- da Silva, R. C., Barboni, R., Dutra, T., Godoy, M. M., & Binotto, R. B. (2012). Footprints of large theropod dinosaurs and implications on the age of Triassic biotas from Southern Brazil. *Journal of South American Earth Sciences*, *39*, 16-23.
- Daegling, D. J. Biomechanical scaling of the hominoid mandibular symphysis. *J. Morphol.*, **25**, 12-23 (2001).
- Dal Corso, J., Bernardi, M., Sun, Y., Song, H., Seyfullah, L.J., Preto, N., Gianolla, P., Ruffell, A., Kustatscher, E., Roghi, G. and Merico, A., (2020). Extinction and dawn of the modern world in the Carnian (Late Triassic). *Science Advances*, *6*(38), p.eaba0099.
- D'Amore, D. C. (2015). Illustrating ontogenetic change in the dentition of the N ile monitor lizard, V aranus niloticus: a case study in the application of geometric morphometric methods for the quantification of shape–size heterodonty. *Journal of Anatomy*, *226*(5), 403-419.
- Damuth, J. D., DiMichele, W. A., & Potts, R. (1992). Terrestrial ecosystems through time: evolutionary paleoecology of terrestrial plants and animals.
- Darwin, C. (1859). On the Origin of Species by Means of Natural Selection, or Preservation of Favoured Races in the Struggle for Life. London :John Murray.
- Davidson, E. B. (1998). Managing bite wounds in dogs and cats. II. *Compendium on continuing education for the practicing veterinarian*.
- Day, M. O., Ramezani, J., Bowring, S. A., Sadler, P. M., Erwin, D. H., Abdala, F., & Rubidge, B. S. (2015). When and how did the terrestrial mid-Permian mass extinction occur? Evidence from the tetrapod record of the Karoo Basin, South Africa. *Proceedings of the Royal Society B: Biological Sciences*, *282*(1811), 20150834.
- De Cuyper, A., Clauss, M., Carbone, C., Codron, D., Cools, A., Hesta, M., & Janssens, G. P. (2019). Predator size and prey size–gut capacity ratios determine kill frequency and carcass production in terrestrial carnivorous mammals. *Oikos*, 128(1), 13-22.
- Demar, R., & Bolt, J. R. (1981). Dentitional organization and function in a Triassic reptile. Journal of Paleontology, 967-984.
- Desojo, J. B., & Vizcaíno, S. F. (2009). Jaw biomechanics in the South American aetosaur Neoaetosauroides engaeus. *Paläontologische Zeitschrift*, *83*(4), 499.
- Desojo, J. B., Heckert, A. B., Martz, J. W., Parker, W. G., Schoch, R. R., Small, B. J., & Sulej, T. (2013). Aetosauria: a clade of armoured pseudosuchians from the Upper Triassic continental beds. *Geological Society, London, Special Publications*, *379*(1), 203-239.

- Dilcher, David L., Lott T. A., Wang, X. & Wang, Q.. (2004). A history of tree canopies. *Forest canopies* (eds Lowman, M. D., and Rinker, H. B.), 118–137. Elsevier, Amsterdam.
- DiMichele, W. A., Montanez, I. P., Poulsen, C. J., and Tabor, N., (2009), Climate and vegetational regime shifts in the late Paleozoic ice age earth: *Geobiology* 7, 200–226.
- Dróżdż, D. (2018). Osteology of a forelimb of an aetosaur Stagonolepis olenkae (Archosauria: Pseudosuchia: Aetosauria) from the Krasiejów locality in Poland and its probable adaptations for a scratch-digging behavior. *PeerJ*, *6*, e5595.
- Dubiel, R. F., Hasiotis, S. T., Davidson, S. K., Leleu, S., & North, C. P. (2011). Deposystems, paleosols, and climatic variability in a continental system: the Upper Triassic Chinle Formation, Colorado Plateau, USA. *From River to Rock Record: The Preservation of Fluvial Sediments and their Subsequent Interpretation: SEPM (Society for Sedimentary Geology) Special Publication*, *97*, 393-421.
- Dunhill, A. M., Hannisdal, B. and Benton, M. J. (2014). Disentangling rock record bias and common-cause from redundancy in the British fossil record. *Nature Communications*, 5, 4818.
- Dunhill, A. M. & Wills, M. A. (2015). Geographic range did not confer resilience to extinction in terrestrial vertebrates at the end-Triassic crisis. *Nature Communications*, 6, 7980
- Dunne, E. M., Close, R. A., Button, D. J., Brocklehurst, N., Cashmore, D. D., Lloyd, G. T., & Butler, R. J. (2018). Diversity change during the rise of tetrapods and the impact of the 'Carboniferous rainforest collapse'. *Proceedings of the Royal Society B: Biological Sciences*, *285*(1872), 20172730.
- Durant, S. M. (1998). Competition refuges and coexistence: an example from Serengeti carnivores. Journal of Animal Ecology 67: 370– 386.
- Durant, S. M. (2000). Living with the enemy: avoidance of hyenas and lions by cheetahs in the Serengeti. *Behavioral ecology*, *11*(6), 624-632.
- Dray S, Dufour A (2007). "The ade4 Package: Implementing the Duality Diagram for Ecologists." *Journal of Statistical Software*, *22*(4), 1-20. doi: 10.18637/jss.v022.i04
- Dzik, J., Sulej, T., & Niedźwiedzki, G. (2008). A dicynodont-theropod association in the latest Triassic of Poland. *Acta Palaeontologica Polonica*, *53*(4), 733-738.
- Eble, G. J. (2000) Contrasting evolutionary flexibility in sister groups: Disparity and diversity in Mesozoic atelostomate echinoids. Paleobiology 26(1):56–79.
- Ernst, R.E., Bond, D.P., Zhang, S.H., Buchan, K.L., Grasby, S.E., Youbi, N., El Bilali, H., Bekker, A. and Doucet, L.S., (2020). Large Igneous Province Record Through Time and Implications for Secular Environmental Changes and Geological Time-Scale Boundaries. *Large Igneous Provinces: A Driver of Global Environmental and Biotic Changes*, 1-26.

- Eronen, J.T., Polly, P.D., Fred, M., Damuth, J., Frank, D.C., Mosbrugger, V., Scheidegger, C., Stenseth, N.C. and Fortelius, M., (2010). Ecometrics: the traits that bind the past and present together. *Integrative Zoology*, *5*(2), 88-101.
- Erwin, D. H., Bowring, S. A., Yugan, J., & Koeberl, C. (2002). End-Permian mass extinctions: a review. Special Papers-Geological Society of America, 363-384.
- Evans A. R., Wilson G. P., Fortelius M, Jernvall J. (2007). High-level similarity of dentitions in carnivorans and rodents. *Nature* 445:78–81.
- Ezard, T.H.G., Quental, T.B. & Benton, M.J. (2016). The challenges to inferring the regulators of biodiversity in deep time. *Philosophical Transactions of the Royal Society of London B 371: 20150216.*
- Ezcurra, M. D. (2016). The phylogenetic relationships of basal archosauromorphs, with an emphasis on the systematics of proterosuchian archosauriforms. *PeerJ*, *4*, e1778.
- Ezcurra, M. D., & Butler, R. J. (2018). The rise of the ruling reptiles and ecosystem recovery from the Permo-Triassic mass extinction. *Proceedings of the Royal Society B: Biological Sciences*, *285*(1880), 20180361.
- Ezcurra, M. D., Jones, A.S., Gentil, A.R., Butler, R.J. (2020). Early Archosauromorphs: the Crocodile and Dinosaur Precursors (second ed.), Encyclopedia of Geology.
- Ezcurra, M. D., Montefeltro, F., & Butler, R. J. (2016). The early evolution of rhynchosaurs. *Frontiers in Ecology and Evolution*, *3*, 142.
- Falcon-Lang, H. J., & Dimichele, W. A. (2010). What happened to the coal forests during Pennsylvanian glacial phases?. *Palaios*, *25*(9), 611-617.
- Farlow, J. O. (1987). Speculations about the diet and digestive physiology of herbivorous dinosaurs. *Paleobiology*, *13*(1), 60-72.
- Faure-Brac, M. G., & Cubo, J. (2020). Were the synapsids primitively endotherms? A palaeohistological approach using phylogenetic eigenvector maps. *Philosophical Transactions of the Royal Society B*, *375*(1793), 20190138.
- Fedriani, J., Fuller, T., Sauvajot, R. & York, E. (2000). Competition and intraguild predation among three sympatric carnivores. Oecologia 125, 258–270.
- Fielding, C. R., Frank, T. D., & Isbell, J. L. (2008). The late Paleozoic ice age—A review of current understanding and synthesis of global climate patterns. In *Resolving the late Paleozoic ice age in time and space* (Vol. 441, pp. 343-354). Special Paper.
- Finke, D. L. & Snyder, W. E. Niche partitioning increases resource exploitation by diverse communities. *Science* 321, 1488–1490 (2008).

- Flynn, J. J., Nesbitt, S. J., Michael Parrish, J., Ranivoharimanana, L., & Wyss, A. R. (2010). A new species of Azendohsaurus (Diapsida: Archosauromorpha) from the Triassic Isalo Group of southwestern Madagascar: cranium and mandible. *Palaeontology*, *53*(3), 669-688.
- Foffa, D., Young, M. T., Stubbs, T. L., Dexter, K. G., & Brusatte, S. L. (2018). The long-term ecology and evolution of marine reptiles in a Jurassic seaway. *Nature Ecology & Evolution*, *2*(10), 1548-1555.
- Foote, M. (1994). Morphological disparity in Ordovician-Devonian crinoids and the early saturation of morphological space. *Paleobiology*, 320-344.
- Ford, D. P., & Benson, R. B. (2020). The phylogeny of early amniotes and the affinities of Parareptilia and Varanopidae. *Nature Ecology & Evolution*, *4*(1), 57-65.
- Freeman, B. G. (2015). Competitive interactions upon secondary contact drive elevational divergence in tropical birds. *The American Naturalist,* 186(4), 470-479.
- Friscia A., Van Valkenburgh B., (2010). Ecomorphology of North American Eocene carnivores: evidence for competition between carnivorans and creodonts. In: Goswami A, Friscia A (eds) Carnivoran Evolution: New Views on Phylogeny, Form, and Function. Cambridge University Press, Cambridge and New York. 311–341.
- Fritz, J., et al. Gizzard vs. teeth, it's a tie: food-processing efficiency in herbivorous birds and mammals and implications for dinosaur feeding strategies. *Paleobiology* 37, 577–586 (2011).
- Fröbisch, J. (2008). Global taxonomic diversity of anomodonts (Tetrapoda, Therapsida) and the terrestrial rock record across the Permian-Triassic boundary. *PLoS One,* 3, e3733
- Fröbisch, J. (2013). Vertebrate diversity across the end-Permian mass extinction—separating biological and geological signals. *Palaeogeography, Palaeoclimatology, Palaeoecology*, *372*, 50-61.
- Galton P.M. (1985). Diet of prosauropod dinosaurs from the Late Triassic and Early Jurassic. *Lethaia* 18, 105-123.
- Gaston, K. J. (1998). Species-range size distributions: products of speciation, extinction and transformation. *Philosophical Transactions of the Royal Society of London. Series B: Biological Sciences*, *353*(1366), 219-230.
- Gill, F. L., Hummel, J., Sharifi, A. R., Lee, A. P., & Lomax, B. H. (2018). Diets of giants: the nutritional value of sauropod diet during the Mesozoic. *Palaeontology*, *61*(5), 647-658.
- Goswami, Anjali, and Anthony Friscia, eds. (2010). *Carnivoran evolution: new views on phylogeny, form and function*. Vol. 1. Cambridge University Press.
- Gould, S. J. (1967). Evolutionary patterns in pelycosaurian reptiles: a factor-analytic study. *Evolution*, 385-401.

- Gow. C.E. (1978). The advent of herbivory in certain reptilian lineages during the Triassic. Palaeontologica Africana. 21, 133–141.
- Graffelman, J. (2013). calibrate: Calibration of Scatterplot and Biplot Axes. R package version 1.7.2., https://CRAN.R–project.org/package=calibrate
- Grant, P. R., and Grant R. B. (2011). How and Why Species Multiply: The Radiation of Darwin's Finches. Princeton, NJ: Princeton Univ. Press
- Grimaldi, D., and Engel, M.S., (2005), Evolution of the insects: New York, Cambridge University Press. 772.
- Grossnickle, D. M., and Newham, E. (2016). Therian mammals experience an ecomorphological radiation during the Late Cretaceous and selective extinction at the K–Pg boundary. *Proceedings of the Royal Society B: Biological Sciences*, *283*(1832), 20160256.
- Guillerme T. (2018) dispRity: A modular R package for measuring disparity. *Methods in Ecology and Evolution*, 00:1-9.
- Guillerme, T. and Cooper, N. (2018), Time for a rethink: time sub-sampling methods in disparity-through-time analyses. *Palaeontology*, 61: 481-493.
- Guillerme, T., Puttick, M. N., Marcy, A. E., & Weisbecker, V. (2020). Shifting spaces: Which disparity or dissimilarity measurement best summarize occupancy in multidimensional spaces?. *Ecology and evolution*, *10*(14), 7261-7275.
- Hallam, A. (1994). Jurassic climates as inferred from the sedimentary and fossil record. In *Palaeoclimates and their Modelling* (pp. 79-88). Springer, Dordrecht.
- Halliday T. J. D., Goswami A., (2015). Eutherian morphological disparity across the end-Cretaceous mass extinction. Biol. J. Linn. Soc. Lond. 118, 152– 168.
- Hammer, Ø., D. Harper, A. T. & Ryan, P. D., (2001). Paleontological statistics software package for education and data analysis. *Palaeontologia Electronica* 4, 9.
- Hardin, G. (1960). The competitive exclusion principle. *Science* 131, 1292–1297.
- Harmon, L. J., J. B. Losos, T. Jonathan Davies, R. G. Gillespie, J. L. Gittleman, W. Bryan Jennings, K. H. Kozak, M. A. McPeek, F. Moreno-Roark, T. J. Near, et al. (2010). Early bursts of body size and shape evolution are rare in comparative data. *Evolution,* 64:2385–2396.
- Hautmann, M. (2020). What is macroevolution?. *Palaeontology* 63(1), 1-11.
- Hayward, M. W., and Kerley, G. I. (2008). Prey preferences and dietary overlap amongst Africa's large predators. *African Journal of Wildlife Research*, *38*(2), 93-108.
- He, B., Xu, Y. G., Huang, X. L., Luo, Z. Y., Shi, Y. R., Yang, Q. J., & Yu, S. Y. (2007). Age and duration of the Emeishan flood volcanism, SW China: geochemistry and SHRIMP zircon U–Pb dating of

silicic ignimbrites, post-volcanic Xuanwei Formation and clay tuff at the Chaotian section. *Earth and Planetary Science Letters*, *255*(3-4), 306-323.

- Hedman, M. M. (2010). Constraints on clade ages from fossil outgroups. *Paleobiology*, *36*(1), 16-31.
- Hendrickx, C., Mateus, O., & Araújo, R. (2015). A proposed terminology of theropod teeth (Dinosauria, Saurischia). *Journal of Vertebrate Paleontology*, *35*(5), e982797.
- Hennig, C. (2019). fpc: Flexible Procedures for Clustering. R package version 2.2.3. https://CRAN.R-project.org/package=fpc
- Hesselbo, S. P., Robinson, S. A., Surlyk, F., & Piasecki, S. (2002). Terrestrial and marine extinction at the Triassic-Jurassic boundary synchronized with major carbon-cycle perturbation: A link to initiation of massive volcanism?. *Geology*, *30*(3), 251-254.
- Hoffman, D. K., Edwards, H. R., Barrett, P. M. & Nesbitt, S. J. (2019). Reconstructing the archosaur radiation using a Middle Triassic archosauriform tooth assemblage from Tanzania. *PeerJ* 7, e7970.
- Hopson, J. A., (1964). Tooth replacement in cynodont, dicynodont and therocephalian reptiles. *Proceedings of the Zoological Society of London*. 142, 4. 625–54.
- Hopson, J. A. (2012). The role of foraging mode in the origin of therapsids: implications for the origin of mammalian endothermy. *Fieldiana Life and Earth Sciences*, *2012*(5), 126-148.
- Hotton, N. III., Olson, E. C., Beerbower, R., Sumida, S. S., & Martin, K. L. M. (1997). Amniote origins and the discovery of herbivory. *Amniote origins*, 207-264.
- Hull, P. (2015). Life in the aftermath of mass extinctions. *Current Biology*, *25*(19), R941-R952.
- Hummel, J., Gee, C. T., Südekum, K. H., Sander, P. M., Nogge, G., & Clauss, M. (2008). In vitro digestibility of fern and gymnosperm foliage: implications for sauropod feeding ecology and diet selection. *Proceedings of the Royal Society B: Biological Sciences*, *275*(1638), 1015-1021.
- Hutchinson, G. E. (1959). Homage to Santa Rosalia or why are there so many kinds of animals? *The American Naturalist.* 93, 145–159.
- Huttenlocker, A. K. (2014). Body size reductions in nonmammalian eutheriodont therapsids (Synapsida) during the end-Permian mass extinction. *PLoS One,* 9(2), e87553.
- Irmis, R. B., & Whiteside, J. H. (2012). Delayed recovery of non-marine tetrapods after the end-Permian mass extinction tracks global carbon cycle. *Proceedings of the Royal Society B: Biological Sciences*, *279*(1732), 1310-1318.
- Ivakhnenko, M. F. (2008). Cranial morphology and evolution of Permian Dinomorpha (Eotherapsida) of eastern Europe. *Paleontological Journal,* 42(9), 859-995.
- Jablonski, D. (2003). The interplay of physical and biotic factors in macroevolution. *Evolution on planet Earth*, 235-252.

- Jablonski, D. (2008). Biotic interactions and macroevolution extensions and mismatches across scales and levels. *Evolution*, 62, 715–739.
- Jablonski, D. and Sepkoski Jr, J.J., 1996. Paleobiology, community ecology, and scales of ecological pattern. *Ecology*, *77*(5).1367-1378.
- Janis, C. (1995). Correlations between craniodental morphology and feeding behavior in ungulates: reciprocal illumination between living and fossil taxa. *Functional Morphology in Vertebrate Paleontology* (Eds Thomason J. J.), 76-98 Cambridge University Press, Cambridge.
- Janis, C. M., & Carrano, M. (1992). Scaling of reproductive turnover in archosaurs and mammals: why are large terrestrial mammals so rare?. In *Annales zoologici fennici*. 28. 201.
- Janis, C. M., & Keller, J. C. (2001). Modes of ventilation in early tetrapods: Costal aspiration as a key feature of amniotes. *Acta Palaeontologica Polonica*, *46*(2).
- Jansson, I. M., Mcloughlin, S., Vajda, V., & Pole, M. (2008). An Early Jurassic flora from the Clarence-Moreton Basin, Australia. *Review of Palaeobotany and Palynology*, *150*(1-4), 5-21.
- Joachimski, M.M., Lai, X., Shen, S., Jiang, H., Luo, G., Chen, B., Chen, J. and Sun, Y., (2012). Climate warming in the latest Permian and the Permian–Triassic mass extinction. *Geology*, *40*(3), pp.195-198.
- Jones, K.E., Angielczyk, K.D., Polly, P.D., Head, J.J., Fernandez, V., Lungmus, J.K., Tulga, S. and Pierce, S.E., (2018). Fossils reveal the complex evolutionary history of the mammalian regionalized spine. *Science*, *361*(6408), 1249-1252.
- Jones, M. E., O'higgins, P., Fagan, M. J., Evans, S. E., & Curtis, N. (2012). Shearing mechanics and the influence of a flexible symphysis during oral food processing in Sphenodon (Lepidosauria: Rhynchocephalia). *The Anatomical Record.* 295, 1075-1091
- Kammerer, C. F. (2009). *Cranial disparity in the non-mammalian Synapsida*. The University of Chicago.
- Kammerer, C. F. (2011). Systematics of the anteosauria (Therapsida: Dinocephalia). *Journal of Systematic Palaeontology,* 9(2), 261-304.
- Kammerer, C. F. (2014). Theriodontia: introduction. In *Early Evolutionary History of the Synapsida*. 165-169. Springer, Dordrecht.
- Kammerer, C. F. (2016). Systematics of the Rubidgeinae (Therapsida: Gorgonopsia). *PeerJ*, 4, e1608.
- Kammerer, C. F., & Masyutin, V. (2018). Gorgonopsian therapsids (Nochnitsa gen. nov. and Viatkogorgon) from the Permian Kotelnich locality of Russia. *PeerJ*, 6, e4954.
- Karagic, N., Meyer, A., & Hulsey, C. D. (2020). Phenotypic plasticity in vertebrate dentitions. *Integrative and Comparative Biology*, *60*(3), 608-618.

- Karatzoglou, A., Smola, A., Hornik, K., & Zeileis, A. (2004). kernlab-an S4 package for kernel methods in R. *Journal of statistical software*, *11*(9), 1-20.
- Kassambara A. & Mundt F. (2017). factoextra: Extract and Visualize the Results of Multivariate Data Analyses. R package version 105. https://CRAN.R-project.org/package=factoextra
- Kaufman, L. & Rousseeuw, P. J. (2009). *Finding groups in data: an introduction to cluster analysis.* 344, John Wiley & Sons, Hoboken.
- Kemp, T. S. (1969). On the functional morphology of the gorgonopsid skull. *Philosophical Transactions of the Royal Society of London. B, Biological Sciences*, 256(801), 1-83.
- Kemp, T. S. (1978). Stance and gait in the hindlimb of a therocephalian mammal-like reptile. Journal of Zoology, 186(2), 143-161.
- Kemp, T. S., & Kemp, D. F. (1982). *Mammal-like reptiles and the origin of mammals*. Academic Press.
- Kemp, T. S. (2005). *The origin and evolution of mammals*. Oxford University Press on Demand.
- Kemp, T. S. (2006a). The origin and early radiation of the therapsid mammal-like reptiles: a palaeobiological hypothesis. Journal of evolutionary biology, 19(4), 1231-1247.
- Kemp, T. S. (2006b). The origin of mammalian endothermy: a paradigm for the evolution of complex biological structure. *Zoological Journal of the Linnean Society*, *147*(4), 473-488.
- Keyser, A. W. (1974). Evolutionary trends in Triassic Dicynodontia. *Palaeontologia africana.* 17, 57–68.
- Kidwell, S. M., & Holland, S. M. (2002). The quality of the fossil record: implications for evolutionary analyses. Annual Review of Ecology and Systematics, 33(1), 561-588.
- Kilbourne, B. M., & Hutchinson, J. R. (2019). Morphological diversification of biomechanical traits: mustelid locomotor specializations and the macroevolution of long bone cross-sectional morphology. *BMC evolutionary biology*, *19*(1), 1-16.
- King G. (1988). Encyclopedia of paleoherpetology. Stuttgart: Gustav Fischer Verlag.
- King, G. M., Oelofsen, B. W., & Rubidge, B. S. (1989). The evolution of the dicynodont feeding system. *Zoological Journal of the Linnean Society*, *96*(2), 185-211.
- Kleiman, D. G., & Eisenberg, J. F. (1973). Comparisons of canid and felid social systems from an evolutionary perspective. *Animal behaviour,* 21(4), 637-659.
- Kravchinsky, V. A. (2012). Paleozoic large igneous provinces of Northern Eurasia: Correlation with mass extinction events. *Global and Planetary Change*, *86*, 31-36.
- Krings, M., Kerp, H., Taylor, T. N., & Taylor, E. L. (2003). How Paleozoic vines and lianas got off the ground: on scrambling and climbing Carboniferous-Early Permian pteridosperms. *The Botanical Review*, *69*(2), 204-224.

- Krupandan, E., Chinsamy-Turan, A., & Pol, D. (2018). The long bone histology of the sauropodomorph, Antetonitrus ingenipes. *The Anatomical Record*, *301*(9), 1506-1518.
- Kustatscher, E., Ash, S.R., Karasev, E., Pott, C., Vajda, V., Yu, J. and McLoughlin, S., (2018). Flora of the Late Triassic. In *The Late Triassic World*. 545-622. Springer, Cham.
- Labandeira, C.C., (2006). The four phases of plant- arthropod associations in deep time. *Geológica Acta,* 4, 409–438.
- Labandeira, C. C., Kustatscher, E., & Wappler, T. (2016). Floral assemblages and patterns of insect herbivory during the Permian to Triassic of Northeastern Italy. *PloS one*, *11*(11), e0165205.
- Labandeira, C.C., and Sepkoski, J.J., Jr., (1993). Insect diversity in the fossil record. *Science*, 261, 310–315.
- Lallensack, J. N., Klein, H., Milàn, J., Wings, O., Mateus, O., & Clemmensen, L. B. (2017). Sauropodomorph dinosaur trackways from the Fleming Fjord Formation of East Greenland: evidence for Late Triassic sauropods. *Acta Palaeontologica Polonica*, *62*(4), 833-843.
- Langer, M. C., Ezcurra, M. D., Bittencourt, J. S., & Novas, F. E. (2010). The origin and early evolution of dinosaurs. *Biological Reviews*, *85*(1), 55-110.
- Larson, D. W., Brown, C. M., & Evans, D. C. (2016). Dental disparity and ecological stability in bird-like dinosaurs prior to the end-Cretaceous mass extinction. *Current Biology*, *26*(10), 1325-1333.
- Laurin, M., & de Buffrénil, V. (2016). Microstructural features of the femur in early ophiacodontids: a reappraisal of ancestral habitat use and lifestyle of amniotes. *Comptes Rendus Palevol*, *15*(1-2), 115-127.
- Lautenschlager, S. (2017). Functional niche partitioning in Therizinosauria provides new insights into the evolution of theropod herbivory. *Palaeontology*, *60*(3), 375-387.
- Lautenschlager, S., Gill, P., Luo, Z. X., Fagan, M. J., & Rayfield, E. J. (2017). Morphological evolution of the mammalian jaw adductor complex. *Biological Reviews*, *92*(4), 1910-1940.
- Lautenschlager, Stephan, Pamela G. Gill, Zhe-Xi Luo, Michael J. Fagan, and Emily J. Rayfield. The role of miniaturization in the evolution of the mammalian jaw and middle ear. *Nature* 561, no. 7724 (2018): 533-537.
- Lautenschlager, S., Figueirido, B., Cashmore, D. D., Bendel, E. M., & Stubbs, T. L. (2020). Morphological convergence obscures functional diversity in sabre-toothed carnivores. *Proceedings of the Royal Society B*, *287*(1935), 20201818.
- Lê, S., Josse, J., & Husson, F. (2008). FactoMineR: an R package for multivariate analysis. *Journal of statistical software*, *25*(1), 1-18.
- Li, M., Huang, C., Hinnov, L., Ogg, J., Chen, Z. Q., & Zhang, Y. (2016). Obliquity-forced climate during the Early Triassic hothouse in China. *Geology*, *44*(8), 623-626.

- Lindström, S., Irmis, R. B., Whiteside, J. H., Smith, N. D., Nesbitt, S. J., & Turner, A. H. (2016). Palynology of the upper Chinle Formation in northern New Mexico, USA: implications for biostratigraphy and terrestrial ecosystem change during the Late Triassic (Norian–Rhaetian). Review of Palaeobotany and Palynology, 225, 106-131.
- Linnell, J. D., and Strand, O. (2000). Interference interactions, co-existence and conservation of mammalian carnivores. *Diversity and Distributions*, *6*(4), 169-176.
- Liow L. H., Reitan T., Harnik P. G., (2015). Ecological interactions on macroevolutionary time scales: Clams and brachiopods are more than ships that pass in the night. Ecol. Lett. 18, 1030–1039.
- Liu, J., Angielczyk, K. D., & Abdala, F. (2021). Permo-Triassic tetrapods and their climate implications. *Global and Planetary Change*, *205*, 103618.
- Lloyd, G. T., Bapst, D. W., Friedman, M., & Davis, K. E. (2016). Probabilistic divergence time estimation without branch lengths: dating the origins of dinosaurs, avian flight and crown birds. *Biology letters*, *12*(11), 20160609.
- Losos, J. B. (2011). *Lizards in an evolutionary tree: ecology and adaptive radiation of anoles*. Vol. 10. University of California Press.
- Losos, J. B., & Mahler, D. L. (2010). Adaptive radiation: the interaction of ecological opportunity, adaptation, and speciation. *Evolution since Darwin: the first*, *150*, 381-420.
- Lu, P.J., Yogo, M. & Marshall, C.R. (2006). Phanerozoic marine biodiversity dynamics in light of the incompleteness of the fossil record. *Proceedings of the National Academy of Sciences*, 103 (8), 2736–2739.
- Lucas, S. G. (2017). Permian tetrapod extinction events. Earth-Science Reviews, 170, 31-60.
- Lucas, S. G., Klein, H., Lockley, M. G., Spielmann, J. A., Gierlinski, G. D., Hunt, A. P., & Tanner, L. H. (2006). Triassic-Jurassic stratigraphic distribution of the theropod footprint ichnogenus Eubrontes. *New Mexico Museum of Natural History and Science Bulletin*, *37*, 86-93.
- Lungmus, J. K., & Angielczyk, K. D. (2019). Antiquity of forelimb ecomorphological diversity in the mammalian stem lineage (Synapsida). Proceedings of the National Academy of Sciences, 116(14), 6903-6907.
- Luo, Z. X. (2007). Transformation and diversification in early mammal evolution. *Nature*, *450* (7172), 1011-1019.
- Ma, W., Pittman, M., Butler, R. J., & Lautenschlager, S. (2021). Macroevolutionary trends in theropod dinosaur feeding mechanics. *Current Biology.*
- MacArthur, R. H. (1972). *Geographical ecology: patterns in the distribution of species.* Princeton Univ. Press, Princeton.

- Macdonald, D. W., Loveridge, A. J., & Nowell, K. (2010). Dramatis personae: an introduction to the wild felids. *Biology and conservation of wild felids*, *1*, 3-58.
- MacDougall, M. J., Brocklehurst, N., & Fröbisch, J. (2019). Species richness and disparity of parareptiles across the end-Permian mass extinction. *Proceedings of the Royal Society B*, *286*(1899), 20182572.
- MacLaren, J. A., Anderson, P. S., Barrett, P. M. & Rayfield, E. J. (2017). Herbivorous dinosaur jaw disparity and its relationship to extrinsic evolutionary drivers. *Paleobiology* 43, 15–33.
- Maddison, W. P. and D.R. Maddison. (2018). Mesquite: a modular system for evolutionary analysis. Version 3.51 http://www.mesquiteproject.org
- Madhulatha, T. S., (2011). Comparison between k-means and k-medoids clustering algorithms. *International Conference on Advances in Computing and Information Technology* 472–481. Springer, Heidelberg,
- Maidment, S.C., Sennikov, A.G., Ezcurra, M.D., Dunne, E.M., Gower, D.J., Hedrick, B.P., Meade, L.E., Raven, T.J., Paschchenko, D.I. and Butler, R.J., (2020). The postcranial skeleton of the erythrosuchid archosauriform Garjainia prima from the Early Triassic of European Russia. *Royal Society Open Science*, 7(12), p.201089.
- Mallon, J.C. and Anderson, J.S., (2013). Skull ecomorphology of megaherbivorous dinosaurs from the Dinosaur Park Formation (upper Campanian) of Alberta, Canada. *PLoS One*, *8*(7), p.e67182.
- Mallon, J. C., Evans, D. C., Ryan, M. J., & Anderson, J. S. (2013). Feeding height stratification among the herbivorous dinosaurs from the Dinosaur Park Formation (upper Campanian) of Alberta, Canada. *BMC ecology*, *13*(1), 14.
- Mancuso, A. C., Benavente, C. A., Irmis, R. B., & Mundil, R. (2020). Evidence for the Carnian pluvial episode in Gondwana: new multiproxy climate records and their bearing on early dinosaur diversification. *Gondwana Research*, *86*, 104-125.
- Mander, L., Kürschner, W. M., & McElwain, J. C. (2013). Palynostratigraphy and vegetation history of the Triassic–Jurassic transition in East Greenland. *Journal of the Geological Society*, *170*(1), 37-46.
- Mander, L. and McElwain, J.C. (2019). Toarcian land vegetation loss. *Nature Geoscience.* 12, 405–406.
- Mannion, P. D., Upchurch, P., Carrano, M. T., & Barrett, P. M. (2011). Testing the effect of the rock record on diversity: a multidisciplinary approach to elucidating the generic richness of sauropodomorph dinosaurs through time. *Biological Reviews*, *86*(1), 157-181.
- Martin, M. M., & Harding, J. (1981). Evidence for the evolution of competition between two species of annual plants. *Evolution*, 975-987

- Martinelli, A. G., Francischini, H., Dentzien-Dias, P. C., Soares, M. B., & Schultz, C. L. (2017). The oldest archosauromorph from South America: postcranial remains from the Guadalupian (mid-Permian) Rio do Rasto Formation (Paraná basin), southern Brazil. *Historical Biology*, *29*(1), 76-84.
- Martz, J. W., & Small, B. J. (2019). Non-dinosaurian dinosauromorphs from the Chinle Formation (Upper Triassic) of the Eagle Basin, northern Colorado: Dromomeron romeri (Lagerpetidae) and a new taxon, Kwanasaurus williamparkeri (Silesauridae). *PeerJ*, *7*, e7551.
- Marzoli, A., Callegaro, S., Dal Corso, J., Davies, J.H., Chiaradia, M., Youbi, N., Bertrand, H., Reisberg, L., Merle, R. and Jourdan, F., (2018). The Central Atlantic magmatic province (CAMP): A review. *The Late Triassic World*, pp.91-125.
- McElwain, J. C., Beerling, D. J., & Woodward, F. I. (1999). Fossil plants and global warming at the Triassic-Jurassic boundary. Science, 285(5432), 1386-1390.
- McElwain, J. C., Popa, M. E., Hesselbo, S. P., Haworth, M., & Surlyk, F. (2007). Macroecological responses of terrestrial vegetation to climatic and atmospheric change across the Triassic/Jurassic boundary in East Greenland. *Paleobiology*, *33*(4), 547-573.
- McPhee, B. W., Benson, R. B., Botha–Brink, J., Bordy, E. M. & Choiniere, J. N. (2018). A giant dinosaur from the earliest Jurassic of South Africa and the transition to quadrupedality in early sauropodomorphs. *Current Biology*. 28, 3143–3151
- McPhee, B. W., Bittencourt, J. S., Langer, M. C., Apaldetti, C., & Da Rosa, Á. A. (2020). Reassessment of Unaysaurus tolentinoi (Dinosauria: Sauropodomorpha) from the Late Triassic (early Norian) of Brazil, with a consideration of the evidence for monophyly within non-sauropodan sauropodomorphs. *Journal of Systematic Palaeontology*, *18*(3), 259-293.
- McPhee, B. W., Bonnan, M. F., Yates, A. M., Neveling, J. & Choiniere, J. N. (2015). A new basal sauropod from the pre-Toarcian Jurassic of South Africa: evidence of niche–partitioning at the sauropodomorph-sauropod boundary? *Scientific Reports.* 5, 13224.
- McPhee, B. W., Yates, A. M., Choiniere, J. N., & Abdala, F. (2014). The complete anatomy and phylogenetic relationships of Antetonitrus ingenipes (Sauropodiformes, Dinosauria): implications for the origins of Sauropoda. Zoological Journal of the Linnean Society, 171(1), 151-205.
- Meloro, C., Raia, P., Carotenuto, F., & Cobb, S. N. (2011). Phylogenetic signal, function and integration in the subunits of the carnivoran mandible. *Evolutionary Biology*, *38*(4), 465-475.
- Melstrom, K. M. (2017). The relationship between diet and tooth complexity in living dentigerous saurians. Journal of morphology, 278(4), 500-522.
- Melstrom, K. M., & Irmis, R. B. (2019). Repeated evolution of herbivorous crocodyliforms during the age of dinosaurs. *Current Biology*, *29*(14), 2389-2395.

- Meng, J. (2014). Mesozoic mammals of China: implications for phylogeny and early evolution of mammals. *National Science Review*, *1*(4), 521-542.
- Meredith, R.W., Janečka, J.E., Gatesy, J., Ryder, O.A., Fisher, C.A., Teeling, E.C., Goodbla, A., Eizirik, E., Simão, T.L., Stadler, T. and Rabosky, D.L., (2011). Impacts of the Cretaceous Terrestrial Revolution and KPg extinction on mammal diversification. *Science*, *334*(6055), 521-524.
- Metcalfe, I., Crowley, J. L., Nicoll, R. S., and Schmitz, M. (2015). High-precision U-Pb CA-TIMS calibration of Middle Permian to Lower Triassic sequences, mass extinction and extreme climate-change in eastern Australian Gondwana. *Gondwana Research,* 28(1), 61-81.
- Midgley, J. J., Midgley, G., & Bond, W. J. (2002). Why were dinosaurs so large? A food quality hypothesis. Evolutionary Ecology Research, 4(7), 1093-1095.
- Miller, C. S., & Baranyi, V. (2019). Triassic climates. *Reference module in earth systems and environmental sciences*, 1-11.
- Millien, V. & Bovy, H. (2010). When teeth and bones disagree: body mass estimates in a giant extinct rodent. *Journal of Mammalogy* **91**, 11–18.
- Montañez, I. P., & Poulsen, C. J. (2013). The Late Paleozoic ice age: an evolving paradigm. *Annual Review of Earth and Planetary Sciences*, *41*, 629-656.
- Montanucci, R. R. (1968). Comparative dentition in four iguanid lizards. Herpetologica, 24(4), 305-315.
- Müller, R.T., and Garcia. M.S. (2019). Rise of an empire: analysing the high diversity of the earliest sauropodomorph dinosaurs through distinct hypotheses. *Historical Biology.* 1-6.
- Müller, R. T., & Garcia, M. S. (2020). A paraphyletic 'Silesauridae'as an alternative hypothesis for the initial radiation of ornithischian dinosaurs. *Biology letters*, *16*(8), 20200417.
- Murray, D. L., Boutin, S., O'Donoghue, M., & Nams, V. O. (1995). Hunting behaviour of a sympatric felid and canid in relation to vegetative cover. *Animal Behaviour*, *50*(5), 1203-1210.
- Myers, C. E., & Saupe, E. E. (2013). A macroevolutionary expansion of the modern synthesis and the importance of extrinsic abiotic factors. *Palaeontology*, *56*(6), 1179-1198.
- Nabavizadeh, A. (2020). Cranial musculature in herbivorous dinosaurs: A survey of reconstructed anatomical diversity and feeding mechanisms. *The Anatomical Record*, *303*(4), 1104-1145.
- Nesbitt, S.J., Butler, R.J., Ezcurra, M.D., Barrett, P.M., Stocker, M.R., Angielczyk, K.D., Smith, R.M., Sidor, C.A., Niedźwiedzki, G., Sennikov, A.G. and Charig, A.J., (2017). The earliest bird-line archosaurs and the assembly of the dinosaur body plan. *Nature*, *544*(7651), 484-487.
- Nordén, K. K., Stubbs, T. L., Prieto-Márquez, A. & Benton, M. J. (2018). Multifaceted disparity approach reveals dinosaur herbivory flourished before the end–Cretaceous mass extinction. *Paleobiology* 44, 620–637.

- Nowell K., and Jackson P. (Eds.), (1996). Panthera onca. Wild Cats: Status Survey and Conservation Action Plan, IUCN/SSC Cat Specialist Group, IUCN, Gland, Switzerland. 118-122.
- Oksanen, J., F. G. Blanchet, M. Friendly, R. Kindt, P. Legendre, D. McGlinn, P. R. Minchin et al. (2019). vegan: Community Ecology Package. R package version 2.5. 4. 2019.
- Olson, E. C. (1961). Jaw mechanisms: rhipidistians, amphibians, reptiles. *American Zoologist*, 205-215.
- Olson, E. C. (1962). Late Permian terrestrial vertebrates, USA and USSR. Transactions of the American Philosophical Society, 52(2), 1-224.
- Olson E. C. (1966). Community evolution and the origin of mammals. Ecology 47, 291–302.
- Olson E. C. (1982). Extinctions of Permian and Triassic nonmarine vertebrates. *GSA Special Papers* 190, 501–512.
- O'Meara B.C., Ane C., Sanderson M.J., Wainwright P.C. (2006). Testing for different rates of continuous trait evolution. *Evolution*. 60:922-933.
- Otero, A., Cuff, A. R., Allen, V., Sumner-Rooney, L., Pol, D., & Hutchinson, J. R. (2019). Ontogenetic changes in the body plan of the sauropodomorph dinosaur Mussaurus patagonicus reveal shifts of locomotor stance during growth. *Scientific reports*, *9*(1), 1-10.
- Pacheco, C., Müller, R. T., Langer, M., Pretto, F. A., Kerber, L., & da Silva, S. D. (2019). Gnathovorax cabreirai: a new early dinosaur and the origin and initial radiation of predatory dinosaurs. *PeerJ*, *7*, e7963.
- Pagel, M. (1994) Detecting correlated evolution on phylogenies: a general method for the comparative analysis of discrete characters. *Proceedings of the Royal Society of London. Series B. Biological Sciences*, **255**, 37–45.
- Pagel, M., & Meade, A. (2013). BayesTraits v. 2.0. *Reading: University of Reading*.
- Palomares, F. & Caro, T. M. (1999). Interspecific killing among mammalian carnivores. *The American Naturalist,* 153, 492–508.
- Paradis, E., Blomberg, S., Bolker, B., Brown, J., Claude, J., Cuong, H.S., Desper, R. and Didier, G., (2015). Package 'ape'. *Analyses of phylogenetics and evolution, version*, *2*, 4-1.
- Paradis, E., & Schliep, K. (2019). ape 5.0: an environment for modern phylogenetics and evolutionary analyses in R. *Bioinformatics*, *35*(3), 526-528.
- Pardo, J. D., Small, B. J., Milner, A. R., & Huttenlocker, A. K. (2019). Carboniferous–Permian climate change constrained early land vertebrate radiations. *Nature ecology & evolution*, *3*(2), 200-206.
- Parrington, F. R. (1955). On the cranial anatomy of some gorgonopsids and the synapsid middle ear. *Proceedings of the Zoological Society of London.* 125(1), 1-40.

- Parrish, J. T. (1995). Geologic evidence of Permian climate. In *The Permian of Northern Pangea*. 53-61. Springer, Berlin, Heidelberg.
- Parrish, J. M. (2006). The origins of high browsing and the effects of phylogeny and scaling on neck length in sauropodomorphs. *Amniote paleobiology: perspectives on the evolution of mammals, birds and reptiles, The University of Chicago Press, Chicago*, 201-244.
- Patzkowsky M. E., (1995). A hierarchical branching model of evolutionary radiations. *Paleobiology* 21, 440– 460.
- Paterson, N. W., & Mangerud, G. (2015). Late Triassic (Carnian–Rhaetian) palynology of Hopen, Svalbard. *Review of Palaeobotany and Palynology*, *220*, 98-119.
- Patterson, B. D., Willig, M. R., & Stevens, R. D. (2003). Trophic strategies, niche partitioning, and patterns of ecological organization. *Bat ecology*, *9*, 536-557.
- Payne J. L & Kump L. R. (2007). Evidence for recurrent Early Triassic massive volcanism from quantitative interpretation of carbon isotope fluctuations. *Earth Planet. Sci. Lett*. 256, 264–277.
- Payne, J. L., Lehrmann, D. J., Wei, J., Orchard, M. J., Schrag, D. P., & Knoll, A. H. (2004). Large perturbations of the carbon cycle during recovery from the end-Permian extinction. *Science*, *305*(5683), 506-509.
- Périquet, S., Fritz, H., & Revilla, E. (2015). The Lion King and the Hyaena Queen: large carnivore interactions and coexistence. *Biological reviews*, *90*(4), 1197-1214.
- Pfefferkorn, H. W., Gastaldo, R. A., DiMichele, W. A., & Phillips, T. L. (2008). Pennsylvanian tropical floras from the United States as a record of changing climate. *Resolving the Late Paleozoic Ice Age in time and space. Special Papers/Geological Society of America*, *441*, 305-316.
- Pfennig, D. W., & Murphy, P. J. (2000). Character displacement in polyphenic tadpoles. *Evolution*, *54*(5), 1738-1749.
- Pigot, A. L., Tobias, J. A., and Jetz, W. (2016). Energetic constraints on species coexistence in birds. *PLoS biology*, *14*(3), e1002407.
- Pinheiro, J., Bates, D., DebRoy, S., Sarkar, D., Heisterkamp, S., Van Willigen, B., & Maintainer, R. (2017). Package 'nlme'. *Linear and nonlinear mixed effects models, version*, *3*(1).
- Pires, M. M., Silvestro, D., and Quental, T. B. (2015). Continental faunal exchange and the asymmetrical radiation of carnivores. *Proceedings of the Royal Society B: Biological Sciences*, *282*(1817), 20151952.
- Pires, M.M., Silvestro, D. and Quental, T.B., (2017). Interactions within and between clades shaped the diversification of terrestrial carnivores. *Evolution*, *71*(7), 1855-1864.

- Pol, D., Otero, A., Apaldetti, C. A., & Martínez, R. J. (2021). Triassic sauropodomorph dinosaurs from South America: The origin and diversification of dinosaur dominated herbivorous faunas. Journal of South American Earth Sciences, 103145.
- Pol, D., J. Ramezani, K. Gomez, J. L. Carballido, A. Paulina Carabajal, O. W. M. Rauhut, I. H. Escapa, and N. R. Cúneo. (2020). Extinction of herbivorous dinosaurs linked to Early Jurassic global warming event. *Proceedings of the Royal Society B.* 287, 1939: 20202310.
- Porro, L. B., Butler, R. J., Barrett, P. M., Moore-Fay, S., & Abel, R. L. (2010). New heterodontosaurid specimens from the Lower Jurassic of southern Africa and the early ornithischian dinosaur radiation. *Earth and Environmental Science Transactions of the Royal Society of Edinburgh*, *101*(3-4), 351-366.
- Porro, L. B., Holliday, C. M., Anapol, F., Ontiveros, L. C., Ontiveros, L. T., & Ross, C. F. (2011). Free body analysis, beam mechanics, and finite element modeling of the mandible of *Alligator mississippiensis*. *Journal of Morphology.* 272, 910-937.
- Preto, N., Kustatscher, E., & Wignall, P. B. (2010). Triassic climates—state of the art and perspectives. *Palaeogeography, Palaeoclimatology, Palaeoecology*, *290*(1-4), 1-10.
- Pringle, R. M., Palmer, T. M., Goheen, J. R., McCauley, D. J., & Keesing, F. (2011). Ecological importance of large herbivores in the Ewaso ecosystem. *Smithsonian contributions to zoology*. 55-71.
- Pritchard, J. R., & Schluter, D. (2001). Declining interspecific competition during character displacement: summoning the ghost of competition past. *Evolutionary Ecology Research*, *3*(2), 209-220.
- Purnell, M. A., & Donoghue, P. C. (2005). Between death and data: biases in interpretation of the fossil record of conodonts. *Special Papers in Palaeontology*, 73, 7-25.
- Puttick, M. N. (2018). Mixed evidence for early bursts of morphological evolution in extant clades. *Journal of evolutionary biology*, *31*(4), 502-515.
- Pyron, R. A., Costa, G. C., Patten, M. A., & Burbrink, F. T. (2015). Phylogenetic niche conservatism and the evolutionary basis of ecological speciation. *Biological Reviews*, *90*(4), 1248-1262.
- Quental T. B., and Marshall C. R., (2013). How the Red Queen drives terrestrial mammals to extinction. *Science* 341, 290–292.
- R Core Team. (2018) R: A Language and Environment for Statistical Computing (R Foundation for Statistical Computing); http://www.R–project.org/
- Rabosky, D. L. (2013). Diversity-dependence, ecological speciation, and the role of competition in macroevolution. *Annual Review of Ecology, Evolution, and Systematics*, 44, 481-502.

- Rabosky, D. L., & Lovette, I. J. (2008). Density-dependent diversification in North American wood warblers. *Proceedings of the Royal Society B: Biological Sciences*, *275*(1649), 2363-2371.
- Racki, G., & Lucas, S. G. (2020). Timing of dicynodont extinction in light of an unusual Late Triassic Polish fauna and Cuvier's approach to extinction. *Historical Biology*, *32*(4), 452-461.
- Raia, P., Carotenuto, F., Meloro, C., Piras, P. & Pushkina, D. (2010). The shape of contention: adaptation, history, and contingency in ungulate mandibles. *Evolution* 64, 1489–1503.
- Ramesh, T., Kalle, R., Sankar, K., & Qureshi, Q. (2012). Dietary partitioning in sympatric large carnivores in a tropical forest of Western Ghats, India. Mammal Study, 37(4), 313-321.
- Ramiadantsoa, T., Hanski, I., & Ovaskainen, O. (2018). Responses of generalist and specialist species to fragmented landscapes. *Theoretical population biology*, *124*, 31-40.
- Rampino, M. R., & Shen, S. Z. (2021). The end-Guadalupian (259.8 Ma) biodiversity crisis: the sixth major mass extinction?. *Historical Biology*, *33*(5), 716-722.
- Ramsay, J. B., & Wilga, C. D. (2007). Morphology and mechanics of the teeth and jaws of white-spotted bamboo sharks (*Chiloscyllium plagiosum*). *Journal of Morphoogyl.* 268, 664-682.
- Rauhut, O.W., Fechner, R.E., Remes, K.R., & Reis, K.A. (2011). How to get big in the Mesozoic: the evolution of the sauropodomorph body plan. Biology of the sauropod dinosaurs: Understanding the life of giants. *Biological Reviews.* 22, 119–149.
- Rauhut, O. W., & Pol, D. (2019). Probable basal allosauroid from the early Middle Jurassic Cañadón Asfalto Formation of Argentina highlights phylogenetic uncertainty in tetanuran theropod dinosaurs. *Scientific Reports*, *9*(1), 1-9.
- Raup, D. M. (1972). Taxonomic diversity during the Phanerozoic. Science, 177, 1065–1071.
- Reisz, R. R. (1972). Pelycosaurian reptiles from the middle Pennsylvanian of North America. *Bulletin of the Museum of Comparative Zoology at Harvard College*. 144. 27-62.
- Reisz, R. R., and Fröbisch J. (2014). The oldest caseid synapsid from the Late Pennsylvanian of Kansas, and the evolution of herbivory in terrestrial vertebrates. *PLoS ONE,* 9: e94518. doi:10.1371/journal. pone.0094518.
- Reisz, R. R. & Sues, H. D. (2000). Herbivory in late Paleozoic and Triassic terrestrial vertebrates. *Evolution of Herbivory in Terrestrial Vertebrates: Perspectives from the fossil record* (eds Sues, H. D.), 9-41. Cambridge University Press, Cambridge.
- Reisz, R.R., LeBlanc, A.R., Maddin, H.C., Dudgeon, T.W., Scott, D., Huang, T., Chen, J., Chen, C.M. and Zhong, S., 2020. Early Jurassic dinosaur fetal dental development and its significance for the evolution of sauropod dentition. *Nature communications*, *11*(1), 1-9.
- Reisz, R. R., Scott, D., Sues, H. D., Evans, D. C., & Raath, M. A. (2005). Embryos of an Early Jurassic prosauropod dinosaur and their evolutionary significance. *Science*, *309*(5735), 761-764.

- Renne, P. R., Black, M. T., Zichao, Z., Richards, M. A., & Basu, A. R. (1995). Synchrony and causal relations between Permian-Triassic boundary crises and Siberian flood volcanism. *Science*, *269*(5229), 1413-1416.
- Retallack, G. J., Metzger, C. A., Greaver, T., Jahren, A. H., Smith, R. M., & Sheldon, N. D. (2006). Middle-Late Permian mass extinction on land. *GSA Bulletin*, 118(11-12), 1398-1411.
- Revell L. J., Collar D. C. (2009). Phylogenetic analysis of the evolutionary correlation using likelihood. *Evolution*. 63:1090-1100.
- Rey, K., Amiot, R., Fourel, F., Abdala, F., Fluteau, F., Jalil, N.E., Liu, J., Rubidge, B.S., Smith, R.M., Steyer, J.S. and Viglietti, P.A., (2017). Oxygen isotopes suggest elevated thermometabolism within multiple Permo-Triassic therapsid clades. *Elife*, *6*, e28589.
- Reyes, W. A., Parker, W. G., & Marsh, A. D. (2020). Cranial anatomy and dentition of the aetosaur Typothorax coccinarum (Archosauria: Pseudosuchia) from the Upper Triassic (Revueltian–mid Norian) Chinle Formation of Arizona. *Journal of Vertebrate Paleontology*, *40*(6), e1876080.
- Rigo, M., Onoue, T., Tanner, L., Lucas, S.G., Godfrey, L., Katz, M.E., Zaffani, M., Grice, K., Cesar, J., Yamashita, D. and Maron, M., (2020). The Late Triassic Extinction at the Norian/Rhaetian boundary: Biotic evidence and geochemical analysis. *Earth-Science Reviews*, 103180.
- Rivals, F. and Lister, A.M., (2016). Dietary flexibility and niche partitioning of large herbivores through the Pleistocene of Britain. *Quaternary Science Reviews*, *146*, 116-133.
- Rohlf, F. (2010) tpsDig v.2.16 (Department of Ecology and Evolution, State Univ. New York at Stony Brook).
- Rohlf, F. (2013). tpsUTIL v.1.56 (Department of Ecology and Evolution, State Univ. New York at Stony Brook).
- Rohlf, F.J., (2015). tpsRelw, version 1.49 (Department of Ecology and Evolution, State University of New York, Stony Brook).
- Romano, M. (2017). Long bone scaling of caseid synapsids: a combined morphometric and cladistic approach. *Lethaia*, 50(4), 511-526.
- Romano, M., & Manucci, F. (2019). Resizing Lisowicia bojani: volumetric body mass estimate and 3D reconstruction of the giant Late Triassic dicynodont. *Historical Biology*. 32, 452-461.
- Romer, A.S. (1966): Vertebrate Paleontology. University of Chicago Press, Chicago.
- Romer, A. S. (1967). Major steps in vertebrate evolution. Science, 158(3809), 1629-1637.
- Romer, A. S., and Price, L. W., (1940). *Review of the Pelycosauria* (Vol. 28). *Geological Society of America.*
- Roopnarine P. D., Angielczyk K. D. (2012). The evolutionary palaeoecology of species and the tragedy of the commons. *Biology Letters*, 8, 147– 150.

- Roopnarine, P. D., Angielczyk, K. D., Wang, S. C., & Hertog, R. (2007). Trophic network models explain instability of Early Triassic terrestrial communities. *Proceedings of the Royal Society B: Biological Sciences*, *274*(1622), 2077-2086.
- Roopnarine, P. D., Angielczyk, K. D., Weik, A., & Dineen, A. (2019). Ecological persistence, incumbency and reorganization in the Karoo Basin during the Permian-Triassic transition. *Earth-Science Reviews,* 189, 244-263.
- Roy, K. (1996) The roles of mass extinction and biotic interaction in large-scale replacements: A reexamination using the fossil record of stromboidean gastropods. Paleobiology 22(3):436–452. 3.
- Ruben, J. A., W. J. Hillenius, T. S. Kemp, and D. E. Quick. (2012). The evolution of mammalian endothermy. 273–286 in A. Chinsamy-Turan (ed.), Forerunners of Mammals: Radiation-Histology-Biology. Indiana University Press, Bloomington, Indiana.
- Rubidge, B. S., & Sidor, C. A. (2001). Evolutionary patterns among Permo-Triassic therapsids. *Annual Review of Ecology and Systematics,* 32(1), 449-480.
- Ruebsam, W., & Schwark, L. (2021). Impact of a northern-hemispherical cryosphere on late Pliensbachian–early Toarcian climate and environment evolution. *Geological Society, London, Special Publications*, *514*(1), 359-385.
- Ruhl, M., Bonis, N. R., Reichart, G. J., Damsté, J. S. S., & Kürschner, W. M. (2011). Atmospheric carbon injection linked to end-Triassic mass extinction. *Science*, *333*(6041), 430-434.
- Ruta, M., Angielczyk, K. D., Fröbisch, J., & Benton, M. J. (2013a). Decoupling of morphological disparity and taxic diversity during the adaptive radiation of anomodont therapsids. *Proceedings of the Royal Society B: Biological Sciences*, *280*(1768), 20131071.
- Ruta, M., Botha-Brink, J., Mitchell, S. A., & Benton, M. J. (2013b). The radiation of cynodonts and the ground plan of mammalian morphological diversity. *Proceedings of the Royal Society B: Biological Sciences,* 280(1769), 20131865.
- Ruta, M., Cisneros, J. C., Liebrecht, T., Tsuji, L. A., Müller, J. (2011). Amniotes through major biological crises: faunal turnover among parareptiles and the end-Permian mass extinction. *Palaeontology* 54, 1117–1137.
- Sahney S. and Benton, M. J. (2008). Recovery from the most profound mass extinction of all time. Proc. R. Soc. B 275, 759–765.
- Sahney, S., Benton, M. J., & Falcon-Lang, H. J. (2010). Rainforest collapse triggered Carboniferous tetrapod diversification in Euramerica. *Geology*, *38*(12), 1079-1082.
- Sakamoto, M. (2010). Jaw biomechanics and the evolution of biting performance in theropod dinosaurs. *Proceedings of the Royal Society B: Biological Sciences*, *277*(1698), 3327-3333.

- Sakamoto, M., Ruta, M., & Venditti, C. (2019). Extreme and rapid bursts of functional adaptations shape bite force in amniotes. *Proceedings of the Royal Society B*, *286*(1894), 20181932.
- Sakamoto, M., & Venditti, C. (2018). Phylogenetic non-independence in rates of trait evolution. *Biology letters*, *14*(10), 20180
- Salgado, L., Coria, R. A., & Calvo, J. O. (1997). Evolution of titanosaurid sauropods: Phytogenetic analysis based on the postcranial evidence. *Ameghiniana*, *34*(1), 3-32.
- Sander, P. M. (2013). An evolutionary cascade model for sauropod dinosaur gigantism-overview, update and tests. *PloS one*, *8*(10), e78573.
- Sander, P.M., Christian, A., Clauss, M., Fechner, R., Gee, C.T., Griebeler, E.M., Gunga, H.C., Hummel, J., Mallison, H., Perry, S.F. and Preuschoft, H., (2011). Biology of the sauropod dinosaurs: the evolution of gigantism. *Biological Reviews*, *86*(1), 117-155.
- Sanson, G. (2006). The biomechanics of browsing and grazing. American Journal of Botany, 93(10), 1531-1545.
- Saunders, A., & Reichow, M. (2009). The Siberian Traps and the End-Permian mass extinction: a critical review. *Chinese Science Bulletin*, *54*(1), 20-37.
- Savage R. J. G., (1977). Evolution in carnivorous mammals. *Palaeontology.* 20: 237–271
- Schaller G. B., and Vasconselos J. M. C. (1978) Jaguar predation on capybara. Z Saugetierk, 43, 296-301.
- Schluter, D. (1994). Experimental evidence that competition promotes divergence in adaptive radiation. *Science*, *266*(5186), 798-801.
- Schluter, D. (2000). *The ecology of adaptive radiation*. OUP Oxford.
- Schneider, C. A., Rasband, W. S., & Eliceiri, K. W. (2012). NIH Image to ImageJ: 25 years of image analysis. *Nature methods*, *9*(7), 671-675.
- Schölkopf, B., Mika, S., Smola, A., Rätsch, G., & Müller, K. R. (1998). Kernel PCA pattern reconstruction via approximate pre-images. In *International Conference on Artificial Neural Networks* (pp. 147-152). Springer, London.
- Seilacher, A. (1970). Arbeitskonzept zur konstruktions-morphologie. *Lethaia3*:393–396.
- Sen, K., (2005). A new rauisuchian archosaur from the Middle Triassic of India. *Palaeontology,* 48(1), pp.185-196.
- Sennikov, A. G. (1996). Evolution of the Permian and Triassic tetrapod communities of Eastern Europe. *Palaeogeography, Palaeoclimatology, Palaeoecology*, 120(3-4), 331-351.
- Sennikov, A. G., Golubev, V. K. (2006). Vyazniki biotic assemblage of the terminal Permian. *Journal of Paleontology*. 40, S475–S481

- Sephton, M. A., Amor, K., Franchi, I. A., Wignall, P. B., Newton, R., & Zonneveld, J. P. (2002). Carbon and nitrogen isotope disturbances and an end-Norian (Late Triassic) extinction event. *Geology*, *30*(12), 1119-1122.
- Sepkoski J. J. (1996). Competition in macroevolution: The double wedge revisited in Evolutionary Paleobiology, D. Jablonski, D. H. Erwin, J. H. Lipps, Eds. 211–255 (University of Chicago Press, Chicago, IL).
- Sereno, P.C., Dutheil, D.B., Iarochene, M., Larsson, H.C., Lyon, G.H., Magwene, P.M., Sidor, C.A., Varricchio, D.J. and Wilson, J.A., (1996). Predatory dinosaurs from the Sahara and Late Cretaceous faunal differentiation. *Science*, *272* (5264), 986-991.
- Shcherbakov, D. E. (2008). On Permian and Triassic insect faunas in relation to biogeography and the Permian-Triassic crisis. Paleontological Journal, 42(1), 15-31.
- Shear, W.A., and Kukaloveck, J., (1990). The ecology of Paleozoic terrestrial arthropods: The fossil evidence. *Canadian Journal of Zoology,* v. 68, p. 1807–1834.
- Shipley, L. A., Forbey, J. S., & Moore, B. D. (2009). Revisiting the dietary niche: when is a mammalian herbivore a specialist?. *Integrative and Comparative Biology*, *49*(3), 274-290.
- Sidor, C.A., Vilhena, D.A., Angielczyk, K.D., Huttenlocker, A.K., Nesbitt, S.J., Peecook, B.R., Steyer, J.S., Smith, R.M. and Tsuji, L.A., 2013. Provincialization of terrestrial faunas following the end-Permian mass extinction. *Proceedings of the National Academy of Sciences,* 110(20), 8129-8133.
- Sugiura, N. (1978). Further analysts of the data by akaike's information criterion and the finite corrections: Further analysts of the data by akaike's. Communications in Statistics-Theory and Methods, 7(1), 13-26.
- Sigogneau-Russell, D. (1989). Theriodontia I. In P. Wellnhofer (Ed.), Handbuch der Paläoherpetologie (Vol. 17 B/I). Stuttgart: Gustav Fischer Verlag.
- Sigurdsen, T., Huttenlocker, A. K., Modesto, S. P., Rowe, T. B., & Damiani, R. (2012). Reassessment of the morphology and paleobiology of the therocephalian Tetracynodon darti (Therapsida), and the phylogenetic relationships of Baurioidea. *Journal of Vertebrate Paleontology*, *32*(5), 1113-1134.
- Silvestro, D., Antonelli, A., Salamin, N. and Quental, T.B., (2015). The role of clade competition in the diversification of North American canids. *Proceedings of the National Academy of Sciences*, *112*(28), 8684-8689.
- Simms, M. J., & Ruffell, A. H. (1990). Climatic and biotic change in the late Triassic. *Journal of the Geological Society*, *147*(2), 321-327.
- Simpson, G. G. *Tempo and Mode in Evolution* (Columbia University Press, 1944).
- Simpson, G. G. (1953). *The Major Features of Evolution.* Columbia University Press, New York.

- Slater, G. J., & Friscia, A. R. (2019). Hierarchy in adaptive radiation: A case study using the Carnivora (Mammalia). *Evolution*, *73*(3), 524-539.
- Slater, S. M., Twitchett, R. J., Danise, S., & Vajda, V. (2019). Substantial vegetation response to Early Jurassic global warming with impacts on oceanic anoxia. *Nature Geoscience*, *12*(6), 462-467.
- Smith, A. B. (2001). Large–scale heterogeneity of the fossil record: implications for Phanerozoic biodiversity studies. *Philosophical Transactions of the Royal Society of London B*: Biological Sciences, 356(1407), 351-367.
- Smith, A. B. (2007). Marine diversity through the Phanerozoic: problems and prospects. *Journal of the Geological Society*, *164*(4), 731-745.
- Smith, J. M., & Szathmary, E. (1997). *The major transitions in evolution*. Oxford University Press.
- Smithwick, F. M. & Stubbs, T. L. (2018). Phanerozoic survivors: actinopterygian evolution through the Permo-Triassic and Triassic-Jurassic mass extinction events. *Evolution* 72, 348–362.
- Soh, W.K., Wright, I.J., Bacon, K.L., Lenz, T.I., Steinthorsdottir, M., Parnell, A. C. & McElwain, J. C. (2017). Palaeo leaf economics reveal a shift in ecosystem function associated with the end-Triassic mass extinction event. *Nature Plants* 3, 17104.
- Sookias, R. B., Butler, R. J. & Benson, R. B. (2012). Rise of dinosaurs reveals major body–size transitions are driven by passive processes of trait evolution. *Proceedings of the Royal Society B: Biological Sciences.* 279, 2180–2187.
- Spalletti, L. A., Artabe, A. E., & Morel, E. M. (2003). Geological factors and evolution of southwestern Gondwana Triassic plants. *Gondwana Research*, *6*(1), 119-134.
- Spiekman, S. N., Neenan, J. M., Fraser, N. C., Fernandez, V., Rieppel, O., Nosotti, S., & Scheyer, T. M. (2020). Aquatic habits and niche partitioning in the extraordinarily long-necked Triassic reptile Tanystropheus. *Current Biology*, *30*(19), 3889-3895.
- Spindler, F. (2020). The skull of Tetraceratops insignis (Synapsida, Sphenacodontia). Palaeovertebrata, 43(1):e1.
- Stayton, C. T. (2006). Testing hypotheses of convergence with multivariate data: morphological and functional convergence among herbivorous lizards. *Evolution*, *60*(4), 824-841.
- Stephens D. W., and Krebs J. R., (1986). *Foraging Theory*. Princeton University Press, Princeton.
- Steinthorsdottir, M., Jeram, A. J., & McElwain, J. C. (2011). Extremely elevated CO2 concentrations at the Triassic/Jurassic boundary. *Palaeogeography, Palaeoclimatology, Palaeoecology*, *308*(3-4), 418-432.
- Stocker, M.R., Nesbitt, S.J., Criswell, K.E., Parker, W.G., Witmer, L.M., Rowe, T.B., Ridgely, R. and Brown, M.A., (2016). A dome-headed stem archosaur exemplifies convergence among dinosaurs and their distant relatives. *Current Biology*, *26*(19), 2674-2680.

- Stocker, M. R., Zhao, L. J., Nesbitt, S. J., Wu, X. C., & Li, C. (2017). A short-snouted, Middle Triassic phytosaur and its implications for the morphological evolution and biogeography of Phytosauria. *Scientific Reports*, *7*(1), 1-9.
- Strotz, L. C., Simões, M., Girard, M. G., Breitkreuz, L., Kimmig, J., & Lieberman, B. S. (2018). Getting somewhere with the Red Queen: chasing a biologically modern definition of the hypothesis. *Biology letters*, *14*(5), 20170734.
- Stubbs, T. L., Pierce, S. E., Rayfield, E. J., & Anderson, P. S. (2013). Morphological and biomechanical disparity of crocodile-line archosaurs following the end-Triassic extinction. *Proceedings of the Royal Society B: Biological Sciences*, *280*(1770), 20131940.
- Sues H. D. (1986) Locomotion and body form in early therapsids (Dinocephalia, Gorgonopsia, and Therocephalia). The Ecology and Biology of Mammal-Like Reptiles (Smithsonian Institution Press, Washington, DC), 61–70.
- Sues, H. D. & Fraser, N. C. (2010). *Triassic life on land: the great transition.* Columbia University Press, New York.
- Sues, H. D., and Reisz, R. R. (1998), Origins and early evolution of herbivory in tetrapods. *Trends in Ecology and Evolution*, 13, 141–145.
- Sulej, T. & Niedźwiedzki, G. (2019). An elephant-sized Late Triassic synapsid with erect limbs. *Science*. 363, 78–80.
- Sun, Y., Joachimski, M.M., Wignall, P.B., Yan, C., Chen, Y., Jiang, H., Wang, L. and Lai, X., (2012). Lethally hot temperatures during the Early Triassic greenhouse. *Science*, 338(6105), 366-370.
- Tanner, L. H., Lucas, S. G., & Chapman, M. G. (2004). Assessing the record and causes of Late Triassic extinctions. *Earth-Science Reviews*, *65*(1-2), 103-139.
- Tegner, C., Marzoli, A., McDonald, I., Youbi, N., & Lindström, S. (2020). Platinum-group elements link the end-Triassic mass extinction and the Central Atlantic Magmatic Province. *Scientific reports*, *10*(1), 1-8.
- Tewari, R., Pandita, S. K., Agnihotri, D., Pillai, S. S. K., & Bernardes-de-Oliveira, M. E. (2012). An Early Permian Glossopteris flora from the Umrer Coalfield, Wardha Basin, Maharashtra, India. *Alcheringa: An Australasian Journal of Palaeontology*, *36*(3), 355-371.
- Thomason, J. (Ed.). (1997). Functional morphology in vertebrate paleontology. Cambridge University Press.
- Throckmorton, G. Y. S. (1976). Oral food processing in two herbivorous lizards, Iguana iguana (Iguanidae) and Uromastix aegyptius (Agarnidae). Journal of Morphology, 148(3), 363-390.
- Thompson, J.N. (2005). *The Geographic Mozaic of Coevolution*. The University of Chicago Press, Chicago and London.

- Tilman, D. (1982). *Resource competition and community structure* (Princeton Univ. Press, Princeton.
- Toljagić, O., & Butler, R. J. (2013). Triassic–Jurassic mass extinction as trigger for the Mesozoic radiation of crocodylomorphs. *Biology Letters*, *9*(3), 20130095.
- Trotter, J. A., Williams, I. S., Nicora, A., Mazza, M., & Rigo, M. (2015). Long-term cycles of Triassic climate change: a new δ18O record from conodont apatite. *Earth and Planetary Science Letters*, *415*, 165-174.
- Troyer, K. (1982). Transfer of fermentative microbes between generations in a herbivorous lizard. Science, 216(4545), 540-542.
- Tucker, M. A., & Rogers, T. L. (2014). Examining the prey mass of terrestrial and aquatic carnivorous mammals: minimum, maximum and range. *PloS one*, *9*(8), e106402.
- Turner, G. F. (2007). Adaptive radiation of cichlid fish. *Current Biology*, *17*(19), R827-R831.
- Upchurch, P., Mannion, P. D., Benson, R. B., Butler, R. J., & Carrano, M. T. (2011). Geological and anthropogenic controls on the sampling of the terrestrial fossil record: a case study from the Dinosauria. *Geological Society, London, Special Publications*, *358*(1), 209-240.
- Van de Schootbrugge, B., Quan, T.M., Lindström, S., Püttmann, W., Heunisch, C., Pross, J., Fiebig, J., Petschick, R., Röhling, H.G., Richoz, S. and Rosenthal, Y., (2009). Floral changes across the Triassic/Jurassic boundary linked to flood basalt volcanism. *Nature Geoscience*, 2(8), 589-594.
- Van Valen, L.M. (1973). A new evolutionary law. *Evolutionary Theory*, 1, 1–30.
- Van Valen, L. M. (1984). A resetting of Phanerozoic community evolution. *Nature.* 307, 50–52.
- Van Valkenburgh, B. (2007). Déjà vu: the evolution of feeding morphologies in the Carnivora. *Integrative and Comparative Biology*, 47(1), 147-16.
- Van Valkenburgh, B., & Ruff, C. B. (1987). Canine tooth strength and killing behaviour in large carnivores. *Journal of Zoology*, *212*(3), 379-397.
- Van Valkenburgh B. (1999). Major patterns in the history of carnivorous mammals. *Annual Review of Earth and Planetary Science,* 27: 463–493
- Van Valkenburgh, B., & Jenkins, I. (2002). Evolutionary patterns in the history of Permo-Triassic and Cenozoic synapsid predators. *Paleontological Society Papers*, 8, 267-288.
- Van Valkenburgh, B., Wang, X., & Damuth, J. (2004). Cope's rule, hypercarnivory, and extinction in North American canids. *Science*, *306*(5693), 101-104.
- Van Valkenburgh, B., & Wayne, R. K. (2010). Carnivores. *Current biology*, *20*(21), R915-R919.
- Valentine, J. W., Jablonski, D., Kidwell, S., & Roy, K. (2006). Assessing the fidelity of the fossil record by using marine bivalves. *Proceedings of the National Academy of Sciences*, 103(17), 6599-6604.

- Veevers, J. J., & Powell, C. M. (1987). Late Paleozoic glacial episodes in Gondwanaland reflected in transgressive-regressive depositional sequences in Euramerica. *Geological Society of America Bulletin*, *98*(4), 475.
- Venditti, C., Meade, A., & Pagel, M. (2010). Phylogenies reveal new interpretation of speciation and the Red Queen. *Nature*, 463(7279), 349-352.
- Venditti, C., Meade, A., & Pagel, M. (2011). Multiple routes to mammalian diversity. *Nature*, *479*(7373), 393-396.
- Voigt, S., and Ganzelewski, M. (2009). Toward the origin of amniotes: Diadectomorph and synapsid footprints from the early Late Carboniferous of Germany. *Acta Palaeontologica Polonica*, *55*(1), 57-72.
- Voje, K. L., Holen, Ø. H., Liow, L. H., & Stenseth, N. C. (2015). The role of biotic forces in driving macroevolution: beyond the Red Queen. *Proceedings of the Royal Society B: Biological Sciences*, *282*(1808), 20150186.
- Wagner, P. J., & Estabrook, G. F. (2014). Trait-based diversification shifts reflect differential extinction among fossil taxa. *Proceedings of the National Academy of Sciences*, *111*(46), 16419-16
- Wainwright, P. C. (2007). Functional versus morphological diversity in macroevolution. *Annual Review of Ecology, Evolution, and Systematics*, *38*.
- Wainwright, P. C., & Richard, B. A. (1995). Predicting patterns of prey use from morphology of fishes. *Environmental biology of fishes*, *44*(1), 97-113.
- Walmsley, C.W., et al. Why the long face? The mechanics of mandibular symphysis proportions in crocodiles. *PLoS One*, **8**, e53873 (2013).
- Wang X., Tedford R., and Antón M. (2008). Dogs: Their Fossil Relatives and Evolutionary History. Columbia University Press, Chichester.
- Warnes G. R., Bolker B., and Lumley T. (2020). gtools: Various R Programming Tools. R package version 3.8.2. https://CRAN.R-project.org/package=gtools
- Weber, M. G., Wagner, C. E., Best, R. J., Harmon, L. J., and Matthews, B. (2017). Evolution in a community context: on integrating ecological interactions and macroevolution. *Trends in ecology and evolution*, *32*(4), 291-304.
- Wei, H., Shen, J., Schoepfer, S. D., Krystyn, L., Richoz, S., & Algeo, T. J. (2015). Environmental controls on marine ecosystem recovery following mass extinctions, with an example from the Early Triassic. *Earth-Science Reviews*, *149*, 108-135.
- Weishampel, D. B. (1984). Interactions between Mesozoic plants and vertebrates: fructifications and seed predation. *Neues Jahrbuch für Geologie und Paläontologie. Abhandlungen*, *167*(2), 224-250.

- Weishampel, D. B., & Norman, D. B. (1989). Vertebrate herbivory in the Mesozoic. *Jaws, plants, and evolutionary metrics. Paleobiology of the Dinosaurs, ed Farlow JO (Geological Society of America, Boulder, CO), Special Paper*, *238*, 87-100.
- Westneat, M. W. (1994). Transmission of force and velocity in the feeding mechanisms of labrid fishes (Teleostei, Perciformes). *Zoomorphology*, 114, 103-118.
- Westneat, M. W. (2004). Evolution of levers and linkages in the feeding mechanisms of fishes. Integrative and Comparative Biology, 44(5), 378-389.
- White, E. P., Ernest, S. M., Kerkhoff, A. J. & Enquist, B. J. (2007). Relationships between body size and abundance in ecology. *Trends in Ecology & Evolution*. 22, 323–330
- Wickham. H. (2016). ggplot2: Elegant Graphics for Data Analysis. Springer-Verlag New York.
- Wignall, P. B., & Atkinson, J. W. (2020). A two-phased end-triassic mass extinction. *Earth-Science Reviews*, 103282.
- Williams, T.M., Wolfe, L., Davis, T., Kendall, T., Richter, B., Wang, Y., Bryce, C., Elkaim, G.H. and Wilmers, C.C., (2014). Instantaneous energetics of puma kills reveal advantage of felid sneak attacks. *Science*, 346(6205), .81-85.
- Wilson G. P., Evans A. R., Corfe IJ, Smits P. D., Fortelius M, Jernvall J. (2012). Adaptive radiation of multituberculate mammals before the extinction of dinosaurs. *Nature* 483:457–460.
- Wings, O., & Sander, P. M. (2007). No gastric mill in sauropod dinosaurs: new evidence from analysis of gastrolith mass and function in ostriches. *Proceedings of the Royal Society B: Biological Sciences*, *274*(1610), 635-640.
- Wu, Y., Chu, D., Tong, J., Song, H., Dal Corso, J., Wignall, P.B., Song, H., Du, Y. and Cui, Y., (2021). Six-fold increase of atmospheric pCO2 during the Permian–Triassic mass extinction. *Nature communications*, *12*(1), pp.1-8.
- Xie, W., Lewis, P. O., Fan, Y., Kuo, L., & Chen, M. H. (2011). Improving marginal likelihood estimation for Bayesian phylogenetic model selection. *Systematic biology*, *60*(2), 150-160.
- Xu, X., Upchurch, P., Mannion, P.D., Barrett, P.M., Regalado-Fernandez, O.R., Mo, J., Ma, J. and Liu, H., (2018). A new Middle Jurassic diplodocoid suggests an earlier dispersal and diversification of sauropod dinosaurs. *Nature communications*, *9*(1), 1-9.
- Yin, H., & Song, H. (2013). Mass extinction and Pangea integration during the Paleozoic-Mesozoic transition. *Science China Earth Sciences*, *56*(11), 1791-1803.
- Yu, G., Smith, D. K., Zhu, H., Guan, Y., & Lam, T. T. Y. (2017). ggtree: an R package for visualization and annotation of phylogenetic trees with their covariates and other associated data. Methods in Ecology and Evolution, 8(1), 28-36.

- Yuan, M. L., Jung, C., Wake, M. H., and Wang, I. J. (2020). Habitat use, interspecific competition and phylogenetic history shape the evolution of claw and toepad morphology in Lesser Antillean anoles. *Biological Journal of the Linnean Society*, *129*(3), 630-643.
- Zawiskie, J. M. (1986). Terrestrial vertebrate faunal succession during the Triassic. *The Beginning of the Age of Dinosaurs: Faunal Change Across the Triassic-Jurassic Boundary* (eds Padian, K.) 353–362. Cambridge University Press, Cambridge.

Appendix

A1.1 R code

Morphometric Analysis Code:

```
#Principal Component Analyses:
#Shape data (landmarks)
library(geomorph)
THbTr_GML.as<-arrayspecs(THbTr_GML.ds, 59, 2) #create 3d array from 2d landmark dataframe

plotAllSpecimens(THbTr_GML.as, mean = TRUE, links = NULL,) #pointscale = 0.5, meansize = 1) ### plot all specimens
PCA<-plotTangentSpace(THbTr_GML.as, warpgrids=T,) #label=TRUE, verbose=TRUE) ### make a simple morphospace of pc1 and pc2

PCA$pc.summary  ### variation on each axis
PCA$pc.scores   ### pc scores for each taxon on each morphospace axis
GMPCscores<-PCA$pc.scores #create PC scores object

#Functional data
library(FactoMineR)
THbTr_Fm<-read.csv(#read in raw functional data)
```

```
Thbt.pca.Zsc<-PCA(THbTr_Fm, scale.unit=T, ncp=10) #PCA of raw data includes z transformation (no logit transformation)
```

Mantel Test:

```
library(factoextra)
library(cluster)

#Shape PC scores
TArchM_PCscores<-TArch_tree.data[1:176, 9:115]
TArchM_PCscores
#Functional PC scores
TArchM_fPCscores<-TArch_tree.data[1:176, 116:123]
TArchM_fPCscores
#Generate Distance matrix of scaled data.
TArchM_FmPC_DM<-get_dist(TArchM_fPCscores, method="euclidean", stand=F)
TArch_GmPC_DM<-get_dist(TArchM_PCscores, method="euclidean", stand=F)
#View distance matrices.
heatmap(as.matrix(TArchM_FmPC_DM))
heatmap(as.matrix(TArch_GmPC_DM))

library(ade4)
Mantel.res<-mantel.rtest(TArch_GmPC_DM, TArchM_FmPC_DM, nrepet = 1000)
Mantel.res
```

DispRity Sum of Variance Disparity Analysis Code:

```
#Set working directory
library(ggplot2)
library(geoscale)
library(strap)
library(dispRity)

Arch.tree<-readRDS("Archosauromorpha_time-scaled_tree.rds")
TArch_tree.data<-read.csv("TArch_Phenogram_data.csv", row.names=1,header=T) #masterfile
```

```
PCdata<-TArch_tree.data[,9:115] #Shape data - pick one or the other
#PCdata<-TArch_tree.data[,116:123] #functional data
head(PCdata)
PCdataT<-as.matrix(PCdata)

fADlAD=TArch_tree.data[,124:125]

timesbinAge<-c(251.9, 251.2, 247.2, 242, 237, 232, 227, 220.83, 214.67, 208.5, 201.3, 199.3, 190.8,
182.7, 174.1) #2 Carnian & 3 Norian TB

##############Disparity calculations with bootstrapping and rarefaction##############
#Non-phylo method example
##TArch_disparity_data_PC<-dispRity(boot.matrix(chrono.subsets(PCdataT, Arch.tree, time =
timesbinAge, method = "discrete", FADLAD=fADlAD),
##                                  bootstraps = 1000, rarefaction = 2),
##                          metric = c(sum, variances))

#Phylogenetic example
###clade Subsets
TArchM_CldSubS_TreeALData<-read.csv("TArchM_CladeSubset_TreeALigned_Data.csv", header=T,
row.names = 1)

 #AvM
DinoPhyloData<-TArch_tree.data[1:73,]
DinoPhyloDataT<-as.matrix(DinoPhyloData)
DinoPhyloDataCleanUP<-clean.data(DinoPhyloDataT, Arch.tree.new.label)
DinoPD_Tree<-DinoPhyloDataCleanUP$tree
DinoPD_Tree$root.time<-245.5
geoscalePhylo(DinoPD_Tree, show.node.label = T)

AvMData<-TArchM_CldSubS_TreeALData[1:143,]
AvMDataPC<-AvMData[,9:115]
AvMDataPC<-AvMData[,116:123]
AvMDataBSz<-AvMData[,128]
```

```
AvMDataFADLAD<-AvMData[,124:125]

AvM_disparity_data_PC<-dispRity(boot.matrix(chrono.subsets(as.matrix(AvMDataPC), DinoPD_Tree,
time = timesbinAge, model="proximity", method = "c", FADLAD=AvMDataFADLAD),
                                    bootstraps = 1000, rarefaction = 2),
                          metric = c(sum, variances))
AvM_disparity_data_PC
plot(AvM_disparity_data_PC, type = "continuous")

#Psd
PsDPhyloData<-TArch_tree.data[74:137,]
PsDPhyloDataT<-as.matrix(PsDPhyloData)
PsDPhyloDataCleanUP<-clean.data(PsDPhyloDataT, Arch.tree.new.label)
PsDPD_Tree<-PsDPhyloDataCleanUP$tree
PsDPD_Tree$root.time<-250.7
geoscalePhylo(PsDPD_Tree, show.node.label = T)

PsDData<-TArchM_CldSubS_TreeALData[144:267,]
PsDDataPC<-PsDData[,9:115]
PsDDataPC<-PsDData[,116:123]
PsDDataBSz<-PsDData[,128]
PsDDataFADLAD<-PsDData[,124:125]

PsD_disparity_data_PC<-dispRity(boot.matrix(chrono.subsets(as.matrix(PsDDataPC), PsDPD_Tree,
time = timesbinAge, model="proximity", method = "c", FADLAD=PsDDataFADLAD),
                                    bootstraps = 1000, rarefaction = 2),
                          metric = c(sum, variances))
PsD_disparity_data_PC
plot(PsD_disparity_data_PC, type = "continuous")

#NCrArchM
NCrArchMPhyloData<-TArch_tree.data[138:176,]
NCrArchMPhyloDataT<-as.matrix(NCrArchMPhyloData)
NCrArchMPhyloDataCleanUP<-clean.data(NCrArchMPhyloDataT, Arch.tree.new.label)
```

```
NCrArchMPD_Tree<-NCrArchMPhyloDataCleanUP$tree
geoscalePhylo(NCrArchMPD_Tree, show.node.label = T)

NCrArchMData<-TArchM_CldSubS_TreeALData[268:345,]
NCrArchMDataPC<-NCrArchMData[,9:115]
NCrArchMDataPC<-NCrArchMData[,116:123]
NCrArchMDataBSz<-NCrArchMData[,128]
NCrArchMDataFADLAD<-NCrArchMData[,124:125]

NCrArchM_disparity_data_PC<-dispRity(boot.matrix(chrono.subsets(as.matrix(NCrArchMDataPC),
NCrArchMPD_Tree, time = timesbinAge, model="proximity", method = "c",
FADLAD=NCrArchMDataFADLAD),
                                bootstraps = 1000, rarefaction = 2),
                        metric = c(sum, variances))
NCrArchM_disparity_data_PC
plot(NCrArchM_disparity_data_PC, type = "continuous")

TArch_disparity_data_PC<-dispRity(boot.matrix(chrono.subsets(PCdataT, Arch.tree.new.label, time =
timesbinAge, model="proximity", method = "c", FADLAD=fADlAD),
                                 bootstraps = 1000, rarefaction = 2),
                         metric = c(sum, variances))
TArch_disparity_data_PC
plot(TArch_disparity_data_PC, type = "continuous")

#####Creating results output##########
#Get disparity values.
TArch.SOV.final <- summary(TArch_disparity_data_PC, quantiles = c(50,90,95), cent.tend = mean,
digits = 10)
###
#SAVE THESE INTO AN EXCEL FILE - COPY AND PASTE.
TArch.metric.plot <- TArch.SOV.final # i do this here so it is easier to change the metric I plot - you can
cut and paste
TArch.metric.plot
```

```
TArch.plot.data <-
c(as.integer(rownames(TArch.metric.plot[match(unique(TArch.metric.plot$subset),
TArch.metric.plot$subset),])))
TArch.plot.data
TArch.main.res <- TArch.metric.plot[, "bs.mean"][TArch.plot.data] # select rows required
TArch.lower <- TArch.metric.plot[, "2.5%"][TArch.plot.data] # select rows required
TArch.upper <- TArch.metric.plot[, "97.5%"][TArch.plot.data] # select rows required

####NPMANOVA Between Timebins##########
Time_subsets<-(chrono.subsets(PCdataT, Arch.tree, time = timesbinAge, method = "discrete",
FADLAD=fADlAD))
TArch_disp_NPMNV<-#adonis.dispRity(Time_subsets)
 adonis.dispRity(Time_subsets, matrix ~ chrono.subsets)
#Uses the adonis function from Vegan R package.
TArch_disp_NPMNV
```

Macroevolutionary model fitting:

```
TArchModel_stasis_disp_time <- model.test(data = TArch_disparity_data_PC, model = c("BM", "EB",
"OU", "Stasis", "Trend"),
                                pool.variance = NULL)
NCrArchModel_stasis_disp_time <- model.test(data = NCrArchM_disparity_data_PC, model =
c("BM", "EB", "OU", "Stasis", "Trend"),
                                  pool.variance = NULL)
PsdModel_stasis_disp_time <- model.test(data = PsD_disparity_data_PC, model = c("BM", "EB",
"OU", "Stasis", "Trend"),
                               pool.variance = NULL)
DinoModel_stasis_disp_time <- model.test(data = AvM_disparity_data_PC, model = c("BM", "EB",
"OU", "Stasis", "Trend"),
                               pool.variance = NULL)
```

Mean Pairwise Distance Disparity Analysis Code:

```
## This function isolates one half of a distance matrix
upperTriangle<-function (x, diag = FALSE, byrow = FALSE)
{
```

```
  if (byrow)
    t(x)[rev(upper.tri(x, diag = diag))]
  else x[upper.tri(x, diag = diag)]
}

## This function calculates the mean pairwise distance within a bin and runs bootstrapping to create
error bars around mean
bootstrapMPD <- function(dissim) {

  dissim <- upperTriangle(dissim)

  mean <- mean(dissim, na.rm=TRUE)

  Z <- length(dissim[complete.cases(dissim)])

  boot.mean <- vector()

  for(i in 1:10000) {
    boot.mean[i] <- mean(dissim[complete.cases(dissim)][sample.int(Z,Z,replace=TRUE)])
  }

  #Lower 0.05 for the mean
  lower <- sort(boot.mean)[length(boot.mean)*0.05]

  #Upper 0.95 for the mean
  upper <- sort(boot.mean)[length(boot.mean)*0.95]

  return(cbind(mean,lower,upper))

}

### This function can extract certain groups from distance matrix
extractPairwise <- function(dMat, listGroups) {
```

```
  dMatNames <- rownames(dMat)
  outputList <- c()
  for(i in 1:length(listGroups)) {
    rowColName <- match(listGroups[[i]], dMatNames)
    rowColName <- rowColName[complete.cases(rowColName)]
    outputList[[i]] <- dMat[rowColName, rowColName]
  }
  names(outputList) <- names(listGroups)
  return(outputList)
}

###Load data - distance matrices of shape or standardised functional data
#######Assign data
proc.dist <- #read.csv(Distance matrix object)
head(proc.dist)
dim(proc.dist)

#assign taxa to bin based on taxon ranges
#Taxa MUST be in same order and names must match exactly!
taxon.ranges <- read.table("taxon.ranges.txt", header=T, row.names=1)

# Rearrange taxon ages object to match the order of the procustes distances object
# The proc dist object is usually ordered based on the sequence which the landmarks were acquired
taxon.ranges <- as.data.frame(taxon.ranges[rownames(proc.dist),])
dim(taxon.ranges)
taxon.ranges # does this still look OK?

# are the row names of the taxon ages and dissim matrix identical?
identical(rownames(taxon.ranges), rownames(proc.dist))

# Need object denoting the range of time bins to place taxa in
bin.ranges <- #read.table(timebin ranges)
bin.ranges
```

```
# Assign the taxa to bins based on the range and dates, in the object 'taxon.bins'
taxon.bins <- list()
for (i in 1:length(rownames(bin.ranges))) {taxon.bins[[i]] <-
rownames(taxon.ranges)[which(taxon.ranges$FAD > bin.ranges[i,"min.age"] & taxon.ranges$LAD <
bin.ranges[i,"max.age"])]}
names(taxon.bins) <- rownames(bin.ranges)
taxon.bins # view the object, does it look OK?

# note the taxon bins object could be time bins or clade bins etc, to make clade file you would need
to use different code to make list
# something like
# inputList <- list(group_1_list, group_2_list,group_3_list ,group_4_list)
# names(inputList) <- c("group_1", "group_2", "group_3", "group_4")
# inputList # does this look correct, are the correct names in the correct group?

### Within bin Mean Pairwise Procrustes Distances
# Using the function I made earlier 'extractPairwise' I will now create a separate Procruestes
distances object object for each time bin
binned.proc.dist <- extractPairwise(proc.dist, taxon.bins)
binned.proc.dist # this is a large object with a distance matrix for each time bin

binned.proc.dist[[1]] # view the distance object for time bin 1
# you could always save the original full distance matrix outside of R and check to see that the
distances in there are the same as those in these bin subsets

# Now I will use the bootstrapMPD function to calculate the mean Procrustes distance between taxa
in each time bin that I have

# Make empty results object to save
MPD.results <-  matrix(NA, nrow=length(taxon.bins), ncol=3)

# for each time bin, it will calculated the MPD for the taxa within it
for(i in 1:length(taxon.bins)) {
  MPD.results [i,] <- bootstrapMPD(binned.proc.dist[[i]])
```

```
}

colnames(MPD.results) <- c("mean", "lower", "upper")
rownames(MPD.results) <- names(taxon.bins)
MPD.results
```

WANG's Permutation test code:

```
TArch_tree.data <-read in csv file.

#Set data
TArchM_Mfile<-TArch_tree.data[1:176,]
#Shape PC scores
TArchM_PCscores<-TArch_tree.data[1:176, 9:115]
TArchM_PCscores
#Functional PC scores
TArchM_fPCscores<-TArch_tree.data[1:176, 116:123]
TArchM_fPCscores

#Groups
Clade2<-TArch_tree.data[1:176, 127]
Clade3<-TArch_tree.data[1:176, 128]
pc.scores<-as.matrix(TArchM_PCscores)
groups.list<-Clade3

#pc.scores <- as.matrix(all.data[,1:10]) # select pc scores
#groups.list <-  all.data[,17] # select column with group names - just two groups

 group2 <- row.names(TArchM_Mfile)[TArchM_Mfile [,'Clade3'] == "B_PsD"]
group1 <- row.names(TArchM_Mfile)[TArchM_Mfile [,'Clade3'] == "A_BArchM"]
groups.list <-list(group1, group2)
groups.list

# This is where the calculation is performed.
disparity.data <- dispRity.per.group(pc.scores, group = groups.list, metric = c(sum, variances))
```

```
#Print and summarise the disparity.data object
disparity.data
summary(disparity.data)

obsdiff <- summary(disparity.data)$obs[2] - summary(disparity.data)$obs[1]
obsdiff # the difference in disparity between group 1 and group 2
plot(disparity.data) # this plots the bootstrapped results
numreps <- 500            # number of repetitions to run for permutations
results <- rep(NA, numreps)  # vector to store results

# loop over repetitions
for(rep in 1:numreps)  {

  groups.list.rand <- list()
  all.taxa <- c(groups.list[[1]], groups.list[[2]])
  groups.list.rand$group1  <- sample(all.taxa, size=length(groups.list[[1]]))
  groups.list.rand$group2  <- sample(all.taxa , size=length(groups.list[[2]]))

  disparity.results <- dispRity.per.group(pc.scores, group = groups.list.rand, metric = c(sum,
variances))
  summary(disparity.results)$obs
  shufdiff <- summary(disparity.results)$obs[2] - summary(disparity.results)$obs[1]
  # store result
  results[rep] <- shufdiff
}

results # here are the disparity differences from randomized groupings
# this is where we do the stats - is there a significant difference between the observed
#difference in disparity between groups 1 and 2. We calcualted earlier (obsdiff) when compared
#to differences in disparity between randomly generated groupings.

# empirical mean of simulated results
expdiff <- mean(results)
```

```
expdiff

# determine empirical (Monte Carlo) p-value
# this is a two-sided p-value; adjust accordingly for one-sided
pval <- sum(abs(results-expdiff) >= abs(obsdiff-expdiff)) / numreps
pval

# output results
cat('observed difference');  obsdiff
cat('expected difference');  expdiff
cat('p-value');  pval
```

Cluster Analysis Code:

```
library(factoextra)
Fdata<- #Read in the functional measurement data
Fdata<-scale(Ing_Gen_dat, center=T, scale=T) #scale and center the data

#Hierarchical Analysis - Exploratory.
FMres.hc <- eclust(Fdata, FUNcluster = "hclust",  k.max=10, hc_metric="euclidean",
hc_method="ward.D2", nboot=4000)
#Specify range of cluster numbers to consider classifying taxa into. #Cluster range set as used in
analysis for ingestion generalists).
FMres.hc.IG_RV <- eclust(Fdata, FUNcluster = "hclust",  k.max=2,3,4,5,6,7,8, hc_metric="euclidean",
hc_method="ward.D2", nboot=4000)

FMres.hc
FMres.hc_$cluster #View cluster assignments for each taxon
FMres.hc.PG_RV$cluster

plot(FMres.hc, cex = 0.5)
plot(FMres.hc.IG_RV, cex = 0.5)

#############Partition Cluster Methods
#K-means Analysis #for PAM, in FUNcluster replace “kmeans” with “pam”
```

```
##Cluster range set as used in analysis for all taxa.
FMres.Km<-eclust(Fdata, FUNcluster = "kmeans", k.max=4,5,6,7,8, nstart=200, nboot=4000)
#Cluster range set as used in analysis for ingestion generalists.
FMres.Km.PG_RV<-eclust(Fdata, FUNcluster = "kmeans", k.max=2,3,4,5,6,7,8, nstart=200,
nboot=4000)

FMres.Km
FMres.Km$cluster #View cluster assignments for each taxon
```

Ancestral State Reconstruction Code:

```
#Continuous data
library(mvMORPH)
NA_test<-na.omit(TArchTre.data)
fit<-mvBM(tree.test, NA_test, model="BMM", method="sparse")
Test_reconstr<-estim(tree.test, TArchTre.data, fit, error=NULL, asr=FALSE)
Test_reconstr$estimates

#Discrete data
library(phytools)
library(strap)

#Load tree
SPM.tree.data<-load("Sauropodomorpha.timescaled.Workspace.RData")
SPM.tree<-myclade.ts.trees[[1]]

SPM.tree$tip.label

#load data
SPM.data<-read.csv('SauPM_PhyloData_08_2021.csv')

#Set data
feed.mode<-setNames(SPM.data[,81],(SPM.data[,1]))
x<- feed.mode
```

```
#Fit Equal Rates (ER) model
fitER<-ace(feed.mode,SPM.tree, model="ER",type="discrete")
fitER
fitER$lik.anc

#Fit All Rates Different (ARD) model
fitARD<-ace(x, SPM.tree,model="ARD",type="discrete")
fitARD

#######fit Symmetrical (SYM) model
fitSYM<-ace(x, SPM.tree, model="SYM",type="discrete", CI=T)
fitSYM
```

A1.2 Complete taxon sampling for mandibular data in each chapter with additional clade and duration data.

Inclusion in chapter indicated by Y (yes) or N (no). Clade abbreviations: AETO, Aetosauria. ALK, Allokotosauria. ANO, Anomodontia. APH, Aphanosauria. ARCHM, Archosauromorpha. ARF, Archosauriformes. BIA, Biarmosuchia. CAS, Caseasauria. Ch, Chapter. CROC, Crocodylomorpha. CYN, Cynodontia. DNC, Dinocephalia. EDA, Edaphosauridae. ERP, Erpetosuchidae. GRA, Gracilisuchidae. GRG, Gorgonopsia, HRR, Herrerasauridae. MML, Mammaliamorpha. OPH, Ophiacodontidae. ORN, Ornithischia. ORS, Ornithosuchidae. OW, Owenettidae. PARA, Paracrocodylomorpha. PHYT, Phytosauria. PROCL, Procolophonoidea. PROL, Prolacertidae. PTR, Pterosauria. RHYN, Rhynchosauria. SIL, Silesauridae. SPD, Sauropodomorpha. SPH, Sphenacodontia. THC, Therocephalia. THP, Theropoda. TNY, Tanystropheidae. VAR, Varanopidae.

Taxa	**Clade**	**Sub-clade**	**FAD**	**LAD**	**Ch. 1**	**Ch. 2.1**	**Ch. 3.1**	**Ch. 3.2**	**Ch. 4.1**
Casea Broilii	Synapsida	CAS	283.5	272.95	Y	Y	N	N	N
Cotylorhynchus romeri	Synapsida	CAS	272.3	268.8	Y	Y	N	N	N
Ennatosaurus tecton	Synapsida	CAS	268.8	265.1	Y	Y	N	N	N

Martensius bromackerensis	Synapsida	CAS	290.1	283.5	Y	Y	N	N	N
Edaphosaurus boanerges	Synapsida	EDA	290.1	283.5	Y	Y	N	N	N
Edaphosaurus cruciger	Synapsida	EDA	290.1	272.95	Y	Y	N	N	N
Edaphosaurus pogonias	Synapsida	EDA	283.5	272.95	Y	Y	N	N	N
Glaucosaurus megalops	Synapsida	EDA	283.5	272.95	Y	Y	N	N	N
Gordodon kraineri	Synapsida	EDA	303.7	298.9	Y	Y	N	N	N
Eothyris parkeyi	Synapsida	CAS	290.1	283.5	Y	Y	Y	N	N
Vaughnictis smithae	Synapsida	CAS	298.9	295	Y	Y	Y	N	N
Ophiacodon uniformis	Synapsida	OPH	295	272.95	Y	Y	Y	N	N
Ophiacodon mirus	Synapsida	OPH	303.7	295	Y	Y	Y	N	N
Ophiacodon retroversus	Synapsida	OPH	295	283.5	Y	Y	Y	N	N
Stereorachis dominans	Synapsida	OPH	303.7	298.9	Y	Y	Y	N	N
Varanosaurus acutirostris	Synapsida	OPH	290.1	272.95	Y	Y	Y	N	N
Cutleria wilmarthi	Synapsida	SPH	298.9	295	Y	Y	Y	N	N
Dimetrodon grandis	Synapsida	SPH	283.5	272.95	Y	Y	Y	N	N
Dimetrodon limbatus	Synapsida	SPH	290.1	283.5	Y	Y	Y	N	N
Dimetrodon loomisi	Synapsida	SPH	283.5	272.95	Y	Y	Y	N	N
Dimetrodon milleri	Synapsida	SPH	295	290.1	Y	Y	Y	N	N
Dimetrodon natalis	Synapsida	SPH	290.1	283.5	Y	Y	Y	N	N
Haptodus garnettensis	Synapsida	SPH	307	303.7	Y	Y	Y	N	N
Haptodus baylei	Synapsida	SPH	295	290.1	Y	Y	Y	N	N
Ianthodon schultzei	Synapsida	SPH	307	303.7	Y	Y	Y	N	N
Palaeohatteria longicaudata	Synapsida	SPH	290.1	283.5	Y	Y	Y	N	N
Pantelosaurus saxonicus	Synapsida	SPH	298.9	295	Y	Y	Y	N	N
Secodontosaurus obtusidens	Synapsida	SPH	290.1	272.95	Y	Y	Y	N	N

Sphenacodon ferocior	Synapsida	SPH	298.9	295	Y	Y	Y	N	N
Sphenacodon ferox	Synapsida	SPH	298.9	290.1	Y	Y	Y	N	N
Tetraceratops insignis	Synapsida	SPH	283.5	272.95	Y	Y	Y	N	N
Aerosaurus wellesi	Synapsida	VAR	298.9	295	Y	Y	Y	N	N
Anningia megalops	Synapsida	VAR	265.1	259.1	Y	Y	Y	N	N
Archaeovenator hamiltonensis	Synapsida	VAR	303.7	298.9	Y	Y	Y	N	N
Ascendonanus nestleri	Synapsida	VAR	295	290.1	Y	Y	Y	N	N
Elliotsmithia longiceps	Synapsida	VAR	265.1	259.1	Y	Y	Y	N	N
Euromycter rutenus	Synapsida	VAR	272.95	265.1	Y	Y	Y	N	N
Heleosaurus scholtzi	Synapsida	VAR	265.1	259.1	Y	Y	Y	N	N
Mesenosaurus romeri	Synapsida	VAR	268.8	265.1	Y	Y	Y	N	N
Microvaranops parentis	Synapsida	VAR	265.1	259.1	Y	Y	Y	N	N
Mycterosaurus longiceps	Synapsida	VAR	290.1	272.95	Y	Y	Y	N	N
Varanodon agilis	Synapsida	VAR	272.95	268.8	Y	Y	Y	N	N
Varanops brevirostris	Synapsida	VAR	290.1	272.95	Y	Y	Y	N	N
Anomocephalus africanus	Synapsida	ANO	265.1	259.1	Y	Y	N	N	N
Biseridens qilianicus	Synapsida	ANO	268.8	265.1	Y	Y	N	N	N
Angonisaurus cruickshanki	Synapsida	ANO	247.2	237	Y	Y	N	Y	N
Aulacephalodon bainii	Synapsida	ANO	259.1	251.9	Y	Y	N	N	N
Australobarbarus kotelnitshi	Synapsida	ANO	265.1	259.1	Y	Y	N	N	N
Basilodon woodwardi	Synapsida	ANO	259.1	251.9	Y	Y	N	N	N
Brachyprosopus broomi	Synapsida	ANO	265.1	259.1	Y	Y	N	N	N
Bulbasaurus phylloxyron	Synapsida	ANO	259.1	254.14	Y	Y	N	N	N
Cistecephaloides boonstrai	Synapsida	ANO	259.1	254.14	Y	Y	N	N	N

Cistecephalus microrhinus	Synapsida	ANO	259.1	254.14	Y	Y	N	N	N
Daptocephalus leoniceps	Synapsida	ANO	259.1	251.9	Y	Y	N	N	N
Daqingshanodon limbus	Synapsida	ANO	254.14	251.9	Y	Y	N	N	N
Dicynodon angielczyki	Synapsida	ANO	259.1	254.14	Y	Y	N	N	N
Dicynodon lacerticeps	Synapsida	ANO	259.1	251.9	Y	Y	N	N	N
Dicynodontoides nowacki	Synapsida	ANO	265.1	251.9	Y	Y	N	N	N
Diictodon feliceps	Synapsida	ANO	265.1	251.9	Y	Y	N	N	N
Diictodontoides skaios	Synapsida	ANO	259.1	254.14	Y	Y	N	N	N
Dinanomodon gilli	Synapsida	ANO	259.1	251.9	Y	Y	N	N	N
Dinodontosaurus pedroanum	Synapsida	ANO	242	232	Y	Y	N	Y	N
Dolichuranus primaevus	Synapsida	ANO	247.2	242	Y	Y	N	Y	N
Emydops oweni	Synapsida	ANO	265.1	251.9	Y	Y	N	N	N
Endothiodon mahalanobisi	Synapsida	ANO	265.1	254.14	Y	Y	N	N	N
Eodicynodon oelofseni	Synapsida	ANO	268.8	265.1	Y	Y	N	N	N
Eosimops newtoni	Synapsida	ANO	265.1	259.1	Y	Y	N	N	N
Galechirus scholtzi	Synapsida	ANO	265.1	259.1	Y	Y	N	N	N
Gordonia traquairi	Synapsida	ANO	254.14	251.9	Y	Y	N	N	N
Idelesaurus tataricus	Synapsida	ANO	259.1	254.14	Y	Y	N	N	N
Ischigualastia jenseni	Synapsida	ANO	232	201.3	Y	Y	N	Y	N
Jachaleria colorata	Synapsida	ANO	227	220.83	Y	Y	N	Y	N
Jimusaria sinkianensis	Synapsida	ANO	254.14	251.9	Y	Y	N	N	N
Kannemeyeria latirostris	Synapsida	ANO	247.2	242	Y	Y	N	Y	N
Katumbia parringtoni	Synapsida	ANO	259.1	254.14	Y	Y	N	N	N
Kawingasaurus fossilis	Synapsida	ANO	259.1	254.14	Y	Y	N	N	N
Kembawacela kitchingi	Synapsida	ANO	259.1	251.9	Y	Y	N	N	N

Kitchinganomodon crassus	Synapsida	ANO	254.14	251.2	Y	Y	N	N	N
Lisowicia bojani	Synapsida	ANO	208.5	201.3	Y	Y	N	Y	N
Lystrosaurus hedini	Synapsida	ANO	254.14	251.2	Y	Y	N	Y	N
Lystrosaurus maccaigi	Synapsida	ANO	254.14	251.2	Y	Y	N	Y	N
Lystrosaurus murrayi	Synapsida	ANO	251.9	247.2	Y	Y	N	Y	N
Lystrosaurus robustus	Synapsida	ANO	251.9	251.2	Y	Y	N	Y	N
Moghreberia nmachouensis	Synapsida	ANO	232	227	Y	Y	N	Y	N
Myosaurus gracilis	Synapsida	ANO	251.9	251.2	Y	Y	N	Y	N
Niassodon mfumukasi	Synapsida	ANO	259.1	254.14	Y	Y	N	N	N
Odontocyclops whaitsi	Synapsida	ANO	259.1	254.14	Y	Y	N	N	N
Oudenodon bainii	Synapsida	ANO	259.1	251.9	Y	Y	N	N	N
Parakannemeyeria ningwuensis	Synapsida	ANO	247.2	242	Y	Y	N	Y	N
Peramodon amalitzkii	Synapsida	ANO	259.1	251.9	Y	Y	N	N	N
Placerias hesternus	Synapsida	ANO	232	214.67	Y	Y	N	Y	N
Pristerodon mackayi	Synapsida	ANO	265.1	251.9	Y	Y	N	N	N
Prosictodon dubei	Synapsida	ANO	265.1	259.1	Y	Y	N	N	N
Rastodon procurvidens	Synapsida	ANO	265.1	259.1	Y	Y	N	N	N
Rhachiocephalus magnus	Synapsida	ANO	259.1	251.9	Y	Y	N	N	N
Rhinodicynodon gracile	Synapsida	ANO	247.2	242	Y	Y	N	Y	N
Robertia broomiana	Synapsida	ANO	265.1	259.1	Y	Y	N	N	N
Sangusaurus parringtonii	Synapsida	ANO	242	237	Y	Y	N	N	N
Sauroscaptor tharavati	Synapsida	ANO	259.1	254.14	Y	Y	N	N	N
Shaanbeikannemeyeria buerdongia	Synapsida	ANO	247.2	242	Y	Y	N	Y	N
Shansiodon wangi	Synapsida	ANO	247.2	242	Y	Y	N	Y	N
Sinokannemeyeria yingchiaoensis	Synapsida	ANO	247.2	242	Y	Y	N	Y	N
Stahleckeria potens	Synapsida	ANO	242	232	Y	Y	N	Y	N

Tetragonias njalilus	Synapsida	ANO	242	237	Y	Y	N	Y	N
Thliptosaurus imperforatus	Synapsida	ANO	254.14	251.9	Y	Y	N	N	N
Tropidostoma dubium	Synapsida	ANO	259.1	254.14	Y	Y	N	N	N
Vivaxosaurus trautscholdi	Synapsida	ANO	259.1	251.9	Y	Y	N	N	N
Wadiasaurus indicus	Synapsida	ANO	247.2	242	Y	Y	N	Y	N
Xiyukannemeyeria brevirostris	Synapsida	ANO	247.2	242	Y	Y	N	Y	N
Galeops whaitsi	Synapsida	ANO	265.1	259.1	Y	Y	N	N	N
Galepus jouberti	Synapsida	ANO	265.1	259.1	Y	Y	N	N	N
Geikia elginensis	Synapsida	ANO	259.1	251.9	Y	Y	N	N	N
Patranomodon nyaphulii	Synapsida	ANO	268.8	265.1	Y	Y	N	N	N
Suminia getmanovi	Synapsida	ANO	265.1	259.1	Y	Y	N	N	N
Ulemica invisa	Synapsida	ANO	268.8	259.1	Y	Y	N	N	N
Venyukovia prima	Synapsida	ANO	268.8	265.1	Y	Y	N	N	N
Alrausuchus tagax	Synapsida	BIA	268.8	265.1	Y	Y	Y	N	N
Biarmosuchus tener	Synapsida	BIA	268.8	265.1	Y	Y	Y	N	N
Herpetoskylax hopsoni	Synapsida	BIA	259.1	254.14	Y	Y	Y	N	N
Hipposaurus boonstrai	Synapsida	BIA	265.1	259.1	Y	Y	Y	N	N
Ictidorhinus martinsi	Synapsida	BIA	254.14	251.9	Y	Y	Y	N	N
Lemurosaurus pricei	Synapsida	BIA	259.1	254.14	Y	Y	Y	N	N
Lende chiweta	Synapsida	BIA	259.1	254.14	Y	Y	Y	N	N
Leucocephalus wewersi	Synapsida	BIA	259.1	254.14	Y	Y	Y	N	N
Lobalopex mordax	Synapsida	BIA	259.1	254.14	Y	Y	Y	N	N
Niaftasuchus zekkeli	Synapsida	BIA	268.8	265.1	Y	Y	Y	N	N
Nikkasaurus tatarinovi	Synapsida	BIA	268.8	265.1	Y	Y	Y	N	N
Phthinosuchus discors	Synapsida	BIA	268.8	265.1	Y	Y	Y	N	N
Proburnetia viatkensis	Synapsida	BIA	265.1	259.1	Y	Y	Y	N	N
Reiszia gubini	Synapsida	BIA	268.8	265.1	Y	Y	Y	N	N
Charassognathus gracilis	Synapsida	CYN	259.1	254.14	Y	Y	Y	N	N

Dvinia prima	Synapsida	CYN	259.1	251.9	Y	Y	Y	N	N
Galesaurus planiceps	Synapsida	CYN	251.9	251.2	Y	Y	Y	N	N
Lumkuia fuzzi	Synapsida	CYN	247.2	242	Y	Y	N	N	N
Madysaurus sharovi	Synapsida	CYN	237	232	Y	Y	N	N	N
Nanictosaurus kitchingi	Synapsida	CYN	259.1	251.9	Y	Y	Y	N	N
Platycraniellus elegans	Synapsida	CYN	251.9	251.2	Y	Y	Y	N	N
Procynosuchus delaharpeae	Synapsida	CYN	259.1	251.9	Y	Y	Y	N	N
Progalesaurus lootsbergensis	Synapsida	CYN	251.9	251.2	Y	Y	Y	N	N
Thrinaxodon liorhinus	Synapsida	CYN	251.9	247.2	Y	Y	Y	N	N
Trucidocynodon riograndensis	Synapsida	CYN	232	227	Y	Y	N	N	N
Vetusodon elikhulu	Synapsida	CYN	254.14	251.9	Y	Y	Y	N	N
Andescynodon mendozensis	Synapsida	CYN	247.2	242	Y	Y	N	Y	N
Boreogomphodon jeffersoni	Synapsida	CYN	232	220.83	Y	Y	N	Y	N
Cricodon metabolus	Synapsida	CYN	247.2	232	Y	Y	N	Y	N
Cynognathus crateronotus	Synapsida	CYN	251.2	232	Y	Y	N	Y	N
Dadadon isaloi	Synapsida	CYN	237	232	Y	Y	N	Y	N
Diademodon tetragonus	Synapsida	CYN	247.2	232	Y	Y	N	Y	N
Etjoia dentitransitus	Synapsida	CYN	247.2	242	Y	Y	N	Y	N
Exaeretodon argentinus	Synapsida	CYN	232	220.83	Y	Y	N	Y	N
Langbergia modisei	Synapsida	CYN	251.2	247.2	Y	Y	N	Y	N
Luangwa drysdalli	Synapsida	CYN	242	232	Y	Y	N	Y	N
Massetognathus pascuali	Synapsida	CYN	242	232	Y	Y	N	Y	N
Menadon besairiei	Synapsida	CYN	237	232	Y	Y	N	Y	N

Pascualgnathus polanskii	Synapsida	CYN	237	232	Y	Y	N	Y	N
Ruberodon roychowdhurii	Synapsida	CYN	232	227	Y	Y	N	Y	N
Sinognathus gracilis	Synapsida	CYN	247.2	242	Y	Y	N	Y	N
Siriusgnathus niemeyerorum	Synapsida	CYN	232	220.83	Y	Y	N	Y	N
Traversodon stahleckeri	Synapsida	CYN	242	232	Y	Y	N	Y	N
Trirachodon berryi	Synapsida	CYN	247.2	242	Y	Y	N	Y	N
Aleodon cromptoni	Synapsida	CYN	242	232	Y	Y	N	N	N
Bonacynodon schultzi	Synapsida	CYN	242	232	Y	Y	N	N	N
Chiniquodon sanjuanensis	Synapsida	CYN	220.83	214.67	Y	Y	N	N	N
Cromptodon mamiferoides	Synapsida	CYN	242	227	Y	Y	N	N	N
Dromatherium sylvestre	Synapsida	CYN	247.2	242	Y	Y	N	N	N
Ecteninion lunensis	Synapsida	CYN	199.3	190.8	Y	Y	N	N	N
Microconodon tenuirostris	Synapsida	CYN	227	220.83	Y	Y	N	N	N
Probainognathus jenseni	Synapsida	CYN	232	227	Y	Y	N	N	N
Protheriodon estudianti	Synapsida	CYN	232	220.83	Y	Y	N	N	N
Prozostrodon brasiliensis	Synapsida	CYN	208.5	190.8	Y	Y	N	N	N
Chaliminia musteloides	Synapsida	CYN	237	232	Y	Y	N	N	N
Diarthrognathus broomi	Synapsida	CYN	242	232	Y	Y	N	N	N
Pachygenelus monus	Synapsida	CYN	232	227	Y	Y	N	N	N
Riograndia guaibensis	Synapsida	CYN	227	220.83	Y	Y	N	N	N
Bienotherium yunnanense	Synapsida	MML	199.3	190.8	Y	Y	N	Y	N

Bocatherium mexicanum	Synapsida	MML	190.8	182.7	Y	Y	N	Y	N
Kayentatherium wellesi	Synapsida	MML	190.8	182.7	Y	Y	N	Y	N
Oligokyphus major	Synapsida	MML	208.5	182.7	Y	Y	N	Y	N
Tritylodon longaevus	Synapsida	MML	201.3	190.8	Y	Y	N	Y	N
Yunnanodon brevirostre	Synapsida	MML	199.3	190.8	Y	Y	N	Y	N
Brasilitherium riograndensis	Synapsida	MML	227	220.83	Y	Y	N	N	N
Brasilodon quadrangularis	Synapsida	MML	227	220.83	Y	Y	N	N	N
Minicynodon maieri	Synapsida	MML	227	220.83	Y	Y	N	N	N
Sinoconodon rigneyi	Synapsida	MML	199.3	190.8	Y	Y	N	N	N
Erythrotherium parringtoni	Synapsida	MML	201.3	190.8	Y	Y	N	N	N
Megazostrodon rudnerae	Synapsida	MML	208.5	190.8	Y	Y	N	N	N
Morganucodon watsoni	Synapsida	MML	208.5	190.8	Y	Y	N	N	N
Argentoconodon fariasorum	Synapsida	MML	182.7	174.1	Y	Y	N	N	N
Dinnetherium nezorum	Synapsida	MML	190.8	182.7	Y	Y	N	N	N
Hadrocodium wui	Synapsida	MML	199.3	190.8	Y	Y	N	N	N
Haramiyavia clemmenseni	Synapsida	MML	208.5	201.3	Y	Y	N	N	N
Kuehneotherium praecursoris	Synapsida	MML	208.5	190.8	Y	Y	N	N	N
Anteosaurus magnificus	Synapsida	DNC	265.1	259.1	Y	Y	Y	N	N
Australosyodon nyaphuli	Synapsida	DNC	268.8	265.1	Y	Y	Y	N	N
Deuterosaurus biarmicus	Synapsida	DNC	268.8	265.1	Y	Y	Y	N	N

Estemmenosuchus uralensis	Synapsida	DNC	268.8	265.1	Y	Y	N	N	N
Jonkeria truculenta	Synapsida	DNC	265.1	259.1	Y	Y	Y	N	N
Mormosaurus seeleyi	Synapsida	DNC	265.1	259.1	Y	Y	N	N	N
Moschognathus whaitsi	Synapsida	DNC	265.1	259.1	Y	Y	N	N	N
Moschops capensis	Synapsida	DNC	265.1	259.1	Y	Y	N	N	N
Pampaphoneus biccai	Synapsida	DNC	265.1	259.1	Y	Y	Y	N	N
Phthinosaurus borissiaki	Synapsida	DNC	272.3	268.8	Y	Y	Y	N	N
Riebeeckosaurus longirostris	Synapsida	DNC	265.1	259.1	Y	Y	N	N	N
Sinophoneus yumenensis	Synapsida	DNC	268.8	265.1	Y	Y	Y	N	N
Styracocephalus platyrhynchus	Synapsida	DNC	265.1	259.1	Y	Y	N	N	N
Syodon biarmicum	Synapsida	DNC	268.8	265.1	Y	Y	Y	N	N
Tapinocaninus pamelae	Synapsida	DNC	268.8	265.1	Y	Y	Y	N	N
Tapinocephalus	Synapsida	DNC	265.1	259.1	Y	Y	N	N	N
Titanophoneus potens	Synapsida	DNC	268.8	259.1	Y	Y	Y	N	N
Ulemosaurus svijagensis	Synapsida	DNC	268.8	259.1	Y	Y	N	N	N
Aelurognathus tigriceps	Synapsida	GRG	259.1	251.9	Y	Y	Y	N	N
Aelurosaurus felinus	Synapsida	GRG	259.1	251.9	Y	Y	Y	N	N
Aloposaurus gracilis	Synapsida	GRG	259.1	254.14	Y	Y	Y	N	N
Aloposaurus tenuis	Synapsida	GRG	259.1	251.9	Y	Y	Y	N	N
Arctognathus curvimola	Synapsida	GRG	259.1	251.9	Y	Y	Y	N	N
Arctops willistoni	Synapsida	GRG	259.1	254.14	Y	Y	Y	N	N
Clelandina rubidgei	Synapsida	GRG	259.1	251.9	Y	Y	Y	N	N
Cynariops robustus	Synapsida	GRG	259.1	254.14	Y	Y	Y	N	N
Cyonosaurus longiceps	Synapsida	GRG	259.1	254.14	Y	Y	Y	N	N

Dinogorgon rubidgei	Synapsida	GRG	259.1	251.9	Y	Y	Y	N	N
Dixeya nasuta	Synapsida	GRG	259.1	254.14	Y	Y	Y	N	N
Eriphostoma microdon	Synapsida	GRG	265.1	259.1	Y	Y	Y	N	N
Gorgonops torvus	Synapsida	GRG	265.1	254.14	Y	Y	Y	N	N
Inostrancevia alexandri	Synapsida	GRG	259.1	251.9	Y	Y	Y	N	N
Inostrancevia latifrons	Synapsida	GRG	259.1	251.9	Y	Y	Y	N	N
Leontosaurus vanderhorsti	Synapsida	GRG	259.1	251.9	Y	Y	Y	N	N
Lycaenops ornatus	Synapsida	GRG	259.1	251.9	Y	Y	Y	N	N
Nochnitsa geminidens	Synapsida	GRG	265.1	259.1	Y	Y	Y	N	N
Pravoslavlevia parva	Synapsida	GRG	254.14	251.9	Y	Y	Y	N	N
Rubidgea atrox	Synapsida	GRG	259.1	251.9	Y	Y	Y	N	N
Sauroctonus parringtoni	Synapsida	GRG	259.1	254.14	Y	Y	Y	N	N
Sauroctonus progressus	Synapsida	GRG	259.1	254.14	Y	Y	Y	N	N
Scylacops capensis	Synapsida	GRG	259.1	254.14	Y	Y	Y	N	N
Smilesaurus ferox	Synapsida	GRG	259.1	254.14	Y	Y	Y	N	N
Suchogorgon golubevi	Synapsida	GRG	265.1	254.14	Y	Y	Y	N	N
Sycosaurus nowaki	Synapsida	GRG	259.1	251.9	Y	Y	Y	N	N
Viatkogorgon ivakhnenkoi	Synapsida	GRG	265.1	259.1	Y	Y	Y	N	N
Annatherapsidus petri	Synapsida	THC	259.1	251.9	Y	Y	Y	N	N
Bauria cynops	Synapsida	THC	247.2	242	Y	Y	N	Y	N
Choerosaurus dejageri	Synapsida	THC	259.1	254.14	Y	Y	Y	N	N
Ericiolacerta parva	Synapsida	THC	251.9	251.2	Y	Y	Y	N	N
Glanosuchus macrops	Synapsida	THC	268.8	259.1	Y	Y	Y	N	N
Gorynychus masyutinae	Synapsida	THC	265.1	259.1	Y	Y	Y	N	N
Hazhenia concava	Synapsida	THC	251.2	242	Y	Y	N	N	N
Hofmeyria atavus	Synapsida	THC	265.1	254.14	Y	Y	Y	N	N
Ictidosaurus angusticeps	Synapsida	THC	268.8	259.1	Y	Y	Y	N	N

Ictidosuchoides longiceps	Synapsida	THC	265.1	251.9	Y	Y	Y	N	N
Jiufengia jiai	Synapsida	THC	254.14	251.2	Y	Y	Y	N	N
Karenites ornamentatus	Synapsida	THC	265.1	259.1	Y	Y	Y	N	N
Lycideops longiceps	Synapsida	THC	259.1	251.9	Y	Y	Y	N	N
Lycosuchus vanderrieti	Synapsida	THC	265.1	259.1	Y	Y	Y	N	N
Microgomphodon oligocynus	Synapsida	THC	251.2	232	Y	Y	N	N	N
Mirotenthes digitipes	Synapsida	THC	259.1	254.14	Y	Y	Y	N	N
Moschorhinus kitchingi	Synapsida	THC	259.1	251.2	Y	Y	Y	N	N
Mupashi migrator	Synapsida	THC	259.1	254.14	Y	Y	Y	N	N
Nothogomphodon danilovi	Synapsida	THC	247.2	242	Y	Y	N	N	N
Olivierosuchus parringtoni	Synapsida	THC	251.9	251.2	Y	Y	Y	N	N
Ophidostoma tatarinovi	Synapsida	THC	259.1	254.14	Y	Y	Y	N	N
Ordosiodon youngi	Synapsida	THC	247.2	242	Y	Y	N	N	N
Pristerognathus polyodon	Synapsida	THC	265.1	259.1	Y	Y	Y	N	N
Promoschorhynchus platyrhinus	Synapsida	THC	254.14	251.2	Y	Y	Y	N	N
Purlovia maxima	Synapsida	THC	254.14	251.9	Y	Y	Y	N	N
Scalopodon tenuisfrons	Synapsida	THC	265.1	259.1	Y	Y	Y	N	N
Scalopolacerta hoffmanni	Synapsida	THC	251.9	251.2	Y	Y	Y	N	N
Scaloposaurus constrictus	Synapsida	THC	251.9	247.2	Y	Y	Y	N	N
Scylacosaurus sclateri	Synapsida	THC	265.1	259.1	Y	Y	Y	N	N
Tetracynodon darti	Synapsida	THC	259.1	251.2	Y	Y	Y	Y	N
Theriognathus microps	Synapsida	THC	259.1	251.9	Y	Y	Y	N	N
Traversodontoides wangwuensis	Synapsida	THC	247.2	242	Y	Y	N	Y	N

Viatkosuchus sumini	Synapsida	THC	265.1	259.1	Y	Y	Y	N	N
Zorillodontops gracilis	Synapsida	THC	251.9	251.2	Y	Y	Y	N	N
Abrictosaurus consors	ARCHM	ORN	201.3	190.8	Y	N	N	N	N
Emausaurus ernsti	ARCHM	ORN	182.7	174.1	Y	N	N	N	N
Eocursor parvus	ARCHM	ORN	201.3	199.3	Y	N	N	N	N
Heterodontosaurus tucki	ARCHM	ORN	199.3	190.8	Y	N	N	N	N
Lesothosaurus diagnosticus	ARCHM	ORN	201.3	190.8	Y	N	N	N	N
Manidens condorensis	ARCHM	ORN	182.7	174.1	Y	N	N	N	N
Scelidosaurus harrisonii	ARCHM	ORN	199.3	190.8	Y	N	N	N	N
Eoraptor	ARCHM	SPD	232	227	Y	N	N	Y	Y
Pampadromaeus barberenai	ARCHM	SPD	232	227	Y	N	N	Y	Y
Panphagia protos	ARCHM	SPD	232	227	Y	N	N	Y	Y
Aardonyx celestae	ARCHM	SPD	201.3	190.8	Y	N	N	Y	Y
Adeopapposaurus mognai	ARCHM	SPD	201.3	190.8	Y	N	N	Y	Y
Anchisaurus	ARCHM	SPD	199.3	190.8	Y	N	N	Y	Y
Bagualosaurus agudoensis	ARCHM	SPD	232	227	Y	N	N	Y	Y
Buriolestes schultzi	ARCHM	SPD	232	227	Y	N	N	Y	Y
Coloradisaurus	ARCHM	SPD	220.83	214.67	Y	N	N	Y	Y
Efraasia minor	ARCHM	SPD	220.83	214.67	Y	N	N	Y	Y
Jingshanosaurus	ARCHM	SPD	201.3	199.3	Y	N	N	Y	Y
Lamplughsaura dharmaramensis	ARCHM	SPD	199.3	190.8	Y	N	N	Y	Y
Leyesaurus marayensis	ARCHM	SPD	201.3	190.8	Y	N	N	Y	Y
Lufengosaurus	ARCHM	SPD	201.3	190.8	Y	N	N	Y	Y
Macrocollum itaquii	ARCHM	SPD	227	220.83	Y	N	N	Y	Y
Massospondylus carinatus	ARCHM	SPD	201.3	190.8	Y	N	N	Y	Y

Melanorosaurus	ARCHM	SPD	214.67	201.3	Y	N	N	Y	Y
Mussaurus patagonicus	ARCHM	SPD	214.67	208.5	Y	N	N	Y	Y
Ngwevu intloko	ARCHM	SPD	199.3	190.8	Y	N	N	Y	Y
Pantydraco caducus	ARCHM	SPD	208.5	201.3	Y	N	N	Y	Y
Plateosaurus engelhardti	ARCHM	SPD	227	201.3	Y	N	N	Y	Y
Riojasaurus	ARCHM	SPD	220.83	214.67	Y	N	N	Y	Y
Sarahsaurus aurifontanalis	ARCHM	SPD	190.8	182.7	Y	N	N	Y	Y
Tazoudasaurus naimi	ARCHM	SPD	182.7	174.1	Y	N	N	Y	Y
Thecodontosaurus sp	ARCHM	SPD	208.5	201.3	Y	N	N	Y	Y
Unaysaurus tolentinoi	ARCHM	SPD	227	220.83	Y	N	N	Y	Y
Xixiposaurus suni	ARCHM	SPD	201.3	199.3	Y	N	N	Y	Y
Yimenosaurus	ARCHM	SPD	201.3	190.8	Y	N	N	Y	Y
Yizhousaurus sunae	ARCHM	SPD	199.3	190.8	Y	N	N	Y	Y
Yunnanosaurus huangi	ARCHM	SPD	201.3	190.8	Y	N	N	Y	Y
Coelophysis bauri	ARCHM	THP	214.67	201.3	Y	N	N	N	N
Daemonosaurus chauliodus	ARCHM	THP	208.5	201.3	Y	N	N	N	N
Dilophosaurus sinensis	ARCHM	THP	199.3	190.8	Y	N	N	N	N
Dilophosaurus wetherilli	ARCHM	THP	190.8	182.7	Y	N	N	N	N
Eodromaeus murphi	ARCHM	THP	232	227	Y	N	N	N	N
Liliensternus liliensterni	ARCHM	THP	214.67	201.3	Y	N	N	N	N
Megapnosaurus kayentakatae	ARCHM	THP	201.3	182.7	Y	N	N	N	N
Notatesseraeraptor frickensis	ARCHM	THP	214.67	208.5	Y	N	N	N	N
Panguraptor lufengensis	ARCHM	THP	201.3	199.3	Y	N	N	N	N
Tawa hallae	ARCHM	THP	214.67	208.5	Y	N	N	N	N
Zupaysaurus rougieri	ARCHM	THP	220.83	214.67	Y	N	N	N	N

Gnathovorax cabreirai	ARCHM	HRR	232	227	Y	N	N	N	N
Herrerasaurus ischigualastensis	ARCHM	HRR	232	227	Y	N	N	N	N
Sanjuansaurus gordilloi	ARCHM	HRR	232	227	Y	N	N	N	N
Smok wawelski	ARCHM	HRR	214.67	201.3	Y	N	N	N	N
Staurikosaurus pricei	ARCHM	HRR	232	227	Y	N	N	N	N
Asilisaurus kongwe	ARCHM	SIL	242	237	Y	N	N	Y	Y
Lagosuchus talampayensis	ARCHM	SIL	237	232	Y	N	N	Y	Y
Lewisuchus admixtus	ARCHM	SIL	237	232	Y	N	N	Y	Y
Pisanosaurus mertii	ARCHM	SIL	232	220.83	Y	N	N	Y	Y
Silesaurus opolensis	ARCHM	SIL	232	227	Y	N	N	Y	Y
Austriadactylus cristatus	ARCHM	PTR	220.83	214.67	Y	N	N	N	N
Austriadraco dallavecchiai	ARCHM	PTR	220.83	214.67	Y	N	N	N	N
Caelestiventus hanseni	ARCHM	PTR	208.5	201.3	Y	N	N	N	N
Campylognathoides liasicus	ARCHM	PTR	182.7	174.1	Y	N	N	N	N
Carniadactylus rosenfeldi	ARCHM	PTR	220.83	214.67	Y	N	N	N	N
Caviramus schesaplanensis	ARCHM	PTR	214.67	208.5	Y	N	N	N	N
Dimorphodon macronyx	ARCHM	PTR	201.3	182.7	Y	N	N	N	N
Dorygnathus banthensis	ARCHM	PTR	182.7	174.1	Y	N	N	N	N
Eudimorphodon ranzii	ARCHM	PTR	227	220.83	Y	N	N	N	N
Peteinosaurus zambelli	ARCHM	PTR	220.83	214.67	Y	N	N	N	N
Preondactylus buffarinii	ARCHM	PTR	220.83	214.67	Y	N	N	N	N
Raeticodactylus filisurensis	ARCHM	PTR	227	220.83	Y	N	N	N	N
Seazzadactylus venieri	ARCHM	PTR	214.67	208.5	Y	N	N	N	N

Scleromochlus taylori	ARCHM	PTR	232	227	Y	N	N	N	N
Yarasuchus	ARCHM	APH	247.2	242	Y	N	N	N	N
Angistorhinus grandis	ARCHM	PHYT	232	227	Y	N	N	N	N
Brachysuchus megalodon	ARCHM	PHYT	232	220.83	Y	N	N	N	N
Diandongosuchus fuyuanensis	ARCHM	PHYT	242	237	Y	N	N	N	N
Leptosuchus crosbiensis	ARCHM	PHYT	227	220.83	Y	N	N	N	N
Machaeroprosopus gregorii	ARCHM	PHYT	227	201.3	Y	N	N	N	N
Mystriosuchus planirostris	ARCHM	PHYT	220.83	214.67	Y	N	N	N	N
Nicrosaurus kapffi	ARCHM	PHYT	220.83	214.67	Y	N	N	N	N
Paleorhinus	ARCHM	PHYT	232	227	Y	N	N	N	N
Parasuchus hislopi	ARCHM	PHYT	232	227	Y	N	N	N	N
Protome batalaria	ARCHM	PHYT	220.83	214.67	Y	N	N	N	N
Rutiodon carolinensis	ARCHM	PHYT	227	220.83	Y	N	N	N	N
Smilosuchus adamanensis	ARCHM	PHYT	227	214.67	Y	N	N	N	N
Aetosaurus ferratus	ARCHM	AETO	227	208.5	Y	N	N	Y	N
Desmatosuchus haplocerus	ARCHM	AETO	227	208.5	Y	N	N	Y	N
Longosuchus meadei	ARCHM	AETO	232	227	Y	N	N	Y	N
Neoaetosauroides engaeus	ARCHM	AETO	220.83	214.67	Y	N	N	Y	N
Paratypothorax andressorum	ARCHM	AETO	227	208.5	Y	N	N	Y	N
Stagonolepis robertsoni	ARCHM	AETO	232	227	Y	N	N	Y	N
Stenomyti huangae	ARCHM	AETO	220.83	208.5	Y	N	N	Y	N
Typothorax coccinarum	ARCHM	AETO	227	208.5	Y	N	N	Y	N

Revueltosaurus callenderi	ARCHM	AETO	227	208.5	Y	N	N	Y	N
Dynamosuchus collisensis	ARCHM	ORS	232	227	Y	N	N	N	N
Ornithosuchus woodwardi	ARCHM	ORS	232	227	Y	N	N	N	N
Riojasuchus tenuisceps	ARCHM	ORS	220.83	214.67	Y	N	N	N	N
Venaticosuchus rusconii	ARCHM	ORS	232	220.83	Y	N	N	N	N
Dyoplax arenaceus	ARCHM	ERP	237	232	Y	N	N	N	N
Erpetosuchus granti	ARCHM	ERP	232	220.83	Y	N	N	N	N
Pagosvenator candelariensis	ARCHM	ERP	242	232	Y	N	N	N	N
Parringtonia gracilis	ARCHM	ERP	242	237	Y	N	N	N	N
Tarjadia ruthae	ARCHM	ERP	242	232	Y	N	N	N	N
Gracilisuchus stipanicicorum	ARCHM	GRA	237	232	Y	N	N	N	N
Turfanosuchus dabanensis	ARCHM	GRA	247.2	242	Y	N	N	N	N
Yonghesuchus sangbiensis	ARCHM	GRA	242	237	Y	N	N	N	N
Arizonasaurus babbitti	ARCHM	PARA	247.2	242	Y	N	N	N	N
Effigia okeeffeae	ARCHM	PARA	208.5	201.3	Y	N	N	Y	N
Lotosaurus adentus	ARCHM	PARA	242	237	Y	N	N	Y	N
Qianosuchus mixtus	ARCHM	PARA	247.2	242	Y	N	N	N	N
Xilousuchus sapingensis	ARCHM	PARA	251.2	242	Y	N	N	N	N
Ticinosuchus ferox	ARCHM	PARA	247.2	242	Y	N	N	N	N
Apatosuchus orbitoangulatus	ARCHM	PARA	220.83	214.67	Y	N	N	N	N
Batrachotomus kupferzellensis	ARCHM	PARA	242	237	Y	N	N	N	N
Prestosuchus chiniquensis	ARCHM	PARA	242	232	Y	N	N	N	N

Saurosuchus galilei	ARCHM	PARA	232	227	Y	N	N	N	N
Decuriasuchus quartacolonia	ARCHM	PARA	242	232	Y	N	N	N	N
Polonosuchus silesiacus	ARCHM	PARA	232	227	Y	N	N	N	N
Postosuchus kirkpatricki	ARCHM	PARA	227	214.67	Y	N	N	N	N
Tikisuchus romeri	ARCHM	PARA	232	227	Y	N	N	N	N
Youngosuchus sinensis	ARCHM	PARA	247.2	242	Y	N	N	N	N
Dibothrosuchus elaphros	ARCHM	CROC	199.3	190.8	Y	N	N	N	N
Dromicosuchus grallator	ARCHM	CROC	227	220.83	Y	N	N	N	N
Pedeticosaurus leviseuri	ARCHM	CROC	201.3	190.8	Y	N	N	Y	N
Pseudhesperosuchus jachaleri	ARCHM	CROC	220.83	214.67	Y	N	N	N	N
Saltoposuchus connectens	ARCHM	CROC	220.83	214.67	Y	N	N	N	N
Sphenosuchus acutus	ARCHM	CROC	201.3	190.8	Y	N	N	N	N
Terrestrisuchus gracilis	ARCHM	CROC	208.5	201.3	Y	N	N	N	N
Trialestes romeri	ARCHM	CROC	232	220.83	Y	N	N	N	N
Pelagosaurus typus	ARCHM	THAL	182.7	174.1	Y	N	N	N	N
Platysuchus multiscrobiculatus	ARCHM	THAL	182.7	174.1	Y	N	N	N	N
Steneosaurus bollensis	ARCHM	THAL	182.7	174.1	Y	N	N	N	N
Coloradisuchus abelini	ARCHM	CROC	220.83	214.67	Y	N	N	N	N
Edentosuchus sp	ARCHM	CROC	190.8	182.7	Y	N	N	Y	N
Hemiprotosuchus leali	ARCHM	CROC	220.83	214.67	Y	N	N	N	N
Orthosuchus stormbergi	ARCHM	CROC	199.3	190.8	Y	N	N	N	N
Protosuchus richardsoni	ARCHM	CROC	208.5	199.3	Y	N	N	N	N

Erythrosuchus africanus	ARCHM	ARF	247.2	242	Y	N	N	N	N
Garjainia prima	ARCHM	ARF	251.2	247.2	Y	N	N	N	N
Shansisuchus shansisuchus	ARCHM	ARF	247.2	242	Y	N	N	N	N
Euparkeria capensis	ARCHM	ARF	247.2	242	Y	N	N	N	N
Osmolskina czatkowicensis	ARCHM	ARF	251.2	247.2	Y	N	N	N	N
Cerritosaurus binsfeldi	ARCHM	ARF	232	227	Y	N	N	N	N
Chanaresuchus bonapartei	ARCHM	ARF	237	232	Y	N	N	N	N
Doswellia sixmilensis	ARCHM	ARF	232	220.83	Y	N	N	N	N
Gualosuchus reigi	ARCHM	ARF	237	232	Y	N	N	N	N
Litorosuchus somnii	ARCHM	ARF	242	237	Y	N	N	N	N
Proterochampsa barrionuevoi	ARCHM	ARF	232	227	Y	N	N	N	N
Tropidosuchus romeri	ARCHM	ARF	237	232	Y	N	N	N	N
Vancleavea campi	ARCHM	ARF	227	201.3	Y	N	N	N	N
Chasmatosaurus yuani	ARCHM	ARF	251.9	247.2	Y	N	N	N	N
Proterosuchus fergusi	ARCHM	ARF	251.9	251.2	Y	N	N	N	N
Teyujagua paradoxa	ARCHM		251.9	247.2	Y	N	N	N	N
Azendohsaurus madagaskarensis	ARCHM	ALK	237	227	Y	N	N	Y	N
Pamelaria dolichotrachela	ARCHM	ALK	247.2	242	Y	N	N	Y	N
Teraterpeton hrynewichorum	ARCHM	ALK	232	227	Y	N	N	Y	N
Trilophosaurus buettneri	ARCHM	ALK	232	214.67	Y	N	N	Y	N
Boreopricea funerea	ARCHM	PROL	251.2	247.2	Y	N	N	N	N
Jesairosaurus lehmani	ARCHM	PROL	251.2	242	Y	N	N	N	N
Malerisaurus robinsonae	ARCHM	PROL	232	227	Y	N	N	N	N
Prolacerta broomi	ARCHM	PROL	251.9	251.2	Y	N	N	N	N

Dinocephalosaurus orientalis	ARCHM	TNY	247.2	242	Y	N	N	N	N
Macrocnemus bassanii	ARCHM	TNY	247.2	237	Y	N	N	N	N
Pectodens zhenyuensis	ARCHM	TNY	247.2	242	Y	N	N	N	N
Tanystropheus longobardicus	ARCHM	TNY	247.2	237	Y	N	N	N	N
Eohyosaurus wolvaardti	ARCHM	RHYN	247.2	242	Y	N	N	Y	N
Fodonyx	ARCHM	RHYN	247.2	242	Y	N	N	Y	N
Hyperodapedon gordoni	ARCHM	RHYN	232	227	Y	N	N	Y	N
Hyperodapedon huxleyi	ARCHM	RHYN	232	227	Y	N	N	Y	N
Hyperodapedon sanjuanensis	ARCHM	RHYN	232	227	Y	N	N	Y	N
Isalorhynchus genovefae	ARCHM	RHYN	237	232	Y	N	N	Y	N
Langeronyx brodiei	ARCHM	RHYN	247.2	242	Y	N	N	Y	N
Mesosuchus browni	ARCHM	RHYN	247.2	242	Y	N	N	Y	N
Rhynchosaurus articeps	ARCHM	RHYN	247.2	242	Y	N	N	Y	N
Stenaulorhynchus sp	ARCHM	RHYN	242	237	Y	N	N	Y	N
Teyumbaita sulcognathus	ARCHM	RHYN	232	227	Y	N	N	Y	N
Candelaria barbouri	Parareptilia	OW	242	237	N	N	N	Y	N
Owenetta kitchingorum	Parareptilia	OW	251.9	251.2	N	N	N	Y	N
Owenetta rubidgei	Parareptilia	OW	259.8	251.2	N	N	N	Y	N
Coletta seca	Parareptilia	PROCL	251.9	251.2	N	N	N	Y	N
Contritosaurus simus	Parareptilia	PROCL	251.9	251.2	N	N	N	Y	N
Eumetabolodon bathycephalus	Parareptilia	PROCL	251.2	242	N	N	N	Y	N
Hypsognathus fenneri	Parareptilia	PROCL	214.67	201.3	N	N	N	Y	N
Kapes bentoni	Parareptilia	PROCL	247.2	242	N	N	N	Y	N

Kapes majmesculae	Parareptilia	PROCL	251.2	242	N	N	N	Y	N
Kitchingnathus untabeni	Parareptilia	PROCL	251.2	247.2	N	N	N	Y	N
Lasasaurus beltanae	Parareptilia	PROCL	251.9	247.2	N	N	N	Y	N
Leptopleuron lacertinum	Parareptilia	PROCL	232	227	N	N	N	Y	N
Mandaphon nadra	Parareptilia	PROCL	242	237	N	N	N	Y	N
Orenburgia bruma	Parareptilia	PROCL	251.2	247.2	N	N	N	Y	N
Pentaedrusaurus ordosianus	Parareptilia	PROCL	251.2	242	N	N	N	Y	N
Phaanthosaurus ignatjevi	Parareptilia	PROCL	251.9	251.2	N	N	N	Y	N
Procolophon trigoniceps	Parareptilia	PROCL	251.9	247.2	N	N	N	Y	N
Samaria concinna	Parareptilia	PROCL	251.2	247.2	N	N	N	Y	N
Sauropareion anoplus	Parareptilia	PROCL	251.9	251.2	N	N	N	Y	N
Soturnia caliodon	Parareptilia	PROCL	227	220.83	N	N	N	Y	N
Thelephon contritus	Parareptilia	PROCL	247.2	242	N	N	N	Y	N
Timanophon raridentatus	Parareptilia	PROCL	251.2	247.2	N	N	N	Y	N
Tichvinskia vjatkensis	Parareptilia	PROCL	251.2	247.2	N	N	N	Y	N